VENOMS, ANIMAL AND MICROBIAL TOXINS

EDITED BY: Jean-Marc Sabatier, Zhijian Cao, Jing-Lin Wang, Patrick Michael McNutt, Yuri N. Utkin, Herve Kovacic, Delavar Shahbazzadeh and Heike Wulff

PUBLISHED IN: Frontiers in Pharmacology and Frontiers in Molecular Biosciences

frontiers Research Topics

frontiers

ISSN 1664-8714
ISBN 978-2-88966-991-2
DOI 10.3389/978-2-88966-991-2

About Frontiers

Frontiers is more than just an open-access publisher of scholarly articles: it is a pioneering approach to the world of academia, radically improving the way scholarly research is managed. The grand vision of Frontiers is a world where all people have an equal opportunity to seek, share and generate knowledge. Frontiers provides immediate and permanent online open access to all its publications, but this alone is not enough to realize our grand goals.

Frontiers Journal Series

The Frontiers Journal Series is a multi-tier and interdisciplinary set of open-access, online journals, promising a paradigm shift from the current review, selection and dissemination processes in academic publishing. All Frontiers journals are driven by researchers for researchers; therefore, they constitute a service to the scholarly community. At the same time, the Frontiers Journal Series operates on a revolutionary invention, the tiered publishing system, initially addressing specific communities of scholars, and gradually climbing up to broader public understanding, thus serving the interests of the lay society, too.

Dedication to Quality

Each Frontiers article is a landmark of the highest quality, thanks to genuinely collaborative interactions between authors and review editors, who include some of the world's best academicians. Research must be certified by peers before entering a stream of knowledge that may eventually reach the public - and shape society; therefore, Frontiers only applies the most rigorous and unbiased reviews.
Frontiers revolutionizes research publishing by freely delivering the most outstanding research, evaluated with no bias from both the academic and social point of view. By applying the most advanced information technologies, Frontiers is catapulting scholarly publishing into a new generation.

What are Frontiers Research Topics?

Frontiers Research Topics are very popular trademarks of the Frontiers Journals Series: they are collections of at least ten articles, all centered on a particular subject. With their unique mix of varied contributions from Original Research to Review Articles, Frontiers Research Topics unify the most influential researchers, the latest key findings and historical advances in a hot research area! Find out more on how to host your own Frontiers Research Topic or contribute to one as an author by contacting the Frontiers Editorial Office: frontiersin.org/about/contact

VENOMS, ANIMAL AND MICROBIAL TOXINS

Topic Editors:
Jean-Marc Sabatier, Aix-Marseille Université, France
Zhijian Cao, Wuhan University, China
Jing-Lin Wang, Beijing Institute of Microbiology and Epidemiology, China
Patrick Michael McNutt, Wake Forest Institute for Regenerative Medicine, United States
Yuri N. Utkin, Institute of Bioorganic Chemistry (RAS), Russia
Herve Kovacic, Aix Marseille Université, France
Delavar Shahbazzadeh, Pasteur Institute of Iran (PII), Iran
Heike Wulff, University of California, Davis, United States

Citation: Sabatier, J.-M., Cao, Z., Wang, J.-L., McNutt, P. M., Utkin, Y. N., Kovacic, H., Shahbazzadeh, D., Wulff, H., eds. (2021). Venoms, Animal and Microbial Toxins. Lausanne: Frontiers Media SA. doi: 10.3389/978-2-88966-991-2

Table of Contents

frontiers in Pharmacology

EDITORIAL
published: 26 May 2021
doi: 10.3389/fphar.2021.706573

Editorial: Venoms, Animal and Microbial Toxins

*Zhijian Cao[1], Jing-Lin Wang[2], Patrick Michael McNutt[3], Yuri N. Utkin[4], Delavar Shahbazzadeh[5], Heike Wulff[6], Hervé Kovacic[7] and Jean-Marc Sabatier[7]**

[1]College of Life Sciences, Wuhan University, Wuhan, China, [2]Beijing Institute of Microbiology and Epidemiology, Beijing, China, [3]Wake Forest Institute for Regenerative Medicine, Winston-Salem, NC, United States, [4]Shemyakin-Ovchinnikov Institute of Bioorganic Chemistry RAS, Moscow, Russia, [5]Pasteur Institute of Iran (PII), Tehran, Iran, [6]Department of Pharmacology, University of California, Davis, Davis, CA, United States, [7]UMR7051 Institut de NeuroPhysiopathologie, Aix-Marseille Université, Marseille, France

Keywords: animal toxin, plant toxin, venom, bacterial toxin, viral toxin

Editorial on the Research Topic

Venoms, Animal and Microbial Toxins

The Research Topic titled "Venoms, Animal and Microbial Toxins" is focused on the structural and functional properties of animal derived venoms, plant and microbial toxins, as well as their molecular/cellular targets. It compiles seventeen key research articles and up-to-date reviews in the field to better describe venoms, the structural features of toxins (and derivatives thereof) and their various modes of action, through the analyses of their structural characteristics, structure-function relationship, and pharmacology.

Venomous animals such as scorpions, snakes, sea anemones, cone snails, worms, wasps, lizards and frogs, and microbes (e.g., bacteria, viruses and fungi) are the natural sources of diverse toxins to neutralize or kill their preys/hosts. These toxins (of various nature and size) are exhibiting a variety of modes of action by targeting ion channels, receptors, enzymes, neurotransmitter release, etc. Because of their potencies and wide range of bioactivities, researchers are actively studying toxins (and derivatives) focusing on their potential as candidate chemotherapeutic drugs (to treat pain, cancer, microbial infections, neurological and immune disorders) or as biological weapons (anthrax, ricin, conotoxins, etc.).

In this Research Topic, several articles are focused on the mode of action and/or synergy of toxins as well as venom compounds. For example, the review article by Ullah highlights snake venom L-amino acid oxidases (SV-LAAOs), which are enzymes catalyzing the stereospecific oxidation of L-amino acids to their corresponding α-keto acids. These key compounds are reportedly playing a role in many biological processes (apoptosis, platelet aggregation/inhibition, edema, hemorrhage and anticoagulation) and have been used as antimicrobials and anticancer agents. The author here describes the structure, mechanism of catalysis, and inhibition and substrate specificity of the characterized SV-LAAOs. Another article by Pucca et al. is focused on toxin synergism between phospholipases A_2 (PLA_2) and cytotoxins. The authors show how cytotoxins and PLA_2 from distinct animal species (bees, vipers, elapids) can interact synergistically to enhance cell lysis. They further propose a mechanistic model of enhanced cell lysis by a synergistic action of both PLA_2 and cytotoxins. The research article by Hess Lopes et al. reports on the action of *Loxosceles* spider venom sphingomyelinases D (SMases D) on lipid rafts and the activation of endogenous metalloproteinases from the ADAMs family. The authors found that SMases D alter lipid raft structures resulting in the activation of membrane bound proteases and subsequent proteolysis of cell surface proteins eventually leading to a pathology. The work by Xu et al. describes an action of the ricin toxin binding subunit B (RTB) on mouse macrophages. It was

OPEN ACCESS

Edited and reviewed by:
Desaphy Jean-François, University of Bari Aldo Moro, Bari, Italy

****Correspondence:***
Jean-Marc Sabatier
sabatier.jm1@libertysurf.fr

Received: *07 May 2021*
Accepted: *13 May 2021*
Published: *26 May 2021*

Citation:
Cao Z, Wang J-L, McNutt PM, Utkin YN, Shahbazzadeh D, Wulff H, Kovacic H and Sabatier J-M (2021) Editorial: Venoms, Animal and Microbial Toxins. Front. Pharmacol. 12:706573. doi: 10.3389/fphar.2021.706573

found to stimulate the production of TNF-α through activation of the transcription factor NF-κB via the TLR4 signaling pathway. Such work is important to better understand the mode of action of the highly toxic plant toxin ricin. Gigolaev et al. were able to switch the K^+ channel subtype selectivity of the scorpion toxin MeKTx13-3 from the Asian scorpion *Mesobuthus eupeus* from the voltage-gated Kv1.1 to the Kv1.3 channel subtype using molecular modeling and mutagenesis. Such work helps to define the structural basis of toxin-to-ion channel recognition at the molecular level and illustrates the feasibility of redesigning venom peptides into potential biologic drug candidates since Kv1.3 constitutes an attractive target for immunosuppression. Similar applied work by Alvarado et al. reports on a "novel" insecticidal peptide against house crickets referred to as Osu1, from the venom of spider *Oculicosa supermirabilis*. Recombinantly expressed Osu1 was shown to potently modulate the human voltage-dependent Kv1.5 (hKv1.5) channel subtype, a potential target for atrial fibrillation therapy. Such a compound might serve as a lead to design structural analogs (and candidate drugs) with improved selectivity and/or potency toward this particular human K^+ channel.

Other articles of the Research Topic are focused on the targets and fields of application of toxins or venoms. For example, bee venom-based acupuncture (BVA) is widely used in certain countries to treat a variety of disorders, including inflammatory and pain-related diseases. Adverse reactions such as anaphylaxis can occur. Lee et al. have examined the incidence rate of hypersensitivity reactions during or following BVA. The authors surveyed the medical records of 8,580 individuals treated by BVA (60,654 BVA treatments), and their potential clinical symptoms (allergy) were studied, highlighting a 0.047% incidence rate of anaphylaxis. An "*in-depth*" review article by de Castro Figueiredo Bordon et al., 2020 is also focusing on the various potential applications of toxins/venoms, from diagnostic tools to chemotherapeutic drugs. An overview of the current toxin-based marketed and candidate (non-marketed) drugs is presented. The advances and perspectives of candidate therapeutic molecules from scorpions, snakes, cone snails, sea anemones, spiders, hymenopterans, amphibians, and others marine and non-marine animals (leeches, bats, lizards, ticks, caterpillars, shrews), are critically discussed. An interesting report by Gao et al., 2021 compares the pancreatic damage induced by Paraquat (PQ) -a widely used herbicide in rats following two methods of PQ administration (intragastric infusion vs. intraperitoneal injection). The authors found that both methods could cause pancreatic damage, the most severe damage being associated with intragastric infusion. This study indicates that particular attention to the toxicity of PQ should therefore be observed by clinicians when this compound is ingested orally. The article by McArthur et al. highlights that, in addition to the voltage-gated $Na_v1.7$ channel, the analgesic spider venom peptide Pn3a can also block high voltage-activated (HVA) calcium channels. This study reveals that L-, P/Q- and N-type Ca_v channels could be inhibited by Pn3a, contrary to R-type channel. Interestingly, the Pn3a inhibition of neuronal Ca_v currents is reportedly enhanced by opioid receptor activation.

The potential neutralization of the highly pathogenic bacterial toxins TcdA, TcdB and CDT (bacterium *Clostridioides difficile*) by human α-Defensin-5 is described in another article Korbmacher et al.. According to Korbmacher et al., α-defensin-5 should be considered as a candidate drug to treat severe associated human diseases such as pseudomembranous or fulminant colitis, and diarrhea. Thus, the beneficial role of α-defensin-5 would rely on its contribution in the first line host defense mechanism against microbes, as well as its inhibitory action against pathogenic bacterial toxins.

An important review article by Santos Menezes et al. deals with the voltage-gated sodium channelopathies and epilepsy. Indeed, voltage-gated sodium (Na_v) channels are central to the action potential and mutation-induced dysfunction of Na_v channels may result in altered neuronal activity (e.g., epilepsy). Although $Na_v1.1$ channels appear to be "key" regarding epilepsy, the authors provide an up-to-date overview on other epilepsy-related human Na_v channel subtypes (Nav1.1 to Nav1.3, Nav1.6 and Nav1.7).

Another key review article is provided by Osmakov et al.. The authors used animal, plant, and microbial toxins for the structural and functional/pharmacological characterization of membrane-associated acid-sensing ion channels (ASICs), which are sensors of extracellular pH variation involved in regulatory functions of neuronal and non-neuronal cells. The authors addressed the biophysical characteristics, architecture, natural ligands, structure-function relationships and therapeutic perspectives of ASICs.

Three articles of the Research Topic are dealing mainly with the structural aspects of toxins. The article by Ullah and Massod (2020) focuses on the structural features (amino acid sequences and 3D structures) of the poorly-studied snake venom phospholipases B, which are enzymes with the highest hemolytic potential in snake venoms. The authors are finally detailing their molecular model of phospholipase B from the snake *Bothrops moojeni*. The article by Câmara et al. describes a multiomics strategy for the identification, sequencing and preliminary screening of potentially bioactive peptides from the venom of tarantula spider *Acanthoscurria rondoniae*. Such multiomics strategies rely on proteomics, peptidomimetics and transcriptomics data coupled to some *in silico* predictions of antimicrobial and antitumor activities. The authors highlighted their "powerful" approach to discover new toxins in venoms and screen for their potential bioactivities.

The review article by Schmidt et al. is dealing with small, non-peptidic, molecules that are present in the venoms of cone snails in addition to conotoxins and conopeptides. The *Stephanoconus* clade of cone snails was mainly investigated because of its particular richness in small, non-peptidic compounds. So far, these molecules were found to be active on neurons and might be of interest in the potential treatment of specific neuronal disorders.

A last article authored by Jackson and Koludarov is particularly important in the field of toxinology, being centered on a complex but "key" question: how toxins actually got their toxic properties? The so-called "weaponization" of a molecule is reasonably and expectedly addressed by these authors.

Finally, in line with its main goal, this Research Topic clearly contributes to an "*in-depth*" knowledge of the animal/plant/microbial toxins (and derivatives) and their molecular targets expectedly opening the way to new attractive research in toxinology, toxicology and (neuro) pharmacology, in parallel to the design of new candidate drugs and/or appropriate antitoxin countermeasures. We strongly believe that this collection of articles exploring the complex world of toxins/toxic compounds and their targets, as well as venoms, will inspire many researchers and clinicians worldwide to continue working in or enter the exciting field of venoms and toxins.

AUTHOR CONTRIBUTIONS

All authors listed have made a substantial, direct, and intellectual contribution to the work and approved it for publication.

REFERENCES

Ullah, A., and Masood, R. (2020). The Sequence and Three-Dimensional Structure Characterization of Snake Venom Phospholipases B. *Front. Mol. Biosci.* 7, 175. doi:10.3389/fmolb.2020.00175

Conflict of Interest: The authors declare that the research was conducted in the absence of any commercial or financial relationships that could be construed as a potential conflict of interest.

frontiers in Pharmacology

REVIEW
published: 25 February 2020
doi: 10.3389/fphar.2020.00110

Structure–Function Studies and Mechanism of Action of Snake Venom L-Amino Acid Oxidases

Anwar Ullah *

Department of Biosciences, COMSATS University Islamabad, Islamabad, Pakistan

Snake venom L-amino acid oxidases (SV-LAAOs) are the least studied venom enzymes. These enzymes catalyze the stereospecific oxidation of an L-amino acid to their corresponding α-keto acid with the liberation of hydrogen peroxide (H_2O_2) and ammonia (NH_3). They display various pathological and physiological activities including induction of apoptosis, edema, platelet aggregation/inhibition, hemorrhagic, and anticoagulant activities. They also show antibacterial, antiviral and leishmanicidal activity and have been used as therapeutic agents in some disease conditions like cancer and anti-HIV drugs. Although the crystal structures of six SV-LAAOs are present in the Protein Data Bank (PDB), there is no single article that describes all of them in particular. To better understand their structural properties and correlate it with their function, the current work describes structure characterization, structure-based mechanism of catalysis, inhibition and substrate specificity of SV-LAAOs. Sequence analysis indicates a high sequence identity (>84%) among SV-LAAOs, comparatively lower sequence identity with Pig kidney D-amino acid oxidase (<50%) and very low sequence identity (<24%) with bacterial LAAOs, Fugal (L-lysine oxidase), and *Zea mays* Polyamine oxidase (PAAO). The three-dimensional structure of these enzymes are composed of three-domains, a FAD-binding domain, a substrate-binding domain and a helical domain. The sequence and structural analysis indicate that the amino acid residues in the loops vary in length and composition due to which the surface charge distribution also varies that may impart variable substrate specificity to these enzymes. The active site cavity volume and its average depth also vary in these enzymes. The inhibition of these enzymes by synthetic inhibitors will lead to the production of more potent antivenoms against snakebite envenomation.

Keywords: snake venom L-amino acid oxidases, sequence and three-dimensional structure analysis, structure-based mechanism of action, inhibition and substrate specificity, L-amino acid oxidases and membrane interaction

OPEN ACCESS

Edited by:
Jean-Marc Sabatier, UMR7051 Institut de Neurophysiopathologie, France

Reviewed by:
Andreimar Martins Soares, Fiocruz Rondonia, Brazil
Ayobami Matthew Olajuyin, Henan Provincial People's Hospital, China
Carlos Chavez Olortegui, Federal University of Minas Gerais, Brazil

***Correspondence:**
Anwar Ullah
anwar.ms90@yahoo.com;
anwarullah@comsats.edu.pk

Specialty section:
This article was submitted to Pharmacology of Ion Channels and Channelopathies, a section of the journal Frontiers in Pharmacology

Received: *16 October 2019*
Accepted: *28 January 2020*
Published: *25 February 2020*

Citation:
Ullah A (2020) Structure–Function Studies and Mechanism of Action of Snake Venom L-Amino Acid Oxidases. Front. Pharmacol. 11:110. doi: 10.3389/fphar.2020.00110

INTRODUCTION

Snake venom LAAO (LAAOs, EC 1.4.3.2) is an FAD-containing dimeric enzyme that stereospecifically deaminates an L-amino acid to an α-keto acid with the concomitant production of hydrogen peroxide and ammonia (Pawelek et al., 2000; Du and Clemetson, 2002; Moustafa et al., 2006; Ullah et al., 2012b; Ullah et al., 2014; Costal-Oliveira et al., 2019). These enzymes are widely distributed in the snake venom and have been found to be toxic (Li et al., 1994; Torii et al., 1997).

Upon snakebite envenomation these enzymes causes many physiological and pathological activities including induction of apoptosis (Torii et al., 1997; Ali et al., 2000; Zainal Abidin et al., 2018; Costal-Oliveira et al., 2019; Machado et al., 2019), edema (Stábeli et al., 2007; Lazo et al., 2017), platelet aggregation/inhibition (Li et al., 1994; Takatsuka et al., 2001; Sakurai et al., 2001; Stabeli et al., 2004; Izidoro et al., 2006; Toyama et al., 2006), hemorrhagic (Souza et al., 1999; Alves et al., 2008), and anticoagulant activities (Sakurai et al., 2003; Tonismagi et al., 2006). Costal-Oliveira et al. (2019) has demonstrated that LAAO from *Bothrops atrox* snake venom causes autophagy, apoptosis and necrosis in normal human keratinocytes. They also display antibacterial (Stiles et al., 1991; Stabeli et al., 2004; Toyama et al., 2006; Tonismagi et al., 2006; Stábeli et al., 2007; Abdelkafi-Koubaa et al., 2016; Rey-Suárez et al., 2018), antiviral (Zhang et al., 2003) antifungal (Costa Torres et al., 2010; Cheng et al., 2012) and leishmanicidal activity (Fernandez-Gomez et al., 1994; Tempone et al., 2001; Toyama et al., 2006; Izidoro et al., 2006; Wiezel et al., 2019).

These enzymes have anti-cancer (Sun et al., 2003; Lee et al., 2014; Tássia et al., 2017) and anti-HIV activity (Sant'Ana et al., 2008) and may be used as therapeutic agents in many disease conditions like anti-cancer and anti-HIV drugs (Sakurai et al., 2003; Zhang et al., 2004; Teixeira et al., 2016; Tan et al., 2017; Costa et al., 2017; Salama et al., 2018; Tan et al., 2018) (Sun et al., 2003; Zhang and Wei, 2007; Lee et al., 2014; Costa et al., 2014; Tássia et al., 2017; Costa et al., 2017). Besides snake venom, LAAO has been found in the insects, fungi (Nuutinen and Timonen, 2008; Yang et al., 2009; Žun et al., 2017), green algae (Schriek et al., 2009), bacteria (Arima et al., 2009), plants (Nishizawa et al., 2005) and mammals (Blanchard et al., 1944; Du and Clemetson, 2002; Kasai et al., 2010). The yellow color of most of the crude venom is due to the presence of LAAO (Tempone et al., 2001; Stábeli et al., 2007) that contains oxidized flavin adenine dinucleotide (FAD) in their structure (Pawelek et al., 2000; Moustafa et al., 2006).

LAAO is a glycoprotein with molecular mass ranging from 120–150 kDa in native (dimeric) form and 55–66 kDa in the denatured (monomeric form) (Tan and Saifuddin, 1989; Abe et al., 1998). Some reports have also shown their tetrameric existence (Georgieva et al., 2011; Feliciano et al., 2017), however, SV-LAAO is mostly present as a dimer in the solution and it is active in this state (Moustafa et al., 2006; Ullah et al., 2012b). The p*I* of these enzymes ranges from 4.4 to 8.0 (Tan, 1998). Most of the SV-LAAOs are stable when kept at room temperature (25°C) and 4°C, however, exposure to the low-temperature (–5°C and –60°C) for long period inactivates these enzymes (Curti et al., 1968; Tan, 1998). The inactivation is caused by a change in the three-dimensional structure of LAAO particularly around the active site (Soltysik et al., 1987). Interestingly, LAAOs from *Ophiophagus hannah* and *Calloselasma rhodostoma* are not inactivated by low temperature treatment (Tan, 1998).

Currently, the crystal structures of six LAAOs have been deposited to the PDB (Zhang et al., 2004; Moustafa et al., 2006; Georgieva et al., 2011; Ullah et al., 2012b; Feliciano et al., 2017). They all share the same structural fold which contains three domains: a FAD-binding domain, a substrate-binding domain and a helical domain (Moustafa et al, 2006; Georgieva et al., 2011; Ullah et al., 2012a; Zhang et al., 2004; Feliciano et al., 2017). SV-LAAOs are usually glycosylated and contain about 3–4% carbohydrates in their structure (deKok and Rawitch (1969); Hayes and Wellner, 1969) and in some cases, the carbohydrate contents may be up to 12% of the total molecular mass of the protein (Alves et al., 2008).

These enzymes hydrolyze the substrate through an oxidation-reduction reaction in which His223 act as a base abstracting a proton from the substrate (amino acid) and converting it to an imino acid (Pawelek et al., 2000; Moustafa et al., 2006). In the next step, the FAD is reduced by transferring a proton from His223. The reoxidation of FAD occurs with the addition of electrons from the oxygen. The imino acid is converted to a α-keto acid with the production of hydrogen peroxide and ammonia (Pawelek et al., 2000; Moustafa et al., 2006).

Although the crystal structures of six SV-LAAOs have been determined, no article describes all of these with comprehensive details. The current work describes the three-dimensional structural features of SV-LAAOs with special reference to their structure-based substrate specificity, mechanism of action and inhibition.

RESULTS AND DISCUSSION

Sequence Alignment Analysis

The primary structure of SV-LAAOs contains 503–516 amino acid residues in the precursor or zymogen form and 485–498 amino acid residues in the mature form (Takatsuka et al., 2001). The amino acid sequence alignment analysis indicates a high degree of sequence identity among SV-LAAOs (>84%), relatively moderate identity with Pig kidney D-amino acid oxidase (DAAOs) (~50%) and very low identity (<24%) with the bacterial (LAAO), fugal (L-lysine oxidase), and *Zea mays* Polyamine oxidase (PAAO) (**Figures 1** and **S1** and **Table 1**). The average sequence identities among SV-LAAOs and LAAOs/PAO/DAAO from other organisms are 86.80 and 31.29% respectively. The differences in amino acid residues are mostly confined to N- and C-termini in SV-LAAOs (**Figure 1**). The amino acid residues belonging to the active site (Arg90, His223, Phe227 and Lys326), FAD-binding (Ser44/Ala44 (1F8R), Glu63, Arg71/Gln71 (4E0V), Met89, Arg90, Glu457, Ileu457 and Thr469) and the substrate/ligand binding (Arg90, Tyr372 and Gly464) are fully conserved among the aligned SV-LAAOs except for Ser44 in *C. rhodostoma* and *Bothrops jararacussu* LAAOs where these have been substituted by Ala44 and Gln71 respectively (**Figures 1** and **S1**). The Cysteine residues (Cys10, Cys173, Cys293, Cys331, Cys390, and Cys413) are fully conserved in all SV-LAAOs and make two disulfide bridges (Cys10-Cys173 and Cys331-Cys413), while Cys293 and Cys390

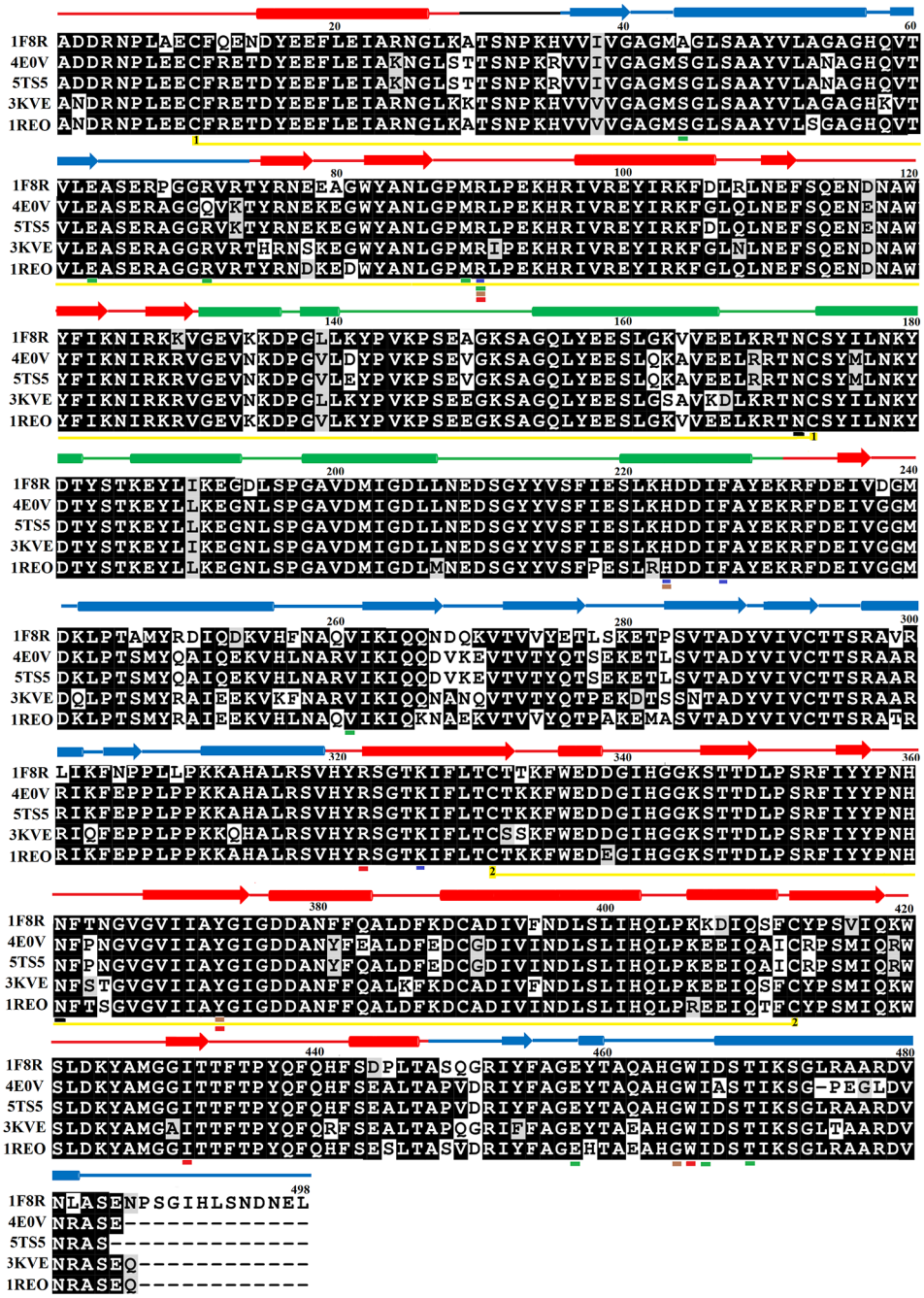

FIGURE 1 | Sequences alignment among snake venom L-amino acid oxidases. 1F8R; crystal structure of L-amino acid oxidase from *Calloselasma rhodostoma*, 4E0V; Structure of L-amino acid oxidase from the *Bothrops jararacussu* venom, 5TS5; Crystal structure of L-amino acid oxidase from *Bothrops atrox*, 3KVE: Structure of native L-amino acid oxidase from *Vipera ammodytes ammodytes*, 1REO; L-amino acid oxidase from *Agkistrodon halys pallas*. The amino acid residues involved in catalysis, metal ion binding and amino acid (substrate) recognition are underlined with blue, brown, and red respectively. The FAD-binding residues are underlined in green. The cysteine residues which make disulfide bridges are linked (yellow lines). The putative N-glycosylation amino acid residues are underlined in black. The amino acid residues in FAD-binding, substrate-binding and helical domain, are colored in blue, red, and green, respectively. The secondary structure elements (alpha helices and beta strands) are shown above the sequence.

don't form any disulfide bridge. The glycosylation sites (Asn172 and Asn361) are also conserved. The C-terminal of LAAO from *C. rhodostoma* has twelve amino acid residues more (extension) than all the other aligned SV-LAAOs sequence.

The Sequence logo generated from multiple sequence alignment of SV-LAAOs indicates that the amino acid residues around the active sites and FAD-binding site are highly conserved among all the aligned enzymes (**Figure S2**).

TABLE 1 | Percent sequence identity among snake venom LAAOs, bacterial (L-Glutamate Oxidase), *Zea mays* (polyamine oxidase), Fungi (L-lysine oxidase) and pig kidney (D-amino acid oxidase).

Proteins	1F8R	4E0V	5TS5	3KVE	1REO	2E1M	2JAE	1B37	3X0V	1KIF
1F8R	–	84.74	86.57	86.60	88.27	34.21	26.60	25.24	24.60	45.83
4E0V	84.74	–	97.93	86.39	87.84	23.47	26.24	24.07	25.20	48.00
5TS5	86.57	97.93	–	87.60	89.26	24.38	26.42	24.38	25.25	48.00
3KVE	86.60	86.39	87.60	–	89.30	33.10	26.15	24.12	25.91	50.00
1REO	88.27	87.84	89.26	89.30	–	35.17	26.71	25.15	25.30	50.00
2E1M	34.21	23.47	24.38	33.10	35.17	–	26.67	45.00	33.11	32.00
2JAE	26.60	26.24	26.42	26.15	26.71	26.67	–	19.55	21.58	37.50
1B37	25.24	24.07	24.38	24.12	25.15	45.00	19.55	–	36.17	50.00
3X0V	24.60	25.20	25.25	25.91	25.30	33.11	21.58	36.17	–	40.00
1KIF	45.83	48.00	48.00	50.00	50.00	32.00	37.50	50.00	40.00	–

1F8R: Calloselasma rhodostoma LAAO, 4E0V: Bothrops jararacussu LAAO, 5TS5: Bothrops atrox LAAO, 3KVE: Vipera ammodytes ammodytes LAAO, 1REO: Agkistrodon halys pallas LAAO, 2E1M: Streptomyces sp. L-Glutamate Oxidase, 2JAE: R. opacus L-amino acid oxidase, 1B37: Zea mays polyamine oxidase, 3X0V: Hypocrea rufa L-lysine oxidase, 1KIF: Pig kidney D-amino acid oxidase.

Overall Structure

SV-LAAO belongs to the family of enzymes called NAD(P)/FAD-dependent oxidoreductase that also comprises polyamine oxidase (PAO), flavin-containing monoamine oxidases (MAOs), D-amino acid dehydrogenase, and linoleic acid isomerase (CDD/SPARCLE; Marchler-Bauer et al., 2017).

The mature protein of SV-LAAO contains 486 amino acid residues that fold into a multidomain protein comprising of three distinct domains namely: a FAD-binding domain, a substrate-binding domain and a helical domain (**Figures 2A–D**) (Moustafa et al, 2006; Georgieva et al., 2011; Ullah et al., 2012a; Zhang et al., 2004; Feliciano et al., 2017). The overall three-dimensional structure of LAAO is composed of seventeen alpha-helices, twenty-two beta-strands and many loops that fold into three well-defined domains. The domains architecture of SV-LAAO is briefly described below:

FAD-Binding Domain

The FAD-binding domain is composed of amino acid residues 35–72, 240–318 and 446–486 (**Figures 1**, **2A**, and **3**, **Table 3**). The secondary structure of this domain contains six beta-strands and five alpha-helices with the insertion of additional short beta-strands (two) and alpha-helix (one). Of the six beta-strands, four are parallel and two are antiparallel, while the two short beta-strands are parallel to one another. The consensus sequence of glycine residues (G40XG42XXG45) present in this domain gives close access to the negatively charged phosphate group of the cofactor and stabilizes the charge by the helix dipole. This domain is stabilized by five salt bridges that exist between the amino acid residues within this domain (Arg71-Glu457, Lys270-Asp288), and with the amino acid residues from the substrate-binding domain (Lys471-Glu13, Arg478-Glu18, Arg478-Asp15) (Sarakatsannis and Duan, 2005) (**Table 2**).

Substrate-Binding Domain

The substrate-binding domain is composed of amino acid residues 5–25, 73–129, 233–236, and 323–420 (**Figures 1**, **2B**, and **3**, **Table 3**). It contains six alpha-helices and eleven beta-strands (**Figure 3**). This domain is stabilized by an intrachain disulfide bridge (Cys331-Cys412) and an interchain disulfide bridge (Cys10-Cys173) with further stabilization by salt bridges (Lys471-Glu13, Glu18-Arg478, Asp15-Arg478, Arg71-Glu457, Arg73-Glu457, Arg99-Asp234, Arg103-Glu100, Lys334-Glu337, Arg353-Asp377, Lys405-Asp391). It also contains an N-linked N-acetylglucosamine.

Helical Domain

This domain is continuous in the amino acid sequence and comprises of amino acids residues 130-230 and is located in between FAD-binding and substrate-binding domain (**Figure 3**, **Table 3**). The secondary structure of this domain contains six alpha-helices with one short alpha-helix and many loops. It is stabilized by an interchain disulfide bridges with the substrate-binding domain (Cys10-Cys173) and intrachain slat bridges (Lys134-Asp117, Lys151-Glu159, Lys179-Glu167).

The Threading-based Protein Domain Prediction online web server identifies seven discontinuous regions from the primary amino acid sequence of SV-LAAOs belonging to these domains. The analysis indicates that these three domains are highly conserved in all SV-LAAOs and with the others proteins containing the similar structure folds in the Protein Data Bank (PDB) (**Figure S3**) (Xue et al., 2013).

The N-terminal of LAAO is stabilized by a hydrogen bond formed between Asn5 (FAD-binding domain) and Asp225 (helical domain) and the C-terminal Ser484 and His57.

Active Site

A funnel-shaped channel is formed between the helical and substrate binding domain that starts from the surface of the protein and extends towards the active site providing access of substrate to the active site. The active site of SV-LAAO comprises FAD and the amino acid residues Arg90, His223, Phe227, Lys326, Tyr372, and Trp375 and a conserved water molecule near FAD and Lys326 (**Figure 2D**). The FAD, Lys326, and the conserved water molecule form a triad Lys326-Water-N5 (FAD) upon substrate binding. The His233 deprotonates the α-amino group of the substrate (amino acid) during the deamination reaction.

Ligand/Substrate-Binding Sites

The FAD is located in between the cofactor and substrate binding domains and is buried deep in the protein. The FAD makes intensive contacts with the amino acid residues from both

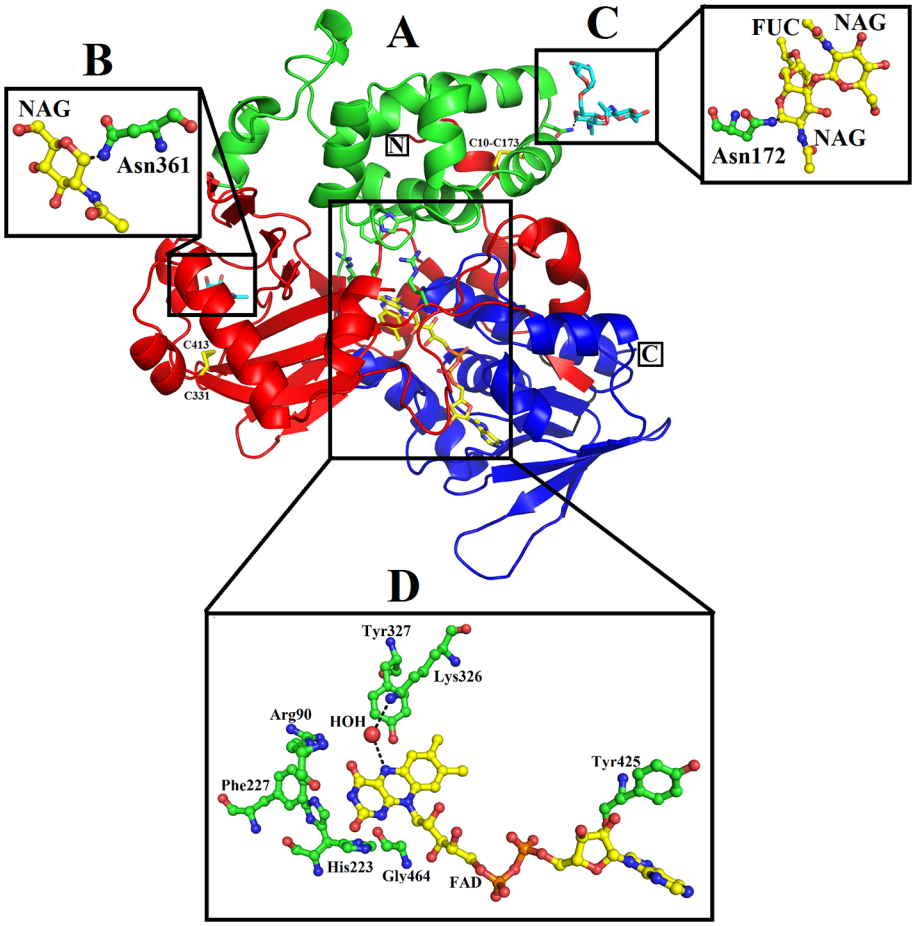

FIGURE 2 | Overall structure of SV-LAAO (PDB ID: 1F8R; *Calloselasma rhodostoma* LAAO) **(A)** cartoon representation. The active site, FAD-binding and glycosylation amino acid residues are shown as green sticks. *T*he disulfide bridges are represented by yellow sticks. **(B–D)**, residues involved in glycosylation and FAD-binding highlighted. The parts of the secondary structure belonging to FAD-binding, substrate-binding and helical domains are colored in blue, red, and green, respectively.

of these domains and several water molecules. These amino acid residues include Ala44, Glu63, Arg71, Met89, Arg90, Val261, Ileu466, and Thr469 (**Figure 4**). The flavin or Isoalloxazine ring makes contact with Met89, Arg90 and Ileu466. The adenine moiety of FAD is bonded to Glu63 and Val261 while the phosphate and sugar part is bonded to Arg71, Ala44, Glu467, and Thr469 (**Figure 4**).

The structure of LAAO from *C. rhodostoma* determined with the bound citrate, 2-amino benzoic acid and L-phenylalanine provides insights into the inhibitors/substrate binding (**Figures 5A–C**). In all three cases the amino acid residues involved are Arg90, Tyr372 and Gly464 (**Figures 5A–C**). Sequence alignment analysis indicates that the ligand/substrate binding amino acid residues are fully conserved among the SV-LAAOs (**Figure 1**).

Zinc Binding Sites

Zinc ions have been found in the crystal structure of LAAOs from *Vipera ammodytes ammodytes* and *B. atrox* (Georgieva et al., 2011; Feliciano et al., 2017). Both enzymes were crystallized in the presence of zinc (zinc acetate and zinc sulfate) (Georgieva et al., 2011; Feliciano et al., 2017). However, LAAOs from *B. jararacussu* and *C. rhodostoma* have no zinc ion in the solution or crystal form (Ullah et al., 2012a; Moustafa et al., 2006), which indicates that the LAAOs from *V. ammodytes ammodytes* and *B. atrox* may have taken the zinc ions from the crystallization solution (Feliciano et al., 2017).

In the tetrameric structure of *V. ammodytes ammodytes* LAAO, the four zinc ions are tetrahedrally coordinated. The zinc ions that connect the monomer A to monomer D are coordinated by His75, Glu279 and two water molecules (**Figure 6A**), while the other zinc ion connecting monomer B and C is also coordinated by His75, Glu279 and two water molecules (**Figure 6B**). The crystal structure of *B. atrox* contains eight zinc ions in which the two zinc ions that connect monomers A and B and monomers C and D are correctly coordinated (**Figures 6C, D**). The remaining six zinc ions are located at the surface of the protein and they are poorly coordinated as confirmed by CheckMyMetal (CMM) (Zheng et al., 2014). In the LAAOs from *V. ammodytes ammodytes* and

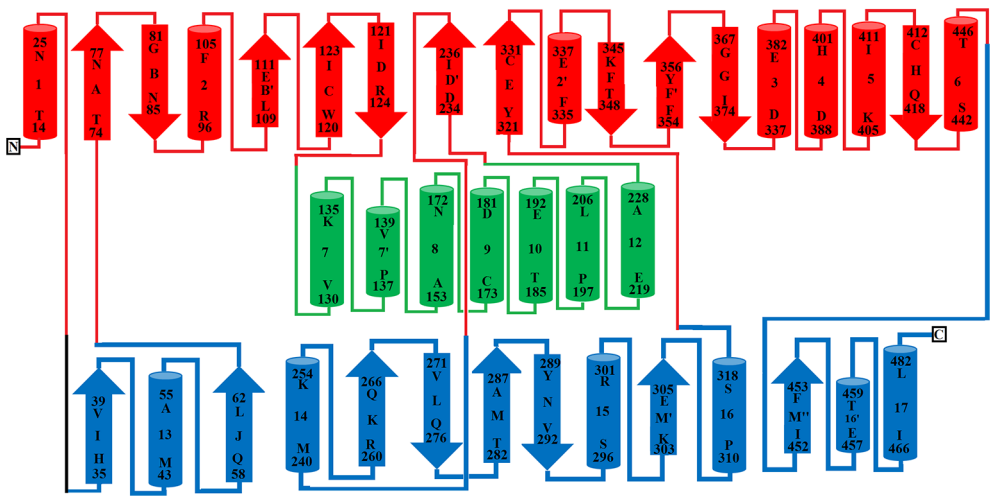

FIGURE 3 | Topology diagram of SV-LAAO. The alpha helices (numbered 1–17) and beta strands (named A–N) are represented as cylinders and arrows, respectively. The short alpha helices and beta strands are shown with primes. The secondary structures and the amino acid residues in alpha helices and beta strands were assigned using the program DSSP from the primary sequence and were confirmed by PyMOL from the tertiary structure. The parts of the secondary structure belonging to FAD-binding, substrate-binding and helical domains are colored in blue, red, and green respectively.

TABLE 2 | Salt bridges in SV-LAAO. NH1 and NH2: Nitrogen atoms (amino groups) of the arginine side chain, OD1, and OD2: Oxygen atoms of aspartic acid side chains, OE: Oxygen atoms of glutamic acid side chains, NZ: Nitrogen atoms (amino groups) of lysine side chains.

Residue 1	Residue 2	Distance
NH1 ARG A 71	OE1 GLU A 457	2.88
NH2 ARG A 71	OE1 GLU A 457	3.58
NH1 ARG A 73	OD1 ASP A 423	3.04
NH2 ARG A 73	OD1 ASP A 423	3.19
NH1 ARG A 76	OD1 ASP A 241	2.82
NH1 ARG A 76	OD2 ASP A 241	2.73
NH2 ARG A 76	OD1 ASP A 241	2.80
NH1 ARG A 99	OD2 ASP A 234	3.63
NH2 ARG A 99	OD2 ASP A 234	2.77
NH1 ARG A 103	OE1 GLU A 100	3.13
NZ LYS A 134	OD1 ASP A 117	2.87
NZ LYS A 134	OD2 ASP A 117	3.82
NZ LYS A 151	OE1 GLU A 159	2.88
NZ LYS A 179	OE1 GLU A 167	3.86
NH2 ARG A 232	OD1 ASP A 234	2.84
NZ LYS A 270	OD1 ASP A 288	2.64
NZ LYS A 270	OD2 ASP A 288	3.82
NZ LYS A 334	OE1 GLU A 337	3.98
NH2 ARG A 353	OD2 ASP A 377	3.76
ND1 HIS A 360	OE1 GLU A 235	3.57
ND1 HIS A 401	OD2 ASP A 339	2.87
NZ LYS A 405	OD1 ASP A 391	2.68
NZ LYS A 405	OD2 ASP A 391	3.81
NZ LYS A 471	OE1 GLU A 13	2.96
NH1 ARG A 478	OE1 GLU A 18	2.60
NH1 ARG A 478	OD2 ASP A 15	3.33

B. atrox zinc ions have been found to stabilize the dimers and these are considered important for the biological activities of these enzymes (Georgieva, et al., 2008; Feliciano et al., 2017). The inhibition and activation by metal ions have been investigated for LAAOs from *Crotalus adamanteus*, *Lachesis muta, Bothrops*

TABLE 3 | Domains of SV-LAAO.

Domains	Amino acid residues range	Total amino acid residues
FAD-Binding domain	35–64, 242–318, 446–471	130
Substrate-binding domain	5–25, 73–129, 233–236, 323–420	176
Helical domain	130–230	100

Brazili, and *Agkistrodon blomhoffii ussurensis* (Bender and Brubacher, 1977; Cisneros, 1996; Solis et al., 1999; Sun et al., 2010). The enzymatic activity of *C. adamanteus* LAAO is enhanced by Mg^{+2} and that of *L. muta* and *B. brazili* LAAOs is inhibited by zinc ion. The zinc ion does not affect the enzymatic activity of *A. blomhoffii ussurensis* LAAO; however, it is important for the structural integrity of the protein (Sun et al., 2010).

Glycosylation

SV-LAAOs are glycosylated proteins with 3–4% carbohydrate moiety (deKok and Rawitch 1969; Hayes and Wellner, 1969). In some cases, the carbohydrate contents may reach up to 12% of the total molecular mass of the protein (Alves et al., 2008). The LAAOs from *C. rhodostoma* and *Agkistrodon halys pallas* contain two glycosylation sites (Asn172 and Asn361) (**Figures 7A, B**) and that of *V. ammodytes ammodytes* and *B. atrox* have a single glycosylation site (Asn172) (**Figures 7C, D**). The glycosylation sites are fully conserved in SV-LAAOs (**Figure 1**). In the case of LAAOs from *C. rhodostoma* and *B. atrox* Asn172 has three carbohydrate moieties, NAG-FUC-NAG (NAG: N-Acetyl-D-Glucosamine; FUC: alfa-L-Fucose) (**Figures 7A, D**), while Asn361 has one NAG in the former and the latter lacks a carbohydrate moiety at this position. The LAAOs from *A. halys pallas* has a single carbohydrate moiety at both positions 172 and 361 (**Figure 7B**). The *V. ammodytes ammodytes* LAAO has a single

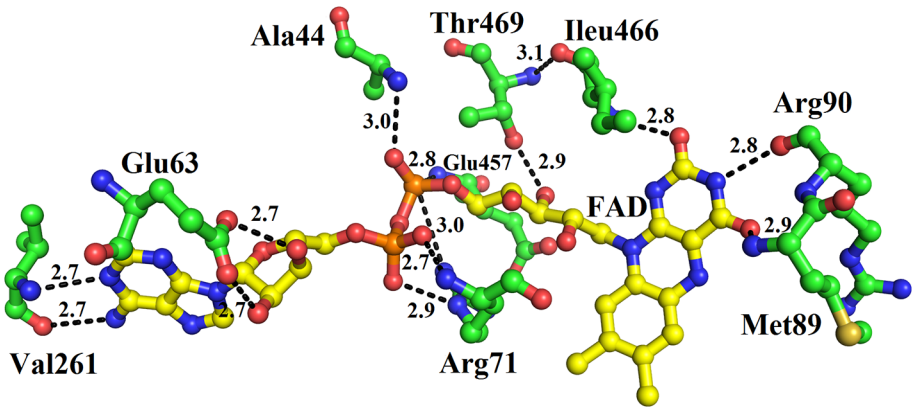

FIGURE 4 | FAD-binding amino acid residues of SV-LAAO. The FAD is shown as yellow sticks and the amino acid residues as green sticks.

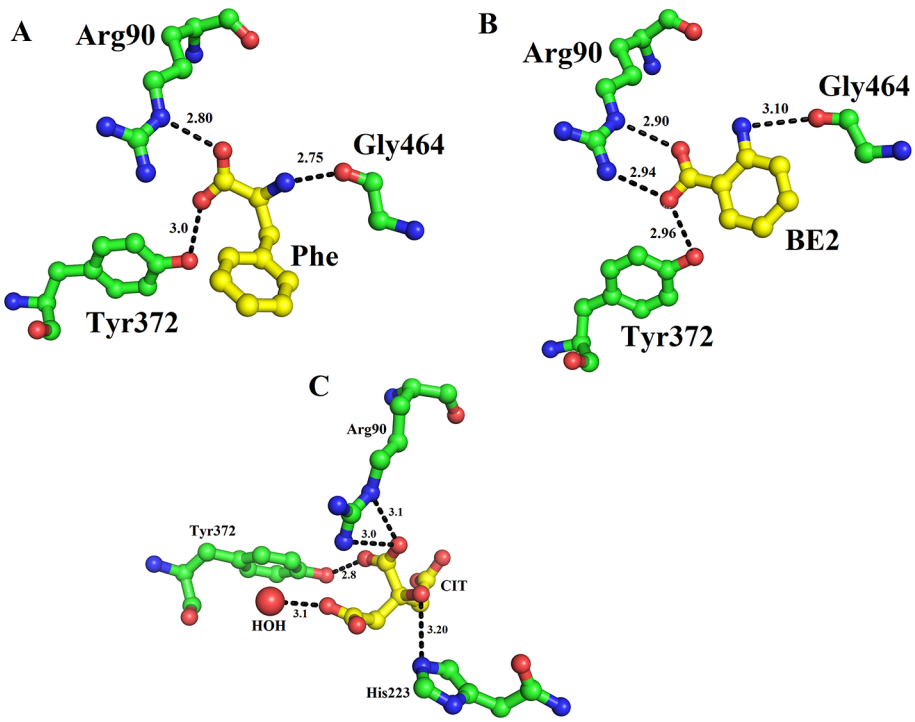

FIGURE 5 | Substrate/ligand bind amino acid residues of SV-LAAOs. Structure of *Calloselasma rhodostoma* with bound **(A)** L-Phenylalanine **(B)** BE2- 2-aminobenzoic acid **(C)** Citrate. The substrate/ligands are shown as yellow sticks and the amino acid residues as green sticks.

glycosylation site (Asn172) and only one NAG molecule (**Figure 7D**). The *B. jararacussu* LAAO lacks carbohydrates at both positions 172 and 361 however; biochemical study has shown that *B. jararacussu* LAAO contains carbohydrates (França et al., 2007; Carone et al., 2017). The LAAOs from *Daboia russelii* and *Trimeresurus stejnegeri* venom have been shown to contain three glycosylation sites at Asn172, 194, and 361 (Zhang et al., 2003; Chen et al., 2012). The glycan moiety in SV-LAAOs is bis-sialylated, biantennary, and core-fucosylated dodecasaccharides (Geyer et al., 2001). The glycan moiety, particularly at the position 172 lies near to the O_2 entrance and H_2O_2 exit tunnel and have been implicated to increases the concentration of the later upon attachment to the cell surface (Suhr and Kim, 1996; Torii et al., 1997; Ande et al., 2006). Thus the glycan moiety plays an important role in the attachment of LAAO to the cell surface thereby increasing the concentration of H_2O_2 which leads to the apoptosis (Ande et al., 2006). Evidence for the direct attachment of SV-LAAOs to mouse lymphocytic leukemia and endothelial KN-3 cells (Suhr and Kim, 1996), human umbilical vein endothelial cell and promyelocytic leukemia HL-60, and human ovarian carcinoma A2789 cells have

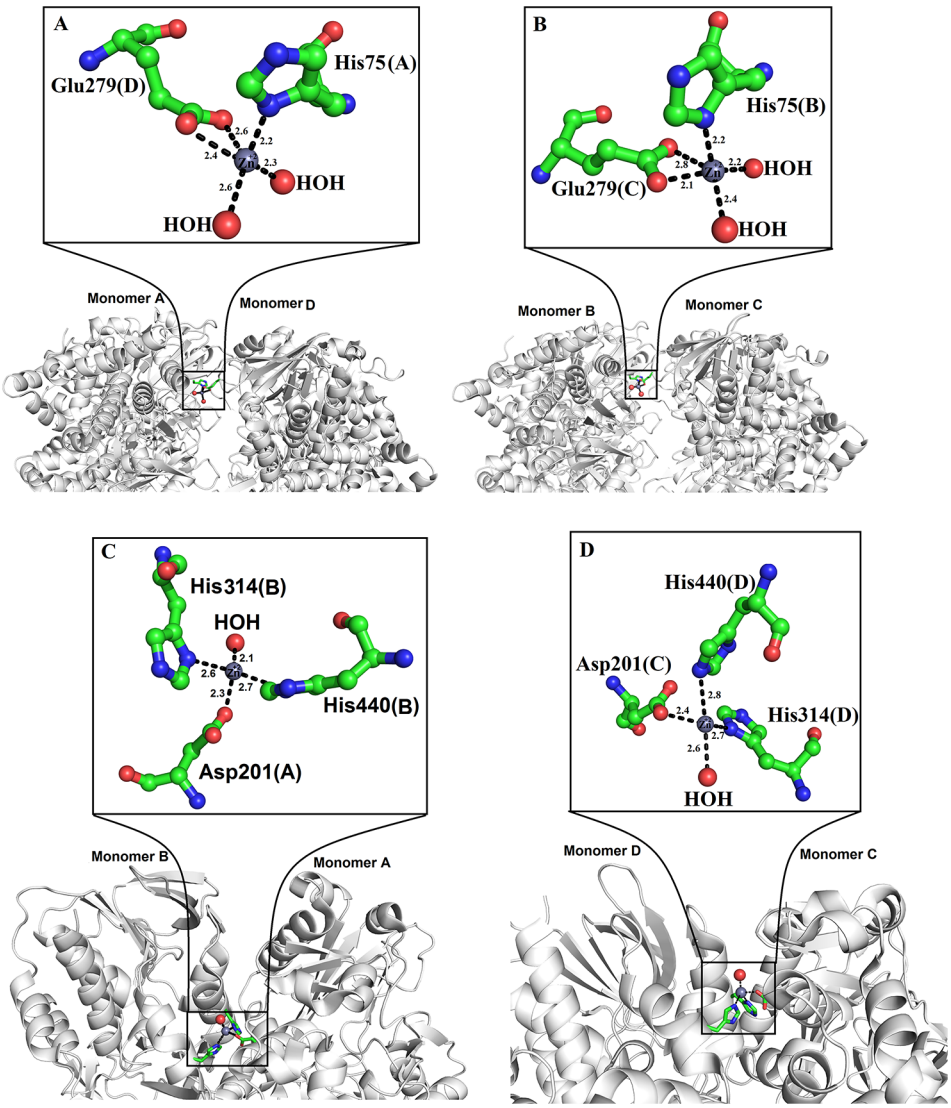

FIGURE 6 | Zinc binding sites of SV-LAAOs **(A**, **B)** Zinc binding site of L-amino acid oxidase from *Vipera ammodytes ammodytes*, (monomers A and D and B and C) **(C**, **D)** Zinc binding site of L-amino acid oxidase from *Bothrops atrox* (monomers A and B and C and D). The zinc ions and water molecules are shown as gray and red spheres respectively and the amino acid residues as green sticks.

been confirmed using Fluorescence microscopy with a fluorescence label LAAO (Suhr and Kim, 1996). The removal of glycan moiety from the SV-LAAOs drastically decreases the apoptotic activity of these enzymes; however, it does not affect their catalytic activity (Geyer et al., 2001; Stabeli et al., 2004; Izidoro et al., 2006; Chen et al., 2012).

Structural Comparison Among SV-LAAOs

The overall three-dimensional structures of SV-LAAOs align well to each other (**Figures 8A–J**). They have the same three-dimensional structural folds that contain three domains namely FAD-binding domain, substrate-binding domain and a helical domain. The Root Mean Square Deviation (RMSD) value for the structural alignment among SV-LAAOs range from 0.30–0.66 Å, with an average RMSD value of 0.46 Å (**Table 4**). The main differences are found in the loop regions (**Figures 8A–J**). The amino acid sequence and length of the loops vary in these regions. This may be important in variable substrate specificity.

In the crystal structure of all SV-LAAOs the adenosyl group of FAD has a normal canonical form in which it is stabilized by Van der Waals contacts and the ribose and di-phosphoryl groups that are tightly bonded to E63, Q71 and E457 side chains and backbone N atoms from M43 and S44 (**Figures 9A, B, D, E**). However, in the crystal structure of *B. jararacussu* LAAO the adenosyl group was found in different conformation from the normal canonical binding mode (**Figures 9B, C**). In this novel conformation, the adenosyl group of the FAD flips towards loop 62–71 and is stabilized by the interaction with amino acid

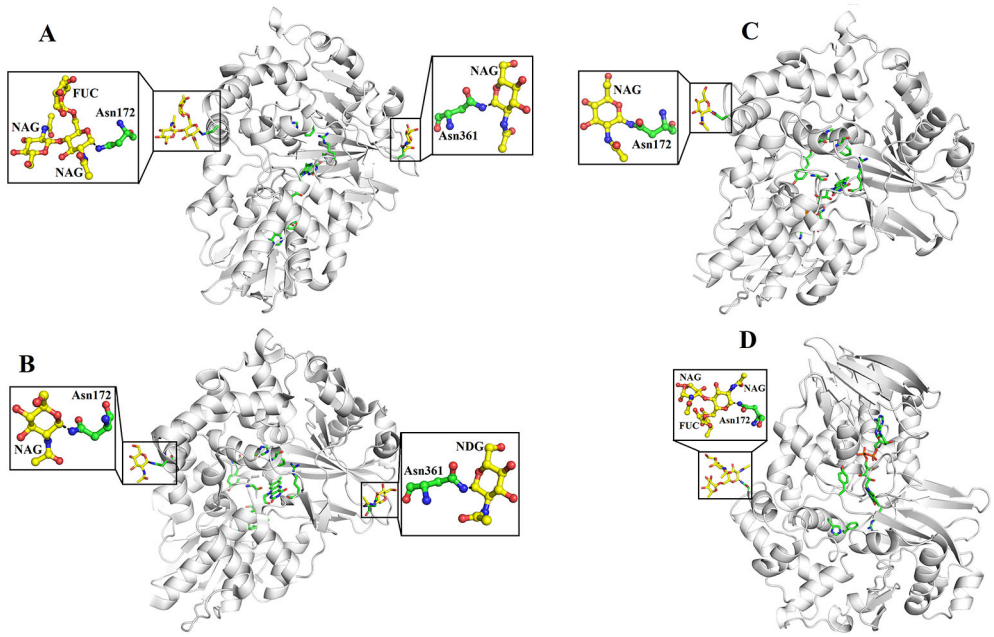

FIGURE 7 | Glycosylation sites of **(A)** L-amino acid oxidase from *Calloselasma rhodostoma* **(B)** L-amino acid oxidase from *Agkistrodon halys pallas* **(C)** Structure of native L-amino acid oxidase from *Vipera ammodytes ammodytes* **(D)** Crystal structure of L-amino acid oxidase from *Bothrops atrox*. The carbohydrate moiety (NAG, FUC) is shown as yellow sticks and the Asn (Asn172 and Asn361) are shown as green sticks.

residues (E63, S65 and R67, and a large number of hydrophobic contacts) from this loop (**Figure 9C**). Due to this new conformation, the active site cleft volume of *B. jararacussu* LAAO increases which further modifies the solvent accessibility to the FAD-binding domain that was previously occupied by the adenosyl group in the canonical-binding mode. This may also contribute to the variable substrate specificity of this enzyme (Ullah et al., 2012b).

Variable Substrate Specificity Among SV-LAAOs

The substrate (amino acid) recognition amino acid residues comprising Arg90, Arg322, Tyr372, Ileu430, and Trp465 are fully conserved among all SV-LAAOs (**Figure 1**). However, LAAOs from various snake species displayed variable substrate specificity (Moustafa et al., 2006; Ullah et al., 2012b; Bregge-Silva et al., 2012; Chen et al., 2012). For example LAAOs from *B. jararacussu*, *L. muta* and *R. viper* display preference for hydrophobic amino acid (L-Met, L-Leu, L-Phe, L-Ileu, L-Trp, and L-Tyr) with large side chain (Bregge-Silva et al., 2012; Chen et al., 2012; Ullah et al., 2012b) while the LAAO from *C. rhodostoma* shows broad specificity toward their substrate (Moustafa et al., 2006). Interestingly the *O. hannah* LAAO has shown a high substrate preference for L-Lysin (Tan and Saifuddin, 1991). The narrow and broad specificity of SV-LAAOs can be explained based on the amino acid residues difference in the loop regions, active site cavity volume and its average depth and surface charge distribution.

The analysis of structural alignment among SV-LAAOs from various snake species shows some differences in their three-dimensional structure that is confined to the loop regions (**Figures 8A–J**). Due to these differences, the surface charge distribution varies in these enzymes (**Figures 10A–E**). The surface charge distribution analysis indicates that LAAOs having broad specificity have their surfaces partially negative and partially positive (**Figures 10A–C**). While others having specificity for hydrophobic amino acids have highly negatively charged surface around the active site cleft (**Figures 10D–F**).

The active site cavity volume and average depth also vary in these enzymes (**Table 5**). It has been shown that the SV-LAAOs with broad substrate specificity (LAAO from *C. rhodostoma*) have small active site cavity volume (4719.94 $Å^3$) and average depth (16.55 Å) (**Table 5**). However, the others SV-LAAOs with narrow substrate specificity have large active site cavity volume (8,469.14–13,670.44 $Å^3$) and average depth (18.23–23.58 Å) (**Table 5**). The unique preference of *O. hannah* LAAO toward L-lysine (basic amino acid, with a positive charge) as a substrate can also be explained based on the surface charge distribution (**Figure 10H**) and active site cavity volume and its average depth (**Table 5**). The overall surface charge of this enzyme is highly negatively charged which attract this amino acid (**Figure 10H**). However, in the case of other SV-LAAOs, the overall surface charge is partially negative and partially positive (**Figures 10A–G**). The average active site cavity volume and depth is also very small for O. *hannah* LAAO when compared to the other SV-LAAOs (**Table 5**).

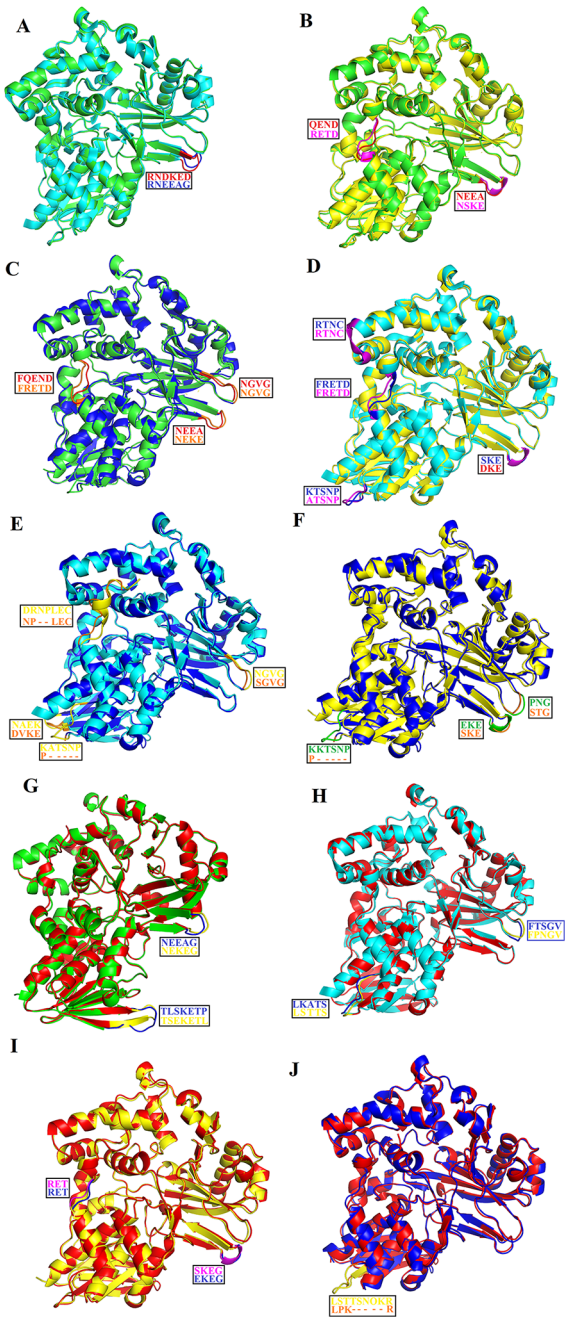

FIGURE 8 | Structural alignment among SV-LAAOs **(A)** *Calloselasma rhodostoma* LAAO (green) align with *Agkistrodon halys pallas* LAAO (cyan) **(B)** *C. rhodostoma* LAAO (green) align with *Vipera ammodytes ammodytes* LAAO (yellow) **(C)** *C. rhodostoma* LAAO (green) align with *Bothrops jararacussu* LAAO (blue) **(D)** *A. halys pallas* LAAO (cyan) align with *V. ammodytes ammodytes* LAAO (yellow) **(E)** *A. halys pallas* LAAO (cyan) align with *B. jararacussu* LAAO (blue) **(F)** *V. ammodytes ammodytes* LAAO (yellow) align with *B. jararacussu* LAAO (blue) **(G)** *C. rhodostoma* LAAO (green) align with *Bothrops atrox* LAAO (red) **(H)** *A. halys pallas* LAAO (cyan) align with *B. atrox* LAAO (red) **(I)** *V. ammodytes ammodytes* LAAO (yellow) align with *B. atrox* LAAO (red) **(J)** *B. jararacussu* LAAO (blue) align with *B. atrox* LAAO (red). The loops showing variable amino acid residues and length are highlighted. The amino acid residues showing differences are shown in the box.

Catalytic Mechanism

The active site of SV-LAAO is located deeply within the enzyme with a long funnel-like entrance (25 Å). The walls of the funnel are lined with the hydrophilic and hydrophobic amino acid residues that direct the substrate to the active site (Pawelek et al., 2000; Moustafa et al., 2006). The active site comprises of the cofactor FAD and amino acid residues Arg90, His223, Phe227, Lys324, Tyr372, Ileu374, Ileu430, and Trp465 (**Figures 1**, **2D**, and **4**) (Georgieva et al., 2011; Pawelek et al., 2000; Moustafa et al., 2006).

TABLE 4 | Root mean square deviation of SV-LAAOs structural alignment.

Protein	RMSD (Å)
1F8R align 1REO	0.30
1F8R align 3KVE	0.51
1F8R align 4E0V	0.61
1F8R align 5TS5	0.36
1REO align 3KVE	0.49
1REO align 4E0V	0.50
1REO align 5TS5	0.34
3KVE align 4E0V	0.66
3KVE align 5TS5	0.36
4E0V align 5TS5	0.51

The alignment of the two structures was carried out using the PyMOL Molecular graphic visualization program and the all-atom RMSD values were calculated using the same program.

The cofactor FAD (substrate-bound and reduced state) acts as a receptor of the hydride from the substrate C-alpha atom to the N5 atom of the flavin isoalloxazine ring system (Moustafa et al., 2006). The Arg90 interact with the carboxylic acid group of the amino acid substrate and keeps it in the specific orientation for the catalysis (Georgieva et al., 2010). The amino acid residues Phe227, Tyr372 and Trp465 stabilize the isoalloxazine part of the FAD cofactor. The Ile374 and Ile430 constitute the hydrophobic substrate-binding site and preferably bind the amino acids (substrate) with non-polar side chains. A conserved water molecule near Lys322 and FAD cofactor (N5 atom of the flavin isoalloxazine ring) has been encountered in the crystal structure of *C. rhodostoma* LAAO with bound L-phenylalanine (Moustafa et al., 2006) and also in the native structure of *V. ammodytes ammodytes* (Georgieva, et al., 2010). This water molecule makes a triad Lys322-Water- N5 of FAD (Isoalloxazine ring), only upon substrate binding (Moustafa et al., 2006; Georgieva, et al., 2010). This water molecule is important for FAD reduction and the formation of H_2O_2 (Moustafa et al., 2006).

The catalytic mechanism involves two reactions namely reductive half-reaction and oxidative half-reaction. The protonated amino acid (substrate) in the zwitterionic form enters the active site of the enzyme through the funnel-shaped channel (Pawelek et al., 2000). In the funnel, His233 and Arg322 block the substrate as they change their conformation due to the zwitterionic form of the substrate (**Figure 11**) (Moustafa et al., 2006). The His233 then removes a proton from the α-amino group of the substrate. After deprotonation, the substrate is further modified by transferring the electrons from the α-

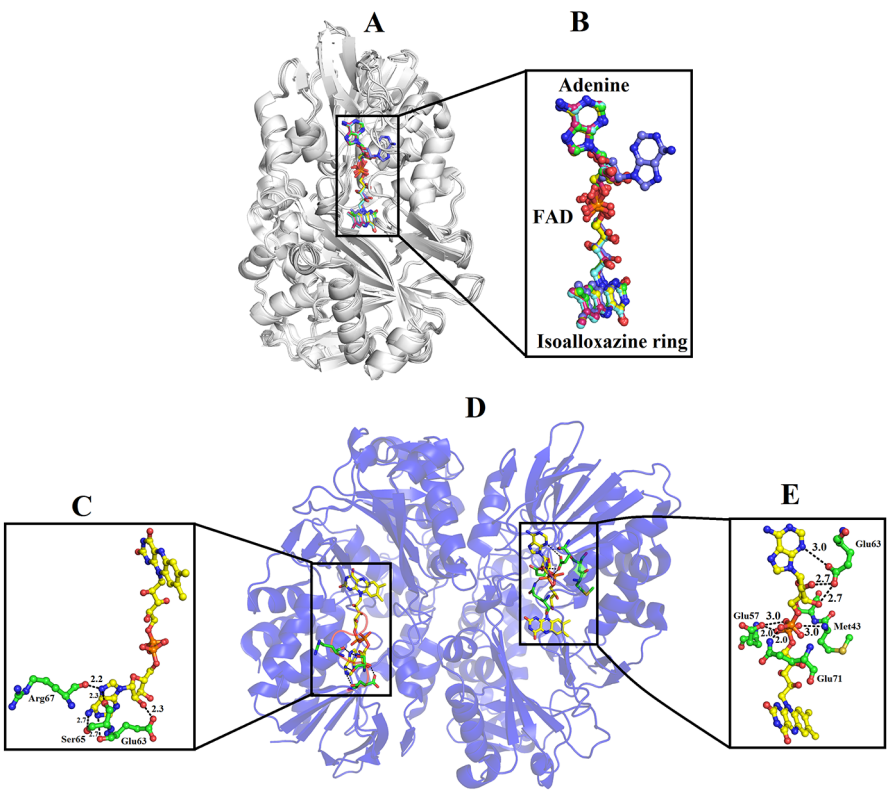

FIGURE 9 | Binding mode of FAD in SV-LAAOs **(A)** structural alignment among SV-LAAOs **(B)** FAD-binding in SV-LAAO **(D)** Two ways of FAD-binding in *Bothrops jararacussu* LAAO **(C)** FAD-binding in monomer A **(E)** FAD-binding in monomer B. The FAD has been shown as yellow sticks and the amino acid residues as green sticks.

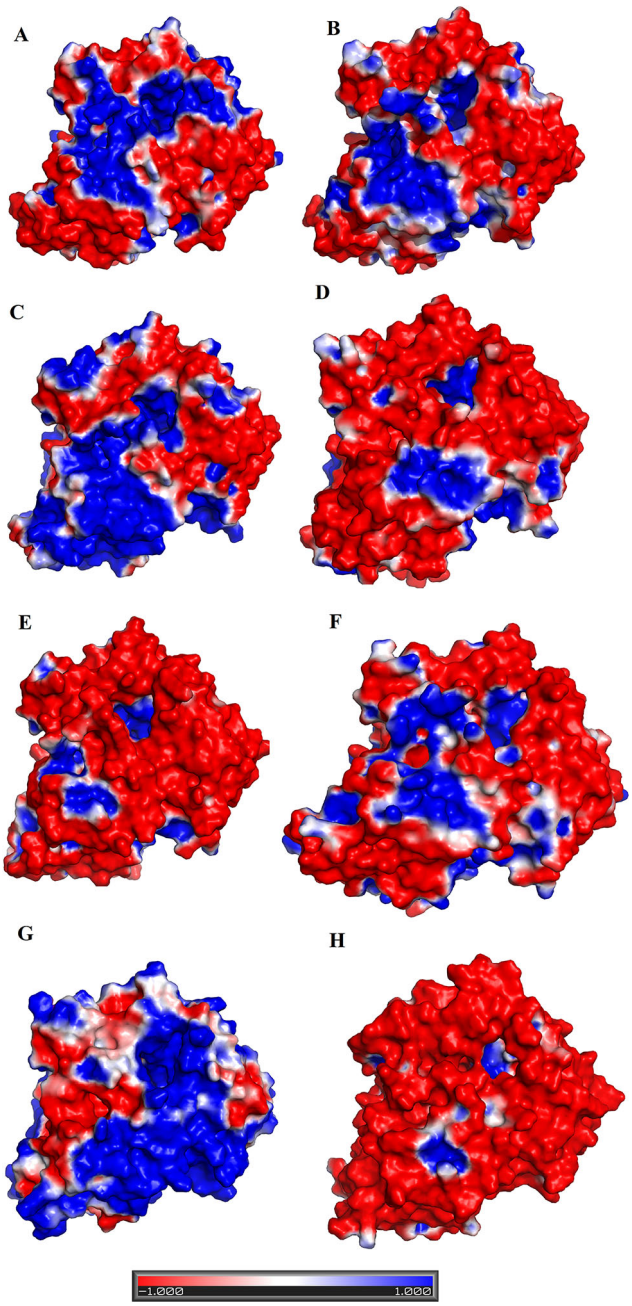

FIGURE 10 | Surface charge distribution of SV-LAAOs **(A)** *Calloselasma rhodostoma* LAAO **(B)** *Agkistrodon halys pallas* LAAO **(C)** *Vipera ammodytes ammodytes* LAAO **(D)** *Bothrops jararacussu* LAAO **(E)** *Bothrops atrox* LAAO **(F)** *Lachesis muta* LAAO (homology model) **(G)** *R. viper* LAAO (homology model) **(H)** *Ophiophagus hannah* LAAO (homology model). The red, blue and white colors represent negative, positive and neutral charges respectively.

nitrogen to the α-carbon atom of the substrate. This makes the substrate more active and thus it transfers a hydride ion to the N5 of the FAD cofactor and reduces it. The substrate changes to the imino form during this step. During the oxidative half-reaction, the FAD is oxidized by O_2. The O_2 takes one electron from the FAD π-electrons and becomes attached to the other electron. In the same time, the O_2 also abstracts a hydrogen ion from the water molecule (hydronium ion) and hydrogen from the FAD which it has taken previously from His223. In this way, an H-O-O-H (H_2O_2) is formed. The bond between the H_2O_2 and FAD breaks and the H_2O_2 is released. The water molecule near Lys322 provides oxygen to the imino acid changing it to keto acid and the hydrogen to the NH_2 converting it to NH_3.

TABLE 5 | Average active site cavity volume and average active site cavity depth of SV-LAAOs and their mammalian and bacterial counterpart.

Protein	Average volume (Å^3)	Average depth (Å)
1F8R	4719.94	16.55
1REO	10710.98	21.84
3KVE	7425.42	23.58
4E0V	8469.14	18.23
5TS5	12895.45	21.67
RV-LAAO- homology model	13670.44	21.85
LM-LAAO- homology model	9656.30	21.91
O. hannah- homology model	2688.61	8.54

1F8R: Calloselasma rhodostoma LAAO, 1REO: Agkistrodon halys pallas LAAO, 3KVE: Vipera ammodytes ammodytes LAAO, 4E0V: Bothrops jararacussu LAAO, 5TS5: Bothrops atrox LAAO, R. viper LAAO (homology model), Lachesis muta LAAO (homology model), Ophiophagus Hannah LAAO (homology model). The average active site cavity volume and average active site cavity depth of the proteins were calculated using the Pdbsum online server (Laskowski et al., 2018).

Inhibition of SV-LAAO

SV-LAAOs are inhibited by L-propargylglycin, Aristocholic acid and suramin (Mitra and Bhattacharyya, 2013; Bhattacharjee et al., 2017). The L-propargylglycin reversibly inhibits the *C. adamanteus* and *C. atrox* LAAOs by covalent modification (Mitra and Bhattacharyya, 2013). This inhibitor binds to amino acid residues Arg90, His233 and Leu207 (**Figure 12A**). The Arg90 and His233 are important for SV-LAAO activity as inhibiting these two leads to the inhibition of the enzyme. The Aristocholic acid and its derivatives bind to the amino acid residues Arg90, Asn208, Arg322, and Thr431 (**Figure 12B**), while suramin binds to Arg90, Glu149, Ser152, His223, Asn208, Lys345, and Arg322, Gly464, and FAD (**Figure 12C**). The Aristocholic acid and its derivatives and suramin inhibit the function of these enzymes by binding to the key amino acid residues (Arg90, His223, and Arg322).

INTERACTION OF SV-LAAO WITH MEMBRANE

The binding between membrane and SV-LAAO was predicted using PPM server (Lomize et al., 2012). The SV-LAAO membrane interaction is mediated by the contacts from FAD, glycan moiety from Asn172 and the amino acid residues from the loops (**Figure 13A**). The amino acid residues that make contact with membrane include Glu265, Glu266, Asn267, Asn305, Pro306, Pro307, Leu309, and Pro310 (**Figure 13B**). The interaction of SV-LAAO with membrane increases the concentration of H_2O_2 that is considered important for the apoptotic activity of this enzyme (Suhr and Kim, 1996; Torii et al., 1997; Ande et al., 2006).

CONCLUSION AND FUTURE DIRECTIONS

SV-LAAO is the most potent apoptotic agents in snake venom. The earliest study of these enzymes was concerned with their enzymatic properties and industrial applications; however, recently more attention has been given to their structure-functional relationship, mechanism of action, therapeutic potentials and biotechnological applications. Sequence analysis indicates a high sequence identity among SV-LAAOs and low identity with the bacterial, fungal, plants and mammalian homologs. Their three-dimensional structure has three well-defined domains namely a FAD-binding domain, a substrate-

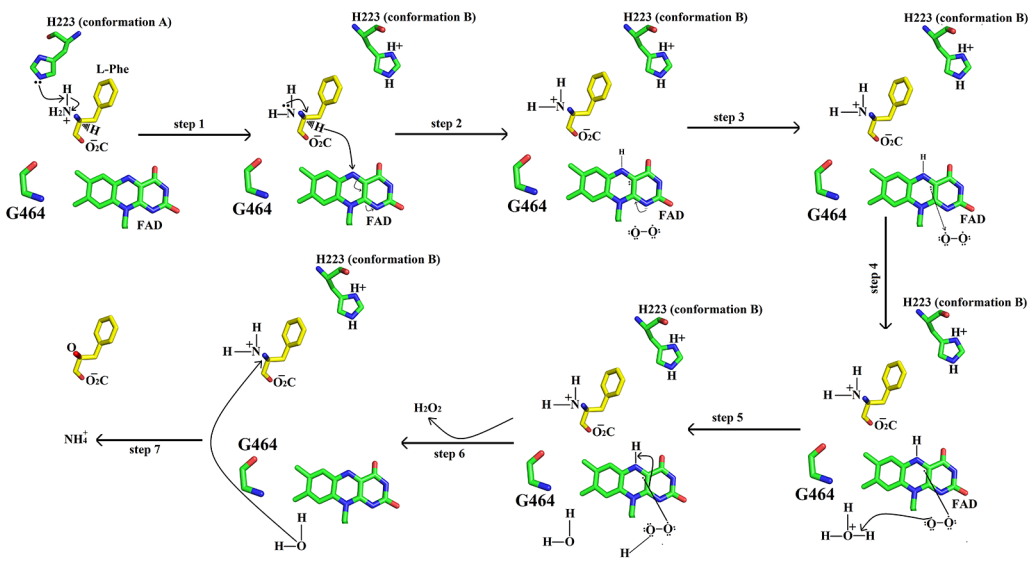

FIGURE 11 | Catalytic mechanism of SV-LAAO. The amino acid residues (His223, Gly464) and FAD are displayed as green sticks. The substrate (L-phenylalanine) is shown as yellow sticks. Only isoalloxazine ring of FAD has been shown here.

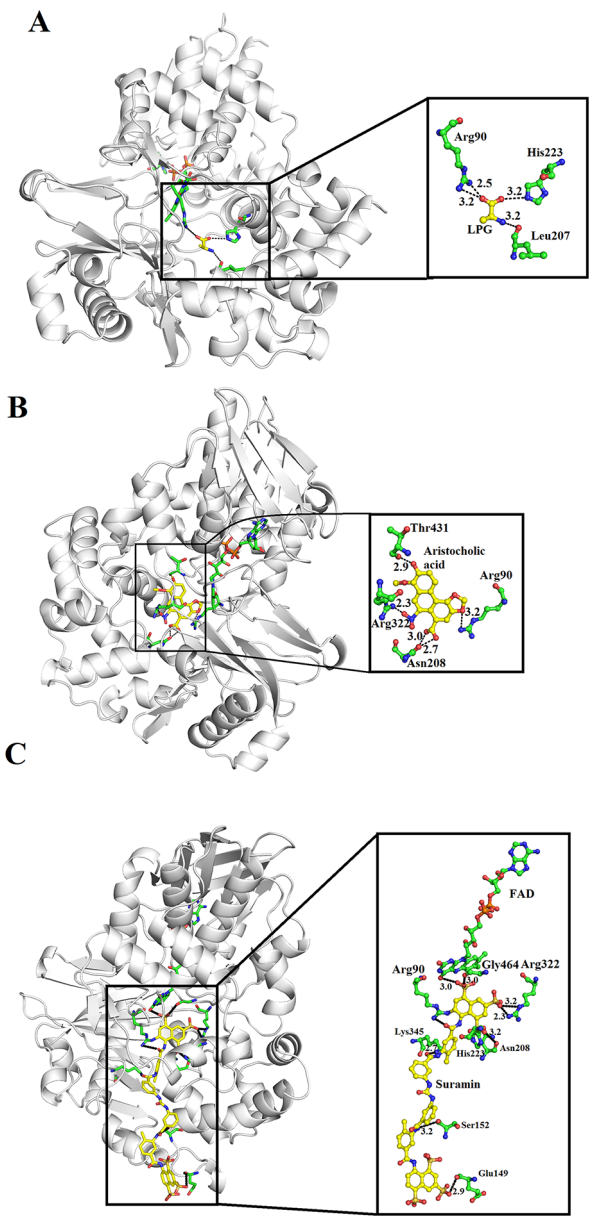

FIGURE 12 | Inhibition of SV-LAAOs by L-propargylglycin, Aristocholic acid and suramin **(A)** *Vipera ammodytes ammodytes* LAAO with bound L-propargylglycin **(B)** *V. ammodytes ammodytes* LAAO with bound Aristocholic acid **(C)** *V. ammodytes ammodytes* LAAO with bound suramin. The amino acid residues interacting with the inhibitors are shown as green sticks. The inhibitors are shown as yellow sticks.

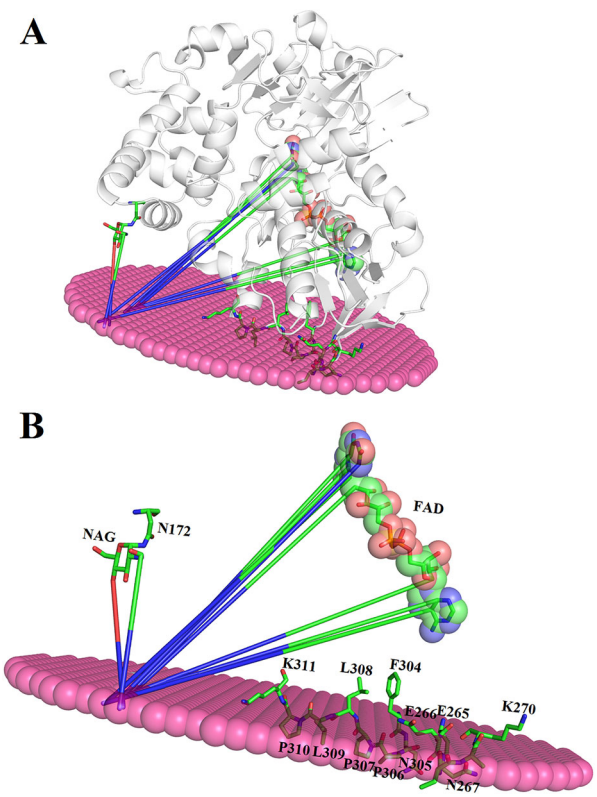

FIGURE 13 | (A) Interaction of SV-LAAO with membrane. The binding was predicted using PPM server **(B)** Parts (amino acid residues, FAD and NAG) of the SV-LAAO interacting with the membrane.

binding domain and a helical domain. The helical domain makes a funnel-like structure that directs the substrate to the active site of these enzymes. The sequence and structural analysis indicate some differences in amino acid residues in the loop regions. These differences change the surface charge distribution, average active site cavity volume and depth which may impart variable substrate specificity to these enzymes. The inhibition of these enzymes by synthetic inhibitors (L-propargylglycin, Aristocholic acid and its derivatives and suramin) can lead to better treatment of snakebite envenomation. Further investigations are necessary to use these enzymes as a therapeutic agent in cancer and HIV-AIDS treatment.

AUTHOR CONTRIBUTIONS

AU has designed the project, written, drafted, and reviewed the current manuscript.

SUPPLEMENTARY MATERIAL

The Supplementary Material for this article can be found online at: https://www.frontiersin.org/articles/10.3389/fphar.2020.00110/full#supplementary-material

REFERENCES

Abdelkafi-Koubaa, Z., Aissa, I., Morjen, M., Kharrat, N., El Ayeb, M., Gargouri, Y., et al. (2016). Interaction of a snake venom L-amino acid oxidase with different cell types membrane. *Int. J. Biol. Macromol.* 82, 757–764. doi: 10.1016/j.ijbiomac.2015.09.065

Abe, Y., Shimoyama, Y., Munakata, H., Ito, J., Nagata, N., and Ohtsuki, K. (1998). Characterization of an apoptosis-inducing factor in Habu snake venom as a glycyrrhizin (GL)-binding protein potently inhibited by GL *in vitro*. *Biol. Pharm. Bull.* 21 (9), 924–927. doi: 10.1248/bpb.21.924

Ali, S. A., Stoeva, S., Abbasi, A., Alam, J. M., Kayed, R., Faigle, M., et al. (2000). Isolation, structural and functional characterization of an apoptosis-inducing L-amino acid oxidasefrom leaf-nosed viper (*Eristocophis macmahoni*) snake venom. *Arch. Biochem. Biophys.* 384, 216–226. doi: 10.1006/abbi.2000.2130

Alves, R. M., Antonucci, G. A., Paiva, H. H., Cintra, A. C. O., Franco, J. J., Mendonca-Franqueiro, E. P., et al. (2008). Evidence of caspase-mediated apoptosis induced by L-amino acid oxidase isolated from. *Bothrops. atrox snake venom.Comp. Biochem. Physiol. A-Mol. Integr. Physiol.* 151 (4). doi: 10.1016/j.cbpa.2008.07.007

Ande, S. R., Kommoju, P. R., Draxl, S., Murkovic, M., Macheroux, P., Ghisla, S., et al. (2006). Mechanisms of cell death induction by l-amino acid oxidase, a major component of ophidian venom. *Apoptosis* 11, 1439–1451. doi: 10.1007/s10495-006-7959-9

Arima, J., Sasaki, C., Sakaguchi, C., Mizuno, H., Tamura, T., Kashima, A., et al. (2009). Structural characterization of L-glutamate oxidase from *Streptomyces* sp. X-119-6. *FEBS J.* 276 (14), 3894–3903. doi: 10.1111/j.1742-4658.2009.07103.x

Bender, M., and Brubacher, L. (1977). *Cat´alisis y acci´on enzim´atica. 1st edition* (Barcelona: EDITORIAL REVERTÉ).

Bhattacharjee, P., Bera, I., Chakraborty, S., Ghoshal, N., and Bhattacharyya, D. (2017). Aristolochic acid and its derivatives as inhibitors of snake venom L-amino acid oxidase. *Toxicon* 138, 1–17. doi: 10.1016/j.toxicon.2017.08.003

Blanchard, M., Green, D., Nocito, V., and Ratner, S. (1944). L-Amino acid oxidase of animal tissue. *J. Biol. Chem.* 155, 421–440.

Bregge-Silva, C., Nonato, M. C., de Albuquerque, S., Ho, P. L., Junqueira de Azevedo, I. L., Vasconcelos, D. M. R., et al. (2012). Isolation and biochemical, functional and structural characterization of a novel L-amino acid oxidase from Lachesis muta snake venom. *Toxicon* 60 (7), 1263–1276. doi: 10.1016/j.toxicon.2012.08.008

Carone, S. E. I., Costa, T. R., Burin, S. M., Cintra, A. C. O., Zoccal, K. F., Bianchini, F. J., et al. (2017). A new l-amino acid oxidase from *Bothrops jararacussu* snake venom: isolation, partial characterization, and assessment of pro-apoptotic and antiprotozoal activities. *Int. J. Biol. Macromol.* 103, 25–35. doi: 10.1016/j.ijbiomac.2017.05.025

Chen, H. S., Wang, Y. M., Huang, W. T., Huang, K. F., and Tsai, I. H. (2012). Cloning, characterization and mutagenesis of *Russell's viper* venom L-amino acid oxidase: Insights into its catalytic mechanism. *Biochimie* 94 (2), 335–344. doi: 10.1016/j.biochi.2011.07.022

Cheng, C.-H., Yang, C.-A., Liu, S.-Y., Lo, C.-T., and Peng, K.-C. (2012). L-Amino acid oxidase-induced apoptosis in filamentous *Botrytis cinerea*. *Anal. Biochem.* 420, 93–95. doi: 10.1016/j.ab.2011.09.003

Cisneros, Y. (1996). Caracter´ısticas bioqu´ımicas de una prote´ına antibacteriana aislada del veneno de Lachesis Muta "Shushupe" [Tesis para optar al Titulo profesional de Bi´ologo], UNMSM, Lima, Peru,.

Costa, T. R., Burin, S. M., Menaldo, D. L., de Castro, F. A., and Sampaio, S. V. (2014). Snake venom L-amino acid oxidases: an overview on their antitumor effects. *J. Venom Anim. Toxins Incl. Trop. Dis.* 20, 23. eCollection 2014. doi: 10.1186/1678-9199-20-23

Costa, T. R., Menaldo, D. L., Zoccal, K. F., Burin, S. M., Aissa, A. F., Castro, F. A., et al. (2017). CR-LAAO, an L-amino acid oxidase from *Calloselasma rhodostoma* venom, as a potential tool for developing novel immunotherapeutic strategies against cancer. *Sci. Rep.* 7, 42673. doi: 10.1038/srep42673

Costa Torres, A. F., Dantas, R. T., Toyama, M. H., Diz Filho, E., Zara, F. J., de QueirozaNadia, M. G. R., et al. (2010). Antibacterial and antiparasitic effects of *Bothrops marajoensis* venom and its fractions: phospholipase A2 and l-amino acid oxidase. *Toxicon* 55 (4), 795–804. doi: 10.1016/j.toxicon.2009.11.013

Costal-Oliveira, F., Stransky, S., Guerra-Duarte, C., Naves de Souza, D. L., Vivas-Ruiz, D. E., Yarlequé, A., et al. (2019). L-amino acid oxidase from *Bothrops atrox* snake venom triggers autophagy, apoptosis and necrosis in normal human keratinocytes. *Sci. Rep.* 9 (1), 781.

Curti, B., Massey, V., and Zmudha., M. (1968). Inactivation of snake venom L-amino acid oxidase by freezing. *J. Biol. Chem.* 243, 2306–2314.

deKok, A., and Rawitch, A. B. (1969). Studies on L-amino acid oxidase. II. Dissociation and characterization of its subunits. *Biochemistry* 8, 1405e1411.

Du, X. Y., and Clemetson, K. J. (2002). Snake venom L-amino acid oxidases. *Toxicon* 40, 659–665. doi: 10.1016/S0041-0101(02)00102-2

Feliciano, P. R., Rustiguel, J. K., Soares, R. O., Sampaio, S. V., and Cristina Nonato, M. (2017). Crystal structure and molecular dynamics studies of L-amino acid oxidase from *Bothrops atrox*. *Toxicon* 15 (128), 50–59. doi: 10.1016/j.toxicon.2017.01.017

Fernandez-Gomez, R., Zerrouk, H., Sebti, F., Loyens, M., Benslimane, A., and Ali Ouaissi, M. (1994). Growth inhibition of *Trypanosoma cruzi* and *Leishmania donovani infantum* by different snake venoms: preliminary identification of proteins from *Cerastes cerastes* venom which interact with the parasites. *Toxicon* 32 (8), 875–882. doi: 10.1016/0041-0101(94)90366-2

França, S. C., Kashima, S., Roberto, P. G., Marins, M., Ticli, F. K., Pereira, J. O., et al. (2007). Molecular approaches for structural characterization of Bothrops L-amino acid oxidases with antiprotozoal activity: cDNA cloning, comparative sequence analysis, and molecular modeling. *Biochem. Biophys. Res. Commun.* 355 (2), 302–306. doi: 10.1016/j.bbrc.2006.12.217

Georgieva, D., Murakami, M., Perband, M., Arni, R., and Betzel, C. (2011). The structure of a native l-amino acid oxidase, the major component of the *Vipera ammodytes ammodytes* venomic, reveals dynamic active site and quaternary structure stabilization by divalent ions. *Mol. Biosyst.* 7 (2), 379–384. doi: 10.1039/C0MB00101E

Geyer, A., Fitzpatrick, T. B., Pawelek, P. D., Kitzing, K., Vrielink, A., Ghisla, S., et al. (2001). Structure and characterization of the glycan moiety of L-amino-acid oxidase from the Malayan pit viper *Calloselasma rhodostoma*. *Eur. J. Biochem.* 268 (14), 4044–4053. doi: 10.1046/j.1432-1327.2001.02321.x

Hayes, M. B., and Wellner, D. (1969). Microheterogeneity of L-amino acid oxidase. *J. Biol. Chem.* 244, 6636–6644.

Izidoro, L. F. M., Ribeiro, M. C., Souza, G. R. L., Sant'Ana, C. D., Hamaguchi, A., Homsi-Brandeburgo, M. I., et al. (2006). Biochemical and functional characterization of an L-amino acid oxidase isolated from *Bothrops pirajai* snake venom. *Bioorg. Med. Chem.* 14, 7034–7043. doi: 10.1016/j.bmc.2006.06.025

Kasai, K., Ishikawa, T., Komata, T., Fukuchi, K., Chiba, M., Nozaka, H., et al. (2010). Novel L-amino acid oxidase with antibacterial activity against methicillin-resistant Staphylococcus aureus isolated from epidermal mucus of the flounder *Platichthys stellatus*. *FEBS J.* 277 (2), 453–465. doi: 10.1111/j.1742-4658.2009.07497.x

Laskowski, R. A., Jabłońska, J., Pravda, L., Vařeková, R. S., and Thornton, J. M. (2018). PDBsum: Structural summaries of PDB entries. *Prot. Sci.* 27, 129–134. doi: 10.1002/pro.3289

Lazo, F., Vivas-Ruiz, D. E., Sandoval, G. A., Rodríguez, E. F., Kozlova, E. E. G., Costal-Oliveira, F., et al. (2017). Biochemical, biological and molecular characterization of an L-Amino acid oxidase (LAAO) purified from *Bothrops pictus* Peruvian snake venom. *Toxicon* 1 (139), 74–86. doi: 10.1016/j.toxicon.2017.10.001

Lee, M. L., Fung, S. Y., Chung, I., Pailoor, J., Cheah, S. H., and Tan, N. H. (2014). King Cobra (*Ophiophagus hannah*) venom l-amino acid oxidase induces apoptosis in pc-3 cells and suppresses pc-3 solid tumor growth in a tumor xenograft mouse model. *Int. J. Med. Sci.* 11 (6), 593–601. doi: 10.7150/ijms.8096

Li, Z. Y., Yu, T. F., and Lian, E. C. (1994). Purification and characterization of L-amino acid oxidase from king cobra (*Ophiophagus hannah*) venom and its effects on human platelet aggregation. *Toxicon* 32 (11), 1349–1358. doi: 10.1016/0041-0101(94)90407-3

Lomize, M. A., Pogozheva, I. D., Joo, H., Mosberg, H. I., and Lomize, A. L. (2012). OPM database and PPM web server: resources for positioning of proteins in membranes. *Nucleic Acids Res.* 40, D370–D376. doi: 10.1093/nar/gkr703

Machado, A. R. T., Aissa, A. F., Ribeiro, D. L., Costa, T. R., Ferreira, R. S.Jr., Sampaio, S. V., et al. (2019). Cytotoxic, genotoxic, and oxidative stress-inducing effect of an l-amino acid oxidase isolated from *Bothrops jararacussu* venom in a co-culture model of HepG2 and HUVEC cells. *Int. J. Biol. Macromol.* 127, 425–432. doi: 10.1016/j.ijbiomac.2019.01.059

Marchler-Bauer, A., Bo, Y., Han, L., He, J., Lanczycki, C. J., Lu, S., et al. (2017). CDD/SPARCLE: functional classification of proteins *via* subfamily domain architectures. *Nucleic Acids Res.* 45 (D1), D200–D203. doi: 10.1093/nar/gkw1129

Mitra, J., and Bhattacharyya, D. (2013). Irreversible inactivation of snake venom l-amino acid oxidase by covalent modification during catalysis of l-propargylglycine. *FEBS Open Bio.* 3, 135–143. doi: 10.1016/j.fob.2013.01.010

Moustafa, I. M., Foster, S., Lyubimov, A. Y., and Vrielink, A. (2006). Crystal structure of LAAO from *Calloselasma rhodostoma* with an L-phenylalanine substrate: insight into structure and mechanism. *J. Mol. Biol.* 15, 991–1002. doi: 10.1016/j.jmb.2006.09.032

Nishizawa, T., Aldrich, C. C., and Sherman, D. H. (2005). Molecular analysis of the rebeccamycin L-amino acid oxidase from *Lechevalieria aerocolonigenes* ATCC 39243. *J. Bacteriol.* 187 (6), 2084–2092. doi: 10.1128/JB.187.6.2084-2092.2005

Nuutinen, J. T., and Timonen, S. (2008). Identification of nitrogen mineralization enzymes, l-amino acid oxidases, from the ectomycorrhizal fungi *Hebeloma* spp. and *Laccaria bicolor*. *Mycol. Res.* 112 (12), 1453–1464. doi: 10.1016/j.mycres.2008.06.023

Pawelek, P. D., Cheah, J., Coulombe, R., Macheroux, P., Ghisla, S., and Vrielink, A. (2000). The structure of L-amino acid oxidase reveals the substrate trajectory into an enantiomerically conserved active site. *EMBO J.* 19, 4204–4215. doi: 10.1093/emboj/19.16.4204

Rey-Suárez, P., Acosta, C., Torres, U., Saldarriaga-Córdoba, M., Lomonte, B., and Núñez, V. (2018). MipLAAO, a new L-amino acid oxidase from the redtail coral snake *Micrurus mipartitus*. *Peer J.* 6, e4924. eCollection 2018. doi: 10.7717/peerj.4924

Sakurai, Y., Takatsuka, H., Yoshioka, A., Matsui, T., Suzuki, M., Titani, K., et al. (2001). Inhibition of human platelet aggregation by L-amino acid oxidase purified from *Naja naja kaouthia* venom. *Toxicon* 39, 1827–1833. doi: 10.1016/S0041-0101(01)00133-7

Sakurai, Y., Shima, M., Matsumoto, T., Takatsuka, H., Nishiya, K., Kasuda, S., et al. (2003). Anticoagulant activity of M-LAO, L-amino acid oxidase purified from *Agkistrodon halys blomhoffii*, through selective inhibition of factor IX. *Biochim. Biophys. Acta* 1649, 51–57. doi: 10.1016/S1570-9639(03)00157-2

Salama, W. H., Ibrahim, N. M., El Hakim, A. E., Bassuiny, R. I., Mohamed, M. M., Mousa, F. M., et al. (2018). l-Amino acid oxidase from *Cerastes vipera* snake venom: Isolation, characterization and biological effects on bacteria and tumor cell lines. *Toxicon* 150, 270–279. doi: 10.1016/j.toxicon.2018.06.064

Sant'Ana, C. D., Menaldo, D. L., Costa, T. R., Godoy, H., Muller, V. D., Aquino, V. H., et al. (2010). Antiviral and antiparasite properties of an l-amino acid oxidase from the Snake Bothrops jararaca: cloning and identification of a complete cDNA sequence. *Biochem. Pharmacol.* 76, 279–288. doi: 10.1016/j.bcp.2008.05.003

Sarakatsannis, J. N., and Duan, Y. (2005). Statistical characterization of salt bridges in proteins. *Proteins* 60, 732–739. doi: 10.1002/prot.20549

Schriek, S., Kahmann, U., Staiger, D., Pistorius, E. K., and Michel, K. P. (2009). Detection of an L-amino acid dehydrogenase activity in *Synechocystis* sp. PCC 6803. *J. Exp. Bot.* 60 (3), 1035–1046.

Solis, C., Escobar, E., Yarleque, A., Gutiérrez, S., et al. (1999). Purificaci'on y caracterizacion de la L-amino'acido oxidasa del veneno de la serpiente *Bothrops brazili* 'Jerg'on shushupe. *Rev. Peru. Biologia.* 6, 75–84.

Soltysik, S., Byron, C. M., Einarsdottir, G. H., and Stankovich, M. T. (1987). The effects of reversible freezing inactivation and inhibitor binding on redox properties of L-amino acid oxidase. *Biochim. Biophys. Acta* 911, 201–208. doi: 10.1016/0167-4838(87)90009-4

Souza, D. H. F., Eugenio, L. M., Fletcher, J. E., Jiang, M. S., Garratt, R. C., Oliva, G., et al. (1999). Isolation and structural characterization of a cytotoxic L-amino acid oxidase from Agkistrodon contortrix laticinctus snake venom: preliminary crystallographic data. *Arch. Biochem. Biophys.* 368, (2), 285–290. doi: 10.1006/abbi.1999.1287

Stábeli, R. G., Sant'Ana, C. D., Ribeiro, P. H., Costa, T. R., Ticli, F. K., Pires, M. G., et al. (2007). Cytotoxic L-amino acid oxidase from *Bothrops moojeni*: biochemical and functional characterization. *Int. J. Biol. Macromol.* 41 (2), 132–140. doi: 10.1016/j.ijbiomac.2007.01.006

Stabeli, R. G., Marcussi, S., Carlos, G. B., Pietro, R. C. L. R., Selistre-de-Araujo, H. S., Giglio, J. R., et al. (2004). Platelet aggregation and antibacterial effects of an L-amino acid oxidase purified from *Bothrops alternatus* snake venom. *Bioorg. Med. Chem.* 12, 2881–2886. doi: 10.1016/j.bmc.2004.03.049

Stiles, B. G., Sexton, F. W., and Weinstein, S. A. (1991). Antibacterial effect in different snake venoms: Purification and characterization of antibacterial protein from *Pseudechis australis* (Australian king or mulga snake) venom. *Toxicon* 29, 1129–1141. doi: 10.1016/0041-0101(91)90210-I

Suhr, S. M., and Kim, D. S. (1996). Identification of the snake venom substance that induces apoptosis. *Biochem. Biophys. Res. Commun.* 224, 134–139. doi: 10.1006/bbrc.1996.0996

Sun, L. K., Yoshii, Y., Hyodo, A., Tsurushima, H., Saito, A., Harakuni, T., et al. (2003). Apoptotic effect in the glioma cells induced by specific protein extracted from Okinawa habu (*Trimeresurus flavoviridis*) venom in relation to oxidative stress. *Toxicol. In Vitro.* 17, 169–177. doi: 10.1016/S0887-2333(03)00010-9

Sun, M. Z., Guo, C., Tian, Y., Chen, D., Greenaway, F. T., and Liu, S. (2010). Biochemical, functional and structural characterization of Akbu-LAAO: a novel snake venom L-amino acid oxidase from *Agkistrodon blomhoffii ussurensis*. *Biochimie* 92 (4), 343–349. doi: 10.1016/j.biochi.2010.01.013

Tássia, R., Menaldo, L., Karina, F. Z., Sandra, M. B., Alexandre, F. A., de Castro, F. A., et al. (2017). CR-LAAO, an L-amino acid oxidase from *Calloselasma rhodostoma* venom, as a potential tool for developing novel immunotherapeutic strategies against cancer. *Sci. Rep.* 7, 42673. doi: 10.1038/srep42673

Takatsuka, H., Sakurai, Y., Yoshioka, A., Kokubo, T., Usami, Y., Suzuki, M., et al. (2001). Molecular characterization of L-amino acid oxidase from *Agkistrodon halys blomhoffii* with special reference to platelet aggregation. *Biochim. Biophys. Acta* 1544, 267–277. doi: 10.1016/S0167-4838(00)00229-6

Tan, N. H., and Saifuddin, M. N. (1989). Isolation and characterization of an unusual form of L-amino acid oxidase from King cobra (*Ophiophagus hannah*) venom. *Biochem. Int.* 19 (4), 937–944.

Tan, N. H., and Saifuddin, M. N. (1991). Substrate specificity of king cobra (Ophiophagus hannah) venom L-amino acid oxidase. *Int. J. Biochem.* 23 (3), 323–327. doi: 10.1038/srep42673

Tan, K. K., Ler, S. G., Gunaratne, J., Bay, B. H., and Ponnampalam, G. (2017). *In vitro* cytotoxicity of L-amino acid oxidase from the venom of *Crotalus mitchellii pyrrhus*. *Toxicon* 139, 20–30. doi: 10.1016/j.toxicon.2017.09.012

Tan, K. K., Bay, B. H., and Gopalakrishnakone, P. (2018). L-amino acid oxidase from snake venom and its anticancer potential. *Toxicon* 144, 7–13. doi: 10.1016/j.toxicon.2018.01.015

Tan, N. H. (1998). "L-amino acid oxidases and lactate dehydrogenases," in *Enzymes from snake venom*, vol. 19 . Ed. G. S. Bailey (Alaken: Fort Collins, CO), 579–598.

Teixeira, T. L., Oliveira Silva, V. A., da Cunha, D. B., Polettini, F. L., Thomaz, C. D., Pianca, A. A., et al. (2016). Isolation, characterization and screening of the *in vitro* cytotoxic activity of a novel L-amino acid oxidase (LAAOcdt) from *Crotalus durissus terrificus* venom on human cancer cell lines. *Toxicon* 119, 203–217. doi: 10.1016/j.toxicon.2016.06.009

Tempone, A. G., Andrade, H. F.Jr., Spencer, P. J., Lourenço, C. O., Rogero, J. R., and Nascimento, N. (2001). *Bothrops moojeni* venom kills *Leishmania* spp. with hydrogen peroxide generated by its L-amino acid oxidase. *Biochem. Biophys. Res. Commun.* 280 (3), 620–624.

Tonismagi, K., Samel, M., Trummal, K., Ronnholm, G., Sugiir, J., Kalkkinen, N., et al. (2006). L-amino acid oxidase from *Vipera lebetina* venom: Isolation, characterization, effects on platelets and bacteria. *Toxicon* 48, 227–237. doi: 10.1016/j.toxicon.2006.05.004

Torii, S., Naito, M., and Tsuruo, T. (1997). Apoxin I, a novel apoptosis-inducing factor with L-amino acid oxidase activity purified from Western diamondback rattlesnake venom. *J. Biol. Chem.* 272 (14), 9539–9542. doi: 10.1074/jbc.272.14.9539

Toyama, M. H., Toyama, D., de, O., Passero, L. F. D., Laurenti, M. D., Corbett, C. E., et al. (2006). Isolation of a new L-amino acid oxidase from *Crotalus durissus cascavella* venom. *Toxicon* 47, 47–57. doi: 10.1016/j.toxicon.2005.09.008

Ullah, A., Coronado, M., Murakami, M. T., Betzel, C., and Arni, R. K. (2012a). Crystallization and preliminary X-ray diffraction analysis of an L-amino-acid oxidase from Bothrops jararacussu venom. *Acta Crystallogr. Sect. F. Struct. Biol. Cryst. Commun.* 68 (Pt. 2), 211–3. doi: 10.1107/S1744309111054923

Ullah, A., Souza, T. A., Abrego, J. R., Betzel, C., Murakami, M. T., and Arni, R. K. (2012b). Structural insights into selectivity and cofactor binding in snake venom L-amino acid oxidases. *Biochem. Biophys. Res. Commun.* 421 (1), 124–128. doi: 10.1016/j.bbrc.2012.03.129

Ullah, A., Masood, R., Spencer, P. J., Murakami, M. T., and Arni, R. K. (2014). Crystallization and preliminary X-ray diffraction studies of an L-amino-acid oxidase from *Lachesis muta* venom. *Acta Crystallogr. F Struct. Biol. Commun.* 70 (Pt 11), 1556–1559. doi: 10.1107/S2053230X14017877

Wiezel, G. A., Rustiguel, J. K., Morgenstern, D., Zoccal, K. F., Faccioli, L. H., Nonato, M. C., et al. (2019). Insights into the structure, function and stability of bordonein-L, the first L-amino acid oxidase from *Crotalus durissus terrificus* snake venom. *Biochimie* 163, 33–49. doi: 10.1016/j.biochi.2019.05.009

Xue, Z., Xu, D., Wang, Y., and Zhang, Y. (2013). ThreaDom: extracting protein domain boundary information from multiple threading alignments. *Bioinformatics* 29 (13), i247–i256. doi: 10.1093/bioinformatics/btt209

Yang, H. H., Yang, S. L., Peng, K. C., Lo, C. T., and Liu, S. Y. (2009). Induced proteome of *Trichoderma harzianum* by *Botrytis cinerea*. *Mycol Res.* 113 (Pt 9), 924–932. doi: 10.1016/j.mycres.2009.04.004

Zainal Abidin, S. A., Rajadurai, P., Chowdhury, M. E. H., Ahmad Rusmili, M. R., Othman, I., and Naidu, R. (2018). Cytotoxic, Antiproliferative and Apoptosis-inducing activity of L-Amino Acid Oxidase from Malaysian Calloselasma rhodostoma on Human Colon cancer cells. *Basic Clin. Pharmacol. Toxicol.* 123 (5), 577–588. doi: 10.1111/bcpt.13060

Zhang, L., and Wei, L. J. (2007). ACTX-8, a cytotoxic L-amino acid oxidase isolated from *Agkistrodon acutus* snake venom, induces apoptosis in Hela cervical cancer cells. *Life Sci.* 80 (13), 1189–1197. doi: 10.1016/j.lfs.2006.12.024

Zhang, Y. J., Wang, J. H., Lee, W. H., Wang, Q., Liu, H., Zheng, Y. T., et al. (2003). Molecular characterization of *Trimeresurus stejnegeri* venom L-amino acid oxidase with potential anti-HIV activity. *Biochem. Biophys. Res. Commun.* 309 (3), 598–604. doi: 10.1016/j.bbrc.2003.08.044

Zhang, H., Teng, M., Niu, L., Wang, Y., Wang, Y., Liu, Q., et al. (2004). Purification, partial characterization, crystallization and structural determination of AHP-LAAO, a novel L-amino-acid oxidase with cell apoptosis-inducing activity from *Agkistrodon halys pallas* venom. *Acta Crystallogr. Sect.* D60, 974–977. doi: 10.1107/S0907444904000046

Zheng, H., Chordia, M. D., Cooper, D. R., Chruszcz, M., Müller, P., Sheldrick, G. M., et al. (2014). Validation of metal-binding sites in macromolecular structures with the CheckMyMetal web server. *Nat. Protoc.* 9 (1), 156–170. doi: 10.1038/nprot.2013.172

Žun, G., Kos, J., and Sabotič, J. (2017). Higher fungi are a rich source of L-amino acid oxidases. *3 Biotech.* 7 (3), 230.

Conflict of Interest: The author declares that the research was conducted in the absence of any commercial or financial relationships that could be construed as a potential conflict of interest.

frontiers in Pharmacology

ORIGINAL RESEARCH
published: 07 May 2020
doi: 10.3389/fphar.2020.00611

Unity Makes Strength: Exploring Intraspecies and Interspecies Toxin Synergism between Phospholipases A_2 and Cytotoxins

Manuela B. Pucca[1,2†], Shirin Ahmadi[2,3†], Felipe A. Cerni[2,4], Line Ledsgaard[2], Christoffer V. Sørensen[2], Farrell T. S. McGeoghan[2], Trenton Stewart[2,5], Erwin Schoof[2], Bruno Lomonte[6], Ulrich auf dem Keller[2], Eliane C. Arantes[4], Figen Çalışkan[3,7] and Andreas H. Laustsen[2]*

[1] Medical School, Federal University of Roraima, Boa Vista, Brazil, [2] Department of Biotechnology and Biomedicine, Technical University of Denmark, Kongens Lyngby, Denmark, [3] Department of Biotechnology and Biosafety, Graduate School of Natural and Applied Sciences, Eskişehir Osmangazi University, Eskişehir, Turkey, [4] Department of BioMolecular Sciences, School of Pharmaceutical Sciences of Ribeirão Preto, University of São Paulo, Ribeirão Preto, Brazil, [5] Department of Biology, Lund University, Lund, Sweden, [6] Facultad de Microbiología, Instituto Clodomiro Picado, Universidad de Costa Rica, San José, Costa Rica, [7] Department of Biology, Faculty of Science and Art, Eskişehir Osmangazi University, Eskişehir, Turkey

Toxin synergism is a complex biochemical phenomenon, where different animal venom proteins interact either directly or indirectly to potentiate toxicity to a level that is above the sum of the toxicities of the individual toxins. This provides the animals possessing venoms with synergistically enhanced toxicity with a metabolic advantage, since less venom is needed to inflict potent toxic effects in prey and predators. Among the toxins that are known for interacting synergistically are cytotoxins from snake venoms, phospholipases A_2 from snake and bee venoms, and melittin from bee venom. These toxins may derive a synergistically enhanced toxicity *via* formation of toxin complexes by hetero-oligomerization. Using a human keratinocyte assay mimicking human epidermis *in vitro*, we demonstrate and quantify the level of synergistically enhanced toxicity for 12 cytotoxin/melittin-PLA_2 combinations using toxins from elapids, vipers, and bees. Moreover, by utilizing an interaction-based assay and by including a wealth of information obtained *via* a thorough literature review, we speculate and propose a mechanistic model for how toxin synergism in relation to cytotoxicity may be mediated by cytotoxin/melittin and PLA_2 complex formation.

Keywords: toxin synergism, phospholipase A_2, toxin complexes, cytotoxins, melittin, cytotoxicity, toxin interactions, venom

OPEN ACCESS

Edited by:
Yuri N. Utkin, Institute of Bioorganic Chemistry (RAS), Russia

Reviewed by:
Choo Hock Tan, University of Malaya, Malaysia
Sardar Gasanov, Lomonosov Moscow State University, Russia

****Correspondence:***
Andreas H. Laustsen
ahola@bio.dtu.dk

†These authors have contributed equally to this work

Specialty section:
This article was submitted to Pharmacology of Ion Channels and Channelopathies, a section of the journal Frontiers in Pharmacology

Received: *14 December 2019*
Accepted: *20 April 2020*
Published: *07 May 2020*

Citation:
Pucca MB, Ahmadi S, Cerni FA, Ledsgaard L, Sørensen CV, McGeoghan FTS, Stewart T, Schoof E, Lomonte B, auf dem Keller U, Arantes EC, Çalışkan F and Laustsen AH (2020) Unity Makes Strength: Exploring Intraspecies and Interspecies Toxin Synergism between Phospholipases A_2 and Cytotoxins. Front. Pharmacol. 11:611. doi: 10.3389/fphar.2020.00611

INTRODUCTION

The venomous animals that pose a threat to human health are classified in six major groups: cnidarians, venomous fish, scorpions, spiders, hymenopterans, and snakes (Ericsson et al., 2006). Their venoms are complex cocktails of toxic proteins, peptides, and small organic and inorganic molecules. In general, venoms derive their toxicity from proteins known as toxins. These toxins are

in themselves a diverse and complex group, including smaller neurotoxic peptides, larger phospholipases, and venom proteases, along with many other protein families (Ducancel, 2016). In fact, it is estimated that between 19,000 and 25,000 snake toxins, 100,000 scorpion toxins, more than 10 million spider toxins, and a large unknown number of toxins from other venomous creatures exist (Laustsen et al., 2016a; Laustsen et al., 2016b).

Venoms are produced for defensive and/or predatory purposes to provide a survival benefit to the species possessing them. However, the production and replenishment of these venoms come with a metabolic cost for the venomous animals (Morgenstern and King, 2013). This metabolic cost has forced venomous animals to evolve mechanisms for minimizing venom expenditure, such as the venom optimization hypothesis (Wigger et al., 2002) and toxin synergism (Laustsen, 2016). Indeed, snakes (Strydom, 1976; Mora-Obando et al., 2014; Lauridsen et al., 2016), spiders (Chan et al., 1975; Wullschleger, 2005), scorpions (Lazarovici et al., 1984), and bees (Mingarro et al., 1995) have evolved to produce venoms with potencies that are larger than the sum of the individual toxins (toxin synergism). One of the most prominent examples of this phenomenon is the synergy between cytotoxins and phospholipases, which was reported for the first time more than half a century ago (Condrea et al., 1964). Cytotoxins from snakes belong to the three-finger toxin (3FTx) superfamily of proteins and share a common scaffold of three loops of β-strands extending from a central globular core reticulated by four highly conserved disulphide bridges (Kessler et al., 2017). Researchers have used different names for categorizing these toxins, including membrane-active polypeptides, membrane-disruptive polypeptides, membrane toxins, membranotoxins, cardiotoxins (Harvey, 2018), direct lytic factors (DLF) (Slotta and Vick, 1969), and cobramines (Wolff et al., 1968). However, in 1988, Dufton and Hider adopted the name "cytotoxin," which underlines the fact that this group of toxins can kill different cell types by interacting with and disrupting their membranes (Dufton and Hider, 1988). The term "cytotoxin" has since then been more widely adopted in the literature and will be the term used in this study. Melittin, the main toxic component of bee venoms, was also first identified as a DLF, and as its mechanism closely resembles that of cytotoxins (Dempsey, 1990), it may be considered as a "cytotoxin-like" peptide.

While snake cytotoxins are mainly found in the genera *Naja* and *Hemachatus* (Dufton and Hider, 1988), snake venom phospholipases A_2 (svPLA$_2$s) are found in all venomous snake families (i.e., Viperidae, Elapidae, Atractaspididae, and Colubridae) (Kini, 1997; Xiao et al., 2017). Catalytically active svPLA$_2$s hydrolyze membrane glycerophospholipids at the *sn*-2 site of these molecules (Xiao et al., 2017), however, many svPLA$_2$s have over the course of evolution lost their catalytic activity, yet retain toxicity via other functions, such as an ability to disrupt cellular membranes very selectively (Arni and Ward, 1996; Kini, 2003). Based on their molecular structure, svPLA$_2$s can be classified into three groups. 1) Group IA contains seven disulfide bridges and a characteristic surface loop between residues 63 and 67, called the elapidic loop. This group is primarily found in Elapidae, although some have also been reported for Colubridae. 2) Group IIA contains a seven-residue C-terminal extension and seven conserved disulfide bonds and is found in Viperidae. 3) Group IIB has a six-residue C-terminal extension and only six disulfide bridges, which means it lacks an otherwise universally conserved 61–95 disulfide bond. This group of svPLA$_2$s is found in vipers (Six and Dennis, 2000). A different group of phospholipases A_2, group III, can be found in lizard and bee venoms. Group III PLA$_2$s have molecular masses that are higher than the molecular masses of PLA$_2$s from snakes (15–18 kDa compared to 13–15 kDa, respectively) and contain eight disulfide bridges (Dennis et al., 2011).

The first synergistic effect between PLA$_2$s and cytotoxins was reported by Condrea and Mager in 1964. Their study (Condrea et al., 1964) demonstrated, using erythrocytes, that when lower concentrations of *Naja naja* PLA$_2$ causing no significant hemolysis or phospholipid hydrolysis (3.3% hemolysis, 0% phospholipid hydrolysis) were combined with a cobra cytotoxin with no phospholipase activity, significant hemolysis and phospholipid hydrolysis was observed (86.5% hemolysis, 77% phospholipid hydrolysis) (Condrea et al., 1964). In a later study (Klibansky et al., 1968), it was shown that synergism also occurred between PLA$_2$s from *Vipera palestinae* and cytotoxins from cobras, implying that synergism was not restricted to toxins from the same animal. In 1995, the occurrence of synergism between cytotoxin P4 from *N. nigricollis* and homologous PLA$_2$s along with many heterologous PLA$_2$s was investigated using melanoma tumor cells. Here, sublytic concentrations of cytotoxin P4 combined with non-lytic concentrations of PLA$_2$s from *N. nigricollis, N. atra, N. melanoleuca, Walterinnesia aegyptia, Bitis arietans*, and *Pseudocerastes persicus,* along with porcine pancreas and bee venom, were demonstrated to cause 100% cell lysis (Chaim-Matyas et al., 1995). For bees, similar examples have been reported, where PLA$_2$ from bee venom (bvPLA$_2$) has been shown to synergistically increase the lytic effect of melittin (Yunes et al., 1977; Frangieh et al., 2019; Pucca et al., 2019).

Despite the considerable amount of research that has been performed in the field of toxinology, little is still known about the phenomenon of toxin synergism. In particular, the synergistic effects between cytotoxins and PLA$_2$s, as well as other toxin-toxin combinations, remain understudied, and the molecular mode of interaction between many of these toxins, as well as their combined mechanism of action, are yet to be completely elucidated. In this study, we demonstrate how several different combinations between all three PLA$_2$ groups (I, II, and III) and different cytotoxins from *N. nigricollis*, *N. mossambica*, *N. melanoleuca*, as well as melittin from bee venom interact synergistically using a cytotoxicity assay involving immortalized human keratinocytes. Based on the synergistically enhanced cytotoxic effects observed on the keratinocytes, an interaction-based assay, and a thorough literature review, this study also proposes a mechanistic model for how cell lysis is synergistically enhanced by cytotoxin and PLA$_2$ complex formation.

MATERIALS AND METHODS

Toxins

Venoms of *N. nigricollis* (the black-necked spitting cobra), *N. melanoleuca* (the forest cobra), and *N. mossambica* (the Mozambique spitting cobra) were purchased from Latoxan (Valence, France). Melittin (P01501) and bvPLA$_2$ (P00630) were purchased from Sigma-Aldrich (Cotia, SP, Brazil, and St Louis, MO, USA, respectively). *Bothrops asper* myotoxin II (MII, lacking PLA$_2$ activity, P24605) was isolated as previously described (Lomonte and Gutiérrez, 1989). Venoms of *N. nigricollis, N. melanoleuca*, and *N. mossambica* were fractionated by reversed-phase high-performance liquid chromatography (RP-HPLC) as described elsewhere (Lauridsen et al., 2017), and peaks were numbered according to (Petras et al., 2011; Lauridsen et al., 2017; Dehli, 2018), respectively. In order to evaluate toxin purities, the fractionated toxins were sent to the Proteomics Core at the Technical University of Denmark where *De Novo* sequencing was performed. The subsequent peptide spectra were screened against the Uniprot database using *N. naja* or *B. asper* as the identifier species. The snake cytotoxins were screened against *N. naja* and MII was screened against *Bothrops asper*. The cytotoxin and phospholipase A$_2$ purities are shown in **Supplementary Table 1** and **Supplementary Figure 1**.

Cell Culture and Synergy Assessment

An immortalized human keratinocyte cell line (N/TERT) (kindly provided by Edel O'Toole from the Queen Mary University of London) (Dickson et al., 2000) was cultured in Dulbecco's modified Eagle's medium (DMEM:F12; Grand Island, NY, USA) supplemented with 10% (v/v) fetal bovine serum (FBS), 1% (v/v) penicillin-streptomycin (Sigma, St. Louis, MO, USA), and 1 × RMplus supplement (McGeoghan, 2017), under standard conditions (37°C, 5% CO_2, and 85% humidity). Sub-culturing was performed by incubating with 0.05% Trypsin-EDTA (Life technologies, Grand Island, NY, USA) for 5 to 10 min at 37°C to detach adherent cells. The cell suspension was diluted 1:1 with medium to neutralize the trypsin, and then centrifuged at 1,300*g* for 5 min. Approximately 4×10^3 cells diluted in 100 µl of medium were seeded per well in 96-well polystyrene black opaque-plates (Thermo Fisher Scientific, Roskilde, DK) and incubated overnight under the standard conditions. The medium was aspirated and replaced by media (100 µl per well) containing different combinations of PLA$_2$s (bvPLA$_2$, MII, or Nmo12) and cytotoxins (fraction 18 from *N. nigricollis* (Nn18), fraction 20 from *N. nigricollis* (Nn20), fraction 17 from *N. melanoleuca* (Nm17), fraction 9 from *N. mossambica* (Nmo9)) or melittin, which had been co-incubated for 30 min at 37°C before addition. Controls consisted of wells without cells, cells incubated without addition of toxins, and cells incubated with only individual toxins. The plates were incubated under the standard conditions for 24 h. Cytotoxicity was evaluated by the CellTiter-Glo luminescent cell viability assay (Promega, Madison, WI, USA) which uses adenosine triphosphate (ATP) levels to measure living cells (Riss et al., 2011). The manufacturer's protocol was followed. Experiments were performed in triplicate with two technical replicates for each combination, and results were expressed as mean ± SD. Data were evaluated through an analysis of variance (ANOVA) test followed by a Bonferroni post-test, and a significance level of $p < 0.05$ was used for statistical testing. All statistical analyses were performed using GraphPad-Prism 6 software (GraphPad-Prism Software Inc., San Diego, CA, USA).

Combination Index

The Coefficient of Drug Interaction or Combination of Drug Index (CDI) (Zhao et al., 2014), here named Combination of Toxin Index (CTI), was calculated by the equation CTI = $(E)_{1,2}/E_1 \times E_2$, where $(E)_{1,2}$ is the measured effect of the combination effect; E_1 and E_2 are the individual effects of each toxin. Thus, CTI values of <1, =1, or >1 indicate that the toxin–toxin interactions are synergistic, additive, or antagonistic, respectively.

Toxin Biotinylation and Protein-Complex Isolation

The toxins MII, Nm17, and melittin were biotinylated using PEG$_4$-conjugated biotin (EZ-Link™ NHS-PEG$_4$-Biotin, Thermo Fisher Scientific, Rockford, IL, USA) with 1:1.5 molar ratio (toxin/biotin), as described elsewhere (Laustsen et al., 2017). In order to evaluate if the synergistically-acting toxins interact with each other and generate complexes, a pull-down assay was performed. Different combinations of toxins were used: biotinylated MII (bio-MII) + Nm17, biotinylated Nm17 (bio-Nm17) + bvPLA$_2$, and biotinylated melittin (bio-melittin) + bvPLA$_2$. The mixtures containing 5 µg of each toxin diluted in phosphate-buffered saline (PBS) pH 7.2 (final volume, 100 µl) were co-incubated for 1 h at 37°C and transferred to 30 µl of Dynabeads M-280 Streptavidin (Invitrogen, Trondheim, Norway). Beads and mixtures were incubated for 30 min at room temperature and mixed gently each 10 mins. As control, the same combinations were used with non-biotinylated toxins. Magnetic separation was used to collect the beads. The beads were washed three times with 200 µl of PBS pH 7.2. For elution of the toxins, 30 µl of PBS pH 7.2 containing lithium dodecyl sulphate loading buffer (NuPAGE LDS, Thermo Fisher Scientific, Rockford, IL, USA), and 0.1 M of dithiothreitol (DTT, Thermo Fisher Scientific, Rockford, IL, USA) were added to the beads and incubated 10 min at 70°C, after which the toxins were recovered from the supernatant. The samples obtained from the pull-down assay were analyzed through electrophoresis for low molecular weight proteins according to the method of Schagger and von Jagow (Schägger and von Jagow, 1987). Samples were run on a 16% Tris-Tricine SDS-PAGE gel (Novex Tricine Gels, Invitrogen, Carlsbad, CA, USA) at 149 V and 150 mA. The gel was stained with silver (SilverXpress, Life Technologies, Carlsbad, CA, USA).

RESULTS

Cytotoxic Effects of Cross-Species Synergistic Combinations of Toxins

Immortalized human keratinocytes (N/TERTs) were challenged with individual cytotoxins in different concentrations and analyzed for cell survival (data not shown). Based on these experiments, doses resulting in low cytotoxicity (0–20%), were used for challenging N/TERT cells. The isolated cytotoxins (Nn18, Nm17, Nn20, Nmo9) and melittin, as well as these cytotoxins in combination with three PLA_2s (Nmo12, MII, and $bvPLA_2$) from different species were added to the culture medium of the N/TERT cells and incubated for 24 h (**Figure 1**). Exposure of N/TERT cells to *Naja* spp. cytotoxins showed an average of seven-fold higher cytotoxic activity in combination with MII (~62%), five-fold higher in combination with Nmo12 (~50%), and four-fold higher when combined to $bvPLA_2$ (~45%) (**Figure 1**). In contrast, melittin showed the highest cytotoxic effect in combination with $bvPLA_2$, with five-fold higher cytotoxicity (~90%), and a three-fold higher cytotoxicity when combined with MII (~60%) and Nmo12 (~55%).

To provide evidence of the synergistically potentiated effects of the toxins in combination compared to the effects obtained by the single toxins, the CTI was calculated. All 12 cytotoxin/melittin-PLA_2 combinations demonstrated a strong synergistic effect (CTI < 0.5). Moreover, three of the combinations (melittin + $bvPLA_2$, Nn18 + MII, and Nn20 + MII) presented very strong synergism (CTI < 0.2) (**Figure 2**).

Evidence of Formation of Phospholipase A_2-Cytotoxin Complex

To investigate the possible occurrence of cytotoxin-PLA_2 complexes, a pull-down assay was performed. The results indicated that formation of a complex took place between cytotoxins and PLA_2s independent of the tested toxin combination (**Figure 3**). Thus, these data demonstrate that

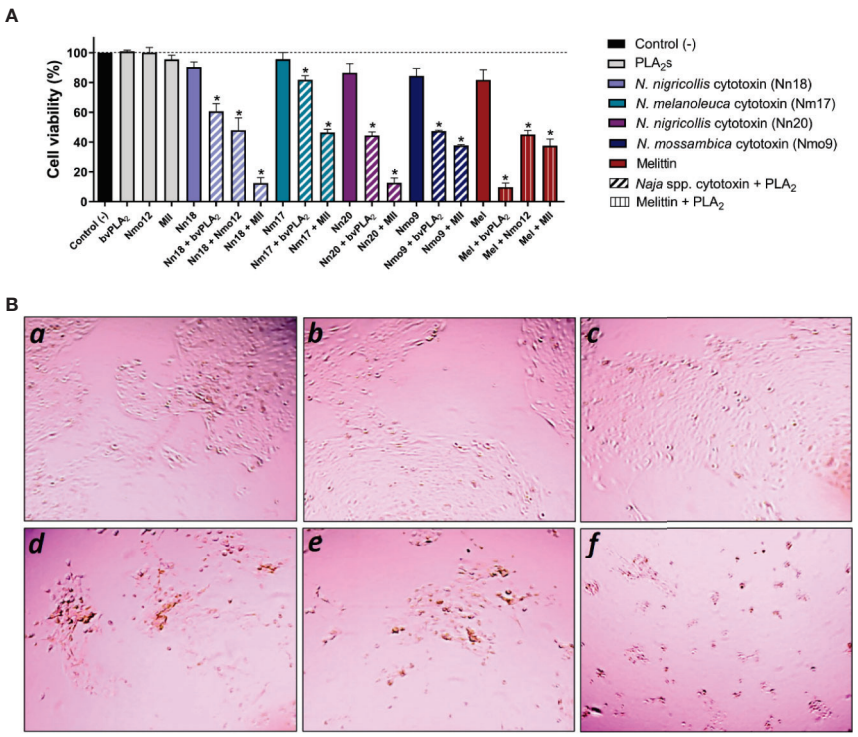

FIGURE 1 | Synergistically enhanced lytic effects of combinations of cytotoxins and PLA_2s from the same and different species. **(A)** Low lytic concentrations of cytotoxins (Nn18: 8 μg/ml, Nm17: 6 μg/ml, Nn20: 20 μg/ml, Nmo9: 1 μg/ml, and melittin: 5 μg/ml) were mixed with sublytic concentrations of PLA_2s (Nmo12: 50 μg/ml, $bvPLA_2$: 50 μg/ml, and MII: 12 μg/ml) and the combinations were added to human keratinocytes (N/TERT). Controls were performed with N/TERT cells not subjected to the toxins. Synergistically enhanced cytotoxicity was examined after 24 h of incubation by determination of adenosine triphosphate (ATP) levels through a luminescent cell viability assay. Experiments were performed in triplicates with two replicates for each combination, and results are expressed as mean ± SD. Data was analyzed by an analysis of variance (ANOVA) test followed by a Bonferroni post-test. (*$p < 0.001$ compared to the respective effect with the individual cytotoxin). **(B)** Representative morphological features of N/TERT cells captured by Evo XL imaging system using a 4× objective lens. (*a-c*) Standard N/TERT cell cultures forming islands of adherent and flattened keratinocytes, indicating viable cells: *a*: control; *b:* $bvPLA_2$, and *c:* Nn18. (*d-f*) N/TERT cell cultures forming separated clusters of keratinocytes (fragmentation) and presenting several rounded cells, indicating cell damage and lysis: *d:* Nn18 + $bvPLA_2$; *e:* Nn18 + Nmo12, and *f:* Nn18 + MII. Similar patterns were seen for other toxins.

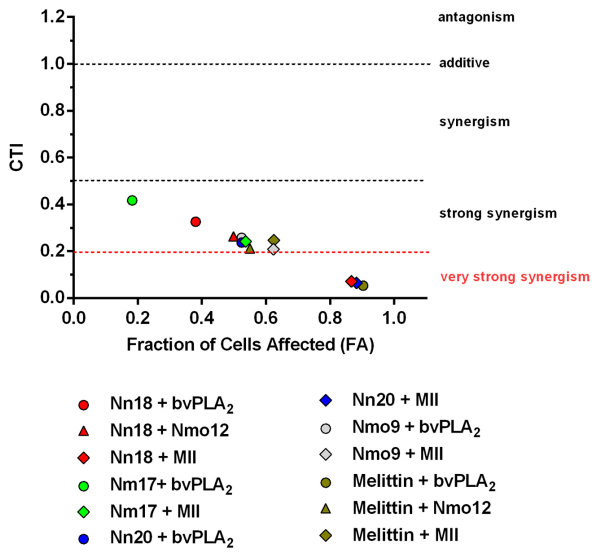

FIGURE 2 | Combination effect of cytotoxins and PLA_2s. The Combination of Toxin Index (CTI) was calculated for 12 different combinations of melittin/cytotoxins and PLA_2s. The X axis shows the level of cytotoxicity, where 0 = 100% of viable cells, and 1 = 0% of viable cells. The Y axis shows the CTI values, where values <1, =1, or >1 indicate that the toxins act synergistically, additively, or antagonistically, respectively. CTI <0.5 indicates strong synergism, and CTI <0.2 very strong synergism. Triangles, diamonds, and circles represent melittin/cytotoxin combinations with PLA_2s from group I (Nmo12), II (MII), and III ($bvPLA_2$), respectively.

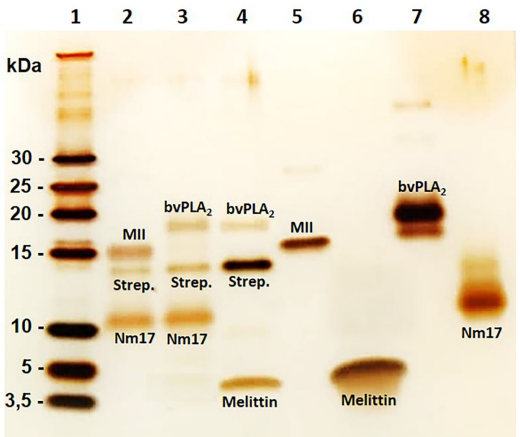

FIGURE 3 | Electrophoresis profiles of toxins and toxin complexes isolated in a pull-down experiment. Different combinations of cytotoxins and PLA_2s (5 µg of each and one of them biotinylated) were co-incubated for 1 h at 37°C. This was followed by a pull-down experiment using Dynabeads M280 Streptavidin. Toxins were eluted with lithium dodecyl sulphate (LDS) and dithiothreitol (DTT) and heated at 70°C for 10 min. Eluted toxins were evaluated using a Tris-Tricine SDS-PAGE 16% and silver staining. Lane 1: Ladder; Lane 2: bio-MII + Nm17; Lane 3: bio-Nm17 + $bvPLA_2$; Lane 4: bio-melittin + $bvPLA_2$; Lane 5: MII; Lane 6: melittin (control); Lane 7: $bvPLA_2$ (control); Lane 8: Nm17 (control). No protein band was seen when combinations with non-biotinylated toxins were used (data not shown). Strep. means streptavidin.

cytotoxins and PLA_2s from the same and different species can form complexes, and that these complexes could be responsible for the synergistically enhanced cytotoxic effects observed on keratinocyte bilayer membranes. The hypothesized mechanism of hetero-oligomer complex interaction with membranes and complex-induced lytic effect is represented in **Figure 4**.

DISCUSSION

Toxin synergism between groups of toxins is a vast field of study that remains largely unexplored, since most toxin-toxin interactions are yet to be studied. However, cytotoxins, PLA_2s, snake venom metalloproteinases (SVMPs), and snake venom serine proteases (SVSPs) are among the toxin families that possess the ability to interact synergistically with other toxins, which has been investigated in previous studies (Xiong and Huang, 2018). For instance, it has been demonstrated that a combination of acidic and basic $svPLA_2$s (including Asp49 and Lys49 subtypes) can be found in a single snake species (Angulo and Lomonte, 2009), having synergistic effects (Mora-Obando et al., 2014; Bustillo et al., 2019). This is in agreement with the belief that toxin synergism can be identified whenever predominant protein families of snake venoms are co-administered (Xiong and Huang, 2018). In this relation, cobra snake venoms are known to be dominated by cytotoxins and PLA_2s. In fact, around 95% of *N. nigricollis* and *N. mossambica* venom is composed of cytotoxins (72.8% and 67.7%, respectively) and PLA_2s (21.9% and 27.1%, respectively) (Petras et al., 2011). Bee venom is also dominated by melittin (50%) and PLA_2 (15%) toxins (Prado et al., 2010). Thus, due to the high abundance in venoms of cytotoxins and PLA_2s, their interactions have been studied for decades and are considered great examples of protein complementation serving to potentiate biological activity (Gasanov et al., 2014). However, the mechanism behind this synergism phenomenon has not been elucidated.

Toxin synergism can be achieved through several mechanisms, mainly divided into intermolecular synergism, where toxins act on different targets or processes causing increased toxicity, or through supramolecular synergism, where toxins either interact with the same target or associate into a complex with increased toxicity (Laustsen, 2016). Gasanov et al. dedicated many efforts to propose a model for cytotoxin-PLA_2 interaction (Gasanov et al., 1995; Gasanov et al., 1997; Gasanov et al., 2014). Moreover, methods like chromatography (gel filtration) (Mukherjee, 2010), ELISA (Saini et al., 1997), and functional assays (Louw and Visser, 1978; Chaim-Matyas et al., 1995) have been used successfully to prove that formation of non-covalent complexes between cytotoxins and PLA_2 occurs. Here, we demonstrate that MII, a basic Lys49 PLA_2 from *B. asper* with no enzymatic activity, produced a strong or very strong synergistic effect with different cytotoxins (Nn18, Nm17, Nn20, Nmo9) and melittin. The interaction of cytotoxins with this type of viper PLA_2 has never been studied before. Our data with non-enzymatic MII are also supported by a recent study, which demonstrated that Asp49 and Lys49 PLA_2s from *Bothrops*

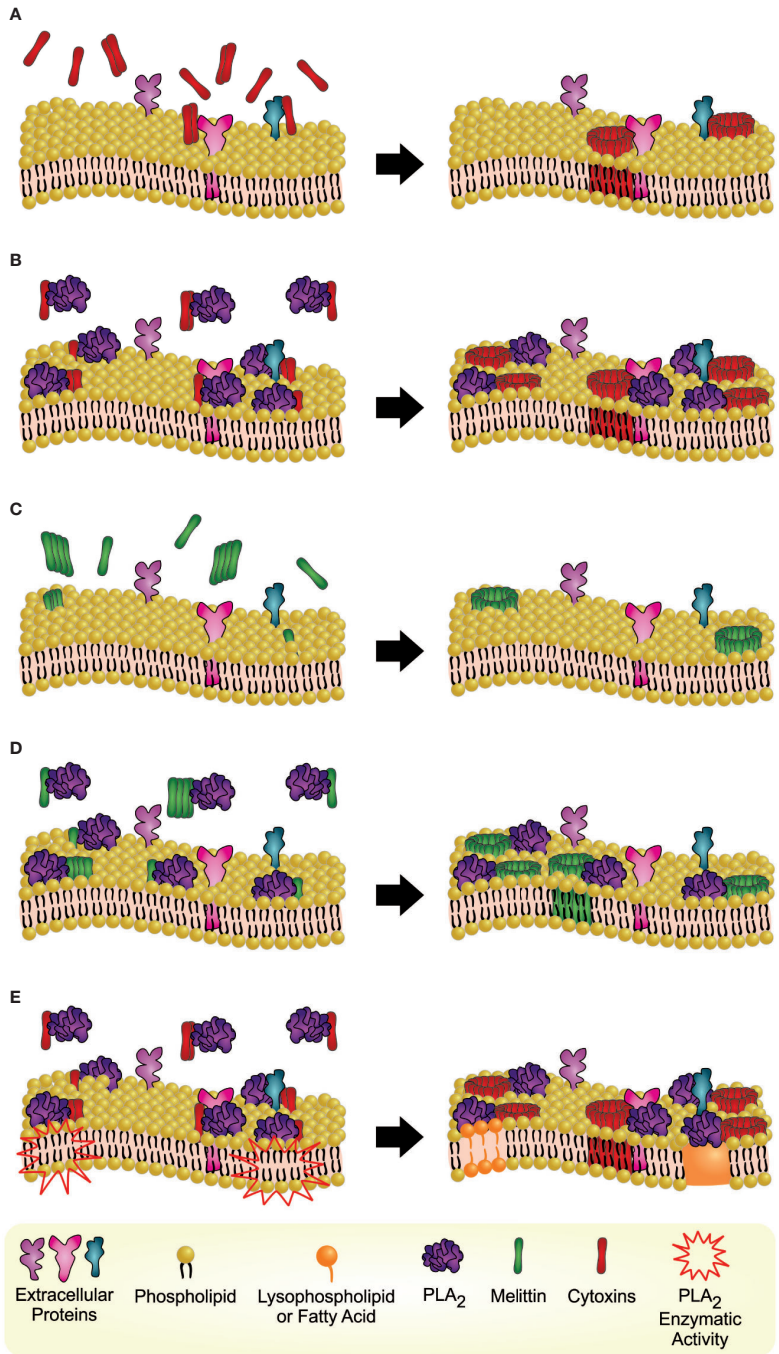

FIGURE 4 | Hypothetical phenomena of synergistically enhanced cell lysis mediated by cytotoxin-PLA_2 or melittin-PLA_2 hetero-oligomers on phospholipid bilayer membranes. **(A)** Cytotoxins (monomers or oligomers) likely bind to anionic extracellular proteins or carbohydrates (Harvey, 2018), which may lead to further oligomerization and formation of membrane pores, leading to cell lysis (Forouhar et al., 2003; Konshina et al., 2011). **(B)** When combined with PLA_2s, cytotoxins are more likely to easily bind to the neutral outer membrane on the lipid binding surface of the molecule (Singer et al., 2002; Burke and Dennis, 2009), resulting in synergistically enhanced lysis. **(C)** Different to cytotoxins, which are proteins of predominantly beta sheet structure, the helical structure of melittin provides better opportunities for melittin interaction with neutral membranes (Dempsey, 1990; Kleinschmidt et al., 1997), which is possibly mediated *via* electrostatic attraction between basic amino acid residues of melittin and the phosphate group of phosphatidylcholine (Dempsey, 1990; Kleinschmidt et al., 1997). The melittin-phospholipid binding enables melittin oligomerization, formation of membrane pores, and lysis (Yang et al., 2001; Pucca et al., 2019). **(D)** As for cytotoxins, PLA_2s can also facilitate melittin binding in the cell membrane, resulting in synergistically enhanced lysis. **(E)** PLA_2-induced hydrolysis also affects membrane integrity through the detergent action of the hydrolytic products of phospholipids, which may also contribute to the lytic effects (Lomonte and Gutiérrez, 2011). The last hypothetical phenomenon is unlikely to account for the synergistic effects observed for MII, since this toxin lacks enzymatic activity.

diporus venom present synergistic effects, and that the Lys49 variant (lacking enzymatic activity) has greater myotoxicity, cytotoxicity, anti-adhesion activity, and causes stronger inhibition of cell migration (Bustillo et al., 2019). In addition, to the best of our knowledge, it is the first time that the presence of supramolecular synergistic interaction between cytotoxins and PLA_2 is demonstrated using a pull-down assay. In this study we demonstrate that independently of the animal species from which the tested venom toxin is derived, cytotoxins and PLA_2s interacted and formed hetero-oligomers. Hence, we speculate that cytotoxin-PLA_2 oligomers are generated in the venom gland and their cytotoxic effect is synergistically enhanced by this formation of hetero-oligomers. To support our hypothesis, a literature review was performed.

Due to their cationic nature, cytotoxins are likely to have no or very weak electrostatic interaction with phospholipids on the outer membrane leaflet of a mammalian cell, mostly composed of neutral components, unfavorable for interacting with the cytotoxins (Harvey, 1985). Since most of the negatively charged lipids are located in inner membrane leaflet (cytoplasmic face), cytotoxins likely first bind to anionic extracellular proteins or carbohydrates (e.g., oligosaccharides) (Harvey, 2018). Thus, cytotoxins (monomers or oligomers) seek and interact with unknown membrane anionic moieties through their basic electrostatic field. The cytotoxin–protein binding may enable cytotoxins to penetrate the membrane through their hydrophobic first loop and interact with negatively charged lipids from the inner membrane leaflet, which may lead to further oligomerization and formation of membrane pores, leading to cell lysis (Forouhar et al., 2003; Konshina et al., 2011). The cytotoxin-mediated mechanism of pore formation is like the perforin polymerization used by cytotoxic effector cells (Natural Killer cells and cytotoxic T lymphocytes) (Abbas et al., 2016). No specific protein targets have yet been identified for cytotoxins (Gasanov et al., 2014).

Different from cytotoxins, all three groups of PLA_2s tested (IA, IIA, and III) bind readily to the neutral outer membrane through interactions with a group of hydrophobic residues on the lipid binding surface of the molecule (Singer et al., 2002; Burke and Dennis, 2009). Moreover, in case of MII, it was demonstrated that the toxin can also bind to fifteen different proteins, including nucleolin (Massimino et al., 2018). Thus, within the complex formation, PLA_2s likely facilitate cytotoxin binding and penetration into the membrane, thereby enhancing the cytotoxin activity, which results in synergistically enhanced lysis. Supporting the synergistic activity, most PLA_2s hydrolyze the ester bond of glycerophospholipids located at position two (*sn*-2), resulting in a structural change of the cell membrane and lysis. Although the composition of glycerophospholipids is diverse among mammalian cells and their distribution is different in the inner or outer plasma membrane leaflets (Hishikawa et al., 2014), PLA_2-induced hydrolysis also affects membrane integrity through the detergent action of the hydrolytic products of phospholipids (i.e., lysophospholipids and fatty acids) contributing to the lytic effect as well (Lomonte and Gutiérrez, 2011). In addition, the augmentation of lysophospholipids facilitates flip-flopping of phospholipids and better exposure of acidic lipids to cytotoxins on the outer membrane leaflet (Gasanov et al., 1997).

Chaim-Matyas and co-authors have shown that among all different combinations of the P4 cytotoxin from *N. nigricollis* and PLA_2s from different origins, the highest synergistic activity is seen between P4 and one of the basic PLA_2s found in the same venom (Chaim-Matyas et al., 1995). Very strong synergism between intraspecies toxins was also observed in our study, where melittin and bvPLA_2 combinations exhibited the highest cytotoxicity in N/TERT cells (>90% cytotoxicity and CTI <0.2). Interspecies toxin combinations were also tested, and interestingly, for snakes, we found that Nmo12, an acidic PLA_2 from *N. mossambica*, exhibited less synergistic effects when combined with *Naja* spp. cytotoxins, compared to when it was combined with MII from the *B. asper* pit viper. Although more studies must be conducted for the evaluation of interfamily synergism, our results might indicate that synergism is not solely dependent on the toxins co-evolving within the same genus but may be a more universal feature co-evolving across genera and families. On the other hand, combinations employing cobra cytotoxins and bvPLA_2 resulted in lower synergism compared to combinations with cobra cytotoxins and snake-derived PLA_2s. This observation is not surprising, as it is to be expected that PLA_2s and cytotoxins originating from snakes have co-evolved to result in the highest level of toxicity, just as the case is for PLA_2s and melittin from bees. All in all, our data from 12 cross-species combinations indicate that synergistic effects of toxin-toxin combinations may be less dependent on species and more related to the fundamental structural and biochemical characteristics of the proteins themselves. Notably, in this study, not all toxins were isolated in high purity upon venom fractionation. Some of the cytotoxins and phospholipases were observed to have co-eluted in some fractions. However, synergistic effects were still observed when either fractionated or purified toxins were combined.

This is the first study that evaluates the cytotoxic effects of co-administration of cytotoxins and PLA_2s on human keratinocytes. Many other cell types have been used for assessment of cytotoxic effects of venom cytotoxins and/or PLA_2s, including erythrocytes, lymphocytes, cardiac myocytes, spleen cells, endothelial cells, skeletal muscle myoblasts/myotubes, and various tumor cells (Chaim-Matyas et al., 1991; Gasanov et al., 1997; Gasanov et al., 2014). However, to the best of our knowledge, there exists no studies reporting the effect of these individual toxins (or in combination) on human keratinocytes, which are among the most affected cells in cases of cobra bite-induced dermonecrosis (Rivel et al., 2016) or skin necrosis caused by bee venom (Palm and Medzhitov, 2013). The lack of studies using human keratinocyte cell lines could be justified by the limited availability of primary keratinocytes to generate epidermal models. Here, we demonstrate that N/TERT cells can be a biologically relevant target for *in vitro* studies with toxins (Smits et al., 2017).

CONCLUSION AND FINAL REMARKS

This study demonstrates how cytotoxins and PLA_2s from different species (elapids, vipers, and bees) may interact synergistically to enhance cell lysis, explored via the use of a human keratinocyte assay mimicking human skin *in vitro*. The results indicate that strong to very strong synergism may result from the hetero-oligomerization of cytotoxins and PLA_2s to potentiated toxin complexes, which are speculated to be better posed to interact with and disrupt cellular membranes. Finally, based on the results obtained in this work combined with findings extracted from prior art, we propose a mechanistic model for how cytotoxin and PLA_2 complex formation may possibly mediate synergistically enhanced cell lysis. We further demonstrate that toxin synergism between cytotoxins, cytotoxin-like toxins, and PLA_2s may occur across snake genera, snake families, and even entirely different species (snakes and bees) due to the fundamental structural and biochemical characteristics of the toxins themselves.

DATA AVAILABILITY STATEMENT

All datasets generated for this study are included in the article/ **Supplementary Material**.

AUTHOR CONTRIBUTIONS

MP, SA, FÇ, TS, and ES performed experiments and analyzed results. UK and FM provided the cell line and FM helped with the cell culture experiments. SA, CS, and BL purified and biotinylated the toxins. FAC performed the figure illustration. MP, SA, LL, and AL wrote the paper. BL, UK, EA, and FÇ gave their valuable and professional suggestions. All authors corrected the manuscript and provided revisions.

FUNDING

We thank Conselho Nacional de Desenvolvimento Científico e Tecnológico (CNPq, The National Council for Scientific and Technological Development, grant no. 307155/2017-0); Fundação de Amparo à Pesquisa do Estado de São Paulo (FAPESP, São Paulo Research Foundation, grant no. 2017/04724-4, scholarship to FAC no. 2017/14035-1 and 2018/14158-9), and the Villum Foundation (grant 00025302).

ACKNOWLEDGMENTS

N/TERT cells were kindly provided by Edel O'Toole (Queen Mary University of London).

SUPPLEMENTARY MATERIAL

The Supplementary Material for this article can be found online at: https://www.frontiersin.org/articles/10.3389/fphar.2020.00611/full#supplementary-material

SUPPLEMENTARY TABLE 1 | Toxin purities. Snake cytotoxin (CTx) and phospholipase A_2 (PLA_2) purities were evaluated using *De Novo* sequencing. The abundance results received were filtered to exclude results with low reliability. Results with less than two peptide matches and lower than 30% sequence coverage were removed from the dataset. In order to obtain purities, the abundance results for each fraction were summed and divided by each respective protein that matched the peptide sequences from the screen. The cytotoxin and phospholipase A_2 purities from each fraction were grouped to determine the purities relative to their toxin families. The Uniprot IDs listed made up the primary abundances for each fraction when screened from the Uniprot database during *De Novo* sequencing. Melittin and honeybee phospholipase A_2 ($bvPLA_2$) were purchased from Sigma-Aldrich and are displayed with their listed purities.

SUPPLEMENTARY FIGURE 1 | Electrophoretic profiles of toxins. Toxins (Nn18, Nn20, Nn25, Nn17, Nmo9, Nmo12, melittin, Bee-PLA2, and M-II – 2 µg) were evaluated using Tris-Tricine SDS-PAGE 16% under reducing conditions using Coomassie blue staining.

REFERENCES

Abbas, A. K., Lichtman, A. H., and Pillai, S. (2016). *Basic immunology: functions and disorders of the immune system. Fifth edition.* (St. Louis, Missouri: Elsevier).

Angulo, Y., and Lomonte, B. (2009). Biochemistry and toxicology of toxins purified from the venom of the snake *Bothrops asper*. *Toxicon* 54, 949–957. doi: 10.1016/j.toxicon.2008.12.014

Arni, R. K., and Ward, R. J. (1996). Phospholipase A2–a structural review. *Toxicon* 34, 827–841. doi: 10.1016/0041-0101(96)00036-0

Burke, J. E., and Dennis, E. A. (2009). Phospholipase A2 structure/function, mechanism, and signaling. *J. Lipid Res.* 50, S237–S242. doi: 10.1194/jlr.R800033-JLR200

Bustillo, S., Fernández, J., Chaves-Araya, S., Angulo, Y., Leiva, L. C., and Lomonte, B. (2019). Isolation of two basic phospholipases A2 from *Bothrops diporus* snake venom: Comparative characterization and synergism between Asp49 and Lys49 variants. *Toxicon* 168, 113–121. doi: 10.1016/j.toxicon.2019.07.004

Chaim-Matyas, A., Borkow, G., and Ovadia, M. (1991). Isolation and characterization of a cytotoxin P4 from the venom of *Naja nigricollis nigricollis* preferentially active on tumor cells. *Biochem. Int.* 24, 415–421.

Chaim-Matyas, A., Borkow, G., and Ovadia, M. (1995). Synergism between cytotoxin P4 from the snake venom of *Naja nigricollis nigricollis* and various phospholipases. *Comp. Biochem. Physiol. Part B* 110, 83–89. doi: 10.1016/0305-0491(94)00130-M

Chan, T. K., Geren, C. R., Howell, D. E., and Odell, G. V. (1975). Adenosine triphosphate in tarantula spider venoms and its synergistic effect with the venom toxin. *Toxicon* 13, 61–66. doi: 10.1016/0041-0101(75)90159-2

Condrea, E., De Vries, A., and Mager, J. (1964). Hemolysis and splitting of human erythrocyte phospholipids by snake venoms. *Biochim. Biophys. Acta (BBA) Specialized Section Lipids Related Subj.* 84, 60–73. doi: 10.1016/0926-6542(64)90101-5

Dehli, R. I. (2018). *Recombinant antivenom against the spitting cobra. Unpublished master"s thesis* (Lyngby, Denmark: Technical University of Denmark).

Dempsey, C. E. (1990). The actions of melittin on membranes. *Biochim. Biophys. Acta* 1031, 143–161. doi: 10.1016/0304-4157(90)90006-x

Dennis, E. A., Cao, J., Hsu, Y.-H., Magrioti, V., and Kokotos, G. (2011). Phospholipase A2 enzymes: physical structure, biological function, disease implication, chemical inhibition, and therapeutic intervention. *Chem. Rev.* 111, 6130–6185. doi: 10.1021/cr200085w

Dickson, M. A., Hahn, W. C., Ino, Y., Ronfard, V., Wu, J. Y., Weinberg, R. A., et al. (2000). Human keratinocytes that express hTERT and also bypass a

p16INK4a-enforced mechanism that limits life span become immortal yet retain normal growth and differentiation characteristics. *Mol. Cell Biol.* 20, 1436–1447. doi: 10.1128/MCB.20.4.1436-1447.2000

Ducancel, F. (2016). Venoms and medical research. *Biol. Aujourdhui* 210, 89–99. doi: 10.1051/jbio/2016016

Dufton, M. J., and Hider, R. C. (1988). Structure and pharmacology of elapid cytotoxins. *Pharmacol. Ther.* 36, 1–40. doi: 10.1016/0163-7258(88)90111-8

Ericsson, C. D., Hatz, C., Junghanss, T., and Bodio, M. (2006). Medically important venomous animals: Biology, prevention, first aid, and clinical management. *Clin. Infect. Dis.* 43, 1309–1317. doi: 10.1086/508279

Forouhar, F., Huang, W.-N., Liu, J.-H., Chien, K.-Y., Wu, W., and Hsiao, C.-D. (2003). Structural basis of membrane-induced cardiotoxin A3 oligomerization. *J. Biol. Chem.* 278, 21980–21988. doi: 10.1074/jbc.M208650200

Frangieh, J., Salma, Y., Haddad, K., Mattei, C., Legros, C., Fajloun, Z., et al. (2019). First characterization of the venom from *Apis mellifera syriaca*, a honeybee from the Middle East region. *Toxins* 11, 191. doi: 10.3390/toxins11040191

Gasanov, S. E., Gasanov, N. E., and Rael, E. D. (1995). Phospholipase A2 and cobra venom cytotoxin Vc5 interactions and membrane structure. *Gen. Physiol. Biophys.* 14, 107–123.

Gasanov, S. E., Alsarraj, M. A., Gasanov, N. E., and Rael, E. D. (1997). Cobra venom cytotoxin free of phospholipase A2 and its effect on model membranes and T leukemia cells. *J. Membrane Biol.* 155, 133–142. doi: 10.1007/s002329900165

Gasanov, S. E., Dagda, R. K., and Rael, E. D. (2014). Snake venom cytotoxins, phospholipase A2s, and Zn2+-dependent metalloproteinases: Mechanisms of action and pharmacological relevance. *J. Clin. Toxicol.* 4, 1000181. doi: 10.4172/2161-0495.1000181

Harvey, A. L. (1985). Cardiotoxins from Cobra venoms: Possible mechanisms of action. *J. Toxicol.* 4, 41–69. doi: 10.3109/15569548509014413

Harvey, A. L. (2018). "Cardiotoxins from Cobra venoms," in *Handbook of Natural Toxins*. Routledge. doi: 10.1201/9780203752715-3

Hishikawa, D., Hashidate, T., Shimizu, T., and Shindou, H. (2014). Diversity and function of membrane glycerophospholipids generated by the remodeling pathway in mammalian cells. *J. Lipid Res.* 55, 799–807. doi: 10.1194/jlr.R046094

Kessler, P., Marchot, P., Silva, M., and Servent, D. (2017). The three-finger toxin fold: a multifunctional structural scaffold able to modulate cholinergic functions. *J. Neurochem.* 142, 7–18. doi: 10.1111/jnc.13975

Kini, R. M. (1997). *Venom phospholipase A2 enzymes : structure, function, and mechanism.* (Chichester ; New York: John Wiley). Available at: https://trove.nla.gov.au/version/17566700 [Accessed November 25, 2019].

Kini, R. M. (2003). Excitement ahead: structure, function and mechanism of snake venom phospholipase A2 enzymes. *Toxicon* 42, 827–840. doi: 10.1016/j.toxicon.2003.11.002

Kleinschmidt, J. H., Mahaney, J. E., Thomas, D. D., and Marsh, D. (1997). Interaction of bee venom melittin with zwitterionic and negatively charged phospholipid bilayers: a spin-label electron spin resonance study. *Biophys. J.* 72, 12. doi: 10.1016/S0006-3495(97)78711-3

Klibansky, C., London, Y., Frenkel, A., and De Vries, A. (1968). Enhancing action of synthetic and natural basic polypeptides on erythrocyte-ghost phospholipid hydrolysis by phospholipase A. *Biochim. Biophys. Acta (BBA) Biomembranes* 150, 15–23. doi: 10.1016/0005-2736(68)90003-5

Konshina, A. G., Boldyrev, I. A., Utkin, Y. N., Omel'kov, A. V., and Efremov, R. G. (2011). Snake cytotoxins bind to membranes via interactions with phosphatidylserine head groups of lipids. *PloS One* 6, e19064. doi: 10.1371/journal.pone.0019064

Lauridsen, L. P., Laustsen, A. H., Lomonte, B., and Gutiérrez, J. M. (2016). Toxicovenomics and antivenom profiling of the Eastern green mamba snake (*Dendroaspis angusticeps*). *J. Proteomics* 136, 248–261. doi: 10.1016/j.jprot.2016.02.003

Lauridsen, L. P., Laustsen, A. H., Lomonte, B., and Gutiérrez, J. M. (2017). Exploring the venom of the forest cobra snake: Toxicovenomics and antivenom profiling of *Naja melanoleuca*. *J. Proteomics* 150, 98–108. doi: 10.1016/j.jprot.2016.08.024

Laustsen, A. H., Engmark, M., Milbo, C., Johannesen, J., Lomonte, B., Gutiérrez, J. M., et al. (2016a). From fangs to pharmacology: The future of snakebite envenoming therapy. *Curr. Pharm. Des.* 22, 5270–5293. doi: 10.2174/1381612822666160623073438

Laustsen, A. H., Solà, M., Jappe, E. C., Oscoz, S., Lauridsen, L. P., and Engmark, M. (2016b). Biotechnological trends in spider and scorpion antivenom development. *Toxins* 8, 1-33. doi: 10.3390/toxins8080226

Laustsen, A. H., Lauridsen, L. P., Lomonte, B., Andersen, M. R., and Lohse, B. (2017). Pitfalls to avoid when using phage display for snake toxins. *Toxicon* 126, 79–89. doi: 10.1016/j.toxicon.2016.12.010

Laustsen, A. H. (2016). Toxin synergism in snake venoms. *Toxin Rev.* 35, 165–170. doi: 10.1080/15569543.2016.1220397

Lazarovici, P., Menashe, M., and Zlotkin, E. (1984). Toxicity to crustacea due to polypeptide-phospholipase interaction in the venom of a chactoid scorpion. *Arch. Biochem. Biophysics* 229, 270–286. doi: 10.1016/0003-9861(84)90153-X

Lomonte, B., and Gutiérrez, J. (1989). A new muscle damaging toxin, myotoxin II, from the venom of the snake *Bothrops asper* (terciopelo). *Toxicon* 27, 725–733. doi: 10.1016/0041-0101(89)90039-1

Lomonte, B., and Gutiérrez, J. M. (2011). Phospholipases A2 from viperidae snake venoms: How do they induce skeletal muscle damage? *Acta Chem. Slov* 58, 647–659.

Louw, A. I., and Visser, L. (1978). The synergism of cardiotoxin and phospholipase A2 in hemolysis. *Biochim. Biophys. Acta (BBA) Biomembranes* 512, 163–171. doi: 10.1016/0005-2736(78)90227-4

Massimino, M. L., Simonato, M., Spolaore, B., Franchin, C., Arrigoni, G., Marin, O., et al. (2018). Cell surface nucleolin interacts with and internalizes *Bothrops asper* Lys49 phospholipase A2 and mediates its toxic activity. *Sci. Rep.* 8, 1–14. doi: 10.1038/s41598-018-28846-4

McGeoghan, F. T. S. (2017). Using RNA seq to identify novel pathomechanisms in recessive X-linked ichthyosis (Unpublished doctoral dissertation). Queen Mary University of London.

Mingarro, I., Pérez-Payá, E., Pinilla, C., Appel, J. R., Houghten, R. A., and Blondelle, S. E. (1995). Activation of bee venom phospholipase A2 through a peptide-enzyme complex. *FEBS Lett.* 372, 131–134. doi: 10.1016/0014-5793(95)00964-B

Mora-Obando, D., Fernández, J., Montecucco, C., Gutiérrez, J. M., and Lomonte, B. (2014). Synergism between basic Asp49 and Lys49 phospholipase A2 myotoxins of viperid snake venom *in vitro* and *in vivo*. *PloS One* 9, e109846. doi: 10.1371/journal.pone.0109846

Morgenstern, D., and King, G. F. (2013). The venom optimization hypothesis revisited. *Toxicon* 63, 120–128. doi: 10.1016/j.toxicon.2012.11.022

Mukherjee, A. K. (2010). Non-covalent interaction of phospholipase A2 (PLA2) and kaouthiotoxin (KTX) from venom of *Naja kaouthia* exhibits marked synergism to potentiate their cytotoxicity on target cells. *J. Venom. Res.* 1, 37–42.

Palm, N. W., and Medzhitov, R. (2013). Role of the inflammasome in defense against venoms. *Proc. Natl. Acad. Sci.* 110, 1809–1814. doi: 10.1073/pnas.1221476110

Petras, D., Sanz, L., Segura, A., Herrera, M., Villalta, M., Solano, D., et al. (2011). Snake venomics of African spitting cobras: toxin composition and assessment of congeneric cross-reactivity of the pan-African EchiTAb-Plus-ICP antivenom by antivenomics and neutralization approaches. *J. Proteome Res.* 10, 1266–1280. doi: 10.1021/pr101040f

Prado, M., Solano-Trejos, G., and Lomonte, B. (2010). Acute physiopathological effects of honeybee (*Apis mellifera*) envenoming by subcutaneous route in a mouse model. *Toxicon* 56, 1007–1017. doi: 10.1016/j.toxicon.2010.07.005

Pucca, M. B., Cerni, F. A., Oliveira, I. S., Timothy Jenkins, T. P., Argemí, L. M., Sørensen, C. V., et al. (2019). Bee updated: Current knowledge on bee venom and bee envenoming therapy. *Front. Immunol.* 10, 1-15. doi: 10.3389/fimmu.2019.02090

Riss, T. L., Moravec, R. A., and Niles, A. L. (2011). "Cytotoxicity testing: measuring viable cells, dead cells, and detecting mechanism of cell death," in *Mammalian Cell Viability*. Ed. M. J. Stoddart (Totowa, NJ: Humana Press), 103–114. doi: 10.1007/978-1-61779-108-6_12

Rivel, M., Solano, D., Herrera, M., Vargas, M., Villalta, M., Segura, Á, et al. (2016). Pathogenesis of dermonecrosis induced by venom of the spitting cobra, *Naja nigricollis*: An experimental study in mice. *Toxicon* 119, 171–179. doi: 10.1016/j.toxicon.2016.06.006

Saini, S. S., Peterson, J. W., and Chopra, A. K. (1997). Melittin binds to secretory phospholipase A2 and inhibits its enzymatic activity. *Biochem. Biophys. Res. Commun.* 238, 436–442. doi: 10.1006/bbrc.1997.7295

Schägger, H., and von Jagow, G. (1987). Tricine-sodium dodecyl sulfate-polyacrylamide gel electrophoresis for the separation of proteins in the range from 1 to 100 kDa. *Anal. Biochem.* 166, 368–379. doi: 10.1016/0003-2697(87)90587-2

Singer, A. G., Ghomashchi, F., Le Calvez, C., Bollinger, J., Bezzine, S., Rouault, M., et al. (2002). Interfacial kinetic and binding properties of the complete set of human and mouse groups I, II, V, X, and XII secreted phospholipases A2. *J. Biol. Chem.* 277, 48535–48549. doi: 10.1074/jbc.M205855200

Six, D. A., and Dennis, E. A. (2000). The expanding superfamily of phospholipase A2 enzymes: classification and characterization. *Biochim. Biophys. Acta (BBA) Mol. Cell Biol. Lipids* 1488, 1–19. doi: 10.1016/S1388-1981(00)00105-0

Slotta, K. H., and Vick, J. A. (1969). Identification of the direct lytic factor from cobra venom as cardiotoxin. *Toxicon* 6, 167–173. doi: 10.1016/0041-0101(69)90116-0

Smits, J. P. H., Niehues, H., Rikken, G., Vlijmen-Willems, I. M. J. J., van, Zande, GWHJF, van de, et al. (2017). Bogaard EH van den. Immortalized N/TERT keratinocytes as an alternative cell source in 3D human epidermal models. *Sci. Rep.* 7, 1–14. doi: 10.1038/s41598-017-12041-y

Strydom, D. J. (1976). Snake Venom Toxins. *Eur. J. Biochem.* 69, 169–176. doi: 10.1111/j.1432-1033.1976.tb10870.x

Wigger, E., Kuhn-Nentwig, L., and Nentwig, W. (2002). The venom optimisation hypothesis: a spider injects large venom quantities only into difficult prey types. *Toxicon* 40, 749–752. doi: 10.1016/S0041-0101(01)00277-X

Wolff, J., Salabè, H., Ambrose, M., and Larsen, P. R. (1968). The basic proteins of cobra venom II. Mechanism of action of cobramine B on thyroid tissue. *J. Biol. Chem.* 243, 1290–1296.

Wullschleger, B. (2005). Spider venom: enhancement of venom efficacy mediated by different synergistic strategies in *Cupiennius salei*. *J. Exp. Biol.* 208, 2115–2121. doi: 10.1242/jeb.01594

Xiao, H., Pan, H., Liao, K., Yang, M., and Huang, C. (2017). Snake Venom PLA2, a Promising Target for Broad-Spectrum Antivenom Drug Development. *BioMed. Res. Int.* 1-10. doi: 10.1155/2017/6592820

Xiong, S., and Huang, C. (2018). Synergistic strategies of predominant toxins in snake venoms. *Toxicol. Lett.* 287, 142–154. doi: 10.1016/j.toxlet.2018.02.004

Yang, L., Harroun, T. A., Weiss, T. M., Ding, L., and Huang, H. W. (2001). Barrel-stave model or toroidal model? A case study on melittin pores. *Biophys. J.* 81, 1475–1485. doi: 10.1016/S0006-3495(01)75802-X

Yunes, R., Goldhammer, A. R., Garner, W. K., and Cordes, E. H. (1977). Phospholipases: Melittin facilitation of bee venom phospholipase A2-catalyzed hydrolysis of unsonicated lecithin liposomes. *Arch. Biochem. Biophysics* 183, 105–112. doi: 10.1016/0003-9861(77)90424-6

Zhao, Y., Gao, J.-L., Ji, J.-W., Gao, M., Yin, Q.-S., Qiu, Q.-L., et al. (2014). Cytotoxicity enhancement in MDA-MB-231 cells by the combination treatment of tetrahydropalmatine and berberine derived from *Corydalis yanhusuo* W. T. Wang. *J. Intercult. Ethnopharmacol.* 3, 68–72. doi: 10.5455/jice.20140123040224

Conflict of Interest: The authors declare that the research was conducted in the absence of any commercial or financial relationships that could be construed as a potential conflict of interest.

frontiers in Pharmacology

ORIGINAL RESEARCH
published: 13 May 2020
doi: 10.3389/fphar.2020.00636

Sphingomyelinases D From *Loxosceles* Spider Venoms and Cell Membranes: Action on Lipid Rafts and Activation of Endogenous Metalloproteinases

Priscila Hess Lopes[1], *Carmen W. van den Berg*[2] *and Denise V. Tambourgi*[1]*

[1] Laboratório de Imunoquímica, Instituto Butantan, São Paulo, Brazil, [2] Centre for Medical Education, School of Medicine, Cardiff University, Cardiff, United Kingdom

OPEN ACCESS

Edited by:
Yuri N. Utkin,
Institute of Bioorganic Chemistry (RAS), Russia

Reviewed by:
Masataka Oda,
Kyoto Pharmaceutical University, Japan
Christoph Arenz,
Humboldt University of Berlin, Germany

***Correspondence:**
Denise V. Tambourgi
denise.tambourgi@butantan.gov.br

Specialty section:
This article was submitted to Translational Pharmacology, a section of the journal Frontiers in Pharmacology

Received: 17 December 2019
Accepted: 21 April 2020
Published: 13 May 2020

Citation:
Lopes PH, Berg CWvd and Tambourgi DV (2020) Sphingomyelinases D From Loxosceles Spider Venoms and Cell Membranes: Action on Lipid Rafts and Activation of Endogenous Metalloproteinases. Front. Pharmacol. 11:636. doi: 10.3389/fphar.2020.00636

Loxosceles spider venom contains Sphingomyelinase D (SMase D), the key toxin causing pathology. SMase D hydrolyzes the main component of lipid rafts, sphingomyelin, which changes the membrane microenvironment resulting in the activation of endogenous metalloproteinase from the ADAMs family. Alterations in membrane microenvironment of lipid rafts contribute to the activation of several cell surface molecules. Serine proteinases convertases acting on the pro-domain of membrane metalloproteinases, such as ADAMs, increase the cleavage and the release of proteins ectodomains and receptors located at the cell surface areas containing lipid rafts. We, therefore, investigated the interaction of SMases D with these membrane microdomains (lipid rafts) in human keratinocytes, to better understand the molecular mechanism of SMases D action, and identify the ADAM(s) responsible for the cleavage of cell surface molecules. Using specific inhibitors, we observed that ADAMs 10 and 17 are activated in the cell membrane after SMase D action. Furthermore, proproteins convertases, such as furin, are involved in the SMase D induced ADAMs activation. One of the signaling pathways that may be involved in the activation of these proteases is the MAPK pathway, since phosphorylation of ERK1/2 was observed in cells treated with SMase D. Confocal analysis showed a strong colocalization between SMase D and GM_1 ganglioside present in rafts. Analysis of structural components of rafts, such as caveolin-1 and flotillin-1, showed that the action of SMase D on cell membranes leads to a reduction in caveolin-1, which is possibly degraded by toxin-induced superoxide production in cells. The action of the toxin also results in flotilin-1 increased detection in the cell membrane. These results indicate that SMases D from *Loxosceles* venoms alter membrane rafts structure, leading to the activation of membrane bound proteases, which may explain why the lipase action of this toxin can result in proteolytic cleavage of cell surface proteins, ultimately leading to pathology.

Keywords: lipid rafts, *Loxosceles*, Sphingomyelinases D, ADAMs, proprotein convertases

INTRODUCTION

Loxosceles spiders envenomation (Sicariidae Family) occur in temperate and tropical regions of North, Central, and South America, Africa, Asia, and Europe (Wasserman and Anderson, 1983; Platnick, 2011). Bites by these spiders commonly result in local necrotic skin lesions and more rarely cause systemic effects including hemolysis, intravascular coagulation, and thrombocytopenia, which may result in renal failure (Barretto et al., 1985; Schenone et al., 1989; Tambourgi et al., 1998).

Forrester et al. (1978), analyzing *Loxosceles reclusa* venom, showed the association of venom toxicity with sphingomyelinase activity, and sphingomyelinase D (SMase D) is now considered the most important component for the establishment of this spider envenomation pathology (Tambourgi et al., 1998). We previously showed that SMases D from *Loxosceles* venom induced activation of membrane-bound metalloproteinases from the Adamalysin family, by indirect action on the cell surface in a variety of cells (Tambourgi et al., 2000; van den Berg et al., 2002). This resulted in e.g. the cleavage and ectodomain shedding of Glycophorins (GPs), endothelial protein C receptor (EPCR), and Thrombomodulin (TM), explaining the observed complement mediated hemolysis and intravascular coagulation (Tambourgi et al., 2000; van den Berg et al., 2002; Paixão-Cavalcante et al., 2006). In addition, we demonstrated that SMase D induces the ADAM (ADAM: a desintegrin and metalloprotease) mediated ectodomain shedding of numerous other cell surface molecules including MCP (Membrane Cofactor Protein: MCP; CD46), Major Histocompatibility Complex class I (MHCI), β2-microglobulin (associated with MHCI), Epidermal Growth Factor Receptor (EGFR), and the C5a receptor (CD88) in many cell types, including keratinocytes (reviewed by [Tambourgi et al., 2010]). We have used keratinocytes successfully as a model to study the molecular mechanisms operating in cutaneous loxoscelism (Paixão-Cavalcante et al., 2006; Paixão-Cavalcante et al., 2007; Corrêa et al., 2016; Lopes et al., 2019).

ADAMs are transmembrane proteases belonging to the family of Metzicins, subfamily of Adamlysins. They induce ectodomain shedding of a number of cell surface proteins and are considered crucial in modulating various physiological and pathophysiological processes (van Goor et al., 2009). The mechanism by which the *Loxosceles* venom induces activation of these ADAMs is not yet understood.

The metalloprotease domain of ADAMs is protected by a pro-domain and the primary pathway of activation and removal of the pro-domain is performed by proprotein convertases (PCs) such as furin, PC7, PC5/6B, and SKI-1 (Seidah, 2006; Klein and Bischoff, 2011). These proprotein convertases belong to a family of serine proteinases of the Subtilisins type (Seidah et al., 2008) and play an important role in the regulation of ADAMs (Reviewed by [Seals and Courtneidge, 2003]). Several studies showed that inhibition of furin transport from the Golgi to the cell membrane, by Brefeldin A and monensin, resulted in a decrease in activity of ADAM-17 (Lum et al., 1998; Roghani et al., 1999; Howard et al., 2000; Kang et al., 2002). Overexpression of PC7 increased the activity of ADAM-10 (Anders et al., 2001), and the genetic modification of the furin binding site of ADAMs 10, 12, and 19 prevented their activation (Loechel et al., 1998; Anders et al., 2001; Kang et al., 2002).

The shedding of ectodomains of surface molecules by ADAMs proteins may occur or increase due to various cellular stimuli (Walev et al., 1996; Müllberg et al., 2000; Chalaris et al., 2007), including those that result in the activation of MAPK and ERK signaling pathways (Xu et al., 2012). Furthermore, the cleavage and release of ectodomains are influenced by the spatial organization of the transmembrane molecule and protease within the lipid microenvironment of membranes (Walev et al., 2000; Kojro et al., 2001; Matthews et al., 2003; von Tresckow et al., 2004; Zimina et al., 2007). Maturation of ADAM-17 occurs in lipid rafts and the mechanisms that regulate the hydrolytic activity of this protease, on various substrates, involve the re-distribution of the target proteins within the lipid rafts (Walev et al., 2000; Kojro et al., 2001; Matthews et al., 2003; von Tresckow et al., 2004; Zimina et al., 2007).

Lipid analysis has revealed that over 70% of all cellular sphingomyelin (SM), the main substrate for *Loxosceles* SMase D, is located in lipid rafts (Smart et al., 1999) and that SM, as well as other sphingolipids, play an important role in the physical properties of biological membranes (Giocondi et al., 2004), and are necessary to maintain the integrity of the lipid rafts. A sphingomyelinase, from *Staphylococcus aureus*, altered the properties of lipid rafts in peripheral blood derived mononuclear cells, resulting in a concomitant reduction of cholesterol content of the rafts (Diaz et al., 2005). In addition, the composition and function of membrane rafts can be modulated in response to a number of factors and conditions (Simons and Ikonen, 1997) including Reactive Oxygen Species production (Park et al., 2009; Mougeolle et al., 2015) and ceramide generation (Zhang et al., 2009) and their functions are closely related to the associated proteins.

Considering that (*i*) interference with organization of lipid rafts or SM-hydrolysis can lead to changes in various biological processes in the cell, (*ii*) that shedding of cell surface molecules depends on the membrane microenvironment and (*iii*) that SMases D in the venoms of *Loxosceles* hydrolyze SM, we aimed to investigate the effects of *Loxosceles* SMase D on the activation of metalloproteinases, proprotein convertases, and lipid raft structure in human keratinocytes, in order to elucidate the complex action of this toxin.

MATERIAL AND METHODS

Reagents, Antibodies, and Buffers

Broad spectrum matrix metalloprotease inhibitor Galardin (GM6001) (Li et al., 2002), proprotein convertases inhibitors, FI (Furin inhibitor); FII (Furin, PACE4 and PC1 inhibitor); ProproC (Furin, PACE4, PC1/3, PC4, and PC5/6 inhibitor) were obtained from Merck-Millipore (Darmstadt, Germany). Specific inhibitors for ADAM-10 (GI254023 abbreviated GI) and ADAM17 (GW280264; abbreviated GW) (Ludwig et al., 2005) were kindly provided by Prof. Ann Ager (Cardiff University, UK). PMSF (serineprotease inhibitor) and Monensin (Golgi transport inhibitor), Bovine serum albumin (BSA), paraformaldehyde

were purchased from Sigma Aldrich (St. Louis, MO, USA). Dimethyl sulfoxide (DMSO) and Tween-20 were obtained from Merck-Millipore (Darmstadt, Germany), "Prolong Gold antifade" containing 4',6-diamidino-2-phenylindole (DAPI) nuclear stain was from Invitrogen (Paisley, UK). EIA Titerzime Phospho-ERK1/2 Enzyme Immunometric Assay was from Assay Designs (Ann Arbor, MI, USA). Reagents for analysis of ROS and RNOS production, Dihydroethidium (DHE) and Dihydrorhodamine-123 (DHR) respectively, were obtained from Sigma-Aldrich (MO, USA) and Alexa555-conjugated Cholera Toxin subunit b (CTx-b/Alexa555)-was obtained from Molecular Probes (Eugene, Oregon, USA). Rabbit antibodies against Flotilin-1 and Caveolin-1, FITC-conjugated secondary antibodies as rabbit anti-mouse IgG (RAM/FITC) or goat anti-rabbit IgG (GAR/FITC) were obtained from Sigma-Aldrich (Saint Louis, MI, USA). Mouse monoclonal antibodies (MoAbs) against human EGFR (Epidermal Growth Factor Receptor), MCP (CD46: Membrane Cofactor Protein), β_2-microglobulin, TNF-RI (CD120a: Tumor Necrosis Factor–Receptor 1), and streptavidin-PE were purchased from BD Biosciences (San Jose, CA, USA). MoAbs against human ADAM-17 and ADAM-10, rabbit IgG against GM_1 ganglioside, and Goat anti-rabbit conjugated Alexa 488 (GAR/Al488) were from Abcam (Cambridge, UK). MoAb against human CD59 (Bric229) was from International Blood Group Reference Laboratory (IBGRL, Bristol, UK). Rabbit IgG anti-*Loxosceles* SMase D was produced in house. DMEM (Dulbecco's Modified Eagle Medium) and penicillin-streptomycin were purchased from Gibco, Invitrogen Corp. (Eugene, Oregon, USA), and Fetal bovine serum (FBS) was from Cultilab (São Paulo, Brazil). ATV (Trypsin 0.2% and Versene 0.02%) was purchased from Adolpho Lutz Institute (São Paulo, Brazil). Buffers: Veronal buffered saline–VBS^{2+} (2.8 mM barbituric acid, 145.5 mM NaCl, 0.8 mM $MgCl_2$, 0.3 mM $CaCl_2$, 0.9 mM Na-barbital, pH 7.2), Phosphate buffered saline–PBS (8.1 mM Na_2HPO_4; 1.5 mM KH_2PO_4; 137 mM NaCl; 2.7 mM KCl, pH 7.4), FACS buffer (PBS buffer containing 1% of albumin and 0.1% of sodium azide), and FACS fixing solution (FACS buffer containing paraformaldehyde 1%).

Expression and Purification of Recombinant Sphingomyelinase D

The recombinant Sphingomyelinase D (SMase D) from *L. laeta* venom was prepared as described by Fernandes-Pedrosa et al. (Fernandes Pedrosa et al., 2002). The permission to access to genetic resources register n° AEE9AEA 11/01/2018 was provided by National System of Management of Genetic Heritage and Associated Traditional Knowledge (SisGen).

Cells Culture

Human keratinocyte cell line HaCaT (obtained from Banco de Células do Rio de Janeiro - BCRJ) were grown in 75 cm^2 flasks (Corning Inc., New York, USA) in DMEM supplemented with 10% fetal bovine serum and 1% penicillin-streptomycin, at 37°C and 5% CO_2.

Treatment of Cells

HaCaT cells were trypsinized with ATV and resuspended in VBS^{2+} buffer. Cells (1×10^6 cells/ml), pre-incubated for 5 min with Galardin (GM6001, 90 μM), ADAM-10 (GI, 45 μM) or ADAM-17 (GW, 45 μM) inhibitors, PMSF (1 mM), Monensin (10 μg/ml); proprotein convertases inhibitor (FI, FII and ProproC, 20 μM) or their vehicles, were further incubated with SMase D (25 μg/ml) or buffer, for 2 h at 37°C under slight agitation.

Cell Surface Markers Analyses

Cells treated as described in *Treatment of Cells*, were incubated for 30 min at 4°C with monoclonal antibodies against EGFR (1:200), MCP (1 μg/ml), β2-microglobulin (1:200), CD59 (1:250), ADAM-10 (1:1,000), ADAM-17 (1:100), GM_1 ganglioside (1:50), Flotilin-1 (10 μg/ml), Caveolin-1 (8 μg/ml), and rabbit anti *Loxosceles* SMase D IgG (1:200). After washing, cells were incubated for 30 min at 4°C with secondary antibodies (RAM/FITC or GAR/FITC, 1:100). Some cells were also incubated for 30 min at 4°C with anti-TNF-RI biotin-labeled antibody (1:50), washed and, then, incubated with streptavidin-PE (1:200). Fluorescence intensity of 10,000 cells was analyzed in a flow cytometer (FACSCanto, Becton Dickinson, CA, USA).

Analysis of the Production of Reactive Oxygen (ROS) and Reactive Nitrogen Oxide Species (RNOS) and Intracellular Signaling Pathway Activation in Human Keratinocytes

Analysis of RNOS and ROS production by human keratinocytes treated with SMase D was analyzed by flow cytometry. HaCaT (10^6 cells) were treated with SMase D or buffer and incubated with 5 μmol/L of DHE (for superoxide, $O2^{\bullet-}$), or DHR (for peroxynitrite, $ONOO^-$) for 1 h at 37 and 30°C, respectively and 5% CO_2. Cells were spun (1,500 rpm, 5 min), and resuspended in 300 μl FACS fixing solution and fluorescence intensity was measured in the flow cytometer (FACScanto, Becton Dickinson, CA, USA).

Activation of pERK1/2 by SMase D was analysed using the EIA Titerzime Phospho-ERK1/2 Enzyme Immunometric Assay kit, according to the manufacturer's recommendations. The reaction was read in a plate reader (Multiskan-EX, Labsystems, Helsinki, Finland) at a wavelength of λ 450 nm. The calculation of the pERK1/2 concentration in the samples was performed using the pERK recombinant standard curve (62.5 to 2,000 pg/ml) with subtraction of the value of the blank. Protein concentration of cell lysates was determined by the method of Lowry et al. (1951).

Analysis of SMase D Binding to Lipid Rafts

HaCaT cells (1.5×10^4/well) were cultured in four well Culture slides (BD) for 24 h in complete medium, followed by culture for 24 h in serum free medium. Cells were treated with SMase D (5 μg/ml) or buffer in serum free medium for 2 h at 37°C and 5% CO_2. Wells were washed five times using serum free medium, followed by incubation in PBS containing 5% BSA for 1 h at room temperature and brief washing with PBS for 5 min.

Binding of SMase D to the cells was assessed by incubation with rabbit IgG anti-SMase D (1:200 PBS/2% BSA, 30 min, RT), followed by three washes with PBS/Tween20 (0.01%) and incubation with GAR/Al488 (1:500 in PBS/2% BSA, 30 min, RT).

For the visualization of lipid rafts, cells were incubated with Alexa555-conjugated Cholera toxin subunit b (CTx-b/Al555) (1.3 μg/200 μl, 30 min, RT) (Harder et al., 1998; Gniadecki et al., 2002). Cells were washed three times in PBS/Tween20 (0.01%) and fixed in 1% paraformaldehyde for 20 min at 37°C. Slides were counterstained with "Prolong Gold antifade" containing DAPI nuclear stain and covered with coverslips for microscopy.

The effect of SMase D treatment on the colocalization of CD59 and ADAM-17 with GM_1, in lipid rafts, was investigated by incubating the cells with MoAbs against human CD59 (1:250) or anti-human ADAM-17 (10 μg/ml). The colocalization of SMase D, CD59, and ADAM-17 proteins and CTx-b was assessed using BioImageXD v1.0 software (Kankaanpää et al., 2012) and threshold values were calculated by the method of Costes (Costes et al., 2004). Colocalization coefficients, according to Manders (Manders et al., 1993), were chosen since they represent the true degree of colocalization. M1 denotes the colocalization index of the green with red marking and M2 the colocalization index of the red with green marking. An average of ten different images, in three different focal planes, were analyzed *per* experiment in four independent experiments.

Alternatively, to evaluate whether the labeling was restricted to the membrane, cells were detached and treated with SMase D or buffer, in suspension for 2 h at 37°C followed by cytospin centrifugation (400 rpm for 5 min) (Cytospin 4, Thermo Scientific, Massachusetts, USA) to fix the cells to the microscopy slides and then incubated with antibodies as described above.

The photomicrographs were acquired in laser scanning confocal microscopy system (LSCM) (LSM 510 meta, Carl Zeiss, Jena, Germany) using objective C-Apochromat 63×/1.2W corr.

Statistical Analysis

Data were expressed as mean ± standard error and statistically analyzed with GraphPad Prism, version 6.1 for Windows (San Diego, USA). Comparisons between more than two groups in relation to one variable were performed by One Way ANOVA and multiple comparisons performed by *post-hoc* Tukey HSD. Comparison of two or more variables between more than two groups was performed using Two Way ANOVA followed by *post-hoc* Bonferroni test. Comparisons between two groups were performed by Student's t test.

RESULTS

ADAM-10 and 17 Are Activated as Consequence of SMase D Action on Keratinocyte Cell Membrane

To investigate the role of ADAMs in the SMase D induced shedding of cell surface molecules from the human keratinocyte cell line HaCaT, the effects of a broad spectrum metalloproteinase inhibitor (Galardin: GM) and specific inhibitors of ADAM-10 (GI) and ADAM-17 (GW) were investigated. **Figures 1B–F** show that SMase D treatment of HaCaT cells resulted in reduced surface expression, likely as a consequence of shedding, of the membrane bound molecules EGFR, β2-microglobulin (associated with MHCI), MCP, and TNF-RI, but not CD59. This was significantly inhibited by the pre-incubation with GM and also by GI or GW, as well as a combination of both. This demonstrates that ADAMs-10 and -17 are activated as consequence of the action of SMase D from *Loxosceles* on cell membranes. As previously described by us (Paixão-Cavalcante et al., 2006), using anti-*Loxosceles* SMases D specific antibodies we could observe that the toxin binds to human keratinocytes membrane (**Figure 1A**).The use of ADAM inhibitors did not affect the cell viability nor the binding of the toxin to the cell membrane and the vehicle of the inhibitors did not produce any interference with the cleavage of the markers (data not shown).

Proprotein Convertases Participate of the ADAMs Activation After SMase D Action on Keratinocyte Cell Membrane

ADAMs are zymogens and require cleavage of the prodomain, by certain serine proteinases, also known as proprotein convertases, such as furin (Seidah, 2006; Klein and Bischoff, 2011). In order to investigate whether furin is involved in the SMase D induced ADAMs activation, HaCaT cells were pre-treated with the broad-spectrum serine proteinase inhibitor PMSF. Furin itself is also a zymogen and has to enter the Golgi to become activated, which can be prevented by monensin, an inhibitor of transport to the Golgi (Vey et al., 1994). Thus, to investigate the activation of furin, cells were also pre-treated with monensin, prior to incubation with SMase D. **Figure 2** shows that both PMSF and monensin were effective in reducing the shedding of membrane markers by ADAMs, suggesting the involvement of serine proteinases and Furin in the mechanism of activation of ADAMs, on the keratinocytes membrane, after SMases D action. Reduction in shedding was not as effective as with the metalloprotease inhibitors.

In an attempt to identify the proprotein convertases that participates in this process, the cells were treated with three different inhibitors of proprotein convertases groups, *i. e.*, FI: specific furin inhibitor (Vey et al., 1995); FII: Furin, PACE4, and PC1 inhibitor (Cameron et al., 2000); and ProproC: Furin, PACE4, PC1/3, PC4, and PC5/6 inhibitor (Becker et al., 2012). **Figure 3** shows that the three inhibitors prevented the cleavage of membrane markers, to some extent, being most effective at inhibiting the release of cell surface β2-microglobulin and MCP. These results indicate that proproteins as furin, PACE4, PC1, PC7, and PC5B may be involved in the activation of ADAMs, induced by the action of SMase D in the membrane. The inhibitors did not have any effect on the cell surface expression of the molecules analyzed on the keratinocytes treated with buffer only, indicating that the observed effect was not due to an effect on the natural turnover of cell surface molecules (data not shown). The inhibitors or their solvents (DMSO, ethanol or PBS) did affect neither the cell viability nor the binding of the toxin to the cell membrane. Furthermore, the solvents of the inhibitors did not interfere with the cleavage of the cell surface markers induced by SMase D action on the cell membrane (data not shown).

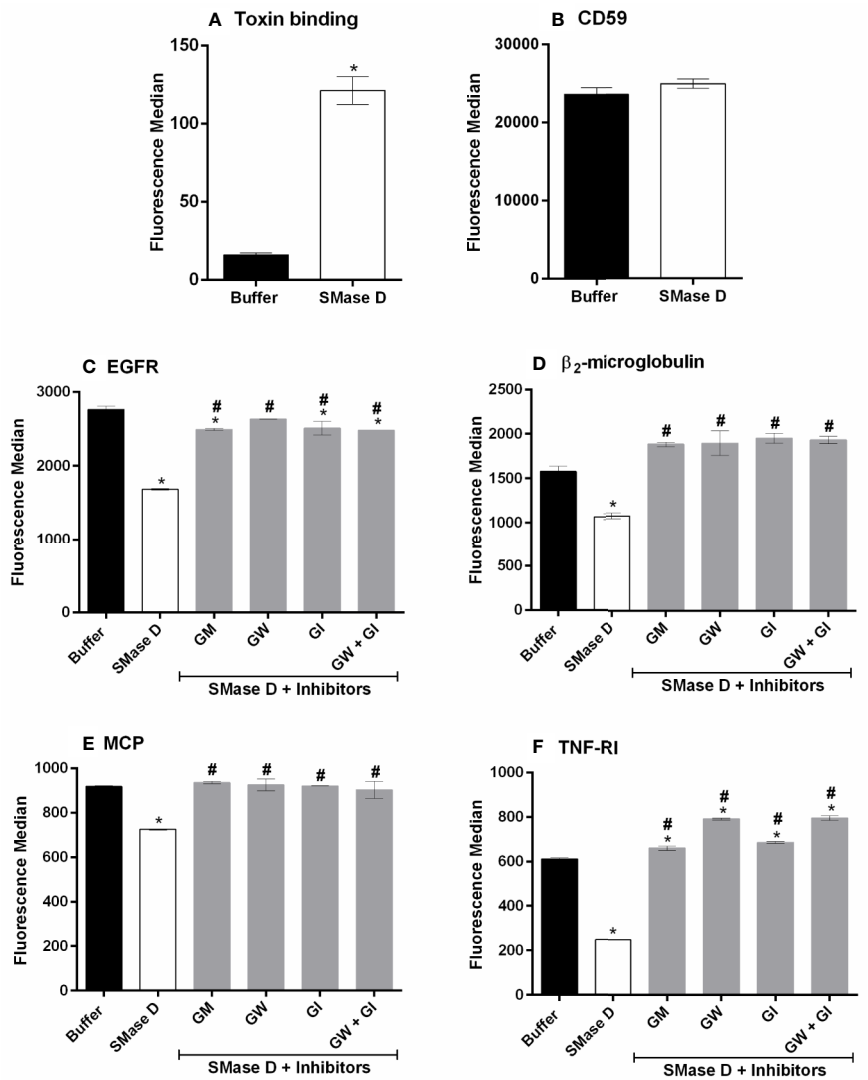

FIGURE 1 | Involvement of ADAMs in the shedding of surface markers, induced by SMase D. HaCaT cells were pre-incubated for 5 min with Galardin (GM: 90 μM), ADAM-10 (GW: 45 μM), or ADAM-17 (GI: 45 μM) inhibitors followed by SMase D (25 μg/ml) or buffer for 2 h. Binding of the SMase D to keratinocytes surface **(A)**, Expression of CD59 in cells treated or not with SMase D **(B)**, EGFR **(C)**, β2-microglobulin **(D)**, MCP **(E)**, and TNF-RI **(F)** cell surface expression was analyzed by flow cytometry. Data are presented as mean ± standard error of duplicates being representative of two independent experiments. Statistically analyzed by one-way ANOVA, followed by Tukey's HSD test or t Test of Student in case of CD59 and toxin binding, using GraphPad Prism 6.1 Software. (*) Significant difference compared to buffer ($p < 0.05$). (#) significant difference in relation to SMase D ($p < 0.05$).

SMase D Modulates the Expression of ADAMs and Induces the Activation of ERK1/2 Signaling Pathway

The results of the experiments, with ADAM-10 and ADAM-17 inhibitors, suggest an increase expression/function of these ADAMs and indeed, using flow-cytometry, we show that SMase D increases the detection/expression of ADAMs 10 and 17 on the cell surface (**Figures 4A, B**).

The shedding of surface molecules by ADAMs proteins may occur or increase due to specific signaling pathways such as MAPK and ERK (Xu et al., 2012). Based on this, we investigated the possible activation of ERK1/2 pathway after SMase D action on keratinocytes. **Figure 4C** shows that SMase D activated this signaling pathway, as demonstrated by an increased detection of ERK1/2 phosphorylation in SMase D-treated keratinocytes.

SMase D Changes the Expression of Structural Lipid Rafts Components GM_1 Ganglioside, Flotilin-1, and Caveolin-1 on Keratinocytes Membrane

Since the maturation of ADAM-17 occurs in lipid rafts and the mechanisms that regulate the hydrolytic activity of this and other

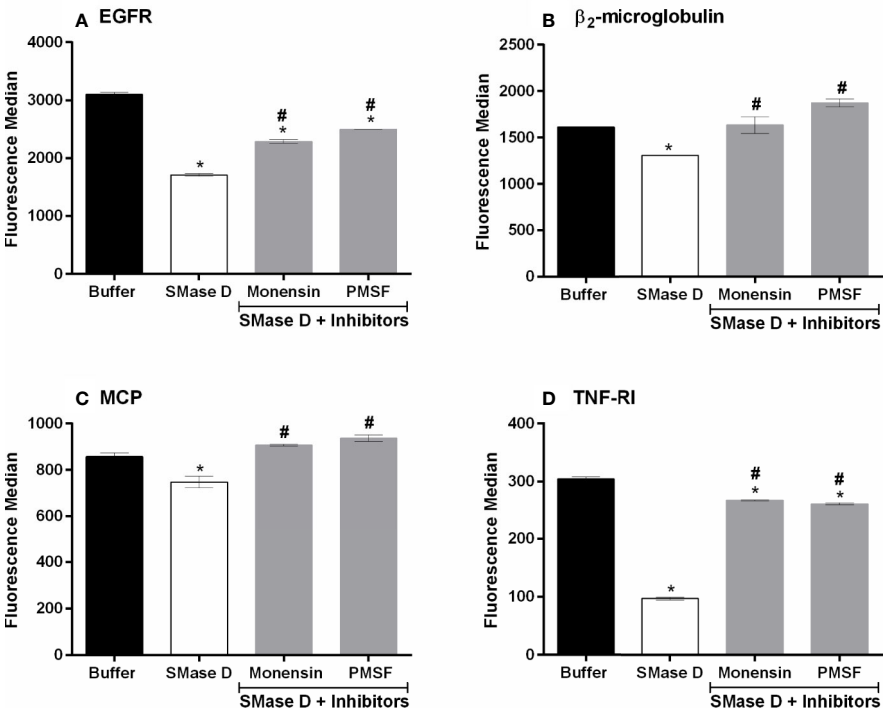

FIGURE 2 | PMSF and Monensin inhibit the SMase D-induced shedding of surface markers. HaCaT cells were pre-incubated for 5 min with PMSF (1 mM) or Monensin (10 μg/ml) followed by SMase D (25 μg/ml) or buffer for 2 h. Expression of EGFR **(A)**, β2-microglobulin **(B)**, MCP **(C)**, and TNF-RI **(D)** was analyzed by flow cytometry. Data are presented as mean ± standard error of duplicates, representative of two independent experiments. Statistically analyzed by one-way ANOVA followed by Tukey HSD test using GraphPad Prism 6.1 Software. (*) Significant difference compared to buffer ($p < 0.05$). (#) Significant difference in relation to SMase D ($p < 0.05$).

proteases, involve proteins within the lipid rafts (Walev et al., 2000; Kojro et al., 2001; Matthews et al., 2003; von Tresckow et al., 2004; Zimina et al., 2007), we analyzed the effect of SMase D on the expression of the lipid raft markers GM_1 ganglioside, flotillin-1, and caveolin-1 using flow cytometry. **Figures 5A, B** show that SMase D increased the detection or expression of GM_1 ganglioside and flotillin-1, while it reduced the expression or detection of caveolin-1 (**Figure 5C**), an important component of a different lipid domain named as caveolae.

SMase D Induces Superoxide Production in Human Keratinocytes

Considering that oxidative stress may contribute to the modification of lipid raft structural components (Park et al., 2009; Mougeolle et al., 2015) and that we observed a reduction in caveolin-1 expression after the SMase D treatment, we investigated the ability of SMase D to induce reactive oxygen and nitrogen species production. **Figure 5D** shows that SMase D induced a significant increase in superoxide production by human keratinocytes. However, the production of peroxynitrite was not affected by SMase D (**Figure 5E**).

SMase D Binds to Lipid Rafts on Human Keratinocytes Membrane and Changes the Behavior of Other Proteins Present in the Microenvironment

As structural components of lipid rafts were altered by the action of SMase D, we analyzed if the binding of SMase D on the cell membrane would colocalize with GM_1 ganglioside, a marker of lipid rafts. Confocal microscopy, using SMase D specific antibodies and fluorescently labeled Choleratoxin b (CTx-b), which binds to GM_1 was performed. **Figures 6A, B** showed that SMase D strongly colocalizes (about 85%) with GM_1 ganglioside, with a Manders' colocalization coefficient of M1 = 0.84 and M2 = 0.85. Z-stack analysis showed that the bindings of SMase D and CTx-b occur mainly at the cell surface, since, as the depth of the focal planes in the Z-axis increased, the level of colocalization reduced (**Figures 6C, D**).

To analyze the behavior of proteins known for their location or concentration of their activities in lipid rafts, we evaluated the colocalization of SMase D, CD59 (typically lipid raft associated) and ADAM-17, with GM_1, in cells before and after SMase D incubation. **Figures 7A, B** show that SMase D significantly reduced the colocalization of CD59 and GM_1 (Manders' colocalization coefficient M1 = 0.64; M2 = 0.61) when

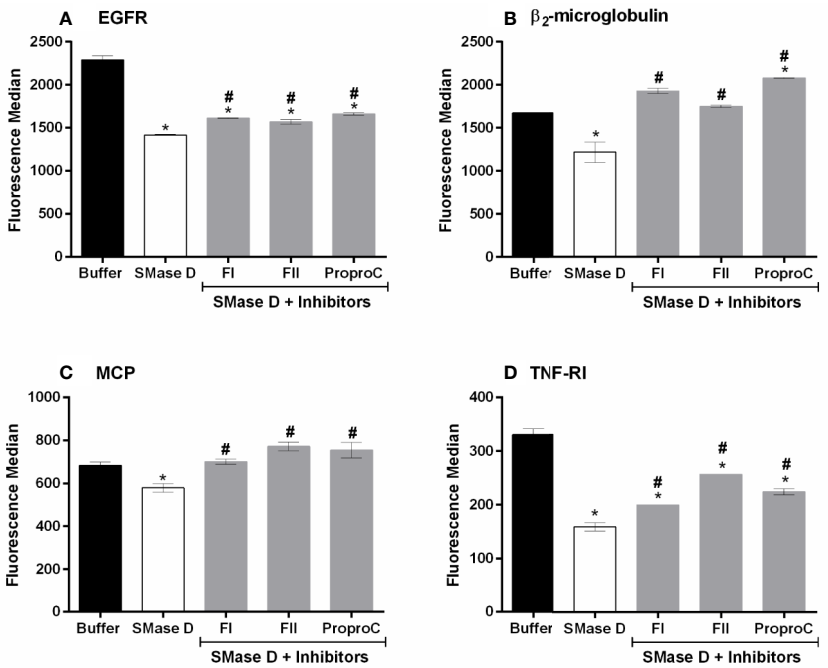

FIGURE 3 | Proprotein convertases inhibitors partially prevent SMase D-induced shedding of surface markers. HaCaT cells were pre-incubated for 5 min with 20 μM of each inhibitor followed by SMase D (25 μg/ml) or buffer for 2 h. Expression of EGFR **(A)**, β2-microglobulin **(B)**, MCP **(C)**, and TNF-RI **(D)** was analyzed by flow cytometry. Data are presented as mean ± standard error of duplicates representative of two independent experiments. Statistically analyzed by one-way ANOVA followed by Tukey HSD test using GraphPad Prism 6.1 Software. (*) Significant difference compared to buffer ($p < 0.05$). (#) Significant difference in relation to SMase D ($p < 0.05$).

compared to cells treated with buffer alone (Manders' colocalization coefficient M1 = 0.76; M2 = 0.76). In contrast, **Figure 8** shows that SMase D significantly increased the colocalization of ADAM-17 and GM_1 (Manders' colocalization coefficient M1 = 0.78; M2 = 0.83) when compared to cells treated with buffer (Manders' colocalization coefficient M1 = 0.60; M2 = 0.47).

DISCUSSION

Various interventions have been proposed as a treatment for loxoscelism, however, a definitive and fully effective therapy has not yet been established. A better understanding of the molecular mechanism of venom/toxins action is important to the establishment of more effective therapeutic approaches for the *Loxosceles* spider envenomation.

In previous studies, using a broad-spectrum metalloproteinase inhibitor Galardin (GM6001), we demonstrated that *Loxosceles* venom/SMases D activated metalloproteinases of the Adamalysin family on nucleated cells surface resulting in cleavage of various transmembrane anchored molecules (van den Berg et al., 2002; van den Berg et al., 2012). Here, we show that in addition to Galardin, specific ADAM-10 and -17 inhibitors significantly reduced the cleavage of the cell surface markers EGFR, β2-microglobulin and MCP. As also previously described by us (van den Berg et al., 2002), CD59 was not affected by the action of SMase D (**Figure 1B**). Furthermore, we show here for the first time that TNF-RI is also cleaved by the indirect action of SMase D on keratinocytes. Thus, data obtained with these inhibitors indicate that both ADAM-10 and -17 are activated by SMase D and contribute to the cleavage/shedding of cell surface molecules. Combined inhibition of these enzymes did not provide a complete inhibition of the shedding, suggesting that other ADAMs may be involved. According to Ari-Pekka et al. (Huovila et al., 2005), while ADAM-10 and -17 are the main sheddases, several other ADAMs contribute to the shedding of membrane bound proteins.

The results presented here show that proteins cleaved after the action of the SMases D are part of the group of specific substrates of ADAM-10 and -17. Shedding of surface molecules by ADAMs proteins may occur or increase in response to cellular stimulation with phorbol esters (Müllberg et al., 2000), bacterial toxins (Walev et al., 1996), apoptotic stimuli (Chalaris et al., 2007), and activation of MAPK and ERK (Xu et al., 2012). Our results showing SMase D-induced activation of MAPK ERK1/2 signaling pathway (**Figure 4C**) in keratinocytes, may suggest that the activation of this pathway may contribute to the ADAMs activity.

The metalloprotease domain of ADAMs is protected by a pro-domain in the inactive zymogens, which is removed by proprotein convertases (PCs) such as furin, PC7, PC5/6B, SKI-1. These PCs, which are serine proteases (Seidah, 2006; Klein and Bischoff, 2011), are activated themselves during transport through the Golgi. Inhibiting serine protease activity with the broad-spectrum

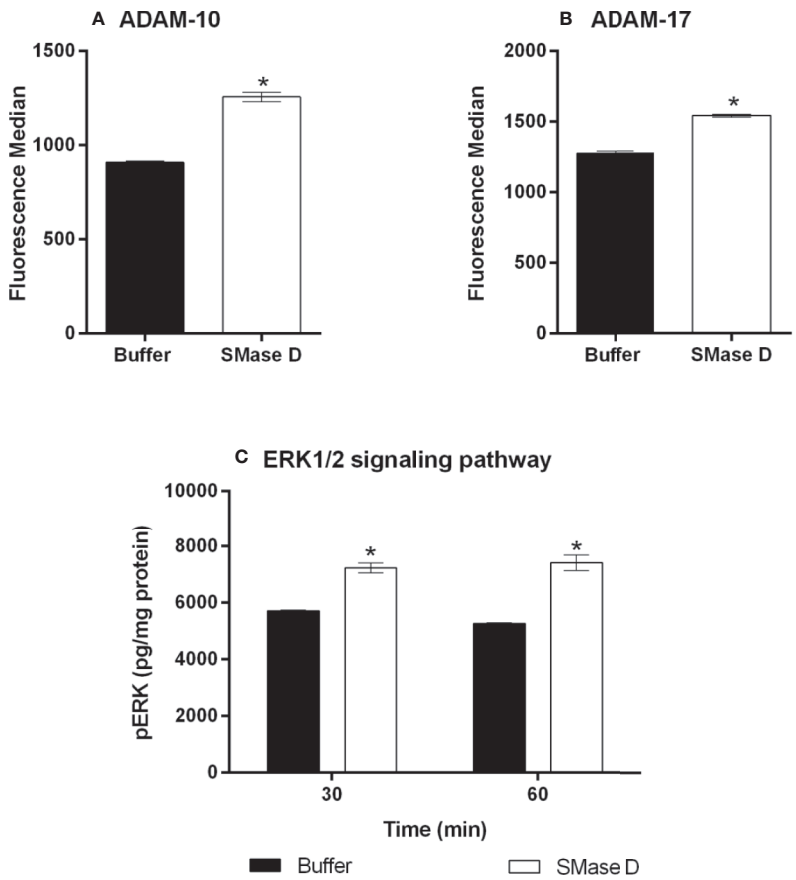

FIGURE 4 | Expression of ADAM-10 and 17 and detection of ERK1/2 phosphorylation in human keratinocytes after treatment with SMase D. HaCaT cells were treated for 2 h with SMase D (25 μg/ml) or buffer and analyzed for the expression of ADAM-10 **(A)** and ADAM-17 **(B)** by flow cytometry. Alternatively, cells were treated with SMase D or buffer for 30 and 60 min and ERK1/2 phosphorylation was evaluated by using the EIA kit Titerzime Phospho-ERK1/2 **(C)**. Data are expressed as mean ± standard error of duplicates, representative of two independent experiments. Statistically analyzed by Two Way ANOVA followed by Tukey HSD test for the evaluation of ERK1/2 and analyzed by Student's t test for ADAMs expression, using the GraphPad Prism 5.1. (*) Significant difference compared to buffer ($p < 0.05$).

inhibitor PMSF and inhibiting Golgi transport, using monensin, resulted in a partial (EGFR, TNF-RI) to complete (MCP and β_2-microglobulin) inhibition of SMase D-induced shedding, suggesting the involvement of proprotein convertases (**Figure 2**). Using more specific inhibitors of the proprotein convertases, including furin, their roles were confirmed, especially in the shedding of MCP and β_2-microglobulin, which cleavages were completely inhibited (**Figure 3**). We thus show here for the first time the participation of proprotein convertases in the SMase D-induced shedding of cell surface molecules.

The furin specific inhibitor FI showed, in most cases, to be equally efficient to the broader spectrum inhibitors FII and ProproC, suggesting that furin is the main proprotein convertase activated and involved in this process. However, in the case of EGFR and TNF-RI, we did not observe a complete inhibition and other mechanisms may contribute to the shedding of these molecules.

Lipid raft disruption has been shown to increase shedding by ADAMs-10 and -17 (Matthews et al., 2003; von Tresckow et al., 2004). Tellier et al. (2006) showed that the zymogen pro-domain of ADAM-17 is cleaved by furin in lipid rafts, which results in concentration of the shedding activity of ADAM-17 in lipid rafts and inhibition of ADAM-17 resulted in increase in its substrates within the rafts. Our results presented here also showed that SMase D-induced cleavage of several cell surface proteins, in the cell membrane, was prevented by ADAMs inhibitors. Corroborating these findings, our confocal microscopy data showed that SMase D changed the behavior of molecules located in the lipid rafts, resulting in an increased lipid raft colocalization index of ADAM-17 and a decreased CD59 colocalization (**Figures 8** and **7**, respectively).

Diaz and colleagues (2005) showed that sphingomyelinase C from *Staphylococcus aureus*, altered the properties of lipid rafts in peripheral blood derived mononuclear cells, resulting in a concomitant reduction of sphingomyelin and cholesterol content of the rafts. We have tried to emulate the action of SMase D and the subsequent cleavage of various cell surface molecules with commercial purified Sphingomyelinase C and with ceramide-1-phosphate, but while the Sphingomyelinase C did not induce cleavage of cell surface molecules, the ceramide-1-phosphate was toxic to the cells and results were inconclusive (unpublished

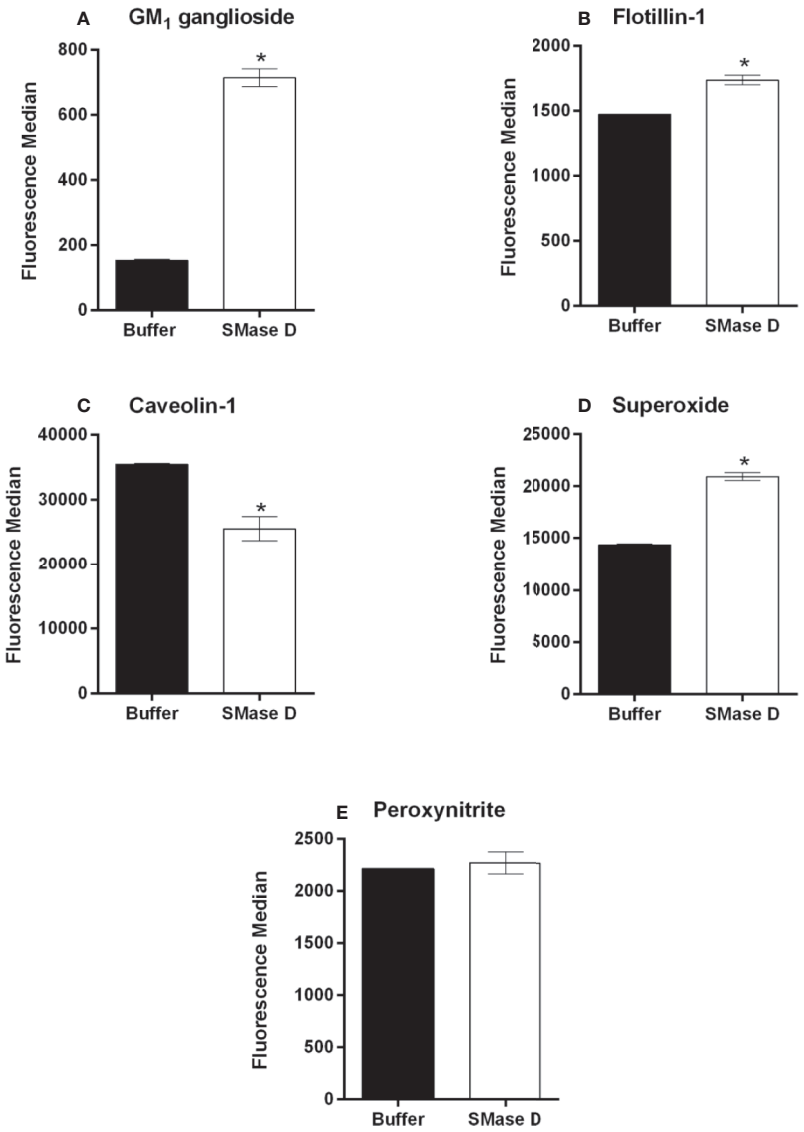

FIGURE 5 | Analysis of GM_1 ganglioside, flotillin-1, and caveolin-1 and ROS production in human keratinocytes, treated with SMase D. HaCaT cells were treated for 2 h with SMase D (25 μg/ml) or buffer and analyzed for the expression of GM_1 ganglioside **(A)**, flotillin-1 **(B)**, and caveolin-1 **(C)** by flow cytometry or for the presence of superoxide ($O_2^{\bullet -}$) **(D)** and peroxynitrite ($ONOO^-$) **(E)**, by flow cytometry. Data are expressed as mean ± standard error of duplicates, representative of two independent experiments. Statistically analyzed by Student t test, using the GraphPad Prism 5.1. (*) Significant difference compared to buffer ($p < 0.001$).

observations). Therefore our observation that SMase D changes the lipid raft composition and stability and increases the activity of ADAMs, suggest that this is a unique property of this SMase D and also reveals the importance of these microdomains in controlling this process, as demonstrated by Tellier et al. (2006).

Since the shedding process by ADAMs occurs in the lipid rafts following "perturbation" of the cell membrane environment, we evaluated the expression of the major component of lipid rafts GM_1 ganglioside, after treatment with SMase D. We observed that the ganglioside detection increased significantly after the action of SMase D, suggesting possible lipid raft disruption leading to an enhanced binding of CTx-b to GM_1 ganglioside, probably due to increased molecule accessibility (Slaughter et al., 2003).

There are two types of rafts: those containing the structural protein caveolin-1 that form caveolae, and those that lack this protein but express two different raft-specific proteins, called flotillin-1 and 2 (Volonté et al., 1999). As both caveolar and non-caveolar rafts are highly enriched in sphingolipids and glycosphingolipids, they are also known as glycolipid-enriched microdomains. These rafts are also highly enriched in gangliosides, especially GM_1 which has almost been exclusively identified in these structures (Cremesti et al., 2002). Thus, we have demonstrated that SMase D is capable of interfering with both types

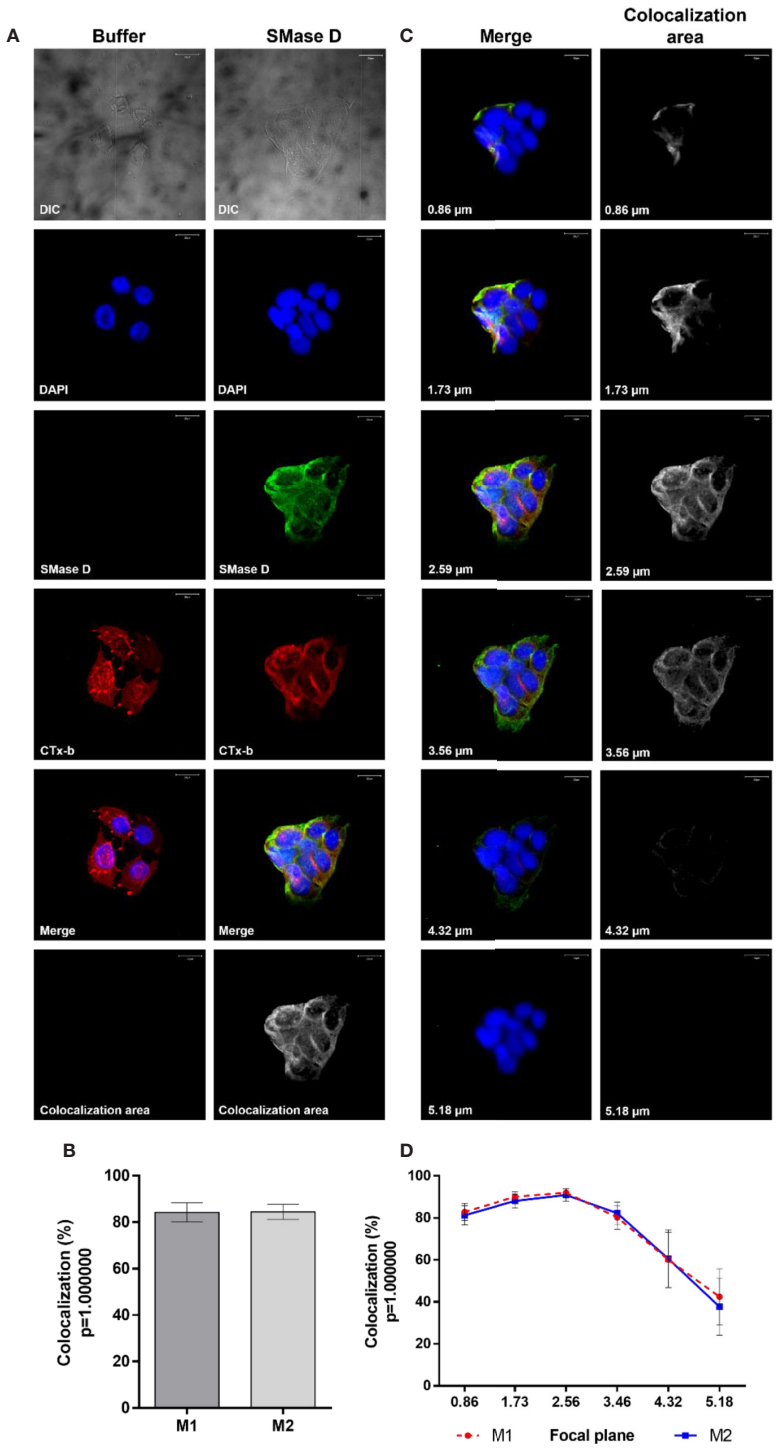

FIGURE 6 | Colocalization of SMase D and Cholera Toxin subunit b in human keratinocytes membrane. HaCaT cells cultured on slides were treated, for 2 h, with buffer or SMase D (5 µg/ml). Binding of SMase D was analyzed using rabbit IgG anti-SMase D (1:200), followed by anti-rabbit secondary antibody conjugated with Alexa-488 (1:200). Lipid rafts were visualized using Cholera toxin subunit b-AlexaFluor 555 and the nuclei counterstained with DAPI and slides were analyzed by CLSM. Scale bars represent 20 µm. **(A)** Cells treated with buffer or SMase D, at focal plane of 2.59 µm. Colocalization areas are shown as grayscale images. **(B)** average percentage SMase D/CTx-b colocalization represent means ± SEM from, at least, 10 images in two independent experiments and three different focal plans. **(C)** Cells treated with SMase D at focal planes from 0.86 to 5.18 µm. Colocalization areas are shown as grayscale images. **(D)** Percentage of SMase D/CTx-b colocalization at the different focal planes analyzed. Data on the graphs represent means ± SEM from, at least, 10 images in two independent experiments and three different focal plans.

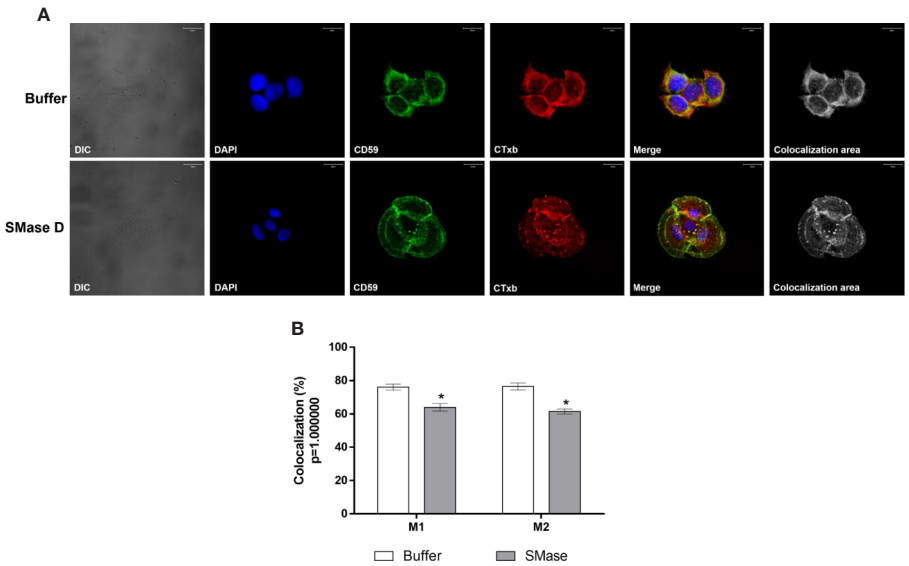

FIGURE 7 | Colocalization of CD59 and Cholera Toxin subunit b in human keratinocytes, treated with SMase D. HaCaT cells were cultured on slides and treated for 2 h with buffer or SMase D (5μg/ml). Cells were stained with Moab anti-CD59 (1:250), followed by RAM-FITC (1:50). GM_1 containing lipid rafts were visualized using Ctx-b/Alexa Fluor 555 and nuclei counterstained with DAPI and slides were analyzed by CLSM. Scale bars represent 20 μm. **(A)** Colocalization of CD59 and GM_1 at the focal plane of 3.02 μm analyzed in cells treated with buffer or SMase D. Colocalization areas are shown as grayscale images. The graph **(B)** shows a comparison between the colocalization of CD59 and CTx-b, in cells treated with SMase D or buffer and represents the mean ± SEM from, at least, 10 images in two independent experiments and three different focal plans. Statistically analyzed by Two Way ANOVA followed by Tukey HSD test, using the GraphPad Prism 5.1. (*) Significant difference compared to buffer ($p < 0.05$).

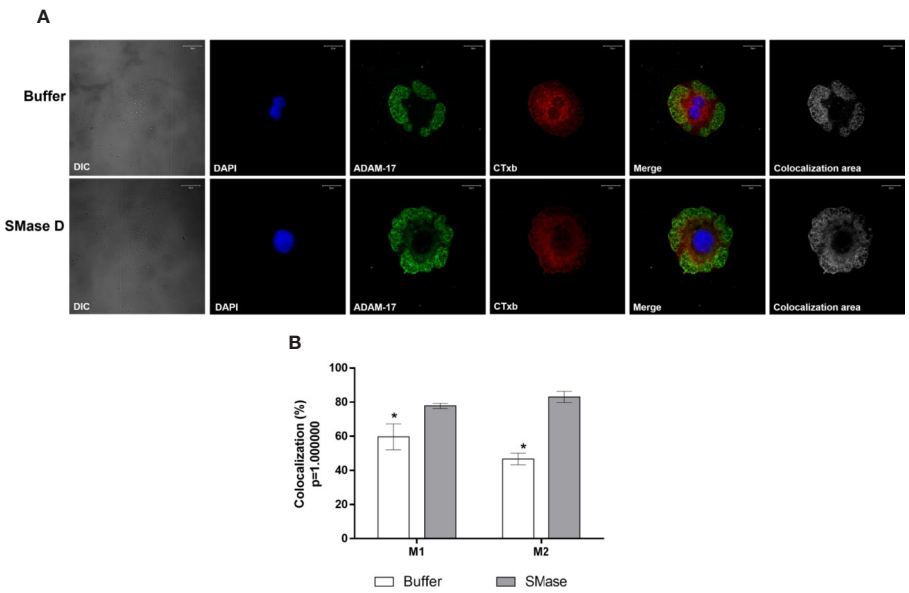

FIGURE 8 | Colocalization of ADAM-17 and Cholera Toxin subunit b in human keratinocytes, treated with SMase D. HaCaT cells were cultured on slides and treated for 2 h with buffer or SMase D (5μg/ml). Cells were stained with Moab anti-ADAM-17 (20 μg/ml), followed by RAM-FITC (1:50). GM_1 containing lipid rafts were visualized, using the CTx-b/Alexa Fluor 555 and the nuclei counterstained with DAPI and slides were analyzed by CLSM. Scale bars represent 20 μm. **(A)** Colocalization of ADAM-17 and GM_1 at the focal plane of 3.02 μm analyzed in cells treated with buffer or SMase D. Colocalization areas are shown as grayscale images. **(B)** Comparison between the colocalization of ADAM-17 and Cholera Toxin subunit b in cells treated with SMase D or buffer and represent means ± SEM from at least 10 images in two independent experiments and three different focal plans. Statistically analyzed by Two Way ANOVA followed by Tukey HSD test, using the GraphPad Prism 5.1. (*) Significant difference compared to SMase D ($p < 0.05$).

of rafts, since a reduction in caveolin-1 expression/detection and increase in flotilin-1 was observed in cells treated with SMase D. Mougeolle et al. (2015) demonstrated that oxidative stress induces caveolin-1 degradation. We have previously shown that SMase D induces oxidative stress in leukocytes with production of superoxide and peroxynitrite (Manzoni-de-Almeida et al., 2018), and corroborating this data, we show here that SMase D induces superoxide production in human keratinocytes (**Figures 5C, D**). Regarding the flotillin-1, its increase may indicate an augmented synthesis and recruitment of raft components to the membrane after degradation or perturbation. In the absence of caveolins, flotillins has been shown to assume the role of a structural protein assisting lipid rafts assembly (Slaughter et al., 2003).

To confirm the action of SMase D on lipid rafts, we sought to analyze the possible toxin binding to the microdomains, which were indirectly visualized by Cholera toxin labeling, which binds to GM_1 gangliosides. We observed a high colocalization index between SMase D in the membrane and the GM_1 ganglioside, suggesting that the SMase D acts on the membrane and preferably in these microdomains.

In conclusion, we have elucidated more of the mechanism by which SMase D exerts its actions and our observation that SMase D changes the rafts dynamics leading to activation of proproteases such as furin and, consequently, the metalloproteases ADAM-10 and -17, opens up pathways for novel therapeutic interventions to prevent and treat systemic and local pathologies after *Loxosceles* spider envenomation.

DATA AVAILABILITY STATEMENT

All datasets generated for this study are included in the article/supplementary material.

AUTHOR CONTRIBUTIONS

PL conceived the project, performed all the experiments, analyzed the data, discussed the results, and wrote the manuscript. CB discussed the results and wrote the manuscript. DT conceived the project, discussed the results, and wrote the manuscript. All authors read, revised, and approved the submitted manuscript.

FUNDING

This work was supported by São Paulo Research Foundation (FAPESP) to Centre of Toxins, Immune Response and Cell Signalling (CeTICS) (grant 2013/07467-1) and to PL (grant 2015/17053-5) and CNPq (grant 162570/2013-9). DT is recipient of CNPq Research Productivity Fellowship. The funding agencies had no influence on study design, data interpretation, or form of the manuscript.

REFERENCES

Anders, A., Gilbert, S., Garten, W., Postina, R., and Fahrenholz, F. (2001). Regulation of the α-secretase ADAM10 by its prodomain and proprotein convertases. *FASEB J.* 15, 1837–1839. doi: 10.1096/fj.01-0007fje

Barretto, O. C., Cardoso, J. L., and De Cillo, D. (1985). Viscerocutaneous form of loxoscelism and erythrocyte glucose-6-phosphate deficiency. *Rev. Inst. Med. Trop. Sao Paulo.* 27, 264–267. doi: 10.1590/S0036-46651985000500006

Becker, G. L., Lu, Y., Hardes, K., Strehlow, B., Levesque, C., Lindberg, I., et al. (2012). Highly potent inhibitors of proprotein convertase furin as potential drugs for treatment of infectious diseases. *J. Biol. Chem.* 287, 21992–22003. doi: 10.1074/jbc.M111.332643

Cameron, A., Appel, J., Houghten, R. A., and Lindberg, I. (2000). Polyarginines are potent furin inhibitors. *J. Biol. Chem.* 275, 36741–36749. doi: 10.1074/jbc.M003848200

Chalaris, A., Rabe, B., Paliga, K., Lange, H., Laskay, T., Fielding, C. A., et al. (2007). Apoptosis is a natural stimulus of IL6R shedding and contributes to the proinflammatory trans-signaling function of neutrophils. *Blood.* 110, 1748–1755. doi: 10.1182/blood-2007-01-067918

Corrêa, M. A., Okamoto, C. K., Gonçalves de Andrade, R. M., van den Berg, C. W., and Tambourgi, D. V. (2016). Sphingomyelinase D from Loxosceles laeta venom induces the expression of MMP7 in human keratinocytes: Contribution to dermonecrosis. *PloS One* 11, 1–14. doi: 10.1371/journal.pone.0153090

Costes, S. V., Daelemans, D., Cho, E. H., Dobbin, Z., Pavlakis, G., and Lockett, S. (2004). Automatic and Quantitative Measurement of Protein-Protein Colocalization in Live Cells. *Biophys. J.* 86, 3993–4003. doi: 10.1529/biophysj.103.038422

Cremesti, A. E., Goni, F. M., and Kolesnick, R. (2002). Role of sphingomyelinase and ceramide in modulating rafts: Do biophysical properties determine biologic outcome? *FEBS Lett.* 531, 47–53. doi: 10.1016/S0014-5793(02)03489-0

Diaz, O., Mébarek-Azzam, S., Benzaria, A., Dubois, M., Lagarde, M., Némoz, G., et al. (2005). Disruption of lipid rafts stimulates phospholipase d activity in human lymphocytes: implication in the regulation of immune function. *J. Immunol.* 175, 8077–8086. doi: 10.4049/jimmunol.175.12.8077

Fernandes Pedrosa, M. F., Junqueira de Azevedo, I. L. M., Gonçalves de Andrade, R. M., van den Berg, C. W., Ramos, C. R. R., Lee Ho, P., et al. (2002). Molecular cloning and expression of a functional dermonecrotic and haemolytic factor from Loxosceles laeta venom. *Biochem. Biophys. Res. Commun.* 298, 638–645. doi: 10.1016/S0006-291X(02)02521-4

Forrester, L. J., Barrett, J. T., and Campbell, B. J. (1978). Red blood cell lysis induced by the venom of the brown recluse spider. The role of sphingomyelinase D. *Arch. Biochem. Biophys.* 187, 355–365. doi: 10.1016/0003-9861(78)90046-2

Giocondi, M. C., Boichot, S., Plénat, T., and Le Grimellec, C. (2004). Structural diversity of sphingomyelin microdomains. *Ultramicroscopy* 100, 135–143. doi: 10.1016/j.ultramic.2003.11.002

Gniadecki, R., Christoffersen, N., and Wulf, H. C. (2002). Cholesterol-rich plasma membrane domains (lipid rafts) in keratinocytes: Importance in the baseline and UVA-induced generation of reactive oxygen species. *J. Invest. Dermatol.* 118, 582–588. doi: 10.1046/j.1523-1747.2002.01716.x

Harder, T., Scheiffele, P., Verkade, P., and Simons, K. (1998). Lipid Domain Structure of the Plasma Membrane Revealed by Patching of Membrane Components, *J. Cell Biol.* 141, 929–942. doi: 10.1083/jcb.141.4.929

Howard, L., Maciewicz, R. A., and Blobel, C. P. (2000). Cloning and characterization of ADAM28: Evidence for autocatalytic pro-domain removal and for cell surface localization of mature ADAM28. *Biochem. J.* 348, 21–27. doi: 10.1042/0264-6021:3480021

Huovila, A. P. J., Turner, A. J., Pelto-Huikko, M., Kärkkäinen, I., and Ortiz, R. M. (2005). Shedding light on ADAM metalloproteinases. *Trends Biochem. Sci.* 30, 413–422. doi: 10.1016/j.tibs.2005.05.006

Kang, T., Zhao, Y. G., Pei, D., Sucic, J. F., and Sang, Q. X. A. (2002). Intracellular activation of human adamalysin 19/disintegrin and metalloproteinase 19 by furin occurs via one of the two consecutive recognition sites. *J. Biol. Chem.* 277, 25583–25591. doi: 10.1074/jbc.M203532200

Kankaanpää, P., Paavolainen, L., Tiitta, S., Karjalainen, M., Päivärinne, J., Nieminen, J., et al. (2012). BioImageXD: An open, general-purpose and high-throughput image-processing platform. *Nat. Methods* 9, 683–689. doi: 10.1038/nmeth.2047

Klein, T., and Bischoff, R. (2011). Active metalloproteases of the a disintegrin and metalloprotease (ADAM) family: Biological function and structure. *J. Proteome Res.* 10, 17–33. doi: 10.1021/pr100556z

Kojro, E., Gimpl, G., Lammich, S., März, W., and Fahrenholz, F. (2001). Low cholesterol stimulates the nonamyloidogenic pathway by its effect on the α-secretase ADAM 10. *Proc. Natl. Acad. Sci. U. S. A.* 98, 5815–5820. doi: 10.1073/pnas.081612998

Li, C., Cantor, W. J., Nili, N., Robinson, R., Fenkell, L., Le Tran, Y., et al. (2002). Arterial repair after stenting and the effects of GM6001, a matrix metalloproteinase inhibitor. *J. Am. Coll. Cardiol.* 39, 1852–1858. doi: 10.1016/S0735-1097(02)01873-9

Loechel, F., Gilpin, B. J., Engvall, E., Albrechtsen, R., and Wewer, U. M. (1998). Human ADAM 12 (Meltrin α) is an active metalloprotease. *J. Biol. Chem.* 273, 16993–16997. doi: 10.1074/jbc.273.27.16993

Lopes, P. H., Murakami, M. T., Portaro, F. C. V., Mesquita Pasqualoto, K. F., van den Berg, C., and Tambourgi, D. V. (2019). Targeting Loxosceles spider Sphingomyelinase D with small-molecule inhibitors as a potential therapeutic approach for loxoscelism. *J. Enzyme Inhib. Med. Chem.* 34, 310–321. doi: 10.1080/14756366.2018.1546698

Lowry, O. H., Rosebrough, N. J., Farr, A. L., and Randall, R. J. (1951). Protein measurement with the Folin-Phenol Reagent. *J. Biol. Cemistry* 193, 265–275. doi: 10.1016/0304-3894(92)87011-4

Ludwig, A., Hundhausen, C., Lambert, M., Broadway, N., Andrews, R., Bickett, D., et al. (2005). Metalloproteinase Inhibitors for the Disintegrin-Like Metalloproteinases ADAM10 and ADAM17 that Differentially Block Constitutive and Phorbol Ester-Inducible Shedding of Cell Surface Molecules. *Comb. Chem. High Throughput Screen.* 8, 161–171. doi: 10.2174/1386207053258488

Lum, L., Reid, M. S., and Blobel, C. P. (1998). Intracellular maturation of the mouse metalloprotease disintegrin MDC15. *J. Biol. Chem.* 273, 26236–26247. doi: 10.1074/jbc.273.40.26236

Manders, E. M. M., Verbeek, F. J., and Aten, J. A. (1993). Measurement of co-localization of objects in dual-colour confocal images. *J. Microsc.* 169, 375–382. doi: 10.1111/j.1365-2818.1993.tb03313.x

Manzoni-de-Almeida, D., Squaiella-Baptistão, C. C., Lopes, P. H., van den Berg, C. W., and Tambourgi, D. V. (2018). Loxosceles venom Sphingomyelinase D activates human blood leukocytes: Role of the complement system. *Mol. Immunol.* 94, 45–53. doi: 10.1016/j.molimm.2017.12.009

Matthews, V., Schuster, B., Schütze, S., Bussmeyer, I., Ludwig, A., Hundhausen, C., et al. (2003). Cellular cholesterol depletion triggers shedding of the human interleukin-6 receptor by ADAM10 and ADAM17 (TACE). *J. Biol. Chem.* 278, 38829–38839. doi: 10.1074/jbc.M210584200

Mougeolle, A., Poussard, S., Decossas, M., Lamaze, C., Lambert, O., and Dargelos, E. (2015). Oxidative stress induces Caveolin 1 degradation and impairs Caveolae functions in skeletal muscle cells. *PloS One* 10, 1–19. doi: 10.1371/journal.pone.0122654

Müllberg, J., Althoff, K., Jostock, T., and Rose-John, S. (2000). The importance of shedding of membrane proteins for cytokine biology. *Eur. Cytokine Netw.* 11, 27-38.

Paixão-Cavalcante, D., van den Berg, C. W., Fernandes-Pedrosa, M. F., Gonçalves de Andrade, R. M., and Tambourgi, ,. D. V. (2006). Role of matrix metalloproteinases in HaCaT keratinocytes apoptosis induced by Loxosceles venom sphingomyelinase D. *J. Invest. Dermatol.* 126, 61–68. doi: 10.1038/sj.jid.5700049

Paixão-Cavalcante, D., van den Berg, C. W., Gonçalves-de-Andrade, R. M., Fernandes-Pedrosa, M. F., Okamoto, C. K., and Tambourgi, ,. D. V. (2007). Tetracycline protects against dermonecrosis induced by Loxosceles spider venom. *J. Invest. Dermatol.* 127, 1410–1418. doi: 10.1038/sj.jid.5700688

Park, S. J., Kim, H. Y., Kim, H., Park, S. M., Joe, E.H, Jou, I., et al. (2009). Oxidative stress induces lipid-raft-mediated activation of Src homology 2 domain-containing protein-tyrosine phosphatase 2 in astrocytes. *Free Radic. Biol. Med.* 46, 1694–1702. doi: 10.1016/j.freeradbiomed.2009.03.026

Platnick, N. I. (2011). *The World Spider Catalogue, version 10.0. Am. Museum Nat. Hist.* American Museum of Natural History. Available at: http://research.amnh.org/entomology/spiders/ catalogue/index.html [Accessed April 7, 2018].

Roghani, M., Becherer, J. D., Moss, M. L., Atherton, R. E., Erdjument-Bromage, H., Arribas, J., et al. (1999). Metalloprotease-disintegrin MDC9: Intracellular maturation and catalytic activity. *J. Biol. Chem.* 274, 3531-3540. doi: 10.1074/jbc.274.6.3531

Schenone, H., Saavedra, T., Rojas, A., and Villarroel, F. (1989). Loxoscelismo en Chile: estudios epidemiológicos, clínicos y experimentales. *Rev. Inst. Med. Trop. Sao Paulo* 31, 403–415. doi: 10.1590/S0036-46651989000600007

Seals, D. F., and Courtneidge, S. A. (2003). The ADAMs family of metalloproteases: Multidomain proteins with multiple functions. *Genes Dev.* 17, 7–30. doi: 10.1101/gad.1039703

Seidah, N. G., Mayer, G., Zaid, A., Rousselet, E., Nassoury, N., Poirier, S., et al. (2008). The activation and physiological functions of the proprotein convertases. *Int. J. Biochem. Cell Biol.* 40, 1111–1125. doi: 10.1016/j.biocel.2008.01.030

Seidah, N. G. (2006). Unexpected similarity between the cytosolic West Nile virus NS3 and the secretory furin-like serine proteinases. *Biochem. J.* 393, e1–e3. doi: 10.1042/BJ20051787

Simons, K., and Ikonen, E. (1997). Functiomal rafts in cell membranes. *Nature* 387, 569–572. doi: 10.1038/42408

Slaughter, N., Laux, I., Tu, X., Whitelegge, J., Zhu, X., Effros, R., et al. (2003). The flotillins are integral membrane proteins in lipid rafts that contain TCR-associated signaling components: Implications for T-cell activation. *Clin. Immunol.* 108, 138–151. doi: 10.1016/S1521-6616(03)00097-4

Smart, E. J., Graf, G. A., McNiven, M. A., Sessa, W. C., Engelman, J. A., Scherer, P. E., et al. (1999). Caveolins, Liquid-Ordered Domains, and Signal Transduction. *Mol. Cell. Biol.* 19, 7289–7304. doi: 10.1128/mcb.19.11.7289

Tambourgi, D. V., Magnoli, F. C., van den Berg, C. W., Morgan, B. P., de Araujo, P. S., Alves, E. W., et al. (1998). Sphingomyelinases in the venom of the spider Loxosceles intermedia are responsible for both dermonecrosis and complement-dependent hemolysis. *Biochem. Biophys. Res. Commun.* 251, 366–373. doi: 10.1006/bbrc.1998.9474

Tambourgi, D. V., Morgan, B. P., de Andrade, R. M., Magnoli, F. C., and van Den Berg, C. W. (2000). Loxosceles intermedia spider envenomation induces activation of an endogenous metalloproteinase, resulting in cleavage of glycophorins from the erythrocyte surface and facilitating complement-mediated lysis. *Blood* 95, 683–691. doi: 10.1182/blood.V95.2.683

Tambourgi, D. V., Gonçalves de Andrade, R. M., and van den Berg, C. W. (2010). Loxoscelism: From basic research to the proposal of new therapies. *Toxicon* 56, 1113–1119. doi: 10.1016/j.toxicon.2010.01.021

Tellier, E., Canault, M., Rebsomen, L., Bonardo, B., Juhan-Vague, I., Nalbone, G., et al. (2006). The shedding activity of ADAM17 is sequestered in lipid rafts. *Exp. Cell Res.* 312, 3969–3980. doi: 10.1016/j.yexcr.2006.08.027

van den Berg, C. W., Gonçalves De Andrade, R. M., Magnoli, F. C., Marchbank, K. J., and Tambourgi, D. V. (2002). Loxosceles spider venom induces metalloproteinase mediated cleavage of MCP/CD46 and MHCI and induces protection against C-mediated lysis. *Immunology* 107, 102–110. doi: 10.1046/j.1365-2567.2002.01468.x

van den Berg, C. W., Gonçalves-de-Andrade, R. M., Okamoto, C. K., and Tambourgi, D. V. (2012). C5a receptor is cleaved by metalloproteases induced by sphingomyelinase D from Loxosceles spider venom. *Immunobiology* 217, 935–941. doi: 10.1016/j.imbio.2012.01.005

van Goor, H., Melenhorst, W. B. W. H., Turner, A. J., and Holgate, S. T. (2009). Adamalysins in biology and disease. *J. Pathol.* 219, 277–286. doi: 10.1002/path.2594

Vey, M., Schäfer, W., Berghöfer, S., Klenk, H. D., and Garten, W. (1994). Maturation of the trans-Golgi network protease furin: Compartmentalization of propeptide removal, substrate cleavage, and COOH-terminal truncation. *J. Cell Biol.* 127, 1829–1842. doi: 10.1083/jcb.127.6.1829

Vey, M., Schäfer, W., Reis, B., Ohuchi, R., Britt, W., Garten, W., et al. (1995). Proteolytic processing of human cytomegalovirus glycoprotein B (gpUL55) is mediatedby the human endoprotease furin. *Virology*. 206, 746–749. doi: 10.1016/S0042-6822(95)80002-6

Volonté, D., Galbiati, F., Li, S., Nishiyama, K., Okamoto, T., and Lisanti, M. P. (1999). Flotillins/cavatellins are differentially expressed in cells and tissues and form a hetero-oligomeric complex with caveolins in vivo: Characterization and epitope-mapping of a novel flotillin-1 monoclonal antibody probe. *J. Biol. Chem.* 274, 12702–12709. doi: 10.1074/jbc.274.18.12702

von Tresckow, B., Kallen, K.-J., von Strandmann, E. P., Borchmann, P., Lange, H., Engert, A., et al. (2004). Depletion of Cellular Cholesterol and Lipid Rafts Increases Shedding of CD30. *J. Immunol.* 172, 4324–4331. doi: 10.4049/jimmunol.172.7.4324

Walev, I., Vollmer, P., Palmer, M., Bhakdi, S., and Rose-John, S. (1996). Pore-forming toxins trigger shedding of receptors for interleukin 6 and lipopolysaccharide. *Proc. Natl. Acad. Sci. U. S. A.* 93, 7882–7887. doi: 10.1073/pnas.93.15.7882

Walev, I., Tappe, D., Gulbins, E., and Bhakdi, S. (2000). Streptolysin O-permeabilized granulocytes shed L-selectin concomitantly with ceramide generation via neutral sphingomyelinase. *J. Leukoc. Biol*. 68, 865–872. doi: 10.1189/jlb.68.6.865

Wasserman, G. S., and Anderson, P. C. (1983). Loxoscelism and Necrotic Arachnidism. *J. Toxicol. Clin. Toxicol.* 21, 451–472. doi: 10.3109/15563658308990434

Xu, P., Liu, J., Sakaki-Yumoto, M., and Derynck, R. (2012). TACE activation by MAPK-mediated regulation of cell surface dimerization and TIMP3 association. *Sci. Signal*. 5, ra34. doi: 10.1126/scisignal.2002689

Zhang, Y., Li, X., Becker, K. A., and Gulbins, E. (2009). Ceramide-enriched membrane domains-Structure and function. *Biochim. Biophys. Acta - Biomembr.* 1788, 178–183. doi: 10.1016/j.bbamem.2008.07.030

Zimina, E. P., Fritsch, A., Schermer, B., Bakulina, A. Y., Bashkurov, M., Benzing, T., et al. (2007). Extracellular phosphorylation of collagen XVII by ecto-casein kinase 2 inhibits ectodomain shedding. *J. Biol. Chem*. 282, 22737–22746. doi: 10.1074/jbc.M701937200

Conflict of Interest: The authors declare that the research was conducted in the absence of any commercial or financial relationships that could be construed as a potential conflict of interest.

frontiers in Pharmacology

BRIEF RESEARCH REPORT
published: 07 July 2020
doi: 10.3389/fphar.2020.01010

Tuning Scorpion Toxin Selectivity: Switching From $K_V1.1$ to $K_V1.3$

Andrei M. Gigolaev[1†], Alexey I. Kuzmenkov[1†], Steve Peigneur[2†], Valentin M. Tabakmakher[1,3†], Ernesto L. Pinheiro-Junior[2], Anton O. Chugunov[1,4,5], Roman G. Efremov[1,4,5], Jan Tytgat[2] and Alexander A. Vassilevski[1,5]*

[1] Shemyakin-Ovchinnikov Institute of Bioorganic Chemistry, Russian Academy of Sciences, Moscow, Russia, [2] Toxicology and Pharmacology, KU Leuven, Leuven, Belgium, [3] School of Biomedicine, Far Eastern Federal University, Vladivostok, Russia, [4] Department of Applied Mathematics, National Research University Higher School of Economics, Moscow, Russia, [5] Moscow Institute of Physics and Technology (State University), Dolgoprudny, Russia

Voltage-gated potassium channels (K_Vs) perform vital physiological functions and are targets in different disorders ranging from ataxia and arrhythmia to autoimmune diseases. An important issue is the search for and production of selective ligands of these channels. Peptide toxins found in scorpion venom named KTx excel in both potency and selectivity with respect to some potassium channel isoforms, which may present only minute differences in their structure. Despite several decades of research the molecular determinants of KTx selectivity are still poorly understood. Here we analyze MeKTx13-3 (Kalium ID: α-KTx 3.19) from the lesser Asian scorpion *Mesobuthus eupeus*, a high-affinity $K_V1.1$ blocker (IC_{50} ~2 nM); it also affects $K_V1.2$ (IC_{50} ~100 nM), 1.3 (~10 nM) and 1.6 (~60 nM). By constructing computer models of its complex with $K_V1.1$–1.3 channels we identify specific contacts between the toxin and the three isoforms. We then perform mutagenesis to disturb the identified contacts with $K_V1.1$ and 1.2 and produce recombinant MeKTx13-3_AAAR, which differs by four amino acid residues from the parent toxin. As predicted by the modeling, this derivative shows decreased activity on $K_V1.1$ (IC_{50} ~550 nM) and 1.2 (~200 nM). It also has diminished activity on $K_V1.6$ (~1500 nM) but preserves $K_V1.3$ affinity as measured using the voltage-clamp technique on mammalian channels expressed in *Xenopus* oocytes. In effect, we convert a selective $K_V1.1$ ligand into a new specific $K_V1.3$ ligand. MeKTx13-3 and its derivatives are attractive tools to study the structure-function relationship in potassium channel blockers.

Keywords: scorpion venom, neurotoxin, voltage-gated potassium channel, potassium channel blocker, molecular modeling, molecular dynamics

OPEN ACCESS

Edited by:
Heike Wulff,
University of California, Davis, United States

Reviewed by:
Yonghua Ji,
Shanghai University, China
Craig Doupnik,
USF Health, United States

****Correspondence:***
Alexander A. Vassilevski
avas@ibch.ru

†These authors have contributed equally to this work

Specialty section:
This article was submitted to Pharmacology of Ion Channels and Channelopathies, a section of the journal Frontiers in Pharmacology

Received: *14 April 2020*
Accepted: *23 June 2020*
Published: *07 July 2020*

Citation:
Gigolaev AM, Kuzmenkov AI, Peigneur S, Tabakmakher VM, Pinheiro-Junior EL, Chugunov AO, Efremov RG, Tytgat J and Vassilevski AA (2020) Tuning Scorpion Toxin Selectivity: Switching From $K_V1.1$ to $K_V1.3$. Front. Pharmacol. 11:1010. doi: 10.3389/fphar.2020.01010

INTRODUCTION

It is believed that potassium (K^+) channels arose near the time of life origin on the earth. K^+ channels are key membrane proteins of all living organisms, and about 80 genes encoding the main α-subunits are found in mammalian genomes (Alexander et al., 2019). The most prevalent family of K^+ channels in mammals is voltage-gated potassium channels (K_Vs) that includes 40 isoforms (Attali et al., 2019). These proteins control neuronal excitability, heart rate, muscle contraction,

hormonal secretion, cell proliferation, etc. It is not surprising that modulation of K_Vs provokes changes in the physiology of a cell or even of the whole organism (Hille, 2001).

K_V1.3 is one of the most studied and pharmacologically important isoforms of K^+ channels. At least two major directions of biomedical research are associated with this type of channel. First, K_V1.3 in T lymphocytes is a validated target for diverse autoimmune diseases, such as multiple sclerosis, rheumatoid arthritis, and type 1 diabetes (Chandy et al., 2004; Beeton et al., 2006; Feske et al., 2012). Second, this protein is a crucial participant in a number of cancers because it is necessary for cell proliferation, malignant angiogenesis, and metastasis (Pardo and Stühmer, 2014; Chandy and Norton, 2016; Teisseyre et al., 2019). For both of these directions selective and effective inhibitors of K_V1.3 are desirable. Novel ligands and their derivatives are considered as promising molecular instruments in K_V1.3 research and are exploited as templates in drug design (Wulff and Zhorov, 2008; Chandy and Norton, 2017; Prosdocimi et al., 2019). Active compounds affecting K_V1.3 can be obtained from different natural sources, such as plant extracts and animal venoms (King, 2011; Norton and Chandy, 2017), as well as synthesized *de novo* (Schmitz et al., 2005; Hendrickx et al., 2020).

Scorpion venom serves as an abundant source of toxins acting as K^+ channel ligands (KTx), which have evolved and been selected for a highly efficient interaction with their molecular targets, including K_Vs (Kuzmenkov et al., 2015a). According to Kalium database (https://kaliumdb.org/), these compounds are polypeptides containing 23 to 78 amino acid residues and cross-linked by two to four intramolecular disulfide bonds (Kuzmenkov et al., 2016a; Tabakmakher et al., 2019). A dominating number of known KTx adopts the CSα/β (cysteine-stabilized α-helix and β-sheet) fold, but some of them present other types of fold (Mouhat et al., 2004; Kuzmenkov et al., 2015a). A number of structural and pharmacological findings pinpointed important determinants in the interfaces of K_Vs and KTx contact that contribute to toxin selectivity (Aiyar et al., 1995; Hidalgo and MacKinnon, 1995; Gross and MacKinnon, 1996; Giangiacomo et al., 2004). Perhaps most importantly, obtaining the crystal structure of the K_V1.2/K_V2.1 paddle chimera in complex with charybdotoxin (ChTx) (Banerjee et al., 2013) highlighted the key amino acids involved in the interaction and opened new opportunities for scaffold engineering of more selective KTx (Han et al., 2008; Kuzmenkov et al., 2018).

Earlier, we identified and purified MeKTx13-3 toxin (Kalium ID: a-KTx 3.19, UniProt ID: C0HJQ6, 37 residues, three disulfide bonds) from the venom of the lesser Asian scorpion *Mesobuthus eupeus* (Kuzmenkov et al., 2015b). We performed pharmacological profiling of this KTx on several isoforms of K_Vs and found that it is active on K_V1.1–1.3 and 1.6 with half-maximal inhibitory concentration (IC_{50}) values of ~2, 100, 10, and 60 nM, respectively. The toxin preferably blocked K_V1.1, however, cross-reactivity with K_V1.3 was also observed (Kuzmenkov et al., 2019). Since a large number of KTx inhibits both K_V1.1 and 1.3 in a similar manner (Mouhat et al., 2005; Takacs et al., 2009; Gao et al., 2010), the goal of our present work is to identify molecular determinants responsible for the interaction with different channel isoforms and switch the selectivity of MeKTx13-3 from K_V1.1 to K_V1.3.

MATERIALS AND METHODS

Ethics Statement

This study strictly complied with the World Health Organization's International Guiding Principles for Biomedical Research Involving Animals. The research was carried out in AAALAC accredited organization according to the standards of the Guide for Care and Use of Laboratory Animals (8th edition, Institute for Laboratory Research of Animals). All experiments were approved by the Institutional Policy on the Use of Laboratory Animals of the Shemyakin-Ovchinnikov Institute of Bioorganic Chemistry Russian Academy of Sciences (Protocol Number 267/2018; date of approval: 28 February 2019).

Homology Modeling of Toxins and Their Complexes With K_Vs

Since the amino acid sequence of MeKTx13-3 is identical to that of BmKTX (Romi-Lebrun et al., 1997), the known 3D structure of the latter (PDB ID: 1BKT) (Renisio et al., 2000) was used in our work. K_V1.1 model was generated in MODELLER 9.19 (Webb and Sali, 2016) using the K_V1.2 structure (PDB ID: 3LUT) (Chen et al., 2010) as a template. K_V1.3 model has been generated previously (Kuzmenkov et al., 2017; Kuzmenkov et al., 2018; Berkut et al., 2019) using an analogous procedure.

Complexes of MeKTx13-3 with K_Vs were modeled considering that the toxin interacts with the channels similarly to ChTx, one of the most thoroughly studied KTx (Goldstein et al., 1994). The model of the complex of MeKTx13-3 with K_V1.2 was built on the basis of the K_V1.2/2.1–ChTx complex crystal structure (Banerjee et al., 2013): the structure of MeKTx13-3 was spatially aligned with the structure of channel-bound ChTx, which was subsequently replaced by the aligned toxin. Complexes with K_V1.1 and 1.3 were generated similarly, but the first step was spatial alignment of the channel models with the K_V1.2/2.1 chimera (Kuzmenkov et al., 2017; Kuzmenkov et al., 2018; Berkut et al., 2019).

Molecular Dynamics Simulations

The resulting complexes of MeKTx13-3 with K_Vs were placed inside a lipid bilayer mimicking a neuronal membrane. We used a pre-equilibrated fragment of bilayer ($7.0 \times 7.0 \times 13.5$ nm^3; 1-palmitoyl-2-oleoyl-sn-glycero-3-phosphocholine/1-palmitoyl-2-oleoyl-sn-glycero-3-phosphoethanolamine/cholesterol, POPC : POPE : Chl; 100:50:50 molecules, respectively, solvated with 14172 water molecules) that has been described in detail in our previous works (Berkut et al., 2019); some phospholipid and Chl molecules were removed to provide room for the protein. The TIP3P water model (Jorgensen et al., 1983) and the required number of Na^+ ions (to maintain electroneutrality) were used for resolvation. All systems were equilibrated (heated up to 37°C) during 100 ps of molecular dynamics (MD) simulation. Positions

of the channel C^{α} atoms of residues not involved in the channel pore vestibule, as well as the N^{ϵ} atom of Lys26 in MeKTx13-3 were restrained during the equilibration to prevent destabilization of the initial complex. Systems were then subjected to 500 ns of MD. All simulations were performed with the GROMACS software (Abraham et al., 2015) (version 2018) using the AMBER99SB-ILDN parameters set (Klepeis et al., 2010). Simulations were carried out with a time step of 2 fs, imposing 3D periodic boundary conditions, in the isothermal-isobaric (NPT) ensemble with a semi-isotropic pressure of 1 bar using the Berendsen pressure coupling algorithm (Berendsen et al., 1984), and at a constant temperature of 37°C using the V-rescale thermostat (Bussi et al., 2007). Van der Waals interactions were truncated using a 1.5-nm spherical cut-off function. Electrostatic interactions were treated with the PME algorithm. During the simulation, the position of the N^{ϵ} atom of Lys26 in each complex was restrained inside the channel pore.

Determination of Interaction Energy and Intermolecular Contacts

We determined the intermolecular contacts during MD and estimated residual contributions to intermolecular interaction energy based on MD trajectory using our in-house software package IMPULSE (Krylov et al., in preparation) analogously to the procedures described in our previous study (Berkut et al., 2019). Briefly, H-bonds were assigned using the parameters set from the hbond utility of GROMACS software (Abraham et al., 2015) (the distance D—A ≤ 0.35 nm and the angle D—H—A ≥ 150° for the hydrogen bond D—H···A, where D and A are the hydrogen bond donor and acceptor, respectively); salt bridges, cation-π, stacking, and hydrophobic contacts were calculated using algorithms described in our previous works (Pyrkov and Efremov, 2007; Pyrkov et al., 2009). The AMBER99SB-ILDN parameters set (Klepeis et al., 2010) and 1.5 nm cutoff distance for Lennard-Jones and electrostatic interactions were used during the intermolecular short-range non-bonded interaction energy estimation, the latter being the sum of the Lennard-Jones and electrostatic terms. All drawings of 3D structures were prepared with the PyMOL Molecular Graphics System, version 1.8 (Schrödinger, LLC). Graphical representation of interaction energy profiles was performed using Python built-in libraries and the NumPy package.

Toxin Isolation From Scorpion Venom

Natural MeKTx13-3 (α-KTx 1.19) was isolated from the same stock of *M. eupeus* venom and following the same procedure as described previously (Kuzmenkov et al., 2015b; Kuzmenkov et al., 2019).

Recombinant Peptide Production

Recombinant MeKTx13-3 and its derivative were produced using an approach elaborated previously (Pluzhnikov et al., 2007). Briefly, the peptides were produced in a bacterial expression system as fusions with the carrier protein thioredoxin (Trx) (McCoy and LaVallie, 1994) and recombinant human enteropeptidase light chain (Gasparian et al., 2011) was used to cleave the fusions.

DNA sequences encoding MeKTx13-3 and its derivative were constructed from synthetic oligonucleotides by PCR in two steps (see **Supplemental Figure S1**). On the first step the target PCR fragments were amplified in 5 cycles using two forward primers and two reverse primers (F1, F2, R1, and R2). The four primers altogether constitute a full gene sequence. For the second step, PCR mixtures from the first step were diluted 100 times, and 1 μl of the dilution was used as a matrix; only the terminal primers (F1 and R1) were used for the amplification (**Supplemental Table S1**). The resulting PCR fragments were cloned into the expression vector pET-32b (Novagen) using *Kpn*I and *Bam*HI restriction enzymes to produce the vectors coding for the target polypeptides.

Escherichia coli SHuffle T7 Express cells (New England Biolabs) were transformed using the corresponding expression vectors and cultured at 30°C in LB medium to the mid-log phase. Expression was then induced by 0.2 mM Isopropyl β-d-1-thiogalactopyranoside. Cells were cultured at room temperature (24°C) overnight (16 h) and harvested by centrifugation. The cell pellet was resuspended in 300 mM NaCl, 50 mM Tris-HCl buffer (pH 8.0) and ultrasonicated. The lysate was applied to a HisPur Cobalt Resin (ThermoFisher Scientific); and the Trx-fusion proteins were purified according to the manufacturer's protocol.

Fusion proteins were dissolved in 50 mM Tris-HCl (pH 8.0) to a concentration of 1 mg/ml. Protein cleavage with human enteropeptidase light chain (1 U of enzyme per 1 mg of substrate) was performed overnight (16 h) at 37°C. Recombinant peptides were purified by reversed-phase HPLC on a Jupiter C_5 column (4.6 × 250 mm; Phenomenex) in a linear gradient of acetonitrile concentration (0–60% in 60 min) in the presence of 0.1% trifluoroacetic acid. The purity of the target peptides was checked by MALDI MS and analytical chromatography on a Vydac C_{18} column (4.6 × 250 mm; Separations Group) in the same acetonitrile gradient.

Mass Spectrometry

Molecular mass measurements for natural and recombinant peptides were performed using MALDI on an Ultraflex TOF-TOF (Bruker Daltonik) spectrometer as described earlier (Kuzmenkov et al., 2016b). 2,5-Dihydroxybenzoic acid (Sigma-Aldrich) was used as a matrix. Measurements were carried out in both linear and reflector modes. Mass spectra were analyzed with the Data Analysis 4.3 and Data Analysis Viewer 4.3 software (Bruker).

Ion Channel Expression in *Xenopus* Oocytes

All procedures were performed in agreement with the guidelines of ARRIVE (Animal Research: Reporting of In Vivo Experiments) and the "European convention for the protection of vertebrate animals used for experimental and other scientific purposes" (Strasbourg, 18.III.1986).

The major pipeline of ion channel expression in oocytes was described previously (Peigneur et al., 2011). Briefly, for the expression of K_V genes (rat (r)K_V1.1, rK_V1.2, human (h)K_V1.3, rK_V1.4, rK_V1.5, and rK_V1.6) in *Xenopus laevis* oocytes, linearized

plasmids containing the respective gene sequences were transcribed using the T7 mMESSAGE-mMACHINE transcription kit (Ambion). 50 nl of cRNA solution (1 ng/nl) were injected into oocytes using a micro-injector (Drummond Scientific). The oocytes were incubated in ND96 solution: 96 mM NaCl, 2 mM KCl, 1.8 mM $CaCl_2$, 2 mM $MgCl_2$ and 5 mM HEPES, pH 7.4, supplemented with 50 mg/l gentamycin sulfate.

Electrophysiological Recordings

Two-electrode voltage-clamp recordings were performed at room temperature (18–22°C) using a Geneclamp 500 amplifier (Molecular Devices) controlled by a pClamp data acquisition system (Axon Instruments) as described (Peigneur et al., 2011). Bath solution composition was ND96. K_V currents were evoked by 250-ms depolarization to 0 mV from a holding potential of −90 mV, followed by 250-ms pulses to −50 mV. For current–voltage relationship studies, currents were evoked by 10-mV depolarization steps. Concentration–response curves were constructed, in which the percentage of current inhibition was plotted as a function of toxin concentration. Data were fitted with the Hill equation: $y = 100/[1 + (IC_{50}/[toxin])^h]$, where y is the amplitude of the toxin-induced effect, [toxin] is toxin concentration, and h is the Hill coefficient. Comparison of two sample means was performed using a paired Student's t-test (p-value of 0.05 was used as a threshold of significance). All data were obtained in at least three independent experiments ($n \geq 3$) and are presented as mean ± standard error of the mean.

RESULTS

Computational Study

Amino acid sequence of MeKTx13-3 is identical to BmKTX that was isolated from *Mesobuthus martensii*, a close relative of *M. eupeus* (Romi-Lebrun et al., 1997). Since the 3D structure of BmKTX is known (PDB ID: 1BKT) (Renisio et al., 2000), we used it to generate models of MeKTx13-3 in complex with K_V1.1–1.3. The models were then subjected to MD simulations (**Figures 1A–C**).

To shed light on the molecular differences in MeKTx13-3 interaction with K_V isoforms, we analyzed intermolecular contacts and residual contributions to interaction energy during the MD simulations using our in-house software package IMPULSE (Krylov et al., in preparation). It was observed that in complex with K_V1.2 the toxin does not form any cation-π or stacking contacts, unlike in complex with K_V1.1 or 1.3 (see **Supplemental Table S2**). This observation is in good agreement with electrophysiological measurements that displayed the preferred activity of MeKTx13-3 against K_V1.1 and 1.3 (Kuzmenkov et al., 2019). We noted the following specific contacts between the toxin and particular channel isoforms.

(1) MeKTx13-3 residue Lys15 forms an H-bond and a salt bridge with K_V1.1 residue Glu353 (**Figure 1B**). Analogous contact with Asp351 (**Figure 1D**) is not observed in complex with K_V1.2, apparently due to the fact that the neighboring residue Arg350 repulses Lys15 and prevents this contact formation. No contact with Thr375 was found in complex with K_V1.3 either, presumably due to the small size of the threonine side chain and the lack of electrostatic attraction to reach Lys15.

(2) MeKTx13-3 residue Lys18 forms an H-bond with K_V1.1 residue Ser354 and a cation-π contact with His355; in complex with K_V1.2 it forms an H-bond with Gln353 (**Figures 1B, C**). In the complex of MeKTx13-3 with K_V1.3 the conformation of the loop containing channel-specific residues Thr375 and Gly377 (**Figure 1D**) during MD is such that it does not reach Lys18, so no specific contacts are observed.

(3) MeKTx13-3 residue Gln12 forms an H-bond with K_V1.2 residue Asp351 (**Figure 1C**). Analogous contact with Thr375 (**Figure 1D**) is not observed in complex with K_V1.3 because the short threonine side chain does not reach Gln12. No contact with Glu353 is found in complex with K_V1.1 because the conformation of the loop containing channel-specific residues during MD prevents reaching Gln12.

In addition to the observed channel-specific contacts, MeKTx13-3 residue Asp33 makes a significant positive contribution to the binding energy (negatively affects the affinity) (see **Supplemental Figure S2**) due to electrostatic repulsion with a conserved negatively charged residue in the channel vestibule (Asp377/375/399 in K_V1.1/1.2/1.3, see **Figure 1D**).

Pharmacological profiling and detailed complex structure analysis allow us to propose several point substitutions in MeKTx13-3 for switching toxin selectivity. Since Gln12, Lys15, and Lys18 form hydrogen bonds, salt bridges, and cation-π interactions in complexes with K_V1.1 and 1.2, the general idea of the modifications was to abolish the formation of these polar contacts. Moreover, since these toxin residues do not form specific contacts with K_V1.3, it is reasonable to assume that such modifications will not affect the affinity to this channel isoform significantly. Therefore, we suggested a derivative of MeKTx13-3 in which Gln12, Lys15, and Lys18 are replaced by Ala to reduce toxin affinity to K_V1.1 and 1.2, and Asp33 is replaced by Arg to increase its affinity to K_Vs (**Figure 2A**).

Recombinant Toxin Production

The natural toxin was purified from crude venom as we described previously (Kuzmenkov et al., 2015b; Kuzmenkov et al., 2019). Recombinant MeKTx13-3 and its derivative MeKTx13-3_AAAR (MeKTx13-3 with the following replacements: Gln12Ala, Lys15Ala, Lys18Ala, and Asp33Arg) were obtained according to our common protocol (Pluzhnikov et al., 2007) using *E. coli* SHuffle B strain as an expression system. Synthetic genes encoding the peptides were cloned into the pET-32b expression vector, and Trx was used as a fusion partner to ensure a high yield of the disulfide-containing peptides with native conformation. The target peptides were produced as a result of fusion protein cleavage by enteropeptidase followed by separation using reversed-phase HPLC and identification by MALDI MS (**Figures 2B, C**). The measured molecular masses of the purified peptides were equal to the calculated values. The final yield of the peptides was ~5 mg per 1 l of bacterial culture.

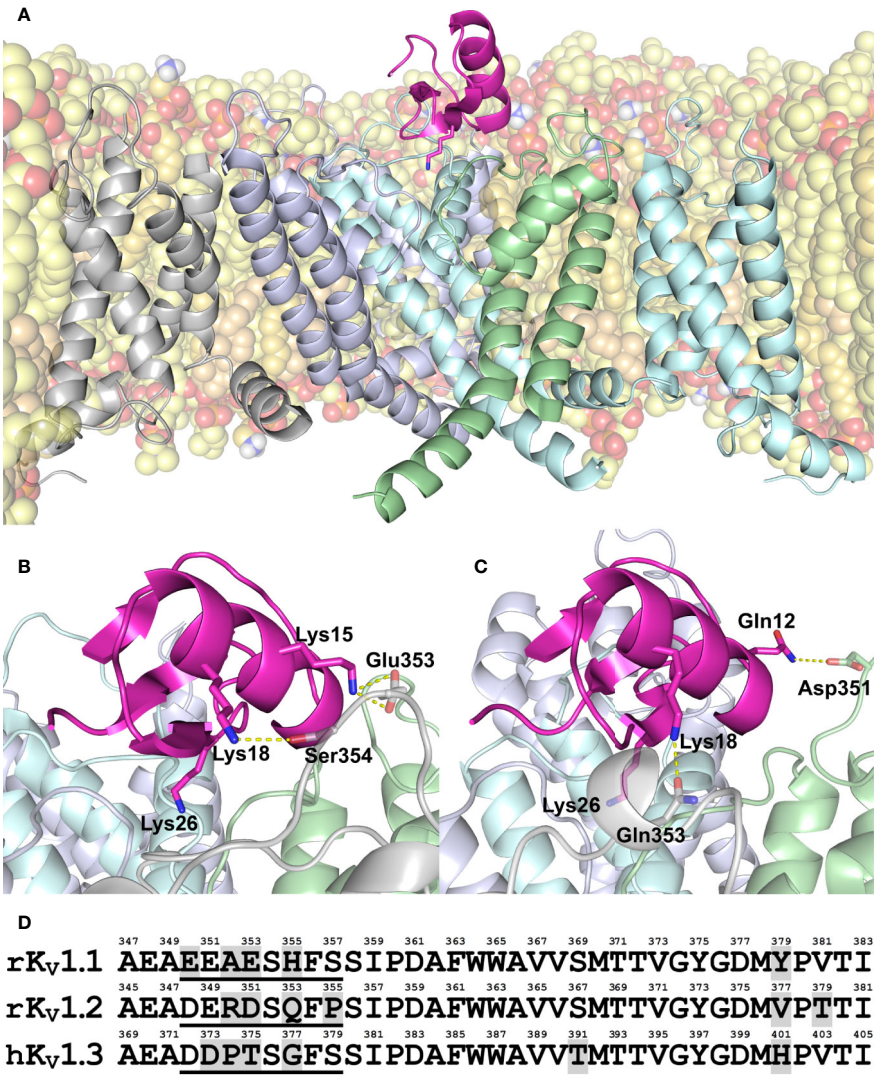

FIGURE 1 | (A–C) Modeled structure of MeKTx13-3 in complex with K_V1.1–1.3. **(A)** Overall structure of the K_V1.3–MeKTx13-3 complex after 100-ns MD simulation inside a hydrated lipid bilayer membrane. Four channel α-subunits with identical sequences are color-coded. The pore domain helices of the channel subunit in the foreground and voltage-sensing domain (VSD) of the adjacent subunit, as well as extended extracellular loops of the VSDs are omitted for clarity. Lipids are shown in a semi-transparent space-filling representation; atoms are colored: oxygen, *red*; phosphorus, *orange*; nitrogen, *blue*; hydrogen of amino group, *white*; carbon of POPC, *light-yellow*; carbon of POPE, *yellow*; and carbon of cholesterol, *beige*. Some lipids are omitted for clarity. MeKTx13-3 is presented in pink; residue Lys26 (plugs the channel pore) is shown as sticks. **(B, C)** Close-up view on the channel pore vestibule area in complexes K_V1.1–MeKTx13-3 and K_V1.2–MeKTx13-3, respectively. Channels are shown in a semi-transparent representation. Lys26 and residues involved in the intermolecular contacts not present in the K_V1.3–MeKTx13-3 complex are shown as sticks. Hydrogen bonds and salt bridges are shown as dashed yellow lines. Lipids are omitted for clarity. **(D)** Amino acid sequence alignment of the extracellular pore region of K_V1.1–1.3 channels. Residue numbering is above each sequence; different residues are shaded gray; sequences of S5-P loops containing channel-specific residues are underlined.

Note that the natural toxin is C-terminally amidated (Kuzmenkov et al., 2015b), whereas this modification is missing from the recombinant peptides.

Electrophysiology

We first compared the activity of the natural and recombinant MeKTx13-3 (**Supplemental Figure S3** and **Supplemental Table S3**) on K_V1.1. Recombinant peptide was less active than the native toxin (IC_{50} values of 6.7 ± 2.7 and 1.9 ± 0.2 nM, respectively), which is probably due to the lack of C-terminal amidation in the former.

We then estimated the activities of the obtained recombinant peptides MeKTx13-3 and MeKTx13-3_AAAR at a concentration of 10 nM against six isoforms of K_Vs (K_V1.1–1.6) expressed in *X. laevis* oocytes (**Figure 3A**). Recombinant MeKTx13-3 as well as the natural toxin inhibited almost completely (by >95%) potassium currents through K_V1.1; ~25%, ~50%, and ~15% of current through

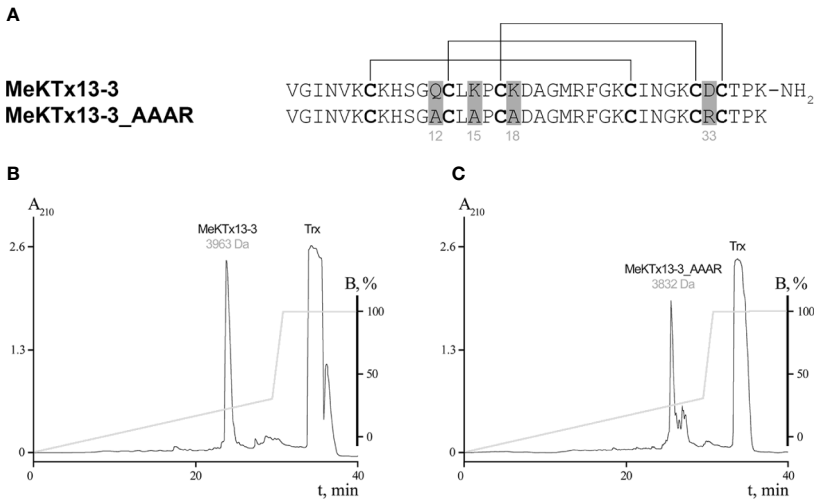

FIGURE 2 | Production of MeKTx13-3 and its derivative. **(A)** Amino acid sequence alignment of MeKTx13-3 and MeKTx13-3_AAAR. Gray shading indicates the positions where replacements were introduced. Cysteine residues are in bold, and lines above the sequences indicate disulfide bonds. Take a note that recombinant analogue of MeKTx13-3 does not bear the C-terminal amidation of the natural toxin. **(B, C)** Reversed-phase HPLC separation of recombinant MeKTx13-3 and MeKTx13-3_AAAR after digestion by enteropeptidase. For target peptides the measured molecular masses are indicated.

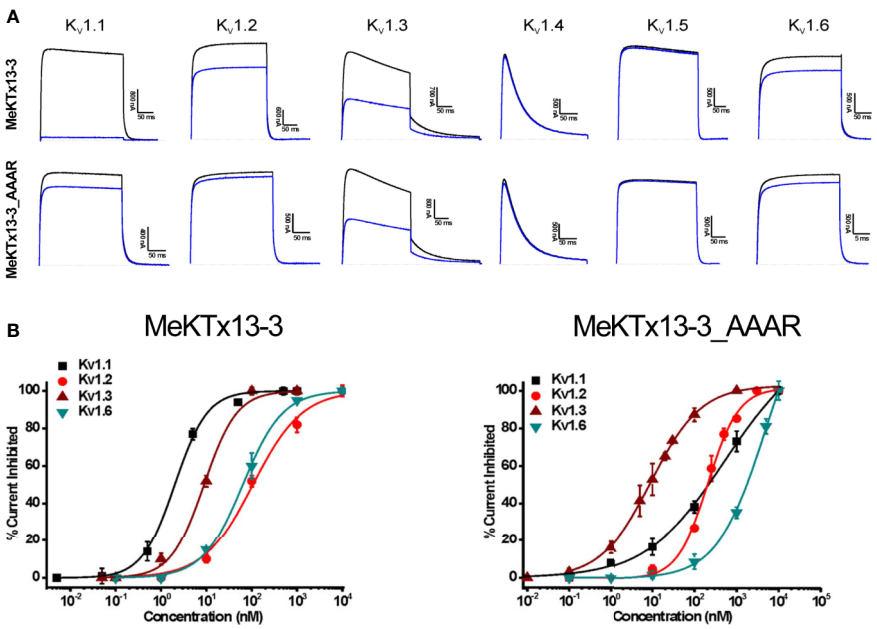

FIGURE 3 | Electrophysiological profiling of MeKTx13-3 and MeKTx13-3_AAAR activities. **(A)** Representative traces of currents through KV1.1–1.6 in control (black) and after application of 10 nM toxin (blue). **(B)** Concentration–response curves of MeKTx13-3 (left) and MeKTx13-3_AAAR (right) on KV1.1–1.3 and 1.6 obtained by electrophysiological measurements. IC50 values are listed in **Table 1**.

K_V1.2, 1.3, and 1.6 was blocked. At the same concentration of 10 nM MeKTx13-3_AAAR blocked K_V1.3 by ~50%, whereas only ~15%, ~5% and ~10% was blocked in K_V1.1, 1.2 and 1.6. Neither K_V1.4 nor K_V1.5 were affected by any of the peptides.

Finally, we constructed dose–response curves for the susceptible channels (**Figure 3B**; see **Table 1** for IC_{50} values and Hill coefficients). MeKTx13-3_AAAR demonstrated a comparable activity with native MeKTx13-3 on K_V1.3 (IC_{50} = 8.9 ± 0.9 nM for the natural toxin and 9.1 ± 0.4 nM for the

TABLE 1 | IC_{50} Values (in nM) Calculated for MeKTx13-3 and Its Derivative against K_V1.1–1.6.

Toxin	K_V1.1	K_V1.2	K_V1.3	K_V1.4	K_V1.5	K_V1.6
MeKTx13-3	1.9 ± 0.2 *(0.9 ± 0.1)*	105.9 ± 14.6 *(1.3 ± 0.3)*	8.9 ± 0.9 *(0.8 ± 0.2)*	N/A	N/A	63.4 ± 4.5 *(1.0 ± 0.1)*
MeKTx13-3_AAAR	541.5 ± 48.6 *(0.7 ± 0.1)*	208.2 ± 15.2 *(1.2 ± 0.1)*	9.1 ± 0.4 *(0.7 ± 0.2)*	N/A	N/A	1522.3 ± 183.4 *(1.4 ± 0.3)*

N/A means toxin was not active up to 1 μM concentration. Hill coefficient values are given in parenthesis.

mutant), whereas its affinity to K_V1.1 decreased dramatically (IC_{50} = 541.5 ± 48.6 nM instead of 1.9 ± 0.2 nM for natural MeKTx13-3). MeKTx13-3_AAAR also showed reduced activity on K_V1.2 (IC_{50} = 208.2 ± 15.2 nM compared to 105.9 ± 14.6 nM for MeKTx13-3) and K_V1.6 (IC_{50} = 1522.3 ± 183.4 nM instead of 63.4 ± 4.5 nM).

DISCUSSION

Animal venom serves a rich source of promising compounds affecting ion channels, which can be utilized as potential drug hits (Wulff et al., 2019). Detailed studies based on either toxin or channel mutagenesis are essential for (i) the understanding of fine molecular contacts between the toxins and very close channel isoforms, and (ii) design and production of more selective ligands. Hence prediction of critical amino acids involved in toxin–channel complex formation *in silico* is a convenient and powerful approach for following mutagenesis studies (Kuyucak and Norton, 2014). For instance, such computationally guided assay helped to design highly selective peptide drug hits or leads, such as ShK-192 (Pennington et al., 2009) and HsTX1[R14A] (Rashid et al., 2015).

Here, we have designed and produced a derivative of scorpion toxin MeKTx13-3 with its selectivity switched from K_V1.1 to K_V1.3. MeKTx13-3 is one of a limited number of known animal toxins that possess selectivity to homotetrameric K_V1.1 (Kuzmenkov et al., 2019). We introduced several substitutions according to computer modeling experiments. To convert the selectivity of MeKTx13-3 we replaced three amino acids by alanine (Gln12Ala, Lys15Ala, and Lys18Ala) to abolish the formation of H-bonds, salt bridges, or cation-π interactions in the complexes with K_V1.1 and 1.2. Moreover, to prevent the electrostatic repulsion between the negatively charged Asp33 in MeKTx13-3 and the conserved aspartic acid residue in the P-S6 loop of K_Vs we introduced the Asp33Arg replacement.

We produced not only MeKTx13-3_AAAR, but also recombinant MeKTx13-3 to confirm that (i) the peptide folding is correct, and (ii) lack of the C-terminal amidation does not impact toxin activity dramatically. These points are of importance, because misfolded toxins usually lose activity, whereas C-terminal amidation can boost ligand potency (Lebrun et al., 1997; Coelho et al., 2014). Voltage-clamp recordings in *X. laevis* oocytes showed that recombinant MeKTx13-3 is ~3.5 times less potent than the natural toxin. We attribute this decrease in activity to the amidation. It is well known that this post-translational modification can affect the activity of peptides. The effects may vary from dramatic to negligible, with most apparent cases found in hormones (Merkler, 1994). As for potassium channel blockers, the C-terminal amidation of ShK from the sea anemone *Stichodactyla helianthus* resulted in ~4 times decreased potency against K_V1.3 (Pennington et al., 2012). Conversely, the amidation of HsTX1 (α-KTx 6.3) from the scorpion *Heterometrus spinifer* increases the activity against K_V1.3 five-fold (Lebrun et al., 1997). The effects in our case are subtle, and we decided to use the recombinantly produced peptide MeKTx13-3 lacking the amidation in further studies.

The designed derivative MeKTx13-3_AAAR was also tested on six K_V isoforms and as we expected the selectivity of this analogue shifted towards K_V1.3. A graphic approach to estimate toxin specificity to a particular channel isoform (K_V1.3 in our case) is using the selectivity factor, i.e. the ratio of IC_{50} (or K_d) values for two channels. MeKTx13-3 displays K_V1.1/K_V1.3 selectivity factor of approximately 0.2, while for MeKTx13-3_AAAR this parameter has changed to 60 (**Supplemental Figure S4**). There is a number of more K_V1.3-specific toxins and their derivatives, for instance, HsTX1, Vm24, or moka1, demonstrating selectivity factors (K_V1.1/K_V1.3) of 500 or even 1000 (Romi-Lebrun et al., 1997; Takacs et al., 2009; Varga et al., 2012).

We aligned the sequences of several dozen toxins from KTx subfamilies α-KTx1–4, 11, 12, 15–18, and 21–24 with comparable length and cysteine pattern to MeKTx13-3 and found that two of the residues mutated in our study (Gln12, the first amino acid before the second Cys residue; and Lys18, the first amino acid after the third Cys) are quite conserved. In numerous toxins Gln/Glu and Lys/Arg are located in these positions, respectively. On the other hand, Lys15 between second and third Cys and Asp33 between the fifth and sixth Cys are variable. Within α-KTx 3 subfamily (to which MeKTx13-3 belongs) these positions display a similar pattern (see **Supplemental Figure S4**). All four residues seem to contribute to the bioactive surface of the toxins, and at present, there is no apparent explanation as to why two of them are more conserved than the other two. Moreover, we cannot infer any correlation between these residues and toxin potency or selectivity.

One may argue that the same substitutions as we introduced to MeKTx13-3 might bring about similar changes of selectivity in other α-KTx 3 toxins. However, and quite unfortunately, our current understanding of K_V–KTx interactions does not allow to predict the specificity of toxins from primary structure. It appears that in each case molecular modeling experiments and a detailed analysis of the contacts are required. This is because

one change in the sequence may actually affect how other residues interact—due to sterical hindrances or packing effects, electrostatic attraction or repulsion, H-bond reshuffling, or local folding rearrangements, all of which are not easily discernible from primary structures. For instance, in case of MeKTx13-3 Lys15 seems to make a salt bridge with Glu353 in $K_V1.1$ (**Figure 1B**). Simple consideration of the primary structures would predict the same salt bridge in $K_V1.2$ since it has Asp351 in the same position of the alignment (**Figure 1D**). This contact is not established in molecular modeling however, due to the neighboring Arg350, which repulses Lys15. Similarly, MeKTx13-3 residues Lys18 and Gln12 make channel-specific contacts due to the different folding of the channel extracellular loops, not just the amino acid substitutions. In conclusion, we hope to have demonstrated here the possibility of switching toxin specificity between two very close channel isoforms based on careful *in silico* design.

DATA AVAILABILITY STATEMENT

The datasets generated for this study can be found in the article/ **Supplementary Material**.

ETHICS STATEMENT

This study strictly complied with the World Health Organization's International Guiding Principles for Biomedical Research Involving Animals. The research was carried out in AAALAC accredited organization according to the standards of the Guidefor Care and Use of Laboratory Animals (8th edition, Institute forLaboratory Research of Animals). The use of the frogs was in accordance with the license number LA1210239 of the Laboratory of Toxicology & Pharmacology, University of Leuven. The use of Xenopus laevis was approved by the Ethical Committee for animal experiments of the University of Leuven (P186/2019). All animal care and experimental procedures agreed with the guidelines of 'European convention for the protection of vertebrate animals used for experimental and other scientific purposes' (Strasbourg, 18.III.1986).

AUTHOR CONTRIBUTIONS

AK and AV designed research. AG, AK, EP-J, SP, VT, and AV analyzed data. AJK, EP-J, SP, VT, AG, and AC performed research. AK, VT, and AV wrote the paper. RE and JT supervised molecular modeling and electrophysiology, respectively.

FUNDING

This work was supported by the Russian Science Foundation (grant no. 18-74-00125). JT was funded by grants G0E7120N, GOC2319N and GOA4919N from the F.W.O Vlaanderen. SP was supported by KU Leuven funding (PDM/19/164). Fundação de Amparo à Pesquisa do Estado de São Paulo (São Paulo Research Foundation, Brazil, scholarship to EP-J n. 2016/04761-4), and Coordenação de Aperfeiçoamento de Pessoal de Nível Superior (Coordination for the Improvement of Higher Education Personnel, Brazil; scholarship to EP-J n. 88881.186830/2018-01).

ACKNOWLEDGMENTS

The molecular dynamics simulations were carried out using the computational facilities of the Supercomputer Center "Polytechnical" at the St. Petersburg Polytechnic University and IACP FEB RAS Shared Resource Center "Far Eastern Computing Resource" equipment (https://cc.dvo.ru). Supercomputer calculations were sponsored in the framework of the Basic Research Program at the National Research University Higher School of Economics and Russian Academic Excellence Project "5-100". We thank O. Pongs for sharing the rKv1.2, rKv1.4, rKv1.5, and rKv1.6 cDNA and we are grateful to M.L. Garcia for sharing the hKv1.3 clone.

SUPPLEMENTARY MATERIAL

The Supplementary Material for this article can be found online at: https://www.frontiersin.org/articles/10.3389/fphar.2020.01010/full#supplementary-material

REFERENCES

Abraham, M. J., Murtola, T., Schulz, R., Páll, S., Smith, J. C., Hess, B., et al. (2015). GROMACS: High performance molecular simulations through multi-level parallelism from laptops to supercomputers. *SoftwareX* 1, 19–25. doi: 10.1016/j.softx.2015.06.001

Aiyar, J., Withka, J. M., Rizzi, J. P., Singleton, D. H., Andrews, G. C., Lin, W., et al. (1995). Topology of the pore-region of a K+ channel revealed by the NMR-derived structures of scorpion toxins. *Neuron* 15, 1169–1181. doi: 10.1016/0896-6273(95)90104-3

Alexander, S. P. H., Mathie, A., Peters, J. A., Veale, E. L., Striessnig, J., Kelly, E., et al. (2019). THE CONCISE GUIDE TO PHARMACOLOGY 2019/20: Ion channels. *Br. J. Pharmacol.* 176, S142–S228. doi: 10.1111/bph.14749

Attali, B., Chandy, K. G., Giese, M. H., Grissmer, S., Gutman, G. A., Jan, L. Y., et al. (2019). "Voltage-gated potassium channels (version 2019.4) in the IUPHAR/BPS Guide to Pharmacology Database," Available at: http://journals.ed.ac.uk/gtopdb-cite/article/view/3233. doi: 10.2218/gtopdb/F81/2019.4

Banerjee, A., Lee, A., Campbell, E., and Mackinnon, R. (2013). Structure of a pore-blocking toxin in complex with a eukaryotic voltage-dependent K(+) channel. *Elife* 2, e00594. doi: 10.7554/eLife.00594

Beeton, C., Wulff, H., Standifer, N. E., Azam, P., Mullen, K. M., Pennington, M. W., et al. (2006). Kv1.3 channels are a therapeutic target for T cell-mediated autoimmune diseases. *Proc. Natl. Acad. Sci. U. S. A.* 103, 17414–17419. doi: 10.1073/pnas.0605136103

Berendsen, H. J. C., Postma, J. P. M., van Gunsteren, W. F., DiNola, A., and Haak, J. R. (1984). Molecular dynamics with coupling to an external bath. *J. Chem. Phys.* 81, 3684–3690. doi: 10.1063/1.448118

Berkut, A. A., Chugunov, A. O., Mineev, K. S., Peigneur, S., Tabakmakher, V. M., Krylov, N. A., et al. (2019). Protein surface topography as a tool to enhance the selective activity of a potassium channel blocker. *J. Biol. Chem.* 294, 18349–18359. doi: 10.1074/jbc.RA119.010494

Bussi, G., Donadio, D., and Parrinello, M. (2007). Canonical sampling through velocity rescaling. *J. Chem. Phys.* 126, 014101. doi: 10.1063/1.2408420

Chandy, K. G., and Norton, R. S. (2016). Channelling potassium to fight cancer. *Nature* 537, 497–499. doi: 10.1038/nature19467

Chandy, K. G., and Norton, R. S. (2017). Peptide blockers of Kv1.3 channels in T cells as therapeutics for autoimmune disease. *Curr. Opin. Chem. Biol.* 38, 97–107. doi: 10.1016/j.cbpa.2017.02.015

Chandy, G., Wulff, H., Beeton, C., Pennington, M., Gutman, G. A., and Cahalan, M. D. (2004). K+ channels as targets for specific immunomodulation. *Trends Pharmacol. Sci.* 25, 280–289. doi: 10.1016/j.tips.2004.03.010

Chen, X., Wang, Q., Ni, F., and Ma, J. (2010). Structure of the full-length Shaker potassium channel Kv1.2 by normal-mode-based X-ray crystallographic refinement. *Proc. Natl. Acad. Sci. U. S. A.* 107, 11352–11357. doi: 10.1073/pnas.1000142107

Coelho, V. A., Cremonez, C. M., Anjolette, F. A. P., Aguiar, J. F., Varanda, W. A., and Arantes, E. C. (2014). Functional and structural study comparing the C-terminal amidated β-neurotoxin Ts1 with its isoform Ts1-G isolated from Tityus serrulatus venom. *Toxicon* 83, 15–21. doi: 10.1016/j.toxicon.2014.02.010

Feske, S., Skolnik, E. Y., and Prakriya, M. (2012). Ion channels and transporters in lymphocyte function and immunity. *Nat. Rev. Immunol.* 12, 532–547. doi: 10.1038/nri3233

Gao, B., Peigneur, S., Tytgat, J., and Zhu, S. (2010). A potent potassium channel blocker from Mesobuthus eupeus scorpion venom. *Biochimie* 92, 1847–1853. doi: 10.1016/j.biochi.2010.08.003

Gasparian, M. E., Bychkov, M. L., Dolgikh, D. A., and Kirpichnikov, M. P. (2011). Strategy for improvement of enteropeptidase efficiency in tag removal processes. *Protein Expr. Purif.* 79, 191–196. doi: 10.1016/j.pep.2011.04.005

Giangiacomo, K. M., Ceralde, Y., and Mullmann, T. J. (2004). Molecular basis of α-KTx specificity. *Toxicon* 43, 877–886. doi: 10.1016/j.toxicon.2003.11.029

Goldstein, S. A., Pheasant, D. J., and Miller, C. (1994). The charybdotoxin receptor of a Shaker K+ channel: peptide and channel residues mediating molecular recognition. *Neuron* 12, 1377–1388. doi: 10.1016/0896-6273(94)90452-9

Gross, A., and MacKinnon, R. (1996). Agitoxin Footprinting the Shaker Potassium Channel Pore. *Neuron* 16, 399–406. doi: 10.1016/S0896-6273(00)80057-4

Han, S., Yi, H., Yin, S.-J., Chen, Z.-Y., Liu, H., Cao, Z.-J., et al. (2008). Structural basis of a potent peptide inhibitor designed for Kv1.3 channel, a therapeutic target of autoimmune disease. *J. Biol. Chem.* 283, 19058–19065. doi: 10.1074/jbc.M802054200

Hendrickx, L. A., Dobričić, V., Toplak, Ž., Peigneur, S., Mašič, L. P., Tomašič, T., et al. (2020). Design and characterization of a novel structural class of Kv1.3 inhibitors. *Bioorg. Chem.* 98, 103746. doi: 10.1016/j.bioorg.2020.103746

Hidalgo, P., and MacKinnon, R. (1995). Revealing the architecture of a K+ channel pore through mutant cycles with a peptide inhibitor. *Science* 268, 307–310. doi: 10.1126/science.7716527

Hille, B. (2001). *Ion Channels of Excitable Membranes*. Sinauer Associates, Inc.

Jorgensen, W. L., Chandrasekhar, J., Madura, J. D., Impey, R. W., and Klein, M. L. (1983). Comparison of simple potential functions for simulating liquid water. *J. Chem. Phys.* 79, 926–935. doi: 10.1063/1.445869

King, G. F. (2011). Venoms as a platform for human drugs: translating toxins into therapeutics. *Expert Opin. Biol. Ther.* 11, 1469–1484. doi: 10.1517/14712598.2011.621940

Klepeis, J. L., Lindorff-Larsen, K., Shaw, D. E., Palmo, K., Dror, R. O., Maragakis, P., et al. (2010). Improved side-chain torsion potentials for the Amber ff99SB protein force field. *Proteins Struct. Funct. Bioinforma.* 78, 1950–1958. doi: 10.1002/prot.22711

Kuyucak, S., and Norton, R. S. (2014). Computational approaches for designing potent and selective analogs of peptide toxins as novel therapeutics. *Future Med. Chem.* 6, 1645–1658. doi: 10.4155/FMC.14.98

Kuzmenkov, A.II, Grishin, E. V., and Vassilevski, A. A. (2015a). Diversity of Potassium Channel Ligands: Focus on Scorpion Toxins. *Biochem (Mosc.)* 80, 1764–1799. doi: 10.1134/S0006297915130118

Kuzmenkov, A.II, Vassilevski, A. A., Kudryashova, K. S., Nekrasova, O. V., Peigneur, S., Tytgat, J., et al. (2015b). Variability of potassium channel blockers in Mesobuthus eupeus scorpion venom with focus on Kv1.1: An integrated transcriptomic and proteomic study. *J. Biol. Chem.* 290, 12195–12209. doi: 10.1074/jbc.M115.637611

Kuzmenkov, A.II, Krylov, N. A., Chugunov, A. O., Grishin, E. V., and Vassilevski, A. A. (2016a). Kalium: a database of potassium channel toxins from scorpion venom. *Database (Oxford)* 2016, pii: baw056. doi: 10.1093/database/baw056

Kuzmenkov, A.II, Sachkova, M. Y., Kovalchuk, S.II, Grishin, E. V., and Vassilevski, A. A. (2016b). Lachesana tarabaevi, an expert in membrane-active toxins. *Biochem. J.* 473, 2495–2506. doi: 10.1042/BCJ20160436

Kuzmenkov, A.II, Peigneur, S., Chugunov, A. O., Tabakmakher, V. M., Efremov, R. G., Tytgat, J., et al. (2017). C-Terminal residues in small potassium channel blockers OdK1 and OSK3 from scorpion venom fine-tune the selectivity. *Biochim. Biophys. Acta Proteins Proteomics* 1865, 465–472. doi: 10.1016/j.bbapap.2017.02.001

Kuzmenkov, A.II, Nekrasova, O. V., Peigneur, S., Tabakmakher, V. M., Gigolaev, A. M., Fradkov, A. F., et al. (2018). KV1.2 channel-specific blocker from Mesobuthus eupeus scorpion venom: Structural basis of selectivity. *Neuropharmacology* 143, 228–238. doi: 10.1016/j.neuropharm.2018.09.030

Kuzmenkov, A.II, Peigneur, S., Tytgat, J., and Vassilevski, A. A. (2019). Pharmacological Characterisation of MeKTx13-2 and MeKTx13-3, Peptide Ligands of Potassium Channels From the Scorpion Mesobuthus eupeus Venom. *Russ. J. Physiol.* 105, 1452–1462. doi: 10.1134/S0869813919110074

Lebrun, B., Romi-Lebrun, R., Martin-Eauclaire, M. F., Yasuda, A., Ishiguro, M., Oyama, Y., et al. (1997). A four-disulphide-bridged toxin, with high affinity towards voltage-gated K+ channels, isolated from Heterometrus spinnifer (Scorpionidae) venom. *Biochem. J.* 328, 321–327. doi: 10.1042/bj3280321

McCoy, J., and LaVallie, E. (1994). Expression and Purification of Thioredoxin Fusion Proteins. *Curr. Protoc. Mol. Biol.* 28, Unit16.8. doi: 10.1002/0471142727.mb1608s28

Merkler, D. (1994). C-terminal Amidated Peptides: Production by the in Vitro Enzymatic Amidation of Glycine-Extended Peptides and the Importance of the Amide to Bioactivity. *Enzyme Microb. Technol.* 16, 450–456. doi: 10.1016/0141-0229(94)90014-0

Mouhat, S., Jouirou, B., Mosbah, A., De Waard, M., and Sabatier, J.-M. (2004). Diversity of folds in animal toxins acting on ion channels. *Biochem. J.* 378, 717–726. doi: 10.1042/bj20031860

Mouhat, S., Visan, V., Ananthakrishnan, S., Wulff, H., Andreotti, N., Grissmer, S., et al. (2005). K+ channel types targeted by synthetic OSK1, a toxin from Orthochirus scrobiculosus scorpion venom. *Biochem. J.* 385, 95–104. doi: 10.1042/BJ20041379

Norton, R. S., and Chandy, K. G. (2017). Venom-derived peptide inhibitors of voltage-gated potassium channels. *Neuropharmacology* 127, 124–138. doi: 10.1016/j.neuropharm.2017.07.002

Pardo, L. A., and Stühmer, W. (2014). The roles of K(+) channels in cancer. *Nat. Rev. Cancer* 14, 39–48. doi: 10.1038/nrc3635

Peigneur, S., Billen, B., Derua, R., Waelkens, E., Debaveye, S., Béress, L., et al. (2011). A bifunctional sea anemone peptide with Kunitz type protease and potassium channel inhibiting properties. *Biochem. Pharmacol.* 82, 81–90. doi: 10.1016/j.bcp.2011.03.023

Pennington, M. W., Beeton, C., Galea, C. A., Smith, B. J., Chi, V., Monaghan, K. P., et al. (2009). Engineering a stable and selective peptide blocker of the Kv1.3 channel in T lymphocytes. *Mol. Pharmacol.* 75, 762–773. doi: 10.1124/mol.108.052704

Pennington, M., Harunur Rashid, M., Tajhya, R., Beeton, C., Kuyucak, S., and Norton, R. (2012). A C-terminally Amidated Analogue of ShK Is a Potent and Selective Blocker of the Voltage-Gated Potassium Channel Kv1.3. *FEBS Lett.* 586, 3996–4001. doi: 10.1016/J.FEBSLET.2012.09.038

Pluzhnikov, K., Vassilevski, A., Korolkova, Y., Fisyunov, A., Iegorova, O., Krishtal, O., et al. (2007). ω-Lsp-IA, a novel modulator of P-type Ca2+ channels. *Toxicon* 50, 993–1004. doi: 10.1016/j.toxicon.2007.07.004

Prosdocimi, E., Checchetto, V., and Leanza, L. (2019). Targeting the Mitochondrial Potassium Channel Kv1.3 to Kill Cancer Cells: Drugs, Strategies, and New Perspectives. *SLAS Discovery Adv. Life Sci. R D* 24, 882–892. doi: 10.1177/2472555219864894

Pyrkov, T., and Efremov, R. (2007). A Fragment-Based Scoring Function to Re-rank ATP Docking Results. *Int. J. Mol. Sci.* 8, 1083–1094. doi: 10.3390/i8111083

Pyrkov, T. V., Chugunov, A. O., Krylov, N. A., Nolde, D. E., and Efremov, R. G. (2009). PLATINUM: a web tool for analysis of hydrophobic/hydrophilic organization of biomolecular complexes. *Bioinformatics* 25, 1201–1202. doi: 10.1093/bioinformatics/btp111

Rashid, M. H., Huq, R., Tanner, M. R., Chhabra, S., Khoo, K. K., Estrada, R., et al. (2015). A potent and Kv1.3-selective analogue of the scorpion toxin HsTX1 as

a potential therapeutic for autoimmune diseases. *Sci. Rep.* 4, 4509. doi: 10.1038/srep04509

Renisio, J. G., Romi-Lebrun, R., Blanc, E., Bornet, O., Nakajima, T., and Darbon, H. (2000). Solution structure of BmKTX, a K+ blocker toxin from the Chinese scorpion Buthus Martensi. *Proteins* 38, 70–78. doi: 10.1002/(SICI)1097-0134(20000101)38:1<70::AID-PROT8>3.0.CO;2-5

Romi-Lebrun, R., Lebrun, B., Martin-Eauclaire, M. F., Ishiguro, M., Escoubas, P., Wu, F. Q., et al. (1997). Purification, characterization, and synthesis of three novel toxins from the Chinese scorpion Buthus martensi, which act on K+ channels. *Biochemistry* 36, 13473–13482. doi: 10.1021/bi971044w

Schmitz, A., Sankaranarayanan, A., Azam, P., Schmidt-Lassen, K., Homerick, D., Hänsel, W., et al. (2005). Design of PAP-1, a Selective Small Molecule Kv1.3 Blocker, for the Suppression of Effector Memory T Cells in Autoimmune Diseases. *Mol. Pharmacol.* 68, 1254–1270. doi: 10.1124/mol.105.015669

Tabakmakher, V. M., Krylov, N. A., Kuzmenkov, A.II, Efremov, R. G., and Vassilevski, A. A. (2019). Kalium 2.0, a comprehensive database of polypeptide ligands of potassium channels. *Sci. Data* 6, 73. doi: 10.1038/s41597-019-0074-x

Takacs, Z., Toups, M., Kollewe, A., Johnson, E., Cuello, L. G., Driessens, G., et al. (2009). A designer ligand specific for Kv1.3 channels from a scorpion neurotoxin-based library. *Proc. Natl. Acad. Sci. U. S. A.* 106, 22211–22216. doi: 10.1073/pnas.0910123106

Teisseyre, A., Palko-Labuz, A., Sroda-Pomianek, K., and Michalak, K. (2019). Voltage-Gated Potassium Channel Kv1.3 as a Target in Therapy of Cancer. *Front. Oncol.* 9, 933. doi: 10.3389/fonc.2019.00933

Varga, Z., Gurrola-Briones, G., Papp, F., Rodríguez de la Vega, R. C., Pedraza-Alva, G., Tajhya, R. B., et al. (2012). Vm24, a natural immunosuppressive peptide, potently and selectively blocks Kv1.3 potassium channels of human T cells. *Mol. Pharmacol.* 82, 372–382. doi: 10.1124/mol.112.078006

Webb, B., and Sali, A. (2016). Comparative Protein Structure Modeling Using MODELLER. *Curr. Protoc. Bioinf.* 54, 5.6.1–5.6.37. doi: 10.1002/cpbi.3

Wulff, H., and Zhorov, B. S. (2008). K+ channel modulators for the treatment of neurological disorders and autoimmune diseases. *Chem. Rev.* 108, 1744–1773. doi: 10.1021/cr078234p

Wulff, H., Christophersen, P., Colussi, P., Chandy, K. G., and Yarov-Yarovoy, V. (2019). Antibodies and venom peptides: new modalities for ion channels. *Nat. Rev. Drug Discovery* 18, 339–357. doi: 10.1038/s41573-019-0013-8

Conflict of Interest: The authors declare that the research was conducted in the absence of any commercial or financial relationships that could be construed as a potential conflict of interest.

frontiers in Pharmacology

REVIEW
published: 08 July 2020
doi: 10.3389/fphar.2020.00991

Animal, Herb, and Microbial Toxins for Structural and Pharmacological Study of Acid-Sensing Ion Channels

Dmitry I. Osmakov[1,2], *Timur A. Khasanov*[1], *Yaroslav A. Andreev*[1,2], *Ekaterina N. Lyukmanova*[1] *and Sergey A. Kozlov*[1]*

[1] *Shemyakin-Ovchinnikov Institute of Bioorganic Chemistry, Russian Academy of Science, Moscow, Russia,* [2] *Institute of Molecular Medicine, Sechenov First Moscow State Medical University, Moscow, Russia*

OPEN ACCESS

Edited by:
Jean-Marc Sabatier, Aix-Marseille Université, France

Reviewed by:
Lachlan Rash, The University of Queensland, Australia
Sergei Noskov, University of Calgary, Canada

***Correspondence:**
Sergey A. Kozlov
serg@ibch.ru

Specialty section:
This article was submitted to Pharmacology of Ion Channels and Channelopathies, a section of the journal Frontiers in Pharmacology

Received: *24 April 2020*
Accepted: *19 June 2020*
Published: *08 July 2020*

Citation:
Osmakov DI, Khasanov TA, Andreev YA, Lyukmanova EN and Kozlov SA (2020) Animal, Herb, and Microbial Toxins for Structural and Pharmacological Study of Acid-Sensing Ion Channels. Front. Pharmacol. 11:991. doi: 10.3389/fphar.2020.00991

Acid-sensing ion channels (ASICs) are of the most sensitive molecular sensors of extracellular pH change in mammals. Six isoforms of these channels are widely represented in membranes of neuronal and non-neuronal cells, where these molecules are involved in different important regulatory functions, such as synaptic plasticity, learning, memory, and nociception, as well as in various pathological states. Structural and functional studies of both wild-type and mutant ASICs are essential for human care and medicine for the efficient treatment of socially significant diseases and ensure a comfortable standard of life. Ligands of ASICs serve as indispensable tools for these studies. Such bioactive compounds can be synthesized artificially. However, to date, the search for such molecules has been most effective amongst natural sources, such as animal venoms or plants and microbial extracts. In this review, we provide a detailed and comprehensive structural and functional description of natural compounds acting on ASICs, as well as the latest information on structural aspects of their interaction with the channels. Many of the examples provided in the review demonstrate the undoubted fundamental and practical successes of using natural toxins. Without toxins, it would not be possible to obtain data on the mechanisms of ASICs' functioning, provide detailed study of their pharmacological properties, or assess the contribution of the channels to development of different pathologies. The selectivity to different isoforms and variety in the channel modulation mode allow for the appraisal of prospective candidates for the development of new drugs.

Keywords: acid-sensing ion channels, natural compounds, ligand receptor interaction, structural features, analgesia, drug development

INTRODUCTION

Natural compounds synthesized by marine and terrestrial inhabitants of three kingdoms (animals, plants, and bacteria) can be considered simultaneously a hazard and a remedy for life quality improvements. Since ancient times, pharmacy has been based inherently on the discovery, examination, and implementation of bioactive molecules, mainly from plants, for treatment of humans. However, the appearance of effective separation methods provided a significant impetus to the promotion of natural compounds from other organisms on the drug market, since it became possible to remove highly toxic components of venoms. The modern growth development of genomics, proteomics, and biotechnology make possible successful study of bioactive molecules, even from very rare animals. As a result, there is an overabundance of structural and functional information of natural compounds that was not confirmed by cellular target specificity. In this review, we only include natural ligands capable of interacting with an acid-sensing ion channels (ASICs).

ASICs are Na^+-selective channels abundantly expressed in neurons of the peripheral and central nervous systems, where they perform an important function in signal transmission associated with a local change in pH. They are of the most sensitive sensors of acidification in the organism. Indirect confirmation of the existence of these channels was first obtained in the early 1980s, when sodium-selective and rapidly activated and desensitized transient current was detected on mammalian sensory neurons in response to a sharp acidification of the extracellular medium (Krishtal and Pidoplichko, 1980; Krishtal, 2015). In the mid-1990s, the channels with such properties were cloned and expressed and then got their modern name of "acid-sensing ion channels" (Waldmann et al., 1997).

Four genes encode six isoforms of ASICs in mammals: ASIC1a, ASIC1b, ASIC2a, ASIC2b, ASIC3, and ASIC4 (Wemmie et al., 2006). In neurons of the peripheral nervous system (PNS), all isoforms and especially ASIC3 have been found, with the exception of ASIC4. In neurons of the central nervous system (CNS), all isoforms (except ASIC1b) have also been detected, and the ASIC1a isoform is predominant (Deval and Lingueglia, 2015; Schuhmacher and Smith, 2016). ASICs can form homo- and heterotrimeric complexes. Thus, heteromeric complexes of all isoforms have been detected in both CNS (ASIC1a/ASIC2a, ASIC1a/ASIC2b, ASIC1a/ASIC4) and PNS neurons (ASIC1a/ASIC1b, ASIC1a/ASIC3, ASIC1b/ASIC3, ASIC2b/ASIC3) (Lingueglia et al., 1997; Alvarez de la Rosa et al., 2002; Askwith et al., 2004; Gautam and Benson, 2013; Wu et al., 2016).

Ligands, controlling the function of ASICs, were found amongst animal polypeptides, microbial metabolites, and in plant extracts pointing on high-relevant evolutionary role of these channels. In this review, we present the widest and most complete list of natural ligands and discuss modern structural aspects and practical applications of these compounds for the study of ASICs physiological and pathological roles in an organism.

Abbreviations: 5-CQA, 5-caffeoylquinic acid; ASICs, acid-sensing ion channels; α-DTx, α-dendrotoxin; BBH, boundless β-hairpin; CNS, central nervous system; CNFs, cono-RFamides; DAU, daurisoline; DRG, dorsal root ganglion; EC_{50}, half-maximal effective concentration; ECDs, extracellular domains; EGCG, (-)-Epigallocatechin gallate; IC_{50}, half-maximal inhibitory concentration; ICK, inhibitor cystine knot; LIN, lindoldhamine; NEO, neomycin; nH, Hill coefficient; NMR, nuclear magnetic resonance; pH_{50}, half-activation pH; PcTx1, psalmotoxin; PNS, peripheral nervous system; SSD, steady-state desensitization; ST, streptomycin; TM, transmembrane; TRPV1, transient receptor potential V1.

BIOPHYSICAL PROPERTIES OF ACID-SENSING ION CHANNELS

The subunit composition of each ASIC determines its pH sensitivity, kinetics, and pharmacology (Escoubas et al., 2000; Diochot et al., 2004; Hesselager et al., 2004). Sensitivity to acidic pH varies between different isoforms as follows: ASIC1a and ASIC3 channels are the most sensitive, with a half-activation pH (pH_{50}) of about 6.4–6.6; ASIC1b channels occupy an intermediate position (pH_{50} 5.9–6.3); and ASIC2a channels are the least sensitive (pH_{50} 4.3–4.9) (Boscardin et al., 2016). ASIC2b and ASIC4 do not respond to the acid stimulus and apparently only form heteromeric channels with other isoforms, thereby influencing the function of the channel as a whole (Deval et al., 2004; Donier et al., 2008; Sherwood et al., 2011). Under the action of an acid pulse, all functional ASICs form a rapidly activated current, which then desensitizes at different rates (**Figure 1A** for ASIC1a subtype) (Gründer and Pusch, 2015; Osmakov et al., 2019a). According to the kinetics of desensitization, the currents of ASIC3 channels stand apart; in other words, a rapidly desensitizing (transient) component is followed by a non-desensitizing current (sustained component), which lasts as long as the stimulating pulse (**Figure 1B** for ASIC3 subtype) (Salinas et al., 2009; Osmakov et al., 2014). A common property of all subtypes is an increase of current amplitude upon more acid stimulation up to a certain saturation level, so the proton activation curve (ligand receptor dependence) has a characteristic shape and pH value of 50% response (**Figure 1D**).

Another property of ASICs is their ability to reach steady-state desensitization (SSD)—that is, to transition into a desensitized state from a closed state, bypassing the activation process (**Figures 1C, E**). This phenomenon is observed when the proton concentration in the environment increases insignificantly and does not cause activation of the channels but the channels respond to the next strong acid stimulus, either much weaker or non-existent (Waldmann et al., 1997; Alijevic and Kellenberger, 2012).

For compounds isolated from natural sources (plant, microbial, and animal peptides; see below), both positive and negative modulating effects on ASICs have been described. Thus, some ligands show the ability to reduce or, conversely, increase the amplitude of the acid-induced current of one or several ASIC isoforms (**Figures 1C, D** orange and blue curves, respectively). Other ligands are able to increase or decrease the desensitization time constant of this current ("narrowing" or "widening" the current trace, respectively), thereby affecting the kinetics of a channel's transition from one state to another. Ligands can also shift the dependence of channel activation (**Figure 1D**). On the graph, the ligand's potentiating effect is expressed as a curve shift

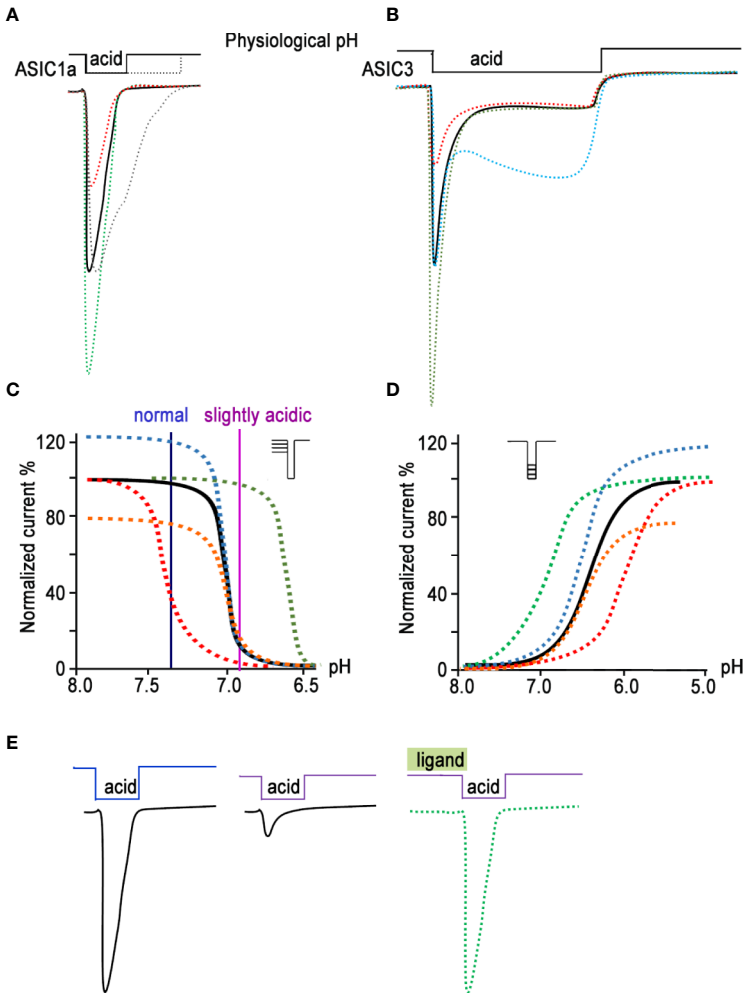

FIGURE 1 | Biophysical properties of ASICs. The characteristic traces of currents recorded in whole-cell configuration are presented for ASIC1a **(A)** and for ASIC3 **(B)** as a black line; currents modified by ligands application are represented in green (potentiation) and red (inhibition). The gray line in **(A)** and cyan line in **(B)** reflect the process of desensitization kinetics change. The pH dependence of the channel gating is shown as a result of steady-state desensitization (SSD) **(C)** and as dependence of currents' amplitude by various acidic stimuli applied **(D)** for the channel alone (black line). The potentiating effect of ligands is demonstrated as green and blue curves, and the inhibiting effect as red and orange curves. **(E)** Current traces reflect the effect of pH-dependent SSD. In a weakly acidic environmental medium, the channel loses its ability to fully respond to a stronger acid stimulus; however, the addition of a ligand is able to restore its properties (green line).

towards higher pH values (green curve), while its inhibitory effect is expressed as a shift towards lower pH values (red curve). Another group of ligands does not act on the activation of the channel directly but produces an effect on the SSD of the channel. In this case, the sensitivity of the channels at resting state to protons either increases (the curve shifts towards higher pH values, and the channel becomes poorly susceptible to acid stimuli; **Figure 1C** red curve) or decreases (the curve shifts towards lower pH values; **Figure 1C** green curve). Toxins usually have a mixed effect, for example combining the amplitude change with a shift of activation or SSD. Moreover, toxins often change the kinetics of activation and inactivation processes, leading to alterations in the slope of curves. Thus, a large arsenal of natural ligands for ASICs has been accumulated to this day, and it is possible to control the biophysical properties of these channels differently.

THE ARCHITECTURE OF ACID-SENSING ION CHANNELS

The structure of an ASIC was first determined in 2007. It was an X-ray crystal structure with 1.9 Å resolution of truncated chicken ASIC1a (cASIC1a), with shortened *N*- and *C*-termini in a low-pH desensitized state (Jasti et al., 2007). Later, in 2009, the structure of desensitized cASIC1a was published with the retained *N*-terminus but still truncated disordered *C*-terminal tail (Gonzales et al., 2009). The cASIC1a structure resembles a bowl formed by three identical subunits (**Figures 2A, B**). Trimers are stabilized by contacts between extracellular domains (ECDs) and transmembrane (TM) helices of adjacent subunits. There is a clear boundary between the ECD and TM part within one subunit formed by a short (3–4 a.a.) linker—also

called a "wrist" region—which serves for the signal transduction from ECDs to the TM domain. The ECD of each subunit protrudes above the membrane ~80 Å and in turn has the domain architecture containing the finger, thumb, palm, β-ball, and knuckle domains (**Figure 2A**). Moreover, the proton-, calcium-, chloride-, and other ligand-binding sites are located within ECDs.

Proton-binding sites are located in the middle of ECDs (~45 Å over the membrane) and consist of four spatially close pairs of side-chains of: Asp238-Asp350 and Glu239-Asp346 from the finger and thumb domains of the same subunit, Glu220-Asp408 from the palm domain of the adjacent subunit (these three pairs form the acidic pocket, **Figure 2B**) and Glu80-Glu417 from the palm domain (Jasti et al., 2007). The residues involved in the acidic pocket are highly conservative in ASICs (**Figure 2E**), demonstrating pKa values significantly different from the isolated pKa of aspartate and glutamate residues. Calcium could stabilize the closed, resting state of ASICs at high pH *via* interaction with these pairs, thus recovering the desensitization state (Todorović et al., 2005). On the other hand, these acidic residues have been identified in proton-insensitive ASICs too (Coric et al., 2005), pointing to the possible existence of other proton-binding sites. It was shown that the acidic pocket plays a modulatory function and is subjected to conformational rearrangement upon the activation of a channel, while the pair of Glu80-Glu417 side chains in the palm domain is responsible for acceleration of desensitization and the appearance of sustained current (Vullo et al., 2017). The acidic pocket has extended conformation at high-pH resting and low-pH desensitized states and collapsed conformation at low-pH open state. Collapsed conformation is characterized by approximation of aspartate and glutamate side-chains for the proton-binding, which in turn results in the rearrangement of ECDs and the TM domain to open the channel (Gonzales et al., 2009; Baconguis and Gouaux, 2012; Yoder et al., 2018).

There is a tunnel piercing through the ASIC from the extracellular top to the cytoplasmic bottom (Hanukoglu, 2017). The main function of this vestibule is ion flow from the extracellular environment into the cell. The vestibule is subdivided into upper, central, and extracellular parts. The hydrophobic residues Leu78 and Ile419 (cASIC1) separate the central and extracellular vestibules, forming a trap in a desensitized-like state (Dawson et al., 2012). The extracellular vestibule, playing the role of a cation reservoir, is significantly expanded in the open state compared to closed or desensitized states (Gonzales et al., 2009; Baconguis and Gouaux, 2012; Baconguis et al., 2014; Yoder et al., 2018).

The extracellular part of the vestibule is bounded with the TM domain located in the phospholipid bilayer (**Figure 2**). The TM domain consists of six α-helices (two from each subunit), has an hourglass shape, and plays a dual role, (i) for stabilization and trimerization of the subunits within the channel trimers and (ii) for pore formation and transfer of ions through the cell membrane. The TM part of each subunit is formed by two α-

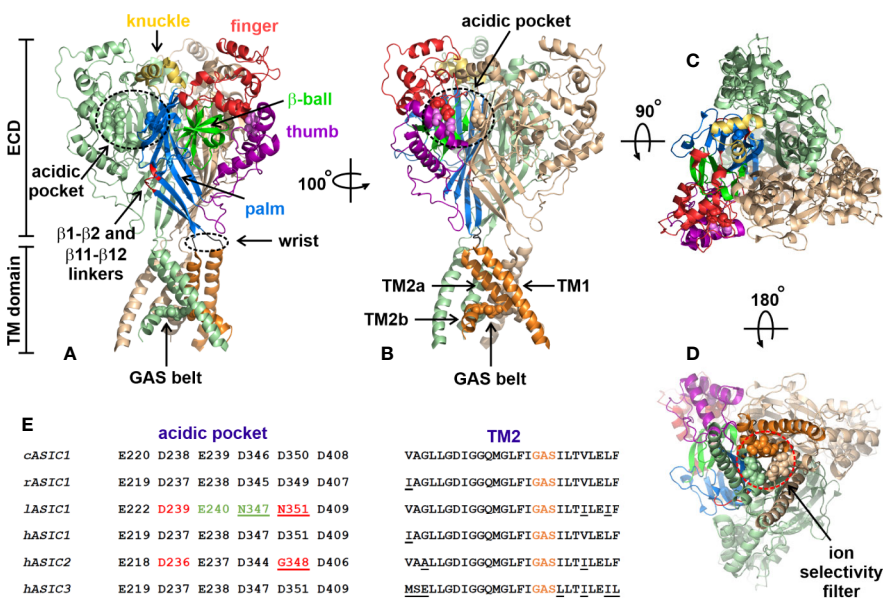

FIGURE 2 | Architecture of chicken ASIC1a channel (PDB code 4NYK). **(A, B)** Side-views of the channel. Two channel subunits are shown by wheat and pale green colors, and the third subunit is colored according its domain structure: the knuckle, finger, b-ball, thumb, palm, and TM part are colored in yellow, dark red, light green, purple, blue, and orange, respectively. Asp and Glu residues forming the acidic pockets (surrounded by black dashed circles) and GAS belts are shown by spheres. The locations of the β1-β2 and β11-β12 linkers are colored by red. **(C)** Top view of the channel. **(D)** View of the channel from an intracellular side. The ion selectivity filter formed by three GAS belts is shown by a red dashed circle. **(E)** Comparison of the residues forming the acidic pocket and TM2 in ASICs of different origin (cASIC1, chicken ASIC1; rASIC1, rat ASIC1; lASIC, lamprey ASIC1; hASIC1,2,3, human ASIC1,2,3).

helices: TM1 and TM2. TM1 contacts TM2 of the same subunit, TM1 and TM2 from the adjacent subunits, and the lipid environment, while TM2 lines the channel pore (Gonzales et al., 2009). TM2 consists of two parts (TM2a and TM2b) separated by three residues—Gly443-Ala444-Ser445 (cASIC1)—that are referred to as a GAS belt (**Figures 2A, B**). In the closed gate, TM2 adopts a kinked conformation, forming a pore "gag" with other TM2s from the adjacent subunits. Straightening of the TM2s transfers the pore to the open state with formation of the ion selectivity filter, formed by three GAS belts from the adjacent subunits (Li et al., 2011). The ion selectivity filter is the narrowest part of the pore and serves for the selection of ion types flowing through the channel. The size of the filter (radius ~3.6 Å) correlates well with the radius of hydrated Na^+ (**Figure 2D**). The TM2 sequence is highly conservative in ASICs, pointing to the similar structure of the pore domain within the whole family (**Figure 2E**).

Presently, the structures of the cASIC1a channel in high-pH resting, low-pH open, and low-pH desensitized states are known (Jasti et al., 2007; Gonzales et al., 2009; Baconguis and Gouaux, 2012; Dawson et al., 2012; Baconguis et al., 2014; Yoder et al., 2018). Two years ago, the structure of the full-length cASIC1a channel was determined by cryo-EM revealing the structural similarity of the full-sized and truncated channels. Based on the cASIC1a structures in all three channel states, the Eric Gouaux group proposed the gating mechanism (Yoder et al., 2018). According to this mechanism, at neutral pH, the channel exists in the closed or resting state. In this state, the acidic pocket is expanded, and the TM domain does not pass the ion flow. When the pH of the extracellular media goes to low values, the acidic pocket changes its conformation from an expanded to a collapsed state, coming closer to carboxyl-carboxylate pairs from the finger and thumb domains and thus binding the protons. This in turn initiates a number of conformational changes in ECDs, with counterclockwise rotation of each subunit, movement of the β1 and β12 strands towards the membrane, and displacement of the TM1 and TM2 helices away from the threefold symmetric axis of the channel. This results in the pore opening and ion flow through the channel. In hundreds of milliseconds (Zhang and Canessa, 2002), the channel switches from its low-pH open state to its low-pH desensitized state, accompanied by reorientation of the β1-β2 and β11-β12 linkers to their initial conformation, and consequently switches movement of TM1 and TM2 back to the center of the pore and closes the channel gate. In other words, the desensitized state of the channel is characterized by simultaneous resting-like conformation of the TM domain and activated-like conformation of the upper half of an ECD with a collapsed acidic pocket and bound protons. This chimeric conformation is reached by rearrangement of the β1-β2 and β11-β12 linkers. Most conformational changes were observed in the β11-β12 linkers, resulting in 9 Å reorientation of the Leu414 residue (cASIC1a) towards the central vestibule. Returning to physiologically high pH values leads to a release of protons from the acidic pocket and its expansion. Thus, the β11-β12 linkers play an important role in channel gating, serving as a bridge between ECDs and the TM domain, within which conformational changes lead to opening or closing of the channel.

In spite of the high relevance of cASIC1a structures in different states and in complexes with various ligands for understanding of the mechanism of channel gating, there are still many blind spots regarding other members of this family. The rat ASIC subunits share ~45–80% of their sequence identities, pointing to a possible difference in the regions responsible for the channel gating. In line with this, the unique Ca^{2+}-binding site was recently identified in ASIC3, located in the channel pore (Zuo et al., 2018). Another example of significant structural and functional differences within the ASIC family is lamprey ASIC1, which does not respond to protons. Substitution of only two residues located in the β1-strand and the β1-β2 linker with the corresponding residues Leu77 and Leu85 from rat ASIC1 recovered the proton activation response, suggesting the importance of other structural elements besides the acidic pockets, which significantly differ between rat and lamprey ASIC1s (Li et al., 2010) (**Figure 2E**). Indeed, two residues in the acidic pocket of lamprey ASIC1 that have positions identical to rat Asp345 and Asp349 from cASIC1a are Asn347 and Asn351, respectively. This means that the acidic pockets of lamprey ASIC1 have lower capability to bind protons at pH values close to 5.0. ASIC2a is a pH-sensitive channel, while its splicing variant ASIC2b is not (Schuhmacher et al., 2015). Both variants have identical acidic pockets, albeit with mutated residue corresponding to Asp350 from cASIC1a (**Figure 2E**). This points to the presence of other important structural domains responsible for channel gating. Such domains located in ECDs immediately after TM1 were recently determined for ASIC2a (Schuhmacher et al., 2015).

There are numerous reports about involvement of membrane lipids into control of the spatial structure and function of different receptors and ion channels including GPCRs (Fantini and Barrantes, 2018), the nicotinic acetylcholine receptors (Baenziger et al., 2000), K^+ and Na^+ voltage-gated ion channels (Agwa et al., 2018; Jiang, 2019), TRPV1 channels (Morales-Lázaro and Rosenbaum, 2019), TREK channels (Hernández-Araiza et al., 2018), and ENAC channels (Kleyman and Eaton, 2020). Interaction with PIP2 is necessary to open ENaCs (Kleyman and Eaton, 2020), which belong to the same degenerin/epithelial Na^+ channel (DEG/ENaC) family as ASICs. In line with it, arachidonic acid was shown to potentiate ASIC1a and ASIC3 by direct interaction with the channels in the rat sensory neurons (Smith et al., 2007), and arachidonic acid and lysophosphatidylcholine (16:0) activate ASIC3 at neutral pH and induce pain behavior in rats pointing on lipid-mediated signaling (Marra et al., 2016). At the same time, no data are available about the role of lipids in modulation of ASIC/toxin or ASIC/drug interactions. ASICs also were reported to be involved in mechanosensation (Page, 2005; Lin et al., 2016) demonstrating dual protein functions: sensing both tissue acidosis and mechanical force, although the mechanical gating mechanism of ASICs is still unclear (Cheng et al., 2018). Thus, the membrane environment could be an important modulator of the ASICs activity and the reason for variety of functional properties of the channel subtypes expressed in different cells. Further study of the lipid bilayer role in the ASICs gating is needed.

NATURAL LIGANDS OF ACID-SENSING ION CHANNELS

Plant Compounds

Low molecular weight ASIC ligands are represented by molecules belonging to various classes of chemical compounds, ranging from relatively simple pyrazines and polyphenolic acids to more complex glycosides and quinoline alkaloids (**Figures 3** and **4**). Most of these ligands are derived from herbs that are well known for their medical properties and used in the traditional medicine of various nations. The most of described below molecules have several other cellular targets, and their therapeutic effects can be associated not only with the modulation of ASICs. Thus, it is important to keep in view these properties to explain possible auxiliary effects of the compounds, and the biological effect exhibited by these molecules *in vivo* should be considered the result of a complex effect on several targets.

5-Caffeoylquinic Acid

5-caffeoylquinic acid (5-CQA) belongs to a group under the general name chlorogenic acids. It is a phenolic compound, an ester of caffeic acid, and one of the stereoisomers of quinic acid. 5-CQA is abundantly present in various plants included in the human diet (for example, green coffee beans) and is well known for its antioxidant, anti-inflammatory, neuroprotective, and analgesic properties (Zhang et al., 2003; dos Santos et al., 2006; Lapchak, 2007; Li et al., 2008). It was demonstrated on rat dorsal root ganglion (DRG) neurons that 5-CQA is concentration-dependent and reversibly inhibits a pH 5.5-induced current with a half-maximal inhibitory concentration (IC_{50}) of 0.235 μM (**Table 1**). To exclude the neuronal acid sensing *via* TRPV1 channels, authors carried out the experiment in the presence of capsazepine (10 μM). Maximal observed inhibitory effect reached 55% that indicated selectivity of 5-CQA to certain ASIC isoforms. The compound also reduces the sensitivity of neurons to various activating pHs, without changing the pH_{50} and Hill coefficient (n_H) parameters of the pH-dependence activation curve (for a graphic example, see **Figure 1D**, orange dashed curve). In this regard authors conclude that the mechanism of the inhibitory effect of 5-CQA is not associated with a decrease in the affinity of ASIC channels to protons. Local administration of 5-CQA at doses of 1 μM and 10 μM attenuates pain induced by intraplantar injection of 20 μl acetic acid (Qu et al., 2014).

Chloroquine

Chloroquine is an antimalarial drug from the group of 4-aminoquinoline derivatives that is first isolated from an extract of cinchona bark. It has an antiproliferative effect on T cells; reduces the production of several pro-inflammatory cytokines and the innate immune system activation; possesses antiviral, antibacterial,

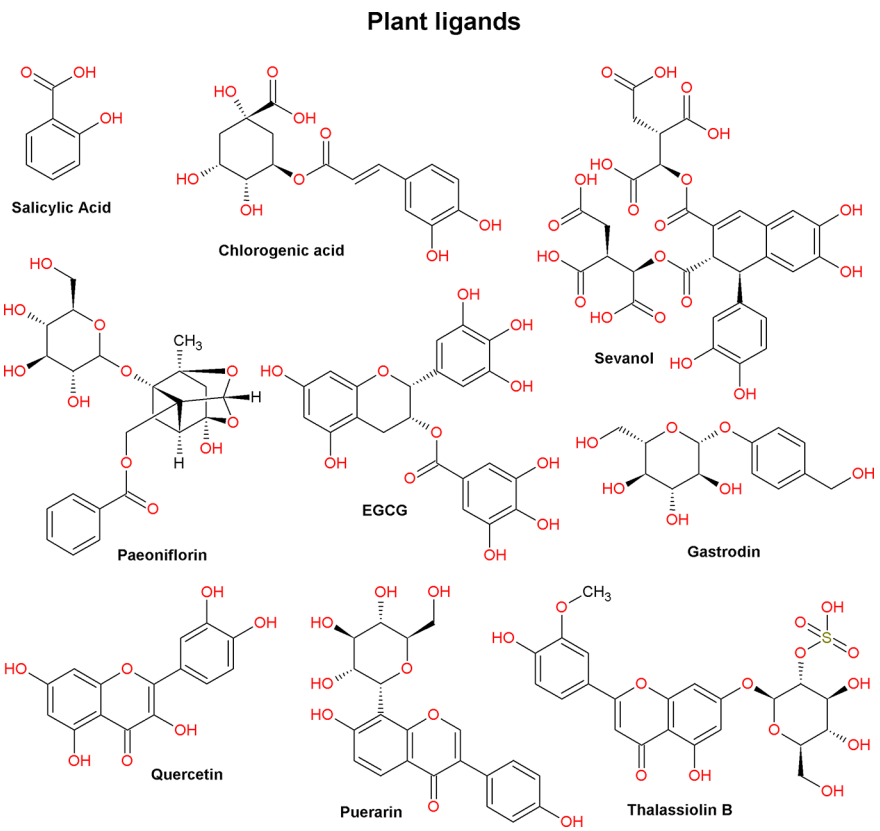

FIGURE 3 | Plant ligands of acid-sensing ion channels (compounds from various chemical classes; see text).

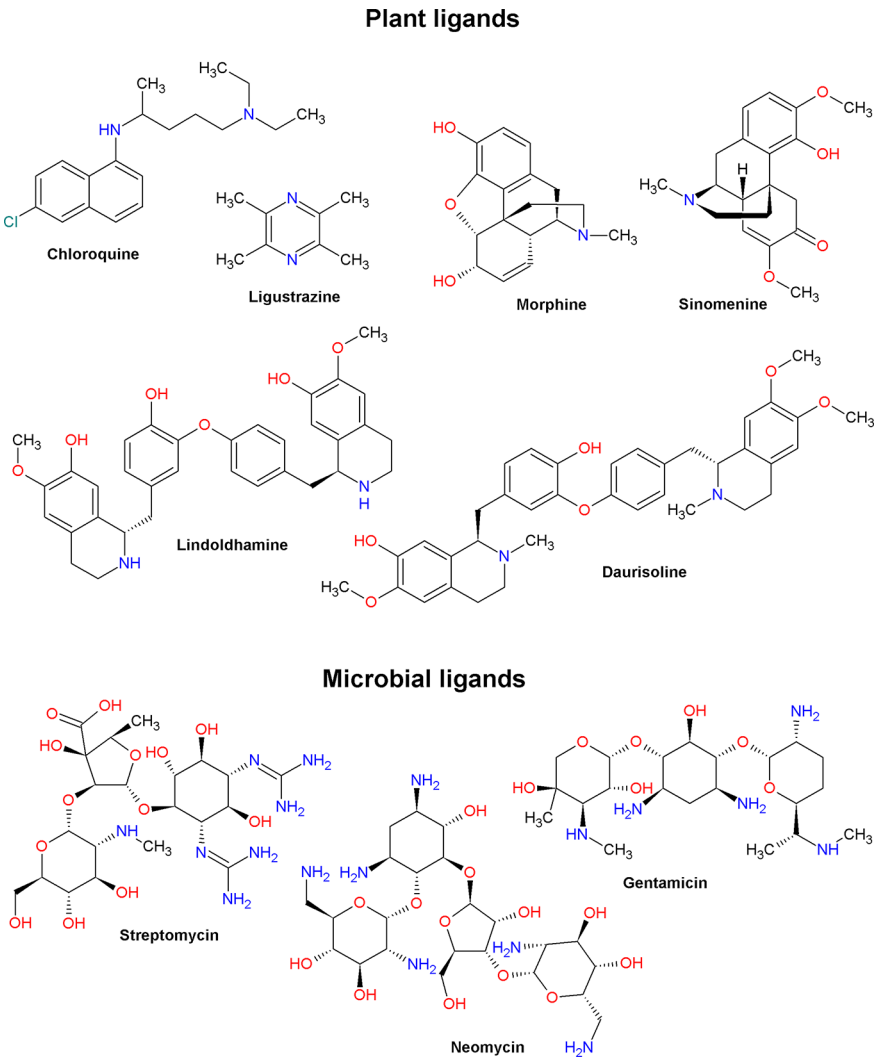

FIGURE 4 | Alkaloid ligands (plant and microbial origin) of acid-sensing ion channels.

and antifungal effects, and have been successfully used to treat several rheumatological, immunological, and infectious diseases (Plantone and Koudriavtseva, 2018). In the heart, chloroquine block of the inward rectifier K^+ currents by inhibiting of $Kir_{2.1}$ channel with IC_{50} 8.7 ± 0.9 μM (Rodriguez-Menchaca et al., 2008). One of its known side effects is retinal toxicity (Hobbs et al., 1959). On retinal ganglion neurons and on CHO cells expressing ASIC1a, it was shown that chloroquine dose dependently and reversibly inhibits the amplitude of a pH 6.5-induced current (IC_{50} 615.9 μM) as well as causes a significant delay in peak maximum and desensitization time constant (**Table 1**). This effect was enhanced with an increase in the concentration of Ca^{2+} ions in the extracellular medium and weakened with an increase in the activating acid stimulus. In the presence of chloroquine, the amplitudes of the main parameters of the electroretinogram, such as the b-wave of scotopic 0.01 and photopic 3.0 and vibrational potentials, decreased (Li et al., 2014). In CHO cells expressing ASIC3 channels and in DRG neurons, it was shown that chloroquine dose dependently potentiates the sustained component (EC_{50} of 425.2 μM and n_H 3.676) without affecting the transient component of the proton-activated current. This effect also depends on the concentration of calcium in the extracellular medium and weakens with an increase in the activating stimulus. Using site-directed mutagenesis, it was possible to demonstrate that chloroquine can activate ASIC3 channels by binding to a non-proton ligand sensor in the palm domain (Lei et al., 2016). In an *in vivo* "cheek" assay model in mice (Shimada and LaMotte, 2008), chloroquine caused combing, and this effect was attenuated in the presence of an ASIC3 inhibitor (Lei et al., 2016).

Lindoldhamine and Daurisoline

Lindoldhamine (LIN) and daurisoline (DAU) are members of the bisbenzylisoquinoline alkaloids group. This is a broad group of biologically active compounds known for their anticancer, antiviral,

TABLE 1 | Effect of plant and microbial ligands *in vitro* on ASICs.

Compound	Trend	Value and object of action	References
(-)-Epigallocatechin gallate	↓	IC_{50} 13.2 μM for mASIC3 in CHO cells	Yan et al., 2019
5-caffeoylquinic acid	↓	IC_{50} 0.235 μM for rASIC in DRG neurons	Qu et al., 2014
Chloroquine	↓	IC_{50} 615.9 μM for rASIC1a in CHO cells	Li et al., 2014
	↑	EC_{50} 425.2 μM for sustained current rASIC3in CHO cells	Lei et al., 2016
Daurisoline	∩	EC_{50} 20 μM for transient current rASIC1a in oocytes	Osmakov et al., 2019b
	↔	EC_{50} 140 μM for rASIC1a in oocytes	
Gastrodin	↓	IC_{50} 0.2 μM for rASIC in DRG neurons	Qiu et al., 2014
Ligustrazine	↓	IC_{50} 270 μM for rASIC in DRG neurons	Zhang et al., 2015
	↓	IC_{50} 97 μM for rASIC1a, 62 μM rASIC1b, 129.4 μM rASIC2a, 239.5 μM rASIC3 in CHO cells	Zhang et al., 2015
Lindoldhamine	↓	IC_{50} 9 μM for rASIC1a oocytes (at pH 6.85 stimulus)	Osmakov et al., 2019c
	Δ	EC_{50} 1.53 mM for hASIC3, 3.2 mM rASIC3 in oocytes	Osmakov et al., 2018
	↑	EC_{50} of 3.8 μM for transient current hASIC3 in oocytes	
Morphine	↓	IC_{50} 2.3 μM for rASIC in DRG neurons	Cai et al., 2014
Neomycin	↓	IC_{50} 45 μM for rASIC in DRG neurons	Garza et al., 2010
Paeoniflorin	↓	IC_{50} 5 μM for rASIC in pheochromocytoma cells	Sun et al., 2011
Puerarin	↓	IC_{50} 38.4 μM for rASIC in hippocampal cells, 9.31 μM for rASIC1a in CHO cells	Gu et al., 2010
Quercetin	↓	IC_{50} 2.4 μM for rASIC1a, 1.3 μM for rASIC2a, 1.8 μM for rASIC3 in CHO cells	Mukhopadhyay et al, 2017
Salicylic acid	↓	IC_{50} 260 μM for rASIC3 in COS cells	Voilley et al., 2001
Sevanol	↓	IC_{50} 353 μM for transient hASIC3, 234 μM for sustained hASIC3 currents in oocytes	Dubinnyi et al., 2012
Sinomenine	↓	IC_{50} 0.3 μM for rASIC1a in CHO cells	Wu et al., 2011
Streptomycin	↓	IC_{50} 30 μM for rASIC in DRG neurons	Garza et al., 2010
Thalassiolin B	↓	IC_{50} 27 μM for rASIC in DRG neurons	Garateix et al., 2011

↓, Inhibition of current; ↑, Potentiating of current; Δ, Activation of current without acidic drop; ∩, Generation of 2nd current component; ↔, Inhibition of steady-state desensitization; IC_{50}, half-maximal inhibitory concentration; EC_{50}, half-maximal effective concentration; hASIC, human ASIC; rASIC, rat ASIC; mASIC, mouse ASIC.

anti-inflammatory, and neuroprotective properties (Tian and Zheng, 2017). LIN was isolated from an acetic acid extract of the plant *Laurus nobilis* L. On *X. laevis* oocytes expressing human and rat ASIC3 channels, it was shown that LIN is capable of inducing sustained incoming currents with EC_{50} of 1.53 mM and n_H 0.93 (for human ASIC3) as well as 3.2 mM and 0.82 (for rat ASIC3) (**Table 1**). Moreover, LIN exerts a potentiating effect on proton-induced currents of human ASIC3, increasing the transient component by more than two times (EC_{50} of 3.8 μM and n_H 1.1) as well as inhibiting SSD and restoring the transient component (EC_{50} of 16 μM and n_H 1) (Osmakov et al., 2018). LIN also exerts a pH-dependent inhibitory effect on rat ASIC1a channels if a weak stimulus (pH 6.85) is applied. Its strongest inhibitory effect (IC_{50} 9 μM and n_H 1.2) weakens with an increase in the acid stimulus. As a result, in the CFA-induced inflammation test, LIN showed a significant anti-inflammatory effect; however, in the acetic acid-induced writhing test, LIN did not show any analgesic effect (Osmakov et al., 2019c).

DAU has a similar structure with LIN but has three more methyl groups (**Figure 4**). DAU is a common compound synthesized by various plants of traditional Chinese medicine. DAU has been shown to have a muscle relaxant and antiarrhythmic effect by inhibiting currents of L-type calcium (active concentration >15 μM) and hERG channels (active concentration >10 μM), respectively (Liu et al., 2010; Liu et al., 2012). On *X. laevis* oocytes expressing the rat ASIC1a channel DAU shows a potentiating effect on a pH 5.5-induced currents, causing the appearance of the second transient component (EC_{50} ~20 μM and n_H 1.8) (**Table 1**). DAU also inhibits SSD with an EC_{50} of ~140 μM and n_H of 0.8. As a result, DAU causes an acidic shift for both the pH-dependence activation curve and the SSD curve (see **Figures 1C, D**). In general, the mechanism of DAU action can be assumed as competition with protons for desensitization sites on the channel (Osmakov et al., 2019b).

(-)-Epigallocatechin Gallate

(-)-Epigallocatechin gallate (EGCG) is an ester of epigallocatechin and gallic acid contained in large quantities in green tea extract. EGCG exhibits pronounced antioxidant activity (Henning et al., 2005), capable to induce apoptosis and inhibit the growth of various types of cancer (Yang et al., 2009). EGCG blocks voltage-gated sodium channel currents at rat hippocampal CA1 neurons (active concentration >100 μM) (Deng et al., 2008) and inhibits the cardiac sodium channel $Nav_{1.5}$ with IC_{50} ~2,1 μM (Amarouch et al., 2020). On CHO cells expressing various isoforms of ASICs, it was shown that EGCG dose dependently and reversibly inhibits the amplitude of the pH 5.0-induced current of mouse ASIC3 with an IC_{50} of 13 μM (Yan et al., 2019). It should be noted that the specificity of the action was checked on isoforms belonging to different species, namely human ASIC1a, rat ASIC1b and 2a, and mouse ASIC3. Thus, this leaves open the question of the species specificity of the action of EGCG. A study of the structure–activity relationship showed that the presence of the gallate part, the presence of the 3-hydroxyl group on the pyrogallol part, and the chirality of the pyrogallol part play an important role in the activity of the molecule. In a hind paw licking test in mice, it was demonstrated that prior local administration of EGCG (100 μM) attenuates (0.6%) acetic acid induced pain-related behaviors (Yan et al., 2019).

Gastrodin

Gastrodin, a gastrodigenin glycoside, is the main bioactive component of the *Gastrodia elata Blume* orchid extract used in traditional Chinese medicine. Gastrodin is known to inhibit of

the M-type K^+ currents in neurons with IC_{50} 19.4 μM (Yang et al., 2019). It has anticonvulsant and analgesic properties alleviating migraine and trigeminal neuralgia, as well demonstrates a neuroprotective effect in ischemia (Kumar et al., 2013; Zeng et al., 2006). On rat DRG neurons, it was demonstrated that gastrodin reversibly and concentration dependently reduced the amplitude of pH 5.5-induced current with an IC_{50} of ~0.2 μM (**Table 1**). At the same time, like 5-CQA (see above), gastrodin in the presence of capsazepine (10 μM) reduces the sensitivity of neurons to various activating pHs but did not change the main parameters (pH_{50} and n_H) of the pH-dependence activation curve. In acid- and formalin-induced pain-related behaviors in rats, gastrodin, having previously been locally administered into the paw (up to concentration of 10 μM), shows analgesic and anti-inflammatory effects (Qiu et al., 2014).

Ligustrazine (Tetramethylpyrazine)

Ligustrazine, a member of the alkylpyrazine group, is a bioactive component found in the extract of the plant *Ligusticum chuanxiong* Hort., used in traditional Chinese medicine. Its neuroprotective, vasodilating, and cardioprotective effect has been described (Liu et al., 1990; Zhou et al., 2004; Cheng et al., 2007). Its inhibitory activity on L-type calcium current of myocytes with IC_{50} varied in 88.19–200 μM range depending to experimental conditions was found as well (Zou et al., 2001; Ren et al., 2012). Also in micromolar range ligustrazine inhibits the transient component of pH 5.0-induced current with an IC_{50} of ~270 μM (**Table 1**) in rat DRG neurons as well as decreases the number of action potentials evoked by acidosis. The specificity of ligustrazine pH-dependent inhibition was studied on CHO cells expressing various asic isoforms, and the following results were obtained: IC_{50} of 97 μM for ASIC1a, 62 μM for ASIC1b, 129.4 μM for ASIC2a, and 239.5 μM for the ASIC3 current. In this instance, ligustrazine does not change the channels' affinity to protons, but reduces their opening efficiency. Ligustrazine repressed the ST segment (at doses of 3 and 10 mg/kg) and coronary artery occlusion-related T-wave (at doses of 20 and 30 mg/kg) in rat angina models and inhibited the myocardial infarction at doses of 3 mg/kg, thus reducing the necrotic area. Ligustrazine also showed a significant analgesic effect in the acetic acid-evoked pain response in rats (Zhang et al., 2015).

Paeoniflorin

Paeoniflorin is a monoterpene glycoside. It is one of the main bioactive components in the root extract of the peony *Paeonia lactiflora*. Antidepressant-like, immunostimulating, anticancer, and pro-apoptotic effects have been shown for this compound (Chen et al., 2012; Hu et al., 2013; Qiu et al., 2013). Paeoniflorin produces an inhibition of L-type calcium current in NG108-15 cells with IC_{50} 14 μM (Tsai et al., 2005) and inhibits $Cav_{1.2}$ channels (the active concentration >50 μM) (Song et al., 2017). On rat pheochromocytoma cells, paeoniflorin demonstrates a cytoprotective effect. This effect is associated with ASICs' inhibition since paeoniflorin dose dependently blocks pH 6.0-induced currents (IC_{50} ~5 μM) and inhibited these channels' expression in the cells, which was estimated by both RT-PCR and ASIC-specific antibody labelling. As a result, it was found that the activity of paeoniflorin leads to increased autophagic degradation of α-synuclein and can serve as evidence of the participation of ASICs in the development of Parkinson's disease (Sun et al., 2011).

Quercetin

Quercetin is a pentahydroxyflavone widely distributed in many vegetables and fruits such as tomato, onion, citrus fruit, and a number of berries. It has anti-inflammatory, anticancer, cardio and neuroprotective, and antibacterial and antiviral properties (Anand David et al., 2016). It can inhibit heart $Na_{V1.5}$ channels with IC_{50} of 19.4 μM (Wallace et al., 2006) and activate vascular smooth muscle L-type calcium channels with EC_{50} ~5 μM (Saponara et al., 2002). On CHO cells expressing various isoforms of rat ASICs, quercetin was shown to equally inhibit pH-induced currents with an IC_{50} of 2.4, 1.3, and 1.8 μM for ASIC1a, ASIC2a, and ASIC3, respectively (**Table 1**). Quercetin prevents a pH 6.0-induced increase of intracellular Ca^{2+} concentration in HEK-293 cells and significantly reduces their mortality. A molecular docking approach with rat ASIC1a site-directed mutagenesis detected the possible involvement of the channels' central vestibule residues Arg369 and Glu416 in the interaction with quercetin (Mukhopadhyay et al., 2017).

Puerarin

The flavonoid consisting of C-glycosyl and hydroxyisoflavone parts is the main bioactive constituent of the leguminous plant *Pueraria lobata* (Willd.) Ohwi extract. Its pharmacological activity as an anti-inflammatory, analgesic, neuroprotective, anticancer, and antioxidant molecule is known (Zhou et al., 2014). Puerarin inhibits potassium channels $Kir_{2.1}$ (IC_{50} 1.27 mM) and $Kv_{7.1}$ (IC_{50} ~55 μM) (Xu H. et al., 2016), and the resting Na_v channels of DRG neurons (IC_{50} 481 μM) (Zhang et al., 2019). Studies on rat hippocampal cells, as well as on CHO cells expressing ASIC1a, showed that puerarin has an inhibitory effect with IC_{50} and nH values of 38.4 μM and 5.97 (hippocampal cells) as well as 9.31 μM and 8.18 (CHO cells) (**Table 1**). Moreover, acceleration of desensitization in the presence of puerarin was observed in both systems because cytoprotector puerarin (100 μM) significantly reduces the mortality of hippocampal neurons exposed to the acidic (pH 6.0) solution (Gu et al., 2010).

Thalassiolin B

Another flavonoid consisting of chrysoeriol and O-glycosyl sulfate moieties abundantly presented in the sea grass *Thalassia testudinum* extract. Thalassiolin B was initially known as the antioxidant (Regalado et al., 2009). Later, it was shown that thalassiolin B inhibits the transient component of the proton-induced current in rat DRG neurons with an IC_{50} of 27 μM (**Table 1**). In a formalin test in mice, thalassiolin B (100 mmol/kg) alleviated pain behavior, reducing the number of licks during the first- and second-phase nociception (Garateix et al., 2011).

Salicylic Acid

Salicylic acid, or 2-hydroxybenzoic acid, is an important signaling component in plant immunity (Marek et al., 2010). This compound is well known for its anti-inflammatory, topical antibacterial, and cosmetic properties (Arif, 2015). It was shown that salicylic acid is able to inhibit the sustained component of current through ASIC3 channels expressed in COS cells with an IC_{50} of 260 μM, as well as the ASIC3/ASIC2b heteromeric current at a concentration of 500 μM (**Table 1**) (Voilley et al., 2001).

Sevanol

Sevanol (or 9,10-diisocytril ester of epiphylic acid) belongs to the group of polyphenolic compounds called lignans. Sevanol was isolated from an acetic acid extract of *Thymus armeniacus*, whereas it was absent in extracts of other representatives of this genus (Osmakov et al., 2015). On *X. laevis* oocytes expressing the human ASIC3 channel, it was shown that sevanol is able to inhibit both components of the ASIC3 current. The transient component of the current is completely inhibited (IC_{50} of 353 μM), whereas the sustained component is inhibited by only 45% (IC_{50} of 234 μM) (**Table 1**). Sevanol also inhibits the rat ASIC1a channel but with less efficacy (Dubinnyi et al., 2012). In models of acetic acid-induced writhing and CFA-induced thermal hyperalgesia tests, sevanol showed dose-dependent (range from 0.001 to 10 mg/kg), pronounced analgesic and anti-inflammatory effects (Andreev et al., 2018).

Morphine

Morphine—a morphinane alkaloid and a tertiary amino heteropentacyclic compound—is the most abundant opiate of the opium poppy (Papaver plant). It is well known as an analgesic, anxiolytic, and vasodilator drug with a number of serious side effects (including addiction) that are a result of its action on opiate receptors (Pathan and Williams, 2012). Studies on rat DRG neurons in the presence of capsazepine showed that morphine reversibly and dose dependently inhibits the pH-induced currents of ASICs with an IC_{50} of 2.3 μM (**Table 1**). The pH dependence of activation does not change significantly in the presence of morphine. Further pharmacological analysis showed that the effect of morphine on neurons is mediated by μ-opioid receptors and depends on the cAMP signaling pathway. In an acid-induced pain test on rats, preliminary local administration of 1–10 μM morphine causes a significant decrease in the number of flinches of the hind paw, but this analgesic effect disappears in the presence of an opioid receptor-inhibitor naloxone (Cai et al., 2014). Morphine can also be synthesized in mammals (Poeaknapo et al., 2004), and it was shown that intermediates in this synthesis pathway—isoquinoline alkaloids tetrahydropapaveroline and reticuline—can directly potentiate ASIC3 channels (Osmakov et al., 2017).

Sinomenine

Sinomenine, by the chemical structure related to the family of morphinane alkaloids, is one of the main biologically active components of the extract of the medicinal plant *Sinomenium acutum*. It has been shown that sinomenine possessed an anti-inflammatory function and regulated the secretion of multiple inflammatory cytokines and monocyte/macrophage subsets (Liu et al., 2018), and it has also been used in the clinic for the treatment of rheumatoid arthritis (Xu et al., 2008). On rat cortical neurons, as well as on CHO cells expressing recombinant channels, it was shown that sinomenine directly and dose dependently inhibits ASIC1a channels with an IC_{50} of ~0.3 μM (**Table 1**). Sinomenine (1 μM) significantly reduces 30 mM KCl, and acidosis-induced increases in intracellular Ca^{2+} concentration, suggesting the inhibitory effect of sinomenine on L-type calcium channels. In the cerebral ischemic insult model, sinomenine exerted a neuroprotective effect and improved brain functional recovery (Wu et al., 2011).

Microbial Compounds

Aminoglycosides (Streptomycin, Neomycin, and Gentamicin)

Aminoglycosides are a group of broad-spectrum antibiotics that exhibit bactericidal action by inhibiting protein biosynthesis. Their structure is based on amino sugars linked together, as well as with aminocyclitol rings, *via* a glycosidic bond (Krause et al., 2016). They also showed a blocking effect on Na^+- and Ca^{2+}-channels (Zhou and Zhao, 2002), as well as on transient receptor potential V1 (TRPV1) channels (Raisinghani and Premkumar, 2005). In DRG neurons, streptomycin (ST) and neomycin (NEO) reversibly but not completely decrease the amplitude of pH 6.1-induced currents with IC_{50} ~30 μM and n_H 1.3 for ST and IC_{50} ~45 μM and n_H 1.7 for NEO (**Table 1**. In this case, ST and NEO, as well as gentamicin, have a slowing effect on the desensitization process, and this effect is enhanced with a decrease in the concentration of Ca^{2+} ions in the extracellular medium. On HEK-293 cells expressing human ASIC1a, only ST shows an incomplete inhibitory effect, without acting, however, on the kinetics of desensitization (Garza et al., 2010).

Animal Venom Toxins

To date, ASIC peptides' modulators have been extracted from the venoms of spiders, snakes, sea anemones, and wasps. Taken together they differ in structure, subtype specificity, and the mode of action onto the channels. Although many of the toxins are not highly specific to ASICs over other cellular targets, a lot of them have adequate affinity for these ion channels. Even if the measured affinity to the channel/receptor is in the micromolar range, this does not exclude such molecules from the list of promising drug seeds (Kozlov, 2018).

RF-Amide Peptides

Cono-RFamides (CNFs) are a group of amides, isolated from cone snails' venom, with particular characteristics: the short length, the *C*-terminal Arg–Phe–NH_2 (RFa) motif, and the lack of cysteine residues (linear peptide) (**Figure 5**). Natural analogues with non-amidated *C*-terminus detected in venoms were inferior in their ability to potentiate ASIC channels.

Two conorfamides As1a and As2a and their non-amidated forms As1b and As2b from *Conus austini* differ by the mutation in the third residue (Lys in As1a and As1b, Arg in As2a, As2b). It

was shown that these compounds modulate proton-induced rat ASIC1a and ASIC3 currents by slowing channel desensitization following a sustained current inducing but they have no effect on homomeric rat ASIC1b or ASIC2a, expressed in *X. laevis* oocytes (Jin et al., 2019). Amidation of *C*-termini is essential for the peptide activity, since non-amidated As1b and As2b show only weak inhibition of transient currents. The most active As2a potentiates ASIC1a with an EC_{50} of 10.9 μM by the mechanism of the shift of the channel-desensitization constant (gray curve on the **Figure 1A**), and the resulting current has an unusual shape with a large amplitude. Similarly, this peptide affects the ASIC3 subtype. The second interesting peptide As1a, up to 200 μM, has a moderate effect on the sustained current generation for rASIC1a and rASIC3.

Another group of CNFs isolated from the venom of *Conus textile* is represented by three peptides (Tx1.1, Tx1.2, Tx1.3) consisting of 4, 6, and 8 amino acid residues, respectively. These CNFs show effects on ASIC3 currents like As2a peptide but also increase the transient current amplitude. The shortest peptide (CNF-Tx1.1) also potentiates the currents of heterotrimers ASIC1a/3, ASIC1b/3, ASIC2a/3, and ASIC2b/3 and has a higher affinity to homotrimer than CNF-Tx1.2. The potentiating effect of CNF-Tx1.1 is implemented by several mechanisms: shifts proton affinity of ASIC3 to higher pH for potentiation (green curve on the **Figure 1D**); lowers pH for desensitization (green curve on the **Figure 1C**); and increases the transient current amplitude 1.48-fold (blue curve on the **Figure 1D**). Intramuscular injection of this CNF in mice increases acid-induced muscle pain (Reimers et al., 2017).

Linear peptides that activate ASIC are not only found in marine snail venoms. Recent studies have described RF-amide modulators of ASICs in wasp venom. Peptide Sa12b extracted from the venom of solitary wasp *Sphex argentatus argentatus* reversibly and pH-independently inhibits the ASIC currents of rat DRG neurons with an IC_{50} ~81 nM when it is applied before the activation stimulus. Peptides' co-application with stimulus does not produce any significant alteration in acid-induced currents, which indicates the peptides binding with the channel closed state. In the same work another peptide Sh5b with a very similar structure (**Figure 5**), purified from the venom of wasp *Isodontia harmandi*, changes the ASIC current parameters in DRG neurons insignificantly (Hernández et al., 2019).

FIGURE 5 | RF-amide peptides family. The same residues are highlighted in green, negatively charged residues Asp and Glu are written in blue, and positively charged residues Lys and Arg are written in red.

Polypeptide Toxins

Polypeptide animal toxins are able to modulate the activity of ASICs with higher affinity at nanomolar concentrations. Historically, two toxins, psalmotoxin (PcTx1) and APETx2, became the basis of numerous scientific works in which they were used as molecular tools to study the function of ion channels ASIC1 and ASIC3 in living organisms. Later, other toxins were discovered, but so far all of them have been isolated from venomous animals such as spiders, sea anemones, and snakes. Toxins differ in their size and spatial organization, which was obtained by the NMR technique as a solution for a number of polypeptide toxins (**Figure 6**), as well as by X-ray structural analysis in the complex with cASIC1a (see section below).

PcTx1-Related Toxins

A 40-amino-acid-long peptide Psalmotoxin 1, isolated from the spider *Psalmopoeus cambridgei*, shares the folding named «inhibitor cystine knot» (ICK), which is a structural motif characterized by a triple-stranded anti-parallel β-sheet connected by three disulfide bonds forming a knotted core (**Figure 6**). This ICK motif is a major type of spider toxin organization, so distribution of the Cys residues like those presented in (**Figure 7**) is utilized for toxins' prediction from modern big data (Kozlov et al., 2005; Kozlov and Grishin, 2011).

PcTx1, a highly basic polypeptide (pI 10.38), was discovered as the first high-affinity and highly selective pharmacological agent to ASIC1a (Escoubas et al., 2000). PcTx1 acts like a selective reversible inhibitor of rat ASIC1a currents (IC_{50} of 0.9 nM), fully blocking it at 10-nM peptide concentration (Escoubas et al., 2000), and of human ASIC1a (IC_{50} of 3.2 nM) (Cristofori-Armstrong et al., 2019). The inhibition mechanism of PcTx1 is increasing its apparent affinity for H^+ through the desensitization of the channel (red curve on the **Figure 1C**) (Chen et al., 2005). It also inhibits mouse ASIC1a/2b (IC_{50} of 2.64 nM) (Sherwood et al., 2011) and rat ASIC1a/2a (Joeres et al., 2016). At the same time, PcTx1 potentiates the ASIC1b isoform with an EC_{50} of ~100 nM (Chen et al., 2006). This toxin has been used many times to study the properties of channels from wild neurons and heterologously expressed channels. In particular, interesting results were obtained in showing that ASIC1a subtypes play an important role in retinal activity (Ettaiche, 2006). Also, due to the successful selective inhibition of the ASIC1a subtype, it was shown that ASIC1b is involved in the development of muscle pain (Chang et al., 2019) and that the ASIC3 subtype is responsible for postoperative pain (Deval et al., 2011).

One more ASIC-active toxin that has an 82% resemblance to PcTx1 (shortened at three *C*-terminal residues and five residues substitution) was named π-TRTX-Hm3a (Hm3a). It was extracted from the venom of a Togo starburst tarantula (*Heteroscodra maculata*) (Er et al., 2017). In general, Hm3a shares the pharmacological profile of PcTx1. It inhibits acid-

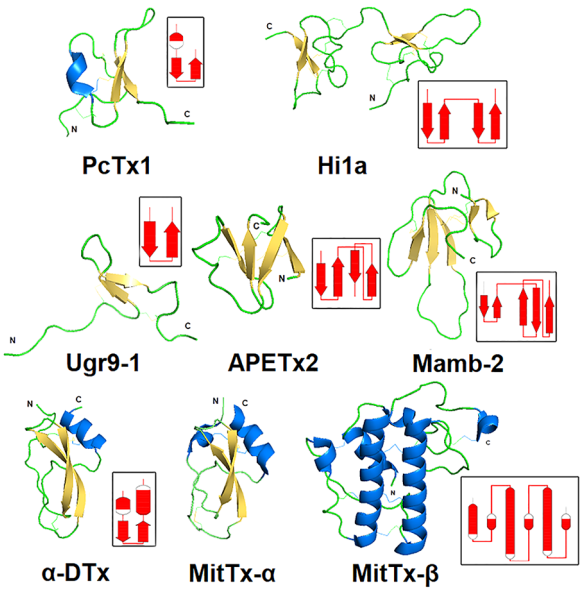

FIGURE 6 | Spatial structure of animal polypeptide toxins. The structures drawn according to the following PDB data: PcTx1 (2KNI), Hi1a (2N8F), Ugr9-1 (2LZO), APETx2 (2MUB), Mamb-2 (2MFA), α-DTx (1DTX), and MitTx-α, MitTx-β (4NTW). The distribution scheme of the secondary structure elements for each toxin is shown next to the 3D structure as an inset.

evoked currents of rASIC1a expressed in *X. laevis* oocytes, with an IC_{50} of 2.6 nM. It potentiates currents of homomeric rASIC1b and heteromeric rASIC1a/ASIC1b with an EC_{50} of 46.5 and 17.4 nM, respectively. This peptide does not show any effect on homomeric rASIC2 or rASIC3. Hm3a also inhibits human ASIC1a (IC_{50} of 39.7 nM) and potentiates human ASIC1b (EC_{50} of 178.1 nM), being ~30-fold and ~3.8-fold less potent to rat isoforms respectively. It was shown that Hm3a is more stable and resistant to thermal, chemical, and enzymatic degradation than PcTx1, becoming a more attractive tool for studying ASICs *in vivo* (Er et al., 2017).

A disulfide-rich polypeptide Hi1a consisting of 75 residues was found in the venom of the Australian funnel-web spider *Hadronyche infensa*. The structure represents two PcTx1-like ICK domains with a short linker connecting them. The *N*- and *C*-terminal moieties have 62 and 50% similarity to the PcTx-1 sequence, respectively, leading to a suggestion that this peptide originated through duplication of a gene encoding PcTx1-like toxin (Chassagnon et al., 2017). Hi1a equipotent inhibits rat and human ASIC1a expressed in *X. laevis* oocytes (IC_{50} of 0.40 and 0.52 nM, respectively), but unlike PcTx1, it does this incompletely even at saturating peptide concentrations. Inhibition of the rASIC1a subtype is more than 2,000 times more potent over other subtypes, with the toxin having no effect on rASIC2a and rASIC3 up to 1 μM and weakly potentiating rASIC1b. Toxin Hi1a has slow current-inhibition reversibility (τ_{off} = 14.2 min for rASIC1a, 31.8 min for hASIC1a after application 10 nM of Hi1a), with ~40% recovery of the current amplitude after a 30-min washout, which was not reported for any ASIC modulators before. Moreover, Hi1a shows less pH-dependent inhibition, which means a small acidic shift (0.18 pH units at 5 nM for hASIC1a) in contrast to PcTx1. *In vitro* tests on primary oxidatively stressed neuron/astrocyte cultures and *in vivo* tests on a rat-focal cerebral ischemia model showed even greater neuroprotective efficacy of Hi1a over PcTx1 (Chassagnon et al., 2017).

This structural group also includes the ICK cnidarians peptide PhcrTx1 purified from the sea anemone *Phymanthus crucifer*. Like PcTx1, this toxin is a basic peptide (pI = 10.89), but its overall homology with PcTx1 is a negligible (only 28%). The peptide reversibly inhibits the transient component of pH 6.1-induced ASIC currents in rat DRG neurons with IC_{50} ~100 nM without significantly affecting the time course of desensitization and with no effect on the sustained component (Rodríguez et al., 2014).

APETx2-Related Toxins

Currently, five peptide modulators of ASICs attributed to the structural class 1b of sea anemone toxins (Kozlov and Grishin, 2012) have been described (**Figure 8**). Polypeptide APETx2 isolated from the venoms of the sea anemones *Anthopleura elegantissima* was positioned for a long time as the specific inhibitor of the ASIC3 subtype. The structure of this small 42-amino-acid-long polypeptide has a large number of positively charged amino acid residues like PcTx1 (pI = 9.59). According to the 3D structure resolved by the NMR technique, APETx2 is a β-defensin-like peptide consisting of a compact disulfide-bonded core from a four-stranded beta-sheet, cross-linked by three disulfide bridges (**Figure 6**) (Chagot et al., 2005).

APETx2 rapidly and reversibly blocks homotrimeric ASIC3 and heterotrimeric channels containing ASIC3 without any effect on homomeric ASIC1a. The IC_{50} values are 63 nM for rASIC3 expressed in *X. laevis* oocytes and 175 nM for human ASIC3

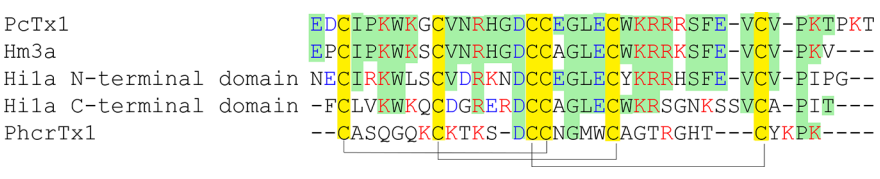

FIGURE 7 | Alignment of primary structures of PcTx1-like toxins. Cysteine residues are highlighted in yellow, and lines represent disulfide bridges' formation. The sequence residues similar to PcTx1 are highlighted in green, negatively charged residues Asp and Glu are written in blue, and positively charged residues Lys and Arg are in red.

expressed in COS cells. Heteromeric ASIC1a/3 and ASIC1b/3 in COS cells are also inhibited by APETx2 but with less affinity (IC_{50} of 2 and 0.9 μM, respectively). The ASIC1a/3 current can only be partly inhibited (~60% by 3 μM concentrations of APETx2). A better result was obtained for ASIC2b/3 heteromers, and the transient current of which was inhibited to approximately 36% of the control amplitude with an IC_{50} of 117 nM (Diochot et al., 2004; Logashina et al., 2020). It was shown that APETx2 potentiates the activity of rASIC1b at concentrations 30- to 100-fold higher than it inhibits rASIC3 homomers, causing an increased current's desensitization, with no effect on the rise time. Moreover, APETx2 potentiates rASIC2a currents using a different method (decrease in the current rise time, with no effect on desensitization time). In both cases, APETx2 appears to provide stabilization of the open state for rASIC1b and rASIC2a (Lee et al., 2018). Furthermore, the toxin weakly inhibits different potassium channels and TTX-resistant currents of DRG neurons (Diochot et al., 2004; Blanchard et al., 2012) but can reduce the $Na_{V1.2}$ and $Na_{V1.8}$ current in oocytes above 50% in nanomolar concentrations (IC_{50} of 114 nM for $Na_{V1.2}$ and 55 nM for $Na_{V1.8}$) (Peigneur et al., 2012). At micromolar concentrations, APETx2 inhibits hERG (IC_{50} of 1.21 μM) reversible with a maximal inhibition of 54%, and this experimental fact would seriously limit its potential as an analgesic (Jensen et al., 2014).

In the venom of the sea anemone *Heteractis crispa*, several toxins were found with related structures to APETx2 and inhibitory activity to ASICs (**Figure 8**). Between themselves, the similarity of these toxins is high (1–9 substitutions from 41 total residues), but their activity to two main isoforms ASIC1a and ASIC3 is different. The most represented in venom peptide π-AnmTX-Hcr1b-1 reversibly inhibits transient component of human ASIC3 currents expressed in *X. laevis* oocytes with an IC_{50} of 5.5 μM (Kozlov et al., 2012). Otherwise, Hcr1b-2 inhibits currents through rat ASIC1a (IC_{50} of 4.8 μM) more prominently than ASIC3 currents (IC_{50} of 15.9 μM). Such possibilities in the reduction of ASIC3 activity in PNS and ASIC1a activity in CNS make this peptide the prospective candidate for analgesia investigation, and Hcr1b-2 showed an analgesic activity *in vivo*, significantly reducing the number of writhing of experimental animals in acetic acid-induced writhing test (Kalina et al., 2018). The peptide Hcr 1b-3, having one residue substitution to the Hcr1b-2 sequence, keeps the same effectiveness for ASIC1a and ASIC3 inhibition with an IC_{50} of 4.95 μM and 17 μM, respectively. The more structurally diverse toxin Hcr1b-4 is capable of inhibiting the rASIC1a with an IC_{50} of 1.25 μM, but with the same potency of EC_{50} of 1.53 μM, it potentiates rASIC3 currents (Kalina et al., 2020). The diverse activity of Hcr1b-4 for two different ASIC isoforms with apparently the same affinity makes it a very interesting tool for structural and bimolecular research.

Toxin Ugr 9-1

Peptide π-AnmTXUgr 9a-1 (Ugr 9-1) isolated from the venom sea anemone *Urticina grebelnyi* consists of 29 amino acid residues and belongs to a structural class 9a (Kozlov and Grishin, 2012). Its spatial structure named "boundless β-hairpin" (BBH) was resolved (**Figure 6**). It is a twisted β-hairpin without interstrand disulfide bonds connected by two S-S bridges, with *C*- and *N*-terminal tails. The peptide shows the reversible inhibition effect on human ASIC3 expressed in *X. laevis* oocytes. It completely blocks the transient component with an IC_{50} of 10 μM, and only by 48% inhibits the sustained component with an IC_{50} of 1.44 μM (Osmakov et al., 2013). Intramuscular or intravenous injection of Ugr 9-1 (0.01–1 mg/kg) produced a significant analgesic effect in the acid-induced pain model and the complete Freund's adjuvant-induced thermal hyperalgesia test (Osmakov et al., 2013; Andreev et al., 2018).

Snake Toxins

Various by structure snake toxins are able to modulate the activity of ASICs. Only a limited number of species produce toxins affecting proton-activated ion channels, and it is obvious that these channels are not primary target for their venom action. The sequences of all currently known toxins are summarized in **Figure 9**, while the spatial organization of toxins is shown in **Figure 6**.

One group of polypeptides was extracted from the venoms of different poisonous snakes. These include mambalgin-1 and mambalgin-2 isolated from the venom of the black mamba *Dendroaspis polylepis*, as well as mambalgin-3 from the venom of the green mamba *Dendroaspis angusticeps*. Toxins utilized a very common fold for snake venom compounds called three-finger toxins, and they contain 57 amino acid residues and 4 disulfide bonds. The sequences of peptides are identical and differ in one residue substitution (mamb-1 to mamb-2/Tyr to Phe in 4th position and mamb-1 to mamb-3/Thr to Ile in 23rd position) (Diochot et al., 2012). According to the authors, despite the similar core, the structure of mamb-2 stands out amongst common short three-finger toxins of a snake as a result of its

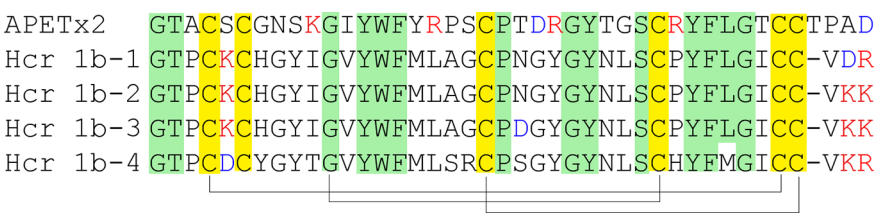

FIGURE 8 | Alignment of primary structures of APETx2-like toxins. Cysteine residues are highlighted in yellow, and lines represent disulfide bridges' formation. The residues similar to APETx2 structure are highlighted in green, negatively charged residues Asp and Glu are in red, and positively charged residues Lys and Arg are in blue.

shortened first and third fingers and elongated middle finger. Mambalgin-1 and mambalgin-2 reversibly inhibit homomeric rASIC1a and heteromeric rASIC1a/2a and rASIC1a/2b expressed in *X. laevis* oocytes with an IC_{50} of 55, 246, and 61 nM, respectively. They act as a gating modifier toxin by decreasing the apparent proton sensitivity of activation (red curve on the **Figure 1D**) and by slightly increasing the apparent proton sensitivity for inactivation (red curve on the **Figure 1C**) (Diochot et al., 2012). Also, they inhibit rASIC1b and rASIC1a/1b with an IC_{50} of 192 and 72 nM, respectively. These peptides inhibit human ASIC1a (IC_{50} of 127–580 nM) (Wen et al., 2015). In addition, it was shown that they inhibit ASIC currents in the spinal cord and sensory and hippocampal neurons but that mambalgins lack any effect on ASIC2a, ASIC3, ASIC1a/3, and ASIC1b/3 (Diochot et al., 2012).

The double-chain toxin MitTx was isolated from the venom of the Texas coral snake (*Micrurus tener tener*). Two non-covalently associated subunits of Kunitz-type protease inhibitors MitTx-α and phospholipase-A2-like MitTx-β are combined in one active molecule to function as a strong and selective agonist for ASICs. The current induced by the toxin is not desensitized but is inhibited by ASICs' selective inhibitors. The selectivity of MitTx depends on pH, whereas at the neutral pH values, the toxin potentiates the predominant ASIC1 subtype but changes selectivity towards ASIC2a at a pH below 6.5. For the homomeric channels expressed in *X. laevis* oocytes, EC_{50} of 9.4 nM for rat ASIC1a, 23 nM for rat ASIC1b, 36 nM for rat ASIC2a, and 830 nM for rat ASIC3 were calculated. It did not show any effect on 2b or 4 subtypes. Heteromeric rASIC1a/2a and rASIC1a/3 expressed in CHO cells are only mild and weakly activated (Bohlen et al., 2011). Injection into the hind paw of wild-type mice resulted in a painful sensation determined by licking the paw. The time of licking was reduced in ASIC1a-knockout mice, meaning that pain-related behavior was mostly linked to the interaction of the toxin with this channel subtype (Bohlen et al., 2011).

One more toxin with Kunitz-type protease inhibitors fold - α-dendrotoxin (α-DTx) is also ASICs modulating peptide. Similar to mambalgin-3, this toxin was isolated from the Eastern green mamba *Dendroaspis angusticeps*, and its main biological targets are voltage-gated potassium channels (specifically of $Kv_{1.1}$, $Kv_{1.2}$ and $Kv_{1.6}$ with IC_{50} of 9.4, 0.38, and 9 nM, respectively) (Tabakmakher et al., 2019). In contrast to MitTx described above, α-DTx reversibly inhibits the transient component of pH 6.1-induced ASIC currents in rat DRG neurons with an IC_{50} of 0.8 μM without remarkable impact on the current desensitization rate, and at 3 μM concentration, α-DTx also inhibits the sustained component (Báez et al., 2015).

STRUCTURE–FUNCTION RELATIONSHIPS IN PEPTIDE TOXINS AND ASICS

There are several structures of the cASIC1a complexes with different peptide ligands playing the role of agonists, inhibitors, and modulators (Jasti et al., 2007; Gonzales et al., 2009; Baconguis and Gouaux, 2012; Dawson et al., 2012; Baconguis et al., 2014; Sun et al., 2018; Yoder et al., 2018). In 2012, two separate groups from Switzerland and the USA published the structures of the cASIC1a complex with PcTx1 (Baconguis and Gouaux, 2012; Dawson et al., 2012). According to their studies, three molecules of PcTx1 bind to cASIC1a at the interfaces of two subunits about 45-50 Å above the membrane bilayer (**Figures 10A, B**). The binding is bimodal: by a hydrophobic patch and basic cluster of the toxin. The hydrophobic patch formed by Trp24, Trp7, Phe30, Val32, Val34, and Pro35 wraps around the thumb domain helix5, whereas the basic cluster formed by Arg26, Arg27, and Arg28 merges into the acidic pocket in contact with Asp350, Asp238, and Glu220, as well as with the palm domain of the adjacent subunit. Thus, PcTx1 simultaneously interacts with the palm, finger, and thumb domains of the channel and blocks their relative arrangement in the desensitized-like state (Baconguis and Gouaux, 2012; Dawson et al., 2012). Alanine-scanning mutagenesis of PcTx1 also showed that residues Trp7, Trp24, Arg26, Arg27, Arg28, and Phe30 are important for interaction with rat ASIC1a (Saez et al., 2015) (**Figures 11** and **12**). Due to the similarity of two Hi1a domains to PcTx1, it was obviously to study the effects of *N*- and *C*-terminal domains individually on ASIC1a (**Figure 12**). It was shown that, in contrast to native Hi1a, the *N*-terminal domain

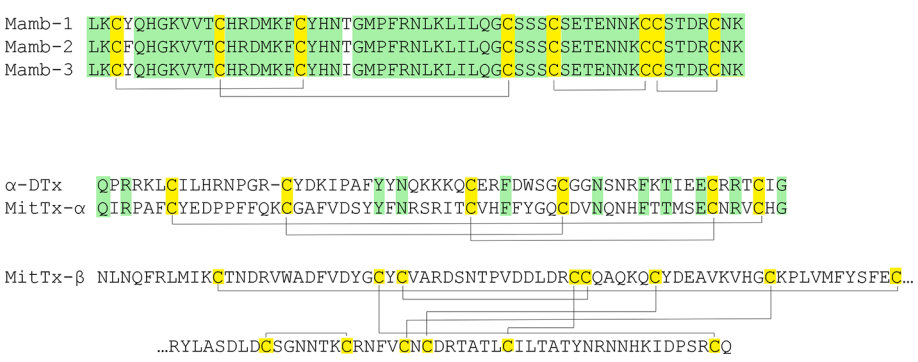

FIGURE 9 | Snake toxins active onto ASICs. Cysteine residues are highlighted in yellow, and lines represent disulfide bridges' formation. The similar residues are highlighted in green.

inhibits rASIC1a fully reversibly and much weaker (IC50 of 1.04 μM), whereas the *C*-terminal domain does not inhibit this channel subtype at all. *N*-terminal serine residues were vestiges of the fusion protein cleavage site (Chassagnon et al., 2017).

The crystal structure of the cASIC1a complex with MitTx revealed the open state of the channel (Baconguis et al., 2014). In this structure, each heterodimer of MitTx exclusively interacts with a single channel subunit forming the numerous contacts with the "wrist" region located near the membrane bilayer and with the β11-β12-linker by its α-subunit, as well as with the thumb domain located 60 Å above the membrane by the toxin's β-subunit (**Figures 10C, D**). Thus, the toxin has a protruding contact area with the channel, although without direct interaction with the acidic pocket. Comparison of the cASIC1a structure in the desensitized state with the structure of the cASIC1a/MitTx complex points to the significantly increased intersubunit distance in the last case with overall expansion of the extracellular vestibule and symmetric open pore (Baconguis et al., 2014). At the same time, the ion selectivity filter does not undergo serious conformational transformations indicating the spatial independence of the channel gate and ion selectivity filter.

A significantly different mechanism of possible ASIC regulation based on the cryo-EM structure of the complex cASIC1a/mambalgin-1 was suggested in 2018 (Sun et al., 2018). In spite of a low resolution of the obtained structure (5.4 Å) without the ability to resolve the TM domain structure, a new mode of a peptide interaction with ASIC1a was revealed. It was shown that three molecules of mambalgin-1 bind to individual subunits of the channel, mainly forming contacts between the first and second loops of peptide and the thumb domain (**Figures 10E, F**). The residues from the first loop of mambalgin-1 (Gln5, His6, Lys8) form electrostatic contacts with the α4-helix of the thumb domain, whereas the second loop interacts with the α5-helix of the thumb domain by electrostatic (Arg28, Lys31) and hydrophobic (Met25, Pro26, Phe27, Leu30, Leu32) contacts. Complex formation with mambalgin-1 changes the conformation of the thumb domain, shifting it away from the threefold molecular axis. It leads to expansion of the acidic pocket and as a result could trap the channel into the closed state. Thus, mambalgin-1 acts as an allosteric negative modulator. This mechanism was confirmed by site-directed mutagenesis and electrophysiology studies of the mambalgin-1 and cASIC mutants (Sun et al., 2018), and it principally differs from the earlier proposed mechanism based on the computational modeling and site-directed mutagenesis, where mambalgin-1 penetrated the acidic pocket and interacted with the thumb domain of rat ASIC1a exclusively by the residues from the

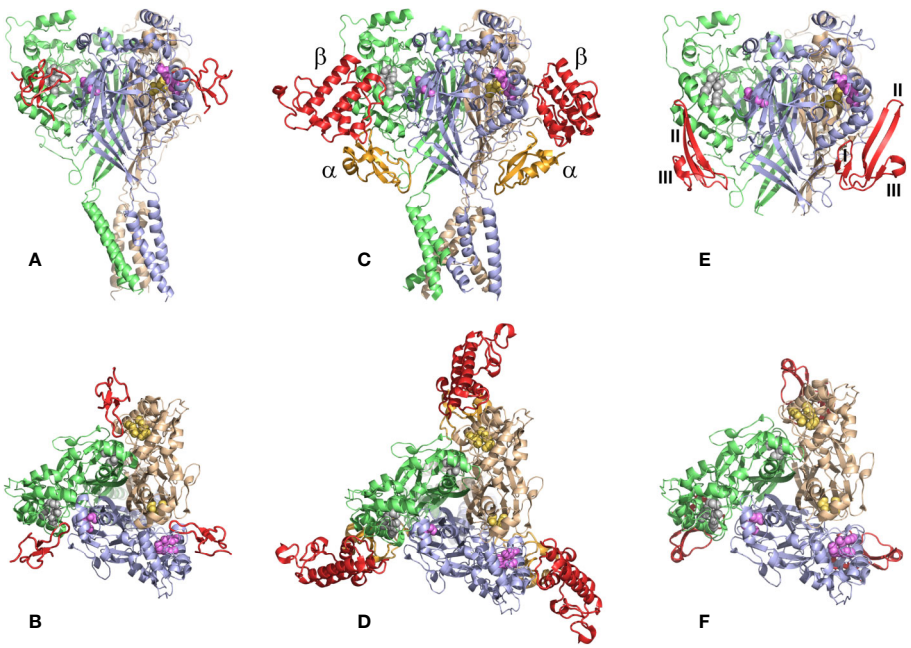

FIGURE 10 | The structures of the cASIC1a complexes with different peptide toxins. The channel subunits are shown by wheat, pale green, and blue colors. Asp and Glu residues forming the acidic pockets in corresponding subunits are shown by spheres colored in yellow, gray, and violet. **(A, B)** The side and top views of the complex cASIC1a/PcTx1 (PDB code 4FZ0). Toxins are shown using a red color. PcTx1 inserts its loop into the acidic pocket, simultaneously interacting with the finger and thumb domains of one channel subunit and the palm domain of adjacent subunit. **(C, D)** The side and top views of the complex cASIC1a/MitTx (PDB code 4NTW). Toxins' α and β subunits are colored light orange and red, respectively. α-Subunit interacts with the wrist region and β1-β2 and β11-β12 linkers, whereas the β-subunit binds to the thumb and finger domains without penetration into the acidic pocket. **(E, F)** The model of the complex cASIC1a/mambalgin-1 is built based on the cryo-EM density map (Sun et al., 2018), crystal channel structure (PDB code 4FZ1), and crystal mambalgin-1 structure (PDB code 5DU1). Mambalgin-1 is shown using a red color. Loops of the polypeptide are numbered, and the mambalgin-1 form the contacts with the thumb domain by the first and second loops without penetration into the acidic pocket.

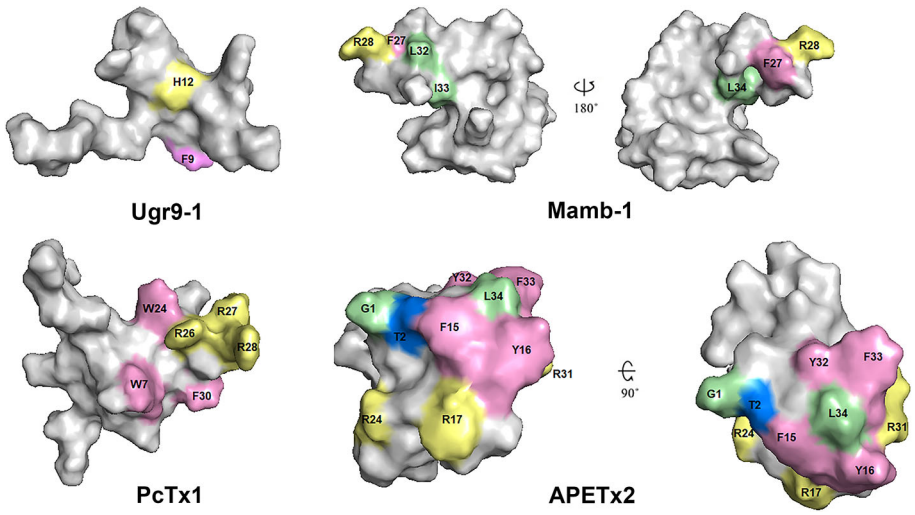

FIGURE 11 | Spatial structure of toxins Ugr9-1 (PDB 2LZO), Mamb-1 (PDB 5DZ5), PcTx1 (PDB 2KNI), and APETx2 (PDB 2MUB). Marked residues play an important role in the activity of toxins on ASICs in accordance with scanning mutagenesis experiments. Basic, aromatic, and hydrophobic residues are indicated by light yellow, light lilac, and light green colors, respectively.

FIGURE 12 | The influence of point mutation in polypeptide modulators on modulating activity to ASICs. Mutations without effect (green), medium affecting (yellow), and destroy the activity (orange) distributed in accordance with publications (references shown in picture). The decrease of mutants' functional activity as part of the wild-type peptide activity for each substitution is presented below as a number except for: X1, loss of ability to inhibit ASICs; X2, loss of ability to inhibit rASIC1a at low concentration and gain of function as a positive modulator at high concentrations (>100 nM); X3, 2,600-fold decrease in inhibition of rASIC1a, and inhibition becomes fully reversible; X4, important decrease in inhibitory potency on cASIC1a; X5 more than 100-fold decrease in ability to inhibit rASIC3; N1, small increase in inhibitory potency on cASIC1a.

second loop (Phe27, Arg28, Leu32, Ile33, and Leu34) (Mourier et al., 2016; Sun et al., 2018) (**Figures 11** and **12**).

Since the ASIC1 subunit shares quite a low sequence identity with ASIC2, ASIC3, and ASIC4 subunits, further functional and structural studies of other members of the ASIC family still have a high challenge and require additional data for understanding of the mechanisms of ion binding, channel gating, and modulation using different ligands. Accordingly, several research groups are working on identification of pharmacophores for that inhibit ASIC3 channels. For example, the importance of *N*-terminus and other residues of APETx2 for an interaction with the channel was revealed (**Figures 11** and **12**). Specifically, Gly1, Thr2, Phe15, Tyr,16, Arg17, Arg24, Arg31, Tyr32, Phe33, and Leu34 are crucial for the inhibition or interaction with rat ASIC3 (Chagot et al., 2005; Jensen et al., 2012; Jensen et al., 2014). As mentioned above, APETx2 also inhibits the off-target hERG channels, and according to the mutagenesis study, surfaces responsible for the effect of the toxin on hERG and ASIC3 partially overlap (Jensen et al., 2014).

Another ligand of the ASIC3 channels is the peptide Ugr 9-1 that is cleaved from the common precursor protein during their maturation together with highly homologous peptides without ASIC3 activity. Mutagenesis of these inactive homologs showed that the key residues in Ugr 9-1 important for interaction with ASIC3 are Phe9 and His12 (**Figure 11**) (Osmakov et al., 2016). Therefore, the basic aromatic cluster of APETx2 and Ugr 9-1 important for interaction with ASIC3 resembles the situation with PcTx1, whose interaction with ASIC1a is also bimodal (Baconguis and Gouaux, 2012).

PERSPECTIVES IN THERAPEUTIC DEVELOPMENT

ASICs being the most sensitive to pH-change channels are at the forefront in the detection of normal and pathological stimuli in the neurons and other cells. Moderate changes in pH, together with a variety of other signals, could be an important signal in normal function (rapid local acidification in synapses during neuronal activity) and a sign of various pathological conditions (ischemia, inflammation, and cancer) (Rash and Rash, 2017). Peptides from venomous animals that are able to inhibit the activation of ASICs or decrease their expression could be considered useful hits for therapy of pathological states. The most studied channels that evidently take part in different normal and pathological processes are ASIC1a and ASIC3, while the significance of other ASICs is less understood, but some of them are also considered suitable for drug development.

Intensive studies of different ASIC modulators and knockout mice disclosed the role of these channels (at least ASIC1a and ASIC3) in detection of acidosis-mediated pain (Rash and Rash, 2017). Several pro-inflammatory endogenous mediators affect ASICs function and potentiate their response to acidification (arachidonic acid and RF-amide peptides (Askwith et al., 2000; Allen and Attwell, 2002), spermine, dynorphins, and histamine for ASIC1a (Babini et al., 2002; Sherwood et al., 2009; Nagaeva et al., 2016), lactate and serotonin for ASIC3 (Immke and McCleskey, 2001), and nocistatine and endogenous isoquinoline alkaloids (Osmakov et al., 2017; Osmakov et al., 2019a). Expression of ASIC1a in DRG neurons is elevated during inflammation and unregulated by inflammatory mediators (Voilley et al., 2001; Mamet et al., 2002). ASIC1a channels in the spinal dorsal horn neurons contribute to inflammatory hypersensitivity to pain (Duan et al., 2007). ASIC3 channels are considered to play a significant role in the perception of external stimuli in free nerve endings. They are present in a most part of muscle afferents and in a significant part of DRG neurons (Molliver et al., 2005; Ikeuchi et al., 2009). The administration of animal toxins can cause significant anti-inflammatory and analgesic effects by inhibiting ASICs' function in PNS or/and CNS, as shown in the variety of animal models (Rash and Rash, 2017).

Peptide APETx2 was reported to produce a significant analgesic effect in several models of pain such as acid-induced pain, CFA-induced hyperalgesia, migraine-related pain, and postoperative pain (Karczewski et al., 2010; Deval et al., 2011; Callejo et al., 2015; Andreev et al., 2018; Lee et al., 2018; Holton et al., 2020). However, it should be taken into consideration that the ability of APETx2 to affect various subtypes of ASICs and several voltage-gated channels (as discussed above) limits connection between the effects of this peptide *in vivo* with ASIC3 function. Nevertheless, more selective to ASIC3, animal toxin Ugr 9-1 significantly reduces inflammatory and acid-induced pain at doses 0.01–1 mg/kg after intravenous or intramuscular administration (Osmakov et al., 2013; Andreev et al., 2018). Sevanol, the compound isolated from thyme, revealed high analgesic activity and was even more effective than peptide inhibitors of ASIC3, as was shown in a comparative study (Andreev et al., 2018). Sevanol efficacy could be a result of its ability to inhibit both components of the ASIC3 current and its additional ability to inhibit ASIC1a. Mambalgins are "multitarget" peptides from the venom of the black mamba and block heteromeric channels of ASIC1a and ASIC2a subunits in CNS neurons and ASIC1b-containing channels in peripheral sensory neurons. Mambalgins relieve the pain in several ways through inhibition of different subtypes of ASICs expressed both in central and peripheral neurons (Diochot et al., 2012; Diochot et al., 2016; Chang et al., 2019). Mambalgins intrathecal administration of ~340 pmol/mouse (~0.1 mg/kg dose) efficiently reduced different types of pain (e.g., acute heat pain, inflammatory hyperalgesia, formalin-induced pain) through an opioid-independent pathway involving ASIC1a and ASIC2a channels. Local injection of the same dose (~0.1 mg/kg) also produced a significant analgesic effect on acute heat pain and reversed carrageenan-induced inflammatory hyperalgesia *via* ASIC1b (Diochot et al., 2012). An intravenous administration 15-30 pmol/mouse (~0.005–0.01 mg/kg dose) of mambalgin-1 was reported to produce a significant analgesic effect in models of acid-induced mechanical hyperalgesia, thus confirming ASIC1b as a perspective pharmacological target on peripheral neurons (Chang et al., 2019).

ASICs play a significant role in a variety of processes in CNS, and the use of selective animal ligands helped to establish pharmacological perspectives of these channels' modulators. In CNS, ASIC1a was involved in synaptic plasticity and learning (Wemmie et al., 2002; Du et al., 2014), fear conditioning, and fear behaviors (Wemmie et al., 2003; Wemmie et al., 2004; Coryell et al., 2008; Ziemann et al., 2009; Wemmie et al., 2013). Pharmacological inhibition of ASIC1a by PcTx1 or genetic deletion of ASIC1a strongly reduced the death of neurons and therefore the infarct volume in the model of ischemic stroke (McCarthy et al., 2015), whereas enhanced ASIC1a activity promoted the neuronal injury during ischemia in the animal model (Duan et al., 2011). PcTx1, injected in CNS, provides activation of the endogenous enkephalin pathway and naloxone-sensitive analgesia (Mazzuca et al., 2007). Also, PcTx1 exhibits neuroprotection activity of the *substantia nigra* in a model of Parkinson's disease (Dwyer et al., 2009).

Low pH of extracellular environment and intracellular acidification accompanies tumor cell proliferation, metastasis, and tumor-related inflammation (Harguindey et al., 2017). Tumor cells express several pH-sensitive ion channels, including ASICs (Xu S. et al., 2016). Down-regulation of ASIC2a augments acidosis-mediated injury of C6 rat glioma cells (Liu et al., 2011). ASIC1a physically interacts with Ca^{2+}/calmodulin-dependent protein kinase II (CaMKII) and integrin-β1 (Xu S. et al., 2016), which are important regulators of intracellular signaling and adhesion. Thus, ASICs can influence glioblastoma cell proliferation by different mechanisms. In addition to gliomas, ASICs are involved in regulation of lung (Wu et al., 2017), and other carcinomas growth, migration, as well as drug resistance (Gupta et al., 2016; Zhang et al., 2017). In line with it, benzamil and PcTx1 demonstrated antiproliferative activity against glioblastoma cells (Rooj et al., 2012), and mambalgin-2 against leukemia cells (Bychkov et al., 2020).

It is an interesting fact that targeted screening of chemical libraries led to only several drug seeds. Some of them, such as A317567 and A317567-10b, exhibited low selectivity to ASICs (Dubé et al., 2005; Kuduk et al., 2010), whereas others possessed limited *in vivo* activity such as NS383 (Munro et al., 2016) and PPC5650 (Nielsen et al., 2015). The most probable way to solve this problem is the modification of natural compounds from plants such as lindoldhamine (Osmakov et al., 2018; Osmakov et al., 2019c), gastrodin (Qiu et al., 2014), sevanol (Dubinnyi et al., 2012; Osmakov et al., 2015), and chlorogenic acid (Qu et al., 2014), as well as some prospective synthetic molecules recently discovered such as CHF5074 (Mango et al., 2014). These scaffolds could be a basis for the creation of the ASIC-oriented chemical libraries for a directed drug development. Noteworthy that the most of natural small molecules affecting ASICs possess activity on other cellular targets including voltage-gated sodium, potassium, and calcium channels with a same effectiveness. Measured *in vivo* effect for these compounds is a combination of different targets regulation that could be beneficial (synergic) in some cases but could be a reason for unpredictable side effects.

Modern medicine is waiting for selective and biologically stable ASIC modulators for the treatment of a great variety of pathological conditions. ASIC inhibitors could serve as effective analgesic and anti-inflammatory drugs, as well as neuroprotective substances for reducing damage from ischemic or traumatic injury of the brain. Moreover, the ASICs channel could play a significant role in the progression of some tumors and could be considered an anticancer target (Bychkov et al., 2020). Further study of the involvement of ASICs in various physiological processes using well-known and new toxins will allow researchers to find new medical problems associated with these channels' functioning. We are convinced that natural compounds will always be extremely useful as tools for studies of animals' main physiological processes and necessarily as remedies for healthcare.

AUTHOR CONTRIBUTIONS

DO, TK, YA, and EL performed bibliography analysis. DO, TK, EL, and SK prepared the figures. DO, TK, YA, EL, and SK wrote the manuscript. SK and YA critically reviewed the manuscript.

FUNDING

The work was supported by the Russian Science Foundation (project # 19-74-20163).

REFERENCES

Agwa, A. J., Peigneur, S., Chow, C. Y., Lawrence, N., Craik, D. J., Tytgat, J., et al. (2018). Gating modifier toxins isolated from spider venom: Modulation of voltage-gated sodium channels and the role of lipid membranes. *J. Biol. Chem.* 293, 9041–9052. doi: 10.1074/jbc.RA118.002553

Alijevic, O., and Kellenberger, S. (2012). Subtype-specific Modulation of Acid-sensing Ion Channel (ASIC) Function by 2-Guanidine-4-methylquinazoline. *J. Biol. Chem.* 287, 36059–36070. doi: 10.1074/jbc.M112.360487

Allen, N. J., and Attwell, D. (2002). Modulation of ASIC channels in rat cerebellar purkinje neurons by ischaemia-related signals. *J. Physiol.* 543, 521–529. doi: 10.1113/jphysiol.2002.020297

Alvarez de la Rosa, D., Zhang, P., Shao, D., White, F., and Canessa, C. M. (2002). Functional implications of the localization and activity of acid-sensitive channels in rat peripheral nervous system. *Proc. Natl. Acad. Sci.* 99, 2326–2331. doi: 10.1073/pnas.042688199

Amarouch, M.-Y., Kurt, H., Delemotte, L., and Abriel, H. (2020). Biophysical Characterization of Epigallocatechin-3-Gallate Effect on the Cardiac Sodium Channel Nav1.5. *Molecules* 25, 902. doi: 10.3390/molecules25040902

Anand David, A., Arulmoli, R., and Parasuraman, S. (2016). Overviews of biological importance of quercetin: A bioactive flavonoid. *Pharmacogn. Rev.* 10, 84. doi: 10.4103/0973-7847.194044

Andreev, Y., Osmakov, D., Koshelev, S., Maleeva, E., Logashina, Y., Palikov, V., et al. (2018). Analgesic Activity of Acid-Sensing Ion Channel 3 (ASIC3) Inhibitors: Sea Anemones Peptides Ugr9-1 and APETx2 versus Low Molecular Weight Compounds. *Mar. Drugs* 16, 500. doi: 10.3390/md16120500

Arif, T. (2015). Salicylic acid as a peeling agent: a comprehensive review. *Clin. Cosmet. Investig. Dermatol.* 26, 455–461. doi: 10.2147/CCID.S84765

Askwith, C. C., Cheng, C., Ikuma, M., Benson, C., Price, M. P., and Welsh, M. J. (2000). Neuropeptide FF and FMRFamide Potentiate Acid-Evoked Currents from Sensory Neurons and Proton-Gated DEG/ENaC Channels. *Neuron* 26, 133–141. doi: 10.1016/S0896-6273(00)81144-7

Askwith, C. C., Wemmie, J. A., Price, M. P., Rokhlina, T., and Welsh, M. J. (2004). Acid-sensing Ion Channel 2 (ASIC2) Modulates ASIC1 H + -activated Currents in Hippocampal Neurons. *J. Biol. Chem.* 279, 18296–18305. doi: 10.1074/jbc.M312145200

Báez, A., Salceda, E., Fló, M., Graña, M., Fernández, C., Vega, R., et al. (2015). α-Dendrotoxin inhibits the ASIC current in dorsal root ganglion neurons from rat. *Neurosci. Lett.* 606, 42–47. doi: 10.1016/j.neulet.2015.08.034

Babini, E., Paukert, M., Geisler, H.-S., and Gründer, S. (2002). Alternative Splicing and Interaction with Di- and Polyvalent Cations Control the Dynamic Range of Acid-sensing Ion Channel 1 (ASIC1). *J. Biol. Chem.* 277, 41597–41603. doi: 10.1074/jbc.M205877200

Baconguis, I., and Gouaux, E. (2012). Structural plasticity and dynamic selectivity of acid-sensing ion channel–spider toxin complexes. *Nature* 489, 400–405. doi: 10.1038/nature11375

Baconguis, I., Bohlen, C. J., Goehring, A., Julius, D., and Gouaux, E. (2014). X-Ray Structure of Acid-Sensing Ion Channel 1–Snake Toxin Complex Reveals Open State of a Na+-Selective Channel. *Cell* 156, 717–729. doi: 10.1016/j.cell.2014.01.011

Baenziger, J. E., Morris, M.-L., Darsaut, T. E., and Ryan, S. E. (2000). Effect of Membrane Lipid Composition on the Conformational Equilibria of the Nicotinic Acetylcholine Receptor. *J. Biol. Chem.* 275, 777–784. doi: 10.1074/jbc.275.2.777

Blanchard, M. G., Rash, L. D., and Kellenberger, S. (2012). Inhibition of voltage-gated Na+ currents in sensory neurones by the sea anemone toxin APETx2. *Br. J. Pharmacol.* 165, 2167–2177. doi: 10.1111/j.1476-5381.2011.01674.x

Bohlen, C. J., Chesler, A. T., Sharif-Naeini, R., Medzihradszky, K. F., Zhou, S., King, D., et al. (2011). A heteromeric Texas coral snake toxin targets acid-sensing ion channels to produce pain. *Nature* 479, 410–414. doi: 10.1038/nature10607

Boscardin, E., Alijevic, O., Hummler, E., Frateschi, S., and Kellenberger, S. (2016). The function and regulation of acid-sensing ion channels (ASICs) and the epithelial Na + channel (ENaC): IUPHAR Review 19. *Br. J. Pharmacol.* 173, 2671–2701. doi: 10.1111/bph.13533

Bychkov, M. L., Shulepko, M. A., Vasileva, V. Y., Sudarikova, A. V., Kirpichnikov, M. P., and Lyukmanova, E. N. (2020). ASIC1a inhibitor mambalgin-2 suppresses growth of leukemia cells by cell cycle arrest. *Acta Naturae* 12, 111–116 doi: 10.32607/actanaturae.10949

Cai, Q., Qiu, C.-Y., Qiu, F., Liu, T.-T., Qu, Z.-W., Liu, Y.-M., et al. (2014). Morphine inhibits acid-sensing ion channel currents in rat dorsal root ganglion neurons. *Brain Res.* 1554, 12–20. doi: 10.1016/j.brainres.2014.01.042

Callejo, G., Castellanos, A., Castany, M., Gual, A., Luna, C., Acosta, M. C., et al. (2015). Acid-sensing ion channels detect moderate acidifications to induce ocular pain. *Pain* 156, 483–495. doi: 10.1097/01.j.pain.0000460335.49525.17

Chagot, B., Escoubas, P., Diochot, S., Bernard, C., Lazdunski, M., and Darbon, H. (2005). Solution structure of APETx2, a specific peptide inhibitor of ASIC3 proton-gated channels. *Protein Sci.* 14, 2003–2010. doi: 10.1110/ps.051378905

Chang, C.-T., Fong, S. W., Lee, C.-H., Chuang, Y.-C., Lin, S.-H., and Chen, C.-C. (2019). Involvement of Acid-Sensing Ion Channel 1b in the Development of Acid-Induced Chronic Muscle Pain. *Front. Neurosci.* 13, 1247. doi: 10.3389/fnins.2019.01247

Chassagnon, I. R., McCarthy, C. A., Chin, Y. K.-Y., Pineda, S. S., Keramidas, A., Mobli, M., et al. (2017). Potent neuroprotection after stroke afforded by a double-knot spider-venom peptide that inhibits acid-sensing ion channel 1a. *Proc. Natl. Acad. Sci.* 114, 3750–3755. doi: 10.1073/pnas.1614728114

Chen, X., Kalbacher, H., and Gr̈nder, S. (2005). The Tarantula Toxin Psalmotoxin 1 Inhibits Acid-sensing Ion Channel (ASIC) 1a by Increasing Its Apparent H+ Affinity. *J. Gen. Physiol.* 126, 71–79. doi: 10.1085/jgp.200509303

Chen, X., Kalbacher, H., and Gründer, S. (2006). Interaction of Acid-sensing Ion Channel (ASIC) 1 with the Tarantula Toxin Psalmotoxin 1 is State Dependent. *J. Gen. Physiol.* 127, 267–276. doi: 10.1085/jgp.200509409

Chen, X., Liu, C., Lu, Y., Yang, Z., Lv, Z., Xu, Q., et al. (2012). Paeoniflorin regulates macrophage activation in dimethylnitrosamine-induced liver fibrosis in rats. *BMC Complement. Altern. Med.* 12, 254. doi: 10.1186/1472-6882-12-254

Cheng, X., Zhang, L., Hu, J., Sun, L., and Du, G. (2007). Neuroprotective effects of tetramethylpyrazine on hydrogen peroxide-induced apoptosis in PC12 cells. *Cell Biol. Int.* 31, 438–443. doi: 10.1016/j.cellbi.2006.10.001

Cheng, Y.-R., Jiang, B.-Y., and Chen, C.-C. (2018). Acid-sensing ion channels: dual function proteins for chemo-sensing and mechano-sensing. *J. Biomed. Sci.* 25, 46. doi: 10.1186/s12929-018-0448-y

Coric, T., Zheng, D., Gerstein, M., and Canessa, C. M. (2005). Proton sensitivity of ASIC1 appeared with the rise of fishes by changes of residues in the region that follows TM1 in the ectodomain of the channel. *J. Physiol.* 568, 725–735. doi: 10.1113/jphysiol.2005.087734

Coryell, M. W., Wunsch, A. M., Haenfler, J. M., Allen, J. E., McBride, J. L., Davidson, B. L., et al. (2008). Restoring Acid-Sensing Ion Channel-1a in the Amygdala of Knock-Out Mice Rescues Fear Memory But Not Unconditioned Fear Responses. *J. Neurosci.* 28, 13738–13741. doi: 10.1523/JNEUROSCI.3907-08.2008

Cristofori-Armstrong, B., Saez, N. J., Chassagnon, I. R., King, G. F., and Rash, L. D. (2019). The modulation of acid-sensing ion channel 1 by PcTx1 is pH-, subtype- and species-dependent: Importance of interactions at the channel subunit interface and potential for engineering selective analogues. *Biochem. Pharmacol.* 163, 381–390. doi: 10.1016/j.bcp.2019.03.004

Dawson, R. J. P., Benz, J., Stohler, P., Tetaz, T., Joseph, C., Huber, S., et al. (2012). Structure of the Acid-sensing ion channel 1 in complex with the gating modifier Psalmotoxin 1. *Nat. Commun.* 3, 936. doi: 10.1038/ncomms1917

Deng, H.-M., Yin, S.-T., Yan, D., Tang, M.-L., Li, C.-C., Chen, J.-T., et al. (2008). Effects of EGCG on voltage-gated sodium channels in primary cultures of rat hippocampal CA1 neurons. *Toxicology* 252, 1–8. doi: 10.1016/j.tox.2008.07.053

Deval, E., and Lingueglia, E. (2015). Acid-Sensing Ion Channels and nociception in the peripheral and central nervous systems. *Neuropharmacology* 94, 49–57. doi: 10.1016/j.neuropharm.2015.02.009

Deval, E., Salinas, M., Baron, A., Lingueglia, E., and Lazdunski, M. (2004). ASIC2b-dependent Regulation of ASIC3, an Essential Acid-sensing Ion Channel Subunit in Sensory Neurons via the Partner Protein PICK-1. *J. Biol. Chem.* 279, 19531–19539. doi: 10.1074/jbc.M313078200

Deval, E., Noel, J., Gasull, X., Delaunay, A., Alloui, A., Friend, V., et al. (2011). Acid-Sensing Ion Channels in Postoperative Pain. *J. Neurosci.* 31, 6059–6066. doi: 10.1523/JNEUROSCI.5266-10.2011

Diochot, S., Baron, A., Rash, L. D., Deval, E., Escoubas, P., Scarzello, S., et al. (2004). A new sea anemone peptide, APETx2, inhibits ASIC3, a major acid-sensitive channel in sensory neurons. *EMBO J.* 23, 1516–1525. doi: 10.1038/sj.emboj.7600177

Diochot, S., Baron, A., Salinas, M., Douguet, D., Scarzello, S., Dabert-Gay, A.-S., et al. (2012). Black mamba venom peptides target acid-sensing ion channels to abolish pain. *Nature* 490, 552–555. doi: 10.1038/nature11494

Diochot, S., Alloui, A., Rodrigues, P., Dauvois, M., Friend, V., Aissouni, Y., et al. (2016). Analgesic effects of mambalgin peptide inhibitors of acid-sensing ion channels in inflammatory and neuropathic pain. *Pain* 157, 552–559. doi: 10.1097/j.pain.0000000000000397

Donier, E., Rugiero, F., Jacob, C., and Wood, J. N. (2008). Regulation of ASIC activity by ASIC4 - new insights into ASIC channel function revealed by a yeast two-hybrid assay. *Eur. J. Neurosci.* 28, 74–86. doi: 10.1111/j.1460-9568.2008.06282.x

dos Santos, M. D., Almeida, M. C., Lopes, N. P., and de Souza, G. E. P. (2006). Evaluation of the Anti-inflammatory, Analgesic and Antipyretic Activities of the Natural Polyphenol Chlorogenic Acid. *Biol. Pharm. Bull.* 29, 2236–2240. doi: 10.1248/bpb.29.2236

Du, J., Reznikov, L. R., Price, M. P., Zha, X., Lu, Y., Moninger, T. O., et al. (2014). Protons are a neurotransmitter that regulates synaptic plasticity in the lateral amygdala. *Proc. Natl. Acad. Sci.* 111, 8961–8966. doi: 10.1073/pnas.1407018111

Duan, B., Wu, L.-J., Yu, Y.-Q., Ding, Y., Jing, L., Xu, L., et al. (2007). Upregulation of Acid-Sensing Ion Channel ASIC1a in Spinal Dorsal Horn Neurons Contributes to Inflammatory Pain Hypersensitivity. *J. Neurosci.* 27, 11139–11148. doi: 10.1523/JNEUROSCI.3364-07.2007

Duan, B., Wang, Y.-Z., Yang, T., Chu, X.-P., Yu, Y., Huang, Y., et al. (2011). Extracellular Spermine Exacerbates Ischemic Neuronal Injury through Sensitization of ASIC1a Channels to Extracellular Acidosis. *J. Neurosci.* 31, 2101–2112. doi: 10.1523/JNEUROSCI.4351-10.2011

Dubé, G. R., Lehto, S. G., Breese, N. M., Baker, S. J., Wang, X., Matulenko, M., et al. (2005). Electrophysiological and in vivo characterization of A-317567, a novel blocker of acid sensing ion channels. *Pain* 117, 88–96. doi: 10.1016/j.pain.2005.05.021

Dubinnyi, M. A., Osmakov, D.II, Koshelev, S. G., Kozlov, S. A., Andreev, Y. A., Zakaryan, N. A., et al. (2012). Lignan from Thyme Possesses Inhibitory Effect on ASIC3 Channel Current. *J. Biol. Chem.* 287, 32993–33000. doi: 10.1074/jbc.M112.366427

Dwyer, J. M., Rizzo, S. J. S., Neal, S. J., Lin, Q., Jow, F., Arias, R. L., et al. (2009). Acid sensing ion channel (ASIC) inhibitors exhibit anxiolytic-like activity in

preclinical pharmacological models. *Psychopharmacol. (Berl).* 203, 41–52. doi: 10.1007/s00213-008-1373-7

Er, S. Y., Cristofori-Armstrong, B., Escoubas, P., and Rash, L. D. (2017). Discovery and molecular interaction studies of a highly stable, tarantula peptide modulator of acid-sensing ion channel 1. *Neuropharmacology* 127, 185–195. doi: 10.1016/j.neuropharm.2017.03.020

Escoubas, P., De Weille, J. R., Lecoq, A., Diochot, S., Waldmann, R., Champigny, G., et al. (2000). Isolation of a Tarantula Toxin Specific for a Class of Proton-gated Na + Channels. *J. Biol. Chem.* 275, 25116–25121. doi: 10.1074/jbc.M003643200

Ettaiche, M. (2006). Silencing Acid-Sensing Ion Channel 1a Alters Cone-Mediated Retinal Function. *J. Neurosci.* 26, 5800–5809. doi: 10.1523/JNEUROSCI.0344-06.2006

Fantini, J., and Barrantes, F. J. (2018). How membrane lipids control the 3D structure and function of receptors. *AIMS Biophys.* 5, 22–35. doi: 10.3934/biophy.2018.1.22

Garateix, A., Salceda, E., Menéndez, R., Regalado, E. L., López, O., García, T., et al. (2011). Antinociception Produced by Thalassia Testudinum Extract BM-21 is Mediated by the Inhibition of Acid Sensing Ionic Channels by the Phenolic Compound Thalassiolin B. *Mol. Pain* 7, 1744-8069-7–10. doi: 10.1186/1744-8069-7-10

Garza, A., Lopez-Ramirez, O., Vega, R., and Soto, E. (2010). The Aminoglycosides Modulate the Acid-Sensing Ionic Channel Currents in Dorsal Root Ganglion Neurons from the Rat. *J. Pharmacol. Exp. Ther.* 332, 489–499. doi: 10.1124/jpet.109.152884

Gautam, M., and Benson, C. J. (2013). Acid-sensing ion channels (ASICs) in mouse skeletal muscle afferents are heteromers composed of ASIC1a, ASIC2, and ASIC3 subunits. *FASEB J.* 27, 793–802. doi: 10.1096/fj.12-220400

Gonzales, E. B., Kawate, T., and Gouaux, E. (2009). Pore architecture and ion sites in acid-sensing ion channels and P2X receptors. *Nature* 460, 599–604. doi: 10.1038/nature08218

Gründer, S., and Pusch, M. (2015). Biophysical properties of acid-sensing ion channels (ASICs). *Neuropharmacology* 94, 9–18. doi: 10.1016/j.neuropharm.2014.12.016

Gu, L., Yang, Y., Sun, Y., and Zheng, X. (2010). Puerarin Inhibits Acid-Sensing Ion Channels and Protects against Neuron Death Induced by Acidosis. *Planta Med.* 76, 583–588. doi: 10.1055/s-0029-1240583

Gupta, S. C., Singh, R., Asters, M., Liu, J., Zhang, X., Pabbidi, M. R., et al. (2016). Regulation of breast tumorigenesis through acid sensors. *Oncogene* 35, 4102–4111. doi: 10.1038/onc.2015.477

Hanukoglu, I. (2017). ASIC and ENaC type sodium channels: conformational states and the structures of the ion selectivity filters. *FEBS J.* 284, 525–545. doi: 10.1111/febs.13840

Harguindey, S., Stanciu, D., Devesa, J., Alfarouk, K., Cardone, R. A., Polo Orozco, J. D., et al. (2017). Cellular acidification as a new approach to cancer treatment and to the understanding and therapeutics of neurodegenerative diseases. *Semin. Cancer Biol.* 43, 157–179. doi: 10.1016/j.semcancer.2017.02.003

Henning, S. M., Niu, Y., Liu, Y., Lee, N. H., Hara, Y., Thames, G. D., et al. (2005). Bioavailability and antioxidant effect of epigallocatechin gallate administered in purified form versus as green tea extract in healthy individuals. *J. Nutr. Biochem.* 16, 610–616. doi: 10.1016/j.jnutbio.2005.03.003

Hernández, C., Konno, K., Salceda, E., Vega, R., Zaharenko, A. J., and Soto, E. J. (2019). Sa12b Peptide from Solitary Wasp Inhibits ASIC Currents in Rat Dorsal Root Ganglion Neurons. *Toxins (Basel).* 11, 585. doi: 10.3390/toxins11100585

Hernández-Araiza, I., Morales-Lázaro, S. L., Canul-Sánchez, J. A., Islas, L. D., and Rosenbaum, T. (2018). Role of lysophosphatidic acid in ion channel function and disease. *J. Neurophysiol.* 120, 1198–1211. doi: 10.1152/jn.00226.2018

Hesselager, M., Timmermann, D. B., and Ahring, P. K. (2004). pH Dependency and Desensitization Kinetics of Heterologously Expressed Combinations of Acid-sensing Ion Channel Subunits. *J. Biol. Chem.* 279, 11006–11015. doi: 10.1074/jbc.M313507200

Hobbs, H. E., Sorsby, A., and Freedman, A. (1959). Retinopathy Following Chloroquine Therapy. *Lancet* 274, 478–480. doi: 10.1016/S0140-6736(59)90604-X

Holton, C. M., Strother, L. C., Dripps, I., Pradhan, A. A., Goadsby, P. J., and Holland, P. R. (2020). Acid-sensing ion channel 3 blockade inhibits durovascular and nitric oxide-mediated trigeminal pain. *Br. J. Pharmacol.* 177, 2478–2486. doi: 10.1111/bph.14990

Hu, S., Sun, W., Wei, W., Wang, D., Jin, J., Wu, J., et al. (2013). Involvement of the prostaglandin E receptor EP2 in paeoniflorin-induced human hepatoma cell apoptosis. *Anticancer. Drugs* 24, 140–149. doi: 10.1097/CAD.0b013e32835a4dac

Ikeuchi, M., Kolker, S. J., and Sluka, K. A. (2009). Acid-Sensing Ion Channel 3 Expression in Mouse Knee Joint Afferents and Effects of Carrageenan-Induced Arthritis. *J. Pain* 10, 336–342. doi: 10.1016/j.jpain.2008.10.010

Immke, D. C., and McCleskey, E. W. (2001). Lactate enhances the acid-sensing Na + channel on ischemia-sensing neurons. *Nat. Neurosci.* 4, 869–870. doi: 10.1038/nn0901-869

Jasti, J., Furukawa, H., Gonzales, E. B., and Gouaux, E. (2007). Structure of acid-sensing ion channel 1 at 1.9 Å resolution and low pH. *Nature* 449, 316–323. doi: 10.1038/nature06163

Jensen, J. E., Mobli, M., Brust, A., Alewood, P. F., King, G. F., and Rash, L. D. (2012). Cyclisation Increases the Stability of the Sea Anemone Peptide APETx2 but Decreases Its Activity at Acid-Sensing Ion Channel 3. *Mar. Drugs* 10, 1511–1527. doi: 10.3390/md10071511

Jensen, J. E., Cristofori-Armstrong, B., Anangi, R., Rosengren, K. J., Lau, C. H. Y., Mobli, M., et al. (2014). Understanding the Molecular Basis of Toxin Promiscuity: The Analgesic Sea Anemone Peptide APETx2 Interacts with Acid-Sensing Ion Channel 3 and hERG Channels via Overlapping Pharmacophores. *J. Med. Chem.* 57, 9195–9203. doi: 10.1021/jm501400p

Jiang, Q.-X. (2019). ""Cholesterol-Dependent Gating Effects on Ion Channels,"," in *Advances in Experimental Medicine and Biology*. Eds. A. Rosenhouse-Dantsker and A. Bukiya (Cham: Springer), 167–190. doi: 10.1007/978-3-030-04278-3_8

Jin, A., Cristofori-Armstrong, B., Rash, L. D., Román-González, S. A., Espinosa, R. A., Lewis, R. J., et al. (2019). Novel conorfamides from Conus austini venom modulate both nicotinic acetylcholine receptors and acid-sensing ion channels. *Biochem. Pharmacol.* 164, 342–348. doi: 10.1016/j.bcp.2019.04.025

Joeres, N., Augustinowski, K., Neuhof, A., Assmann, M., and Gründer, S. (2016). Functional and pharmacological characterization of two different ASIC1a/2a heteromers reveals their sensitivity to the spider toxin PcTx1. *Sci. Rep.* 6, 27647. doi: 10.1038/srep27647

Kalina, R., Gladkikh, I., Dmitrenok, P., Chernikov, O., Koshelev, S., Kvetkina, A., et al. (2018). New APETx-like peptides from sea anemone Heteractis crispa modulate ASIC1a channels. *Peptides* 104, 41–49. doi: 10.1016/j.peptides.2018.04.013

Kalina, R. S., Koshelev, S. G., Zelepuga, E. A., Kim, N. Y., Kozlov, S. A., Kozlovskaya, E. P., et al. (2020). APETx-like peptides from the sea anemone Heteractis crispa, diverse in their effect on ASIC1a and ASIC3 ion channels. *Toxins (Basel).* 12, 266. doi: 10.3390/toxins12040266

Karczewski, J., Spencer, R. H., Garsky, V. M., Liang, A., Leitl, M. D., Cato, M. J., et al. (2010). Reversal of acid-induced and inflammatory pain by the selective ASIC3 inhibitor, APETx2. *Br. J. Pharmacol.* 161, 950–960. doi: 10.1111/j.1476-5381.2010.00918.x

Kleyman, T. R., and Eaton, D. C. (2020). Regulating ENaC's gate. *Am. J. Physiol. Physiol.* 318, C150–C162. doi: 10.1152/ajpcell.00418.2019

Kozlov, S., and Grishin, E. (2011). The mining of toxin-like polypeptides from EST database by single residue distribution analysis. *BMC Genomics* 12, 88. doi: 10.1186/1471-2164-12-88

Kozlov, S., and Grishin, E. (2012). Convenient nomenclature of cysteine-rich polypeptide toxins from sea anemones. *Peptides* 33, 240–244. doi: 10.1016/j.peptides.2011.12.008

Kozlov, S., Malyavka, A., McCutchen, B., Lu, A., Schepers, E., Herrmann, R., et al. (2005). A novel strategy for the identification of toxinlike structures in spider venom. *Proteins Struct. Funct. Bioinforma.* 59, 131–140. doi: 10.1002/prot.20390

Kozlov, S. A., Osmakov, D.II, Andreev, Y. A., Koshelev, S. G., Gladkikh, I. N., Monastyrnaya, M. M., et al. (2012). A sea anemone polypeptide toxin inhibiting the ASIC3 acid-sensitive channel. *Russ. J. Bioorg. Chem.* 38, 578–583. doi: 10.1134/S1068162012060064

Kozlov, S. (2018). Animal toxins for channelopathy treatment. *Neuropharmacology* 132, 83–97. doi: 10.1016/j.neuropharm.2017.10.031

Krause, K. M., Serio, A. W., Kane, T. R., and Connolly, L. E. (2016). Aminoglycosides: An Overview. *Cold Spring Harb. Perspect. Med.* 6, a027029. doi: 10.1101/cshperspect.a027029

Krishtal, O. A., and Pidoplichko, V.II (1980). A receptor for protons in the nerve cell membrane. *Neuroscience* 5, 2325–2327. doi: 10.1016/0306-4522(80)90149-9

Krishtal, O. (2015). Receptor for protons: First observations on Acid Sensing Ion Channels. *Neuropharmacology* 94, 4–8. doi: 10.1016/j.neuropharm.2014.12.014

Kuduk, S. D., Di Marco, C. N., Bodmer-Narkevitch, V., Cook, S. P., Cato, M. J., Jovanovska, A., et al. (2010). Synthesis, Structure–Activity Relationship, and Pharmacological Profile of Analogs of The ASIC-3 Inhibitor A-317567. *ACS Chem. Neurosci.* 1, 19–24. doi: 10.1021/cn9000186

Kumar, H., Kim, I.-S., More, S. V., Kim, B.-W., Bahk, Y.-Y., and Choi, D.-K. (2013). Gastrodin Protects Apoptotic Dopaminergic Neurons in a Toxin-Induced Parkinson's Disease Model. *Evidence-Based Complement. Altern. Med.* 2013, 1–13. doi: 10.1155/2013/514095

Lapchak, P. A. (2007). The phenylpropanoid micronutrient chlorogenic acid improves clinical rating scores in rabbits following multiple infarct ischemic strokes: Synergism with tissue plasminogen activator. *Exp. Neurol.* 205, 407–413. doi: 10.1016/j.expneurol.2007.02.017

Lee, J. Y. P., Saez, N. J., Cristofori-Armstrong, B., Anangi, R., King, G. F., Smith, M. T., et al. (2018). Inhibition of acid-sensing ion channels by diminazene and APETx2 evoke partial and highly variable antihyperalgesia in a rat model of inflammatory pain. *Br. J. Pharmacol.* 175, 2204–2218. doi: 10.1111/bph.14089

Lei, Z., Sami Shaikh, A., Zheng, W., Yu, X., Yu, J., and Li, J. (2016). Non-proton ligand-sensing domain of acid-sensing ion channel 3 is required for itch sensation. *J. Neurochem.* 139, 1093–1101. doi: 10.1111/jnc.13869

Li, Y., Shi, W., Li, Y., Zhou, Y., Hu, X., Song, C., et al. (2008). Neuroprotective effects of chlorogenic acid against apoptosis of PC12 cells induced by methylmercury. *Environ. Toxicol. Pharmacol.* 26, 13–21. doi: 10.1016/j.etap.2007.12.008

Li, T., Yang, Y., and Canessa, C. M. (2010). Two residues in the extracellular domain convert a nonfunctional ASIC1 into a proton-activated channel. *Am. J. Physiol. Physiol.* 299, C66–C73. doi: 10.1152/ajpcell.00100.2010

Li, T., Yang, Y., and Canessa, C. M. (2011). Outlines of the pore in open and closed conformations describe the gating mechanism of ASIC1. *Nat. Commun.* 2, 399. doi: 10.1038/ncomms1409

Li, X., Fei, J., Lei, Z., Liu, K., Wu, J., Meng, T., et al. (2014). Chloroquine impairs visual transduction via modulation of acid sensing ion channel 1a. *Toxicol. Lett.* 228, 200–206. doi: 10.1016/j.toxlet.2014.05.008

Lin, S.-H., Cheng, Y.-R., Banks, R. W., Min, M.-Y., Bewick, G. S., and Chen, C.-C. (2016). Evidence for the involvement of ASIC3 in sensory mechanotransduction in proprioceptors. *Nat. Commun.* 7, 11460. doi: 10.1038/ncomms11460

Lingueglia, E., de Weille, J. R., Bassilana, F., Heurteaux, C., Sakai, H., Waldmann, R., et al. (1997). A Modulatory Subunit of Acid Sensing Ion Channels in Brain and Dorsal Root Ganglion Cells. *J. Biol. Chem.* 272, 29778–29783. doi: 10.1074/jbc.272.47.29778

Liu, S., Cai, Y., Evans, T. W., McCormack, D. G., Barer, G. R., and Barnes, P. J. (1990). Ligustrazine is a vasodilator of human pulmonary and bronchial arteries. *Eur. J. Pharmacol.* 191, 345–350. doi: 10.1016/0014-2999(90)94167-V

Liu, Q.-N., Zhang, L., Gong, P.-L., Yang, X.-Y., and Zeng, F.-D. (2010). Daurisoline Suppressed Early Afterdepolarizations and Inhibited L-Type Calcium Current. *Am. J. Chin. Med.* 38, 37–49. doi: 10.1142/S0192415X1000766X

Liu, X.-Y., Zhang, S.-Z., Ma, X.-Y., Wang, H., Wu, B.-H., Sun, H.-L., et al. (2011). Knockdown of ASIC2a subunit aggravates injury of rat C6 glioma cells in acidosis. *J. Physiol. Biochem.* 67, 275–281. doi: 10.1007/s13105-010-0060-4

Liu, Q., Mao, X., Zeng, F., Jin, S., and Yang, X. (2012). Effect of Daurisoline on hERG Channel Electrophysiological Function and Protein Expression. *J. Nat. Prod.* 75, 1539–1545. doi: 10.1021/np300232b

Liu, W., Zhang, Y., Zhu, W., Ma, C., Ruan, J., Long, H., et al. (2018). Sinomenine Inhibits the Progression of Rheumatoid Arthritis by Regulating the Secretion of Inflammatory Cytokines and Monocyte/Macrophage Subsets. *Front. Immunol.* 9, 2228. doi: 10.3389/fimmu.2018.02228

Logashina, Y. A., Korolkova, Y. V., Maleeva, E. E., Osmakov, D.II, Kozlov, S. A., and Andreev, Y. A. (2020). Refolding of disulfide containing peptides in fusion with thioredoxin. *Mendeleev Commun.* 30, 214–216. doi: 10.1016/j.mencom.2019.11.008

Mamet, J., Baron, A., Lazdunski, M., and Voilley, N. (2002). ProInflammatory Mediators, Stimulators of Sensory Neuron Excitability via the Expression of Acid-Sensing Ion Channels. *J. Neurosci.* 22, 10662–10670. doi: 10.1523/JNEUROSCI.22-24-10662.2002

Mango, D., Barbato, G., Piccirilli, S., Panico, M. B., Feligioni, M., Schepisi, C., et al. (2014). Electrophysiological and metabolic effects of CHF5074 in the hippocampus: Protection against in vitro ischemia. *Pharmacol. Res.* 81, 83–90. doi: 10.1016/j.phrs.2014.02.010

Marek, G., Carver, R., Ding, Y., Sathyanarayan, D., Zhang, X., and Mou, Z. (2010). A high-throughput method for isolation of salicylic acid metabolic mutants. *Plant Methods* 6, 21. doi: 10.1186/1746-4811-6-21

Marra, S., Ferru-Clément, R., Breuil, V., Delaunay, A., Christin, M., Friend, V., et al. (2016). Non-acidic activation of pain-related Acid-Sensing Ion Channel 3 by lipids. *EMBO J.* 35, 414–428. doi: 10.15252/embj.201592335

Mazzuca, M., Heurteaux, C., Alloui, A., Diochot, S., Baron, A., Voilley, N., et al. (2007). A tarantula peptide against pain via ASIC1a channels and opioid mechanisms. *Nat. Neurosci.* 10, 943–945. doi: 10.1038/nn1940

McCarthy, C. A., Rash, L. D., Chassagnon, I. R., King, G. F., and Widdop, R. E. (2015). PcTx1 affords neuroprotection in a conscious model of stroke in hypertensive rats via selective inhibition of ASIC1a. *Neuropharmacology* 99, 650–657. doi: 10.1016/j.neuropharm.2015.08.040

Molliver, D. C., Immke, D. C., Fierro, L., Paré, M., Rice, F. L., and McCleskey, E. W. (2005). ASIC3, an Acid-Sensing Ion Channel, is Expressed in Metaboreceptive Sensory Neurons. *Mol. Pain* 1, 1744-8069-1–35. doi: 10.1186/1744-8069-1-35

Morales-Lázaro, S. L., and Rosenbaum, T. (2019). ""Cholesterol as a Key Molecule That Regulates TRPV1 Channel Function,"," in *Advances in Experimental Medicine and Biology*. Eds. A. Rosenhouse-Dantsker and A. Bukiya (Cham: Springer), 105–117. doi: 10.1007/978-3-030-14265-0_6

Mourier, G., Salinas, M., Kessler, P., Stura, E. A., Leblanc, M., Tepshi, L., et al. (2016). Mambalgin-1 Pain-relieving Peptide, Stepwise Solid-phase Synthesis, Crystal Structure, and Functional Domain for Acid-sensing Ion Channel 1a Inhibition. *J. Biol. Chem.* 291, 2616–2629. doi: 10.1074/jbc.M115.702373

Mukhopadhyay, M., Singh, A., Sachchidanand, S., and Bera, A. K. (2017). Quercetin inhibits acid-sensing ion channels through a putative binding site in the central vestibular region. *Neuroscience* 348, 264–272. doi: 10.1016/j.neuroscience.2017.02.025

Munro, G., Christensen, J. K., Erichsen, H. K., Dyhring, T., Demnitz, J., Dam, E., et al. (2016). NS383 Selectively Inhibits Acid-Sensing Ion Channels Containing 1a and 3 Subunits to Reverse Inflammatory and Neuropathic Hyperalgesia in Rats. *CNS Neurosci. Ther.* 22, 135–145. doi: 10.1111/cns.12487

Nagaeva, E.II, Tikhonova, T. B., Magazanik, L. G., and Tikhonov, D. B. (2016). Histamine selectively potentiates acid-sensing ion channel 1a. *Neurosci. Lett.* 632, 136–140. doi: 10.1016/j.neulet.2016.08.047

Nielsen, L. M., Olesen, A. E., Andresen, T., Simrén, M., Törnblom, H., and Drewes, A. M. (2015). Efficacy and Safety of PPC-5650 on Experimental Rectal Pain in Patients with Irritable Bowel Syndrome. *Basic Clin. Pharmacol. Toxicol.* 116, 140–145. doi: 10.1111/bcpt.12294

Osmakov, D.II, Kozlov, S., Andreev, Y., Koshelev, S. G., Sanamyan, N. P., Sanamyan, K. E., et al. (2013). Sea Anemone Peptide with Uncommon β-Hairpin Structure Inhibits Acid-sensing Ion Channel 3 (ASIC3) and Reveals Analgesic Activity. *J. Biol. Chem.* 288, 23116–23127. doi: 10.1074/jbc.M113.485516

Osmakov, D.II, Andreev, Y. A., and Kozlov, S. A. (2014). Acid-Sensing Ion Channels and Their Modulators. *Biochemistry* 79, 1528–1545. doi: 10.1134/S0006297914130069

Osmakov, D.II, Koshelev, S. G., Belozerova, O. A., Kublitski, V. S., Andreev, Y. A., Grishin, E. V., et al. (2015). Biological Activity of Sevanol and Its Analogues 1. *Russ. J. Bioorg. Chem.* 41, 543–547. doi: 10.1134/S1068162015050106

Osmakov, D.II, Koshelev, S. G., Andreev, Y. A., Dyachenko, I. A., Bondarenko, D. A., Murashev, A. N., et al. (2016). Conversed mutagenesis of an inactive peptide to ASIC3 inhibitor for active sites determination. *Toxicon* 116, 11–16. doi: 10.1016/j.toxicon.2015.11.019

Osmakov, D.II, Koshelev, S. G., Andreev, Y. A., and Kozlov, S. A. (2017). Endogenous isoquinoline alkaloids agonists of acid-sensing ion channel type 3. *Front. Mol. Neurosci.* 10, 282. doi: 10.3389/FNMOL.2017.00282

Osmakov, D.II, Koshelev, S. G., Andreev, Y. A., Dubinnyi, M. A., Kublitski, V. S., Efremov, R. G., et al. (2018). Proton-independent activation of acid-sensing ion channel 3 by an alkaloid, lindoldhamine, from Laurus nobilis. *Br. J. Pharmacol.* 175, 924–937. doi: 10.1111/bph.14134

Osmakov, D.II, Koshelev, S. G., Ivanov, I. A., Andreev, Y. A., and Kozlov, S. A. (2019a). Endogenous Neuropeptide Nocistatin Is a Direct Agonist of Acid-Sensing Ion Channels (ASIC1, ASIC2 and ASIC3). *Biomolecules* 9, 401. doi: 10.3390/biom9090401

Osmakov, D.II, Koshelev, S. G., Lyukmanova, E. N., Shulepko, M. A., Andreev, Y. A., Illes, P., et al. (2019b). Multiple Modulation of Acid-Sensing Ion Channel 1a by the Alkaloid Daurisoline. *Biomolecules* 9, 336. doi: 10.3390/biom9080336

Osmakov, D.II, Koshelev, S. G., Palikov, V. A., Palikova, Y. A., Shaykhutdinova, E. R., Dyachenko, I. A., et al. (2019c). Alkaloid Lindoldhamine Inhibits Acid-Sensing Ion

Channel 1a and Reveals Anti-Inflammatory Properties. *Toxins (Basel).* 11, 542. doi: 10.3390/toxins11090542

Page, A. J. (2005). Different contributions of ASIC channels 1a, 2, and 3 in gastrointestinal mechanosensory function. *Gut* 54, 1408–1415. doi: 10.1136/gut.2005.071084

Pathan, H., and Williams, J. (2012). Basic opioid pharmacology: an update. *Br. J. Pain* 6, 11–16. doi: 10.1177/2049463712438493

Peigneur, S., Béress, L., Möller, C., Marí, F., Forssmann, W., and Tytgat, J. (2012). A natural point mutation changes both target selectivity and mechanism of action of sea anemone toxins. *FASEB J.* 26, 5141–5151. doi: 10.1096/fj.12-218479

Plantone, D., and Koudriavtseva, T. (2018). Current and Future Use of Chloroquine and Hydroxychloroquine in Infectious, Immune, Neoplastic, and Neurological Diseases: A Mini-Review. *Clin. Drug Investig.* 38, 653–671. doi: 10.1007/s40261-018-0656-y

Poeaknapo, C., Schmidt, J., Brandsch, M., Drager, B., and Zenk, M. H. (2004). Endogenous formation of morphine in human cells. *Proc. Natl. Acad. Sci.* 101, 14091–14096. doi: 10.1073/pnas.0405430101

Qiu, F.-M., Zhong, X.-M., Mao, Q.-Q., and Huang, Z. (2013). Antidepressant-like effects of paeoniflorin on the behavioural, biochemical, and neurochemical patterns of rats exposed to chronic unpredictable stress. *Neurosci. Lett.* 541, 209–213. doi: 10.1016/j.neulet.2013.02.029

Qiu, F., Liu, T.-T., Qu, Z.-W., Qiu, C.-Y., Yang, Z., and Hu, W.-P. (2014). Gastrodin inhibits the activity of acid-sensing ion channels in rat primary sensory neurons. *Eur. J. Pharmacol.* 731, 50–57. doi: 10.1016/j.ejphar.2014.02.044

Qu, Z.-W., Liu, T.-T., Qiu, C.-Y., Li, J.-D., and Hu, W.-P. (2014). Inhibition of acid-sensing ion channels by chlorogenic acid in rat dorsal root ganglion neurons. *Neurosci. Lett.* 567, 35–39. doi: 10.1016/j.neulet.2014.03.027

Raisinghani, M., and Premkumar, L. S. (2005). Block of native and cloned vanilloid receptor 1 (TRPV1) by aminoglycoside antibiotics. *Pain* 113, 123–133. doi: 10.1016/j.pain.2004.09.042

Rash, L. D. (2017). "Acid-Sensing Ion Channel Pharmacology, Past, Present, and Future," in *Advances in Pharmacology*. Ed. D. P. Geraghty (Netherlands: Elsevier Inc.), 35–66. doi: 10.1016/bs.apha.2017.02.001

Regalado, E. L., Rodríguez, M., Menéndez, R., Concepción, Á. A., Nogueiras, C., Laguna, A., et al. (2009). Repair of UVB-Damaged Skin by the Antioxidant Sulphated Flavone Glycoside Thalassiolin B Isolated from the Marine Plant Thalassia testudinum Banks ex König. *Mar. Biotechnol.* 11, 74–80. doi: 10.1007/s10126-008-9123-8

Reimers, C., Lee, C.-H., Kalbacher, H., Tian, Y., Hung, C.-H., Schmidt, A., et al. (2017). Identification of a cono-RFamide from the venom of Conus textile that targets ASIC3 and enhances muscle pain. *Proc. Natl. Acad. Sci.* 114, E3507–E3515. doi: 10.1073/pnas.1616232114

Ren, Z., Ma, J., Zhang, P., Luo, A., Zhang, S., Kong, L., et al. (2012). The effect of ligustrazine on L-type calcium current, calcium transient and contractility in rabbit ventricular myocytes. *J. Ethnopharmacol.* 144, 555–561. doi: 10.1016/j.jep.2012.09.037

Rodríguez, A. A., Salceda, E., Garateix, A. G., Zaharenko, A. J., Peigneur, S., López, O., et al. (2014). A novel sea anemone peptide that inhibits acid-sensing ion channels. *Peptides* 53, 3–12. doi: 10.1016/j.peptides.2013.06.003

Rodriguez-Menchaca, A. A., Navarro-Polanco, R. A., Ferrer-Villada, T., Rupp, J., Sachse, F. B., Tristani-Firouzi, M., et al. (2008). The molecular basis of chloroquine block of the inward rectifier Kir2.1 channel. *Proc. Natl. Acad. Sci.* 105, 1364–1368. doi: 10.1073/pnas.0708153105

Rooj, A. K., McNicholas, C. M., Bartoszewski, R., Bebok, Z., Benos, D. J., and Fuller, C. M. (2012). Glioma-specific Cation Conductance Regulates Migration and Cell Cycle Progression. *J. Biol. Chem.* 287, 4053–4065. doi: 10.1074/jbc.M111.311688

Saez, N. J., Deplazes, E., Cristofori-Armstrong, B., Chassagnon, I. R., Lin, X., Mobli, M., et al. (2015). Molecular dynamics and functional studies define a hot spot of crystal contacts essential for PcTx1 inhibition of acid-sensing ion channel 1a. *Br. J. Pharmacol.* 172, 4985–4995. doi: 10.1111/bph.13267

Salinas, M., Lazdunski, M., and Lingueglia, E. (2009). Structural Elements for the Generation of Sustained Currents by the Acid Pain Sensor ASIC3. *J. Biol. Chem.* 284, 31851–31859. doi: 10.1074/jbc.M109.043984

Saponara, S., Sgaragli, G., and Fusi, F. (2002). Quercetin as a novel activator of L-type Ca 2+ channels in rat tail artery smooth muscle cells. *Br. J. Pharmacol.* 135, 1819–1827. doi: 10.1038/sj.bjp.0704631

Schuhmacher, L.-N., and Smith, E. S. J. (2016). Expression of acid-sensing ion channels and selection of reference genes in mouse and naked mole rat. *Mol. Brain* 9, 97. doi: 10.1186/s13041-016-0279-2

Schuhmacher, L.-N., Srivats, S., and Smith, E. S. J. (2015). Structural Domains Underlying the Activation of Acid-Sensing Ion Channel 2a. *Mol. Pharmacol.* 87, 561–571. doi: 10.1124/mol.114.096909

Sherwood, T., Franke, R., Conneely, S., Joyner, J., Arumugan, P., and Askwith, C. (2009). Identification of Protein Domains That Control Proton and Calcium Sensitivity of ASIC1a. *J. Biol. Chem.* 284, 27899–27907. doi: 10.1074/jbc.M109.029009

Sherwood, T. W., Lee, K. G., Gormley, M. G., and Askwith, C. C. (2011). Heteromeric Acid-Sensing Ion Channels (ASICs) Composed of ASIC2b and ASIC1a Display Novel Channel Properties and Contribute to Acidosis-Induced Neuronal Death. *J. Neurosci.* 31, 9723–9734. doi: 10.1523/JNEUROSCI.1665-11.2011

Shimada, S. G., and LaMotte, R. H. (2008). Behavioral differentiation between itch and pain in mouse. *Pain* 139, 681–687. doi: 10.1016/j.pain.2008.08.002

Smith, E. S., Cadiou, H., and McNaughton, P. A. (2007). Arachidonic acid potentiates acid-sensing ion channels in rat sensory neurons by a direct action. *Neuroscience* 145, 686–698. doi: 10.1016/j.neuroscience.2006.12.024

Song, C., Wang, J., Gao, D., Yu, Y., Li, F., Wei, S., et al. (2017). Paeoniflorin, the Main Active Ingredient of Shuyu Capsule, Inhibits Ca v 1.2 and Regulates Calmodulin/Calmodulin-Dependent Protein Kinase II Signalling. *BioMed. Res. Int.* 2017, 1–10. doi: 10.1155/2017/8459287

Sun, X., Cao, Y.-B., Hu, L.-F., Yang, Y.-P., Li, J., Wang, F., et al. (2011). ASICs mediate the modulatory effect by paeoniflorin on alpha-synuclein autophagic degradation. *Brain Res.* 1396, 77–87. doi: 10.1016/j.brainres.2011.04.011

Sun, D., Yu, Y., Xue, X., Pan, M., Wen, M., Li, S., et al. (2018). Cryo-EM structure of the ASIC1a–mambalgin-1 complex reveals that the peptide toxin mambalgin-1 inhibits acid-sensing ion channels through an unusual allosteric effect. *Cell Discovery* 4, 27. doi: 10.1038/s41421-018-0026-1

Tabakmakher, V. M., Krylov, N. A., Kuzmenkov, A.II, Efremov, R. G., and Vassilevski, A. A. (2019). Kalium 2.0, a comprehensive database of polypeptide ligands of potassium channels. *Sci. Data* 6, 73. doi: 10.1038/s41597-019-0074-x

Tian, Y., and Zheng, J. (2017). ""Metabolic Activation and Toxicities of bis-Benzylisoquinoline Alkaloids,"," in *Advances in Molecular Toxicology*. Eds. J. C. Fishbein and J. M. Heilman (Netherlands: Elsevier B.V.), 241–272. doi: 10.1016/B978-0-12-812522-9.00006-3

Todorović, N., Ćorić, T., Zhang, P., and Canessa, C. (2005). Effects of Extracellular Calcium on fASIC1 Currents. *Ann. N. Y. Acad. Sci.* 1048, 331–336. doi: 10.1196/annals.1342.030

Tsai, T.-Y., Wu, S. N., Liu, Y.-C., Wu, A. Z., and Tsai, Y.-C. (2005). Inhibitory action of L-type Ca2+ current by paeoniflorin, a major constituent of peony root, in NG108-15 neuronal cells. *Eur. J. Pharmacol.* 523, 16–24. doi: 10.1016/j.ejphar.2005.08.042

Voilley, N., de Weille, J., Mamet, J., and Lazdunski, M. (2001). Nonsteroid Anti-Inflammatory Drugs Inhibit Both the Activity and the Inflammation-Induced Expression of Acid-Sensing Ion Channels in Nociceptors. *J. Neurosci.* 21, 8026–8033. doi: 10.1523/JNEUROSCI.21-20-08026.2001

Vullo, S., Bonifacio, G., Roy, S., Johner, N., Bernèche, S., and Kellenberger, S. (2017). Conformational dynamics and role of the acidic pocket in ASIC pH-dependent gating. *Proc. Natl. Acad. Sci.* 114, 3768–3773. doi: 10.1073/pnas.1620560114

Waldmann, R., Champigny, G., Bassilana, F., Heurteaux, C., and Lazdunski, M. (1997). A proton-gated cation channel involved in acid-sensing. *Nature* 386, 173–177. doi: 10.1038/386173a0

Wallace, C. H. R., Baczkó, I., Jones, L., Fercho, M., and Light, P. E. (2006). Inhibition of cardiac voltage-gated sodium channels by grape polyphenols. *Br. J. Pharmacol.* 149, 657–665. doi: 10.1038/sj.bjp.0706897

Wemmie, J. A., Chen, J., Askwith, C. C., Hruska-Hageman, A. M., Price, M. P., Nolan, B. C., et al. (2002). The Acid-Activated Ion Channel ASIC Contributes to Synaptic Plasticity, Learning, and Memory. *Neuron* 34, 463–477. doi: 10.1016/S0896-6273(02)00661-X

Wemmie, J. A., Askwith, C. C., Lamani, E., Cassell, M. D., Freeman, J. H., and Welsh, M. J. (2003). Acid-Sensing Ion Channel 1 Is Localized in Brain Regions with High Synaptic Density and Contributes to Fear Conditioning. *J. Neurosci.* 23, 5496–5502. doi: 10.1523/JNEUROSCI.23-13-05496.2003

Wemmie, J. A., Coryell, M. W., Askwith, C. C., Lamani, E., Leonard, A. S., Sigmund, C. D., et al. (2004). Overexpression of acid-sensing ion channel 1a in

transgenic mice increases acquired fear-related behavior. *Proc. Natl. Acad. Sci.* 101, 3621–3626. doi: 10.1073/pnas.0308753101

Wemmie, J. A., Price, M. P., and Welsh, M. J. (2006). Acid-sensing ion channels: advances, questions and therapeutic opportunities. *Trends Neurosci.* 29, 578–586. doi: 10.1016/j.tins.2006.06.014

Wemmie, J. A., Taugher, R. J., and Kreple, C. J. (2013). Acid-sensing ion channels in pain and disease. *Nat. Rev. Neurosci.* 14, 461–471. doi: 10.1038/nrn3529

Wen, M., Guo, X., Sun, P., Xiao, L., Li, J., Xiong, Y., et al. (2015). Site-specific fluorescence spectrum detection and characterization of hASIC1a channels upon toxin mambalgin-1 binding in live mammalian cells. *Chem. Commun.* 51, 8153–8156. doi: 10.1039/C5CC01418B

Wu, W.-N., Wu, P.-F., Chen, X.-L., Zhang, Z., Gu, J., Yang, Y.-J., et al. (2011). Sinomenine protects against ischaemic brain injury: involvement of co-inhibition of acid-sensing ion channel 1a and L-type calcium channels. *Br. J. Pharmacol.* 164, 1445–1459. doi: 10.1111/j.1476-5381.2011.01487.x

Wu, J., Xu, Y., Jiang, Y.-Q., Xu, J., Hu, Y., and Zha, X. (2016). ASIC subunit ratio and differential surface trafficking in the brain. *Mol. Brain* 9, 4. doi: 10.1186/s13041-016-0185-7

Wu, Y., Gao, B., Xiong, Q.-J., Wang, Y.-C., Huang, D.-K., and Wu, W.-N. (2017). Acid-sensing ion channels contribute to the effect of extracellular acidosis on proliferation and migration of A549 cells. *Tumor Biol.* 39, 101042831770575. doi: 10.1177/1010428317705750

Xu, M., Liu, L., Qi, C., Deng, B., and Cai, X. (2008). Sinomenine Versus NSAIDs for the Treatment of Rheumatoid Arthritis: A Systematic Review and Meta-Analysis. *Planta Med.* 74, 1423–1429. doi: 10.1055/s-2008-1081346

Xu, H., Zhao, M., Liang, S., Huang, Q., Xiao, Y., Ye, L., et al. (2016). The Effects of Puerarin on Rat Ventricular Myocytes and the Potential Mechanism. *Sci. Rep.* 6, 35475. doi: 10.1038/srep35475

Xu, S., Liu, C., Ma, Y., Ji, H.-L., and Li, X. (2016). Potential Roles of Amiloride-Sensitive Sodium Channels in Cancer Development. *BioMed. Res. Int.* 2016, 1–6. doi: 10.1155/2016/2190216

Yan, X.-G., Li, W.-G., Qi, X., Zhu, J.-J., Huang, C., Han, S.-L., et al. (2019). Subtype-selective inhibition of acid-sensing ion channel 3 by a natural flavonoid. *CNS Neurosci. Ther.* 25, 47–56. doi: 10.1111/cns.12979

Yang, C. S., Wang, X., Lu, G., and Picinich, S. C. (2009). Cancer prevention by tea: animal studies, molecular mechanisms and human relevance. *Nat. Rev. Cancer* 9, 429–439. doi: 10.1038/nrc2641

Yang, C.-S., Lai, M.-C., Liu, P.-Y., Lo, Y.-C., Huang, C.-W., and Wu, S.-N. (2019). Characterization of the Inhibitory Effect of Gastrodigenin and Gastrodin on M-type K+ Currents in Pituitary Cells and Hippocampal Neurons. *Int. J. Mol. Sci.* 21, 117. doi: 10.3390/ijms21010117

Yoder, N., Yoshioka, C., and Gouaux, E. (2018). Gating mechanisms of acid-sensing ion channels. *Nature* 555, 397–401. doi: 10.1038/nature25782

Zeng, X., Zhang, S., Zhang, L., Zhang, K., and Zheng, X. (2006). A Study of the Neuroprotective Effect of the Phenolic Glucoside Gastrodin during Cerebral Ischemia in vivo and in vitro. *Planta Med.* 72, 1359–1365. doi: 10.1055/s-2006-951709

Zhang, P., and Canessa, C. M. (2002). Single Channel Properties of Rat Acid–sensitive Ion Channel-1α, -2a, and -3 Expressed in Xenopus Oocytes. *J. Gen. Physiol.* 120, 553–566. doi: 10.1085/jgp.20028574

Zhang, L.-Y., Cosma, G., Gardner, H., Vallyathan, V., and Castranova, V. (2003). Effect of chlorogenic acid on hydroxyl radical. *Mol. Cell Biochem.* 247, 205–210. doi: 10.1023/A:1024103428348

Zhang, Z.-G., Zhang, X.-L., Wang, X.-Y., Luo, Z.-R., and Song, J.-C. (2015). Inhibition of acid sensing ion channel by ligustrazine on angina model in rat. *Am. J. Transl. Res.* 7, 1798–1811.

Zhang, Y., Zhang, T., Wu, C., Xia, Q., and Xu, D. (2017). ASIC1a mediates the drug resistance of human hepatocellular carcinoma via the Ca2+/PI3-kinase/AKT signaling pathway. *Lab. Investig.* 97, 53–69. doi: 10.1038/labinvest.2016.127

Zhang, X.-L., Cao, X.-Y., Lai, R.-C., Xie, M.-X., and Zeng, W.-A. (2019). Puerarin Relieves Paclitaxel-Induced Neuropathic Pain: The Role of Nav1.8 β1 Subunit of Sensory Neurons. *Front. Pharmacol.* 9, 1510. doi: 10.3389/fphar.2018.01510

Zhou, Y., and Zhao, Z.-Q. (2002). Effects of neomycin on high-threshold Ca2+ currents and tetrodotoxin-resistant Na+ currents in rat dorsal root ganglion neuron. *Eur. J. Pharmacol.* 450, 29–35. doi: 10.1016/S0014-2999(02)02050-2

Zhou, Y., Hu, C.-P., Deng, P.-Y., Deng, H.-W., and Li, Y.-J. (2004). The Protective Effects of Ligustrazine on Ischemia-Reperfusion and DPPH Free Radical-Induced Myocardial Injury in Isolated Rat Hearts. *Planta Med.* 70, 818–822. doi: 10.1055/s-2004-827229

Zhou, Y.-X., Zhang, H., and Peng, C. (2014). Puerarin: A Review of Pharmacological Effects. *Phyther. Res.* 28, 961–975. doi: 10.1002/ptr.5083

Ziemann, A. E., Allen, J. E., Dahdaleh, N. S., Drebot, I.II, Coryell, M. W., Wunsch, A. M., et al. (2009). The Amygdala Is a Chemosensor that Detects Carbon Dioxide and Acidosis to Elicit Fear Behavior. *Cell* 139, 1012–1021. doi: 10.1016/j.cell.2009.10.029

Zou, L.-Y., Hao, X.-M., Zhang, G.-Q., Zhang, M., Guo, J.-H., and Liu, T.-F. (2001). Effect of tetramethyl pyrazine on L-type calcium channel in rat ventricular myocytes. *Can. J. Physiol. Pharmacol.* 79, 621–626. doi: 10.1139/y01-045

Zuo, Z., Smith, R. N., Chen, Z., Agharkar, A. S., Snell, H. D., Huang, R., et al. (2018). Identification of a unique Ca2+-binding site in rat acid-sensing ion channel 3. *Nat. Commun.* 9, 2082. doi: 10.1038/s41467-018-04424-0

Conflict of Interest: The authors declare that the research was conducted in the absence of any commercial or financial relationships that could be construed as a potential conflict of interest.

frontiers in Pharmacology

ORIGINAL RESEARCH
published: 17 July 2020
doi: 10.3389/fphar.2020.01075

A Multiomics Approach Unravels New Toxins With Possible *In Silico* Antimicrobial, Antiviral, and Antitumoral Activities in the Venom of *Acanthoscurria rondoniae*

*Guilherme A. Câmara[1], Milton Y. Nishiyama-Jr[2], Eduardo S. Kitano[3], Ursula C. Oliveira[2], Pedro I. da Silva Jr[2], Inácio L. Junqueira-de-Azevedo[2] and Alexandre K. Tashima[1,2]**

[1] Departamento de Bioquímica, Escola Paulista de Medicina, Universidade Federal de São Paulo, São Paulo, Brazil, [2] Laboratório Especial de Toxinologia Aplicada, Center of Toxins, Immune-Response and Cell Signaling, Instituto Butantan, São Paulo, Brazil, [3] Laboratory of Immunology, Heart Institute (InCor), Faculty of Medicine, University of Sao Paulo, Sao Paulo, Brazil

OPEN ACCESS

Edited by:
Heike Wulff,
University of California, Davis,
United States

Reviewed by:
Cassandra Marie Modahl,
National University of Singapore,
Singapore
Oscar Moran,
Italian National Research Council, Italy

***Correspondence:**
Alexandre K. Tashima
aktashima@unifesp.br

Specialty section:
This article was submitted to Pharmacology of Ion Channels and Channelopathies, a section of the journal Frontiers in Pharmacology

Received: 20 May 2020
Accepted: 02 July 2020
Published: 17 July 2020

Citation:
Câmara GA, Nishiyama-Jr MY, Kitano ES, Oliveira UC, Silva Jr PI, Junqueira-de-Azevedo IL and Tashima AK (2020) A Multiomics Approach Unravels New Toxins With Possible In Silico Antimicrobial, Antiviral, and Antitumoral Activities in the Venom of Acanthoscurria rondoniae. Front. Pharmacol. 11:1075. doi: 10.3389/fphar.2020.01075

The *Araneae* order is considered one of the most successful groups among venomous animals in the world. An important factor for this success is the production of venoms, a refined biological fluid rich in proteins, short peptides and cysteine-rich peptides (CRPs). These toxins may present pharmacologically relevant biological actions, as antimicrobial, antiviral and anticancer activities, for instance. Therefore, there is an increasing interest in the exploration of venom toxins for therapeutic reasons, such as drug development. However, the process of peptide sequencing and mainly the evaluation of potential biological activities of these peptides are laborious, considering the low yield of venom extraction and the high variability of toxins present in spider venoms. Here we show a robust methodology for identification, sequencing, and initial screening of potential bioactive peptides found in the venom of *Acanthoscurria rondoniae*. This methodology consists in a multiomics approach involving proteomics, peptidomics and transcriptomics analyses allied to *in silico* predictions of antibacterial, antifungal, antiviral, and anticancer activities. Through the application of this strategy, a total of 92,889 venom gland transcripts were assembled and 84 novel toxins were identified at the protein level, including seven short peptides and 10 fully sequenced CRPs (belonging to seven toxin families). *In silico* analysis suggests that seven CRPs families may have potential antimicrobial or antiviral activities, while two CRPs and four short peptides are potentially anticancer. Taken together, our results demonstrate an effective multiomics strategy for the discovery of new toxins and *in silico* screening of potential bioactivities. This strategy may be useful in toxin discovery, as well as in the screening of possible activities for the vast diversity of molecules produced by venomous animals.

Keywords: *Acanthoscurria rondoniae*, cysteine-rich peptides, peptidomics, proteomics, multiomics, antimicrobial peptides, antiviral peptides, antitumoral peptides

INTRODUCTION

Spider venoms are composed of a complex mixture of salts, nucleotides and other small molecules, as well as bioactive molecules such as proteins and peptides, usually referred to as toxins (Escoubas and Rash, 2004; Kuhn-Nentwig et al., 2011; Langenegger et al., 2019). In spiders, toxins are produced and stored in venom glands. These toxins are synthetized in an inactive form and undergo several maturation processes (i.e. signal-peptide cleavage, posttranslational modifications (PTMs) and disulfide-bond formation) before being secreted in its mature form (Mebs, 2001; Kaas and Craik, 2015).

The family of cysteine-rich peptides (CRPs) is the main class of toxins present in spider venoms, typically presenting molecular masses between 3 and 9 kDa. The toxins contain ≥6 cysteine residues that form disulfide-bonds (S-S), which confers high stability to the peptides (Fry et al., 2009; Undheim et al., 2015). CRPs acts in different voltage-gated ion channels (Kuhn-Nentwig et al., 2011; Langenegger et al., 2019), such as calcium (Kubista et al., 2007; Deng et al., 2014), potassium (Lee and MacKinnon, 2004; Liao et al., 2006; Lau et al., 2016) and sodium channels (Corzo et al., 2008; Rates et al., 2013; Zhou et al., 2020), making them valuable tools to investigate physiological processes (Ruta et al., 2003; Osteen et al., 2016). Moreover, through the modulation of these channels, spiders can induce paralysis in insects while having minor effects on other taxa, being potential lead molecules for the development of biopesticides (Windley et al., 2012; King and Hardy, 2013). Another class of spider toxins are the antimicrobial peptides (AMPs), commonly found in spider hemolymphs (Silva et al., 2000; Riciluca et al., 2012) as a component of innate immunity, but also found in spider venoms (Jung et al., 2006; Abreu et al., 2017). Usually, AMPs are small molecules rich in cationic and hydrophobic residues that fold into a cationic amphipathic secondary structure (Edwards et al., 2016). AMPs interacts with the negatively charged outer membrane of microorganisms (Seo et al., 2012) through nonspecific interactions with anionic lipids (Arouri et al., 2009), causing membrane disruption through different pore-forming mechanisms (Fuertes et al., 2011; Paredes-Gamero et al., 2012). Interestingly, anticancer peptides (ACPs) share the same main characteristics of AMPs, such as folding into a cationic amphipathic structure and interacting with the negatively charged outer-membrane (Gaspar et al., 2013). Therefore, there is an increasing interest in studying the application of AMPs for cancer treatment (Felício et al., 2017; Zhang et al., 2019; Pérez-Peinado et al., 2020).

The biochemical arsenal of spider venoms is essential not only in predation and self-defense, but also in feeding, mating and antimicrobial protection, among other possible roles (Schendel et al., 2019). Tarantula spiders are usually harmless to humans (Lucas et al., 1994; Vetter and Isbister, 2008), but their venoms are valuable natural sources of molecules with potential for biotechnological applications and pharmacological research (Escoubas and King, 2009; Mobli et al., 2017). According to the World Spider Catalog, there are more than 48,000 spider species described (http://wsc.nmbe.ch, accessed on May 1st, 2020) and it is estimated that they can produce more than 10 million bioactive toxins (Saez et al., 2010). However, according to the ArachnoServer 3.0 database, about 1,500 spider toxins are cataloged and curated to date (Pineda et al., 2018), representing a small fraction of the estimated universe of spider venom toxins. Thus, the discovery of biologically active peptides derived from spider venoms is still a promising field in toxinology research.

The advances in sensitivity and resolution of mass spectrometers as well as advances in DNA and RNA sequencing techniques have led to a remarkable increase in the number of toxins reported in the last years (Duan et al., 2013; Sanggaard et al., 2014; Zelanis and Keiji Tashima, 2014; Abreu et al., 2017; Zobel-Thropp et al., 2018; Langenegger et al., 2019). However, the increase in toxin identification is not synchronized with the functional description of new toxins, since the functional characterization involves a significant number of experimental processes. Advances in bioinformatics and computational capacity allowed the development of machine-learning algorithms that serve as useful allies in drug discovery (Kaas and Craik, 2015). These machine-learning based tools may be used to predict potential biological activities, such as antimicrobial (Meher et al., 2017) and antitumoral (Manavalan et al., 2017), based on the primary structure of toxins. Thus, they may serve as valuable guides in toxin selection for further investigation.

Our group developed a workflow based on transcriptomic analysis, multiple enzyme digestion of venoms, mass spectrometry and bioinformatic analysis focused on the full sequencing of mature toxins (Abreu et al., 2017; Lomazi et al., 2018). In a previous work, we completely sequenced and determined the number of S-S bonds of new mature CRPs from the venom of *Acanthoscurria gomesiana* (Abreu et al., 2017). In this present study, we used our methodology allied to *in silico* predictions of AMPs and ACPs to investigate the *A. rondoniae* venom, which to the best of our knowledge, remained largely unexplored to date.

MATERIALS AND METHODS

A scheme of the complete methodology used in this work is illustrated as a flow chart (**Figure 1**). Details of each block are given in the following items of this section.

Reagents

All proteolytic enzymes were obtained from Promega (Madison, WI, USA). Dithiothreitol (DTT) and iodoacetamide (IAA) were acquired from GE Healthcare (Chicago, IL, USA). Acetonitrile (ACN) was purchased from Avantor (Center Valley, PA, USA). Unless otherwise stated, all other reagents were acquired from Sigma-Aldrich (Saint-Louis, MO, USA).

Animals

Three adult *Acanthoscurria rondoniae* specimens were kept in captivity in the biotherium of the Laboratório Especial de Toxinologia Aplicada (LETA), Instituto Butantan (SP, Brazil). These animals were collected and maintained under SISBIO/

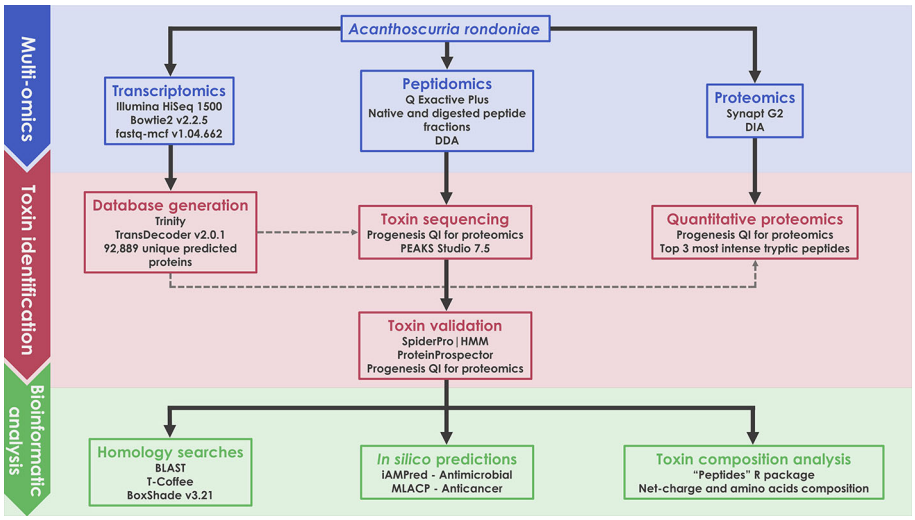

FIGURE 1 | Schematic representation of the multiomics workflow applied in this work.

ICMBio permanent license number 11024-3-IBAMA (Brazilian Institute of Environment and Renewable Natural Resources) and under the SisGen license number A82F014. The spiders were fed on 15-day intervals with cockroaches or crickets and had water *ad libitum*. All procedures were approved by the Research Ethical Committee of the Federal University of Sao Paulo (protocol number 7649061014).

Venom Gland Transcriptome sequencing

One female specimen of *A. rondoniae* was anesthetized with carbon dioxide for about 10 min, euthanized to extract the venom glands, which were immediately stored at −80°C. mRNA from the venom glands was extracted and further processed for cDNA library construction following the stranded TruSeq RNA Sample Prep Kit protocol (Illumina, San Diego, CA, USA) (Freitas-de-sousa et al., 2015). Briefly, selected poly-A-RNA was fragmented and primed with random hexamers. Fragmented RNA was reverse transcribed and the generated first strand cDNA was ligated to indexing adapters for hybridization in the flow cell of a HiSeq 1500 System (Illumina, Inc) for sequencing. The size distribution of the cDNA libraries was measured by 2100 Bioanalyzer with DNA1000 assay (Agilent Technologies, CA, USA). An ABI Step One Plus Real-Time PCR System was used in quantification of the sample library before sequencing. The cDNA libraries were sequenced on the Illumina HiSeq 1500 System, in Rapid paired-end flow cell in a strategy of 300 cycles of 2*150bp paired-end. The RNA-seq raw sequencing reads were pre-processed through an "*in house*" pipeline for the detection of PhiX contaminant, using the software bowtie2 version 2.2.5 (Langmead and Salzberg, 2012), followed by filter quality control, to trim and remove reads with low-complexity and homopolymer enriched regions, poly-A/T/N tails, adapter sequences and low-quality bases with the software fastq-mcf 1.04.662 (Aronesty, 2013). Trimming was performed for reads shorter than 40bp and if mean quality score was lower than 25 in a window size equal to 15 and filtered out those composed by 90% of homopolymers or low-complexity regions. The raw data generated in this project was deposited in the NCBI BioProject section under the accession code PRJNA633430 and BioSample SAMN14943686. This Transcriptome Shotgun Assembly was deposited at NCBI TSA under the accession GIOJ00000000.

Transcriptome Assembly and Database Generation

To generate a nonredundant set of transcripts, we performed a *de novo* assembly by the Trinity software (Grabherr et al., 2011) version r20131110, using 44,559,666 RNA-seq good quality paired-reads, with parameter CuffFly to reduce the number of false-positive isoforms, and minimum transcript length set to 300 bp. The prediction of translated amino acid sequences for the reconstructed transcripts were based on the TransDecoder software, version 2.0.1 (http://transdecoder.sourceforge.net/), considering only predicted proteins with protein length ≥60aa. Each transcript containing the coding sequences was aligned by BLASTp (Altschul, 1997) against the Uniprot/Swissprot protein database and the Transcriptome Shotgun Assembly (TSA) NCBI to assess the protein annotation with cutoff e-value <1e-5. The analysis of PFAM domains for the predicted proteins was based on hmmsearch tool in the software package hmmer (Johnson et al., 2010) against a PFAM domains database (Bateman, 2004), using the cutoff e-value <1e-3. The TransDecoder usually predicts more than one coding sequence by transcript and only one candidate was selected, following the priority order of match for UniProtKB/Swissprot, PFAM and TSA-NCBI for annotating and selecting the best candidate for each transcript.

Venom Extraction and Enrichment

The venom extraction procedure was carried out as previously described (Rocha-e-Silva et al., 2009). Briefly, after one week of fasting, three *A. rondoniae* specimens were anesthetized with

carbon dioxide (CO_2) and had their venom glands electrically stimulated at a frequency of 10 Hz and voltage of 10–25 V. After extraction, the venom was pooled due to the low yield of each individual and then the pool was quantified using the Bradford reagent and bovine serum albumin (BSA) as a standard. After quantification, 500 µg of the pooled venom was submitted to solid-phase extraction using C18 StageTips (Rappsilber et al., 2007), with minor adjustments, in order to enrich the peptide fraction. Briefly, the StageTips were conditioned with 500 µl of methanol, then with 500 µl of methanol:water (1:1) and centrifuged at 2,100 rpm for 2 min in both steps. Then, 500 µl of 80% ACN in 0.1% trifluoroacetic acid (TFA) were added to the StageTips and centrifuged at 1,800 rpm for 3 min. In the following step, 500 µl of 5% ACN in 0.1% TFA were added and the tip was centrifuged for 1800 rpm for 3 min. After conditioning and stabilization, 500 µg of pooled venom (diluted in 5% ACN in 0.1% TFA, to a total volume of 500 µl) were loaded to the StageTip and then centrifuged for 3 min at 1,400 rpm. Three washing steps were performed using 500 µl of 5% ACN in 0.1% TFA and centrifugation at 1,700 rpm for 2 min. Lastly, the peptide fraction was eluted in 500 µl of 40% ACN in 0.1% TFA by centrifugation at 1,700 rpm for 3 min. After enrichment, the sample was divided into six aliquots of equal volumes (83 µl), vacuum-dried using a Concentrator Plus (Eppendorf) and stored at 4°C until the digestion step.

Proteolytic Digestion

For proteomics analyses, a crude venom pool aliquot of 50 µg of proteins was digested with trypsin. For peptidomics analyses, five out of the six aliquots were submitted to proteolytic digestion using a different enzyme for each aliquot. The vacuum-dried aliquots were dissolved to 50 µl of digestion buffer according to the enzyme: NH_4HCO_3 50 mM for trypsin and Asp-N; phosphate buffer 50 mM for Glu-C; Tris/HCl 100 mM, $CaCl_2$ 10 mM for chymotrypsin and Tris/HCl 100 mM, $CaCl_2$ 0.5 mM for thermolysin. The sixth aliquot was directly dissolved in 0.1% formic acid for LC-MS/MS analysis to characterize the toxins in their native (mature) forms.

To digest the toxins, volumes of 25 µl of 0.2% Rapigest surfactant (Waters, MA, USA) were added to each sample, which were incubated at 80°C for 15 min. Samples were reduced with 2.5 µl of DTT 100 mM for 30 min at 60°C and then alkylated with 2.5 µl of IAA 300 mM for 30 min at room temperature in the dark. After reduction and alkylation, the enzymes were added in an enzyme:protein ratio of 1:100 and incubated at 37°C for 30 min. Except for thermolysin, in which a ratio of 1:250 was used and the incubation was performed at 75° C for 15 min. TFA was added to a final concentration of 0.5% to stop the digestions. Samples were filtered using Ultrafree -MC PVDF 0,22 µm filters (Millipore), vacuum-dried and stored at −20°C until MS analysis.

Mass Spectrometry: Peptidomics

For peptidomics analysis, digested and native peptide fractions were dissolved in 0.1% formic acid (solution A). Aliquots of 1 µl were automatically injected by a nano chromatography EASY-nlC 1200 system (Thermo Scientific) into a 15 cm x 50 µm Acclaim PepMap^{TM} C18 column (Thermo Scientific) coupled to a Q Exactive Plus mass spectrometer (Thermo Scientific). Peptides were eluted with a linear gradient of 7%–45% of solution B (80% acetonitrile in 0.1% formic acid) at 300 nl/min for 60 min. Spray voltage was set at 2.5 kV and the mass spectrometer was operated in the data dependent mode, in which one full MS scan was acquired in the m/z range of 300-1,500 followed by MS/MS acquisition using higher energy collision dissociation (HCD) of the five most intense ions from the MS scan. MS and MS/MS spectra were acquired in the Orbitrap analyzer at 70,000 and 17,500 resolution (at 200 m/z), respectively. Unassigned and +1 charge states were not subjected to fragmentation. The maximum injection times and AGC targets were set to 25 ms and 3E6 for full MS, and 40 ms and 1E5 for MS/MS. The minimum signal threshold to trigger fragmentation event, isolation window and stepped normalized collision energy (NCE) were set to, respectively, 2.5E4 cps, 1.4 m/z and 26, 28, and 30. A dynamic peak exclusion was applied to avoid the same m/z selection for the next 5 seconds. All samples were analyzed in duplicates.

Mass Spectrometry: Proteomics

The proteomics analysis of the digested crude venom pool was performed on a Synapt G2 mass spectrometer coupled to a nanoAcquity UPLC system (Waters). Five µl of peptide samples were loaded online in a Symmetry C18 trapping column (5 µm particles, 180 µm x 20 mm length; Waters) for 5 min at a flow rate of 8 µl/min of phase A (0.1% formic acid). The mixtures of trapped peptides were subsequently separated by elution with a gradient of 7%–35% of phase B (0.1% formic acid in acetonitrile) through a BEH 130 C18 column (1.7 µm particles, 75 mm by 150 mm; Waters) over 90 min at 275 nl/min. Data were acquired in the data independent acquisition mode HDMS^E with ion mobility separation in the m/z range of 50–2,000 and in the resolution mode. Peptide ions were fragmented by collision induced dissociation (CID) and energies were alternated between 4 eV and a ramp of 15–65 eV for precursor ion and fragment ions, respectively, using scan times of 1.25 s (Abreu et al., 2017; Pedroso et al., 2017). The ESI source was operated in positive mode with a capillary voltage of 3.0 kV, block temperature of 100°C, and cone voltage of 40 V. For lock mass correction, Glu-Fibrinopeptide B (500 fmol/mL in 50% acetonitrile, 0.1% formic acid; Peptide 2.0) was infused through the reference sprayer at 500 nl/min and sampled for 0.5 s every 60 s. The venom pool was analyzed in triplicate. All mass spectrometry data (DIA and DDA) were deposited to the ProteomeXchange Consortium *via* the PRIDE (Perez-Riverol et al. 2019) partner repository with the dataset identifier PXD019343.

Bioinformatic Analysis

Quantitative Peptidomics and Proteomics

For quantitative peptidomics, mass spectrometry raw data of the native venom peptides were loaded in Progenesis QI for proteomics (Nonlinear Dynamics, Newcastle, UK). Briefly, a

reference run for the duplicates was automatically selected. The retention times of precursor ions were processed for alignment, peak picking and normalized to the reference run using default parameters. The normalized data was exported from Progenesis QI for proteomics in.csv format and further analysis were made in Microsoft Excel (Microsoft), where precursor ions with an intensity below $5.0x10^5$ or with redundant m/z values were excluded from subsequent analysis.

Quantitative proteomics was also performed in Progenesis QI for proteomics with the same processing parameters. After processing, a.mgf file of all MS/MS spectra was exported to PEAKS Studio 7.5 (Bioinformatics Solutions Inc.) for protein identification (as described in "Toxin Sequencing"). The identification results were exported back to Progenesis as a.xml file. Venom proteins were quantified by the average signal intensity of the three most intense tryptic peptides of each protein (Silva et al., 2006). Only proteins identified with a minimum of three peptides and in at least two of the three replicates were considered for further analysis.

Toxin Sequencing

Mass spectrometry raw data of digested venom fractions were loaded and processed in PEAKS Studio 7.5 (Bioinformatic Solutions Inc.). *De novo* analysis was performed according to the following parameters: precursor ion mass tolerance of 10 ppm, fragment ion mass tolerance of 0.025 Da, maximum of one nonspecific cleavage, maximum of two missed cleavages and enzyme set according to the sample. Cys carbamidomethylation was set as fixed modification and Asn/Gln deamidation, Met oxidation and N-terminal acetylation as variable modifications. Database searches were performed with the same parameters of *de novo* analysis against the previously built *A. rondoniae* venom gland transcriptome (92,939 sequences and 251 common contaminants) utilizing *de novo* sequenced peptides with average local confidence (ALC) scores ≥50%. Posttranslational modifications and homology searches were performed through PEAKS PTM and SPIDER modules, respectively. The false discovery rate (FDR) was estimated by the decoy fusion method (Zhang et al., 2012) and set to a maximum of 1%.

Mature Toxin Validation

Primary structures of toxins identified by *de novo* and database search were submitted to analysis on the Spider|ProHMM module of ArachnoServer 3.0 (Pineda et al., 2018) in order to predict the cleavage sites of signal peptide and propeptide, ultimately resulting in the prediction of its mature sequences. The predicted mature sequences were then confronted with the sequences obtained experimentally, and if a correspondence was observed, the toxin was considered fully sequenced by LC-MS/MS. Mature sequences were also submitted to analysis in the MS-Product module of ProteinProspector v5.22 (http://prospector.ucsf.edu/prospector/mshome.htm), which provides theoretical fragmentations and precursor ion m/z values. The theoretical m/z values of precursor ions with charges ranging from +2 to +9 were compared to those assigned in Progenesis QI for proteomics and also manually validated in the raw data of the native toxins through Xcalibur (Thermo Scientific). If a peak corresponding to a m/z value of a mature toxin was found in the raw data and the consensus sequence was supported by MS/MS data, the presence of the toxin in the venom was validated.

Homology Search and Alignment

Validated mature sequences were submitted to homology search through BLAST (https://www.uniprot.org/blast/), aligned with T-Coffee (http://tcoffee.crg.cat/apps/tcoffee/do:regular) and lastly, edited with Boxshade (http://www.ch.embnet.org/software/BOX_form.html).

In Silico Anticancer and Antimicrobial Assays

For the prediction of possible biological activities, *in silico* analysis were performed by two tools. For antimicrobial activity, we utilized iAMPpred (Meher et al., 2017), a sequence-based computational tool which provides a score (ranging from 0 to 1) which reflects potential antibacterial, antiviral and antifungal properties. For this analysis, only scores >0.8 were considered as significant values. Gomesin from *A. gomesiana* hemolymph (Silva et al., 2000) was utilized as a positive control for antibacterial activity. Mouse β-defensin-4 (mBD4) and P9 (Zhao et al., 2016), a peptide derived from mBD4, were utilized as positive controls for antiviral activity. Rondonin from *A. rondoniae* hemolymph (Riciluca et al., 2012) and gomesin were utilized as positive controls for antifungal activity. For the prediction of antitumoral activities, we utilized MLACP (Manavalan et al., 2017), a sequence-based computational tool that utilizes two distinct machine-learning based algorithms, RFACP and SVMACP. Only peptides which presented a consensus with the two algorithms, with both presenting scores >0.5, were considered as potential ACPs, as recommended by the authors (Manavalan et al., 2017). For this analysis, we utilized gomesin (Ikonomopoulou et al., 2018), Aurein 1.2 from the frog *Litoria aurea* (Rozek et al., 2000) and human neutrophil peptide-1 (HNP-1) (Gaspar et al., 2015) as positive controls for anticancer activity.

Net Charge and Amino Acids Composition Analysis

Net charge and amino acid composition were calculated by the R scripts in the package Peptides (Osorio et al., 2015). For net charge analysis, only CRPs were selected and Cys residues were not considered due to disulfide bonds. For amino acids composition, only predicted ACPs were selected.

RESULTS

A. rondoniae Venom Gland Transcriptomics

Sequencing of the venom gland transcriptome of *A. rondoniae* resulted in a total 46,511,000 raw paired-reads. After the quality processing of raw reads, a total of 44,559,666 high-quality reads remained (95.8% of the total). *De novo* assembly using Trinity was performed on high-quality reads generating 150,409

transcripts, with an N50 value of 892 bp, a median length of 473 bp and an average transcript length of 735 bp. These transcripts generated 92,889 unique predicted proteins from the transcriptome, which were used as the reference database for the peptidomics and proteomics analysis.

A. rondoniae Venom Peptidomics

Raw mass spectral files (.raw) of native venom peptides, were initially processed in Progenesis QI for proteomics, resulting in a total of 17,329 mature precursor ions recorded. After manual filtering for threshold establishment and clustering of redundant peptide ions, a total of 2,800 precursor ions were kept for further analysis (**Figure 2A** and **Supplementary Table 1**). Main clusters of precursor ions around 5, 5.5, 6, and 7 kDa, mass values typically observed for CRPs from tarantula venoms (King and Hardy, 2013; Abreu et al., 2017). Also, there is a cluster in a mass range below 1.5 kDa, which represents short peptides also commonly found in tarantulas (King and Hardy, 2013). *De novo* sequencing, database searches and homology analysis of MS/MS spectra of digested venom peptides resulted in the identification of 12,032 peptide spectrum matches corresponding to 2,770 cleaved peptides (**Supplementary Table 2**) belonging to 74 different proteins (**Supplementary Table 3**). Among these 74 proteins, 62 were identified with more than two unique peptides and 12 with two unique peptides. The N-terminal of the mature toxins was determined by our multiple digestion approach, given that the same N-terminal amino acid was identified by consensus MS/MS spectra from different enzymes. Although the solid phase extraction step of our method was focused to enrich venom peptides, we identified 55 proteins with mass above 15 kDa (**Supplementary Table 3**). However, the protein masses from entries in the transcriptomic database are from the complete sequences, with the signal peptide and prodomains, adding the respective masses to the

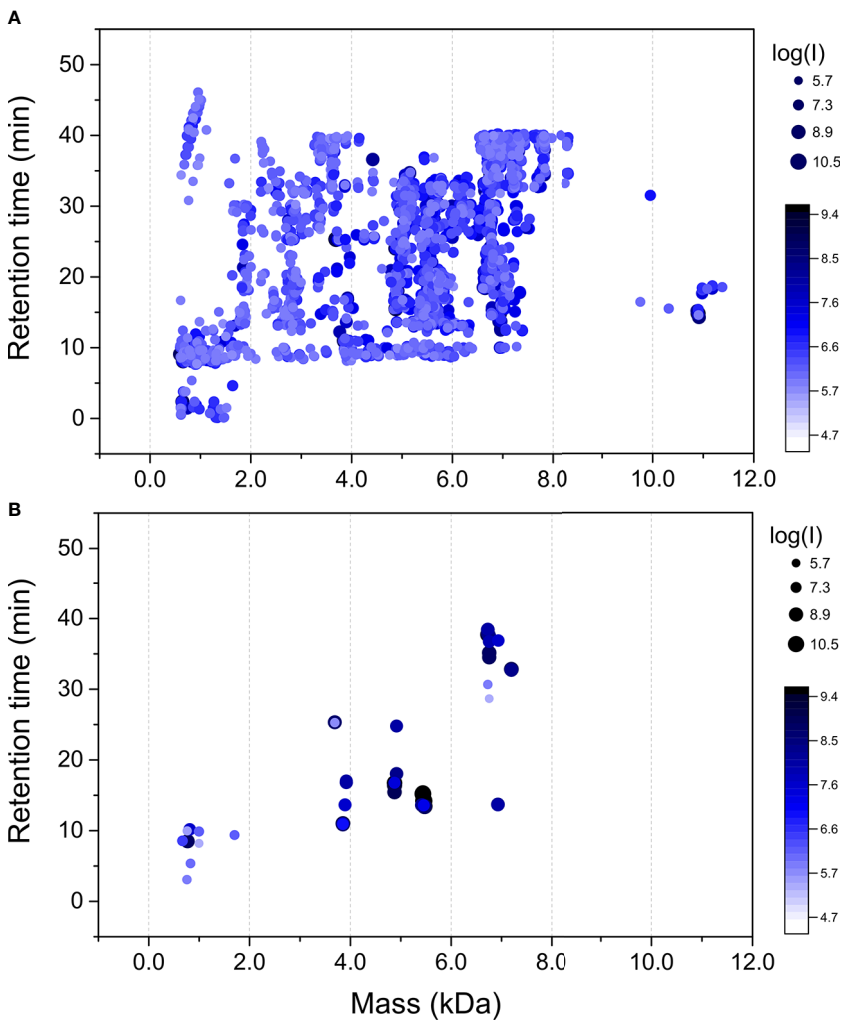

FIGURE 2 | Mass maps of precursor ions identified in *Acanthoscurria rondoniae* peptidomic venom fraction after Progenesis QI for proteomics raw data processing. **(A)** 2,800 precursor ions obtained after manual filtering and clustering of redundant ions. **(B)** Precursor ions corresponding to the 18 mature toxins validated in *A. rondoniae* venom in different charge states.

TABLE 1 | Mature toxins identified and validated in *Acanthoscurria rondoniae* peptidomic venom fraction.

Toxin	Monoisotopic mass (Da)	Mature sequence	AA	S-S	Log (I)	Rank
VLPVFV	670.41	PLPVFV	6	–	6.38	15
VVVPFVV	757.47	VVVPFVV	7	–	8.54	9
VENLAEP	770.39	VENLAEP	7	–	8.78	8
VLPPLKF	812.40	VLPPLKF	7	–	7.60	13
VPPILKY	828.51	VPPILKY	7	–	5.91	18
YPPPPPPPH	997.50	YPPPPPPPH	9	–	6.21	16
FETPNNPDGKVTKQE	1702.82	FETPNNPDGKVTKQE	15	–	6.08	17
U1-TRTX-Agm3a	3690.49	ACGSFMWKCSERLPCCQEYVCSPQWKWCQNP	31	3	9.49	2
U1-TRTX-Ar1a	3852.54	SCVHERETCSKVRGPLCCRGECTCPIYGDCFCYGS	35	4	9.08	4
U1-TRTX-Ar1b	3920.58	SCVYERETCSKVRGPLCCRGECTCPIYGDCFCYGS	35	4	8.05	12
U2-TRTX-Ar1a	4876.02	CATENVPCDENRPGDCCSEYECLKPTGHGWWYASYYCYKKKSG	43	3	8.91	6
U3-TRTX-Ar1a	5439.80	IIECFFSCEIEKDGKSKEGKPCKPKGDKDKDKKCSGGWRCKLKLCLKI	48	3	10.29	10
U3-TRTX-Ar1b	5457.75	IIECFFSCEIEKDGKSKEGKPCKPKGDKDKDKKCSGGWRCKLKMCLKI	48	3	10.54	1
U4-TRTX-Ar1a	6728.19	ECKQLKEKCSNHCDCCGKTVLCATVYVGRNTEMLCKEKRSDDPILNSIGKVINAATKAMSGC	62	4	9.36	3
U4-TRTX-Ar1b	6755.19	ECKQLKEKCNNHCDCCGKTVLCATVYVGRNTEMLCKEKRSDDPILNSIGKVINAATKAMSGC	62	4	8.80	7
U5-TRTX-Ar1a	6928.76	ACTTEADCPNGCCTGGSFHRYCRSYGGEMDQCEPRNDFGSYSTACPCKEEFECSPIKRCQRR	62	5	8.32	11
U6-TRTX-Ar1a	6936.18	NREHCYIPRRRCVTTEQCCKPYDTVNYFVACGKAWPEDKKRKVNKCYICNNELTVCTR	58	4	7.56	14
U7-TRTX-Ar1a	7195.23	ETSCIEELQTCKNSCECCGTTTICSPSWVDGNEIKLCRNEGNKLQKVWHFFQKAYSKMHSCKT	63	4	8.98	5

Intensities are shown in a logarithmic scale (log10) and ranks were assigned based on the intensities. AA, number of amino acids; S-S, number of disulfide bonds.

mature proteins. Besides, part of the heavier venom proteins may have bypassed the enrichment, as it seems to be the case of the 53.3 kDa Ar-CRISP, identified with 202 unique peptides and 80% coverage, and the 82.4 kDa Ar-Neprilysin-1, identified with 193 unique peptides and 81% coverage (**Supplementary Table 3**).

The theoretical m/z values of these 74 proteins were calculated in ProteinProspector and then compared to those present in Progenesis QI for proteomics data (**Supplementary Table 1**). A total of 57 toxins fully sequenced from the overlapping peptide fragments generated by multiple enzyme digestions are possible mutated CRPs and posttranslational modified forms. To validate the identification of mature toxins, precursor ion spectra were manually analyzed in Xcalibur (Thermo Scientific) to confirm monoisotopic peak and charge state assignments. This resulted in the validation of 17 new toxins and also of the U1-TRTX-Agm3a, a toxin described by our group in the *Acanthoscurria gomesiana* venom (Abreu et al., 2017). In total, 18 mature toxins were validated (**Figure 2B** and **Table 1**). The 17 new toxins are distributed in 7 families containing a total of 10 CRPs and seven short peptides (**Table 1**). The CRPs families were named according to the nomenclature proposed by King et al. (King et al., 2008). In order to add another level of validation to the mature CRPs identified, the whole translated sequences predicted by our transcriptome were processed in the SpiderPro|HMM module of ArachnoServer 3.0 (Pineda et al., 2018). The mature sequences of six CRP families were confirmed by the propeptide and signal peptide cleavage site predictions, here represented by the predicted transcript of each family, except for the U6-TRTX-Ar1a, which is two amino acids residues (NR) longer than predicted in the N-terminus (**Supplementary Table 4**).

We could not validate the presence of the mature forms of the other 40 possibly mutated or modified CRPs and thousands of native precursor ions still remained to be identified. We consider that many of these forms are derived from the main CRP families identified, as clusters of masses are observed around the main seven classes reported here (**Figure 2A** and **Table 1**). Posttranslational modifications, mutations and proteolytic processing at alternative sites may result in a complex population of toxin proteoforms present in the spider venoms. Incorrect assignment of monoisotopic peaks and charge state on acquisition may also limit identification and redundant ion clustering. In addition, native toxins of ~11 kDa (**Figure 2A**) could not have their mature forms identified and other CRP families may have been missed in our native peptidomic analysis. For *in silico* analysis, only the 18 validated toxins without any posttranslational modifications were utilized.

A. rondoniae Venom Proteomics

In the proteomics analysis of the *A. rondoniae* venom 33 proteins were quantified. We only considered proteins identified with at least three peptides and present in two out of three replicates (**Table 2**). The most abundant venom protein was the cysteine-rich secretory protein (Ar-CRISP), composing 28% of the venom, followed by the CRP U3-TRTX-Ar1a (26%) and then, the U5-TRTX-Ar1a (15%). These first three toxins represent 69% of the *A. rondoniae* venom toxins. The CRP proteoforms identified in the peptidomics analysis were not included in the quantitative proteomics due to the difficulty to precisely quantify sequences with high homologies. But the U3-TRTX-Ar1b, differing by only one amino acid from the U3-TRTX-Ar1a (L44M), is the most intense peak among the native CRPs, corroborating the proteomics results. The most abundant toxin family is of the CRP, composing 58% of the venom (**Table 2**). The venom also contains significant amounts of the metalloprotease neprilysin-1 (Ar-Neprilysin-1, 8.4%) and hyaluronidase (Ar-Hyaluronidase, 1.5%). The proteins are homologous to those of the *A. geniculata* venom (Sanggaard et al., 2014). The Ar-CRISP is 76% homologous to the putative cysteine-rich protease (L1941_T1/1_Tarantula_S_fr3), Ar-

TABLE 2 | Relative quantification of proteins by proteomic analysis of the venom of *Acanthoscurria rondoniae*.

Accession	Peptide count	Mass (kDa)	Description	NI	%
comp117964_c0_seq1.p1	181	53.3	Ar-CRISP	1.38E+07	27.9%
comp90511_c0_seq1.p1	28	10.7	U3-TRTX-Ar1a	1.29E+07	25.9%
comp105543_c0_seq1.p3	25	9.4	U5-TRTX-Ar1a	7.29E+06	14.7%
comp127239_c0_seq1.p1	101	82.4	Ar-Neprilysin-1	4.16E+06	8.4%
comp57753_c0_seq1.p1	13	12.3	U4-TRTX-Ar1a	4.13E+06	8.3%
comp90508_c2_seq2.p1	5	15	U2-TRTX-Ar1a	2.51E+06	5.1%
comp107050_c0_seq2.p2	12	13	U7-TRTX-Ar1a	1.47E+06	3.0%
comp127127_c4_seq1.p1	46	49.8	Ar-Hyaluronidase	7.49E+05	1.5%
comp125618_c0_seq2.p1	5	6.9	U1-TRTX-Agm3a	6.81E+05	1.4%
comp90482_c0_seq1.p1	26	48.6	PFAM: Serpin (serine protease inhibitor)	4.25E+05	0.9%
comp98439_c0_seq1.p1	4	16.3	PFAM: Thyroglobulin type-1 repeat	3.23E+05	0.7%
comp117041_c0_seq1.p1	28	42.8	PFAM: Tyrosine phosphatase family	2.45E+05	0.5%
comp57865_c0_seq1.p1	7	18.5	Unknown	1.86E+05	0.4%
comp99029_c0_seq1.p1	4	10.8	U6-TRTX-Ar1a	1.62E+05	0.3%
comp117273_c1_seq1.p1	23	45.1	PFAM: Putative serine esterase (DUF676)	1.46E+05	0.3%
comp119317_c0_seq2.p1	20	87.2	PFAM: Peptidase family M13	1.28E+05	0.3%
comp116850_c0_seq2.p1	9	53.1	PFAM: Zinc carboxypeptidase	6.93E+04	0.1%
comp122884_c0_seq2.p1	5	78.9	PFAM: Peptidase S8 pro-domain	4.99E+04	0.1%
comp117075_c0_seq1.p1	3	25.5	PFAM: Tetraspanin family	4.61E+04	0.1%
comp115582_c0_seq1.p1	10	76.4	PFAM: Neutral/alkaline nonlysosomal ceramidase	4.30E+04	0.1%
comp113427_c0_seq1.p1	11	91.1	PFAM: Fasciclin domain	4.15E+04	0.1%
comp87917_c0_seq1.p1	5	12.2	TSA: U3-hexatoxin-Hib [Hadronyche infensa]	1.98E+04	0.0%
comp27569_c0_seq1.p1	3	27.4	TSA: putative uncharacterized protein. partial	1.53E+04	0.0%
comp126642_c0_seq1.p1	3	46.1	PFAM: Cysteine-rich secretory protein family	1.16E+04	0.0%
comp114378_c0_seq1.p1	18	72.2	PFAM: Hemocyanin. copper containing domain	7.96E+03	0.0%
comp120272_c1_seq8.p1	3	39.9	TSA: peptidylglycine alpha-hydroxylating monooxygenase	4.76E+03	0.0%
comp121853_c0_seq2.p1	6	72.3	PFAM: Angiotensin-converting enzyme	4.54E+03	0.0%
comp114378_c0_seq4.p1	17	71.5	PFAM: Hemocyanin. copper containing domain	2.72E+03	0.0%
comp117984_c0_seq2.p1	4	31.1	PFAM: Immunoglobulin I-set domain	2.60E+03	0.0%
comp57921_c1_seq1.p1	4	44.9	PFAM: Hemocyanin. ig-like domain	7.99E+02	0.0%
comp114578_c0_seq3.p1	7	25.1	TSA: tri-cap-1 [Trittame loki]	4.91E+02	0.0%
comp114378_c0_seq2.p1	16	73.7	PFAM: Hemocyanin. ig-like domain	1.71E+02	0.0%
comp86283_c0_seq1.p1	6	78.4	PFAM: Transferrin	0.00E+00	0.0%

Neprilysin-1 is 74% and Ar-Hyaluronidase is 80% to the respective Membrane venom metalloendopeptidase-a (L67_T1/2_Tarantula_V_fr5) and Venom hyaluronidase (L1941_T1/1_Tarantula_S_fr3) from *A. geniculata* (Sanggaard et al., 2014).

In Silico Analysis Suggests Possible Antimicrobial Activities of CRPs and Antitumoral Activities of Short Peptides

For screening of the possible biological activities of *A. rondoniae* toxins, we performed *in silico* simulations using iAMPred (Meher et al., 2017) and MLACP (Manavalan et al., 2017), two machine-learning algorithms to evaluate potential antimicrobial and antitumoral activities, respectively. Both tools give as the output a score from 0 to 1. Higher scores suggest a higher probability of presenting the respective activity.

The results indicate that all new CRPs may have antimicrobial activities (**Table 3**). In general, higher scores were obtained for antimicrobial and antifungal activities (>0.9 for both in all seven families), but all CRPs showed antiviral scores >0.5, with the lowest score being 0.685 for U2-TRTX-Ar1a, while all other toxins had scores higher than 0.8. The U3-TRTX-Ar1x family demonstrated the highest scores for antibacterial (>0.99) and antifungal activities (>0.97). As for short peptides, our results suggest a lower probability of presenting antimicrobial activity, except for the peptide VLPPLKF, which had scores above 0.79 for all three activities. Our positive control for antibacterial activity, gomesin, obtained a score of 0.985, close to those observed for the seven CRPs families. This was also observed for the positive controls of antifungal activity, gomesin and rondonin, with scores of 0.973 and 0.903, respectively (**Table 3**). Lastly, our positive controls for antiviral activity, mBD4 and P9, a peptide derived from mBD4, obtained scores of 0.773 and 0.940, respectively.

On the other hand, the results obtained for antitumoral activities demonstrate that short peptides of *A. rondoniae* are more prone to present antitumoral properties than the CRPs in this *in silico* analysis. From the 7 short peptides, 4 demonstrated a consensus on the two algorithms, indicating potential antitumoral activities (**Table 3**). These short peptides are: PLPVFV, VPPILKY, VVVPFVV and VLPPLKF. The two CRPs indicating potential antitumoral activity are the U1-TRTX-Agm3a and the U1-TRTX-Ar1b. Gomesin, aurein 1.2 and human neutrophil peptide-1 (HNP-1), used as positive controls for anticancer activity, demonstrated consensus on the two algorithms (**Table 3**).

Homology Analysis Indicates Potential Biological Activities for Cysteine-Rich Toxins

In order to identify homologous toxins from other spiders and provide insights of possible biological activities by structural similarity, one toxin of each of the seven families of CRPs were

TABLE 3 | *In silico* predictions of biological activities of validated toxins identified in the venom of *A. rondoniae* spiders.

	Antimicrobial activity			Antitumoral activity			
Peptide	**Bacterial**	**Viral**	**Fungal**	**RFACP**	**Prob.**	**SVMACP**	**Prob.**
Gomesin	0.985	0.898	0.973	ACP	0.668	ACP	0.926
Rondonin	0.671	0.301	0.903	Non-ACP	0.400	Non-ACP	0.447
P9	0.997	0.940	0.992	Non-ACP	0.479	ACP	0.816
mBD4	0.990	0.773	0.968	Non-ACP	0.371	ACP	0.837
Aurein 1.2	0.940	0.913	0.917	ACP	0.870	ACP	0.935
HNP-1	0.920	0.920	0.950	ACP	0.879	ACP	0.938
PLPVFV	0.623	0.586	0.515	ACP	0.639	ACP	0.656
VVVPFVV	0.645	0.538	0.432	ACP	0.637	ACP	0.635
VENLAEP	0.083	0.046	0.028	Non-ACP	0.296	Non-ACP	0.508
VLPPLKF	0.801	0.794	0.828	ACP	0.632	ACP	0.740
VPPILKY	0.751	0.410	0.429	ACP	0.501	ACP	0.528
YPPPPPPPH	0.542	0.382	0.406	Non-ACP	0.442	ACP	0.618
FETPNNPDGKVTKQE	0.133	0.143	0.082	Non-ACP	0.350	Non-ACP	0.164
U1-TRTX-Agm3a	0.843	0.696	0.579	ACP	0.559	ACP	0.878
U1-TRTX-Ar1a	0.994	0.968	0.976	Non-ACP	0.489	ACP	0.862
U1-TRTX-Ar1b	0.987	0.966	0.972	ACP	0.541	ACP	0.903
U2-TRTX-Ar1a	0.940	0.685	0.920	Non-ACP	0.283	ACP	0.624
U3-TRTX-Ar1a	0.996	0.918	0.982	Non-ACP	0.292	Non-ACP	0.360
U3-TRTX-Ar1b	0.997	0.924	0.986	Non-ACP	0.324	Non-ACP	0.381
U4-TRTX-Ar1a	0.981	0.770	0.954	Non-ACP	0.139	Non-ACP	0.121
U4-TRTX-Ar1b	0.978	0.742	0.937	Non-ACP	0.142	Non-ACP	0.128
U5-TRTX-Ar1a	0.996	0.858	0.989	Non-ACP	0.363	ACP	0.519
U6-TRTX-Ar1a	0.986	0.826	0.947	Non-ACP	0.300	ACP	0.538
U7-TRTX-Ar1a	0.991	0.855	0.926	Non-ACP	0.256	Non-ACP	0.302

Antimicrobial activities were predicted by iAMPpred (Meher et al., 2017). Anticancer activities were predicted by MLACP (Manavalan et al., 2017): RFACP, random forest method; SVAMCP, support vector machine method; ACP, anticancer peptide; Non-ACP, nonanticancer peptide.

selected for BLAST analysis. In general, our results demonstrated a high conservation of primary sequences among species of the same genus (Acanthoscurria) and decreasing homology with increasing distance in the phylogenetic tree (**Figure 3**). For instance, the U1-TRTX-Ar1a is 97% homologous to the *A. gomesiana* U1-TRTX-Agm2a (Abreu et al., 2017) and to the *A. geniculata* genicutoxin-D1 (Sanggaard et al., 2014). The next closest homolog is the HNTX-XVII.3, from *Cyriopagopus hainanus* (**Figure 3A**), with 62% homology. U1-TRTX-Agm2a has potential antimicrobial activity (Abreu et al., 2017) and HNTX-XVII.3 presents weak inhibition of Kv1.2/KCNA2 and Kv1.3/KCNA3 voltage-gated potassium channels. U1-TRTX-Ar1a presented high levels of *in silico* antibacterial, antiviral and antifungal scores (>0.96 for all three) and may present potassium channel modulation by homology to the HNTX-XVII.3.

The U2-TRTX-Ar1a is 88% homologous to the genicutoxin-B2 from *A. geniculata* (Sanggaard et al., 2014), 74% to Ω-TRTX-Bs2a from *Brachypelma smithi* (Corzo et al., 2008) (**Figure 3B**), 70% to U11-TRTX-Hhn1k from *Cyriopagopus hainanus* and 69% to Ω-TRTX-Asp3, from *Aphonopelma* sp. *Brachypelma smithi* is a Mexican Theraphosid and the Ω-TRTX-Bs2a has insecticidal activity against crickets, possibly acting on the Para/tipE insect sodium channels (Corzo et al., 2008). As the U2-TRTX-Ar1a, the Ω-TRTX-Bs2a is amidated at the C-terminal Ser. Interesting to notice that the identification of a peptidylglycine alpha-hydroxylating monooxygenase in the venom proteome (comp120272_c1_seq8.p1, **Table 2**) supports this PTM. The U3-TRTX-Ar1a is highly homologous to toxins already reported in other Acanthoscurria spiders, with 96% homology to the *A. gomesiana* U1-TRTX-Agm1a (Abreu et al., 2017), 94% to the *A. paulensis* U1-TRTX-Ap1a (Mourão et al., 2013) and 92% to the *A. natalensis* μ-TRTX-An1a (Rates et al., 2013) (**Figure 3C**). The U3-TRTX-Ar1a levels of antimicrobial scores were >0.98 for antibacterial and antifungal activities, corresponding to the antimicrobial potential of U1-TRTX-Agm1a (Abreu et al., 2017). The U1-TRTX-Ap1a is insecticidal against *Spodoptera frugiperda* caterpillars and *Drosophila melanogaster* (Mourão et al., 2013). And the μ-TRTX-An1a affects insect neuronal voltage-dependent sodium channels (Rates et al., 2013). The U4-TRTX-Ar1a, U5-TRTX-Ar1a, U6-TRTX-Ar1a and U7-TRTX-Ar1a presented different levels of homology to other spider toxins reported mostly at the transcript level (**Figure 3**).

Net Charge Analysis and Amino Acid Composition

From all 11 CRPs analyzed, seven presented positive net charge at physiological pH (7.4), two are negatively charged and two are neutral (**Figure 4**). The U6-TRTX-Ar1a presented the highest net charge at physiological pH (+6,0), followed by the U3-TRTX-Ar1a/b with a net charge of +5,9. The negatively charged CRPs U2-TRTX-Ar1a and U5-TRTX-Ar1a presented net charges values of −0,96, and −0,95, respectively. As for amino acid composition, only the predicted ACPs were selected, totalizing two CRPs and four short peptides. Our main goal was to evaluate the percentage of nonpolar (hydrophobic) residues in those toxins. We observed high percentages of hydrophobic residues

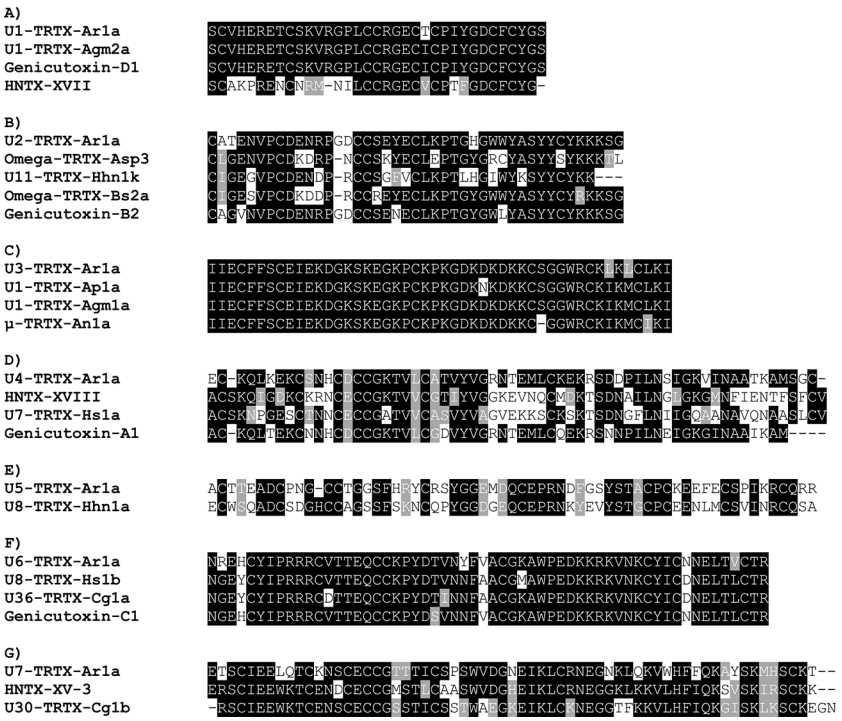

FIGURE 3 | Alignments of the seven families of CRPs validated in *Acanthoscurria rondoniae* peptidomic venom fraction with homologous toxins (>50% primary structure similarity) from other spider species. **(A)** U1-TRTX-Ar1a: *A. rondoniae*; U1-TRTX-Agm2a: *A. gomesiana* (UniProt ID: P0DQJ4); Genicutoxin-D1: *A. geniculata*; HNTX-XVII: *Cyriopagopus hainanus* (UniProt ID: D2Y2C5). **(B)** U2-TRTX-Ar1a: *A. rondoniae*; Omega-TRTX-Asp3: *Aphonopelma sp* (UniProt ID: P0CI04); U11-TRTX-Hhn1k: *Cyriopagopus hainanus* (UniProt ID: D2Y281); Ω-TRTX-Bs2a: *Brachypelma smithi* (UniProt ID: B3FIV1); Genicutoxin-B2: *A. geniculata*. **(C)** U3-TRTX-Ar1a: *A. rondoniae*; U1-TRTX-Ap1a: *A. paulensis* (UniProt ID: B3EWY4); U1-TRTX-Agm1a: *A. gomesiana* (UniProt ID: P0DQJ3); μ-TRTX-An1a: *A. natalensis* (UniProt ID: B3A0P0). **(D)** U4-TRTX-Ar1a: *A. rondoniae*; HNTX-XVIII: *Cyriopagopus hainanus* (UniProt ID: D2Y251); U7-TRTX-Hs1a: *Cyriopagopus schmidti* (UniProt ID: B3FIN4); Genicutoxin-A1: *A. geniculata*. **(E)** U5-TRTX-Ar1a: *A. rondoniae*; U8-TRTX-Hhn1a: *Cyriopagopus hainanus* (UniProt ID: D2Y2C0). **(F)** U6-TRTX-Ar1a: *A. rondoniae*; U8-TRTX-Hs1b: *Cyriopagopus schmidti* (UniProt ID: P82960); U36-TRTX-Cg1a: *Chilobrachys guangxiensis* (UniProt ID: B1P1J5); Genicutoxin-C1: *A. geniculata*. **(G)** U7-TRTX-Ar1a: *A. rondoniae*; HNTX-XV-3: *Cyriopagopus hainanus* (UniProt ID: D2Y2B9); U30-TRTX-Cg1b: *Chilobrachys guangxiensis* (UniProt ID: B1P1I2).

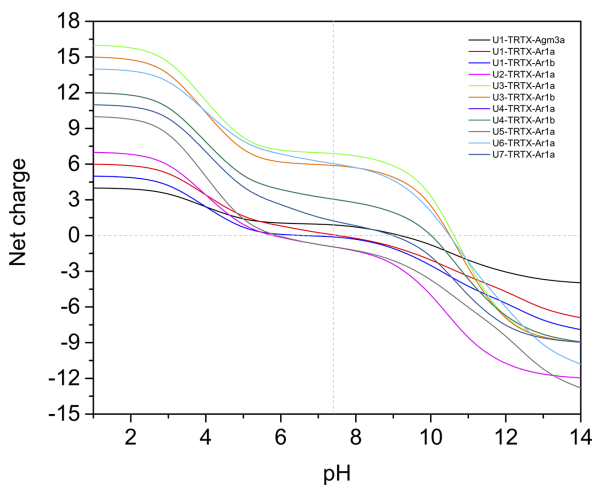

FIGURE 4 | Net-charge analysis of all CRPs validated in *Acanthoscurria rondoniae* peptidomic venom fraction. Net charges were calculated in pH ranges of 0-14 in 0.5 intervals.

(>60%) in CRPs and even higher percentages of hydrophobic residues (>85%) in short peptides (**Table 4**).

DISCUSSION

In this study, we applied a multiomics strategy to explore the venom composition of *A. rondoniae* and *in silico* analysis in order to prospect new toxins with possible therapeutical applications. Previously, one experimental study was conducted to characterize AMPs from *A. rondoniae* spiders, which led to the identification of rondonin, an antifungal peptide present in the spider hemolymph (Riciluca et al., 2012). To our knowledge, this work is the first analysis of *A. rondoniae* venom composition. Through this strategy, we sequenced the venom gland transcriptome, identified and quantified proteins and determined the sequences of mature toxins of 17 new CRPs and short peptides present in the native venom, as well as one previously identified by our group, U1-TRTX-Agm3a (Abreu et al., 2017).

TABLE 4 | Amino acids composition analysis of anticancer peptides (ACPs) predicted by MLACP (Manavalan et al., 2017).

Amino acids class	Peptide											
	U1-TRTX-Agm3a		U1-TRTX-Ar1b		VLPPLKF		PLPVFV		VVVPFVV		VPPILKY	
	#	%	#	%	#	%	#	%	#	%	#	%
Tiny	5	20	9	33.3	0	0	0	0	0	0	0	0
Small	10	40	14	51.9	3	42.9	4	66.7	6	85.7	3	42.9
Aliphatic	3	12	4	14.8	3	42.9	3	50	5	71.4	3	42.9
Aromatic	5	20	4	14.8	1	14.3	1	16.7	1	14.3	1	14.3
Hydrophobic	13	52	14	51.9	6	85.7	6	100	7	100	6	85.7
Hydrophilic	12	48	13	48.1	1	14.3	0	0	0	0	1	14.3
Charged	5	20	8	29.6	1	14.3	0	0	0	0	1	14.3
Cationic	3	12	4	14.8	1	14.3	0	0	0	0	1	14.3
Anionic	2	8	4	14.8	0	0	0	0	0	0	0	0

Homology searches and alignments demonstrated similarities of all seven CRP families to toxins reported in other spider venoms and, as expected, higher similarity to toxins of other Acanthoscurria spiders. The results indicate that these toxins may be biologically essential for the spider survival and also highlights a close phylogeny relationship within the genus. The U3-TRTX-Ar1x family demonstrated a high similarity with the toxins U1-TRTX-Ap1a, U1-TRTX-Agm1a, and μ-TRTX-An1a, all from other Acanthoscurria spiders. It is important to notice that this family also corresponds to the most expressed CRP in *A. rondoniae* venom observed by the quantitative proteomics and peptidomics approaches. The data highlights the relevance of U3-TRTX-Ar1x family for *A. rondoniae* spiders. Similarly to other spider venoms, enzymes as neprilysin, hyaluronidase, and carboxypeptidases, among others were found in the venom of *A. rondoniae* (Sanggaard et al., 2014; Borges et al., 2016; Kuhn-Nentwig et al., 2019). These enzymes may act in synergy with the neurotoxic CRPs to increase the spread and efficiency of the venom in the preys, as hypothesized elsewhere (Kuhn-Nentwig et al., 2019).

Our results from antimicrobial activity prediction demonstrated that all new CRPs identified in *A. rondoniae* venom have a probability of being antimicrobial, while only one short peptide (sequence: VLPPLKF) demonstrated possible antibacterial and antifungal properties. Gomesin was used as a positive control for antibacterial score since it has shown experimental activity against several Gram-positive and Gram-negative bacteria, such as *Escherichia coli*, *Klebsiella pneumoniae*, *Bacillus spp* and *Staphylococcus spp* (Silva et al., 2000). Gomesin scored 0.985 in iAMPpred for antibacterial activity, which is slightly lower than most of CRPs analyzed (**Table 3**). As for antifungal activities, gomesin and rondonin were selected as positive controls. Gomesin demonstrated activity against the filamentous fungi *Tricoderma viridae* as well as the yeast *Candida albicans* (Silva et al., 2000), while rondonin demonstrated activity against *Candida albicans* (Riciluca et al., 2012). The scores for antifungal activity obtained for gomesin and rondonin were 0.973 and 0.903, respectively, while all seven families of CRPs presented antifungal scores >0.92. Taken together, these results suggest the probabilities of the new CRPs identified in this work to present antibacterial and antifungal activities, which should be further explored by *in vitro* and *in vivo* assays. From all seven families of new CRPs, the U3-TRTX-Ar1x family presented the highest scores for antibacterial (>0.99) and antifungal (>0.98) activities, probably due to the high proportion of basic residues (**Table 1**), which impacts directly on net-charge and isoelectric points. These toxins have a net-charge of 5.94 at pH 7.4 (**Figure 4**). The high positive net charges are relevant and possibly increase antimicrobial activity, as evidenced by other studies with cationic peptides (Jiang et al., 2008; Paredes-Gamero et al., 2012). It is also important to notice that these toxins present high isoelectric points of 10.60 and 10.52 for U3-TRTX-Ar1and U6-TRTX-Ar1a, respectively (**Figure 4**). The net positive charges at neutral pH probably increase the efficiency of interaction with negatively charged membranes of microorganisms (Jiang et al., 2008). Future experiments may confirm the antimicrobial activity of the *A. rondoniae* peptides.

Many of the CRPs presented *in silico* antiviral scores, although in lower levels than antifungal and antibacterial, on average (**Table 3**). For antiviral activity prediction, we utilized mBD4 and P9, a peptide derived from mBD4, which has shown a broad activity of antiviral effects on respiratory virus such as H1N1, H3N2, H5N1, H7N7, H7N9, SARS-CoV and MERS-CoV in *in vivo* and *in vitro* assays (Zhao et al., 2016). The scores for antiviral activity of mBD4 and P9 were 0.773 and 0.940, respectively. The toxins from the U1-TRTX-Ar1x family demonstrated higher scores than P9 for antiviral activity, while all other families except U2-TRTX-Ar1x and U4-TRTX-Ar1x demonstrated scores between those obtained from mBD4 and P9, which also suggests a potential antiviral activity and should be further evaluated by *in vitro* and *in vivo* assays. Antiviral peptides may be promising therapeutic drugs (Vilas Boas et al., 2019). Some Arthropod peptides were found to suppress viral gene expression, as the cecropin A from the moth *Hyalophora cecropia*, which inhibited HIV activity (Wachinger et al., 1998), and mucroporin-M1, a peptide derived from the venom of the scorpion *Lychas mucronatus* which inhibited the activities of measles, SARS-CoV and influenza H5N1 viruses (Li et al., 2011). The authors proposed that the antiviral action of the peptide mucroporin-M1 could be by

interaction with the virus envelope, binding to it by surface charge interactions and drastically decreasing the infectivity of the three viruses (Li et al., 2011). Several of the *A. rondoniae* CRPs found in this work present positive net charges at physiological pH and could be promising antiviral peptides, although this is not the only property to be considered.

In regard to *in silico* antitumoral activities, the predictions suggest that only two CRPs, U1-TRTX-Ar1b and U1-TRTX-Agm3a, may present antitumoral properties, as well as four short peptides: VLPPLKF, PLPVFV, VVVPFVV and VPPILKY. For this analysis, we utilized HNP-1 and Aurein 1.2 as positive controls. HNP-1, an human α-defensin AMP, showed cytotoxic activity against prostate tumor cells *in vitro* (Gaspar et al., 2015). Aurein 1.2, derived from the frog *Litoria aurea*, is another example of AMP with anticancer activity, as demonstrated by *in vitro* assays (Rozek et al., 2000). Both controls scored >0.84 in both algorithms of MLACP and, consequently, were predicted as ACPs. From all 11 CRPs, U1-TRTX-Agm3a and U1-TRTX-Ar1b have the shortest amino acids sequences, with 31 and 35 amino acids, respectively. It is also important to highlight that hydrophobicity plays a pivotal role in ACPs activity (Huang et al., 2011) and, as shown in **Table 4**, these potential ACPs are composed of more than 50% hydrophobic residues. It is interesting to note that short peptides indicated potential anticancer activity. In a possible peptide therapy, the potential of short peptides may be advantageous as they are easier to synthesize and modify, present higher ability to penetrate tumors and good biocompatibility (Thundimadathil, 2012). Therefore, the toxins present in the venom of *A. rondoniae* may be promising candidates to the investigation of therapeutic compounds.

The *in silico* anticancer and antimicrobial predictions have demonstrated to be important steps in our methodology, since it enabled a simple and fast screening of potential biological activities. It is important to highlight that the *in silico* predictions are indicatives of potential biological activities. However, the high scores in these predictions may not necessarily imply in real antimicrobial or anticancer activities. To confirm these hypotheses, experimental work should be performed in order to evaluate the biological activities of these peptides *in vitro* and *in vivo*. Although not definitive, the predictions suggest promising peptides and may serve as a guide in target selection for further steps of investigation, which is often a time-consuming task. These results demonstrate the effectiveness of a multiomics approach for toxin discovery, characterization and prospection of biological activities. The next steps would be the synthesis or expression of promising toxins to experimentally validate the activities observed *in silico*.

DATA AVAILABILITY STATEMENT

The datasets generated for this study can be found in the NCBI BioProject section under the accession code PRJNA633430 and BioSample SAMN14943686. The Transcriptome Shotgun Assembly was deposited at NCBI TSA under the accession GIOJ00000000. Mass spectrometry data were deposited to the ProteomeXchange Consortium via the PRIDE partner repository with the dataset identifier PXD019343.

AUTHOR CONTRIBUTIONS

GC and AT designed the concept of this study. MN, PS, IJ-D-A and AT designed experiments. GC, EK, and UO performed experiments. GC, MN and AT analyzed data. GC and AT prepared the draft and final version of the manuscript. All authors contributed to the article and approved the submitted version.

FUNDING

This research was funded by Fundação de Amparo à Pesquisa do Estado de São Paulo (grants 2017/23771-3 to GC, 2013/07467-1 to PS and IJ-D-A, 2016/03839-0 and 2017/20106-9 to AT), Financiadora de Estudos e Projetos (FINEP) and Coordenação de Aperfeiçoamento de Pessoal de Nível Superior - Brasil (CAPES) - Finance Code 001.

ACKNOWLEDGMENTS

The authors thank Prof. Dr. Reinaldo Salomão from UNIFESP for the use of Progenesis QI for proteomics (FAPESP grant 2017/21052-0) and Dr. Ana Marisa Chudzinski-Tavassi from CENTD/Instituto Butantan for the use of the mass spectrometer Q Exactive Plus (grant 2015/50040-4, FAPESP and GlaxoSmithKline).

SUPPLEMENTARY MATERIAL

The Supplementary Material for this article can be found online at: https://www.frontiersin.org/articles/10.3389/fphar.2020.01075/full#supplementary-material

REFERENCES

Abreu, T. F., Sumitomo, B. N., Nishiyama, M. Y., Oliveira, U. C., Souza, G. H. M. F., Kitano, E. S., et al. (2017). Peptidomics of Acanthoscurria gomesiana spider venom reveals new toxins with potential antimicrobial activity. *J. Proteomics* 151, 232–242. doi: 10.1016/j.jprot.2016.07.012

Altschul, S. (1997). Gapped BLAST and PSI-BLAST: a new generation of protein database search programs. *Nucleic Acids Res.* 25, 3389–3402. doi: 10.1093/nar/25.17.3389

Aronesty, E. (2013). Comparison of Sequencing Utility Programs. *Open Bioinforma. J.* 7, 1–8. doi: 10.2174/1875036201307010001

Arouri, A., Dathe, M., and Blume, A. (2009). Peptide induced demixing in PG/PE lipid mixtures: A mechanism for the specificity of antimicrobial peptides towards bacterial membranes? *Biochim. Biophys. Acta Biomembr.* 1788, 650–659. doi: 10.1016/j.bbamem.2008.11.022

Bateman, A. (2004). The Pfam protein families database. *Nucleic Acids Res.* 32, 138D–1141. doi: 10.1093/nar/gkh121

Borges, M. H., Figueiredo, S. G., Leprevost, F. V., De Lima, M. E., Cordeiro, M., do, N., et al. (2016). Venomous extract protein profile of Brazilian tarantula Grammostola iheringi: searching for potential biotechnological applications. *J. Proteomics* 136, 35–47. doi: 10.1016/j.jprot.2016.01.013

Corzo, G., Diego-García, E., Clement, H., Peigneur, S., Odell, G., Tytgat, J., et al. (2008). An insecticidal peptide from the theraposid Brachypelma smithi spider venom reveals common molecular features among spider species from different genera. *Peptides* 29, 1901–1908. doi: 10.1016/j.peptides.2008.07.003

Deng, M., Luo, X., Xiao, Y., Sun, Z., Jiang, L., Liu, Z., et al. (2014). Huwentoxin-XVI, an analgesic, highly reversible mammalian N-type calcium channel antagonist from Chinese tarantula Ornithoctonus huwena. *Neuropharmacology* 79, 657–667. doi: 10.1016/j.neuropharm.2014.01.017

Duan, Z., Cao, R., Jiang, L., and Liang, S. (2013). A combined de novo protein sequencing and cDNA library approach to the venomic analysis of Chinese spider Araneus ventricosus. *J. Proteomics* 78, 416–427. doi: 10.1016/j.jprot.2012.10.011

Edwards, I. A., Elliott, A. G., Kavanagh, A. M., Zuegg, J., Blaskovich, M. A. T. T., and Cooper, M. A. (2016). Contribution of Amphipathicity and Hydrophobicity to the Antimicrobial Activity and Cytotoxicity of β-Hairpin Peptides. *ACS Infect. Dis.* 2, 442–450. doi: 10.1021/acsinfecdis.6b00045

Escoubas, P., and King, G. F. (2009). Venomics as a drug discovery platform. *Expert Rev. Proteomics* 6, 221–224. doi: 10.1586/epr.09.45

Escoubas, P., and Rash, L. (2004). Tarantulas: Eight-legged pharmacists and combinatorial chemists. *Toxicon* 43, 555–574. doi: 10.1016/j.toxicon.2004.02.007

Felício, M. R., Silva, O. N., Gonçalves, S., Santos, N. C., and Franco, O. L. (2017). Peptides with Dual Antimicrobial and Anticancer Activities. *Front. Chem.* 5, 5. doi: 10.3389/fchem.2017.00005

Freitas-de-sousa, L. A., Amazonas, D. R., Sousa, L. F., Sant'Anna, S. S., Nishiyama, J. M. Y., Serrano, S. M. T., et al. (2015). Comparison of venoms from wild and long-term captive Bothrops atrox snakes and characterization of Batroxrhagin, the predominant class PIII metalloproteinase from the venom of this species. *Biochimie* 118, 60–70. doi: 10.1016/j.biochi.2015.08.006

Fry, B. G., Roelants, K., Champagne, D. E., Scheib, H., Tyndall, J. D. A., King, G. F., et al. (2009). The Toxicogenomic Multiverse: Convergent Recruitment of Proteins Into Animal Venoms. *Annu. Rev. Genomics Hum. Genet.* 10, 483–511. doi: 10.1146/annurev.genom.9.081307.164356

Fuertes, G., Giménez, D., Esteban-Martín, S., Sánchez-Muñoz, O. L., and Salgado, J. (2011). A lipocentric view of peptide-induced pores. *Eur. Biophys. J.* 40, 399–415. doi: 10.1007/s00249-011-0693-4

Gaspar, D., Veiga, A. S., and Castanho, M. A. R. B. (2013). From antimicrobial to anticancer peptides. A review. *Front. Microbiol.* 4, 294. doi: 10.3389/fmicb.2013.00294

Gaspar, D., Freire, J. M., Pacheco, T. R., Barata, J. T., and Castanho, M. A. R. B. (2015). Apoptotic human neutrophil peptide-1 anti-tumor activity revealed by cellular biomechanics. *Biochim. Biophys. Acta Mol. Cell Res.* 1853, 308–316. doi: 10.1016/j.bbamcr.2014.11.006

Grabherr, M. G., Haas, B. J., Yassour, M., Levin, J. Z., Thompson, D. A., Amit, I., et al. (2011). Full-length transcriptome assembly from RNA-Seq data without a reference genome. *Nat. Biotechnol.* 29, 644–652. doi: 10.1038/nbt.1883

Huang, Y.-B., Wang, X.-F., Wang, H.-Y., Liu, Y., and Chen, Y. (2011). Studies on Mechanism of Action of Anticancer Peptides by Modulation of Hydrophobicity Within a Defined Structural Framework. *Mol. Cancer Ther.* 10, 416–426. doi: 10.1158/1535-7163.MCT-10-0811

Ikonomopoulou, M. P., Fernandez-Rojo, M. A., Pineda, S. S., Cabezas-Sainz, P., Winnen, B., Morales, R. A. V., et al. (2018). Gomesin inhibits melanoma growth by manipulating key signaling cascades that control cell death and proliferation. *Sci. Rep.* 8, 11519. doi: 10.1038/s41598-018-29826-4

Jiang, Z., Vasil, A.II, Hale, J. D., Hancock, R. E. W., Vasil, M. L., and Hodges, R. S. (2008). Effects of net charge and the number of positively charged residues on the biological activity of amphipathic α-helical cationic antimicrobial peptides. *Biopolymers* 90, 369–383. doi: 10.1002/bip.20911

Johnson, L. S., Eddy, S. R., and Portugaly, E. (2010). Hidden Markov model speed heuristic and iterative HMM search procedure. *BMC Bioinf.* 11, 431. doi: 10.1186/1471-2105-11-431

Jung, H. J., Kim, P., Lee, S. K., Lee, C. W., Eu, Y.-J., Lee, D. G., et al. (2006). Lipid membrane interaction and antimicrobial activity of GsMTx-4, an inhibitor of mechanosensitive channel. *Biochem. Biophys. Res. Commun.* 340, 633–638. doi: 10.1016/j.bbrc.2005.12.046

Kaas, Q., and Craik, D. J. (2015). Bioinformatics-Aided Venomics. *Toxins (Basel)* 7, 2159–2187. doi: 10.3390/toxins7062159

King, G. F., and Hardy, M. C. (2013). Spider-Venom Peptides: Structure, Pharmacology, and Potential for Control of Insect Pests. *Annu. Rev. Entomol.* 58, 475–496. doi: 10.1146/annurev-ento-120811-153650

King, G. F., Gentz, M. C., Escoubas, P., and Nicholson, G. M. (2008). A rational nomenclature for naming peptide toxins from spiders and other venomous animals. *Toxicon* 52, 264–276. doi: 10.1016/j.toxicon.2008.05.020

Kubista, H., Mafra, R. A., Chong, Y., Nicholson, G. M., Beirão, P. S. L., Cruz, J. S., et al. (2007). CSTX-1, a toxin from the venom of the hunting spider Cupiennius salei, is a selective blocker of L-type calcium channels in mammalian neurons. *Neuropharmacology* 52, 1650–1662. doi: 10.1016/j.neuropharm.2007.03.012

Kuhn-Nentwig, L., Stöcklin, R., and Nentwig, W. (2011). "Venom composition and strategies in spiders: is everything possible?," in *Advances in Insect Physiology* (London: Academic Press), 1–86. doi: 10.1016/B978-0-12-387668-3.00001-5

Kuhn-Nentwig, L., Langenegger, N., Heller, M., Koua, D., and Nentwig, W. (2019). The Dual Prey-Inactivation Strategy of Spiders—In-Depth Venomic Analysis of Cupiennius salei. *Toxins (Basel)* 11, 167. doi: 10.3390/toxins11030167

Langenegger, N., Nentwig, W., and Kuhn-Nentwig, L. (2019). Spider venom: Components, modes of action, and novel strategies in transcriptomic and proteomic analyses. *Toxins (Basel)* 11, 611. doi: 10.3390/toxins11100611

Langmead, B., and Salzberg, S. L. (2012). Fast gapped-read alignment with Bowtie 2. *Nat. Methods* 9, 357–359. doi: 10.1038/nmeth.1923

Lau, C. H. Y., King, G. F., and Mobli, M. (2016). Molecular basis of the interaction between gating modifier spider toxins and the voltage sensor of voltage-gated ion channels. *Sci. Rep.* 6, 34333. doi: 10.1038/srep34333

Lee, S.-Y., and MacKinnon, R. (2004). A membrane-access mechanism of ion channel inhibition by voltage sensor toxins from spider venom. *Nature* 430, 232–235. doi: 10.1038/nature02632

Li, Q., Zhao, Z., Zhou, D., Chen, Y., Hong, W., Cao, L., et al. (2011). Virucidal activity of a scorpion venom peptide variant mucroporin-M1 against measles, SARS-CoV and influenza H5N1 viruses. *Peptides* 32, 1518–1525. doi: 10.1016/j.peptides.2011.05.015

Liao, Z., Yuan, C., Deng, M., Li, J., Chen, J., Yang, Y., et al. (2006). Solution structure and functional characterization of jingzhaotoxin-XI: a novel gating modifier of both potassium and sodium channels. *Biochemistry* 45, 15591–15600. doi: 10.1021/bi061457+

Lomazi, R. L., Nishiduka, E. S., Silva, P.II, and Tashima, A. K. (2018). "Identification of Peptides in Spider Venom Using Mass Spectrometry," in *Peptidomics - Methods and Strategies*. Eds. L. D. Fricker and M. Schrader (New York: Springer), 359–367. doi: 10.1007/978-1-4939-7537-2_24

Lucas, S. M., Da Silva, P.II, Bertani, R., and Costa Cardoso, J. L. (1994). Mygalomorph spider bites: A report on 91 cases in the State of São Paulo, Brazil. *Toxicon* 32, 1211–1215. doi: 10.1016/0041-0101(94)90350-6

Manavalan, B., Basith, S., Shin, T. H., Choi, S., Kim, M. O., and Lee, G. (2017). MLACP: machine-learning-based prediction of anticancer peptides. *Oncotarget* 8, 77121–77136. doi: 10.18632/oncotarget.20365

Mebs, D. (2001). Toxicity in animals. Trends in evolution? *Toxicon* 39, 87–96. doi: 10.1016/S0041-0101(00)00155-0

Meher, P. K., Sahu, T. K., Saini, V., and Rao, A. R. (2017). Predicting antimicrobial peptides with improved accuracy by incorporating the compositional, physico-chemical and structural features into Chou's general PseAAC. *Sci. Rep.* 7, 42362. doi: 10.1038/srep42362

Mobli, M., Undheim, E. A. B., and Rash, L. D. (2017). "Modulation of Ion Channels by Cysteine-Rich Peptides," in *Ion Channels DownUnder* (Cambridge: Elsevier Inc.), 199–223. doi: 10.1016/bs.apha.2017.03.001

Mourão, C. B. F., Heghinian, M. D., Barbosa, E. A., Marí, F., Bloch, C., Restano-Cassulini, R., et al. (2013). Characterization of a Novel Peptide Toxin from Acanthoscurria paulensis Spider Venom: A Distinct Cysteine Assignment to the HWTX-II Family. *Biochemistry* 52, 2440–2452. doi: 10.1021/bi4000035

Osorio, D., Rondon-Villarreal, P., and Torres, R. (2015). Peptides: A Package for Data Mining of Antimicrobial Peptides. *R. J.* 7, 4–14. doi: 10.32614/RJ-2015-001

Osteen, J. D., Herzig, V., Gilchrist, J., Emrick, J. J., Zhang, C., Wang, X., et al. (2016). Selective spider toxins reveal a role for the Nav1.1 channel in mechanical pain. *Nature* 534, 494–499. doi: 10.1038/nature17976

Pérez-Peinado, C., Defaus, S., and Andreu, D. (2020). Hitchhiking with Nature: Snake Venom Peptides to Fight Cancer and Superbugs. *Toxins (Basel)* 12, 255. doi: 10.3390/toxins12040255

Perez-Riverol, Y., Csordas, A., Bai, J., Bernal-Llinares, M., Hewapathirana, S., and Kundu, D. J. (2019). The PRIDE database and related tools and resources in

2019: improving support for quantification data. *Nucleic Acids Res* 47, D442–D450. doi: 10.1093/nar/gky1106

Paredes-Gamero, E. J., Casaes-Rodrigues, R. L., Moura, G. E. D. D., Domingues, T. M., Buri, M. V., Ferreira, V. H. C., et al. (2012). Cell-Permeable Gomesin Peptide Promotes Cell Death by Intracellular Ca 2+ Overload. *Mol. Pharm.* 9, 2686–2697. doi: 10.1021/mp300251j

Pedroso, A. P., Souza, A. P., Dornellas, A. P. S., Oyama, L. M., Nascimento, C. M. O., Santos, G. M. S., et al. (2017). Intrauterine Growth Restriction Programs the Hypothalamus of Adult Male Rats: Integrated Analysis of Proteomic and Metabolomic Data. *J. Proteome Res.* 16, 1515–1525. doi: 10.1021/acs.jproteome.6b00923

Pineda, S. S., Chaumeil, P.-A., Kunert, A., Kaas, Q., Thang, M. W. C. C., Le, L., et al. (2018). ArachnoServer 3.0: an online resource for automated discovery, analysis and annotation of spider toxins. *Bioinformatics* 34, 1074–1076. doi: 10.1093/bioinformatics/btx661

Rappsilber, J., Mann, M., and Ishihama, Y. (2007). Protocol for micro-purification, enrichment, pre-fractionation and storage of peptides for proteomics using StageTips. *Nat. Protoc.* 2, 1896–1906. doi: 10.1038/nprot.2007.261

Rates, B., Prates, M. V., Verano-Braga, T., da Rocha, Â. P., Roepstorff, P., Borges, C. L., et al. (2013). μ-Theraphotoxin-An1a: Primary structure determination and assessment of the pharmacological activity of a promiscuous anti-insect toxin from the venom of the tarantula Acanthoscurria natalensis (Mygalomorphae, Theraphosidae). *Toxicon* 70, 123–134. doi: 10.1016/j.toxicon.2013.04.013

Riciluca, K. C. T., Sayegh, R. S. R., Melo, R. L., and Silva, P.II (2012). Rondonin an antifungal peptide from spider (Acanthoscurria rondoniae) haemolymph. *Results Immunol.* 2, 66–71. doi: 10.1016/j.rinim.2012.03.001

Rocha-e-Silva, T. A. A., Sutti, R., and Hyslop, S. (2009). Milking and partial characterization of venom from the Brazilian spider Vitalius dubius (Theraphosidae). *Toxicon* 53, 153–161. doi: 10.1016/j.toxicon.2008.10.026

Rozek, T., Wegener, K. L., Bowie, J. H., Olver, I. N., Carver, J. A., Wallace, J. C., et al. (2000). The antibiotic and anticancer active aurein peptides from the Australian Bell Frogs Litoria aurea and Litoria raniformis. *Eur. J. Biochem.* 267, 5330–5341. doi: 10.1046/j.1432-1327.2000.01536.x

Ruta, V., Jiang, Y., Lee, A., Chen, J., and MacKinnon, R. (2003). Functional analysis of an archaebacterial voltage-dependent K+ channel. *Nature* 422, 180–185. doi: 10.1038/nature01473

Saez, N. J., Senff, S., Jensen, J. E., Er, S. Y., Herzig, V., Rash, L. D., et al. (2010). Spider-venom peptides as therapeutics. *Toxins (Basel)* 2, 2851–2871. doi: 10.3390/toxins2122851

Sanggaard, K. W., Bechsgaard, J. S., Fang, X., Duan, J., Dyrlund, T. F., Gupta, V., et al. (2014). Spider genomes provide insight into composition and evolution of venom and silk. *Nat. Commun.* 5, 3765. doi: 10.1038/ncomms4765

Schendel, V., Rash, L. D., Jenner, R. A., and Undheim, E. A. B. (2019). The Diversity of Venom: The Importance of Behavior and Venom System Morphology in Understanding Its Ecology and Evolution. *Toxins (Basel)* 11, 666. doi: 10.3390/toxins11110666

Seo, M.-D., Won, H.-S., Kim, J.-H., Mishig-Ochir, T., and Lee, B.-J. (2012). Antimicrobial Peptides for Therapeutic Applications: A Review. *Molecules* 17, 12276–12286. doi: 10.3390/molecules171012276

Silva, P.II, Daffre, S., and Bulet, P. (2000). Isolation and characterization of gomesin, an 18-residue cysteine-rich defense peptide from the spider Acanthoscurria gomesiana hemocytes with sequence similarities to horseshoe crab antimicrobial peptides of the tachyplesin family. *J. Biol. Chem.* 275, 33464–33470. doi: 10.1074/jbc.M001491200

Silva, J. C., Gorenstein, M. V., Li, G.-Z., Vissers, J. P. C., and Geromanos, S. J. (2006). Absolute Quantification of Proteins by LCMS E. *Mol. Cell. Proteomics* 5, 144–156. doi: 10.1074/mcp.M500230-MCP200

Thundimadathil, J. (2012). Cancer Treatment Using Peptides: Current Therapies and Future Prospects. *J. Amino Acids* 2012, 1–13. doi: 10.1155/2012/967347

Undheim, E. A. B., Grimm, L. L., Low, C.-F., Morgenstern, D., Herzig, V., Zobel-Thropp, P., et al. (2015). Weaponization of a Hormone: Convergent Recruitment of Hyperglycemic Hormone into the Venom of Arthropod Predators. *Structure* 23, 1–10. doi: 10.1016/j.str.2015.05.003

Vetter, R. S., and Isbister, G. K. (2008). Medical Aspects of Spider Bites. *Annu. Rev. Entomol.* 53, 409–429. doi: 10.1146/annurev.ento.53.103106.093503

Vilas Boas, L. C. P., Campos, M. L., Berlanda, R. L. A., de Carvalho Neves, N., and Franco, O. L. (2019). Antiviral peptides as promising therapeutic drugs. *Cell. Mol. Life Sci.* 76, 3525–3542. doi: 10.1007/s00018-019-03138-w

Wachinger, M., Kleinschmidt, A., Winder, D., Von Pechmann, N., Ludvigsen, A., Neumann, M., et al. (1998). Antimicrobial peptides melittin and cecropin inhibit replication of human immunodeficiency virus 1 by suppressing viral gene expression. *J. Gen. Virol.* 79, 731–740. doi: 10.1099/0022-1317-79-4-731

Windley, M. J., Herzig, V., Dziemborowicz, S. A., Hardy, M. C., King, G. F., and Nicholson, G. M. (2012). Spider-Venom Peptides as Bioinsecticides. *Toxins (Basel)* 4, 191–227. doi: 10.3390/toxins4030191

Zelanis, A., and Keiji Tashima, A. (2014). Unraveling snake venom complexity with 'omics' approaches: Challenges and perspectives. *Toxicon* 87, 131–134. doi: 10.1016/j.toxicon.2014.05.011

Zhang, J., Xin, L., Shan, B., Chen, W., Xie, M., Yuen, D., et al. (2012). PEAKS DB: De Novo Sequencing Assisted Database Search for Sensitive and Accurate Peptide Identification. *Mol. Cell. Proteomics* 11, M111.010587. doi: 10.1074/mcp.M111.010587

Zhang, C., Yang, M., and Ericsson, A. C. (2019). Antimicrobial Peptides: Potential Application in Liver Cancer. *Front. Microbiol.* 10, 1257. doi: 10.3389/fmicb.2019.01257

Zhao, H., Zhou, J., Zhang, K., Chu, H., Liu, D., Poon, V. K.-M., et al. (2016). A novel peptide with potent and broad-spectrum antiviral activities against multiple respiratory viruses. *Sci. Rep.* 6, 22008. doi: 10.1038/srep22008

Zhou, X., Ma, T., Yang, L., Peng, S., Li, L., Wang, Z., et al. (2020). Spider venom-derived peptide induces hyperalgesia in Nav1.7 knockout mice by activating Nav1.9 channels. *Nat. Commun.* 11, 2293. doi: 10.1038/s41467-020-16210-y

Zobel-Thropp, P. A., Bulger, E. A., Cordes, M. H. J., Binford, G. J., Gillespie, R. G., and Brewer, M. S. (2018). Sexually dimorphic venom proteins in long-jawed orb-weaving spiders (Tetragnatha) comprise novel gene families. *PeerJ* 6, e4691. doi: 10.7717/peerj.4691

Conflict of Interest: The authors declare that the research was conducted in the absence of any commercial or financial relationships that could be construed as a potential conflict of interest.

frontiers in Pharmacology

REVIEW
published: 24 July 2020
doi: 10.3389/fphar.2020.01132

From Animal Poisons and Venoms to Medicines: Achievements, Challenges and Perspectives in Drug Discovery

Karla de Castro Figueiredo Bordon[1], Camila Takeno Cologna[1], Elisa Corrêa Fornari-Baldo[2], Ernesto Lopes Pinheiro-Júnior[1], Felipe Augusto Cerni[1], Fernanda Gobbi Amorim[3], Fernando Antonio Pino Anjolette[4], Francielle Almeida Cordeiro[1], Gisele Adriano Wiezel[1], Iara Aimê Cardoso[1], Isabela Gobbo Ferreira[1], Isadora Sousa de Oliveira[1], Johara Boldrini-França[5], Manuela Berto Pucca[6], Mateus Amaral Baldo[2] and Eliane Candiani Arantes[1]**

[1] Laboratory of Animal Toxins, Department of BioMolecular Sciences, School of Pharmaceutical Sciences of Ribeirão Preto, University of São Paulo, Ribeirão Preto, Brazil, [2] Health and Science Institute, Paulista University, São José do Rio Pardo, Brazil, [3] Postgraduate Program in Pharmaceutical Sciences, Vila Velha University, Vila Velha, Brazil, [4] Department of Pharmacy, Federal Institute of Education, Science and Technology of Paraná, Palmas, Brazil, [5] Postgraduate Program in Ecosystem Ecology, Vila Velha University, Vila Velha, Brazil, [6] Medical School, Federal University of Roraima, Boa Vista, Brazil

OPEN ACCESS

Edited by:
Yuri N. Utkin, Institute of Bioorganic Chemistry (RAS), Russia

Reviewed by:
Sakthivel Vaiyapuri, University of Reading, United Kingdom
Helena Safavi, The University of Utah, United States
Zhonghua Liu, Hunan Normal University, China

***Correspondence:**
Karla de Castro Figueiredo Bordon
karla@fcfrp.usp.br
Eliane Candiani Arantes
ecabraga@fcfrp.usp.br

Specialty section:
This article was submitted to Translational Pharmacology, a section of the journal Frontiers in Pharmacology

Received: *18 April 2020*
Accepted: *13 July 2020*
Published: *24 July 2020*

Citation:
Bordon KCF, Cologna CT, Fornari-Baldo EC, Pinheiro-Júnior EL, Cerni FA, Amorim FG, Anjolette FAP, Cordeiro FA, Wiezel GA, Cardoso IA, Ferreira IG, Oliveira IS, Boldrini-França J, Pucca MB, Baldo MA and Arantes EC (2020) From Animal Poisons and Venoms to Medicines: Achievements, Challenges and Perspectives in Drug Discovery. Front. Pharmacol. 11:1132. doi: 10.3389/fphar.2020.01132

Animal poisons and venoms are comprised of different classes of molecules displaying wide-ranging pharmacological activities. This review aims to provide an in-depth view of toxin-based compounds from terrestrial and marine organisms used as diagnostic tools, experimental molecules to validate postulated therapeutic targets, drug libraries, prototypes for the design of drugs, cosmeceuticals, and therapeutic agents. However, making these molecules applicable requires extensive preclinical trials, with some applications also demanding clinical trials, in order to validate their molecular target, mechanism of action, effective dose, potential adverse effects, as well as other fundamental parameters. Here we go through the pitfalls for a toxin-based potential therapeutic drug to become eligible for clinical trials and marketing. The manuscript also presents an overview of the current picture for several molecules from different animal venoms and poisons (such as those from amphibians, cone snails, hymenopterans, scorpions, sea anemones, snakes, spiders, tetraodontiformes, bats, and shrews) that have been used in clinical trials. Advances and perspectives on the therapeutic potential of molecules from other underexploited animals, such as caterpillars and ticks, are also reported. The challenges faced during the lengthy and costly preclinical and clinical studies and how to overcome these hindrances are also discussed for that drug candidates going to the bedside. It covers most of the drugs developed using toxins, the molecules that have failed and those that are currently in clinical trials. The article presents a detailed overview of toxins that have been used as therapeutic agents, including their discovery, formulation, dosage, indications, main adverse effects, and pregnancy and breastfeeding prescription warnings. Toxins in diagnosis, as well as

cosmeceuticals and atypical therapies (bee venom and leech therapies) are also reported. The level of cumulative and detailed information provided in this review may help pharmacists, physicians, biotechnologists, pharmacologists, and scientists interested in toxinology, drug discovery, and development of toxin-based products.

Keywords: poison, venom, toxin, drug discovery, scorpion, snake, toad, *Conus*

INTRODUCTION

Animal poisons and venoms are rich sources of proteins, peptides, neurotransmitters, among other compounds. Together, these molecules can induce major damages in the prey's body, being one of the mechanisms employed by these animals to subdue and/or kill their preys or predators. The main difference between the terms "poison" and "venom" is the delivery method. Poisons are generated by specialized cells or tissues or are acquired from the diet, causing prey toxicity by ingestion or contact with the poisonous animal. On the other hand, venoms are produced by a tissue or organ (venom gland) and are parenterally introduced into the prey by the venomous animal, with a specialized apparatus (fang, stinger, teeth, nematocysts, among others) (Fox and Serrano, 2007). The word "toxin" will be used for both compounds from animal poisons and venoms in the whole article.

As a result of evolution and natural selection, toxins from animal poisons and venoms display wide-ranging pharmacological activities. Since the toxin targets are related to biological functions, with many of them playing important roles in human diseases, several venom components were used in the design of new therapeutic agents. They were also employed as cosmeceuticals, diagnostic tools, and experimental molecules to validate postulated therapeutic targets, improving several drug libraries (Ghosh et al., 2019; Utkin et al., 2019).

Although several biologically active toxins have been reported from terrestrial and marine organisms, there is a large gap between the initial drug discovery phase, including their validation as drug models, and their use in a clinical study. Drug candidates must pass through an extensive range of *in vitro* and *in vivo* tests to establish their pharmacology and biochemistry, carcinogenicity, and effects on the reproductive system, to assess their safety before moving on to the clinical phases (Tamimi and Ellis, 2009). In other words, drug development includes the discovery of a candidate molecule, preclinical and clinical studies, which are usually costly and takes a significant amount of time to attend the requirements stated by the regulatory agencies throughout the world.

This review aims to highlight the key successes and some examples of the obstacles and challenges faced when developing toxin-based drugs. It covers toxins from poisonous and venomous animals, drugs that target diverse pathological conditions, the molecules that have failed, and those that are currently in clinical trials. It also aims to encourage scientists to elucidate the mechanism of action of the already known venom components, discover new molecules with innovative therapeutic potential, and develop strategies to improve their pharmacokinetic and pharmacodynamic properties. Moreover, perspectives on the research and development of a wide range of toxins from several underexploited animal poisons and venoms are also discussed.

ACHIEVEMENTS WITH ANIMAL TOXIN-BASED MOLECULES

Readers and scientists looking for approved drugs must consider the databases from regulatory agencies, such as the US Food and Drug Administration (FDA) and the European Medicines Agency (EMA). Furthermore, valuable information for health professionals and general public can be found at the Drug Information Database. However, the information provided by these databases is significantly limited, since biotechnology companies and pharmaceutical industries usually perform the drug development processes. Thus, much of the information relevant to drug development is not published and/or quite difficult to access.

Therefore, the subsections *Approved Drugs* to *Venom Therapies* will address the toxin-based approved drugs, diagnostic tools, cosmeceuticals and venom therapies, respectively, with the currently available details found at these databases.

Approved Drugs

Among the 11 approved toxin-based molecules marketed, one molecule (ziconotide) is obtained from cone snails, two from lizards (exenatide and lixisenatide), two from leeches (bivalirudin and desirudin), and six from snakes (captopril, enalapril, tirofiban, eptifibatide, batroxobin, and cobratide). Batroxobin and cobratide are native compounds purified from snake venoms, desirudin is a recombinant molecule, and the other drugs (bivalirudin, captopril, enalapril, eptifibatide, exenatide, tirofiban, and ziconotide) are synthetic molecules (**Table 1**).

Most toxin-based approved drugs are derived from snake venoms. One of the possible reasons for this scenario is the larger amount of venoms produced by snakes in comparison to small animals (e.g. scorpions, spiders, and snails) (King, 2011; King, 2013). In parallel, the effect of snake venoms on hemostasis evidenced the cardiovascular system as a pharmacological target for snake venom toxins. Furthermore, the analytical techniques capable of characterizing limited amounts of venom components from small animals were only developed recently. These are some issues that boosted the initial toxinological studies primarily on snake venoms. The advent of more sensitive techniques and the improvement in experimental models in the last years have allowed the study of poorly expressed toxins and their novel pharmacological targets (Boldrini-França et al., 2017).

TABLE 1 | Approved drugs and therapies for human use.

Molecule (brand name)	Species origin of venom toxin	Production	Formulation	Mechanism of action	Use	Dosage(maximum dose per day)*	More frequently reported adverse effects, pregnancy and breastfeeding warnings*	Reference
Batroxobin (Defibrase®) (1)	Brazilian lancehead snake (*Bothrops moojeni*)	Purified from venom	Ampoule contains 10 batroxobin units, NaCl, chlorobutanol, and partially hydrolyzed gelatin in water	Cleaves Aα-chain of fibrinogen	Acute cerebral infarction; unspecific angina pectoris; sudden deafness	40 batroxobin units by i.v. infusion over 1 h.	Microvascular thrombosis	(Stocker, 1978; Vu et al., 2013; Pentapharm DSM Nutritional Products Ltd, 2018)
Batroxobin (Plateltex-Act®) (1)	Common lancehead snake (*Bothrops atrox*)	Purified from venom	Vial of batroxobin (5 batroxobin units/1 ml), and 1 vial of calcium gluconate (940 mg gluconate/10 ml)	Cleaves Aα-chain of fibrinogen	Gelification of blood for topical applications	1 ml (or maximum of 1.5 ml) of calcium gluconate mixed with batroxobin (5 U). This mixture is mixed with 6-10 ml of platelet concentrate. After gel formation (7-10 min), it is applied on the area or in the site to be treated.	No toxicity phenomena are described in the tissues treated with the gel.	(Plateltex, 2018)
Batroxobin - Fibrin sealant (Vivostat®) (1)	Brazilian lancehead snake (*Bothrops moojeni*)	Purified from venom	Medical device used for the preparation of an autologous fibrin; citrate	Cleaves Aα-chain of fibrinogen	Autologous fibrin sealant in surgery	Citrate is added to the device (during surgery or 24 h before), where is drawn 120 ml of the patient's blood. After 25 min, an autologous fibrin is ready for use.	The sealant has no known adverse effects.	(Kjaergard and Trumbull, 1998; Vivostat A/S, 2018)
Bee venom therapy (Apitox®)	Honeybee *Apis mellifera*	Whole venom	100 μg/1 ml (bee venom in 0.9% NaCl)	Anti-inflammatory action; alteration of the immune response *via* antigen competition	Pain associated with osteoarthritis and multiple sclerosis	Monthly s.c. injections; twice weekly range from 1 to 20 intradermal injections (100 μg/0.1 ml saline)—at acupuncture points	Irritation, swollen, reddened skin and severe allergic reactions that can be life-threatening.	(Gotter, 2019; US National Library of Medicine, 2020)
Bivalirudin (Angiomax®) (2)	European medicinal leech (*Hirudo medicinalis*)	Synthetic	Powder for injection, 250 mg, (bivalirudin trifluoroactetate, mannitol and sodium hidroxide)	Reversible direct thrombin inhibitor	Anticoagulant in percutaneous coronary intervention	0.75 mg/kg by direct IV injection, followed by 1.75 mg/kg per hour (300-325 mg daily)	Hemorragic events, back pain, pain (unspecified), nausea, headache, hyper/hypotension, injection site pain, insomnia, vomiting, pelvic pain, anxiety, bradycardia, dyspepsia, abdominal pain, fever, nervouness, urinary retention; pregnancy risk factor B	(US Food and Drug Administration, 2020)
Captopril (Capoten®) (3)	Jararaca pit viper snake (*Bothrops jararaca*)	Synthetic	Oral tablets: 12.5, 25, 50, and 100 mg (inactive ingredients: anhydrous lactose, colloidal silicon dioxide, crospovidone, microcrystalline cellulose, and stearic acid)	Angiotensin-converting enzyme inhibitor	Hypertension, cardiac failure	50 or 100 mg orally 3 times a day (maximum dose: 450 mg/day)	Cough and skin rash; US FDA pregnancy category D; excreted into human milk—discontinue breastfeeding or discontinue the drug, since the effects in the nursing infant are unknown	(US Food and Drug Administration, 2020)
Cobratide (Ketongning,	Chinese cobra (*Naja naja atra*)	Purified from venom	Freeze-dried powder (70 or 140 μg/vial) with dextran and glycine as excipient, for	Blockage of nicotinic receptors	Chronic arthralgia, sciatica,	Minimum and maximum daily dose are 280 μg and 840 μg, respectively—	Fatal side effects, such as respiration inhibition, can occur when it is injected at higher dosage levels.	(Chen et al., 2016; Orientoxin

(Continued)

TABLE 1 | Continued

Molecule (brand name)	Species origin of venom toxin	Production	Formulation	Mechanism of action	Use	Dosage(maximum dose per day)*	More frequently reported adverse effects, pregnancy and breastfeeding warnings*	Reference
cobrotoxin) [2]			injection and cobratide enteric coated capsule		neuropathic headache	enteric coated capsule (CN101381408B)		Biotech Co. Ltd., 2019)
Desirudin (Iprivask®) [2]	European medicinal leech (*Hirudo medicinalis*)	Recombinant	Sterile powder for injection (desirudin-15.75 mg, anhydrous magnesium chloride-1.31 mg, and sodium hydroxide for injection USP)	Selective and near-irreversible inhibitor of thrombin	Prevention of venous thrombotic events	15 mg (5-15 min prior surgery), followed by 15 mg every 12 h up to 12 days	Bleeding, deep vein thrombophlebitis, wound secretion, nausea, vomiting, fever, hematoma, anemia; pregnancy risk factor C; no breastfeeding when using desirudin	(US Food and Drug Administration, 2020)
Enalapril (Vasotec®) [3]	Jararaca pit viper snake (*Bothrops jararaca*)	Synthetic	Oral Tablets, 2.5, 5, 10, and 20 mg; 1.25 mg/ml i.v. (with benzyl alcohol 0.9%)	Angiotensin-converting enzyme inhibitor	Hypertension, cardiac failure	2.5 mg twice daily up to 10-20 mg twice daily. Increased dosage up to 40 mg/day (1 or 2 divided doses)	Increased serum creatinine,hypotension, dizziness, headache, fatigue, skin rash, abdominal pain, anorexia, constipation, diarrhea, nausea, vomiting, cough, dyspnea; US FDA pregnancy category D; excreted into human milk —discontinue breastfeeding or discontinue the drug, since the effects in the nursing infant are unknown	(US Food and Drug Administration, 2020)
Eptifibatide (Integrilin®) [2]	Pigmy rattlesnake (*Sistrurus miliarius*)	Synthetic	I.v. bolus injection (20 mg/ 10 ml); i.v. infusion (75 mg/ 100 ml); i.v. infusion (200 mg/100 ml); Each vial of any dose also contains 5.25 mg/ml citric acid and NaOH to adjust to pH 5.35.	Prevents binding of fibrinogen, von Willebrand factor, and other adhesive ligands to GPIIb/IIIa	Acute coronary syndrome; percutaneous coronary intervention	Initial dose of 180 μg/kg intravenous bolus administered and for maintenance 2 μg/kg/min by a continuous infusion until hospital discharge, or for up 18 to 24 h, whichever comes first. A minimum of 12 h of infusion is recommended by the manufacturer.	Bleeding, dizziness; US FDA pregnancy category B; not known if distributed into human milk	(RxList, 2019; European Medicines Agency, 2020)
Exenatide (Byetta®) [2]	Gila monster lizard (*Heloderma suspectum*)	Synthetic	Prefilled cartridge pen (250 μg/ml; s.c. injection)	Glucagon-like peptide-1 receptor agonist	Type 2 diabetes mellitus	5 or 10 μg twice daily 60 min before two main meals of the day, ~6 h apart	Hypoglycemia, nausea, vomiting, diarrhea, jittery feeling, dizziness, headache, dyspepsia, asthenia, gastroesophageal reflux disease, hyperhidrosis, constipation, abdominal distention, decreased appetite, flatulence; data lacking on the use in pregnancy; not known if excreted into human milk	(US Food and Drug Administration, 2020)
Extended-release exenatide (Bydureon®) [2]	Gila monster lizard (*Heloderma suspectum*)	Synthetic	Exenatide (2 mg) and diluent	Glucagon-like peptide-1 receptor agonist	Type 2 diabetes mellitus	2 mg weekly at any time of the dosing day, with or without meals	Hypoglycemia, nausea, diarrhea, injection-site reactions (pruritus, nodule, erythema, hematoma), vomiting, constipation, headache, viral gastroenteritis, gastroesophageal reflux disease, dyspepsia, fatigue, decreased appetite; data lacking on the use in pregnancy; not known if excreted into human milk	(European Medicines Agency, 2020; US Food and Drug Administration, 2020)
Leech therapy	European medicinal leech	Leech	Leeches drain blood from tissue	Inhibits platelet aggregation	Skin grafts and	Usually 1–10 leeches are used for each treatment, while at the beginning, the patient might need two or more	Lymphadenitis, slight swelling, pain of regional lymph nodes on the side of leech application and subfebrile temperature. Leech therapy is not	(Mumcuoglu, 2014; US Food and Drug

(Continued)

TABLE 1 | Continued

Molecule (brand name)	Species origin of venom toxin	Production	Formulation	Mechanism of action	Use	Dosage(maximum dose per day)*	More frequently reported adverse effects, pregnancy and breastfeeding warnings*	Reference
	(*Hirudo medicinalis*) or other species			and the coagulation cascade	reattachment surgery	treatments per day. Leeches should be applied on the darker spots of the reattached body parts or flaps. Usually the treatment lasts for 2–6 days.	recommended in pregnancy, lactation and in patients with an unstable medical status and disposition to keloid scar formation.	Administration, 2020)
Lixisenatide (Lyxumia® and Adlyxin®) (2)	Gila monster lizard (*Heloderma suspectum*)	Synthetic	0.15 mg/3 ml (0.05 mg/ml) —s.c. 0.3 mg/3 ml (0.1 mg/ml)— s.c.	Glucagon-like peptide-1 receptor agonist	Type 2 diabetes mellitus	Initial dose: 10 µg by s.c. injection once a day. Increase to 20 µg on day 15. This drug should be administered 1 h before the first meal of the day. Concurrent use with short acting insulin has not been studied and is not recommended.	Nausea, vomiting, diarrhea, headache, dizziness, low blood sugar; data lacking on the use in pregnancy; not known if distributed into human milk, but its use is not recommended.	(European Medicines Agency, 2020; US Food and Drug Administration, 2020)
Tirofiban (Aggrastat®) (3)	Saw-scaled viper snake (*Echis carinatus*)	Synthetic	I.v. bolus (3.75 mg in 15 ml —vial); i.v. bolus and infusion (5 mg in 100 ml— vial); i.v. bolus and infusion (12.5 mg/250 ml—bag)	Antagonist of fibrinogen binding to the GPIIb/IIIa receptor	Acute coronary syndrome	Initial dose: 25 µg/kg i.v. within 5 min. Maintenance dose: 0.15 µg/kg/min i.v. infusion for up to 18 h	Dizziness, slow heart rate, leg pain, pelvic pain, swelling, increased sweating; US FDA pregnancy category B; not known if distributed into human milk.	(Medicure Pharma, 2016)
Ziconotide (Prialt®) (2)	Magical cone marine snail (*Conus magus*)	Synthetic	25 or 100 µg/ml (aqueous pH adjusted solution pH 4-5, L-methionine and NaCl); i.t.	Cav2.2 channel antagonist	Severe chronic pain	Initial dose: ≤ 2.4 µg/day (≤ 0.1 µg/h) less than 2 to 3 times/week. Maximum dose: 19.2 µg/day (0.8 µg/h) by day 21.	Dizziness, confusion, drowsiness,abnormal gait, memory impairment, ataxia, speech disorder, headache, aphasia, hallucination, thinking abnormality, amnesia, anxiety, blurred vision, increased creatine phosphokinase, anorexia, nystagmus, fever; pregnancy risk factor C	(US Food and Drug Administration, 2020)

**For complete and detailed information, we suggest consulting Drugs.com and the patient information leaflets provided by the medicine manufacturer; 1), enzyme; 2), peptide; 3), non-protein molecule; i.t., intrathecal; i.v., intravenous; s.c., subcutaneous.*

Additionally, the discovery of many ion channels in the 1970-1980s, and the better understanding of the nervous system, which houses the main molecular targets of small venomous invertebrates, opened up the field to new therapeutic leads for non-cardiovascular targets (King, 2013).

The first animal toxin-based drug approved for human use was captopril in 1981. Captopril (Capoten®, Bristol-Myers Squibb) was developed based on the bradykinin potentiating factor (BPF) present in *Bothrops jararaca* snake venom (Ferreira, 1965; Camargo et al., 2012). BPF is a nonapeptide that acts by blocking the activity of the angiotensin-converting enzyme (ACE), inhibiting the production of the hypertensive molecule angiotensin II and potentiating the action of the hypotensive peptide bradykinin (Ferreira, 1965; Ferreira and Rocha e Silva, 1965; Ferreira et al., 1970a; Ferreira et al., 1970b).

Since the native peptide found in this venom was quite expensive to be synthesized and impossible to be orally administered (Ferreira, 2000), captopril was designed by the miniaturization of the original molecule, and by the addition of a succinyl group to a proline residue, which allowed its oral administration. This amino acid residue located at the C-terminal of BPP5a (one of the most active peptides in the bradykinin potentiating factor) is responsible for interacting with ACE (Cushman et al., 1977; Camargo et al., 2012). Captopril (alone or in combination with other drugs) is suitable and widely used for hypertension treatment (Weber et al., 2014).

After captopril, enalapril (MK-421, enalapril maleate) was approved by the FDA in 1985 for hypertension and congestive heart failure treatments (Patchett, 1984). The mercapto group in captopril structure was believed to be responsible for the skin rash and loss of taste reported as common adverse effects when using this drug. Therefore, the main challenge in enalapril development was to substitute the mercapto by an alkyl group, keeping the interaction with ACE (Patchett, 1984). Enalapril (Vasotec®, Merck) is produced as a prodrug that undergoes *in vivo* de-esterification to give rise to enalaprilat (MK-422), whose potency is greater than captopril, but has limited oral bioavailability (Biollaz et al., 1981; Patchett, 1984). Historically, captopril and enalapril are the hallmark in the development of ACE inhibitors for the treatment of hypertension.

The antiplatelet drug tirofiban (Aggrastat®, Medicure International, Inc.) is based on the RGD motif (Arg-Gly-Asp) from echistatin, a disintegrin found in the venom of the saw-scaled viper *Echis carinatus* (Topol et al., 1999). Tirofiban was approved by the FDA in 1998 for acute coronary syndrome treatment (Hartman et al., 1992). It mimics the RGD sequence and possesses a (S)-$NHSO_2$-C_4H_9 group that enhanced the interactions with the platelet glycoprotein GPIIb/IIIa receptor (Gan et al., 1988). The competition with fibrinogen for the RGD recognition sites on the GPIIb/IIIa complex results in the inhibition of platelet aggregation and other antithrombotic properties (Topol et al., 1999; Lang et al., 2012).

Eptifibatide (Integrilin®, Millennium Pharmaceuticals, Inc.) is another antiplatelet drug approved by the FDA in 1998 and licensed to Schering-Plough in 2005. It was developed during the efforts to create synthetic analogues of barbourin, a disintegrin isolated from *Sistrurus miliarius barbouri* snake venom. Due to its conservative amino acid substitution of arginine (R) for lysine (K), barbourin presents more specificity for platelet glycoprotein GPIIb/IIIa complex than other disintegrins containing the RGD motif (Scarborough et al., 1991). Also, it was verified that the affinity for GPIIb/IIIa is highly influenced by the amino acid residues adjacent to the KGD sequence and the size of the peptide ring created through the disulfide bond formation. From this information, different synthetic peptides with potential clinical use were designed, including eptifibatide (Scarborough, 1999). Eptifibatide is a cyclic heptapeptide (deamino-Cys(1)-hArg-Gly-Asp-Trp-Pro-Cys(1)-NH_2) more resistant to proteolysis due the introduction of a ring in the structure (Scarborough et al., 1993; Tcheng and O'Shea, 2002).

In the middle of 1900s, hirudin was isolated from *Hirudo medicinalis* leech saliva (Lee and Ansell, 2011). This 65-amino acid peptide presents an anticoagulant effect, through direct thrombin inhibition, and it was the only molecule to prevent blood coagulation until the discovery of heparin (Dodt et al., 1984; Markwardt, 1991). The removal of a sulfate group at Tyr63 residue gave rise to desulfatohirudin and increased in 10 times the complex formation with thrombin; however, obtaining this molecule with high activity and yield was a challenge to be overcome to allow clinical studies (Johnson et al., 1989; Markwardt, 1991). Desirudin (Iprivask®, Bausch Health), the recombinant 63-desulfohirudin (variant HV-1) produced in *Saccharomyces cerevisiae* (strain TR 1456), was approved by the FDA in 2003 for prophylaxis of deep vein thrombosis after hip replacement surgery (Warkentin, 2004). Revasc® (Novartis) was approved by EMA in 1997, but it was withdrawn from the market in 2014 for commercial reasons.

In general, hirudins inactivate irreversibly thrombin, causing more bleeding than heparin (Römisch et al., 1993). Therefore, some analogues were developed with the aim of optimizing the therapeutic profile of hirudin based on the interaction with the active site of thrombin (Warkentin, 2004). Bivalirudin (Angiomax®, The Medicines Company) is a synthetic peptide resulted from rational drug design, comprised of 20 amino acids: 4 N-terminal residues from native hirudin which interact with the active site, connected by 4 glycine residues to the last 12 residues present in its C-terminal responsible to interact with the anion exosite (Maraganore et al., 1990). This drug binds reversibly to thrombin, which decreased the risk of bleeding reported to other hirudins (Nutescu and Wittkowsky, 2004). Angiomax® was approved by the FDA in 2000 to patients with unstable angina undergoing percutaneous transluminal coronary angioplasty (Bittl et al., 2001). In Europe it is marketed as Angiox® (Mehrzad et al., 2017).

In 2004, ziconotide (Prialt®, Elan Pharmaceuticals, Inc.) was approved for the management of severe chronic pain by the FDA and by the EMA (Smith and Deer, 2009). Ziconotide (SNX-111) is a synthetic analogue of the omega-conotoxin MVIIA isolated from the venom of the fish-hunting snail *Conus magus*. It is a 25-amino acid peptide that blocks $Ca_v2.2$ channels (N-type voltage-sensitive calcium channels) and, consequently, inhibits the

conduction of nerve impulse and release of neurotransmitters into the thalamus, leading to antinociception (McGivern, 2007; Vink and Alewood, 2012). Ziconotide does not induce dependence or tolerance, which is a valuable advantage in comparison to morphine, which is also less effective than ziconotide (Scott et al., 2002). However, the main limitations of ziconotide use are its intrathecal administration route, which impairs the patient's adherence to the treatment (Smith and Deer, 2009), and narrow therapeutic index (Scott et al., 2002). Recently, the intranasal route has been studied to overcome the challenge of administering ziconotide (Manda et al., 2016).

Exenatide (synthetic exendin-4 from Gila monster, *Heloderma suspectum*) is the first glucagon-like-peptide-1 (GLP-1) analogue (Furman, 2012) and has been used as an adjuvant in the treatment of type 2 diabetes mellitus (Nauck et al., 2007; Henry et al., 2014). It presents a combination of actions: stimulation of insulin and suppression of glucagon secretion that result in blood glucose control, and reduction of body weight and cardiovascular risk factors (Eng et al., 1992; Greig et al., 1999; Alves et al., 2017).

Since GLP-1 is rapidly degraded by serum proteases presenting a very short lifetime, the key point was the development of GLP-1analogues resistant to these enzymes (Lorenz et al., 2013). Indeed the N-terminal (HGE) of exendin-4 is more resistant to peptidases that degrade the endogenous GLP-1 which make that more potent and longer-lasting than GLP-1 (Eng et al., 1992; Greig et al., 1999). The first pharmaceutical form of exenatide (Byetta®) was approved by the FDA in 2005 and in 2009 by the EMA. Even with the N-terminal more resistant to proteases, Byetta® has a half-life of ~2.4 h after administration (Lorenz et al., 2013).

Lixisenatide (Lyxumia® in the Europe and Adlyxin® in the USA., Sanofi S.A.) is a 44-amino acid peptide, with an amide group on its C-terminus. It is comprised of the first 39 amino acids of exendin-4, with a deletion of proline at position 38 and addition of six lysine residues (Christensen et al., 2009). Lixisenatide was approved in 2013 and 2016 by the EMA and the FDA, respectively, as the first once-daily injectable GLP-1 receptor agonist for the treatment of diabetes type II, presenting a half-life of ~3 h (Elkinson and Keating, 2013; Lorenz et al., 2013; US Food and Drug Administration, 2016).

In addition, there is an extended-release form of exenatide (Bydureon®), approved in 2011 and 2012 by the EMA and the FDA, respectively. It has a half-life of 5-6 days due to its encapsulation into poly (D,L-lactide-*co*-glycolide) microspheres, which hydrate *in situ* and slowly degrade to release the drug over time, resulting in less peak-trough variation (DeYoung et al., 2011; Lorenz et al., 2013). Long-acting exenatide has also been developed in a ready-to-use auto injector to facilitate the administration since the former pharmaceutical form needs to be diluted prior to administration (Wysham et al., 2017).

Apart from the marketed drugs in the USA and Europe, there are also those approved by the National Medical Products Administration (NMPA, formerly State FDA and China FDA —SFDA and CFDA, respectively). Batroxobin (also known as hemocoagulase, reptilase, and botropase) is a thrombin-like serine protease obtained from *B. atrox* and *B. moojeni* snake venoms (Itoh et al., 1987; Earps and Shoolingin-Jordan, 1998). It cleaves fibrinogen, resulting in the formation of non-cross-linked fibrin clots. Unlike thrombin, which releases fibrinopeptides A and B from fibrinogen, batroxobin releases only fibrinopeptide A (Holleman and Weiss, 1976). Although the enzyme is not clinically approved in the USA, its defibrinogenating effect is clinically used in other countries for the treatment of various thrombotic diseases including deep vein thrombosis, myocardial infarction, pulmonary embolism, and acute ischemic stroke (You et al., 2004).

Currently, batroxobin has been commercialized with the brand names: Batroxobin and Reptilase (Tobishi Pharmaceutical, China), Defibrase (Tobishi Pharmaceutical, China and DSM Nutritional Products Ltd Branch Pentapharm, Switzerland), Botropase (Hanlim, South Korea and Juggat Pharma, India), Botroclot (Juggat Pharma, India) (Drugs.com, 2020), Plateltex-Act® (Plateltex S.R.O., Czech Republic) (Plateltex, 2018), and Vivostat System (Vivostat A/S, 2018). Therapeutic applications of Defibrase® include acute cerebral infarction, unspecific angina pectoris, and sudden deafness (Pentapharm DSM Nutritional Products Ltd, 2018). Plateltex-Act® is used to prepare autologous platelet-gel, an emerging biotechnology in current tissue engineering and cellular therapy (Mazzucco et al., 2008). Batroxobin from Plateltex-Act® converts fibrinogen into fibrin in the presence of Ca^{2+} ions, and forms a fibrin reticulum that causes the gelling of the product and cooperates with the regenerative and reparative processes of damaged tissues (Mazzucco et al., 2008; Plateltex, 2016). The Vivostat System (Vivostat A/S, Denmark) is a medical device used for the preparation of an autologous fibrin sealant in the operating room by the action of batroxobin upon the fibrinogen in the patient's plasma (Vivostat A/S, 2018).

In 1998, cobratide (a short-chain post-synaptic α-neurotoxin isolated from *Naja naja atra* snake venom, also known as ketongning and cobrotoxin) was approved in combination with synthetic drugs as a pain killer for the treatment of moderate to severe pain (Gazerani and Cairns, 2014; Zhang, 2015). However, pharmacokinetics studies *in vivo* of cobratide injection (China Approval no. H53022101) are still necessary to adjust drug plasma concentrations and to reduce the risk of drug accumulation and fatal side effects (e.g., respiration inhibition) (Chen et al., 2016).

A detailed description of mechanism, pharmacology, pharmacokinetics, and clinical development of most approved toxin-based drugs can be found in specific reviews already published for each compound (Brogden et al., 1988; Tabacova and Kimmel, 2001; Wong, 2005; Zeymer, 2007; Graetz et al., 2011; Pope and Deer, 2013; Serrano, 2013; Knop et al., 2017; Trujillo and Goldman, 2017; Yang et al., 2019).

Diagnostic Tools

Besides its therapeutic applications, batroxobin (Reptilase®) has also been used for decades as a laboratory reagent to measure fibrinogen levels and blood coagulation capability through the *in vitro* clotting time using serine proteases instead of thrombin (Reptilase® time) (Funk et al., 1971). Since Reptilase® does not need Ca^{2+} and phospholipids, some coagulation factors (V, VIII, XI, and XIII) are not activated and the platelet aggregation is not

induced, cleaving only the fibrinopeptide A. Both Reptilase® time and thrombin time are complementary tests to evaluate coagulation disorders. Reptilase® is also used to detect antithrombin activity (Francischetti and Gil, 2019).

RVV-V (Pefakit®) is a 27 kDa factor V-activating serine protease from the Russel's viper (*Daboia russelii*) venom, used to identify factor V levels in plasma (Tokunaga et al., 1988). It is widely used in assays for the diagnosis of resistance to activated protein C, which does not cleaves factors Va and VIIIa (Francischetti and Gil, 2019).

RVV-X (Stypven®) is a 120 kDa factor X-activating metalloprotease from *D. russelii* venom that converts factor X quantitatively into factor Xa (Tans and Rosing, 2001; Morita, 2005). This toxin is dependent of Ca^{2+}, factor V, phospholipids and prothrombin (Francischetti and Gil, 2019).

Ecarin, from *E. carinatus* venom, is a 55 kDa metalloprotease able to activate prothrombin and detect its abnormal types (Morita et al., 1976; Weinger et al., 1980; Braud et al., 2000). Contrary to RVV-X, ecarin is independent of factor V, phospholipids or Ca^{2+}, detecting thrombin with chromogenic substrates (Ecarin chromogenic assay—ECA) or in a clotting assay (Ecarin clotting time—ECT) (Francischetti and Gil, 2019).

RVV-V, RVV-X, and ecarin are used to the diagnosis of lupus anticoagulant (Francischetti and Gil, 2019), one of the clinical manifestations of Antiphospholipid Syndrome, characterized by the presence of antiphospholipid antibodies (Favaloro and Wong, 2014).

Other snake venom toxins used as diagnostic tools include Botrocetin® and Protac®. Venom coagglutinin (Botrocetin®) isolated from *B. jararaca* venom is a 22 kDa C-type lectin-like protein that aggregates platelets by increasing the affinity between the receptor GPIbα and von Willebrand factor (Brinkhous et al., 1983; Beeton, 2013), independent of von Willebrand factor molecule size (Francischetti and Gil, 2019).

ACC-C (Protac®) from *A. contortrix contortrix* venom is a plasma protein C-activating serine protease used to quantify protein S and C levels (Stocker et al., 1988) with chromogenic substrates or by prolongation of the activated partial thromboplastin time (aPTT). These protein levels are used to investigate the cause of a blood clot (thromboembolism), linked to deep vein thrombosis or pulmonary embolism. AAC-C activity is not compromised by the inhibitor of protein C from plasma (Francischetti and Gil, 2019).

Cosmeceuticals

The cosmeceutical field is a profitable venture. For example, the anti-wrinkling effect of the botulinum toxin (Botox®), a toxin isolated from *Clostridium botulinum* bacteria, accounts for striking global sales of about $3 billion per year (Clark et al., 2019). Among the biologically active compounds from animal venoms showing cosmeceuticals applications, we can cite the use of bee venom-containing cosmetics on facial wrinkles in human skin (Han et al., 2015), and the inhibitory activity of melanogenesis of Argiotoxine-636 (ArgTX-636), a polyamine isolated from *Argiope lobata* spider venom (Verdoni et al., 2016), including a deposited patent (US10064814B2) for skin whitening/depigmenting (Mabrouk et al., 2018). Another example is the synthetic tripeptide [dipeptide diaminobutyroyl benzylamide diacetate (H-β-Ala-Pro-Dab-NHBzl x 2 AcOH)], commercialized as the cosmeceutical SYN®-AKE (Pentapharm). It mimics the activity of waglerin 1, a 22-amino acid peptide from *Tropidolaemus wagleri* snake venom, and reduces wrinkles by inhibiting muscle contractions (Zhang and Falla, 2009).

Venom Therapies

Bee venom therapy is an ancient therapy which uses this toxin arsenal as a cream, liniment, ointment, injection, acupuncture, or directly *via* stings of live bees to treat several disorders (Ali, 2012). Those treatments rely on the fact that bee venom is composed of a wide range of components, such as biogenic amines, enzymes (mostly PLA_2s), basic peptides, and non-enzyme proteins (mainly melittin and apamin) (Santos et al., 2011). Bee venom acupuncture corresponds to the most common used method, especially in the Koreas, and can be employed as an alternative treatment to pain, rheumatoid arthritis, osteoarthritis, and multiple sclerosis. The treatment consists of using bee venom in the relevant sites according to the disease or acupuncture points (Lee et al., 2014). A phase II randomized study to evaluate the effects of bee venom acupuncture in 68 participants with adhesive capsulitis (frozen shoulder) (NCT01526031) and another one in 60 patients with chronic cervicalgia (NCT01922466) were completed in 2012 and 2015, respectively.

Bee venom designated as apitoxin (Apitox®) has been marketed by Apimeds, Inc. for osteoarthritis in South Korea since 2016. A phase III randomized study (NCT01112722) in 363 patients with diagnosed osteoarthritis of the knee was completed in 2016 and a phase III randomized study (NCT03710655) for multiple sclerosis is not yet recruiting patients (last update 2018). Apitox® diminishes the pain and swelling associated with rheumatoid arthritis, tendinitis, bursitis, and multiple sclerosis (Bastos et al., 2011; Moreno and Giralt, 2015).

Another therapy for medicinal purposes is the hirudotherapy (medicinal leech therapy), approved in 2004 by the FDA. Since the beginning of civilization, leeches have been used for therapeutic purposes (Koh and Kini, 2008; Abdualkader et al., 2013). They are hematophagous animals that possess about 100 biologically active compounds in their saliva, especially the anticoagulants, but also components with anti-inflammatory, bacteriostatic, and analgesic properties (Singh, 2010). Many of the compounds responsible for those activities have already been identified (Sig et al., 2017), such as hirudin, kallikrein inhibitors, calin, hyaluronidase, collagenase, histamine-like substances, and antimicrobial peptides (e. g. theromacin, theromyzin, peptide B and lumbricin) (Cooper and Mologne, 2017). *H. medicinalis*, also known as the healing leech, is the main species used in the therapy (Abdualkader et al., 2013). The hirudotherapy has been shown to produce statistically significant improvement of arthritic conditions (Cooper and Mologne, 2017) and has also been applied in cardiovascular diseases, reconstructive and microsurgery, cancer and metastasis, diabetes mellitus and its complications, infectious diseases, arthritis, and as analgesic

(Singh, 2010; Abdualkader et al., 2013). For an extensive review regarding these venom therapies, please see (Mumcuoglu, 2014; Jagua-Gualdrón et al., 2020).

The hirudotherapy and all the toxin-based drugs approved by the FDA are chronologically shown in the next timeline (**Figure 1**).

ANIMAL TOXIN-BASED DRUG DEVELOPMENT CHALLENGES

Animal toxins are most often useful as pharmacological tools for target validation. However, in section *Achievements With Animal Toxin-Based Molecules* it was shown that they have also been successfully used as therapeutic agents.

Although there are examples of success, there is a gap between the number of compounds with interesting pharmacological properties obtained from animal poisons and venoms and those that are approved. Drug development programs may be discontinued due to several factors, like intellectual property disputes, changes in the program leadership, lack of funding, among other business decisions. The lack of publications regarding important data, during the different stages of their development, also contributes to several program discontinuations. While we sought to retrieve this information from the scientific literature, this fact impairs most of the process, concealing most of the key events.

The subsections *Challenges Regarding Basic Research* to *Challenges Regarding Clinical Trials* will address the challenges related to basic research, preclinical evaluation and clinical trials during the development of animal toxin-based drugs. However, many challenges faced during these stages are not available in the scientific literature, since much of this information is under intellectual property law for compounds that are still being developed or for which the development stopped because of internal issues.

Challenges Regarding Basic Research

One of the bottlenecks when studying toxins from small or rare venomous species, such as scorpions and spiders, is the hardship in obtaining large amounts of venom and purified toxins. For example, the venom glands from *Cupiennius salei* spider contain only 10 µl of venom, and the venom regeneration in milked animals requires from 8 to 16 days (Wigger et al., 2002). On the other hand, the snake *Lachesis muta muta* is able of injecting large venom amounts (milliliters of venom yielding 200-400 mg of toxins) (Stransky et al., 2018). The higher amount of collected snake venom is one of the reasons that may explain why most of the approved animal toxins-based drugs come from these animals.

Mucus-rich samples, such as toad and frog poisons, is also another issue, which may hinder the use of omic approaches (Shibao et al., 2018). In this context, studies comprising animal toxins are not a simple task since many challenges must be addressed. The small amount obtained from different poisonous and venomous animals, together with the nature of the venom/poison allied with the difficulty in isolating specific toxins, are the main limitations faced during basic research. Overcoming these limitations is thoroughly discussed in section *Filling the Gap Between the Drug Discovery and Its Commercialization—Future Trends*.

Challenges Regarding Preclinical Evaluation

Problems in the development of toxin-based drugs encompass selectivity, mechanism of action, formulation, stability, and production cost (Zhang and Falla, 2009). Besides the modern approaches using omic techniques, molecular biology, bioconjugation, and nanomaterials in animal venom research, venom components do not always meet all the requirements for a potential therapeutic application. Drug metabolism and pharmacokinetics properties of animal toxins, for instance, are key factors that need to be carefully optimized (Kovalainen et al., 2015).

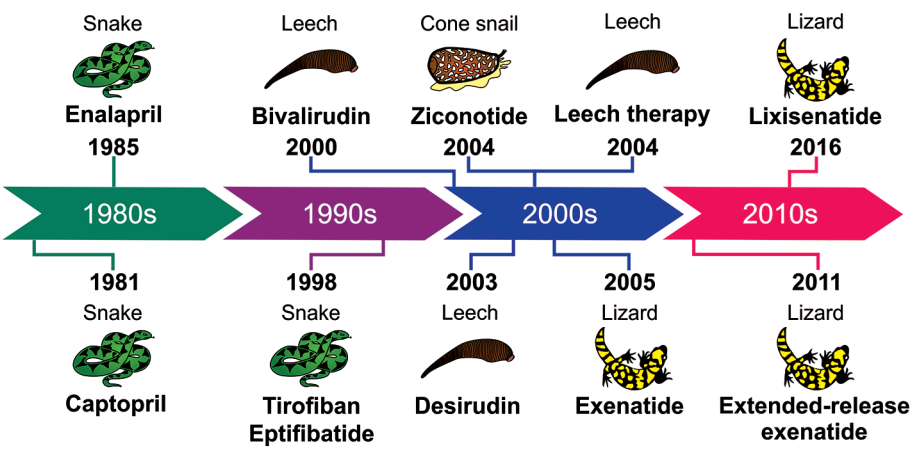

FIGURE 1 | Timeline showing the animal toxin-based drugs and hirudotherapy approved by the FDA.

In this regard, after overcoming the challenges imposed during the basic research, like obtaining enough amount of the toxin, it becomes necessary to stand up against some pitfalls faced during preclinical evaluation. Some compounds lack the ability of crossing pivotal barriers in the organism, including the blood-brain barrier, which may interfere in their delivery. Additionally, the susceptibility to blood proteases, as well as their immunogenicity, which are directly linked to biopharmaceutical degradation *in vivo*, are also important factors to be considered. Due to the relatively large size and other specific physicochemical properties, parenteral administration is currently the most used delivery route for approved venom-based drugs (**Table 1**) (Ibraheem et al., 2014; Duskey et al., 2017).

Considering all the challenges at this phase, preclinical studies are usually costly and lengthy, since they must attend all the requirements stated by the regulatory agencies throughout the world. In this respect, regulatory issues, together with problems related to lack of funding, and manufacturing problems, have been a hindrance for academics pursuing to advance their drug candidates into the clinical trials.

Challenges Regarding Clinical Trials

Randomized clinical trials are the gold standard to evaluate specific drug-related issues such as the efficacy and, to a lesser extent, the safety of new medicines before marketing approval. But these studies are not often able to evaluate special populations, such as children, pregnant women, and the elderly (Trifiro et al., 2019). To overcome these limitations, studies using electronic healthcare records (EHRs) of post-marketing comparative drug safety may complement traditional spontaneous reporting systems to predict which drugs require further epidemiological investigation. For instance, a multi-country healthcare database network identified new signals of potentially drug-induced acute liver injury in children using EHRs (Ferrajolo et al., 2014). A method of enhancing effectiveness of therapeutic agents using taxane nanoparticle co-administered with the therapeutic agent has been recently patented (US10660965B2).

On this point, the obstacles faced during the process of approving a new drug are harder to overcome than just improving its drugability, with two mainly issues contributing at this stage. First, new therapeutic drugs must achieve very high standards to be accepted, since they may have to compete with older and well-known drugs on the market, which may be more effective and cheaper, in most cases (because of the expired patent, for instance) (Scannell et al., 2012). Another problem is when the role of the toxin's target on the disease state is less relevant than previously thought for the manifestation of a particular disease, resulting in low efficacy. Even more, unexpected and unwanted effects could be observed *in vivo* if the target is expressed at different cells or if the toxin binds promiscuously to other targets (Scannell et al., 2012; Harvey, 2014; Vetter et al., 2017). In this context, adverse effects, lack of efficacy and dose-limiting toxicity are responsible for the interruption of many clinical trials (Harvey, 2014; Lewis, 2015).

LEARNING FROM DISCONTINUED TOXIN-BASED DRUGS

Most cases of drugs withdrawn from the market (voluntarily or prohibited by regulatory agencies) are related to different events, ranging from safety issues, like serious side effects, to several non-safety issues, encompassing those related to the manufacturing process, regulatory or business issues, or lack of efficacy. The foreseen toxicity of some toxin-based drugs may not be completely avoided, impairing the process at different stages of drug development. Therefore, understanding the mechanisms of toxicity is of utmost importance as an attempt to prevent post-marketing withdrawals (Siramshetty et al., 2016).

A mimetic peptide isolated from *Naja* spp. cobra venom, ximelagatran (Exanta®, AstraZeneca), was discontinued in 2006, due to hepatotoxic potential (King, 2011). This prodrug anticoagulant agent, orally administered, had been approved in Europe and South America for thrombin inhibition (Eriksson et al., 2003; Koh et al., 2006; Fox and Serrano, 2007; King, 2011). While Ximelagatran was mostly well tolerated in specific trial populations, a small proportion of the treated patients developed elevated liver enzyme levels, during phase II of clinical trials, which caused the FDA to reject its approval.

A phase III study of agkisacutacin (also known as hemocoagulase) in perioperative bleeding (Wei et al., 2010) was ceased due to anaphylactic reactions (Xu et al., 2016). The enzyme, which acts on fibrinogen and fibrin, is a heterodimeric serine protease from *Deinagkistrodon acutus* venom whose monomers A and B are comprised of 123 and 129 amino acid residues, respectively, linked by a disulfide bond (Wei et al., 2010). On the other hand, a phase IV randomized study (NCT03270735) to evaluate the efficacy and safety of hemocoagulase injection in the treatment of moderate to severe hemoptysis is recruiting patients since 2017. However, updated information regarding the evolution of this study could not be retrieved.

Pexiganan, also known as MSI-78 (a 22-residue linear peptide analogue of magainin-2), isolated from the skin of *Xenopus laevis* frog, is an antimicrobial peptide with therapeutic potential in treatment of infected foot ulcers in diabetic patients. The molecule presents *in vitro* activity against both Gram-positive and Gram-negative bacteria. The company Dipexium Pharmaceuticals, Inc. patented a 0.8% pexiganan acetate cream (Locilex® or Cytolex) but, in 1999, FDA denied the approval of this medicine arguing that its efficacy was not proven superior to that of the conventional treatment in any of the clinical trials (Ladram and Nicolas, 2016; Gomes et al., 2017).

Following the approval of ziconotide, other conotoxins, such as leconotide and Xen2174, were synthesized, studied and advanced to clinical trials. Leconotide (AM336 or ω-conotoxin CVID from *Conus catus*) caused side effects when intrathecally administered and would be intravenously evaluated, but the developer company went bankrupt (Harvey, 2014). Xen2174 (χ-CTX MrIA from *C. marmoreus*) progressed to Phase IIb trial (Lewis, 2015), but it showed dose-limiting toxicity in pharmacodynamics and

cerebrospinal fluid pharmacokinetics assays. Thus, it is unlikely that this conotoxin can be used for the treatment of acute pain in humans (Okkerse et al., 2017).

Alfimeprase, a recombinant zinc metalloprotease fibrolase from *Agkistrodon contortrix* with 203 residues and three disulfide bonds, cleaves the Aα- and Bβ-chains of fibrin, releasing fibrinopeptides A and B, respectively (King, 2011; Koh and Kini, 2012; Swenson and Markland, 2013). This molecule reached phase III of clinical trials in catheter occlusion and stroke; however, it was discontinued due to the lack of effectiveness (Shah and Scher, 2007; Markland and Swenson, 2010).

Among the several reasons for the interruption of many drug development programs are also intellectual property conflicts, lack of funding, business issues or changes in development leadership. In the case of lepirudin (Refludan®), for instance, its marketing was discontinued by Bayer in 2012 because the third-party manufacturer of the product had permanently ceased production of the drug (Bayer Healthcare, 2012). But the reasons that led to the manufacturing interruption have not been published, which prevents the proposal of solutions. Lepirudin is a recombinant peptide similar to hirudin, with an isoleucine instead of a leucine at N-terminal region and also lacking a sulfate group at Tyr63. It was marketed for prophylaxis or treatment of thrombosis complicating heparin-induced thrombocytopenia (Lee and Ansell, 2011).

The process of looking for information on drug removals from the market or haltered developments is a difficult task, since some of them are not available for several reasons aforementioned, and the data retrieved from public databases are significantly limited. In other words, factors that have not been published could have contributed to the discontinuation of the program.

PROMISING ANIMAL TOXINS IN PRECLINICAL STAGE AND CLINICAL TRIALS

The database search for toxin-based drugs on clinical trials is challenging. One needs to know the acronym or the abbreviation of the desired active ingredient, since sometimes neither the species nor the generic name is cited to allow a broad search. Furthermore, most of the information on these drugs is confidential and thus not available in the public domain. Another problem is that a lot of available data for some drugs have not been updated for several years, which makes it difficult to find accurate details.

Clinical development is a lengthy and costly process that includes phases I to III of clinical trials (previous regulatory review and approval) and phase IV (post-marketing surveillance) (Chow and Chang, 2008). Phase I recruits healthy volunteers to assess primarily pharmacokinetics, safety and tolerability; phase II evaluates a cohort of patients with the target disease to establish efficacy and dose-response relationship, and the large-scale phase III studies confirm safety and efficacy (Tamimi and Ellis, 2009). Phase IV clinical development focus on the safety rather than efficacy (Chow and Chang, 2008).

The following subsections will address the clinical trial status of some toxin-based drugs from different animal species and additional information about these drugs is available in **Table 2**.

Amphibians

Chansu, the dried toad venom secreted by the skin glands of *Bufo gargarizans* (previously *B. bufo gargarizans*) or *Duttaphrynus melanostictus* (previously *B. melanostictus*), has been used in the Traditional Chinese Medicine for more than 1000 years (Qi et al., 2011). Bufalin, the major digoxin-like immunoreactive component of Chansu, is a cardiotonic glycoside (bufadienolide) present in toad poisons and has demonstrated anticancer activities in several preclinical studies (Miao et al., 2013). Cinobufagin and resibufogenin are also bufadienolides present in Chansu, capable of inhibiting cancer cells growth *in vitro* (Xie et al., 2012; Li et al., 2013).

Huachansu (also known as cinobufacini) is a sterilized aqueous extract of Chansu, designed for intravenous injection, and has been widely used in oncological clinics in China to treat patients with several types of cancer, being approved by the NMPA (formerly China FDA) (Qi et al., 2011; Liu et al., 2015). The major biologically active components present in huachansu are steroidal cardiac glycosides, such as bufalin, resibufogenin, cinobufagin, cinobufotalin, marinobufagin (also known as marinobufagenin) and bufotalin, and indole alkaloids, like bufotenine, bufotenidine, cinobufotenine, and serotonin (Su et al., 2003).

During a phase I clinical study, huachansu was tolerable even at doses 6 times higher than those normally administered, and could slow disease progression in some cancer patients, with no observed significant cardiac toxicity (Meng et al., 2009).

The efficacy and safety of gemcitabine-oxaliplatin (Gemox) combined with huachansu chemotherapy is an effective and well-tolerated regimen for advanced and metastatic gallbladder carcinoma (Qin et al., 2008). Another study showed that huachansu combined with chemotherapy reduced the occurrence of gastrointestinal side effects and leukocytopenia in patients with advanced gastric cancer (Xie et al., 2013).

Many *in vitro* studies demonstrating anticancer properties of huachansu justify its continued evaluation in clinical trials. Phases II and III studies started recruiting participants, in 2016, to evaluate if cinobufacini tablets have synergistic effect in the treatment of diffuse large B cell lymphoma, the most common subtype of non-Hodgkin lymphoma. The estimated date of conclusion of the study is December 2021 (NCT02871869).

Bombesin is a peptide composed of 14 amino acids (EQRLGNQWAVGHLM-NH_2), isolated from the poisonous skin of the frog *Bombina bombina*, that shows high affinity for gastrin-releasing peptide-receptors (Tornesello et al., 2017; Utkin, 2017). Overexpression of members of this receptor family has been documented in several human neoplasms, such as prostate cancer, breast cancer, and small cell lung cancer. In this way, these receptors represent a molecular target for radiolabeled bombesin analogues as diagnostic or radiotherapeutic applications in these tumors (Schwartsmann et al., 2006; Wieser et al., 2014). Gallium-68 (68Ga)-DOTA-bombesin completed phase II in 2017 with 10 patients presenting

TABLE 2 | Toxin-based drugs in clinical trials.

Molecule (NCT number)	Species origin of venom toxin	Production	Formulation	Mechanism of action	Use	Status(last update)	Reference
ACV-1 (α-Vc1.1) – Discontinued [1]	*Conus victoriae*	Synthetic	S.c. injection	Activation of $GABA_B$ receptors	Neuropathic pain	Phase II—discontinued (lack of efficacy)	(Clark et al., 2010; King, 2011)
Agkisacutacin, Hemocoagulase, Recothrom® (NCT not available; NCT03270735) [2]	*Deinagkistrodon acutus*	Recombinant	I.v. infusion (2U)	Fibrinogen and fibrin cleavage	Perioperative bleeding; moderate to severe hemoptysis	Phase III ceased (2016); phase IV recruiting (September 1, 2017)	(Wei et al., 2010)
Alfimeprase – Discontinued (NCT00338585) [2]	*Agkistrodon contortrix contortrix*	Recombinant	Parenteral administration (up to 0.5 mg/kg was tolerated)	Cleaves Aα-chain of fibrin and fibrinogen	Catheter occlusion and stroke	Phase III terminated (based upon preliminary safety and efficacy results from a similar study) (January 15, 2008);	(Swenson et al., 2004; Ouriel et al., 2005)
Ancrod (Viprinex®) (NCT01621256) [2]	*Calloselasma rhodostoma* (Malasyan pit viper)	Recombinant	I.v. infusion (0.167 IU/kg for 6 h)	Reduce fibrinogen	Sudden sensorineural hearing loss	Phases I/II completed (December 21, 2018)	(Hennerici et al., 2006)
Bombesin (NCT02440308) [1]	*Bombina bombina*	Synthetic	I.v.	Attaches to prostate tumor cells with specific receptors on their surfaces	Imaging agent for positron emission tomography/ magnetic resonance imaging	Phase II completed (April 11, 2017)	(US National Library of Medicine, 2020)
Cenderitide, CD-NP (NCT00482937, NCT02603614, NCT02359227 and NCT02071602) [1]	*Dendroaspis angusticeps*	Chimeric natriuretic peptide	I.v. infusion (10, 25, 50, 100, 200, and 300 ng/ kg/min over 4 h) or subcutaneous infusion (0.5, 1.0, 2.0, and 3.0 ng/kg/min) or IV infusion (5 and 10 ng/kg/min over 72 h)	Connection to natriuretic peptide receptor	Congestive cardiac failure, heart failure and myocardial infarction	Phase I completed (June 6, 2007; February 11, 2020 and January 4, 2019)	(Lee et al., 2009)
Chlorotoxin derivates - Tozuleristide (BLZ-100) (NCT02234297) and 131-I-TM-601 (NCT00379132) [1]	*Leiurus quinquestriatus quinquestriatus* (Deathstalker yellow scorpion)	BLZ-100: Synthetic/131-I-TM-601: Recombinant	I.v. infusion (BLZ-100: dose unknown/31-I-TM-601: 0.2, 0.4, and 0.6 mg)	Binds to different targets (membrane type-2 matrix metalloprotease, annexin A2, and CLC-3 chloride channels in glioma cells and other tumors of neuroectodermal origin)	Tumor paint for intraoperative visualization of solid cancer cells	Phase I completed (April 6, 2016 and March 31, 2009)	(Patil et al., 2019; US National Library of Medicine, 2020)
Cinobufacini (Buformin®) (NCT02871869)	*Bufo gargarizans* or *Duttaphrynus melanostictus*	Sterilized water extract of dried toad skin (Chansu)	0.3 g per tablet, three tablets per time	Induction of apoptosis; inhibition of cancer cells	Several types of cancer	Phase II/III recruiting (July 17, 2017)	(US National Library of Medicine, 2020)
Conantokin-G (CGX-1007) – Discontinued [1]	*Conus geographus*	Synthetic	Intrathecal	NMDA receptor antagonist	Intractable epilepsy	Phase I—discontinued (the developer company went bankrupt)	(Han et al., 2008; King, 2011)
Contulakin-G (CGX-1160) – Discontinued [1]	*Conus geographus*	Synthetic	Intrathecal	Neurotensin receptor agonist	Neuropathic pain	Phase II—discontinued (the developer company went bankrupt)	(Han et al., 2008; King, 2011)
Dalazatide, ShK-186, Stichodactyla	*Stichodactyla helianthus* (Sun sea anemone)	Synthetic	S.c. injection twice per week for a total of nine doses	Kv1.3 channel antagonist	Autoimmune diseases (psoriatic arthritis, multiple	Phase I completed (May 6, 2015)	(US National Library of Medicine, 2020)

(Continued)

TABLE 2 | Continued

Molecule (NCT number)	Species origin of venom toxin	Production	Formulation	Mechanism of action	Use	Status(last update)	Reference
toxin ShK (NCT02435342) (1)					sclerosis, lupus, rheumatoid arthritis, etc.)		
Desmoteplase (NCT00790920 and NCT00111852) (2)	Common vampire bat (*Desmodus rotundus*)	Recombinant	I.v. single bolus (90 or 125 μg/kg of body weight)	Plasminogen activator a1 with high fibrin specificity	Acute ischemic stroke	Phase III completed (September 18, 2015 and March 20, 2012)	(US National Library of Medicine, 2020)
Fibrin glue, fibrin sealant (2 and 3)	*Crotalus durissus terrificus* and *Bubalus bubalis*	Thrombin-like serine protease from snake venom and fibrinogen-rich cryoprecipitate from buffalo blood	Topically	Fibrinogen cleavage	Adhesive, sealant, and hemostatic effects	Phase I/II completed by the Clinic of Chronic Ulcers of the Dermatology Service at the Botucatu Medical School, UNESP (November, 11, 2019)	(Ferreira et al., 2017; Buchaim et al., 2019)
Huachansu (NCT00837239 and NCT02647125)	*Bufo gargarizans* or *Duttaphrynus melanostictus*	Sterilized water extract of dried toad skin (Chansu)	20 ml/m^2 for total 500 ml given as a 2-h infusion	Induction of apoptosis; inhibition of cancer cells	Several types of cancer	Phase II completed (July 12, 2012) and active, not recruiting (April 30, 2020)	(US National Library of Medicine, 2020)
Leconotide (AM336 or ω-conotoxin CVID) – Discontinued (1)	*Conus catus*	Synthetic	3–6 μg/h (intrathecal)	Selective blocker of $Ca_V2.2$ channel	Neuropathic pain	Phase I/IIa—discontinued (the developer company went bankrupt)	(Kolosov et al., 2010; King, 2011; Harvey, 2014)
RPI-78M (Receptin®) (NCT not avaiable) (3)	*Naja kaouthia*	Detoxified or chemically modified	Orally (with benzalkonium chloride)	Connetion to nicotinic acetylcholine receptors (nAChRs)	Analgesic applications and multiple sclerosis	Manufacturing for clinical trials (October 28, 2018)	(King, 2011; Drug discovery and development, 2016; Adis Insight, 2018; Ojeda et al., 2018)
RPI-MN (Pepteron®) (NCT not avaiable)(3)	*Naja naja atra*	Detoxified or chemically modified	S.c. injection	Connection to nicotinic acetylcholine receptors (nAChRs) and can protect cells due to its ability to inhibit viral replication	Analgesic applications and HIV	Phase I and II completed (January 28, 2020)	(Biocentury, 2007; King, 2011; Adis Insight, 2020)
Shk-192 – Discontinued (1)	*Stichodactyla helianthus*	Synthetic	10 or 100 μg/kg by s.c. injection once daily	$K_V1.3$ channel blocker	Autoimmune disease	Phase I	(Pennington et al., 2009; King, 2011)
Soricidin, SOR-C13 (NCT01578564 and NCT03784677) (1)	*Blarina brevicauda* (Northern short-tailed shrew)	Synthetic	I.v. infusion (dose range from 1.375 to 6.12 mg/kg)	Inhibitor of the Ca^{2+}-selective transient receptor potential channel TRPV6	Ovarian (and other) cancers	Phase I completed (June 23, 2016) and recruiting (August 6, 2019)	(US National Library of Medicine, 2020)
Tetrodotoxin (Tectin®) (NCT01655823) (4)	*Pufferfish, marine animals and phylogenetically unrelated terrestrial organisms*	Synthetic	Different injectable dosages (1 ml), twice a day for four consecutive days	Sodium channel blocker	Neuropathic pain caused by chemotherapy	Phase II terminated (decided to proceed to Phase III) (October 30, 2018)	(US National Library of Medicine, 2020)
Xen 2174 (χ-CTX MrIA) – Discontinued (1)	*Conus marmoreus*	Synthetic	Intrathecal	Interacts with a large hydrophobic pocket within the norepinephrine transporter	Postoperative pain	Phase IIb (2015)—discontinued	(Brust et al., 2009; King, 2011; Lewis, 2015)
Ximelagatran (Exanta®) –	*Naja* spp.	Synthetic	36 mg orally twice daily.	Direct thrombin inhibitor	Prevention of venous	Phase III terminated (November 15, 2010)—withdrawn from the	(Gulseth, 2005; King, 2011)

(Continued)

TABLE 2 | Continued

Molecule (NCT number)	Species origin of venom toxin	Production	Formulation	Mechanism of action	Use	Status(last update)	Reference
Discontinued (NCT00206089) [4]					thromboembolic events	market and clinical development in February 2006 in the interest of patient safety (hepatic toxicity)	

1), peptide; 2), enzyme; 3), non-enzyme protein; 4), organic molecule; i.v., intravenous; NCT, ClinicalTrials.gov identifier; s.c., subcutaneous.

prostate cancer. It is an imaging agent for positron emission tomography/magnetic resonance imaging and attaches to tumor cells with specific receptors on their surfaces (NCT02440308).

Different chemical modifications have been introduced in the synthetic bombesin to stabilize its structure, increase the binding affinity and to potentiate its agonist/antagonist properties (Cescato et al., 2008; Tornesello et al., 2017). A large variety of bombesin receptor ligands have been preclinically tested, most of which were bombesin agonists (Baratto et al., 2018). However, most of these ligands demonstrated high gastrointestinal uptake and limited metabolic stability *in vivo*, and can cause acute side effects (nausea, abdominal pain and emesis) when administered at higher doses (Accardo et al., 2016).

A synthetic bombesin/gastrin-releasing peptide-receptor antagonist (RC-3095) was able to produce long-lasting tumor regressions in murine and human tumor models *in vitro* and *in vivo*. Due to the occurrence of local toxicity at the injection site during a phase I trial in patients with advanced solid malignancies, a recommended dose of RC-3095 for Phase II trials could not be clearly established (Schwartsmann et al., 2006). Considering its mechanism of action and preclinical antitumor activity, further studies exploiting new formulations of RC-3095 for human use, such as slow-release preparations and analogues with a more favorable pharmacokinetics, are justified.

Epibatidine is an alkaloid extracted from the skin of the Ecuadorian frog *Epipedobatus tricolor* (poison-dart frog). This molecule binds to several nAChR subtypes, including α7, α4β2, and the neuromuscular α1β1δγ subtype. Antinociceptive efficacy of epibatidine is about 100 times more powerful than morphine, but it has induced adverse effects, revealing high toxicity to be used as a pain-relieving drug (Traynor, 1998; Salehi et al., 2019).

Many compounds based on the chemical structure of epibatidine have been developed and tested to become new, powerful pain-reducing drugs (Daly, 2004; Umana et al., 2013). An example is ABT-594 (tebanicline or ebanicline) (Salehi et al., 2019). ABT-594 is of particular interest once it is more powerful than morphine showing no morphine-associated side effects and only mild cardiovascular side effects (Fox and Serrano, 2007). Due to severe gastrointestinal side effects caused by this first analogue of epibatidine, it has not been included in pain therapies in humans (Salehi et al., 2019).

Cone Snails

Conotoxins, isolated from different species of cone snails (*Conus* ssp.), comprise a large family of small cysteine-rich peptides (10–30 amino acid residues) organized in subfamilies according to their structure (cysteine framework) and their mechanism of action (Lewis et al., 2012; Ovsepian et al., 2019). Undoubtedly, omega-conotoxins represent the most notable and famous conotoxin subfamily, in which omega-MVIIA [ziconotide (Prialt®)], previously reported in the section *Achievements With Animal Toxin-Based Molecules*, belongs to.

KCP-400 (also known as RgIA4), derived from Vc1.1, the first toxin isolated from *C. regius* venom, is a novel non-opioid drug for the treatment of chronic pain. Vc1.1 is a highly potent toxin that targets α9α10 nAChR, blocking pain signaling at the site of nerve injury, producing analgesic, anti-inflammatory and neuroprotective effects (Romero et al., 2017). The preclinical safety and efficacy studies of KCP-400 had been conducted by Kineta Inc., which is currently developing the non-opioid KCP-506 (Kineta Inc., 2020).

Because of their high potency and specificity, novel conotoxins can provide additional information on the pharmacology of ion channels, receptors, and transporters (Lewis et al., 2012; Gao et al., 2017).

Hymenopterans

The whole venom of bees (Alyostal ST *Apis mellifera*) completed a randomized phase II study, in 2014, to evaluate its efficacy and potential effects in 50 participants presenting motor symptoms of Parkinson's disease (NCT01341431). The administration of bee venom showed to be safe in non-allergic patients (Hartmann et al., 2016). Following the same direction of bee venom, the whole venom of ants has been employed in therapeutic use. For instance, the extracted material from venom sacs of *Pseudomyrmex triplarinus* could be helpful in relieving the pain caused by rheumatoid arthritis (WO1990003178A1, US4247540A).

The whole venom of wasps, bees and ants are also being used in venom immunotherapy (VIT), which represents a treatment to allergic patients preventing further sting-induced anaphylactic reactions (Kolaczek et al., 2017). Several clinical protocols and guidelines were published and generally consist of injections of small but gradually increasing doses of a specific venom (Bonifazi et al., 2005).

Despite those studies published employing hymenoptera whole venoms, little has been reported on the therapeutic applications of purified toxins. Thus far, the most explored hymenoptera venom components are melittin, apamin (both isolated from bees), and mastoparan (isolated from wasps) (Moreno and Giralt, 2015). All those three components arise as promising drug candidates for several conditions or therapeutic applications, such as antitumor agents (Gajski and

Garaj-Vrhovac, 2013; de Azevedo et al., 2015), learning disabilities (Messier et al., 1991; Ikonen and Riekkinen, 1999), antimicrobial and antiviral activity (Vila-Farres et al., 2012; Sample et al., 2013), cell penetrating-peptides (Jones and Howl, 2012), among other applications.

Concerning melittin, a phase II study of ARC-520 in 79 participants with chronic hepatitis B virus (HBV) was terminated for regulatory and business reasons in 2019 (NCT02577029). The Dynamic Polyconjugate® technology, developed by Arrowhead Therapeutics, uses melittin as an endosomolytic agent to facilitate the delivery of siRNA conjugates to hepatocytes (US8313772; US8501930; US8618277; WO2013003520A1).

Scorpions

Chlorotoxin (CTx) is the only toxin from scorpion venoms undergoing clinical phase trials. The evidence of a venom molecule that interacts with chloride (Cl^-) channels was firstly demonstrated by DeBin and Strichartz, which showed that *Leiurus quinquestriatus quinquestriatus* (the yellow scorpion from the Middle East, also known as death stalker) venom was able to block Cl^- channels of reconstituted rat epithelia and embryonic rat brain (DeBin and Strichartz, 1991). CTx is a peptide with 36 amino acids presenting 4070 Da, 4 disulfide bonds and it is positively charged in pH 7. Moreover its structure was solved by nuclear magnetic resonance spectroscopy: three-stranded antiparallel β-sheet packed against an α-helix (Lippens et al., 1995). The synthetic CTx was also produced successfully (Ojeda et al., 2016).

CTx discovery was marked by a substantial rise of publications using this molecule for different applications, such as insecticide (DeBin et al., 1993), antiangiogenic (Jacoby et al., 2010), and tumor binding (Cohen-Inbar and Zaaroor, 2016). CTx has demonstrated the capability to bind to different targets including chloride channels, membrane type-2 matrix metalloprotease (MMP-2) and annexin A2 (Ojeda et al., 2016). However, a milestone in the CTx discovery was the production of fluorescent molecular probes such as the tumor paint (CTx conjugated with Cy5.5 or CTx : Cy5.5). This bioconjugate can detect cancer foci and metastases from malignant glioma, sarcoma medulloblastoma and prostate and intestinal cancers using mouse models. The specific identification by this fluorescent molecular beacon (CTx : Cy5.5) increases the precision of surgical resection (image guidance) and improves patient prognosis (Veiseh et al., 2007). CTx:800CW (an infrared dye conjugate) was also produced; however, it has failed since the integrity of the blood-brain barrier was compromised even in the early stages of medulloblastoma tumor (Kovar et al., 2013).

Tozuleristide (BLZ-100), a CTx indocyanine green conjugate, demonstrated to bind to tumor cells while sparing healthy tissues (Butte et al., 2014). Phase I studies of BLZ-100 in 17 patients with glioma undergoing surgery were finished in 2016 (NCT02234297). The 131-I-TM-601 is the recombinant version of chlorotoxin (TM-601) radioconjugated with iodine 131 (Hockaday et al., 2005; Kesavan et al., 2010). It has been tested against different cancers (breast cancer, non-small cell lung cancer, melanoma, colorectal cancer, pancreatic cancer, prostate adenocarcinoma, glioma primary and solid tumors). The Phase I with 60 patients presenting recurrent or refractory somatic and/or cerebral metastatic solid tumors was completed in 2009 (NCT00379132). Regarding intellectual property, many patents applications can be detected relating to CTx variants, bioconjugates and methods for use, with an extensive list of records (e.g. WO2011142858A2; WO20006115633A2; US20030021810A1; US20160096869A1; US20080260639A1).

Although solely CTx reached clinical phase so far, other scorpion toxins have demonstrated therapeutic potential. For instance, the scorpion venom active polypeptide (SVAP) from *Mesobuthus martensii* (formerly *B. martensii*) has completed preclinical phase as a potential antithrombotic peptide. The results demonstrated that SVAP (0.125, 0.25, 0.5 mg/ml) inhibited rabbit platelet aggregation *in vitro*. Moreover, this peptide (0.32 and 0.64 mg/kg, intravenous administration) prolonged the occlusion time of carotid artery thrombosis in rats. Thus, SVAP may be considered an interesting molecule to be used in the treatment of cardiocerebral vascular diseases (Song et al., 2005).

Cancer treatment is also explored with other scorpion toxins. Besides CTx, BmKCT, a CTx-like molecule from *M. martensii* venom, reversibly inhibits chloride currents of glioma cells (Yang et al., 2005). BmkTa, also a CTx-like from *M. martensii* venom, is able to abolish the human glioma cells growth in a dose-dependent manner, with an IC_{50} of approximately 0.28 μM (Fu et al., 2007). Although some peptides must be highlighted (AmmTx3, BmTx3, Bekm-1, BmHyA, and IbTx), the list of scorpion toxins with antiproliferative activities is extensive (Das Gupta et al., 2007; Fu et al., 2012; Ding et al., 2014; Ortiz et al., 2015).

Scorpion toxins blocking potassium channels have also been widely investigated. In particular, those inhibiting $K_v1.3$ currents are considered potential bioactive molecules to treat autoimmune diseases (Zhao et al., 2015). To the best of our knowledge, there are 81 scorpion toxins with positive results in inhibiting $K_v1.3$ (Oliveira et al., 2019). Nevertheless, only eight of them present *in vivo* assays (i.e. most of them were studied using solely *in vitro* electrophysiological experiments). 1) HsTX1 from *Heterometrus spinifer* venom demonstrated to reduce inflammation in an active delayed-type hypersensitivity model and in the pristane-induced arthritis using rat models (Tanner et al., 2017). 2) ImKTX88 from *Isometrus maculatus* venom ameliorates pathological severity in rat experimental autoimmune encephalomyelitis (Huang et al., 2017). 3) Kaliotoxin (Ktx) from *Androctonus mauretanicus mauretanicus* venom showed the ability of preventing bone loss through a receptor activator of NF-κB ligand (RANKL)-dependent osteoclastogenesis mechanism, using rat periodontal disease model. Thus, Ktx has been tested to treat periodontal disease and rheumatoid arthritis (Valverde et al., 2004). 4) Margatoxin (MgTX) from *Centruroides margaritatus* venom caused a reduction of tumor volume into a xenograft model using nude mice by blocking $K_v1.3$ channels, and it is being considered as a novel therapeutic target for lung adenocarcinoma therapy (Jang et al., 2011). 5) OSK1 from *Orthochirus scrobilosus* venom displayed blocking activity of $K_v1.3$; however, during *in vivo* experiments, it demonstrated to be neurotoxic since it can diffuse immediately throughout the mouse brain (Mouhat et al., 2005). 6-7) Ts6 and Ts15 from *Tityus serrulatus* venom inhibit the proliferation of effector memory T cells and reduce inflammation in delayed-type hypersensitivity

response using mice model (Pucca et al., 2016). 8) Vm24 from *Vaejovis mexicanus smithi* venom reduces delayed-type hypersensitivity reactions in rats (Varga et al., 2012), as well as impairs the synthesis and secretion of T cell cytokines in response to T-cell receptor engagement (Veytia-Bucheli et al., 2018).

Some reports have shown that maurocalcine from the scorpion *Maurus palmatus*, a toxin active on ryanodine receptors, goes into the cells and can also be used as a vector for the penetration of cell-impermeable cargo molecules. Mutated analogues of maurocalcine have been produced as leads to develop better cell-penetrating peptides (CPPs) (Esteve et al., 2005; Ram et al., 2009). CPPs are short (9-35 residues) cationic or amphipathic molecules with the capability of being rapidly internalized across cell membranes. In this way, they can mediate the translocation of a conjugated drug across plasma membranes, being considered an effective and non-toxic mechanism for drug delivery (Ramsey and Flynn, 2015). The first Ca^{2+} channel toxin from *T. serrulatus* venom, designated as CPP-Ts, exhibited selective internalization properties and specific nuclear delivery, being a potential intranuclear delivery tool to target cancerous cells (de Oliveira-Mendes et al., 2018).

Sea Anemones

Sea anemones, the polyp form of marine coelenterates of the phylum Cnidaria (Watters, 2005), are poorly studied, but represent a rich source of new compounds. ShK-186, originally isolated from *Stichodactyla helianthus* sea anemone venom, inspired the design of dalazatide, a synthetic peptide composed of 37 amino acids, acting as a $K_v1.3$ inhibitor (Beeton et al., 2006). In preclinical tests, dalazatide have significantly reduced the clinical score of rat model of multiple sclerosis (Tarcha et al., 2012). Dalazatide completed phase I trials in 2015 to examine the safety of systemic multiple ascending dose administration in 32 healthy volunteers (NCT02446340) and in 24 patients with plaque psoriasis (NCT02435342). No phase II study has been started since then. However, public databases (e.g., the FDA, Drugs.com, etc.) do not mention what happened to this drug lead.

Snakes

Recently, collinein-1, a SVSP from *Crotalus durissus collilineatus* venom (Boldrini-França et al., 2015) was recombinantly expressed in *Pichia pastoris* system (Boldrini-Franca et al., 2019) and demonstrated to block, independently from its catalytic activity, the hEAG1 ion channel, which is overexpressed in several cell cancer lines. Collinein-1 reduced the viability of human breast cancer cell line MCF7, which displays high expression of hEAG1, but does not affect the HepG2 and MCF10A cell lines, which present low expression of this ion channel, demonstrating that the reduction of cell viability might be connected with hEAG1 inhibition by this protein (Boldrini-França et al., 2020).

Isolated from the Malayan pit viper (*Calloselasma rhodostoma*), ancrod is a thrombin-like enzyme able to release fibrinopeptide A from fibrinogen Aα chain, causing hypofibrinogenemia in humans (Reid, 1971). Structurally, it is composed of 234 amino acids and presents six disulfide bonds (Burkhart et al., 1992). Because of its enzyme activity on fibrinogen (Chan et al., 2016), this toxin was used in stroke treatment (Pizzo et al., 1972), marketed for several decades by Knoll Pharma in Germany and Austria, until it was withdrawn in the 1980s (Chan et al., 2016). In 2002 the rights of this drug were licensed. Two parallel trials (NCT00141001 and NCT00300196) were in phase III of clinical trials by Neurobiological Technologies (NTI), but both studies were terminated due to low efficacy, suboptimal and inconsistent results which led to the dissolution of NTI in 2009 (King, 2011; Liu et al., 2011). A randomized study involving this molecule completed phase II trial in 31 patients with sudden hearing loss to check its effectiveness, safety, and tolerance for this kind of pathology in 2018 (NCT01621256).

The association of 15 residues of the C-terminal portion of *Dendroaspis* natriuretic peptide, isolated from *D. angusticeps* venom, with 22 residues of a human C-type natriuretic peptide, formed the chimeric natriuretic peptide, cenderitide (CD-NP) (Lisy et al., 2008; Lee et al., 2009). It can be applied in congestive heart failure, and its mechanism of action is associated with the connection to natriuretic peptide receptors, leading to hypotension (Wei et al., 1993; Lee et al., 2009). Studies with this peptide completed phase I in 2007, in a non-randomized way, to check its efficacy, safety, and pharmacodynamics in 22 healthy participants (NCT00482937) (Lee et al., 2009; Ichiki et al., 2019). A phase II study in 14 patients with stable chronic heart failure (NCT02359227) and a phase I/II randomized study in 8 patients with chronic stable heart failure and moderate renal impairment (NCT02603614) were completed in February 2020. Another phase I randomized study to maintain the function of left ventricle in 30 participants with myocardial infarction was completed in 2019 (NCT02071602).

Fibrin sealant or fibrin glue, a bioproduct formed by a thrombin-like serine protease from *C. d. terrificus* venom and fibrinogen-rich cryoprecipitate from humans, could transmit infectious diseases and was suspended by the FDA in 1978 (Spotnitz, 2014; Ferreira et al., 2017). To overcome this drawback, the Center for the Study of Venoms and Venomous Animals (CEVAP) at São Paulo State University (UNESP), in Brazil, started studying the aforementioned fibrin sealant using a fibrinogen-rich cryoprecipitate from *Bubalus bubalis* buffaloes blood (Barros et al., 2009; Ferreira et al., 2017), and this bioproduct completed phase I/II of clinical trials with 10 patients in phase I and 30 patients in phase II (Ferreira et al., 2017). The fibrin glue displays adhesive, sealant and hemostatic effects due to its proteolytic activity on fibrinogen, producing fibrin monomers, which forms a clot in the presence of calcium (Barros et al., 2009; Ferreira et al., 2017). Similarly, preliminary studies have been conducted to evaluate the effect of direct application of Vivostat® (autologous fibrin sealant) in controlling cerebral bleeding (Graziano et al., 2015; Graziano et al., 2016).

A 33 kDa-batroxobin from *B. atrox* and *B. moojeni* venoms (Itoh et al., 1987; Earps and Shoolingin-Jordan, 1998) was expressed in *P. pastoris* and exhibited biochemical activities

similar to those of native protein (You et al., 2004). The recombinant batroxobin used with a medical adhesive synergistically accelerated hemostasis in the mouse liver and femoral artery models, reducing bleeding time and blood loss. Hemostasis was more rapidly achieved with increasing concentrations of batroxobin (You et al., 2014). Other dressings using collagen and chitosan with recombinant batroxobin also controlled bleeding and improved the hemostatic properties of collagen and chitosan pads used alone (Seon et al., 2017).

An analgesic preparation containing cobratide and oxycodone for cancer-related pain (CN104645312) and a keluoqu tablet preparation method using tramadol hydrochloride, ibuprofen and cobratide (also known as ketongning and cobrotoxin) (CN105769791) have been patented. The anti-nociceptive effects of cobrotoxin (the *N. n. atra* snake venom short-chain post-synaptic α-neurotoxin cobratide) do not involve muscarinic acetylcholine or opioid receptors and the molecule has high affinity for the α_1 subunit of the nicotinic acetylcholine receptors (nAChR) (Gazerani and Cairns, 2014). Cobratoxin, a long-chain post-synaptic α-neurotoxin isolated from the Thailand cobra (*N. kaouthia*), produces anti-nociceptive and anti-inflammatory effects through decreased production of inflammatory cytokines, for example, TNF-α, IL-1, and IL-2, *via* its high affinity for the α_7 subtype of nAChR (Gazerani and Cairns, 2014).

RPI-78M (Receptin®) and RPI-MN (Pepteron®) are detoxified and chemically modified forms of cobratoxin and cobrotoxin, respectively (King, 2011; Harvey, 2014). RPI-78M has 71 amino acid residues with five disulfide bonds and completed phase I of clinical trials for multiple sclerosis, while RPI-MN presents 62 amino acid residues and four disulfide bonds (King, 2011). Both molecules show analgesic applications and present the nAChRs as molecular target (Chan et al., 2016). Although RPI-MN is parenterally administered *via* subcutaneous injection, RPI-78M can be orally administered, since its absorption through the oral mucosa occurs when it is formulated with benzalkonium chloride (Reid and Raymond, 2010). Chemical modifications that detoxify these molecules can alter their affinity to nAChRs. They may include their oxidation with ozone, formate (also known as methanoate) and hydrogen peroxide, being the latter more adopted (Reid, 2007). RPI-MN has also completed preclinical studies against Human Immunodeficiency Virus (HIV), protecting cells due to its ability to inhibit viral replication (Reid, 2007; King, 2011; Harvey, 2014). However, its mechanism of action has not been elucidated yet (Reid and Raymond, 2010).

Crotamine, a highly cationic and cysteine-rich CPP from *C. d. terrificus* snake venom, displays membrane translocation capabilities, penetrates into the cell and presents cytoplasmatic, vesicular, and nuclear distribution (Kerkis et al., 2004). This toxin is specifically uptaken by actively proliferating cells, being able to permeate several lineages *in vitro* (Nascimento et al., 2007). Additionally, several molecules based on crotamine structure, including fluorescent derivatives (Tansi et al., 2019) and functionalized with gold nanoparticles (Karpel et al., 2018), for instance, are being developed. Crotamine and its analogues have been tested in healthy and tumorous cell lines, and the results indicate they can be used as selective delivery tools of anticancer molecules (Mambelli-Lisboa et al., 2018).

Another component isolated from *C. d. terrificus* venom is crotalphine (Konno et al., 2008), a potent analgesic comprised of 14 amino acid residues. It acts at peripheral opioid receptors (Gutierrez et al., 2008) and selectively targets TRPA1 ion channels (Bressan et al., 2016), being more potent under conditions of acute peripheral sensitization (Zambelli et al., 2014). The potent and long lasting opioid-mediated antinociception of crotalphine has been evaluated in cancer pain (Brigatte et al., 2013).

Spiders

The toxin π-theraphotoxin-Pc1a or π-TRTX-Pc1a (also known as psalmotoxin 1 or PcTx1), obtained from the *Psalmopoeus cambridgei* (Trinidad chevron tarantula) venom, is considered a novel therapeutic molecule for treating pain (Monge-Fuentes et al., 2018). Classified as a specific inhibitor of ASIC1a, the most abundant acid-sensing ion channel, the toxin π-TRTX-Pc1 demonstrated an effective analgesic effect comparable to morphine in rat models of acute pain (Mazzuca et al., 2007). Recently, PcTx1 was also reported as a valuable tool for understanding the functional role of ASIC2a heteromeric channels (ASIC1a/2a) (Liu et al., 2018) and had no effect on acid-induced transient or chronic hyperalgesia in a mouse model of fibromyalgia (Chang et al., 2019).

Hi1a, a PcTx1-related toxin isolated from the Australian funnel-web spider *Hadronyche infensa*, partially inhibits ASIC1a and does not affect ASIC1b (Maatuf et al., 2019). This toxin strongly attenuates brain damage after stroke and could be used to protect the brain from ischemic injury (Chassagnon et al., 2017), being considered as a lead for development of neuroprotective agents (Ren et al., 2018).

Purotoxin-1 (PT1), obtained from the central Asian spider *Geolycosa* sp. venom, has also been studied to pain treatment (Monge-Fuentes et al., 2018). Characterized as a specific antagonist of P2X3 purinergic receptor, which is the most-studied subtype of P2X receptor related to pain, PT1 was able to inhibit nociceptive effect in different rat pain models (Grishin et al., 2010).

Phoneutria nigriventer (the armed spider) presents different toxins with potential pharmaceutical application and under preclinical tests (Peigneur et al., 2018). The toxin Phα1β, classified as P/Q- and N-type voltage-gated calcium channel blocker, and its recombinant form (produced in *E. coli*) demonstrated analgesic effects in rodent models of pain (Souza et al., 2008). Recently, the same toxin (Phα1β) together with PhTx3-3 (also a voltage-gated calcium channel blocker) demonstrated significant inhibitory effects on the proliferation and viability of different glioma cell lines (M059J, U-138MG and U-251MG) at low concentrations (0.3-100 pM). In the same study, Phα1β and its recombinant form named CTK 01512-2 caused significant reductions of tumor areas *in vivo* using mouse glioblastoma model (Nicoletti et al., 2017). Moreover, Phα1β and its recombinant version were able to reduce the inflammatory phase of the formalin-induced nociceptive behavior in rats, to decrease neuropathic pain caused by chronic constriction injury

of sciatic nerve in rats, and to reduce the hyperalgesia caused by melanoma cancer model in mice (Rigo et al., 2017).

P. nigriventer venom became attractive because of its induced-priapism effect. The δ-ctenitoxin-Pn2a toxin, also known as δ-CNTX-Pn2a or Tx2-6, modulates voltage-gated sodium (Na_v) channels and demonstrated an erectile effect in rats (12 μg/kg, subcutaneous or intravenous injection) (Nunes et al., 2008). Interestingly, a minimum dose of 0.006 μg/kg directly injected into the corpus cavernosum can cause erection in mice (Andrade et al., 2008). A synthetic 19-amino acid peptide, PnPP-19, designed from active core of PnTx2-6 tertiary structure, potentiated erection *in vivo* and *ex vivo via* the nitric oxide/cyclic guanosine monophosphate pathway. PnPP-19 is a promising candidate for erectile dysfunction treatment in patients that do not respond to the usual therapies (Silva et al., 2015). Biozeus Biopharmaceutical S.A performed pilot tests with the topical peptide (renamed BZ371) on healthy human beings and has been performing a pilot test with voluntary men with erectile dysfunction associated to hypertension or diabetes. The regulatory toxicological preclinical tests have already started. The next steps involve the final marketing formulation and future clinical trials (Phases 1 and 2) (Biozeus Biopharmaceutical SA, 2018; Johnson & Johnson, 2019){Johnson & Johnson, 2019, Champions of Science® Storytelling Challenge: Latin America and Caribbean Edition;Biozeus Biopharmaceutical SA, 2018, First clinical trial sponsored by Biozeus concluded!}.

Although antimicrobial activities with spider toxins are well documented (for detail see Spider Toxin Database, http://arachnoserver.org), their therapeutic use are limited due to their susceptibility to proteolysis.

Tetraodontiformes

Tetrodotoxin (TTX), a guanidinium neurotoxin with high affinity for voltage-gated sodium (Na_v) channels, had traditionally been known for many years as the main toxin from Tetraodontidae pufferfish (Lago et al., 2015). However, the toxin was present not only in other marine animals such as octopuses, gobies and sea stars, but also in phylogenetically unrelated terrestrial and aquatic organisms, including a dinoflagellate *Alexandrium tamarense*, red calcareous algae, arthropods, echinoderms, molluscs, worms, newts, frogs, and bacteria *Actinomyces*, *Aeromonas*, *Alteromonas*, *Bacillus* and *Pseudomonas* (Lago et al., 2015; Assuncao et al., 2017). The blockage of Na^+ into the cell inhibits the action potentials' propagation in the excitable cell membranes, which causes neuromuscular paralysis (Duran-Riveroll and Cembella, 2017). TTX has been used for the development of analgesic and anesthetic drugs (Assuncao et al., 2017; Vetter et al., 2017) and, under the trade name Tectin® (Wex Pharmaceuticals Inc.), proceeded to phase III of the clinical trials for the treatment of pain resulting from chemotherapy treatment in 2018 (NCT01655823).

Other Animals

The salivary secretion from different animals, such as bats, leeches, lizards, shrews and ticks are considered important sources of biologically active compounds. Other animals, such as caterpillars, have biologically active compounds in their bristles. Many of these compounds are still underexploited, lacking information on their chemical structure, physiological role and therapeutic application. Thus, the study of these compounds increases the chances of discovering new compounds with great pharmaceutical potential. The subsections ***Bats*** to ***Ticks*** will address some potential therapeutic molecules found in the saliva or bristles of these animals.

Bats

Desmoteplase, also known as "*Desmodus rotundus* salivary plasminogen activator" (DPSA), is a thrombolytic agent for acute ischemic stroke derived from vampire-bat saliva (Medcalf, 2012; Shi et al., 2016). This fibrin-dependent plasminogen activator is composed of 441 amino acids with high fibrin specificity, long half-life, low bleeding tendency, nonactivation by β-amyloid and lack of neurotoxicity (Medcalf, 2012; Shi et al., 2016; Li et al., 2017). A phase III randomized study in 492 participants with acute ischemic stroke was completed in 2015. Currently, there is no drug based on desmoteplase available for commercialization.

Caterpillars

Caterpillars from different South American countries, such as Venezuela, Brazil, French Guyana, Peru, Paraguay, Argentina and Colombia, are responsible for a severe bleeding syndrome in humans who touch their bristles (Arocha-Pinango and Guerrero, 2001). *Lonomia obliqua* is the main species of caterpillar found in Southern Brazil and its venom is comprised of molecules with antiviral, procoagulant, fibrinolytic and wound healing activities (Veiga et al., 2005; Reis et al., 2006; Alvarez-Flores et al., 2011; Carmo et al., 2015; Sato et al., 2016). Their toxic compounds are found in the bristle extract, hemolymph, cryosecretion (a crude venomous fluid ejected by the whole secretory tegument of caterpillars, stored at -20°C for 24 h) and tegument extract (Pinto et al., 2006; Veiga et al., 2009). Some compounds with potential therapeutic applications were identified in *Lonomia* sp, e.g. prothrombin or factor X activators, such as Lopap (*L. obliqua* prothrombim activator protease) and Losac (*L. obliqua* Stuart factor activator protease), PLA_2-like, proteases, hyaluronidases, α-fibrinogenases (e.g. Lonofibrase), protease inhibitors, serpins, lipocalins, and lectins (Veiga et al., 2009). Currently, there are three clinical studies on caterpillars recorded at the Clinical Trials website (US National Library of Medicine, 2020). However, these studies are related to their use as a source of protein in the diet and none of them involves the genus *Lonomia*.

Leeches

Two phase II randomized studies involving leech therapy in 118 (NCT00435773) and 60 participants (NCT02612974) with knee osteoarthritis were completed in 2007 and 2015, respectively. Additional information on FDA-approved hirudin analogues from *H. medicinalis* leech saliva and hirudotherapy was reported in section *Achievements With Animal Toxin-Based Molecules*.

Lizards

Exenatide is the synthetic version of the native peptide exendin-4 isolated from the saliva of Gila monster lizard (*H. suspectum*) (Eng et al., 1992; Furman, 2012). According to the Clinical Trials website, there are more than 300 clinical studies about exenatide. So far, there are 207 completed studies, 12 terminated, 25 whose status has not changed for 2 years, 47 recruiting volunteers, 11 that are not yet recruiting, and three enrolled by invitation. Among the clinical studies, exenatide has been used in patients with Parkinson's disease, showing beneficial effects on nerve cells by slowing down or stopping the degenerative process of this disease (NCT03456687). For an extensive review regarding clinical trials involving this drug, please see (Odegard and Desantis, 2009; Bhavsar et al., 2013). Additional information on exenatide was described in section *Achievements With Animal Toxin-Based Molecules*.

Shrews

SOR-C13 is a synthetic selective peptide inhibitor of Transient Receptor Potential Vanilloid 6 (TRPV6) calcium oncochannel (Pennington et al., 2017; Soricimed, 2018). It is comprised of 13 amino acids derived from the C-terminal region of the paralytic peptide soricidin (UniProtKB—P0C2P6), from the submaxillary and sublingual salivary glands of the Northern Short-tailed shrew (*Blarina brevicauda*) (Bowen et al., 2013; Fu et al., 2017). It inhibits the activation of nuclear factor of activated T-cell (NFAT) transcription complex, and induces apoptosis in TRPV6-overexpressing cells (NIH National Cancer Institute, 2018). A phase I of study (NCT01578564) in 23 advanced cancer patients with TRPV6 channel overexpression was completed in 2016 and a phase I study (NCT03784677) started recruiting patients with advanced refractory solid tumors in 2019.

Ticks

There are several studies addressing the importance of tick saliva components. The use of evasins in the treatment of heart diseases, such as myocarditis (Singh et al., 2017) and the use of ixolaris, an anticoagulant protein from *Ixodes scapularis* tick saliva, to reduce HIV-driven coagulopathy, for instance (Schechter et al., 2017).

However, although tick saliva contains many components with therapeutic and biotechnological potentials, there are neither clinical studies involving the use of substances isolated from tick saliva nor drugs available for therapeutic purposes. The 101 clinical studies currently registered on the Clinical Trial website in respect to ticks are related to the development of vaccines against ticks or the use of different antibiotics in Lyme disease.

FILLING THE GAP BETWEEN THE DRUG DISCOVERY AND ITS COMMERCIALIZATION—FUTURE TRENDS

Animal poisons and venoms are comprised of a cocktail of bioactive components with a gamut of different activities. Company pipelines worldwide are expanding the number of peptide-based products currently in development mainly because of the diversity of their application and activity. However, industrial production of toxin-related drugs from natural sources is quite challenging, laborious and presents restricted yield (Boldrini-França et al., 2017). To overcome these limitations, the main options are the chemical synthesis of peptides and the production of biopharmaceuticals *via* heterologous expression using biotechnological tools.

Recent data reinforces the advances in transcriptomics, proteomics and heterologous expression techniques, which allowed the characterization and potential production of low abundant active venom components, presenting low or high molecular mass (Boldrini-França et al., 2017). Additionally, pharmacomics has been gaining ground by integrating "omic" approaches to study dynamic molecular states and monitors disease states and drug responses, improving the development of novel drugs (Wilson and Daly, 2018).

The industry has focused on heterologous expression systems as an interesting alternative for manufacturing biopharmaceuticals of high molecular mass (Merlin et al., 2014). Recombinant protein production processes require extensive design and regulatory control before therapeutic products become commercially available. Regarding heterologous expression, the accurate cysteine bond formation and the proper incorporation of post-translational modifications remain a challenge, and new technologies to assess and mitigate immunogenicity risk of engineered proteins are becoming more common. Therefore, a special attempt should be made to ensure that the recombinant protein presents comparable three-dimensional folding and consistent pharmacological properties when compared to its corresponding native form.

Native chemoselective reaction has been employed in the production of animal toxins with potential therapeutic application, such as mambalgin-2, a 57-amino acid analgesic peptide from three-finger toxins family, from *Dendroaspis polylepis polylepis* venom (Diochot et al., 2012; Harvey, 2014). This approach allows the synthesis of large proteins, since it is based in the production of different unprotected linear peptide fragments, which are condensed in solution *via* chemoselective reactions to originate the entire polypeptide (Kent et al., 2012). Studies to improve the protecting groups, resins, linkers, and activation and coupling reagents may enable the manufacture of larger peptides and even small proteins for therapeutic applications. However, the development of cheaper reagents and methods for the synthesis and purification of peptides are necessary.

Concerning the limitations of peptides in terms of their biopharmaceutical properties, designed approaches that will find molecules with intrinsically more favorable properties will need to be devised. As mentioned earlier in section *Achievements With Animal Toxin-Based Molecules*, the drug design of captopril made oral administration possible. Additionally, designed cationicity-enhanced analogues of natural antimicrobial peptides have exhibited higher potency and spectra of antimicrobial activity (Luna-Ramirez et al., 2017).

Achievements towards successful oral delivery of proteins and peptides by protecting them against degradation and increasing their absorption remain as an active area of research. Regarding toxin-based formulations, intranasal inoculation of hyaluronidase from *T. serrulatus* venom induced mononuclear increase in the bronchoalveolar space and became a promising tool for the treatment of pulmonary fibrosis (Bitencourt et al., 2011).

Some approaches to improve biopharmaceuticals delivery, such as alternative delivery routes, PEGylation and conjugation to (nano) carriers, represent a relevant step towards targeted delivery of toxin-based drugs. It is sobering to realize how little alternative delivery routes and bioconjugation strategies have been exploited to deliver toxin-based drugs, suggesting that studies on routes of distribution, delivery vehicles, cargo molecules, and targeting strategies are fruitful fields for future research.

Collinein-1, a thrombin-like serine protease from *C. d. collilineatus*, was successfully modified by site-specific PEGylation with maleimide-mPEG of 5 kDa and exhibited higher catalytic efficiency and affinity for the substrate than the native form (da-Silva-Freitas et al., 2015). The PEGylated peptide HsTX1[R14A] from *Heterometrus spinnifer* scorpion venom showed higher plasma circulating half-life in rodents compared to the native peptide, which resulted in sustained efficacy in rodent models of multiple sclerosis and rheumatoid arthritis (Tanner et al., 2017).

In the drug development process, formulation patents using advanced drug release systems extend the market exclusivity of drugs, because of the high technical barrier to be overcome by generic manufacturers after the expiration of patents. Focusing on competitiveness, pharmaceutical companies have established strategic partnerships with leading academic institutions that have deep scientific expertise in novel concepts in the main areas of biology or chemistry. Some reports have shown the antitumor potential, among other applications, of animal venoms or their toxins conjugated with a wide variety of nanomaterials, such as silica, gold, chitosan, poly(D,L-Lactide)-based, and supermagnetic iron oxide nanoparticles (Badr et al., 2014; Utkin, 2017).

Studies on cell penetrating peptides (CPPs) have open unprecedented possibilities for vector applications in several fields, such as basic research, therapeutics, technology, and medical imaging. CPP-Ts, the first Ca^{2+} channel toxin from *T. serrulatus* venom, showed to be a potential intranuclear delivery tool to target cancerous cells (de Oliveira-Mendes et al., 2018). WaTx, a cell-penetrating toxin from the Australian black rock scorpion *U. manicatus*, reduced the permeability of the TRPA1 ion channel to Ca^{2+} ions and can be used as a tool to study the mechanisms involved in chronic pain (King et al., 2019).

Another field in ever-growing demand is the cosmeceutical industry, especially in Asia, where Korea is at the forefront of cosmeceutical development. Efficacy and safety studies on these products in humans are on high demand (Juhász et al., 2018).

CONCLUSION

Animal poisons and venoms are rich sources of molecules with a wide range of applications. However, to make the use of these molecules feasible, extensive preclinical trials are necessary, with some applications also requiring clinical trials (**Figure 2**).

Although the research in the field of toxinology tends to be quite challenging and time-consuming, the high selectivity of animal toxins for their targets turns them into promising leads for the development of effective therapeutic drugs. Studies on new engineered molecules with reduced side effects can be reached by untangling the interaction of venom peptides with their target. Therefore, we are still at a beginning phase in comprehending the complexity of animal venoms and poisons. While very few species have been extensively studied, we still have thousands of unexploited organisms, especially marine ones. Novel methods to produce and deliver biopharmaceuticals are expected to be

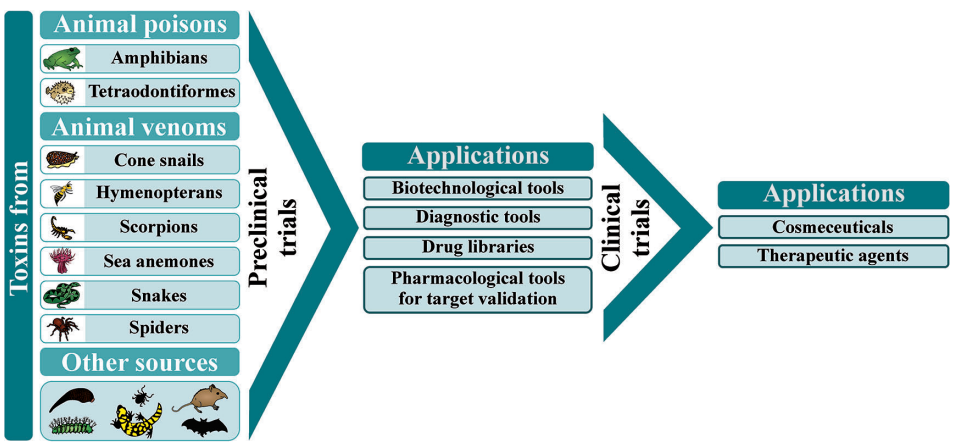

FIGURE 2 | Animal poisons and venoms as sources of candidate molecules for wide-ranging applications, after extensive characterization during preclinical and clinical trials.

developed in the near future. With that in mind, we can get a glimpse of how much work on toxinology and drug discovery is yet to come in the next years.

AUTHOR CONTRIBUTIONS

KB and EA contributed to the conception and design of the study. KB and EP-J wrote the first draft of the manuscript. KB, CC, EF-B, EP-J, FCe, FGA, FPA, FCo, GW, IC, IF, IO, JB-F, MP, MB, and EA wrote sections of the manuscript. FCe created the figures. KB, GW, IC, and IO created the tables. All authors contributed to manuscript revision, read, and approved the submitted version.

FUNDING

This study was supported by the São Paulo Research Foundation (FAPESP, grants 2017/04724-4 and 2019/10173-6, and scholarships to CC 2013/26200-6, EP-J 2016/04761-4; FCe 2017/14035-1 and 2018/14158-9; GW 2017/00586-6; ISO 2017/03580-9 and 2018/21233-7; KB 2013/26619-7), the National Council for Scientific and Technological Development (CNPq, grants 306479/2017-6 and 307155/2017-0 and scholarships to FCo 155276/2018-2 and FGA 150037/2018-0) and the Coordination for the Improvement of Higher Education Personnel (Coordenação de Aperfeiçoamento de Pessoal de Nível Superior—Brasil, CAPES, Finance Code 001, scholarships to EP-J 88881.186830/2018-01, GW, IF, IO, and JB-F).

REFERENCES

Abdualkader, A. M., Ghawi, A. M., Alaama, M., Awang, M., and Merzouk, A. (2013). Leech therapeutic applications. *Indian J. Pharm. Sci.* 75 (2), 127. doi: 10.4103/0250-474X.115456

Accardo, A., Galli, F., Mansi, R., Del Pozzo, L., Aurilio, M., Morisco, A., et al. (2016). Pre-clinical evaluation of eight DOTA coupled gastrin-releasing peptide receptor (GRP-R) ligands for *in vivo* targeting of receptor-expressing tumors. *EJNMMI Res.* 6 (1):17. doi: 10.1186/s13550-016-0175-x

Adis Insight (2018). *RPI-78M*. Available at: https://adisinsight.springer.com/drugs/800020844 (Accessed June 22, 2020).

Adis Insight (2020). *RPI-MN*. Available at: https://adisinsight.springer.com/drugs/800025141 (Accessed June 22, 2020).

Ali, M.A.A.-S.M. (2012). Studies on bee venom and its medical uses. *Int. J. Adv. Res. Technol.* 1 (2), 69–83.

Alvarez-Flores, M. P., Furlin, D., Ramos, O. H. P., Balan, A., Konno, K., and Chudzinski-Tavassi, A. M. (2011). Losac, the first hemolin that exhibits procogulant activity through selective factor X proteolytic activation. *J. Biol. Chem.* 286 (9), 6918–6928. doi: 10.1074/jbc.M110.167718

Alves, P. L., Abdalla, F. M. F., Alponti, R. F., and Silveira, P. F. (2017). Anti-obesogenic and hypolipidemic effects of a glucagon-like peptide-1 receptor agonist derived from the saliva of the Gila monster. *Toxicon* 135, 1–11. doi: 10.1016/j.toxicon.2017.06.001

Andrade, E., Villanova, F., Borra, P., Leite, K., Troncone, L., Cortez, I., et al. (2008). Penile erection induced *in vivo* by a purified toxin from the Brazilian spider *Phoneutria nigriventer*. *BJU Int.* 102 (7), 835–857. doi: 10.1111/j.1464-410X.2008.07762.x

Arocha-Pinango, C. L., and Guerrero, B. (2001). *Lonomia* genus caterpillar envenomation: Clinical and biological aspects. *Haemostasis* 31 (3-6), 288–293. doi: 10.1159/000048075

Assuncao, J., Guedes, A. C., and Malcata, F. X. (2017). Biotechnological and pharmacological applications of biotoxins and other bioactive molecules from dinoflagellates. *Mar. Drugs* 15 (12), 393. doi: 10.3390/md15120393

Badr, G., Sayed, D., Maximous, D., Mohamed, A. O., and Gul, M. (2014). Increased susceptibility to apoptosis and growth arrest of human breast cancer cells treated by a snake venom-loaded silica nanoparticles. *Cell Physiol. Biochem.* 34 (5), 1640–1651. doi: 10.1159/000366366

Baratto, L., Jadvar, H., and Iagaru, A. (2018). Prostate cancer theranostics targeting gastrin-releasing peptide receptors. *Mol. Imaging Biol.* 20 (4), 501–509. doi: 10.1007/s11307-017-1151-1

Barros, L. C., Ferreira, R. S.Jr., Barraviera, S. R. C. S., Stolf, H. O., Thomazini-Santos, I. A., Mendes-Giannini, M. J. S., et al. (2009). A new fibrin sealant from *Crotalus durissus terrificus* venom: applications in medicine. *J. Toxicol. Environ. Health B Crit. Rev.* 12 (8), 553–571. doi: 10.1080/10937400903442514

Bastos, E. M. A. F., Heneine, L. G. D., Pesquero, J. L., and Merlo, L. A. (2011). *Pharmaceutical composition containing an Apitoxin fraction and use thereof*, WO/2011/041865 patent application.

Bayer Healthcare (2012). *Discontinuation of Refludan® [lepirudin (rDNA) for injection]*. Available at: https://www.hrsa.gov/sites/default/files/opa/programrequirements/manufacturerletters/2012/refludan05312012.pdf (Accessed March 19, 2020).

Beeton, C., Wulff, H., Standifer, N. E., Azam, P., Mullen, K. M., Pennington, M. W., et al. (2006). Kv1.3 channels are a therapeutic target for T cell-mediated autoimmune diseases. *Proc. Natl. Acad. Sci. U.S.A.* 103 (46), 17414–17419. doi: 10.1073/pnas.0605136103

Beeton, C. (2013). "Targets and therapeutic properties," in *Handbook of biologically active peptides, 2nd ed.* Ed. A. J. Kastin (Amsterdam: Elsevier), 473–482.

Bhavsar, S., Mudaliar, S., and Cherrington, A. (2013). Evolution of exenatide as a diabetes therapeutic. *Curr. Diabetes Rev.* 9 (2), 161–193. doi: 10.2174/1573399811309020007

Biocentury (2007). *Pepteron (RPI-MN)*. Available at: https://bciq.biocentury.com/products/pepteron_(rpi-mn) (Accessed March 19, 2020).

Biollaz, J., Burnier, M., Turini, G. A., Brunner, D. B., Porchet, M., Gomez, H. J., et al. (1981). Three new long-acting converting-enzyme inhibitors: relationship between plasma converting-enzyme activity and response to angiotensin I. *Clin. Pharmacol. Ther.* 29 (5), 665–670. doi: 10.1038/clpt.1981.92

Biozeus Biopharmaceutical SA (2018). *First clinical trial sponsored by Biozeus concluded!*. Available at: http://biozeus.com.br/first-clinical-trial-sponsored-by-biozeus-concluded/ (Accessed March 29, 2020).

Bitencourt, C. S., Pereira, P. A., Ramos, S. G., Sampaio, S. V., Arantes, E. C., Aronoff, D. M., et al. (2011). Hyaluronidase recruits mesenchymal-like cells to the lung and ameliorates fibrosis. *Fibrogenesis Tissue Repair* 4(1), 3. doi: 10.1186/1755-1536-4-3

Bittl, J. A., Chaitman, B. R., Feit, F., Kimball, W., and Topol, E. J. (2001). Bivalirudin versus heparin during coronary angioplasty for unstable or postinfarction angina: Final report reanalysis of the Bivalirudin Angioplasty Study. *Am. Heart J.* 142 (6), 952–959. doi: 10.1067/mhj.2001.119374

Boldrini-França, J., Santos Rodrigues, R., Santos-Silva, L. K., de Souza, D. L., Gomes, M. S., Cologna, C. T., et al. (2015). Expression of a new serine protease from *Crotalus durissus collilineatus v*enom in P*ichia pastoris* and functional comparison with the native enzyme. *Appl. Microbiol. Biotechnol.* 99 (23), 9971–9986. doi: 10.1007/s00253-015-6836-2

Boldrini-França, J., Cologna, C. T., Pucca, M. B., Bordon, K. C. F., Amorim, F. G., Anjolette, F. A. P., et al. (2017). Minor snake venom proteins: Structure, function and potential applications. *Biochim. Biophys. Acta Gen. Subj.* 1861 (4), 824–838. doi: 10.1016/j.bbagen.2016.12.022

Boldrini-Franca, J., Pinheiro-Junior, E. L., and Arantes, E. C. (2019). Functional and biological insights of rCollinein-1, a recombinant serine protease from *Crotalus durissus collilineatus*. *J. Venom. Anim. Toxins Incl. Trop. Dis.* 25, e147118. doi: 10.1590/1678-9199-jvatitd-1741-18

Boldrini-França, J., Pinheiro-Junior, E. L., Peigneur, S., Pucca, M. B., Cerni, F. A., Borges, R. J., et al. (2020). Beyond hemostasis: a snake venom serine protease with potassium channel blocking and potential antitumor activities. *Sci. Rep.* 10, 4476 (2020). doi: 10.1038/s41598-020-61258-x

Bonifazi, F., Jutel, M., Bilo, B. M., Birnbaum, J., Muller, U., and Hy, E.I.G.I.V. (2005). Prevention and treatment of hymenoptera venom allergy: guidelines for clinical practice. *Allergy* 60 (12), 1459–1470. doi: 10.1111/j.1398-9995.2005.00960.x

Bowen, C. V., DeBay, D., Ewart, H. S., Gallant, P., Gormley, S., Ilenchuk, T. T., et al. (2013). I*n vivo* detection of human TRPV6-rich tumors with anti-cancer peptides derived from soricidin. *PloS One* 8 (3), e58866. doi: 10.1371/journal.pone.0058866

Braud, S., Bon, C., and Wisner, A. (2000). Snake venom proteins acting on hemostasis. *Biochimie* 82 (9-10), 851–859. doi: 10.1016/S0300-9084(00)01178-0

Bressan, E., Touska, F., Vetter, I., Kistner, K., Kichko, T. I., Teixeira, N. B., et al. (2016). Crotalphine desensitizes TRPA1 ion channels to alleviate inflammatory hyperalgesia. *Pain* 157 (11), 2504–2516. doi: 10.1097/j.pain.0000000000000669

Brigatte, P., Konno, K., Gutierrez, V. P., Sampaio, S. C., Zambelli, V. O., Picolo, G., et al. (2013). Peripheral kappa and delta opioid receptors are involved in the antinociceptive effect of crotalphine in a rat model of cancer pain. *Pharmacol. Biochem. Behav.* 109, 1–7. doi: 10.1016/j.pbb.2013.04.012

Brinkhous, K. M., Read, M. S., Fricke, W. A., and Wagner, R. H. (1983). Botrocetin (venom coagglutinin) - Reaction with a broad-spectrum of multimeric forms of factor VIII macromolecular complex. *Proc. Natl. Acad. Sci. U.S.A. -Biol. Sci.* 80 (5), 1463–1466. doi: 10.1073/pnas.80.5.1463

Brogden, R. N., Todd, P. A., and Sorkin, E. M. (1988). Captopril - an update of its pharmacodynamic and pharmacokinetic properties, and therapeutic use in hypertension and congestive heart-failure. *Drugs* 36 (5), 540–600. doi: 10.2165/00003495-198836050-00003

Brust, A., Palant, E., Croker, D. E., Colless, B., Drinkwater, R., Patterson, B., et al. (2009). χ-conopeptide pharmacophore development: toward a novel class of norepinephrine transporter inhibitor (Xen2174) for pain. *J. Med. Chem.* 52 (22), 6991–7002. doi: 10.1021/jm9003413

Buchaim, D. V., Cassaro, C. V., Shindo, J., Della Coletta, B. B., Pomini, K. T., Rosso, M. P. D., et al. (2019). Unique heterologous fibrin biopolymer with hemostatic, adhesive, sealant, scaffold and drug delivery properties: a systematic review. *J. Venom. Anim. Toxins Incl. Trop. Dis.* 25, e20190038. doi: 10.1590/1678-9199-jvatitd-2019-0038

Burkhart, W., Smith, G. F., Su, J. L., Parikh, I., and LeVine, H. (1992). Amino acid sequence determination of ancrod, the thrombin-like alpha-fibrinogenase from the venom of A*gkistrodon rhodostoma*. *FEBS Lett.* 297 (3), 297–301. doi: 10.1016/0014-5793(92)80559-Y

Butte, P. V., Mamelak, A., Parrish-Novak, J., Drazin, D., Shweikeh, F., Gangalum, P. R., et al. (2014). Near-infrared imaging of brain tumors using the Tumor Paint BLZ-100 to achieve near-complete resection of brain tumors. *Neurosurg. Focus* 36 (2), E1. doi: 10.3171/2013.11.FOCUS13497

Camargo, A. C. M., Ianzer, D., Guerreiro, J. R., and Serrano, S. M. T. (2012). Bradykinin-potentiating peptides: Beyond captopril. *Toxicon* 59 (4), 516–523. doi: 10.1016/j.toxicon.2011.07.013

Carmo, A. C. V., Yamasaki, L. H. T., Figueiredo, C. A., Giovanni, D., de Oliveira, M. I., dos Santos, F. C. P., et al. (2015). Discovery of a new antiviral protein isolated L*onomia obliqua* analysed by bioinformatics and real-time approaches. *Cytotechnology* 67 (6), 1011–1022. doi: 10.1007/s10616-014-9740-1

Cescato, R., Maina, T., Nock, B., Nikolopoulou, A., Charalambidis, D., Piccand, V., et al. (2008). Bombesin receptor antagonists may be preferable to agonists for tumor targeting. *J. Nucl. Med.* 49 (2), 318–326. doi: 10.2967/jnumed.107.045054

Chan, Y. S., Cheung, R. C., Xia, L., Wong, J. H., Ng, T. B., and Chan, W. Y. (2016). Snake venom toxins: toxicity and medicinal applications. *Appl. Microbiol. Biotechnol.* 100 (14), 6165–6181. doi: 10.1007/s00253-016-7610-9

Chang, C. T., Fong, S. W., Lee, C. H., Chuang, Y. C., Lin, S. H., and Chen, C. C. (2019). Involvement of acid-sensing ion channel 1b in the development of acid-induced chronic muscle pain. *Front. Neurosci.* 13:1247:1247. doi: 10.3389/fnins.2019.01247

Chassagnon, I. R., McCarthy, C. A., Chin, Y. K. Y., Pineda, S. S., Keramidas, A., Mobli, M., et al. (2017). Potent neuroprotection after stroke afforded by a double-knot spider-venom peptide that inhibits acid-sensing ion channel 1a. *Proc. Natl. Acad. Sci. U.S.A.* 114 (14), 3750–3755. doi: 10.1073/pnas.1614728114

Chen, C. W., Hu, Y. Q., Shi, X. W., Tao, C. H., Zheng, H. Y., Fei, W. D., et al. (2016). A single-label fluorescent derivatization method for quantitative determination of neurotoxin i*n vivo* by capillary electrophoresis coupled with laser-induced fluorescence detection. *Analyst* 141 (14), 4495–4501. doi: 10.1039/c6an00327c

Chow, S. C., and Chang, M. (2008). Adaptive design methods in clinical trials - a review. *Orphanet J. Rare Dis.* 3, 11. doi: 10.1186/1750-1172-3-11

Christensen, M., Knop, F. K., Holst, J. J., and Vilsboll, T. (2009). Lixisenatide, a novel GLP-1 receptor agonist for the treatment of type 2 diabetes mellitus. *Idrugs* 12 (8), 503–513.

Clark, R. J., Jensen, J., Nevin, S. T., Callaghan, B. P., Adams, D. J., and Craik, D. J. (2010). The engineering of an orally active conotoxin for the treatment of neuropathic pain. *Angew. Chem. Int. Ed* 49 (37), 6545–6548. doi: 10.1002/anie.201000620

Clark, G. C., Casewell, N. R., Elliott, C. T., Harvey, A. L., Jamieson, A. G., Strong, P. N., et al. (2019). Friends or foes? Emerging impacts of biological toxins. *Trends Biochem. Sci.* 44 (4), 365–379. doi: 10.1016/j.tibs.2018.12.004

Cohen-Inbar, O., and Zaaroor, M. (2016). Glioblastoma multiforme targeted therapy: The Chlorotoxin story. *J. Clin. Neurosci.* 33, 52–58. doi: 10.1016/j.jocn.2016.04.012

Cooper, E. L., and Mologne, N. (2017). Exploiting leech saliva to treat osteoarthritis: A provocative perspective. *J. Tradit. Complement Med.* 7 (3), 367–369. doi: 10.1016/j.jtcme.2016.11.005

Cushman, D. W., Cheung, H. S., Sabo, E. F., and Ondetti, M. A. (1977). Design of potent competitive inhibitors of angiotensin-converting enzyme. Carboxyalkanoyl and mercaptoalkanoyl amino acids. *Biochemistry* 16 (25), 5484–5491. doi: 10.1021/bi00644a014

Daly, J. (2004). *Chlorine compound of the month: Eptibatidine - natural frog poison with a surprising benefit to humans*. Available at: https://chlorine.americanchemistry.com/Science-Center/Chlorine-Compound-of-the-Month-Library/Epibatidine-Natural-Frog-Poison-with-a-Surprising-Benefit-to-Humans/ (Accessed March 19, 2020).

Das Gupta, S., Debnath, A., Saha, A., Giri, B., Tripathi, G., Vedasiromoni, J. R., et al. (2007). Indian black scorpion (H*eterometrus bengalensis* Koch) venom induced antiproliferative and apoptogenic activity against human leukemic cell lines U937 and K562. *Leuk. Res.* 31 (6), 817–825. doi: 10.1016/j.leukres.2006.06.004

da-Silva-Freitas, D., Boldrini-Franca, J., and Arantes, E. C. (2015). PEGylation: A successful approach to improve the biopharmaceutical potential of snake venom thrombin-like serine protease. *Protein Pept. Lett.* 22 (12), 1133–1139. doi: 10.2174/0929866522666151013130742

de Azevedo, R. A., Figueiredo, C. R., Ferreira, A. K., Matsuo, A. L., Massaoka, M. H., Girola, N., et al. (2015). Mastoparan induces apoptosis in B1 6F10-Nex2 melanoma cells via the intrinsic mitochondrial pathway and displays antitumor activity i*n vivo*. *Peptides* 68, 113–119. doi: 10.1016/j.peptides.2014.09.024

de Oliveira-Mendes, B. B. R., Horta, C. C. R., do Carmo, A. O., Biscoto, G. L., Sales-Medina, D. F., Leal, H. G., et al. (2018). CPP-Ts: a new intracellular calcium channel modulator and a promising tool for drug delivery in cancer cells. *Sci. Rep.* 8, 14739. doi: 10.1038/s41598-018-33133-3

DeBin, J. A., and Strichartz, G. R. (1991). Chloride channel inhibition by the venom of the scorpion L*eiurus quinquestriatus*. *Toxicon* 29 (11), 1403–1408. doi: 10.1016/0041-0101(91)90128-E

DeBin, J. A., Maggio, J. E., and Strichartz, G. R. (1993). Purification and characterization of chlorotoxin, a chloride channel ligand from the venom of the scorpion. *Am. J. Physiol.* 264 (2 Pt 1), C361–C369. doi: 10.1152/ajpcell.1993.264.2.C361

DeYoung, M. B., MacConell, L., Sarin, V., Trautmann, M., and Herbert, P. (2011). Encapsulation of exenatide in poly-(D,L-lactide-co-glycolide) microspheres produced an investigational long-acting once-weekly formulation for type 2 diabetes. *Diabetes Technol. Ther.* 13 (11), 1145–1154. doi: 10.1089/dia.2011.0050

Ding, J., Chua, P. J., Bay, B. H., and Gopalakrishnakone, P. (2014). Scorpion venoms as a potential source of novel cancer therapeutic compounds. *Exp. Biol. Med. (Maywood)* 239 (4), 387–393. doi: 10.1177/1535370213513991

Diochot, S., Baron, A., Salinas, M., Douguet, D., Scarzello, S., Dabert-Gay, A. S., et al. (2012). Black mamba venom peptides target acid-sensing ion channels to abolish pain. *Nature* 490 (7421), 552–555. doi: 10.1038/nature11494

Dodt, J., Müller, H.-P., Seemüller, U., and Chang, J.-Y. (1984). The complete amino acid sequence of hirudin, a thrombin specific inhibitor. Application of colour carboxymethylation. *FEBS* 165 (2), 180–184. doi: 10.1016/0014-5793(84)80165-9

Drug discovery and development (2016). *Nutra Pharma announces manufacturing alliance with Omnia Biologics to produce RPI-78M for clinical trials in pediatric multiple sclerosis*. Available at: https://www.drugdiscoverytrends.com/nutra-pharma-omnias-manufacturing-alliance-to-produce-pediatric-ms-treatment/ (Accessed March 19, 2020).

Drugs.com (2020). *Search*. Available at: https://www.drugs.com/ (Accessed June 25, 2020).

Duran-Riveroll, L. M., and Cembella, A. D. (2017). Guanidinium toxins and their interactions with voltage-gated sodium ion channels. *Mar Drugs* 15 (10), 303. doi: 10.3390/md15100303

Duskey, J. T., Belletti, D., Pederzoli, F., Vandelli, M. A., Forni, F., Ruozi, B., et al. (2017). Current strategies for the delivery of therapeutic proteins and enzymes to treat brain disorders. *Int. Rev. Neurobiol.* 137, 1–28. doi: 10.1016/bs.irn.2017.08.006

Earps, L., and Shoolingin-Jordan, P. M. (1998). Molecular modelling of batroxobin on kallikreins. *Biochem. Soc. Trans.* 26 (3), S283–S283. doi: 10.1042/bst026s283

Elkinson, S., and Keating, G. M. (2013). Lixisenatide: First global approval. *Drugs* 73 (4), 383–391. doi: 10.1007/s40265-013-0033-3

Eng, J., Kleinman, W. A., Singh, L., Singh, G., and Raufman, J. P. (1992). Isolation and characterization of exendin-4, an exendin-3 analogue, from H*eloderma suspectum* venom. Further evidence for an exendin receptor on dispersed acini from guinea pig pancreas. *J. Biol. Chem.* 267 (11), 7402–7405.

Eriksson, U. G., Bredberg, U., Gislén, K., Johansson, L. C., Frison, L., Ahnoff, M., et al. (2003). Pharmacokinetics and pharmacodynamics of ximelagatran, a novel oral direct thrombin inhibitor, in young healthy male subjects. *Eur. J. Clin. Pharmacol.* 59 (1), 35–43. doi: 10.1007/s00228-003-0565-7

Esteve, E., Mabrouk, K., Dupuis, A., Smida-Rezgui, S., Altafaj, X., Grunwald, D., et al. (2005). Transduction of the scorpion toxin maurocalcine into cells - Evidence that the toxin crosses the plasma membrane. *J. Biol. Chem.* 280 (13), 12833–12839. doi: 10.1047/jbc.M412521200

European Medicines Agency (2020). *Search for medicines: Search our database of medicines - including human medicines, veterinary medicines and herbal medicines*. Available at: https://www.ema.europa.eu/en (Accessed June 25, 2020).

Favaloro, E. J., and Wong, R. C. (2014). Antiphospholipid antibody testing for the antiphospholipid syndrome: a comprehensive practical review including a synopsis of challenges and recent guidelines. *Pathology* 46 (6), 481–495. doi: 10.1097/PAT.0000000000000142

Ferrajolo, C., Coloma, P. M., Verhamme, K. M. C., Schuemie, M. J., de Bie, S., Gini, R., et al. (2014). Signal detection of potentially drug-induced acute liver injury in children using a multi-country healthcare database network. *Drug Saf.* 37 (2), 99–108. doi: 10.1007/s40264-013-0132-9

Ferreira, S. H., and Rocha e Silva, M. (1965). Potentiation of bradykinin and eledoisin by BPF (bradykinin potentiating factor) from *Bothrops jararaca* venom. *Experientia* 21 (6), 347–349. doi: 10.1007/BF02144709

Ferreira, S. H., Bartelt, D. C., and Greene, L. J. (1970a). Isolation of bradykinin-potentiating peptides from B*othrops jararaca* venom. *Biochemistry* 9 (13), 2583–2593. doi: 10.1021/bi00815a005

Ferreira, S. H., Greene, L. H., Alabaster, V. A., Bakhle, Y. S., and Vane, J. R. (1970b). Activity of various fractions of bradykinin potentiating factor against angiotensin I converting enzyme. *Nature* 225 (5230), 379–380. doi: 10.1038/225379a0

Ferreira, R. S., de Barros, L. C., Abbade, L. P. F., Barraviera, S. R. C. S., Silvares, M. R. C., de Pontes, L. G., et al. (2017). Heterologous fibrin sealant derived from snake venom: from bench to bedside - an overview. *J. Venom. Anim. Toxins Incl. Trop. Dis.* 23, 21. doi: 10.1186/s40409-017-0109-8

Ferreira, S. H. (1965). A bradykinin-potentiating factor (BPF) present in the venom of B*othrops jararaca*. *Br. J. Pharmacol. Chemother.* 24, 163–169. doi: 10.1111/j.1476-5381.1965.tb02091.x

Ferreira, S. H. (2000). Angiotensin converting enzyme: history and relevance. *Semin. Perinatol.* 24 (1), 7–10. doi: 10.1016/S0146-0005(00)80046-4

Fox, J. W., and Serrano, S. M. T. (2007). Approaching the golden age of natural product pharmaceuticals from venom libraries: An overview of toxins and toxin-derivatives currently involved in therapeutic or diagnostic applications. *Curr. Pharm. Des.* 13 (28), 2927–2934. doi: 10.2174/138161207782023739

Francischetti, I. M., and Gil, M. R. (2019). "Diagnostic use of venoms," in *Transfusion Medicine and Hemostasis*, *3rd ed.* Eds. B. H. Shaz, C. D. Hillyer and M. R. Gil (Amsterdam: Elsevier), 969–975.

Fu, Y. J., Yin, L. T., Liang, A. H., Zhang, C. F., Wang, W., Chai, B. F., et al. (2007). Therapeutic potential of chlorotoxin-like neurotoxin from the Chinese scorpion for human gliomas. *Neurosci. Lett.* 412 (1), 62–67. doi: 10.1016/j.neulet.2006.10.056

Fu, Y., Zheng, S., Huang, R., An, N., Zheng, Y., Zhang, Z., et al. (2012). A potential strategy for high-grade gliomas: combination treatment with lithium chloride and BmK CT. *Biotechnol. Lett.* 34 (1), 9–17. doi: 10.1007/s10529-011-0741-2

Fu, S., Hirte, H., Welch, S., Ilenchuk, T. T., Lutes, T., Rice, C., et al. (2017). First-in-human phase I study of SOR-C13, a TRPV6 calcium channel inhibitor, in patients with advanced solid tumors. *Invest. New Drugs* 35 (3), 324–333. doi: 10.1007/s10637-017-0438-z

Funk, C., Gmur, J., Herold, R., and Straub, P. W. (1971). Reptilase® - a new reagent in blood coagulation. *Br. J. Haematol.* 21 (1), 43–&. doi: 10.1111/j.1365-2141.1971.tb03415.x

Furman, B. L. (2012). The development of Byetta (exenatide) from the venom of the Gila monster as an anti-diabetic agent. *Toxicon* 59 (4), 464–471. doi: 10.1016/j.toxicon.2010.12.016

Gajski, G., and Garaj-Vrhovac, V. (2013). Melittin: A lytic peptide with anticancer properties. *Environ. Toxicol. Pharmacol.* 36 (2), 697–705. doi: 10.1016/j.etap.2013.06.009

Gan, Z. R., Gould, R. J., Jacobs, J. W., Friedman, P. A., and Polokoff, M. A. (1988).). Echistatin. A potent platelet aggregation inhibitor from the venom of the viper E*chis carinatus*. *J. Biol. Chem.* 263 (36), 19827–19832.

Gao, B., Peng, C., Yang, J., Yi, Y., Zhang, J., and Shi, Q. (2017). Cone snails: a big store of conotoxins for novel drug discovery. *Toxins* 9 (12):397. doi: 10.3390/toxins9120397

Gazerani, P., and Cairns, B. E. (2014). Venom-based biotoxins as potential analgesics. *Expert Rev. Neurother.* 14 (11), 1261–1274. doi: 10.1586/14737175.2014.962518

Ghosh, A., Roy, R., Nandi, M., and Mukhopadhyay, A. (2019). Scorpion venom-toxins that aid in drug development: a review. *Int. J. Pept. Res. Ther.* 25 (1), 27–37. doi: 10.1007/s10989-018-9721-x

Gomes, A., Teixeira, C., Ferraz, R., Prudencio, C., and Gomes, P. (2017). Wound-healing peptides for treatment of chronic diabetic foot ulcers and other infected skin injuries. *Molecules* 22 (10), 1743. doi: 10.3390/molecules22101743

Gotter, A. (2019). *Apitherapy*. Available at: https://www.healthline.com/health/apitherapy (Accessed June 25, 2020).

Graetz, T. J., Tellor, B. R., Smith, J. R., and Avidan, M. S. (2011). Desirudin: a review of the pharmacology and clinical application for the prevention of deep vein thrombosis. *Expert Rev. Cardiovasc. Ther.* 9 (9), 1101–1109. doi: 10.1586/erc.11.131

Graziano, F., Certo, F., Basile, L., Maugeri, R., Grasso, G., Meccio, F., et al. (2015). Autologous fibrin sealant (Vivostat®) in the neurosurgical practice: Part I: Intracranial surgical procedure. *Surg. Neurol. Int.* 6, 77. doi: 10.4103/2152-7806.156871

Graziano, F., Maugeri, R., Basile, L., Meccio, F., and Iacopino, D. G. (2016). Aulogous fibrin sealant (Vivostat®) in the neurosurgical practice: Part II: Vertebro-spinal procedures. *Surg. Neurol. Int.* 7 (Suppl 3), S77–S82. doi: 10.4103/2152-7806.174894

Greig, N. H., Holloway, H. W., De Ore, K. A., Jani, D., Wang, Y., Zhou, J., et al. (1999). Once daily injection of exendin-4 to diabetic mice achieves long-term beneficial effects on blood glucose concentrations. *Diabetologia* 42 (1), 45–50. doi: 10.1007/s001250051111

Grishin, E. V., Savchenko, G. A., Vassilevski, A. A., Korolkova, Y. V., Boychuk, Y. A., Viatchenko-Karpinski, V. Y., et al. (2010). Novel peptide from spider venom inhibits P2X3 receptors and inflammatory pain. *Ann. Neurol.* 67 (5), 680–683. doi: 10.1002/ana.21949

Gulseth, M. P. (2005). Ximelagatran: An orally active direct thrombin inhibitor. *Am. J. Health Syst. Pharm.* 62 (14), 1451–1467. doi: 10.2146/ajhp040534

Gutierrez, V. P., Konno, K., Chacur, M., Sampaio, S. C., Picolo, G., Brigatte, P., et al. (2008). Crotalphine induces potent antinociception in neuropathic pain by acting at peripheral opioid receptors. *Eur. J. Pharmacol.* 594 (1-3), 84–92. doi: 10.1016/j.ejphar.2008.07.053

Han, T. S., Teichert, R. W., Olivera, B. M., and Bulaj, G. (2008). Conus venoms - A rich source of peptide-based therapeutics. *Curr. Pharm. Des.* 14 (24), 2462–2479. doi: 10.2174/138161208785777469

Han, S. M., Hong, I. P., Woo, S. O., Chun, S. N., Park, K. K., Nicholls, Y. M., et al. (2015). The beneficial effects of honeybee-venom serum on facial wrinkles in humans. *Clin. Interv. Aging* 10, 1587–1592. doi: 10.2147/cia.s84940

Hartman, G. D., Egbertson, M. S., Halczenko, W., Laswell, W. L., Duggan, M. E., Smith, R. L., et al. (1992). Non-peptide fibrinogen receptor antagonists. 1. Discovery and design of exosite inhibitors. *J. Med. Chem.* 35 (24), 4640–4642. doi: 10.1021/jm00102a020

Hartmann, A., Mullner, J., Meier, N., Hesekamp, H., van Meerbeeck, P., Habert, M. O., et al. (2016). Bee venom for the treatment of Parkinson disease - A randomized controlled clinical trial. *PloS One* 11 (7), e0158235. doi: 10.1371/journal.pone.0158235

Harvey, A. L. (2014). Toxins and drug discovery. *Toxicon* 92, 193–200. doi: 10.1016/j.toxicon.2014.10.020

Hennerici, M. G., Kay, R., Bogousslavsky, J., Lenzi, G. L., Verstraete, M., Orgogozo, J. M., et al. (2006). Intravenous ancrod for acute ischaemic stroke in the European Stroke Treatment with Ancrod Trial: a randomised controlled trial. *Lancet* 368 (9550), 1871–1878. doi: 10.1016/S0140-6736(06)69776-6

Henry, R. R., Rosenstock, J., Logan, D., Alessi, T., Luskey, K., and Baron, M. A. (2014). Continuous subcutaneous delivery of exenatide via ITCA 650 leads to sustained glycemic control and weight loss for 48 weeks in metformin-treated subjects with type 2 diabetes. *J. Diabetes Complicat.* 28 (3), 393–398. doi: 10.1016/j.jdiacomp.2013.12.009

Hockaday, D. C., Shen, S., Fiveash, J., Raubitschek, A., Colcher, D., Liu, A., et al. (2005). Imaging glioma extent with 131I-TM-601. *J. Nucl. Med.* 46 (4), 580–586.

Holleman, W. H., and Weiss, L. J. (1976). The thrombin-like enzyme from B*othrops atrox* snake venom. Properties of the enzyme purified by affinity chromatography on p-aminobenzamidine-substituted agarose. *J. Biol. Chem.* 251 (6), 1663–1669.

Huang, J., Han, S., Sun, Q., Zhao, Y. P., Liu, J. C., Yuan, X. L., et al. (2017). Kv1.3 channel blocker (ImKTx88) maintains blood-brain barrier in experimental autoimmune encephalomyelitis. *CellBiosci* 7, 31. doi: 10.1186/s13578-017-0158-2

Ibraheem, D., Elaissari, A., and Fessi, H. (2014). Administration strategies for proteins and peptides. *Int. J. Pharm.* 477, 578–589. doi: 10.1016/j.ijpharm.2014.10.059

Ichiki, T., Dzhoyashvili, N., and Burnett, J. C. (2019). Natriuretic peptide based therapeutics for heart failure: Cenderitide: A novel first-in-class designer natriuretic peptide. *Int. J. Cardiol.* 281, 166–171. doi: 10.1016/j.ijcard.2018.06.002

Ikonen, S., and Riekkinen, P. (1999). Effects of apamin on memory processing of hippocampal-lesioned mice. *Eur. JPharmacol.* 382 (3), 151–156. doi: 10.1016/s0014-2999(99)00616-0

Itoh, N., Tanaka, N., Mihashi, S., and Yamashina, I. (1987). Molecular cloning and sequence analysis of cDNA for batroxobin, a thrombin-like snake venom enzyme. *J. Biol. Chem.* 262 (7), 3132–3135.

Jacoby, D. B., Dyskin, E., Yalcin, M., Kesavan, K., Dahlberg, W., Ratliff, J., et al. (2010). Potent pleiotropic anti-angiogenic effects of TM601, a synthetic chlorotoxin peptide. *Anticancer Res.* 30 (1), 39–46.

Jagua-Gualdrón, A., Peña-Latorre, J. A., and Fernadez-Bernal, R. E. (2020). Apitherapy for osteoarthritis: perspectives from basic research. *Complement Med. Res.* 27 (3), 184–192. doi: 10.1159/000505015

Jang, S. H., Choi, S. Y., Ryu, P. D., and Lee, S. Y. (2011). Anti-proliferative effect of Kv1.3 blockers in A549 human lung adenocarcinoma i*n vitro* and i*n vivo*. *Eur. J. Pharmacol.* 651 (1-3), 26–32. doi: 10.1016/j.ejphar.2010.10.066

Johnson & Johnson (2019). *Champions of Science® Storytelling Challenge: Latin America and Caribbean Edition*. Available at: https://www.jnj.com/latin-america-caribbean-storytelling-challenge/maria-elena-de-lima (Accessed March 29, 2020).

Johnson, P. H., Sze, P., Winant, R., Payne, P. W., and Lazar, J. B. (1989). Biochemistry and genetic-engineering of hirudin. *Semin. Thromb. Hemost.* 15 (3), 302–315. doi: 10.1055/s-2007-1002723

Jones, S., and Howl, J. (2012). Enantiomer-specific bioactivities of peptidomimetic analogues of mastoparan and mitoparan: Characterization of inverso mastoparan as a highly efficient cell penetrating peptide. *Bioconj. Chem.* 23 (1), 47–56. doi: 10.1021/bc2002924

Juhász, M. L., Levin, M. K., and Marmur, E. S. (2018). The use of natural ingredients in innovative Korean cosmeceuticals. *J. Cosmet. Dermatol.* 17, 1–8. doi: 10.1111/jocd.12492

Karpel, R. L., Liberato, M. D., Campeiro, J. D., Bergeon, L., Szychowski, B., Butler, A., et al. (2018). Design and characterization of crotamine-functionalized gold nanoparticles. *Colloids Surf B Biointerfaces* 163, 1–8. doi: 10.1016/j.colsurfb.2017.12.013

Kent, S., Sohma, Y., Liu, S., Bang, D., Pentelute, B., and Mandal, K. (2012). Through the looking glass - a new world of proteins enabled by chemical synthesis. *J. Pept. Sci.* 18 (7), 428–436. doi: 10.1002/psc.2421

Kerkis, A., Kerkis, I., Radis-Baptista, G., Oliveira, E. B., Vianna-Morgante, A. M., Pereira, L. V., et al. (2004). Crotamine is a novel cell-penetrating protein from the venom of rattlesnake Crotalus durissus terrificus. *FASEB J.* 18 (10), 1407–140+. doi: 10.1096/fj.03-1459fje

Kesavan, K., Ratliff, J., Johnson, E. W., Dahlberg, W., Asara, J. M., Misra, P., et al. (2010). Annexin A2 is a molecular target for TM601, a peptide with tumor-targeting and anti-angiogenic effects. *J. Biol. Chem.* 285 (7), 4366–4374. doi: 10.1074/jbc.M109.066092

Kineta Inc. (2020). *KCP-506 - A novel non-opioid for the treatment of chronic pain*. Available at: https://kinetabio.com/neuroscience/ (Accessed March 29, 2020).

King, J. V. L., Emrick, J. J., Kelly, M. J. S., Herzig, V., King, G. F., Medzihradszky, K. F., et al. (2019). A cell-penetrating scorpion toxin enables mode-specific modulation of TRPA1 and pain. *Cell* 178 (6), 1362–136+. doi: 10.1016/j.cell.2019.07.014

King, G. F. (2011). Venoms as a platform for human drugs: translating toxins into therapeutics. *Expert Opin. Biol. Ther.* 11 (11), 1469–1484. doi: 10.1517/14712598.2011.621940

King, G. F. (2013). Venoms to drugs: translating venom peptides into therapeutics. *Aust. Biochem.* 44 (3), 13–16.

Kjaergard, H. K., and Trumbull, H. R. (1998). Vivostat system autologous fibrin sealant: Preliminary study in elective coronary bypass grafting. *Ann. Thorac. Surg.* 66 (2), 482–486. doi: 10.1016/s0003-4975(98)00470-6

Knop, F. K., Bronden, A., and Vilsboll, T. (2017). Exenatide: pharmacokinetics, clinical use, and future directions. *Expert Opin. Pharmacother.* 18 (6), 555–571. doi: 10.1080/14656566.2017.1282463

Koh, C. Y., and Kini, R. M. (2008). Anticoagulants from hematophagous animals. *Expert Rev. Hematol.* 1 (2), 135–139. doi: 10.1586/17474086.1.2.135

Koh, C. Y., and Kini, R. M. (2012). From snake venom toxins to therapeutics - cardiovascular examples. *Toxicon* 59 (4), 497–506. doi: 10.1016/j.toxicon.2011.03.017

Koh, D. C. I., Armugam, A., and Jeyaseelan, K. (2006). Snake venom components and their applications in biomedicine. *Cell Mol. Life Sci.* 63 (24), 3030–3041. doi: 10.1007/s00018-006-6315-0

Kolaczek, A., Skorupa, D., Antczak-Marczak, M., Kuna, P., and Kupczyk, M. (2017). Safety and efficacy of venom immunotherapy: a real life study. *Postepy DermatolAlergol.* 34 (2), 159–167. doi: 10.5114/ada.2017.67082

Kolosov, A., Goodchild, C. S., and Cooke, I. (2010). CNSB004 (leconotide) causes antihyperalgesia without side effects when given intravenously: a comparison with ziconotide in a rat model of diabetic neuropathic pain. *Pain Med.* 11 (2), 262–273. doi: 10.1111/j.1526-4637.2009.00741.x

Konno, K., Picolo, G., Gutierrez, V. P., Brigatte, P., Zambelli, V. O., Camargo, A. C. M., et al. (2008). Crotalphine, a novel potent analgesic peptide from the venom of the South American rattlesnake C*rotalus durissus terrificus*. *Peptides* 29 (8), 1293–1304. doi: 10.1016/j.peptides.2008.04.003

Kovalainen, M., Monkare, J., Riikonen, J., Pesonen, U., Vlasova, M., Salonen, J., et al. (2015). Novel delivery systems for improving the clinical use of peptides. *Pharmacol. Rev.* 67 (3), 541–561. doi: 10.1124/pr.113.008367

Kovar, J. L., Curtis, E., Othman, S. F., Simpson, M. A., and Olive, D. M. (2013). Characterization of IRDye 800CW chlorotoxin as a targeting agent for brain tumors. *Anal. Biochem.* 440 (2), 212–219. doi: 10.1016/j.ab.2013.05.013

Ladram, A., and Nicolas, P. (2016). Antimicrobial peptides from frog skin: biodiversity and therapeutic promises. *Front. Biosci.* 21, 1341–1371. doi: 10.2741/4461

Lago, J., Rodriguez, L. P., Blanco, L., Vieites, J. M., and Cabado, A. G. (2015). Tetrodotoxin, an extremely potent marine neurotoxin: distribution, toxicity, origin and therapeutical uses. *Mar Drugs* 13 (10), 6384–6406. doi: 10.3390/md13106384

Lang, S., Manning, N., Armstrong, N., Misso, K., Allen, A., Di Nisio, M., et al. (2012). Treatment with tirofiban for acute coronary syndrome (ACS): a systematic review and network analysis. *Curr. Med. Res. Opin.* 28 (3), 351–370. doi: 10.1185/03007995.2012.657299

Lee, C. J., and Ansell, J. E. (2011). Direct thrombin inhibitors. *Br. JClin. Pharmacol.* 72 (4), 581–592. doi: 10.1111/j.1365-2125.2011.03916.x

Lee, C. Y., Chen, H. H., Lisy, O., Swan, S., Cannon, C., Lieu, H. D., et al. (2009). Pharmacodynamics of a novel designer natriuretic peptide, CD-NP, in a first-in-human clinical trial in healthy subjects. *J. Clin. Pharmacol.* 49 (6), 668–673. doi: 10.1177/0091270009336233

Lee, J. A., Son, M. J., Choi, J., Jun, J. H., Kim, J. I., and Lee, M. S. (2014). Bee venom acupuncture for rheumatoid arthritis: a systematic review of randomised clinical trials. *BMJ Open* 4, e006140. doi: 10.1136/bmjopen-2014-006140

Lewis, R. J., Dutertre, S., Vetter, I., and Christie, M. J. (2012). C*onus* venom peptide pharmacology. *Pharmacol. Rev.* 64 (2), 259–298. doi: 10.1124/pr.111.005322

Lewis, R. J. (2015). "Case study 1: development of the analgesic drugs Prialt® and Xen2174 from cone snail venoms," in *Venoms to drugs: venom as a source for the development of human therapeutics*. Ed. G. F. King (London: Royal Society of Chemistry), 245–254.

Li, C., Hashimi, S. M., Cao, S., Mellick, A. S., Duan, W., Good, D., et al. (2013). The mechanisms of chansu in inducing efficient apoptosis in colon cancer cells. *Evid. Based Complement Alternat. Med.* 2013:849054. doi: 10.1155/2013/849054

Li, X., Ling, L., Li, C., and Ma, Q. (2017). Efficacy and safety of desmoteplase in acute ischemic stroke patients: A systematic review and meta-analysis. *Medicine* 96 (18), e6667. doi: 10.1097/md.0000000000006667

Lippens, G., Najib, J., Wodak, S. J., and Tartar, A. (1995). NMR sequential assignments and solution structure of chlorotoxin, a small scorpion toxin that blocks chloride channels. *Biochemistry* 34 (1), 13–21. doi: 10.1021/bi00001a003

Lisy, O., Huntley, B. K., McCormick, D. J., Kurlansky, P. A., and Burnett, J. C. (2008).). Design, synthesis, and actions of a novel chimeric natriuretic peptide: CD-NP. *J. Am. Coll. Cardiol.* 52 (1), 60–68. doi: 10.1016/j.jacc.2008.02.077

Liu, S., Marder, V. J., Levy, D. E., Wang, S. J., Yang, F., Paganini-Hill, A., et al. (2011). Ancrod and fibrin formation: perspectives on mechanisms of action. *Stroke* 42 (11), 3277–3280. doi: 10.1161/STROKEAHA.111.622753

Liu, Y., Ban, L. Y., Su, X., Gao, S., Liu, J. W., and Cui, X. N. (2015). Effects of cinobufacini injection on cell proliferation and the expression of topoisomerases in human HepG-2 hepatocellular carcinoma cells. *Mol. Med. Rep.* 12 (1), 1598–1604. doi: 10.3892/mmr.2015.3552

Liu, Y., Hagan, R., and Schoellerman, J. (2018). Dual actions of Psalmotoxin at ASIC1a and ASIC2a heteromeric channels (ASIC1a/2a). *Sci. Rep.* 8, 7179. doi: 10.1038/s41598-018-25386-9

Lorenz, M., Evers, A., and Wagner, M. (2013). Recent progress and future options in the development of GLP-1 receptor agonists for the treatment of diabesity. *Bioorg. Med. Chem. Lett.* 23 (14), 4011–4018. doi: 10.1016/j.bmcl.2013.05.022

Luna-Ramirez, K., Tonk, M., Rahnamaeian, M., and Vilcinskas, A. (2017). Bioactivity of natural and engineered antimicrobial peptides from venom of the scorpions U*rodacus yaschenkoi a*nd U. *manicatus*. *Toxins* 9 (1), 22. doi: 10.3390/toxins9010022

Maatuf, Y., Geron, M., and Priel, A. (2019). The role of toxins in the pursuit for novel analgesics. *Toxins* 11 (2):131. doi: 10.3390/toxins11020131

Mabrouk, K., Luis, J., De Pomyers, H., Bertin, D., Bengeloune, A. H., Verdoni, M., et al. (2018). *Use of spider venoms for skin whitening/depigmenting and composition comprising spider venoms molecules or synthetic analogs*, WO/2014/037111 patent application.

Mambelli-Lisboa, N. C., Sciani, J. M., da Silva, A., and Kerkis, I. (2018). Co-localization of crotamine with internal membranes and accentuated accumulation in tumor cells. *Molecules* 23 (4), 968. doi: 10.3390/molecules 23040968

Manda, P., Kushwaha, A. S., Kundu, S., Shivakumar, H. N., Jo, S. B., and Murthy, S. N. (2016). Delivery of ziconotide to cerebrospinal fluid via intranasal pathway for the treatment of chronic pain. *J. Control Release* 224, 69–76. doi: 10.1016/j.jconrel.2015.12.044

Maraganore, J. M., Bourdon, P., Jablonski, J., Ramachandran, K. L., and Fenton, J. W. (1990). Design and characterization of hirulogs: a novel class of bivalent peptide inhibitors of thrombin. *Biochemistry* 29 (30), 7095–7101. doi: 10.1021/bi00482a021

Markland, F. S., and Swenson, S. (2010). Fibrolase: trials and tribulations. *Toxins* 2 (4), 793–808. doi: 10.3390/toxins2040793

Markwardt, F. (1991). Past, present and future of hirudin. *Haemostasis* 21 Suppl 1, 11–26. doi: 10.1159/000216258

Mazzuca, M., Heurteaux, C., Alloui, A., Diochot, S., Baron, A., Voilley, N., et al. (2007). A tarantula peptide against pain via ASIC1a channels and opioid mechanisms. *Nat. Neurosci.* 10 (8), 943–945. doi: 10.1038/nn1940

Mazzucco, L., Balbo, V., Cattana, E., and Borzini, P. (2008). Platelet-rich plasma and platelet gel preparation using Plateltex®. *Vox Sang* 94 (3), 202–208. doi: 10.1111/j.1423-0410.2007.01027.x

McGivern, J. G. (2007). Ziconotide: a review of its pharmacology and use in the treatment of pain. *Neuropsychiatr. Dis. Treat* 3 (1), 69–85. doi: 10.2147/nedt.2007.3.1.69

Medcalf, R. L. (2012). Desmoteplase: discovery, insights and opportunities for ischaemic stroke. *Br. J. Pharmacol.* 165 (1), 75–89. doi: 10.1111/j.1476-5381.2011.01514.x

Medicure Pharma (2016). *Aggrastat (Tirofiban hydrochloride) injection premixed and injection prescribing information* (Somerset, USA). Available at: https://www.aggrastathdb.com/product-formats (Accessed March 19, 2020).

Mehrzad, M., Tuktamyshov, R., and Mehrzad, R. (2017). Safety, efficiency and cost effectiveness of Bivalirudin: A systematic review. *World J. Cardiol.* 9 (9), 761–772. doi: 10.4330/wjc.v9.i9.761

Meng, Z., Yang, P., Shen, Y., Bei, W., Zhang, Y., Ge, Y., et al. (2009). Pilot study of huachansu in patients with hepatocellular carcinoma, nonsmall-cell lung cancer, or pancreatic cancer. *Cancer* 115 (22), 5309–5318. doi: 10.1002/cncr.24602

Merlin, M., Gecchele, E., Capaldi, S., Pezzotti, M., and Avesani, L. (2014). Comparative evaluation of recombinant protein production in different biofactories: the green perspective. *BioMed. Res. Int.* 2014:14. doi: 10.1155/2014/136419

Messier, C., Mourre, C., Bontempi, B., Sif, J., Lazdunski, M., and Destrade, C. (1991). Effect of apamin, a toxin that inhibits $Ca2^{+}$dependent K+ channels, on learning and memory processes. *Brain Res.* 551 (1-2), 322–326. doi: 10.1016/0006-8993(91)90950-z

Miao, Q., Bi, L. L., Li, X., Miao, S., Zhang, J., Zhang, S., et al. (2013). Anticancer effects of bufalin on human hepatocellular carcinoma HepG2 cells: roles of apoptosis and autophagy. *Int. J. Mol. Sci.* 14 (1), 1370–1382. doi: 10.3390/ijms14011370

Monge-Fuentes, V., Arenas, C., Galante, P., Goncalves, J. C., Mortari, M. R., and Schwartz, E. F. (2018). Arthropod toxins and their antinociceptive properties: From venoms to painkillers. *Pharmacol. Ther.* 188, 176–185. doi: 10.1016/j.pharmthera.2018.03.007

Moreno, M., and Giralt, E. (2015). Three valuable peptides from bee and wasp venoms for therapeutic and biotechnological use: melittin, apamin and mastoparan. *Toxins* 7 (4), 1126–1150. doi: 10.3390/toxins7041126

Morita, T., Iwanaga, S., and Suzuki, T. (1976). The mechanism of activation of bovine prothrombin by an activator isolated from E*chis carinatus v*enon and characterization of the new active intermediates. *J. Biochem.* 79 (5), 1089–1108. doi: 10.1093/oxfordjournals.jbchem.a131150

Morita, T. (2005). Structures and functions of snake venom CLPs (C-type lectin-like proteins) with anticoagulant-, procoagulant-, and platelet-modulating activities. *Toxicon* 45 (8), 1099–1114. doi: 10.1016/j.toxicon.2005.02.021

Mouhat, S., Visan, V., Ananthakrishnan, S., Wulff, H., Andreotti, N., Grissmer, S., et al. (2005). K+ channel types targeted by synthetic OSK1, a toxin from O*rthochirus scrobiculosus* scorpion venom. *Biochem. J.* 385 (Pt 1), 95–104. doi: 10.1042/BJ20041379

Mumcuoglu, K. Y. (2014). Recommendations for the use of leeches in reconstructive plastic surgery. *Evid. Based Complement Alternat. Med.* 2014, 205929. doi: 10.1155/2014/205929

Nascimento, F. D., Hayashi, M. A. F., Kerkis, A., Oliveira, V., Oliveira, E. B., Radis-Baptista, G., et al. (2007). Crotamine mediates gene delivery into cells through the binding to heparan sulfate proteoglycans. *J. Biol. Chem.* 282 (29), 21349–21360. doi: 10.1074/jbc.M604876200

Nauck, M. A., Duran, S., Kim, D., Johns, D., Northrup, J., Festa, A., et al. (2007). A comparison of twice-daily exenatide and biphasic insulin aspart in patients with type 2 diabetes who were suboptimally controlled with sulfonylurea and metformin: a non-inferiority study. *Diabetologia* 50 (2), 259–267. doi: 10.1007/s00125-006-0510-2

Nicoletti, N. F., Erig, T. C., Zanin, R. F., Roxo, M. R., Ferreira, N. P., Gomez, M. V., et al. (2017). Pre-clinical evaluation of voltage-gated calcium channel blockers derived from the spider P. *nigriventer in* glioma progression. *Toxicon* 129, 58–67. doi: 10.1016/j.toxicon.2017.02.001

NIH National Cancer Institute (2018). *NCI Drug Dictionary - TRPV6 calcium channel inhibitor SOR-C13*. Available at: https://www.cancer.gov/publications/dictionaries/cancer-drug/def/trpv6-calcium-channel-inhibitor-sor-c13 (Accessed April 19, 2018).

Nunes, K. P., Costa-Goncalves, A., Lanza, L. F., Cortes, S. F., Cordeiro, M. N., Richardson, M., et al. (2008). Tx2-6 toxin of the P*honeutria nigriventer* spider potentiates rat erectile function. *Toxicon* 51 (7), 1197–1206. doi: 10.1016/j.toxicon.2008.02.010

Nutescu, E. A., and Wittkowsky, A. K. (2004). Direct thrombin inhibitors for anticoagulation. *Ann. Pharmacother.* 38 (1), 99–109. doi: 10.1345/aph.1D066

Odegard, P. S., and Desantis, A. (2009). Recent results of exenatide use as adjunctive therapy in the treatment of patients with type 2 diabetes. *Diabetes Metab. Syndr. Obes.* 2, 135–144. doi: 10.2147/DMSO.S4444

Ojeda, P. G., Wang, C. K., and Craik, D. J. (2016). Chlorotoxin: Structure, activity, and potential uses in cancer therapy. *Biopolymers* 106 (1), 25–36. doi: 10.1002/bip.22748

Ojeda, P. G., Ramirez, D., Alzate-Morales, J., Caballero, J., Kaas, Q., and Gonzalez, W. (2018). Computational studies of snake venom toxins. *Toxins* 10 (1), 8. doi: 10.3390/toxins10010008

Okkerse, P., Hay, J. L., Sitsen, E., Dahan, A., Klaassen, E., Houghton, W., et al. (2017). Pharmacokinetics and pharmacodynamics of intrathecally administered Xen2174, a synthetic conopeptide with norepinephrine reuptake inhibitor and analgesic properties. *Br. J. Clin. Pharmacol.* 83 (4), 751–763. doi: 10.1111/bcp.13176

Oliveira, I. S., Ferreira, I. G., Alexandre-Silva, G. M., Cerni, F. A., Cremonez, C. M., Arantes, E. C., et al. (2019). Scorpion toxins targeting Kv1.3 channels: insights into immunosuppression. *J. Venom. Anim. Toxins Incl. Trop. Dis.* (25), e148118. doi: 10.1590/1678-9199-JVATITD-1481-18

Orientoxin Biotech Co. Ltd . (2019). *Medicine, cobratide for injection*. Available at: https://orientoxin.en.ec21.com/Medicine_Cobratide_for_Injection–9761674.html (Accessed December 19, 2019).

Ortiz, E., Gurrola, G. B., Schwartz, E. F., and Possani, L. D. (2015). Scorpion venom components as potential candidates for drug development. *Toxicon* 93, 125–135. doi: 10.1016/j.toxicon.2014.11.233

Ouriel, K., Cynamon, J., Weaver, F. A., Dardik, H., Akers, D., Blebea, J., et al. (2005). A phase I trial of alfimeprase for peripheral arterial thrombolysis. *J. Vasc. Interv. Radiol.* 16 (8), 1075–1083. doi: 10.1097/01.RVI.0000167863.10122.2A

Ovsepian, S. V., O'Leary, V. B., Ayvazyan, N. M., Al-Sabi, A., Ntziachristos, V., and Dolly, J. O. (2019). Neurobiology and therapeutic applications of neurotoxins targeting transmitter release. *Pharmacol. Ther.* 193, 135–155. doi: 10.1016/j.pharmthera.2018.08.016

Patchett, A. A. (1984). The chemistry of enalapril. *Br. J. Clin. Pharmacol.* 18 Suppl 2, 201S–207S. doi: 10.1111/j.1365-2125.1984.tb02599.x

Patil, C. G., Walker, D. G., Miller, D. M., Butte, P., Morrison, B., Kittle, D. S., et al. (2019). Phase 1 safety, pharmacokinetics, and fluorescence imaging study of tozuleristide (BLZ-100) in adults with newly diagnosed or recurrent gliomas. *Neurosurgery* 85 (4), E641–E648. doi: 10.1093/neuros/nyz125

Peigneur, S., de Lima, M. E., and Tytgat, J. (2018). P*honeutria nigriventer* venom: A pharmacological treasure. *Toxicon* 151, 96–110. doi: 10.1016/j.toxicon.2018.07.008

Pennington, M. W., Beeton, C., Galea, C. A., Smith, B. J., Chi, V., Monaghan, K. P., et al. (2009). Engineering a stable and selective peptide blocker of the Kv1.3 channel in T lymphocytes. *Mol. Pharmacol.* 75 (4), 762–773. doi: 10.1124/mol.108.052704

Pennington, M. W., Czerwinski, A., and Norton, R. S. (2017). Peptide therapeutics from venom: Current status and potential. *Bioorg. Med. Chem.* 26, 2738–2758. doi: 10.1016/j.bmc.2017.09.029

Pentapharm DSM Nutritional Products Ltd (2018). *Defibrase®*. Available at: http://www.pentapharm.com/content.cfm?nav=21&content=39&CFID=31651415&CFTOKEN=27339979&jsessionid=ae30b7ebec2f381e5bb64c68363f73c6f813 (Accessed March 15, 2018).

Pinto, A. F. M., Silva, K., and Guimaraes, J. A. (2006). Proteases from L*onomia obliqua* venomous secretions: Comparison of procoagulant, fibrin(ogen)olytic and amidolytic activities. *Toxicon* 47 (1), 113–121. doi: 10.1016/j.toxicon.2005.10.004

Pizzo, S. V., Schwartz, M. L., Hill, R. L., and McKee, P. A. (1972). Mechanism of ancrod anticoagulation. A direct proteolytic effect on fibrin. *J. Clin. Invest.* 51 (11), 2841–2850. doi: 10.1172/JCI107107

Plateltex, S. R. O. (2016). *Plateltex - Device for the activation (gelification) of blood components destined to the topical non-transfusional use* (Czech Republic: Praha). Available at: http://www.plateltex.com/data/pdf/IFU4.3plateltex ACTJUNE2016ENG.pdf (Accessed March 19, 2020).

Plateltex, S. R. O. (2018). *Plateltex - biologicals, clinical use, information sheet* (Prague, Czech Republic). Available at: https://www.plateltex.com/ (Accessed April 19, 2018).

Pope, J. E., and Deer, T. R. (2013). Ziconotide: a clinical update and pharmacologic review. *Expert Opin. Pharmacother.* 14 (7), 957–966. doi: 10.1517/14656566.2013.784269

Pucca, M. B., Bertolini, T. B., Cerni, F. A., Bordon, K. C. F., Peigneur, S., Tytgat, J., et al. (2016). Immunosuppressive evidence of T*ityus serrulatus* toxins Ts6 and Ts15: insights of a novel K+ channel pattern in T cells. *Immunology* 147 (2), 240–250. doi: 10.1111/imm.12559

Qi, F., Li, A., Inagaki, Y., Kokudo, N., Tamura, S., Nakata, M., et al. (2011). Antitumor activity of extracts and compounds from the skin of the toad B*ufo bufo gargarizans* Cantor. *Int. Immunopharmacol.* 11 (3), 342–349. doi: 10.1016/j.intimp.2010.12.007

Qin, T. J., Zhao, X. H., Yun, J., Zhang, L. X., Ruan, Z. P., and Pan, B. R. (2008). Efficacy and safety of gemcitabine-oxaliplatin combined with huachansu in patients with advanced gallbladder carcinoma. *World J. Gastroenterol.* 14 (33), 5210–5216. doi: 10.3748/wjg.14.5210

Ram, N., Jaumain, E., Ronjat, M., Pirollet, F., and De Waard, M. (2009). "Maurocalcine-derivatives as biotechnological tools for the penetration of cell-impermeable compounds," in *Animal toxins: state of the art-perspectives in health and biotechnology*, *1st ed.* Eds. M. E. D. Lima, A. M. D. C. Pimenta, M. F. Martin-Eauclaire, R. B. Zingali and H. Rochat (Belo Horizonte: Editora UFMG), 715–732.

Ramsey, J. D., and Flynn, N. H. (2015). Cell-penetrating peptides transport therapeutics into cells. *Pharmacol. Ther.* 154, 78–86. doi: 10.1016/j.pharmthera.2015.07.003

Reid, P. F., and Raymond, L. N. (2010). *Modified elapid venoms as stimulators of the immune reaction*, 11/592896 application number.

Reid, H. A. (1971). Therapeutic defibrination by ancrod (Arvin). *Folia Haematol. Int. Mag. Klin. Morphol. Blutforsch.* 95 (2), 209–215.

Reid, P. F. (2007). Alpha-cobratoxin as a possible therapy for multiple sclerosis: a review of the literature leading to its development for this application. *Crit. Rev. Immunol.* 27 (4), 291–302. doi: 10.1615/CritRevImmunol.v27.i4.10

Reis, C. V., Andrade, S. A., Ramos, O. H. P., Ramos, C. R. R., Ho, P. L., Batista, I. D. C., et al. (2006). Lopap, a prothrombin activator from L*onomia obliqua* belonging to the lipocalin family: recombinant production, biochemical characterization and structure-function insights. *Biochem. J.* 398, 295–302. doi: 10.1042/bj20060325

Ren, Y. D., Li, C. C., Chang, J. L., Wang, R., Wang, Y. H., and Chu, X. P. (2018). Hi1a as a novel neuroprotective agent for ischemic stroke by inhibition of acid-sensing ion channel 1a. *Transl. Stroke Res.* 9 (2), 96–98. doi: 10.1007/s12975-017-0575-x

Rigo, F. K., Trevisan, G., De Pra, S. D. T., Cordeiro, M. N., Borges, M. H., Silva, J. F., et al. (2017). The spider toxin Phα1β recombinant possesses strong analgesic activity. *Toxicon* 133, 145–152. doi: 10.1016/j.toxicon.2017.05.018

Romero, H. K., Christensen, S. B., Mannelli, L. D., Gajewiak, J., Ramachandra, R., Elmslie, K. S., et al. (2017). Inhibition of α9α10 nicotinic acetylcholine receptors prevents chemotherapy-induced neuropathic pain. *Proc. Natl. Acad. Sci. U.S.A.* 114 (10), E1825–E1832. doi: 10.1073/pnas.1621433114

Römisch, J., Diehl, K. H., Hoffmann, D., Krahl-Mateblowski, U., Reers, M., Stüber, W., et al. (1993). Comparison of *in vitro* and *in vivo* properties of rhirudin (HBW 023) and a synthetic analogous peptide. *Haemostasis* 23 (5), 249–258. doi: 10.1159/000216883

RxList (2019). *Search*. Available at: https://www.rxlist.com/script/main/hp.asp (Accessed December 19, 2019).

Salehi, B., Sestito, S., Rapposelli, S., Peron, G., Calina, D., Sharifi-Rad, M., et al. (2019). Epibatidine: a promising natural alkaloid in health. *Biomolecules* 9 (1):6. doi: 10.3390/biom9010006

Sample, C. J., Hudak, K. E., Barefoot, B. E., Koci, M. D., Wanyonyi, M. S., Abraham, S., et al. (2013). A mastoparan-derived peptide has broad-spectrum antiviral activity against enveloped viruses. *Peptides* 48, 96–105. doi: 10.1016/j.peptides.2013.07.014

Santos, L. D., Pieroni, M., Menegasso, A. R. S., Pinto, J., and Palma, M. S. (2011). A new scenario of bioprospecting of Hymenoptera venoms through proteomic approach. *J. Venom. Anim. Toxins Incl. Trop. Dis.* 17 (4), 364–377. doi: 10.1590/S1678-91992011000300004

Sato, A. C., Bosch, R. V., Will, S. E. A., Alvarez-Flores, M. P., Goldfeder, M. B., Pasqualoto, K. F. M., et al. (2016). Exploring the i*n vivo* wound healing effects of a recombinant hemolin from the caterpillar L*onomia obliqua*. *J. Venom. Anim. Toxins Incl. Trop. Dis.* 22, 36. doi: 10.1186/s40409-016-0093-4

Scannell, J. W., Blanckley, A., Boldon, H., and Warrington, B. (2012). Diagnosing the decline in pharmaceutical R&D efficiency. *Nat. Rev. Drug Discovery* 11 (3), 191–200. doi: 10.1038/nrd3681

Scarborough, R. M., Rose, J. W., Hsu, M. A., Phillips, D. R., Fried, V. A., Campbell, A. M., et al. (1991). Barbourin. A GPIIb-IIIa-specific integrin antagonist from the venom of S*istrurus m. barbouri*. *J. Biol. Chem.* 266 (15), 9359–9362.

Scarborough, R. M., Naughton, M. A., Teng, W., Rose, J., Phillips, D., Nannizzi, L., et al. (1993). Design of potent and specific integrin antagonists. Peptide antagonists with high specificity for glycoprotein IIb-IIIa. *J. Biol. Chem.* 268 (2), 1066–1073.

Scarborough, R. M. (1999). Development of eptifibatide. *Am. Heart J.* 138 (6), 1093–1104. doi: 10.1016/s0002-8703(99)70075-x

Schechter, M. E., Andrade, B. B., He, T., Richter, G. H., Tosh, K. W., Policicchio, B. B., et al. (2017). Inflammatory monocytes expressing tissue factor drive SIV and HIV coagulopathy. *Sci. Transl. Med.* 9 (405), eaam5441. doi: 10.1126/scitranslmed.aam5441

Schwartsmann, G., DiLeone, L. P., Horowitz, M., Schunemann, D., Cancella, A., Pereira, A. S., et al. (2006). A phase I trial of the bombesin/gastrin-releasing peptide (BN/GRP) antagonist RC3095 in patients with advanced solid malignancies. *Invest. New Drugs* 24 (5), 403–412. doi: 10.1007/s10637-006-6886-5

Scott, D. A., Wright, C. E., and Angus, J. A. (2002). Actions of intrathecal omega-conotoxins CVID, GVIA, MVIIA, and morphine in acute and neuropathic pain in the rat. *Eur. J. Pharmacol.* 451 (3), 279–286. doi: 10.1016/S0014-2999(02)02247-1

Seon, G. M., Lee, M. H., Kwon, B. J., Kim, M. S., Koo, M. A., Kim, D., et al. (2017). Functional improvement of hemostatic dressing by addition of recombinant batroxobin. *Acta Biomater.* 48, 175–185. doi: 10.1016/j.actbio.2016.10.024

Serrano, S. M. T. (2013). The long road of research on snake venom serine proteinases. *Toxicon* 62, 19–26. doi: 10.1016/j.toxicon.2012.09.003

Shah, A. R., and Scher, L. (2007). Drug evaluation: alfimeprase, a plasminogen-independent thrombolytic. *IDrugs* 10 (5), 329–335.

Shi, L., Liang, F., Li, Y., Shao, A., Zhou, K., Yu, J., et al. (2016). Desmoteplase for acute ischemic stroke within 3 to 9 Hours after symptom onset: Evidence from randomized controlled trials. *Sci. Rep.* 6:33989. doi: 10.1038/srep33989

Shibao, P. Y. T., Cologna, C. T., Morandi, R., Wiezel, G. A., Fujimura, P. T., Ueira-Vieira, C., et al. (2018). Deep sequencing analysis of toad R*hinella schneideri* skin glands and partial biochemical characterization of its cutaneous secretion. *J. Venom. Anim. Toxins Incl. Trop. Dis.* 24, 36. doi: 10.1186/s40409-018-0173-8

Sig, A. K., Guney, M., Uskudar Guclu, A., and Ozmen, E. (2017). Medicinal leech therapy - an overall perspective. *Integr. Med. Res.* 6 (4), 337–343. doi: 10.1016/j.imr.2017.08.001

Silva, C. N., Nunes, K. P., Torres, F. S., Cassoli, J. S., Santos, D. M., Almeida, F. D., et al. (2015). PnPP-19, a synthetic and nontoxic peptide designed from a P*honeutria nigriventer* toxin, potentiates erectile function via NO/cGMP. *J. Urol* 194 (5), 1481–1490. doi: 10.1016/j.juro.2015.06.081

Singh, K., Davies, G., Alenazi, Y., Eaton, J. R. O., Kawamura, A., and Bhattacharya, S. (2017). Yeast surface display identifies a family of evasins from ticks with novel polyvalent CC chemokine-binding activities. *Sci. Rep.* 7 (1), 4267. doi: 10.1038/s41598-017-04378-1

Singh, A. P. (2010). Medicinal leech therapy (hirudotherapy): a brief overview. *Complement Ther. Clin. Pract.* 16 (4), 213–215. doi: 10.1016/j.ctcp.2009.11.005

Siramshetty, V. B., Nickel, J., Omieczynski, C., Gohlke, B. O., Drwal, M. N., and Preissner, R. (2016). Withdrawn - a resource for withdrawn and discontinued drugs. *Nucleic Acids Res.* 44 (D1), D1080–D1086. doi: 10.1093/nar/gkv1192

Smith, H. S., and Deer, T. R. (2009). Safety and efficacy of intrathecal ziconotide in the management of severe chronic pain. *Ther. Clin. Risk Manag.* 5 (3), 521–534. doi: 10.2147/TCRM.S4438

Song, Y. M., Tang, X. X., Chen, X. G., Gao, B. B., Gao, E., Bai, L., et al. (2005). Effects of scorpion venom bioactive polypolypeptides on platelet aggregation and thrombosis and plasma 6-keto-PG F1alpha and TXB2 in rabbits and rats. *Toxicon* 46 (2), 230–235. doi: 10.1016/j.toxicon.2005.04.012

Soricimed (2018). *SOR-C13 clinical development program - A first-in-class drug candidate in development for the treatment of solid-tumor cancer*. Available at: https://www.soricimed.com/sor-c13.htm (Accessed April 19, 2018).

Souza, A. H., Ferreira, J., Cordeiro Mdo, N., Vieira, L. B., De Castro, C. J., Trevisan, G., et al. (2008). Analgesic effect in rodents of native and recombinant Phα1β toxin, a high-voltage-activated calcium channel blocker isolated from armed spider venom. *Pain* 140 (1), 115–126. doi: 10.1016/j.pain.2008.07.014

Spotnitz, W. D. (2014). Fibrin sealant: The only approved hemostat, sealant, and adhesive - a laboratory and clinical perspective. *ISRN Surg.* 2014:203943. doi: 10.1155/2014/203943

Stocker, K., Fischer, H., and Meier, J. (1988). Practical application of the protein C activator Protac from A*gkistrodon contortrix* venom. *Folia Haematol. Int. Mag. Klin. Morphol. Blutforsch.* 115 (3), 260–264.

Stocker, K. (1978). "Defibrinogenation with thrombin-like snake venom enzymes," in *Fibrinolytics and antifibrinolytics*. Ed. F. Markwardt (Berlin, Heidelberg, New York: Springer-Verlag), 451–484.

Stransky, S., Costal-Oliveira, F., Lopes-de-Souza, L., Guerra-Duarte, C., Chavez-Olortegui, C., and Braga, V. M. M. (2018). In vitro assessment of cytotoxic activities of L*achesis muta muta* snake venom. *PloS Negl. Trop. Dis.* 12 (4), e0006427. doi: 10.1371/journal.pntd.0006427

Su, Y., Huang, X., Zhang, D., Zhang, Y., Xie, J., and Linh, C. (2003). HPLC separation and determination of bufadienolide in cinobufacini injection. *Chin. Tradit. Pat. Med.* 25, 24–27.

Swenson, S., Toombs, C. F., Pena, L., Johansson, J., and Markland, F. S. (2004). Alpha-fibrinogenases. *Curr. Drug Targets Cardiovasc. Haematol. Disord.* 4 (4), 417–435. doi: 10.2174/1568006043335754

Swenson, S., and Markland, F. S. (2013). "Fibrolase," in *Handbook of proteolytic enzymes*. Eds. N. D. Rawlings and G. Salvesen (Amsterdam: Elsevier), 972–976.

Tabacova, S. A., and Kimmel, C. A. (2001). Enalapril: pharmacokinetic/dynamic inferences for comparative developmental toxicity - A review. *Reprod. Toxicol.* 15 (5), 467–478. doi: 10.1016/s0890-6238(01)00161-7

Tamimi, N. A. M., and Ellis, P. (2009). Drug development: from concept to marketing! *Nephron Clin. Pract.* 113 (3), C125–C131. doi: 10.1159/000232592

Tanner, M. R., Tajhya, R. B., Huq, R., Gehrmann, E. J., Rodarte, K. E., Atik, M. A., et al. (2017). Prolonged immunomodulation in inflammatory arthritis using the selective Kv1.3 channel blocker HsTX1 R14A and its PEGylated analog. *Clin. Immunol.* 180, 45–57. doi: 10.1016/j.clim.2017.03.014

Tans, G., and Rosing, J. (2001). Snake venom activators of factor X: an overview. *Haemostasis* 31 (3-6), 225–233. doi: 10.1159/000048067

Tansi, F. L., Filatova, M. P., Koroev, D. O., Volpina, O. M., Lange, S., Schumann, C., et al. (2019). New generation CPPs show distinct selectivity for cancer and noncancer cells. *J. Cell Biochem.* 120 (4), 6528–6541. doi: 10.1002/jcb.27943

Tarcha, E. J., Chi, V., Munoz-Elias, E. J., Bailey, D., Londono, L. M., Upadhyay, S. K., et al. (2012). Durable pharmacological responses from the peptide ShK-186, a specific Kv1.3 channel inhibitor that suppresses T cell mediators of autoimmune disease. *J. Pharmacol. Exp. Ther.* 342 (3), 642–653. doi: 10.1124/jpet.112.191890

Tcheng, J. E., and O'Shea, J. C. (2002). Eptifibatide: a potent inhibitor of the platelet receptor integrin glycoprotein IIb/IIIa. *Expert OpinPharmacother.* 3 (8), 1199–1210. doi: 10.1517/14656566.3.8.1199

Tokunaga, F., Nagasawa, K., Tamura, S., Miyata, T., Iwanaga, S., and Kisiel, W. (1988). The factor V-activating enzyme (RVV-V) from Russell's viper venom. Identification of isoproteins RVV-V alpha, -V beta, and -V gamma and their complete amino acid sequences. *J. Biol. Chem.* 263 (33), 17471–17481.

Topol, E. J., Byzova, T. V., and Plow, E. F. (1999). Platelet GPIIb-IIIa blockers. *Lancet* 353 (9148), 227–231. doi: 10.1016/S0140-6736(98)11086-3

Tornesello, A. L., Buonaguro, L., Tornesello, M. L., and Buonaguro, F. M. (2017). New insights in the design of bioactive peptides and chelating agents for imaging and therapy in oncology. *Molecules* 22 (8):1282. doi: 10.3390/molecules22081282

Traynor, J. R. (1998). Epibatidine and pain. *Br. J. Anaesth.* 81 (1), 69–76. doi: 10.1093/bja/81.1.69

Trifiro, G., Gini, R., Barone-Adesi, F., Beghi, E., Cantarutti, A., Capuano, A., et al. (2019). The role of European healthcare databases for post-marketing drug effectiveness, safety and value evaluation: where does Italy stand? *Drug Safe* 42 (3), 347–363. doi: 10.1007/s40264-018-0732-5

Trujillo, J. M., and Goldman, J. (2017). Lixisenatide, a once-daily prandial glucagon-like peptide-1 receptor agonist for the treatment of adults with type 2 diabetes. *Pharmacotherapy* 37 (8), 927–943. doi: 10.1002/phar.1962

Umana, I. C., Daniele, C. A., and McGehee, D. S. (2013). Neuronal nicotinic receptors as analgesic targets: it's a winding road. *Biochem. Pharmacol.* 86 (8), 1208–1214. doi: 10.1016/j.bcp.2013.08.001

US Food and Drug Administration (2016). *FDA approves Adlyxin to treat type 2 diabetes* (Accessed March 30, 2020).

US Food and Drug Administration (2020). *Drugs FDA: FDA approved drug products*. Available at: https://www.accessdata.fda.gov/scripts/cder/daf/ (Accessed June 25, 2020).

US National Library of Medicine (2020). *ClinicalTrials.gov - Find a study*. Available at: https://clinicaltrials.gov/ (Accessed June 25, 2020).

Utkin, Y. N., Vassilevski, A. A., Kudryavtsev, D., and Undheim, E. A. B. (2019). Animal toxins as comprehensive pharmacological tools to identify diverse ion channels. *Front. Pharmacol.* 10, 423. doi: 10.3389/fphar.2019.00423

Utkin, Y. N. (2017). Modern trends in animal venom research - omics and nanomaterials. *World J. Biol. Chem.* 8 (1), 4–12. doi: 10.4331/wjbc.v8.i1.4

Valverde, P., Kawai, T., and Taubman, M. A. (2004). Selective blockade of voltage-gated potassium channels reduces inflammatory bone resorption in experimental periodontal disease. *J. Bone Miner. Res.* 19 (1), 155–164. doi: 10.1359/JBMR.0301213

Varga, Z., Gurrola-Briones, G., Papp, F., Rodriguez de la Vega, R. C., Pedraza-Alva, G., Tajhya, R. B., et al. (2012). Vm24, a natural immunosuppressive peptide, potently and selectively blocks Kv1.3 potassium channels of human T cells. *Mol. Pharmacol.* 82 (3), 372–382. doi: 10.1124/mol.112.078006

Veiga, A. B., Ribeiro, J. M., Guimarães, J. A., and Francischetti, I. M. (2005). A catalog for the transcripts from the venomous structures of the caterpillar L*onomia obliqua:* identification of the proteins potentially involved in the coagulation disorder and hemorrhagic syndrome. *Gene* 355, 11–27. doi: 10.1016/j.gene.2005.05.002

Veiga, A. B. G., Berger, M., and Guimarães, J. A. (2009). "Lonomia obliqua venom: pharmaco-toxicological effects and biotechnological perspectives," in *Animal toxins: state of the art - perspectives in health and biotechnology*, *1st ed.* Eds. M. E. D. Lima, A. M. D. C. Pimenta, M. F. Martin-Eauclaire, R. B. Zingali and H. Rochat (Belo Horizonte: Editora UFMG), 371–390.

Veiseh, M., Gabikian, P., Bahrami, S. B., Veiseh, O., Zhang, M., Hackman, R. C., et al. (2007). Tumor paint: a chlorotoxin:Cy5.5 bioconjugate for intraoperative visualization of cancer foci. *Cancer Res.* 67 (14), 6882–6888. doi: 10.1158/0008-5472.CAN-06-3948

Verdoni, M., Roudaut, H., De Pomyers, H., Gigmes, D., Bertin, D., Luis, J., et al. (2016). ArgTX-636, a polyamine isolated from spider venom: A novel class of melanogenesis inhibitors. *Bioorgan. Med. Chem.* 24 (22), 5685–5692. doi: 10.1016/j.bmc.2016.08.023

Vetter, I., Deuis, J. R., Mueller, A., Israel, M. R., Starobova, H., Zhang, A., et al. (2017). $Na_V1.7$ as a pain target - From gene to pharmacology. *Pharmacol. Ther.* 172, 73–100. doi: 10.1016/j.pharmthera.2016.11.015

Veytia-Bucheli, J. I., Jimenez-Vargas, J. M., Melchy-Perez, E. I., Sandoval-Hernandez, M. A., Possani, L. D., and Rosenstein, Y. (2018). Kv1.3 channel blockade with the Vm24 scorpion toxin attenuates the CD4+ effector memory T cell response to TCR stimulation. *J. Cell Commun. Signal* 16, 45. doi: 10.1186/s12964-018-0257-7

Vila-Farres, X., Giralt, E., and Vila, J. (2012). Update of peptides with antibacterial activity. *Curr. Med. Chem.* 19 (36), 6188–6198. doi: 10.2174/092986712804485818

Vink, S., and Alewood, P. F. (2012). Targeting voltage-gated calcium channels: developments in peptide and small-molecule inhibitors for the treatment of neuropathic pain. *Br. J. Pharmacol.* 167 (5), 970–989. doi: 10.1111/j.1476-5381.2012.02082.x

Vivostat A/S (2018). *Vivostat autologous fibrin sealant* (Medicon Valley: Scandinavia). Available at: https://www.vivostat.com/products/vivostat-fibrin-sealant (Accessed April 19, 2018).

Vu, T. T., Stafford, A. R., Leslie, B. A., Kim, P. Y., Fredenburgh, J. C., and Weitz, J. I. (2013). Batroxobin binds fibrin with higher affinity and promotes clot expansion to a greater extent than thrombin. *J. Biol. Chem.* 288 (23), 16862–16871. doi: 10.1074/jbc.M113.464750

Warkentin, T. E. (2004). Bivalent direct thrombin inhibitors: hirudin and bivalirudin. *Best Pract. Res. Clin. Haematol.* 17 (1), 105–125. doi: 10.1016/j.beha.2004.02.002

Watters, M. R. (2005). Tropical marine neurotoxins: Venoms to drugs. *Semin. Neurol.* 25 (3), 278–289. doi: 10.1055/s-2005-917664

Weber, M. A., Schiffrin, E. L., White, W. B., Mann, S., Lindholm, L. H., Kenerson, J. G., et al. (2014). Clinical practice guidelines for the management of hypertension in the community: a statement by the American Society of Hypertension and the International Society of Hypertension. *J. Clin. Hypertens.* 16 (1), 14–26. doi: 10.1111/jch.12237

Wei, C. M., Aarhus, L. L., Miller, V. M., and Burnett, J. C. (1993). Action of C-type natriuretic peptide in isolated canine arteries and veins. *Am. J. Physiol.* 264 (1 Pt 2), H71–H73. doi: 10.1152/ajpheart.1993.264.1.H71

Wei, J. M., Zhu, M. W., Zhang, Z. T., Jia, Z. G., He, X. D., Wan, Y. L., et al. (2010). A multicenter, phase III trial of hemocoagulase A*gkistrodon:* hemostasis, coagulation, and safety in patients undergoing abdominal surgery. *Chin. Med. J. (Engl)* 123 (5), 589–593.

Weinger, R. S., Rudy, C., Moake, J. L., Olson, J. D., and Cimo, P. L. (1980). Prothrombin Houston: a dysprothrombin identifiable by crossed immunoelectrofocusing and abnormal *Echis carinatus* venom activation. *Blood* 55 (5), 811–816.

Wieser, G., Mansi, R., Grosu, A. L., Schultze-Seemann, W., Dumont-Walter, R. A., Meyer, P. T., et al. (2014). Positron emission tomography (PET) imaging of prostate cancer with a gastrin releasing peptide receptor antagonist - from mice to men. *Theranostics* 4 (4), 412–419. doi: 10.7150/thno.7324

Wigger, E., Kuhn-Nentwig, L., and Nentwig, W. (2002). The venom optimisation hypothesis: a spider injects large venom quantities only into difficult prey types. *Toxicon* 40 (6), 749–752. doi: 10.1016/s0041-0101(01)00277-x

Wilson, D., and Daly, N. L. (2018). Venomics: A mini-review. *High Throughput* 7 (3), 19. doi: 10.3390/ht7030019

Wong, C. K. (2005). Should bivalirudin be the anticoagulant of choice for percutaneous coronary intervention? *Nat. Clin. Pract. Cardiovasc. Med.* 2 (8), 384–385. doi: 10.1038/ncpcardio0277

Wysham, C. H., Rosenstock, J., Vetter, M. L., Dong, F., Öhman, P., and Iqbal, N. (2017). Efficacy and tolerability of the new autoinjected suspension of exenatide once weekly versus exenatide twice daily in patients with type 2 diabetes. *Diabetes Obes. Metab.* 20, 165–172. doi: 10.1111/dom.13056

Xie, X. B., Yin, J. Q., Wen, L. L., Gao, Z. H., Zou, C. Y., Wang, J., et al. (2012). Critical role of heat shock protein 27 in bufalin-induced apoptosis in human osteosarcomas: a proteomic-based research. *PloS One* 7 (10), e47375. doi: 10.1371/journal.pone.0047375

Xie, X., Huang, X., Li, J., Lv, X., Huang, J., Tang, S., et al. (2013). Efficacy and safety of Huachansu combined with chemotherapy in advanced gastric cancer: a meta-analysis. *Med. Hypotheses* 81 (2), 243–250. doi: 10.1016/j.mehy.2013.04.038

Xu, Y. Y., Ma, X. H., and Zhang, S. J. (2016). Hemocoagulase agkistrodon-induced anaphylactic shock: A case report and literature review. *Int. J. Clin. Pharmacol. Ther.* 54 (2), 129–134. doi: 10.5414/CP202296

Yang, R., Peng, F., Liu, H., Cao, Z. J., Li, W. X., Mao, X., et al. (2005). Functional analysis of a gene encoding a chlorotoxin-like peptide derived from scorpion toxin. *Chin. J. Biochem. Mol. Biol.* 21 (1), 19–23.

Yang, M., Huo, X. C., Miao, Z. R., and Wang, Y. J. (2019). Platelet glycoprotein IIb/IIIa receptor inhibitor tirofiban in acute ischemic stroke. *Drugs* 79 (5), 515–529. doi: 10.1007/s40265-019-01078-0

You, W. K., Choi, W. S., Koh, Y. S., Shin, H. C., Jang, Y., and Chung, K. H. (2004). Functional characterization of recombinant batroxobin, a snake venom thrombin-like enzyme, expressed from P*ichia pastoris*. *FEBS Lett.* 571 (1-3), 67–73. doi: 10.1016/j.febslet.2004.06.060

You, K. E., Koo, M. A., Lee, D. H., Kwon, B. J., Lee, M. H., Hyon, S. H., et al. (2014). The effective control of a bleeding injury using a medical adhesive containing batroxobin. *BioMed. Mat.* 9 (2):25002. doi: 10.1088/1748-6041/9/2/025002

Zambelli, V. O., Fernandes, A. C. D., Gutierrez, V. P., Ferreira, J. C. B., Parada, C. A., Mochly-Rosen, D., et al. (2014). Peripheral sensitization increases opioid receptor expression and activation by crotalphine in rats. *PloS One* 9 (3), e90576. doi: 10.1371/journal.pone.0090576

Zeymer, U. (2007). The role of eptifibatide in patients undergoing percutaneous coronary intervention. *Expert Opin. Pharmacother.* 8 (8), 1147–1154. doi: 10.1517/14656566.8.8.1147

Zhang, L. J., and Falla, T. J. (2009). Cosmeceuticals and peptides. *Clin. Dermatol.* 27 (5), 485–494. doi: 10.1016/j.clindermatol.2009.05.013

Zhang, Y. (2015). Why do we study animal toxins? *Zool Res.* 36 (4), 183–222. doi: 10.13918/j.issn.2095-8137.2015.4.183

Zhao, Y., Huang, J., Yuan, X., Peng, B., Liu, W., Han, S., et al. (2015). Toxins targeting the Kv1.3 channel: Potential immunomodulators for autoimmune diseases. *Toxins* 7 (5), 1749–1764. doi: 10.3390/toxins7051749

Conflict of Interest: The authors declare that the research was conducted in the absence of any commercial or financial relationships that could be construed as a potential conflict of interest.

frontiers in Molecular Biosciences

ORIGINAL RESEARCH
published: 05 August 2020
doi: 10.3389/fmolb.2020.00175

The Sequence and Three-Dimensional Structure Characterization of Snake Venom Phospholipases B

Anwar Ullah[1]* *and Rehana Masood*[2]

[1] Department of Biosciences, COMSATS University Islamabad, Islamabad, Pakistan, [2] Department of Biochemistry, Shaheed Benazir Bhutto Women University Peshawar, Peshawar, Pakistan

Snake venom phospholipases B (SVPLBs) are the least studied enzymes. They constitute about 1% of *Bothrops* crude venoms, however, in other snake venoms, it is present in less than 1%. These enzymes are considered the most potent hemolytic agent in the venom. Currently, no structural information is available about these enzymes from snake venom. To better understand its three-dimensional structure and mechanisms of envenomation, the current work describes the first model-based structure report of this enzyme from *Bothrops moojeni* venom named as *B. moojeni* phospholipase B (PLB_*Bm*). The structure model of PLB_*Bm* was generated using model building software like I-TESSER, MODELLER 9v19, and Swiss-Model. The build PLB_*Bm* model was validated using validation tools (PROCHECK, ERRAT, and Verif3D). The analysis of the PLB_*Bm* modeled structure indicates that it contains 491 amino acid residues that form a well-defined four-layer αββα sandwich core and has a typical fold of the N-terminal nucleophile aminohydrolase (Ntn-hydrolase). The overall structure of PLB_*Bm* contains 18 β-strands and 17 α-helices with many connecting loops. The structure divides into two chains (A and B) after maturation. The A chain is smaller and contains 207 amino acid residues, whereas the B chain is larger and contains 266 amino acid residues. The sequence and structural comparison among homologous snake venom, bacterial, and mammals PLBs indicate that differences in the length and sequence composition may confer variable substrate specificity to these enzymes. Moreover, the surface charge distribution, average volume, and depth of the active site cavity also vary in these enzymes. The present work will provide more information about the structure–function relationship and mechanism of action of these enzymes in snakebite envenomation.

Keywords: snake venom phospholipases B, sequence and three-dimensional structure analysis, glycosylation, structural comparison, structure-based substrate specificity and maturation

OPEN ACCESS

Edited by:
Annalisa Pastore,
King's College London,
United Kingdom

Reviewed by:
Piero Andrea Temussi,
University of Naples Federico II, Italy
Delia Picone,
University of Naples Federico II, Italy

***Correspondence:**
Anwar Ullah
anwarullah@comsats.edu.pk;
anwar.ms90@yahoo.com

Specialty section:
This article was submitted to Structural Biology, a section of the journal Frontiers in Molecular Biosciences

Received: *06 May 2020*
Accepted: *06 July 2020*
Published: *05 August 2020*

Citation:
Ullah A and Masood R (2020) The Sequence and Three-Dimensional Structure Characterization of Snake Venom Phospholipases B. Front. Mol. Biosci. 7:175. doi: 10.3389/fmolb.2020.00175

INTRODUCTION

Phospholipases B (PLBs) or lysophospholipases (EC3.1.1.5) are high-molecular-mass enzymes that break ester linkages of glycerophospholipids of membranes at both positions *sn-1* and *sn-2* (Shiloah et al., 1973; Rokyta et al., 2011; Chapeaurouge et al., 2015). These enzymes have been named as PLBs (Doery and Pearson, 1964), phospholipase B-like (Doery and Pearson, 1964; Aird et al., 2013),

lysophospholipases (Takasaki and Tamiya, 1982), and Ntn-hydrolases (Oinonen and Rouvinen, 2000). These are reported to exist in the venom proteomes of various snakes, bee, scorpions, and insects), fungi, bacteria, animal tissues, and rice bran (**Table 1**).

Currently, little is known about the pathological and physiological effects of these enzymes in snake venom (Rokyta et al., 2011; Chapeaurouge et al., 2015; Oliveira et al., 2019; Tang et al., 2019). Upon snakebite envenomation, snake venom PLBs (SVPLBs) display strong hemolytic and cytotoxic activities and cause myoglobinuria and cytotoxicity (Takasaki and Tamiya, 1982; Bernheimer et al., 1986, 1987). The hemolytic activity of these enzymes is related to the hydrolysis of phosphatidylcholine (Bernheimer et al., 1986).

The relative abundance of PLBs varies in snake venoms, and generally, it constitutes a small percentage of the crude venoms; for example, PLBs constitute about 0.34% of the crude venom of Elapidae (Margres et al., 2013) and in the Viperidae, this percentage varies from 0.23 to 2.5 (Sousa et al., 2013). In *Botrops* species, the highest percentage has been reported in *Rhinocerophis cotiara* (2.5% of the crude venom) (Sousa et al., 2013).

SVPLBs are high-molecular-mass proteins (∼55 kDa) (Rokyta et al., 2011; Chapeaurouge et al., 2015; Wiezel et al., 2015) with a *p*I of 6.2 (Bernheimer et al., 1987). These enzymes display maximum catalytic activity in the pH range from 8.5 to 10 (Doery and Pearson, 1964).

Research about the SVPLBs is in nascent stage, and the first sequence report (based on transcriptomic analysis) about this protein came out in 2011 (Chatrath et al., 2011; Rokyta et al., 2011). The primary structure of SVPLB contains 553 amino acids in which the first 36 amino acids form the signal peptides and the remaining 526 make the PLB domain (Rokyta et al., 2011). Both monomeric and dimeric forms of PLBs have been reported to exist in snake venoms (Bernheimer et al., 1987; Chatrath et al., 2011). SVPLBs are stable proteins and show full enzymatic activity in the temperature range of 0–60°C; however, some of these retain 47% of the biological activity even at a temperature of 100°C (Bernheimer et al., 1987).

Although the primary amino acid sequence of PLBs from a number of snake venoms is present in the protein sequence database (UniProt databank), there is no report about their three-dimensional (3D) structure. Owing to this, it is difficult to co-relate their structural properties with the function. Keeping this in view, the current work reports model-based structural characterization of PLBs from *Bothrops moojeni* venom.

RESULTS AND DISCUSSION

Sequence Alignment Analysis

The primary amino acid sequence of PLB_*Bm* contains 553 amino acid residues in the precursor form and 491 amino acid residues in the mature form (Amorim et al., 2017). The sequence alignment analysis indicates a high sequence identity (70–97%) among SVPLBs, moderate sequence identity (63–67%) with cow PLB, and very low sequence identity (34%) with mouse PLB (**Figure 1** and **Table 2**). The primary amino acid sequence of PLB_*Bm* contains seven cysteine residues in the precursor form and five cysteine residues in the mature form (**Figure 1**). Of the five cysteine residues, four make two disulfide bonds (Cys88–Cys500 and Cys499–Cys523), whereas one cysteine (Cys237) remains in the free form. This free cysteine functions as one of the main amino acids in the active site of these enzymes, and they are also called cysteine proteinases (Verma et al., 2016). This cysteine residue is fully conserved in all SVPLBs and also PLBs of cow and mouse (**Figure 1**). The four other cysteine residues are fully conserved among SVPLB and mouse PLB; however, in the cow PLB, the cysteine at positions 501, 502, and 523 are not conserved (**Figure 1**). The amino acid residues belonging to the active sites (Asp303, Lys527, Cys237, His254, and Arg265) are also fully conserved among SVPLBs and mouse and cow PLBs. SVPLBs contain one glycosylation site (Asn69), which is fully conserved with the mouse PLB. The concurrence (consensus) lipase sequence GXSXG is fully conserved among all the aligned PLBs (**Figure 1**). The analysis of the phylogenetic tree generated from the aligned sequence shows a close relationship among SVPLBs and PLBs from mouse and bovine kidneys (**Supplementary Figure S1**).

Domain Analysis

The ThreaDom (Threading-based Protein Domain Prediction) (Xue et al., 2013) analysis indicates that PLB_*Bm* is a single-domain protein. The molecular weights (calculated through ProtParam (Gasteiger et al., 2005) of the precursor and mature protein were 63.88 and 57.09 kDa with the corresponding p*I* of 8.80 and 7.71, respectively. These results indicate that the p*I* of PLB_*Bm* changes from highly basic to slightly basic upon maturation. The theoretically calculated molecular weights and p*I*s agree with the experimentally observed molecular weights and p*I*s of these enzymes (Doery and Pearson, 1964; Takasaki and Tamiya, 1982; Bernheimer et al., 1986, 1987; Chatrath et al., 2011).

Homology Modeling

For the 3D structure characterization of PLB_*Bm*, the homology model was generated using the online modeling servers like the SWISS Model (Waterhouse et al., 2018), I-TESSER (Laskowski et al., 2001), and MODELLER 9v19 program (Webb and Sali, 2016). The atomic coordinates of phospholipase B-like protein 1 from *Bos taurus* (PDB ID: 4BWC; 70% amino acid sequence identity with PLB_*Bm*) (Repo et al., 2014), were applied as a template.

Model Validation

The generated model of PLB_*Bm* was validated using programs like PROCHECK, ERRAT, and Verif3D software (Bowie et al., 1991; Lüthy et al., 1992; Colovos and Yeates, 1993; Laskowski et al., 1993). The best model was selected based on the analysis coming from these programs. The PROCHECK analysis of the best 3D structure model of PLB_*Bm* shows that 95.7% (468 amino acid residues) were in the favored region and 4.3% (21 amino acid residues) were in the allowed region with no amino acid residue in the outlier region of the Ramachandran plot

TABLE 1 | Occurrence of PLBs in various organisms.

Snakes	References
Calloselasma rhodostoma, Trimeresurus insularis, *Porthidium porrasi*, *Hypnale hypnale*, *Crotalus durissus collilineatus, Echis carinatus carinatus*, *Bothrops moojeni*, coral snake, *Naja kaouthia*, *Tropidolaemus wagleri*, Russian Vipers of Pelias Group, *Lachesis muta rhombeata*, *Porthidium lansbergii lansbergii*, *Pseudechis guttatus*, *Austrelaps superbus*, *Ovophis okinavensis*, *Protobothrops flavoviridis*, *Bothropoides jararaca*, *Bothropoides neuwiedi*, *Rhinocerophis alternatus*, *Rhinocerophis cotiara*, *Bothrops jararacussu* and *Bothrops atrox*, *Drysdalia coronoides*, *Pseudechis colletti*	Bernheimer et al., 1987; Aird et al., 2013, 2017; Marcon et al., 2013; Sousa et al., 2013; Viala et al., 2014; Jiménez-Charris et al., 2015; Wiezel et al., 2015; Kovalchuk et al., 2016; Tang et al., 2016, 2019; Zainal Abidin et al., 2016; Amorim et al., 2017; Patra et al., 2017; Tan et al., 2017; Vanuopadath et al., 2018; Jones et al., 2019; Méndez et al., 2019; Oliveira et al., 2019
Scorpion	
Egyptian scorpion	Doery and Pearson, 1964; Mohamed et al., 1969
Insects	
Musca domestica L., Culex pipiens fatigans	Khan and Hodgson, 1967; Rao and Subrahmanyam, 1969
Fungi	
Penicillium notatum	Fairbairn, 1948; Saito, 2014
Bacteria	
Streptomyces sp. strain NA684,	Doery and Pearson, 1964; Matsumoto et al., 2013
Mammals	
Bovine lysosomal phospholipase B-like protein	Repo et al., 2014
Rice bran	Contardi and Ercoli, 1933

PLBs, phospholipases B.

(Lovell et al., 2003; **Supplementary Figure S2**). The overall quality factor of the ERRAT analysis was 96 (**Supplementary Figure S3**), which lies for the best structure quality of the proteins 3D structure according to the writers of the program (Colovos and Yeates, 1993).

Molecular Dynamics Simulation

The programs used for the molecular dynamics (MD) simulation includes GROMACS (Berendsen et al., 1995; Maier et al., 2015), AMBER16 (Case et al., 2005; Salomon-Ferrer et al., 2013), MDWeb, and MDMobby (Hospital et al., 2012). The analysis of the MD simulation coming from all these programs indicates the same results for the modeled structure of PLB_*Bm* (**Supplementary Figures S4A–D**). The important 3D structure parameters like chirality, disulfide bonds, and unusual *cis*/*trans* configuration were correct, and there were no steric clashes in the modeled PLB_*Bm* structure (**Supplementary Figure S4A**). The analysis of the root-mean-square deviation (RMSD) and radius of gyration (RG), the two essential parameters for 3D structure validation, have shown that the PLB_*Bm* has not undergone substantial changes during the modeling process. The RMSD value did not diverge more than 1 Å (**Supplementary Figure S4B**), and the radius of gyration was constant (kept around 21.5 Å) throughout the MD simulation process (**Supplementary Figure S4C**). The B-factor per residue was ∼17 Å (**Supplementary Figure S4D**), which lies in the average B-factor range for the proteins with X-ray resolution (1.8–2.1 Å) (Carugo, 2018).

The Overall Structure of Snake Venom Phospholipase B

The mature protein of PLB_*Bm* contains 491 amino acid residues that fold into a well-defined 3D structure, which contains four-layer αββα sandwich core and has a typical fold of the N-terminal nucleophile aminohydrolase (Ntn-hydrolase) (**Figures 2A,B**; Oinonen and Rouvinen, 2000; Lakomek et al., 2009; Repo et al., 2014). The overall structure of PLB_*Bm* contains 18 β-strands and 17 α-helices with many connecting loops (**Figures 2A,B** and **Supplementary Figure S5**). The structure divides into two chains (A and B) after maturation (Oinonen and Rouvinen, 2000; Repo et al., 2014). The A chain is small and contains 207 amino acid residues, whereas the B chain is large and contains 266 amino acid residues (**Supplementary Figure S5**).

The A chain has four β-strands numbered 1 through 4 and five α-helices named A to E (**Supplementary Figure S5**). The β-strands are anti-parallel to each other. The N-terminal of this chain starts with long β-strands, and the C-terminal ends at α-helix (**Figure 2B** and **Supplementary Figure S5**). This chain is stabilized by four intrachain salt bridges (His110–Asp69, Arg144–Asp167, Arg144–Asp140, and Arg159–Asp55) and two interchain salt bridges (Lys82–Asp259 and Arg157–Asp264) (**Table 3**).

The B chain is more compact, and it contains 14 β-strands and 12 α-helices. Of the 14 β-strands, seven are parallel, whereas the other seven are antiparallel. The N-terminal of this chain starts with a long β-strand, and the C-terminal ends with a short β-strand. The active site is located in this chain (**Figure 2B**). This chain is stabilized by two interchain salt bridges (Lys82–Asp259 and Arg157–Asp264) and 14 intrachain salt bridges (Arg253–Asp285, Arg253–Asp488, Lys358–Asp356, Lys382–Asp403, Lys382–Glu405, Arg391–Asp368, Arg436–Asp459, Lys440–Asp437, Arg473–Asp475, Arg479–Asp477, Lys490–Asp285, and Lys490–Asp488). This chain is further stabilized by two intrachain disulfide bridges (Cys88–Cys500 and Cys499–Cys523) (**Figures 1**, **2B**).

Active Site

A 16-amino-acid-residue segment (208–224) is removed autocatalytically between chains A and B, which opens the active

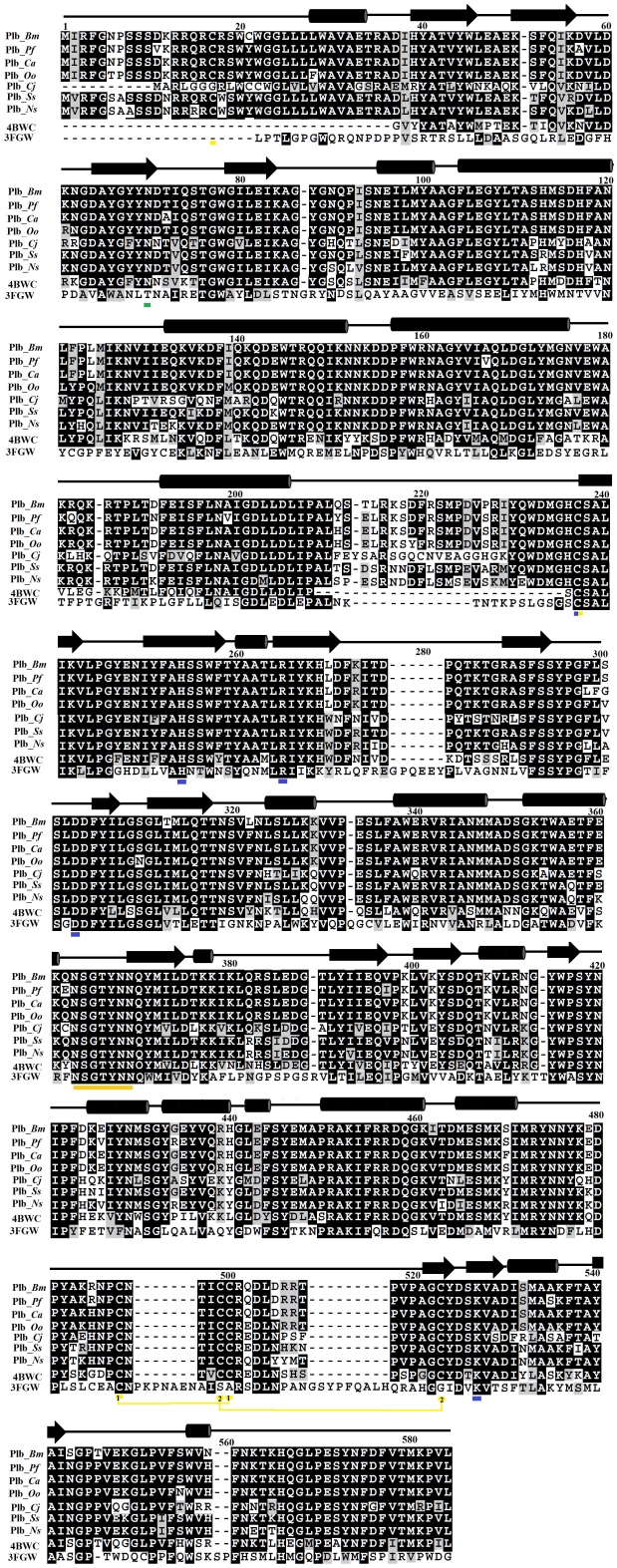

FIGURE 1 | Sequence alignment among snake venom phospholipases B (SVPLBs), PLB from bovine kidneys, and 66.3 kDa protein from *Mus musculus*. PLB_*Bm*, phospholipase B from *Bothrops moojeni*; PLB_*Pf*, *(Continued)*

FIGURE 1 | Continued
phospholipase B from *Protobothrops flavoviridis*; PLB_*Ca*, phospholipase B from *Crotalus atrox*; PLB_*Oo*, phospholipase B from *Ovophis okinavensis*; PLB_*Cj*, phospholipase B from *Coturnix japonica*; PLB_*Ss*, phospholipase B from *Spilotes sulphureus*; PLB_*Ns*, phospholipase B from *Notechis scutatus*; 4BWC, phospholipase B like protein 1 from bovine kidneys; 3FGW, 66.3 kDa protein from *M. musculus*. The amino acid residues involved in catalysis are underlined with blue, and the cysteine residues are underlined with yellow. The consensus lipase sequence is underlined with gold color. The cysteine residues that make disulfide bridges are linked (yellow lines). The putative *N*-glycosylation amino acid residues are underlined in green. The secondary structure elements (α-helices and β-strands) are shown above the sequence.

site and produces a cavity that facilitates the entry of a substrate to the active site (**Figure 2B**). The free cysteine residue (Cys225), which is situated between the key β-sheets in chain B, forms the active site of this enzyme. This cysteine residue functions as both a nucleophile and a general base during catalysis. It is further supported by His242 and Lys490, which is in turn assisted by Asp285, Asp488, and Arg253 (**Figure 2C**). These active site residues are conserved in the PLBs from other organisms as well (**Figure 1** and **Supplementary Figure S6**). The sequence logo produced from the aligned sequence of SVPLBs and PLBs of mouse and bovine kidneys display high sequence identity around the active site (**Supplementary Figure S7**).

Glycosylation

PLB_*Bm* contains carbohydrate moiety like PLBs from other organisms (Lakomek et al., 2009; Repo et al., 2014). The NetNGlyc server1 (Gupta et al., 2004) found a single glycosylation site for this enzyme at Asn69. In the primary amino acid structure of *Drysdalia coronoides* PLB, two putative glycosylation sites have been found (Chatrath et al., 2011). In bovine lysosomal phospholipase B-like protein (PDB ID: 4WBC) (Repo et al., 2014), six glycosylation sites were identified, which include Asn68, Asn211, Asn305, Asn363, Asn408, and Asn523. Of these, only Asn69 that is conserved between PLB_*Bm* and bovine lysosomal phospholipase B-like protein contains *N*-acetylglucosamine (NAG). Although Asn211, Asn305, Asn408, and Asn523 are conserved with PLB_*Bm*, these were found without carbohydrate moiety. In the structure of lysosomal 66.3 kDa protein from mouse (PDB ID: 3FGR) (Lakomek et al., 2009), seven NAG molecules were found, which were attached to Asn93, Asn236, and Asn520 (one NAG each) and Asn115 and Asn441 (two NAGs each). Only Asn93, which corresponds to Asn69 of PLB_*Bm*, is conserved between the two proteins and contains NAG. In SVPLBs, the specific function of the glycan moiety is not fully known; however, it may help the enzyme to specifically bind to the cell surface, thereby facilitating the hydrolysis processes.

Substrate Specificity

SVPLBs have been shown to hydrolyze phosphatidylcholine, phosphatidylethanolamine, and lysophosphatidylcholine, however, they are not active against phosphatidylinositol, phosphatidylserine, sphingomyelin, and cardiolipin (**Supplementary Figure S8**; Bernheimer et al., 1986, 1987).

TABLE 2 | Percent sequence identity among snake venom PLBs, PLB-like protein 1 from bovine kidneys, and 66.3 kDa protein from *Mus musculus*.

Proteins	PLB_*Bm*	PLB_*Ca*	PLB_*Oo*	PLB_*Pf*	PLB_*Ss*	PLB_*Ns*	PLB_*Cj*	4BWC	3FGW
PLB_*Bm*	–	96.93	96.20	95.84	87. 70	84.45	70.58	63.57	34.33
PLB_*Ca*	96.93	–	96.56	96.93	88.79	86.26	70.95	62.98	34.40
PLB_*Oo*	96.20	96.56	–	95.48	87.16	84.99	71.32	63.37	34.24
PLB_*Pf*	95.84	96.93	95.48	–	89.33	85.71	72.63	64.15	33.65
PLB_*Ss*	87. 70	88.79	87.16	89.33	–	96.60	72.02	64.73	34.02
PLB_*Ns*	84.45	86.26	84.99	85.71	96.60	–	64.73	62.40	33.65
PLB_*Cj*	70.58	70.95	71.32	72.63	72.02	70.40	–	67.57	34.19
4BWC	63.57	62.98	63.37	64.15	64.73	62.40	67.57	–	34.46
3FGW	34.33	34.40	34.24	33.65	34.02	33.65	34.19	34.46	–

PLBs, phospholipases B; PLB_Bm, phospholipase B from Bothrops moojeni; PLB_Pf, phospholipase B from Protobothrops flavoviridis; PLB_Ca, phospholipase B from Crotalus atrox; PLB_Oo, phospholipase B from Ovophis okinavensis; PLB_Cj, phospholipase B from Coturnix japonica; PLB_Ss, phospholipase B from Spilotes sulphureus; PLB_Ns, phospholipase B from Notechis scutatus; 4BWC, phospholipase B like protein 1 from bovine kidneys; 3FGW, 66.3 kDa protein from M. musculus.

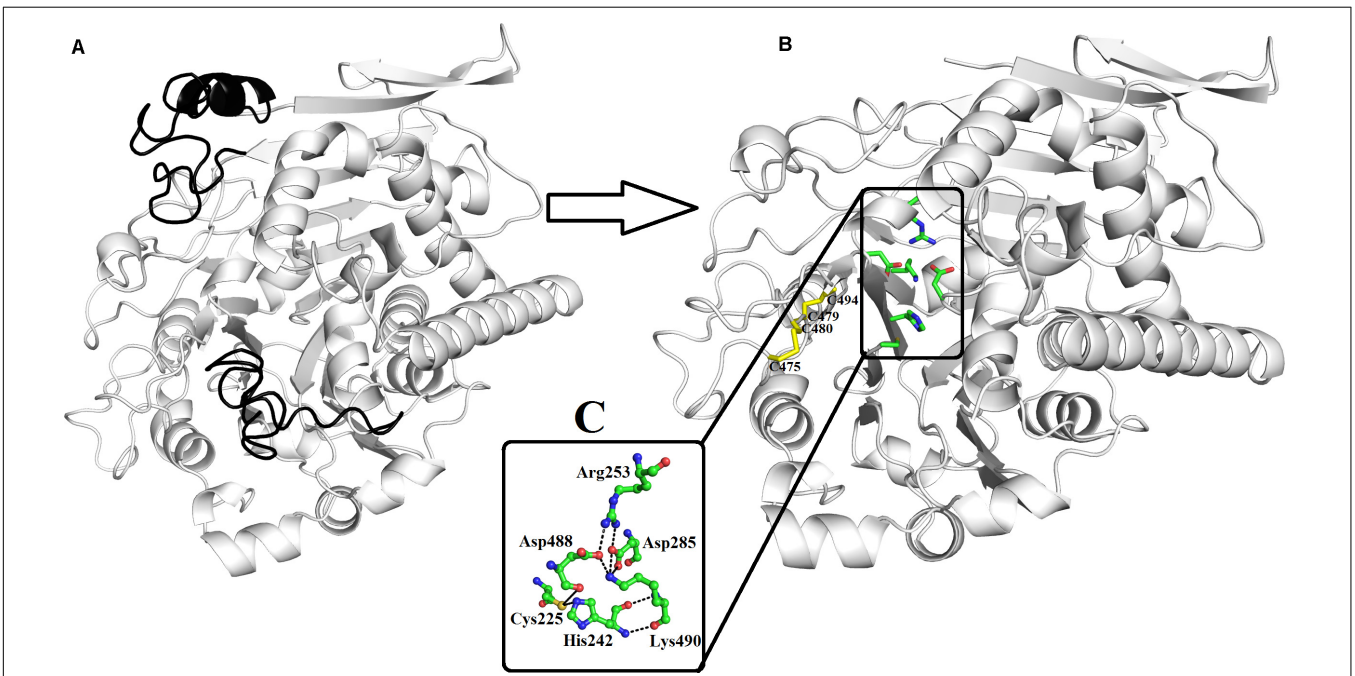

FIGURE 2 | Overall structure of phospholipase B from *Bothrops moojeni* (PLB_*Bm*) cartoon representation of **(A)** zymogen and **(B)** mature protein. The signal and the inner peptides are shown in black color. The active site residues and the disulfide bridges are shown as green and yellow sticks. **(C)** The residues involved in catalysis are highlighted.

On the other hand, PLBs of fungi, bacteria, and mammals have been shown to hydrolyze a broad range of substrates like phosphatidylcholine, phosphatidylinositol, phosphatidylserine, phosphatidylethanolamine, phosphatidic acid, lysophosphatidylcholine, and lysophosphatidylethanolamine (**Supplementary Figure S8**; Morgan et al., 2004; Lakomek et al., 2009; Repo et al., 2014). An explanation for the observed specificity of SVPLBs and PLBs from other organisms can be made on the basis of surface charge distribution around the active site cavity (Ullah et al., 2018, 2019; Ullah, 2020). In SVPLBs, the active site cavity is negatively charged, whereas the entry to the active site is positively charged (**Figure 3A**). In the case of bovine lysosomal phospholipase B-like protein, the active site cavity and its entrance are both neutral and positively charged, respectively (**Figure 3B**), whereas lysosomal 66.3 kDa protein from mouse that is also a PLB has an active site cavity that is highly negatively charged, and its entrance is also negatively charged (**Figure 3C**). A second factor that may involve this substrate specificity is the volume of the active site cavity. The SVPLBs have large active site cavity volumes with long average depth (**Table 4**). Owing to this, the phospholipids with the large polar head group easily reach their active sites, whereas the PLBs from other organisms have relatively small cavity volume with small depth and can accommodate phospholipids with a small polar head group (**Table 4**). The size of the active site cavity gradually decreases in PLB_*Bm* while going from the surface to the interior of the protein (**Figure 3A**). From

TABLE 3 | Salt bridges in the PLB_*Bm* three-dimensional structure.

Residue 1	Residue 2	Distance
NZ LYS A 82	OD2 ASP B 259	3.51
NE2 HIS A 110	OD2 ASP A 69	3.89
NH1 ARG A 144	OD2 ASP A 167	2.87
NH2 ARG A 144	OD2 ASP A 140	3.43
NH2 ARG A 157	OD2 ASP B 264	3.65
NH1 ARG A 179	OD2 ASP A 55	3.59
NH1 ARG B 253	OD2 ASP B 285	3.94
NH1 ARG B 253	OD2 ASP B 488	2.83
NZ LYS B 358	OD2 ASP B 356	3.59
NZ LYS B 382	OD1 ASP B 403	2.84
NZ LYS B 382	OE1 GLU B 405	2.90
NH2 ARG B 391	OD1 ASP B 368	2.72
NH1 ARG B 436	OD1 ASP B 459	2.74
NH2 ARG B 436	OD2 ASP B 437	2.76
NH2 ARG B 436	OD2 ASP B 459	2.70
NZ LYS B 440	OD1 ASP B 437	2.68
NH2 ARG B 473	OD1 ASP B 475	3.77
NH2 ARG B 479	OD1 ASP B 477	3.12
NZ LYS B 490	OD2 ASP B 285	2.93
NZ LYS B 490	OD1 ASP B 488	2.80

PLB_Bm, phospholipase B from Bothrops moojeni.

the above discussion, it is clear that the enzymes showing specificity for phosphatidylcholine, phosphatidylethanolamine, and lysophosphatidylcholine (SVPLBs) have negatively charged active site with a large volume, which can accommodate the phospholipids with large and positively charged head groups (**Supplementary Figure S8**). The other PLBs (fungi, bacteria, and mammals) having broad specificity display surface charge distribution (partially positive and neutral and highly negative), and the active site with a relatively small volume can accommodate phospholipids with head group that is positively and negatively charged or neutral (**Supplementary Figure S8**).

Maturation of Snake Venom Phospholipases B

The SVPLBs like other snake venom enzymes are secreted as zymogen with the signal peptide, an internal peptide, and a phospholipase domain (Rokyta et al., 2011; Amorim et al., 2017; **Figures 4A–D**, **5**). The zymogen or precursor proteins of SVPLBs contain 547–553 amino acid residues in length (Chatrath et al., 2011; Rokyta et al., 2011; Aird et al., 2017). During the maturation process, the SVPLBs lose the signal peptide. The amino acid sequence analysis by signalP-3.0 (Bendtsen et al., 2004) indicates that this part has 36 amino acid residues (**Figure 4A**). The signal peptide is removed cotranslationally or by the action of signal peptidases (Paetzel et al., 2002; **Figure 5**). A second segment (internal peptide) is removed autocatalytically and internally from these enzymes (Oinonen and Rouvinen, 2000). This segment contains 16 amino acid residues (**Figure 1**). After the removal of the internal peptide, the SVPLBs are divided into two chains like bovine lysosomal phospholipase B-like protein

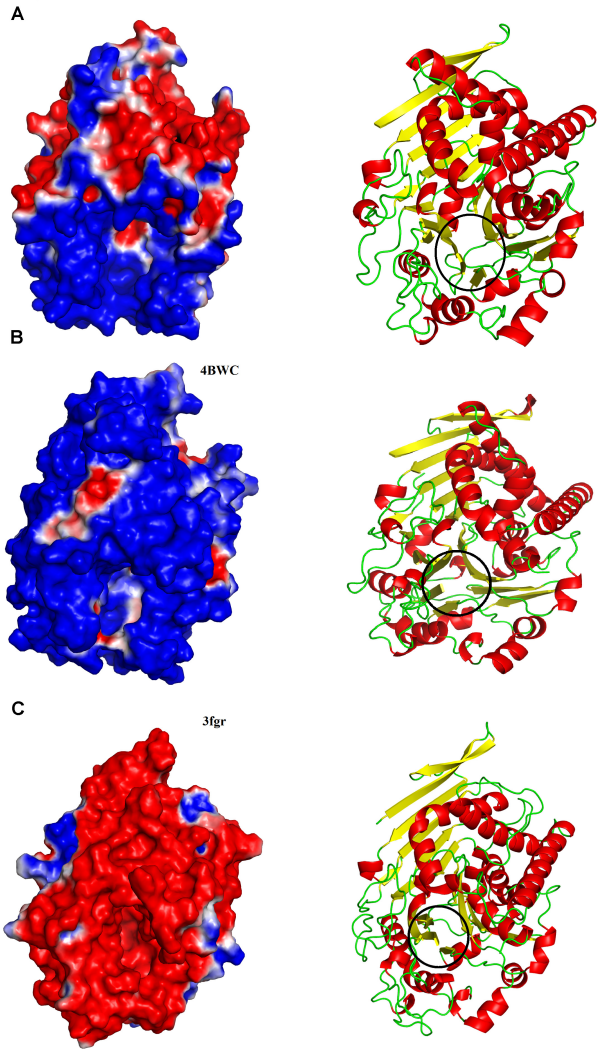

FIGURE 3 | Surface charge distributions of **(A)** phospholipase B from Bothrops moojeni (PLB_Bm), **(B)** phospholipase B like protein 1 from bovine kidneys, and **(C)** 66.3 kDa protein from Mus musculus highlighting the contrasts at the catalytic interface. Black circles indicate the location of the active-site pocket. Blue, red, and white represent positive, negative, and neutral charges, respectively.

TABLE 4 | Average active site cavity volumes and average active site cavity depths of PLB_*Bm* and their mammalian counterparts.

Protein	Average volume (Å^3)	Average depth (Å)
PLB_*Bm* model	5,740.88	15.71
4BWC	2,911.36	11.16
3FGR	4,231.83	13.35

PLB_Bm, phospholipase B from Bothrops moojeni.

and lysosomal 66.3 kDa proteins from mouse (Lakomek et al., 2009). The two chains are connected by many hydrogen bonds and non-bonded contacts between them (Lakomek et al., 2009). The Kyte–Doolittle plot for hydropathy (Gasteiger et al., 2005) and the temperature B-factor analysis indicate that both the signal

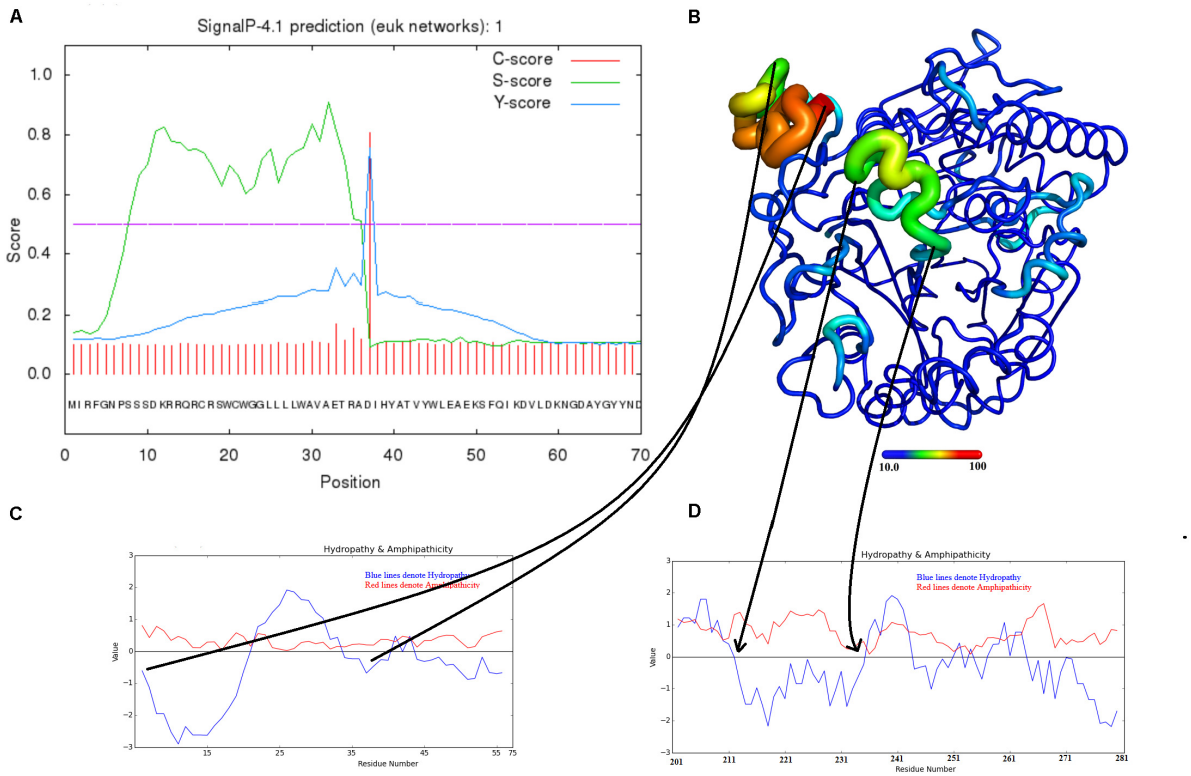

FIGURE 4 | Maturation mechanism for phospholipase B from *Bothrops moojeni* (PLB_*Bm*). **(A)** A signalP-HMM prediction plot, **(B,C)** a Kyte–Doolittle plot for signal and activation peptides, and **(D)** ribbon representation of colored B-factor (temperature)

and internal peptides are present in the hydrophilic region of the protein (**Figures 4B–D**).

CONCLUSION

- The sequence and structural analysis of PLB_*Bm* was carried out using several computational biology programs.
- The sequence alignment analysis indicates a high sequence identity (70–97%) among SVPLBs, average sequence identity (63–67%) with cow PLB, and very low sequence identity (34%) with mouse PLB.
- The 3D structural analysis of PLB_*Bm* indicates that its structure is composed of four-layer αββα sandwich core and has a typical fold of the Ntn-hydrolases.
- Structural comparisons with PLBs from cow and mouse indicated that the surface charge distribution and the average active site cavity volume and depth vary in these enzymes, which may impart variable substrate specificity to these enzymes.
- The maturation process of PLB_*Bm* involves loss of the signal and internal peptides to convert it into the fully active mature form.
- The structure of PLB_*Bm* described in this work is solely a predicted structure, and these observations need to be confirmed with experimental evidence like X-rays crystallography (Ullah et al., 2020).
- This work will provide a good starting point for future experimental studies of these enzymes.

MATERIALS AND METHODS

Sequence Logo Generated From Multiple Sequence Alignment

The Weblogo 3.2 (Schneider and Stephens, 1990; Crooks et al., 2004) was used to generate the sequence logo from multiple sequence alignment using default parameters.

Domain Prediction and Biochemical Properties of the PLB_*Bm*

The domain organization and biochemical properties of PLB_*Bm* were predicted using the program ThreaDomEx (Wang et al., 2017) and ProtParam[1] (Gasteiger et al., 2005), respectively.

Prediction of Ligand Binding

The ligand-binding sites in PLB_*Bm* were predicted using the 3DLigandSite (Wass et al., 2010) with parameters set to default.

[1]http://web.expasy.org/compute_pi/

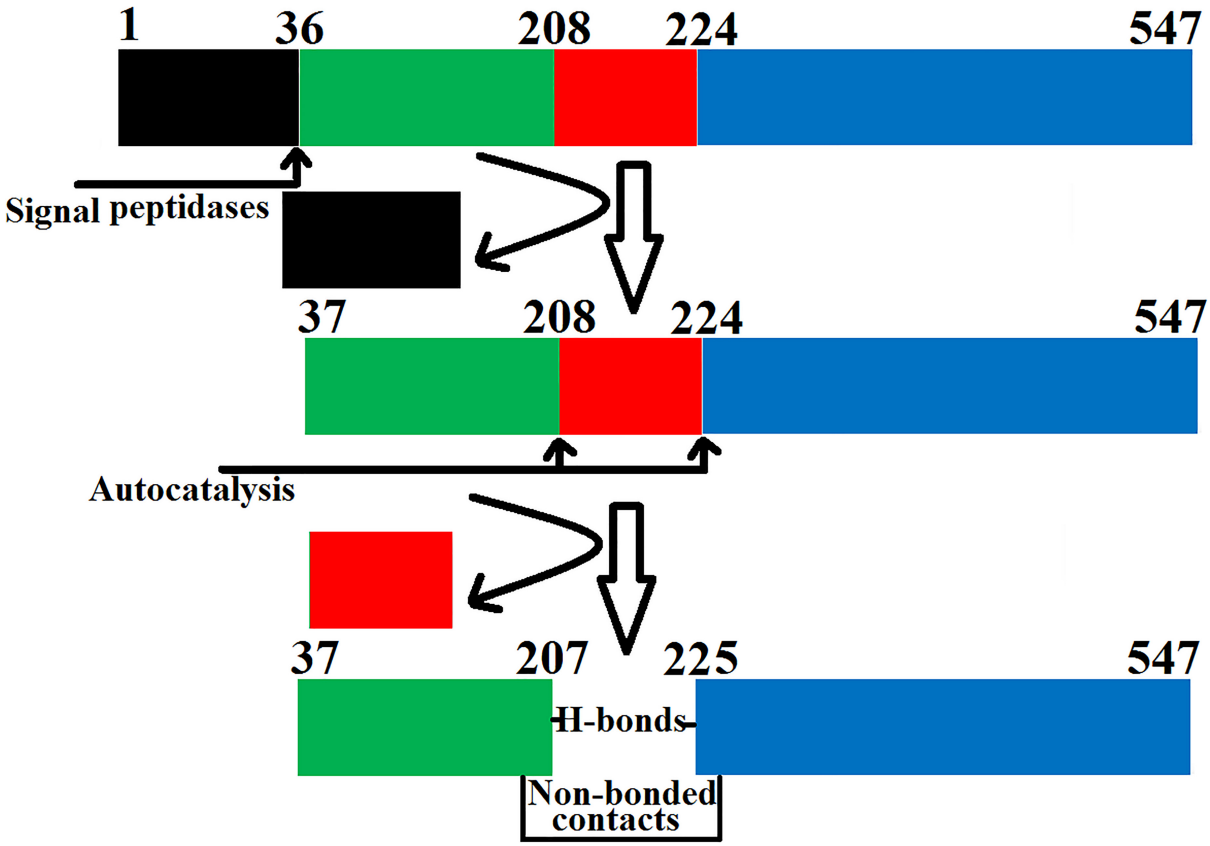

FIGURE 5 | Steps involved in the maturation of phospholipase B from *Bothrops moojeni* (PLB_*Bm*). The prepropeptide of PLB_*Bm* with the signal and internal peptides (colored in black and red, respectively) and the mature protein with chain A (colored in green) and chain B (colored in blue).

Prediction of Glycosylation Sites

The ScanProsite tool (De Castro et al., 2006) and NetNGlyc 1.0 Server (Gupta et al., 2004) were used to predict the putative glycosylation sites of PLB_*Bm*. All the parameters were set to default.

Disulfide Bond Prediction

The disulfide bridges in PLB_*Bm* were checked using the DiANNA webserver (Ferrè and Clote, 2006) and Dinosolve (Darden et al., 1993; DeLano, 2002; Anandakrishnan et al., 2012; Yaseen and Li, 2013; Maier et al., 2015).

Homology Model Building of PLB_*Bm*

The 3D structure model of PLB_Bm was produced using various protein modeling programs, like I-TESSER (Roy et al., 2010), the MODELLER 9v19 program (Colovos and Yeates, 1993), and the SWISS Model (Waterhouse et al., 2018). The atomic coordinates of Phospholipase B-like Protein 1 from bovine kidneys (PDB ID: 4BWC) that display 70% amino acid sequence identity with PLB_Bm were used as a template (Repo et al., 2014). The best model was carefully chosen based on the quality and validation reports produced by PROCHECK (Webb and Sali, 2016).

Molecular Dynamics Simulation

The validation of the modeled 3D structure of PLB_*Bm* was carried out through MD simulation using the programs like GROMACS (Berendsen et al., 1995), MDMoby (Hospital et al., 2012), AMBER16 (Maier et al., 2015), and MDweb (Hospital et al., 2012). The FF14SB force field (Darden et al., 1993) was used for all-atom–protein interaction. The protonation states of the amino acid side chain were determined using the web server H^{++} (Anandakrishnan et al., 2012) at pH 7.0. The system was neutralized with chloride ions, was placed in a rectangular box of TIP3P water, and extended to at least 15 Å from any protein atom. The bad contact from the modeled structure was removed by energy minimization of the system for 500 conjugate gradients steps using a constant force constraint of 15 kcal/mol.$Å^2$. The gradual heating of the system was carried out from 0 to 300 K for 250 ps with a constant atom number, volume, and temperature (NVT) ensemble. The protein was maintained with a constant force of 10 kcal/mol.$Å^2$. The equilibration step was achieved using the constant atom number, pressure, and temperature (NPT) ensemble for 500 ps. The simulation was carried out for 100 ns with a 4-fs time step. The pressure and temperature were kept constant at 1 atm and 300 K, respectively, by Langevin coupling. The particle-mesh Ewald (PME) method (Darden et al., 1993) was used to compute the long-range electrostatic

interactions by keeping the cutoff distance of 10 Å to Van der Waals interactions.

Model Validation

The PROCHECK software (Laskowski et al., 1993, 2001), ERRAT version 2.0 (Colovos and Yeates, 1993), and Verify 3D (Bowie et al., 1991; Lüthy et al., 1992) were used for validation of the built 3D model of PLB_*Bm*.

Structure Superimposition

The PyMOL molecular graphics visualization program (DeLano, 2002) was used to align the build PLB_*Bm* model to other homologous proteins from the Protein Data Bank.

Surface Charge Analysis

The PDB2PQR server program (Dolinsky et al., 2004) was used for charge and radius calculations; and the ABPS Tools from PyMOL was used for surface and charge visualization of the protein (DeLano, 2002).

DATA AVAILABILITY STATEMENT

The raw data supporting the conclusions of this article will be made available by the authors, without undue reservation, to any qualified researcher.

AUTHOR CONTRIBUTIONS

AU designed the project and reviewed the manuscript. RM drafted and thoroughly checked it. Both authors contributed to the article and approved the submitted version.

SUPPLEMENTARY MATERIAL

The Supplementary Material for this article can be found online at: https://www.frontiersin.org/articles/10.3389/fmolb.2020.00175/full#supplementary-material

REFERENCES

Aird, S. D., da Silva, N. J., Qiu, L., Villar-Briones, A., Saddi, V. A., de Campos Telles, M. P., et al. (2017). Coralsnake venomics: analyses of venom gland transcriptomes and proteomes of six Brazilian taxa. *Toxins* 9:187. doi: 10.3390/toxins9060187

Aird, S. D., Watanabe, Y., Villar-Briones, A., Roy, M. C., Terada, K., and Mikheyev, A. S. (2013). Quantitative high-throughput profiling of snake venom gland transcriptomes and proteomes (*Ovophis okinavensis* and *Protobothrops flavoviridis*). *BMC Genomics* 14:790. doi: 10.1186/1471-2164-14-790

Amorim, F. G., Morandi-Filho, R., Fujimura, P. T., Ueira-Vieira, C., and Sampaio, S. V. (2017). New findings from the first transcriptome of the *Bothrops moojeni* snake venom gland. *Toxicon* 140, 105–117. doi: 10.1016/j.toxicon.2017.10.025

Anandakrishnan, R., Aguilar, B., and Onufriev, A. V. (2012). H++ 3.0: automating pK prediction and the preparation of biomolecular structures for atomistic molecular modeling and simulation. *Nucleic Acids Res.* 40, W537–W541.

Bendtsen, J. D., Nielsen, H., von Heijne, G., and Brunak, S. (2004). Improved prediction of signal peptides: signalP 3.0. *J. Mol. Biol.* 340, 783–795. doi: 10.1016/j.jmb.2004.05.028

Berendsen, H. J. C., van der Spoel, D., and van Drunen, R. (1995). GROMACS: a message-passing parallel molecular dynamics implementation. *Comput. Phys. Commun.* 91, 43–56. doi: 10.1016/0010-4655(95)00042-e

Bernheimer, A. W., Linder, R., Weinstein, S. A., and Kim, K. S. (1987). Isolation and characterization of a phospholipase B from venom of Collett's snake, *Pseudechis colletti*. *Toxicon* 25, 547–554. doi: 10.1016/0041-0101(87)90290-x

Bernheimer, A. W., Weinstein, S. A., and Linder, R. (1986). Isoelectric analysis of some Australian elapid snake venoms with special reference to phospholipase B and hemolysis. *Toxicon* 24, 841–849. doi: 10.1016/0041-0101(86)90109-1

Bowie, J., Luthy, R., and Eisenberg, D. (1991). A method to identify protein sequences that fold into a known three-dimensional structure. *Science* 253, 164–170. doi: 10.1126/science.1853201

Carugo, O. (2018). How large B-factors can be in protein crystal structures. *BMC Bioinformatics* 19:61. doi: 10.1186/s12859-018-2083-8

Case, D. A., Cheatham, T. E., Darden, T., Gohlke, H., Luo, R., Merz, K. M., et al. (2005). The Amber biomolecular simulation programs. *J. Computat. Chem.* 26, 1668–1688. doi: 10.1002/jcc.20290

Chapeaurouge, A., Reza, M. A., Mackessy, S. P., Carvalho, P. C., Valente, R. H., Teixeira-Ferreira, A., et al. (2015). Interrogating the venom of the viperid snake sistrurus catenatus edwardsii by a combined approach of electrospray and MALDI mass spectrometry. *PLoS One.* 10:e0092091. doi: 10.1371/journal.pone.0092091

Chatrath, S. T., Chapeaurouge, A., Lin, Q., Lim, T. K., Dunstan, N., Mirtschin, P., et al. (2011). Identification of novel proteins from the venom of a cryptic snake *Drysdalia coronoides* by a combined transcriptomics and proteomics approach. *J. Proteome Res.* 10, 739–750. doi: 10.1021/pr1008916

Colovos, C., and Yeates, T. O. (1993). Verification of protein structures: patterns of nonbonded atomic interactions. *Protein Sci.* 2, 1511–1519. doi: 10.1002/pro.5560020916

Contardi, A., and Ercoli, A. (1933). Enzymatic cleavage of lecithin and lyso-lecithin. *Biochem. Z.* 261:275–302.

Crooks, G. E., Hon, G., Chandonia, J. M., and Brenner, S. E. (2004). WebLogo: a sequence logo generator. *Genome Res.* 14, 1188–1190. doi: 10.1101/gr.849004

Darden, T., York, D., and Pedersen, L. (1993). Particle mesh Ewald: an N log (N) method for Ewald sums in large systems. *J. Chem. Phys.* 98, 10089–10092. doi: 10.1063/1.464397

De Castro, E., Sigrist, C. J. A., Gattiker, A., Bulliard, V., Langendijk-Genevaux, P. S., Gasteiger, E., et al. (2006). ScanProsite: detection of PROSITE signature matches and ProRule-associated functional and structural residues in proteins. *Nucleic Acids Res.* 34, W362–W365.

DeLano, W. L. (2002). *The PyMOL Molecular Graphics System*. San Carlos, CA: DeLano Scientific.

Doery, H. M., and Pearson, J. E. (1964). Phospholipase B in snake venoms and bee venom. *Biochem. J.* 92, 599–602. doi: 10.1042/bj0920599

Dolinsky, T. J., Nielsen, J. E., McCammon, J. A., and Baker, N. A. (2004). PDB2PQR: expanding and upgrading automated preparation of biomolecular structures for molecular simulations. *Nucleic Acids Res.* 32, W665–W667.

Fairbairn, D. (1948). The preparation and properties of a lysophospholipase from *Penicillium notatum*. *J. Biol. Chem.* 173, 705–714.

Ferrè, F., and Clote, P. (2006). DiANNA 1.1: an extension of the DiANNA web server for ternary cysteine classification. *Nucleic Acids Res.* 34(Suppl. 2), W182–W185.

Gasteiger, E., Hoogland, C., Gattiker, A., Duvaud, S., Wilkins, M. R., Appel, R. D., et al. (2005). "Protein identification and analysis tools on the ExPASy server," in *The Proteomics Protocols Handbook*, ed. J. M. Walker (Totowa, NJ: Humana Press), 571–607. doi: 10.1385/1-59259-890-0:571

Gupta, R., Jung, E., and Brunak, S. (2004). *Prediction of N-glycosylation Sites in Human Proteins*. Available online: http://www.cbs.dtu.dk/services/NetNGlyc/ (accessed December 2, 2019).

Hospital, A., Andrio, P., Fenollosa, C., Cicin-Sain, D., Orozco, M., and Gelpí, J. L. (2012). MDWeb and MDMoby: an integrated web-based platform for molecular dynamics simulations. *Bioinformatics* 28, 1278–1279. doi: 10.1093/bioinformatics/bts139

Jiménez-Charris, E., Montealegre-Sanchez, L., Solano-Redondo, L., Mora-Obando, D., Camacho, E., Castro-Herrera, F., et al. (2015). Proteomic and functional analyses of the venom of *Porthidium lansbergii lansbergii* (Lansberg's hognose viper) from the atlantic department of Colombia. *J. Proteomics* 114, 287–299. doi: 10.1016/j.jprot.2014.11.016

Jones, B. K., Saviola, A. J., Reilly, S. B., Stubbs, A. L., Arida, E., Iskandar, D. T., et al. (2019). Venom composition in a phenotypically variable pit viper (*Trimeresurus insularis*) across the Lesser Sunda Archipelago. *J. Proteome. Res.* 18, 2206–2220. doi: 10.1021/acs.jproteome.9b00077

Khan, M. A., and Hodgson, E. (1967). Phospholipase activity in *Musca domestica* L. *Comp. Biochem. Physiol.* 23, 899–910. doi: 10.1016/0010-406x(67)90350-7

Kovalchuk, S. I., Ziganshin, R. H., Starkov, V. G., Tsetlin, V. I., and Utkin, Y. N. (2016). Quantitative proteomic analysis of venoms from russian vipers of pelias group: phospholipases A2 are the main venom components. *Toxins* 8:105. doi: 10.3390/toxins8040105

Lakomek, K., Dickmanns, A., Kettwig, M., Urlaub, H., Ficner, R., and Luebke, T. (2009). Initial insight into the function of the lysosomal 66.3 kDa protein from mouse by means of X-ray crystallography. *BMC Struct. Biol.* 9:56. doi: 10.1186/1472-6807-9-56

Laskowski, R. A., MacArthur, M. W., Moss, D. S., and Thornton, J. M. (1993). PROCHECK: a program to check the stereochemical quality of protein structures. *J. Appl. Crystallogr.* 26, 283–291. doi: 10.1107/s0021889892009944

Laskowski, R. A., MacArthur, M. W., and Thornton, J. M. (2001). "PROCHECK: validation of protein structure coordinates," in *International Tables of Crystallography: Volume F: Crystallography of Biological Macromolecules*, eds M. G. Rossmann and E. Arnold (Dordrecht: Kluwer Academic Publishers), 722–725.

Sousa, L. F., Nicolau, C. A., Peixoto, P. S., Bernardoni, J. L., Oliveira, S. S., Portes-Junior, J. A., et al. (2013). Comparison of phylogeny, venom composition and neutralization by antivenom in diverse species of bothrops complex. *PLoS Negl. Trop. Dis.* 7:e2442. doi: 10.1371/journal.pntd.0002442

Lovell, S. C., Davis, I. W., Arendall, W. B., de Bakker, P. I. W., Word, J. M., Prisant, M. G., et al. (2003). Structure validation by Calpha geometry: phi,psi and C beta deviation. *Proteins* 50, 437–450.

Lüthy, R., Bowie, J. U., and Eisenberg, D. (1992). Assessment of protein models with three-dimensional profiles. *Nature* 356, 83–85. doi: 10.1038/356083a0

Maier, J. A., Martinez, C., Kasavajhala, K., Wickstrom, L., Hauser, K. E., and Simmerling, C. (2015). ff14SB: improving the accuracy of protein side chain and backbone parameters from ff99SB. *J. Chem. Theory Comput.* 11, 3696–3713. doi: 10.1021/acs.jctc.5b00255

Marcon, F., Purtell, L., Santos, J., Hains, P. G., Escoubas, P., Graudins, A., et al. (2013). Characterization of monomeric and multimeric snake neurotoxins and other bioactive proteins from the venom of the lethal Australian common copperhead (*Austrelaps superbus*). *Biochem. Pharmacol.* 85, 1555–1573. doi: 10.1016/j.bcp.2013.02.034

Margres, M. J., Aronow, K., Loyacano, J., and Rokyta, D. R. (2013). The venom-gland transcriptome of the eastern coral snake (*Micrurus fulvius*) reveals high venom complexity in the intragenomic evolution of venoms. *BMC Genomics.* 14:531. doi: 10.1186/1471-2164-14-531

Matsumoto, Y., Mineta, S., Murayama, K., and Sugimori, D. (2013). A novel phospholipase B from *Streptomyces* sp. NA684–purification, characterization, gene cloning, extracellular production and prediction of the catalytic residues. *FEBS J.* 280, 3780–3796. doi: 10.1111/febs.12366

Méndez, R., Bonilla, F., Sasa, M., Dwyer, Q., Fernández, J., and Lomonte, B. (2019). Proteomic profiling, functional characterization, and immunoneutralization of the venom of *Porthidium porrasi*, a pitviper endemic to Costa Rica. *Acta Trop.* 193, 113–123. doi: 10.1016/j.actatropica.2019.02.030

Mohamed, A. H., Kamel, A., and Ayobe, M. H. (1969). Studies of phospholipase A and B activities of Egyptian snake venoms and a scorpion toxin. *Toxicon* 6, 293–298. doi: 10.1016/0041-0101(69)90099-3

Morgan, C. P., Insall, R., Haynes, L., and Cockcroft, S. (2004). Identification of phospholipase B from Dictyostelium discoideum reveals a new lipase family present in mammals, flies and nematodes, but not yeast. *Biochem. J.* 382(Pt 2), 441–449. doi: 10.1042/bj20040110

Oinonen, C., and Rouvinen, J. (2000). Structural comparison of Ntn-hydrolases. *Protein Sci.* 9, 2329–2337. doi: 10.1110/ps.9.12.2329

Oliveira, I. S., Cardoso, I. A., Bordon, K. C. F., Carone, S. E. I., Boldrini-França, J., Berto Pucca, M., et al. (2019). Global proteomic and functional analysis of *Crotalus durissus* collilineatus individual venom variation and its impact on envenoming. *J. Proteomics.* 191, 153–165. doi: 10.1016/j.jprot.2018.02.020

Paetzel, M., Karla, A., Strynadka, N. C., and Dalbey, R. E. (2002). Signal peptidases. *Chem Rev.* 102, 4549–4580.

Patra, A., Kalita, B., Chanda, A., and Mukherjee, A. K. (2017). Proteomics and antivenomics of *Echis carinatus carinatus* venom: correlation with pharmacological properties and pathophysiology of envenomation. *Sci. Rep.* 7:17119.

Rao, R. H., and Subrahmanyam, D. (1969). Characterization of phospholipase B of Culex pipiens fatigans. *J. Lipid Res.* 10, 636–641.

Repo, H., Kuokkanen, E., Oksanen, E., Goldman, A., and Heikinheimo, P. (2014). Is the bovine lysosomal phospholipase B-like protein an amidase? *Proteins* 82, 300–311. doi: 10.1002/prot.24388

Rokyta, D. R., Wray, K. P., Lemmon, A. R., Lemmon, E. M., and Caudle, S. B. (2011). A high-throughput venom-gland transcriptome for the eastern diamondback rattlesnake (*Crotalus Adamanteus*) and evidence for pervasive positive selection across toxin classes. *Toxicon* 57, 657–671. doi: 10.1016/j.toxicon.2011.01.008

Roy, A., Kucukural, A., and Zhang, Y. (2010). I-TASSER: a unified platform for automated protein structure and function prediction. *Nat. Protoc.* 5, 725–738. doi: 10.1038/nprot.2010.5

Saito, K. (2014). Reminiscence of phospholipase B in *Penicillium notatum*. *Proc. Jpn. Acad. Ser. B Phys. Biol. Sci.* 90, 333–346. doi: 10.2183/pjab.90.333

Salomon-Ferrer, R., Case, D. A., and Walker, R. C. (2013). An overview of the Amber biomolecular simulation package. *WIREs Comput. Mol. Sci.* 3, 198–210. doi: 10.1002/wcms.1121

Schneider, T. D., and Stephens, R. M. (1990). Sequence logos: a new way to display consensus sequences. *Nucleic Acids Res.* 18, 6097–6100. doi: 10.1093/nar/18.20.6097

Shiloah, J., Klibansky, C., de Vries, A., and Berger, A. (1973). Phospholipase B activity of a purified phospholipase A from *Vipera palestinae* venom. *J. Lipid. Res.* 14, 267–278.

Takasaki, C., and Tamiya, N. (1982). Isolation and properties of lysophospholipases from the venom of an Australian elapid snake, *Pseudechis australis*. *Biochem. J.* 203, 269–276. doi: 10.1042/bj2030269

Tan, K. Y., Tan, C. H., Chanhome, L., and Tan, N. H. (2017). Comparative venom gland transcriptomics of *Naja kaouthia* (monocled cobra) from Malaysia and Thailand: elucidating geographical venom variation and insights into sequence novelty. *PeerJ* 5:e3142. doi: 10.7717/peerj.3142

Tang, E. L., Tan, C. H., Fung, S. Y., and Tan, N. H. (2016). Venomics of *Calloselasma rhodostoma*, the Malayan pit viper: a complex toxin arsenal unraveled. *J. Proteomics* 148, 44–56. doi: 10.1016/j.jprot.2016.07.006

Tang, E. L. H., Tan, N. H., Fung, S. Y., and Tan, C. H. (2019). Comparative proteomes, immunoreactivities and neutralization of procoagulant activities of *Calloselasma rhodostoma* (Malayan pit viper) venoms from four regions in Southeast Asia. *Toxicon* 169, 91–102. doi: 10.1016/j.toxicon.2019.08.004

Ullah, A. (2020). Structure-function studies and mechanism of action of snake venom L-Amino acid oxidases. *Front. Pharmacol.* 11:110. doi: 10.3389/fphar.2020.00110

Ullah, A., Masood, R., Ali, I., Ullah, K., Ali, H., Akbar, H., et al. (2018). Thrombin-like enzymes from snake venom: Structural characterization and mechanism of action. *Int. J. Biol. Macromol.* 114, 788–811.

Ullah, A., Masood, R., Hayat, Z., and Hafeez, A. (2020). Determining the structures of the snake and spider toxins by x-rays. *Methods Mol. Biol.* 2068, 163–172. doi: 10.1007/978-1-4939-9845-6_8

Ullah, A., Ullah, K., Ali, H., Betzel, C., and Ur Rehman, S. (2019). The sequence and a three-dimensional structural analysis reveal substrate specificity among snake venom phosphodiesterases. *Toxins (Basel).* 11:625. doi: 10.3390/toxins11110625

Vanuopadath, M., Sajeev, N., Murali, A. R., Sudish, N., Kangosseri, N., Sebastian, I. R., et al. (2018). Mass spectrometry-assisted venom profiling of Hypnale hypnale found in the Western Ghats of India incorporating de novo sequencing approaches. *Int. J. Biol. Macromol.* 118(Pt B), 1736–1746. doi: 10.1016/j.ijbiomac.2018.07.016

Verma, S., Dixit, R., and Pandey, K. C. (2016). Cysteine proteases: modes of activation and future prospects as pharmacological targets. *Front. Pharmacol.* 7:107. doi: 10.3389/fphar.2016.00107

Viala, V. L., Hildebrand, D., Trusch, M., Arni, R. K., Pimenta, D. C., Schlüter, H., et al. (2014). Pseudechis guttatus venom proteome: insights into evolution and toxin clustering. *J. Proteomics* 110, 32–44. doi: 10.1016/j.jprot.2014.07.030

Wang, Y., Wang, J., Li, R., Shi, Q., Xue, Z., and Zhang, Y. (2017). ThreaDomEx: a unified platform for predicting continuous and discontinuous protein domains by multiple-threading and segment assembly. *Nucleic Acids Res.* 45, W400–W407.

Wass, M. N., Kelley, L. A., and Sternberg, M. J. (2010). 3DLigandSite: predicting ligand-binding sites using similar structures. *Nucleic Acids Res.* 38, W469–W473.

Waterhouse, A., Bertoni, M., Bienert, S., Studer, G., Tauriello, G., Gumienny, R., et al. (2018). SWISS-MODEL: homology modelling of protein structures and complexes. *Nucleic Acids Res.* 46, W296–W303.

Webb, B., and Sali, A. (2016). Comparative protein structure modeling using modeller. *Curr. Protoc. Protein Sci.* 86, 2.9.1–2.9.37.

Wiezel, G. A., dos Santos, P. K., Cordeiro, F. A., Bordon, K. C., Selistre-de-Araújo, H. S., Ueberheide, B., et al. (2015). Identification of hyaluronidase and phospholipase B in Lachesis muta rhombeata venom. *Toxicon* 107(Pt B), 359–368. doi: 10.1016/j.toxicon.2015.08.029

Xue, Z., Xu, D., Wang, Y., and Zhang, Y. (2013). ThreaDom: extracting protein domain boundary information from multiple threading alignments. *Bioinformatics* 29, i247–i256. doi: 10.1093/bioinformatics/btt209

Yaseen, A., and Li, Y. (2013). Dinosolve: a protein disulfide bonding prediction server using context-based features to enhance prediction accuracy. *BMC Bioinform.* 14:S9. doi: 10.1186/1471-2105-14-S13-S9

Zainal Abidin, S. A., Rajadurai, P., Chowdhury, M. E., Ahmad Rusmili, M. R., Othman, I., and Naidu, R. (2016). Proteomic characterization and comparison of Malaysian *Tropidolaemus wagleri* and *Cryptelytrops purpureomaculatus* venom using shotgun-proteomics. *Toxins* 8:E299.

Conflict of Interest: The authors declare that the research was conducted in the absence of any commercial or financial relationships that could be construed as a potential conflict of interest.

frontiers in Pharmacology

BRIEF RESEARCH REPORT
published: 12 August 2020
doi: 10.3389/fphar.2020.01204

Human α-Defensin-5 Efficiently Neutralizes *Clostridioides difficile* Toxins TcdA, TcdB, and CDT

Michael Korbmacher[1†], *Stephan Fischer*[1*†], *Marc Landenberger*[1], *Panagiotis Papatheodorou*[1], *Klaus Aktories*[2] *and Holger Barth*[1*]

[1] Institute of Pharmacology and Toxicology, University of Ulm Medical Center, Ulm, Germany, [2] Institute of Experimental and Clinical Pharmacology and Toxicology, University of Freiburg, Freiburg, Germany

Infections with the pathogenic bacterium *Clostridioides (C.) difficile* are coming more into focus, in particular in hospitalized patients after antibiotic treatment. *C. difficile* produces the exotoxins TcdA and TcdB. Since some years, hypervirulent strains are described, which produce in addition the binary actin ADP-ribosylating toxin CDT. These strains are associated with more severe clinical presentations and increased morbidity and frequency. Once in the cytosol of their target cells, the catalytic domains of TcdA and TcdB glucosylate and thereby inactivate small Rho-GTPases whereas the enzyme subunit of CDT ADP-ribosylates G-actin. Thus, enzymatic activity of the toxins leads to destruction of the cytoskeleton and breakdown of the epidermal gut barrier integrity. This causes clinical symptoms ranging from mild diarrhea to life-threatening pseudomembranous colitis. Therefore, pharmacological inhibition of the secreted toxins is of peculiar medical interest. Here, we investigated the neutralizing effect of the human antimicrobial peptide α-defensin-5 toward TcdA, TcdB, and CDT in human cells. The toxin-neutralizing effects of α-defensin-5 toward TcdA, TcdB, and CDT as well as their medically relevant combination were demonstrated by analyzing toxins-induced changes in cell morphology, intracellular substrate modification, and decrease of trans-epithelial electrical resistance. For TcdA, the underlying mode of inhibition is most likely based on the formation of inactive toxin-defensin-aggregates whereas for CDT, the binding- and transport-component might be influenced. The application of α-defensin-5 delayed intoxication of cells in a time- and concentration-dependent manner. Due to its effect on the toxins, α-defensin-5 should be considered as a candidate to treat severe *C. difficile*–associated diseases.

Keywords: *C. difficile* infection, large clostridial glucosylating toxins, binary actin ADP-ribosylating toxin, toxin inhibitor, AB-type protein toxins

OPEN ACCESS

Edited by:
Jean-Marc Sabatier, Aix-Marseille Université, France

Reviewed by:
Oscar Moran, Italian National Research Council, Italy
Harald Genth, Hannover Medical School, Germany

***Correspondence:**
Stephan Fischer
stephan-1.fischer@uni-ulm.de
Holger Barth
holger.barth@uni-ulm.de

[†]These authors have contributed equally to this work

Specialty section:
This article was submitted to Pharmacology of Ion Channels and Channelopathies, a section of the journal Frontiers in Pharmacology

Received: *25 March 2020*
Accepted: *23 July 2020*
Published: *12 August 2020*

Citation:
Korbmacher M, Fischer S, Landenberger M, Papatheodorou P, Aktories K and Barth H (2020) Human α-Defensin-5 Efficiently Neutralizes Clostridioides difficile Toxins TcdA, TcdB, and CDT. Front. Pharmacol. 11:1204. doi: 10.3389/fphar.2020.01204

INTRODUCTION

Bacterial AB-type protein toxins belong to the most toxic substances in nature and are able to cause a broad variety of severe diseases in humans and animals. The extraordinary potency of bacterial toxins is based on their inimitable structures harboring enzyme activities and their highly sophisticated uptake mechanisms (Schiavo and van der Goot, 2001; Uptake and Trafficking of

Protein Toxins | Holger Barth | Springer). The toxins serve as important virulence factors, which are directly linked to the clinical symptoms of human diseases as for example diphtheria, anthrax or other severe enteric complications such as medically relevant *Clostridioides* (*C.*, formerly *Clostridium*) *difficile*–associated diseases, in particular diarrhea (CDAD). Especially *C. difficile* infection (CDI) remains a remarkable challenge for affected patients and global health care systems. The characteristic symptoms for CDI range from mild and watery diarrhea up to severe forms of pseudomembranous or fulminant colitis which may ultimately end in multi-organ failure (Spencer, 1998; Goudarzi et al., 2014). In addition to the patients suffering, CDIs also remain a high economic burden. In England, the costs for CDIs have been estimated at €5000 - €15000 per case (Kuijper et al., 2006) accompanied with an increased length of stay in hospital (van Kleef et al., 2014; Wilcox et al., 2017).

The gram-positive, spore-forming anaerobic bacterium *C. difficile* is an important nosocomial gastrointestinal human gut pathogen. The incidence and severity of CDIs have dramatically increased over the last decade. This is mainly attributed to the emergence of new hypervirulent strains. First and foremost, the epidemically occurring *C. difficile* PCR ribotype O27 strain gained more and more attention. This strain is characterized by its comprehensive occurrence in Canada, the USA and continental Europe (Pépin et al., 2004; Pépin et al., 2005; Kuijper et al., 2008) and due to its higher morbidity and mortality mainly caused by the presence of the three proteinaceous AB-type toxins TcdA, TcdB, and CDT (Kuehne et al., 2014). In fact, not the bacterium itself is responsible for the development of clinical disease presentations but rather the produced and secreted AB-type protein toxins. They are responsible for epithelial breakdown of the gut barrier integrity resulting in severe enterotoxicity (Carter et al., 2012; Carter et al., 2015). The main causative determinants of *C. difficile* are the two large single-chain AB-type toxins TcdA and TcdB (Aktories, 2011). They alone are sufficient to develop the full disease pattern (Kuehne et al., 2010; Kuehne et al., 2014). TcdA and TcdB exhibit a high sequence homology and share the same multidomain architecture (von Eichel-Streiber et al., 1992; Jank and Aktories, 2008). However, hypervirulent *C. difficile* strains are able to produce in addition to TcdA and TcdB a third toxin, the binary toxin CDT (*C. difficile* transferase). CDT is a bipartite toxin and is comprised of the enzymatic active component CDTa and the binding- and translocation-component CDTb. CDTb is able to form heptamers to which one single CDTa-molecule can bind (Sheedlo et al., 2020). Although CDT differs in structure and function, all three toxins share some important similarities (Papatheodorou et al., 2018). They are secreted from the bacteria and enter their human target cells *via* receptor-mediated endocytosis. In acidified endosomes, their conformation changes and their catalytic domains are released into the host cell cytosol where they modify their specific intracellular target proteins. TcdA and TcdB glucosylate and thereby inactivate small GTPases of the Rho and Ras families of monomeric GTPases (Just et al., 1995a; Just et al., 1995b; Just et al., 1996) that cause colonic tissue damage by distinct mechanisms (Chumbler et al., 2016), whereas CDT acts as an ADP-ribosyltransferase modifying monomeric G-actin (Perelle et al., 1997; Gülke et al., 2001). Intracellular substrate modification leads to depolymerization of the actin cytoskeleton, and thus to cell rounding and breakdown of the intestinal gut barrier integrity. Therapy of CDI is challenging because an effective antibiotic treatment is mostly limited to broad-spectrum antibiotics such as metronidazole, vancomycin, or the newer anti-CDI drug fidaxomicin (Debast et al., 2014), as first-line treatment (Louie et al., 2011; Tart, 2013). Indeed, application of antibiotics might eventually result in further disturbance of the gut microbiota increasing the risk of recurrent CDIs.

Therefore, novel therapeutic approaches to treat CDI preferentially based on the inactivation of the produced and secreted toxins are urgently needed. In this context, antimicrobial peptides (AMPs) and in particular human defensins play an elevated role. Defensins are small and cationic peptides linked *via* three intra-molecular disulfide bridges (Ganz and Lehrer, 1994; Kagan et al., 1994). In addition to mere microbicidal activity, inactivation and neutralization of several bacterial toxins were reported (Kim et al., 2005; Kim et al., 2006; Giesemann et al., 2008; Lehrer et al., 2009). Especially for α-defensins, an inhibitory potency against several bacterial toxins was reported earlier (Kim et al., 2005; Kim et al., 2006; Giesemann et al., 2008; Fischer et al., 2018; Fischer et al., 2020). Based on these findings, we investigated the effect of the human antimicrobial peptide α-defensin-5 as inhibitor of the *C. difficile* toxins TcdA, TcdB, and CDT and in particular as inhibitor of the medically most relevant combination of all three toxins.

MATERIALS AND METHODS

Protein Expression, Purification, and Used Inhibitor

The recombinant protein toxins used in this work were expressed and purified as described in earlier publications (Schwan et al., 2009; Papatheodorou et al., 2010; Schwan et al., 2011). Native TcdA was purified as described (Giesemann et al., 2008). α-Defensin-5 was purchased from PeptaNova (Sandhausen, Germany) and dissolved as described by the manufacturer.

Cell Culture and Cytotoxicity Experiments

Vero and Caco-2 cells were cultivated in culture dishes at 37°C and 5% CO_2. For cultivation, cells were maintained in their respective media (Vero cells: Minimum Essential Media (MEM) containing 10% fetal calf serum (FCS), 1 mM sodium pyruvate, 2 mM L-glutamine, 0.1 mM non-essential amino acids (NEAA), 10 g/L penicillin/streptomycin; Caco-2 cells: Dulbecco's Modified Eagle's Medium (DMEM) containing 10% FCS, 1 mM sodium pyruvate, 0.1 mM NEAA, 10 g/L penicillin/streptomycin) and split three times a week at a confluency of 80% to 100%. For cytotoxicity experiments, cells were seeded into different well plates ranging from 96- to 8-well cell culture plates and grown for at least 1 day. After reaching the requested density, the cells were treated with the respective toxins in serum-free medium. After defined time points,

pictures were taken using an Axiovert 40CFl microscope from Zeiss connected to a ProgRes C10 CCD camera from Jenoptik to monitor the intoxication process. Cell pictures were processed using the ImageJ software (Schneider et al., 2012; Rueden et al., 2017) in combination with the plug in cell_counter.jar.

Investigation of the Glucosylation Status of Rac1 in Cells After Treatment With TcdA and/or TcdB

After reaching confluency, cells were treated with either TcdA (10 pM), TcdB (10 pM) or the combination of both toxins (each 10 pM) in the presence or absence of α-defensin-5 in concentrations ranging from 1 μM to 6 μM. For control, cells were left untreated. After defined time points, the cells were thoroughly washed, lysed, and transferred to SDS-PAGE followed by Western blot. Native and thereby non-glucosylated Rac1 was detected by using an anti-Rac1-antibody (BD, Bioscience, 610650, 1:1000) combined with the respective secondary antibody (chicken-anti-mouse IgG-HRP, Santa Cruz Biotechnology, 1:2500). Comparable protein loading of the samples was confirmed *via* immunodetection of either Hsp90 (Santa Cruz Biotechnology, 1:500) or GAPDH (Santa Cruz Biotechnology, 1:1000).

Sequential ADP-Ribosylation of Actin in Lysates of CDT-Treated Cells

After reaching confluency, cells were treated with CDT (CDTa/CDTb: 1 nM/1.3 nM) in the presence or absence of α-defensin-5 (1, 3, or 6 μM). For control, cells were left untreated. After 4.5 h, cells were washed and scraped off in 50 μl of ADP-ribosylation-buffer containing 1 mM DTT, 5 mM $MgCl_2$ and 1 mM EDTA, 20 mM Tris-HCl pH 7.5 plus cOmplete™ protease inhibitor cocktail (Roche, Germany). After lysis, 20 μl of the cell lysate was incubated with 10 μM biotinylated NAD^+ (Trevigen, USA) in the presence of 50 ng freshly added CDTa for 30 min at 37°C. After adding SDS sample buffer and inactivation for 10 min at 95°C, samples were analyzed by Western blotting. Biotin-labeled, i.e., ADP-ribosylated actin was detected with a peroxidase-coupled streptavidin (Sigma-Aldrich, USA, 1:2500). To ensure comparable protein loading, GAPDH was detected as described above.

In Vitro Glucosylation of Rac1 by TcdA and *In Vitro* ADP-Ribosylation of Actin by CDTa

For investigation of the *in vitro* glucosylation of Rac1, 40 μg of Caco-2 whole cell lysate was incubated with 300 ng TcdA for 1 h at 37°C in the presence of increasing concentration of α-defensin-5 (6, 12, or 24 μM). For control, cell lysate was either left untreated or incubated with TcdA alone. After heat inactivation, samples were transferred to SDS-PAGE followed by Rac1 immunoblotting. For investigation of the *in vitro* ADP-ribosylation of actin, 40 μg of whole Caco-2 lysate was incubated with 1 ng CDTa for 30 min at 37°C with 10 μM biotinylated NAD^+ and with increasing concentrations of α-defensin-5 (1 μM, 3 μM, and 6 μM). For control, cell lysate was supplemented with 10 μM biotinylated NAD^+, with CDTa of was left untreated. Biotin-labeled, i.e. ADP-ribosylated actin was detected as mentioned above.

Fluorescence Microscopy

Caco-2 cells were seeded in 8-well μ-slide chambers from ibidi (Gräfelfing, Germany) and incubated for 2 days at 37°C until reaching confluency. Afterward, cells were treated with either the combination of TcdA/TcdB (each 10 pM), CDT (2 nM/2.7 nM), or the combination of all three toxins together (TcdA: 10 pM, TcdB: 10 pM, CDT: 2 nM/2.7 nM) in the presence or absence of α-defensin-5 (6 μM). After indicated time intervals of incubation, cells were washed carefully two times with PBS and fixed using 4% paraformaldehyde (PFA) for 20 min at room temperature (RT). After permeabilization with Triton-X 100 (0.4% in PBS) for 5 min and treatment with 100 mM glycine for 2 min at RT, cells were incubated with 5% skim milk powder for 30 min at 37°C. Non-glucosylated Rac1 was stained with a mouse anti-Rac1 antibody (BD Bioscience, 1:100) in combination with a fluorescent labeled secondary antibody (goat-anti-mouse-568, Invitrogen, USA, 1:750). Actin was stained using phalloidin-FITC (Sigma Aldrich, 1:100) and nuclei were stained *via* Hoechst33342 (1:10000) at 37°C for 5 min. Images were taken using iMic digital microscope (FEI, Munich, Germany) and processed using ImageJ software (following wavelength settings were used: **Figure 1C**: channel 1 (Hoechst), 500/1300; channel 2 (F-actin), 600/1200; channel 3 (Rac1), 650/950. **Figure 2C**: channel 1 (Hoechst), 500/1200; channel 2 (F-actin), 520/600; channel 3 (Rac1), 1000/1000. **Figure 3B**: channel 1 (Hoechst), 500/1300; channel 2 (F-actin), 515/600; channel 3 (Rac1), 515/600).

TEER Measurements

Transepithelial electrical resistance (TEER) measurements were used to analyze the integrity of a confluent Caco-2 cell monolayer. Here, 1.2×10^5 Caco-2 cells were seeded in a 24-well hanging cell culture insert (catalogue number MCHT24H48) from Merck Millipore and incubated for 3 days at 37°C until TEER values between 2000 and 3000 Ω/cm^2 were reached. CDT (1.6 nM/2 nM) was added apically in complete growth medium in the presence or absence of α-defensin-5 (6 μM). TEER was measured using the EVOMX apparatus provided with the STX2 electrode (both WPI, USA). Blank resistance (filters only filled with culture medium) was subtracted from raw TEER values and resulting values were multiplied by the effective surface area of the membrane in the filter (here 0.3 cm^2). Additionally, the exploited values were normalized to time point zero (t0 = 100%).

Precipitation Studies With TcdA

After centrifugation at 10000 rpm for 20 min at 4°C, 1 μg of TcdA was incubated for 15 min at 37°C in 30 μl serum-free medium in the presence or absence of α-defensin-5 (6 μM). After an additional centrifugation step at 14000 rpm for 20 min at 4°C, samples were divided into a supernatant and a pellet fraction. The pellet fraction was resuspended in 30 μl MEM, and all fractions were incubated with SDS sample buffer at 95°C for 10 min. Afterward, the samples were transferred to and analyzed by SDS-PAGE.

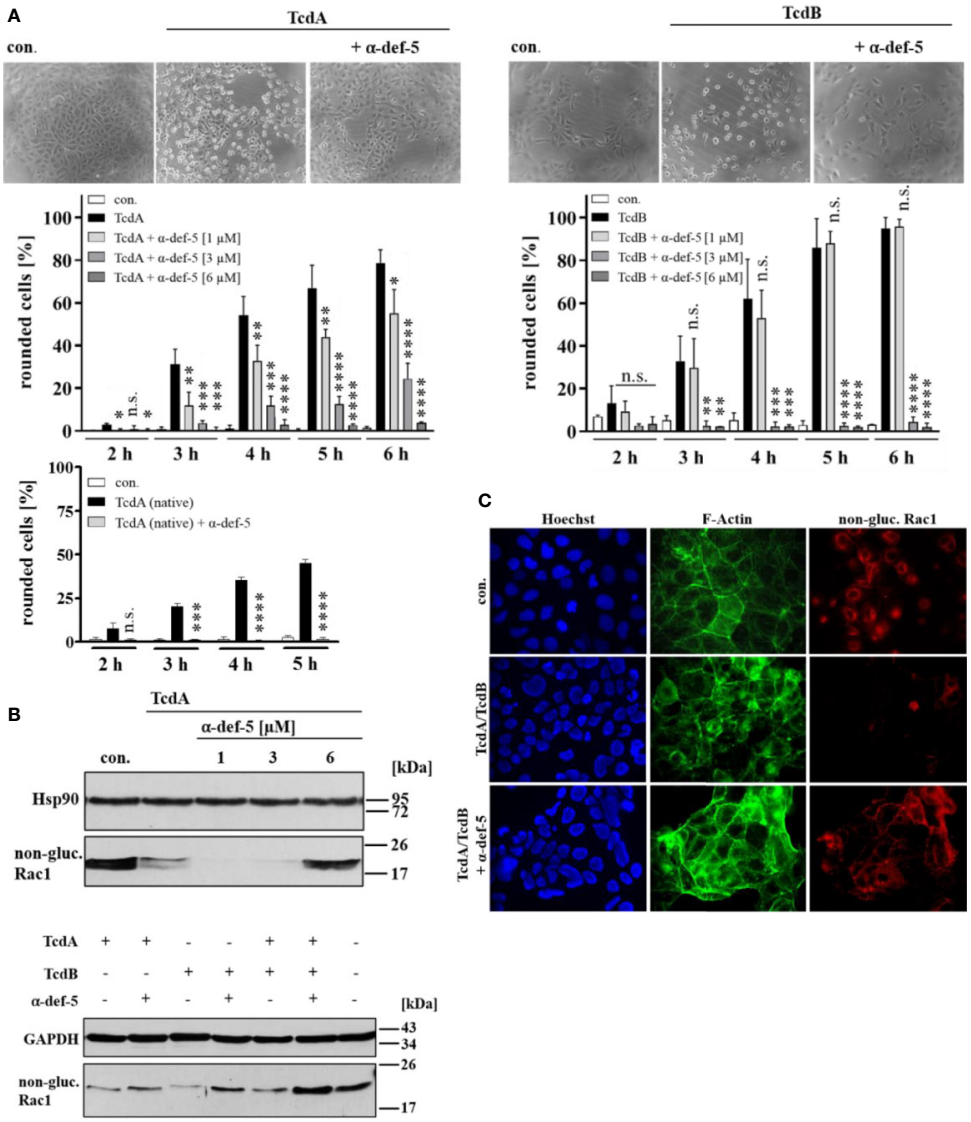

FIGURE 1 | α-Defensin-5 decreases the cytotoxic effects of TcdA, TcdB and of the combination of both toxins. **(A)** Vero cells were either treated with TcdA (10 pM, left panel) or TcdB (10 pM, right panel) in the presence or absence of increasing concentrations of α-defensin-5 (1, 3, 6 µM), and the percentage or rounded cells was determined. For comparison, Vero cells were treated with native TcdA (10 pM, left lower panel) in the presence or absence of α-defensin-5 (6 µM). Values are given as mean ± SD (n = 3). Significance was determined using the one-way ANOVA test (n.s. = not significant, *p < 0.05, **p < 0.01, ***p < 0.001, ****p < 0.0001). **(B)** Vero cells (upper panel) were treated with TcdA (10 pM) and α-defensin-5 with increasing concentrations (1, 3, 6 µM) for 3.5 h. Caco-2 cells (lower panel) were treated with either TcdA (10 pM), TcdB (10 pM) or the combination of both toxins (each 10 pM) with or without α-defensin-5 (6 µM) for 8 h. Afterward, cells were lysed and subjected to Western blot analysis. Non-glucosylated Rac1 was detected using a specific antibody. Hsp90 or GAPDH were used as controls for equal protein loading. **(C)** Caco-2 cells were treated with the combination of TcdA (10 pM) plus TcdB (10 pM) and with/without α-defensin-5 (6 µM) for 8.5 h. For control, cells were left untreated. After incubation, cells were fixed and permeabilized. Non-glucosylated Rac1 was detected using a specific anti-Rac1-antibody, F-actin was stained with phalloidin-FITC, nuclei were stained with Hoechst33342.

Calcium (Ca^{2+}) Imaging

Caco-2 cells were seeded in an 8-well µ-slide plate from ibidi (Gräfelfing, Germany) with a density of 1.5×10^5 cells per well for 2 days. Then, the cells were loaded with 3 µM of Fura-2 AM for 45 min at 37°C and afterward treated with bath solution (containing 140 mM NaCl, 5 mM KCl, 2 mM $CaCl_2$, 1 mM $MgCl_2$, 5 mM Glucose, 10 mM HEPES, pH 7.4). After three washing steps with bath solution, baseline was measured for 2 min, and cells were then treated with CDTb (13 nM) with or without α-defensin-5 (6 µM). Calcium flow was recorded using an iMic digital microscope (FEI, Munich, USA). Resulting ratio images were created with excitation light pulses at 340 and 380 nm followed by subsequent ratio calculations (340/380).

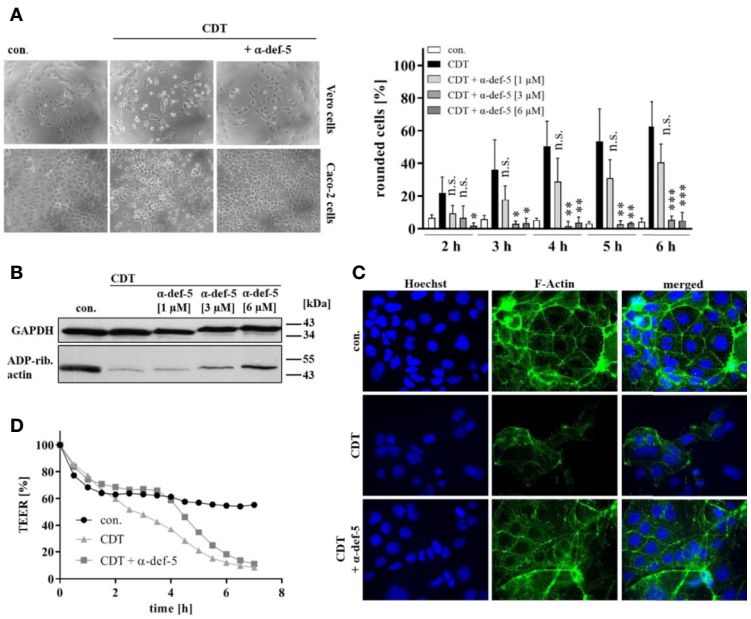

FIGURE 2 | α-Defensin-5 protects cells from intoxication with the binary toxin CDT. **(A)** Vero cells (upper left panel) were treated with CDT (1 nM/1.3 nM) and Caco-2 cells (lower left panel) were treated with CDT (4.1 nM/5.3 nM) in the presence or absence of α-defensin-5 with varying concentrations. Representative images for Vero cells (6 h) and Caco-2 cells (4.5 h) plus/minus α-defensin-5 (6 µM) are depicted. For Vero cells, the amount of rounded cells over time was determined (right panel). Values are given as mean ± SD (n = 3). Significance was determined using the one-way ANOVA test (n.s. = not significant, *p < 0.05, **p < 0.01, ***p < 0.001). **(B)** Caco-2 cells were treated for 4.5 h with CDT (4.1 nM/5.3 nM) with and without α-defensin-5 (6 µM). Afterward, cells were washed, lysed and subjected with 10 µM biotinylated NAD^+ and 50 ng fresh CDTa. Biotin-labeled, e.g. ADP-ribosylated actin was detected by immunoblotting using the ECL system. GAPDH was stained for comparable protein loading. **(C)** Caco-2 cells were treated with CDT (2 nM/2.7 nM) with or without α-defensin-5 (6 µM) for 5 h. For control, cells were left untreated. Then, cells were fixed and permeabilized. Phalloidin-FITC was used to stain F-actin, Hoechst33342 was used to stain nuclei. **(D)** Transepithelial electrical resistance was investigated using Caco-2 cells with CDT (1.6 nM/2 nM) with or without α-defensin-5 (6 µM).

RESULTS

The Human Peptide α-Defensin-5 Decreased the Cytotoxic Activities of TcdA and TcdB

First, the cytopathic effects of TcdA and TcdB under the influence of α-defensin-5 were examined in detail using the mammalian epithelial Vero cell line. After intoxication, Vero cells rapidly display a characteristic change in morphology, i.e. cell rounding, which is a traditional and well-established specific, robust, and sensitive endpoint to monitor the inhibition of bacterial protein toxins. The TcdA- and TcdB-induced changes in cell morphology (cell rounding) in the presence and absence of increasing concentrations of α-defensin-5 were quantified by cell counting. Representative images which clearly show a specific inhibition of TcdA and TcdB by α-defensin-5 are displayed (**Figure 1A**). Since the effect was surprising for TcdA, native toxin A was also tested in this case, which was also inhibited by α-defensin-5 (**Figure 1A**, left lower panel). All subsequent experiments were then performed with recombinant TcdA. In order to further strengthen the inhibitory potential of α-defensin-5 especially on TcdA, the status of Rac1 glucosylation in intoxicated cells was examined. Here, an antibody was used, that is only able to detect non-modified Rac1 from untreated cells. After intoxication and thereby glucosylation, Rac1 is no longer detected by this specific antibody (Genth et al., 2006: Egerer et al., 2007; Fischer et al., 2020). First, TcdA was investigated with increasing amounts of α-defensin-5 and a clear inhibition could be observed with the highest amount (6 µM) of the inhibitor (**Figure 1B**, upper panel). But also for TcdB and more importantly for the medically relevant combination of both toxins, a clear inhibition in the presence of α-defensin-5 could be detected (**Figure 1B**, lower panel). The results for the combination of both toxins were further confirmed *via* fluorescence microscopy (**Figure 1C**).

Human α-Defensin-5 Decreased the Cytotoxic Activity of CDT

Next, the effect of α-defensin-5 toward the binary toxin CDT was examined. First, Vero as well as human colonic Caco-2 cells were treated with CDT in the presence and absence of α-defensin-5 and a clear time- and concentration-dependent inhibition became obvious (**Figure 2A**). Especially for the higher concentrations of the peptide, the inhibition of CDT could be clearly confirmed *via* investigating the effect on actin modification in CDT-treated Caco-2 cells (**Figure 2B**). After visualization of the actin cytoskeleton *via* fluorescence microscopy, it became evident, that CDT caused a dramatic

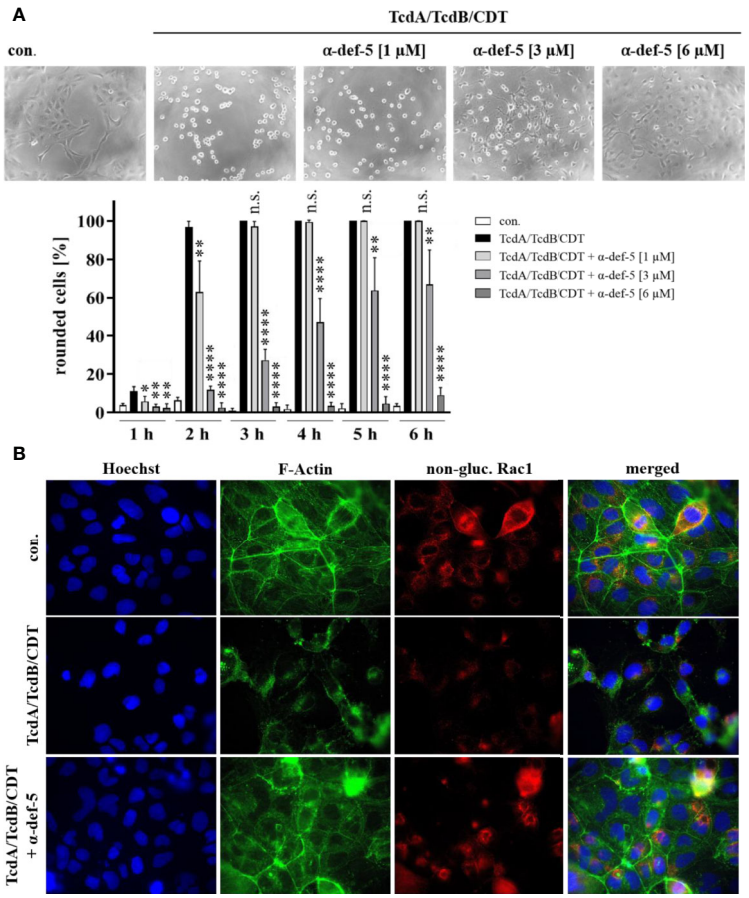

FIGURE 3 | α-Defensin-5 protects cells in a time- and concentration-dependent manner from intoxication with the combination of TcdA, TcdB, and CDT. **(A)** Vero cells were treated with the combination of all three *C. difficile* toxins (TcdA: 10 pM, TcdB: 10 pM, CDT: 1 nM/1. 3 nM) and increasing concentrations of α-defensin-5 (1, 3, 6 µM). Representative images after 6 h are shown (upper panel). The amount of rounded cells was determined over time (lower panel). Values are given as mean ± SD (n=3). Significance was determined using the one-way ANOVA test (n.s. = not significant, *p < 0.05, **p < 0.01, ****p < 0.0001). **(B)** Caco-2 cells were treated with the combination of TcdA (10 pM), TcdB (10 pM), and CDT (2 nM/2.7 nM) in the presence or absence of α-defensin-5 (6 µM). After 5.5 h, cells were fixed, permeabilized and non-glucosylated Rac1 was stained using a specific antibody. Phalloidin-FITC was used to stain F-actin, Hoechst33342 was used to stain nuclei.

disorganization of actin which is characterized by a lower actin signal in total. In the presence of α-defensin-5, the cytoskeleton was almost completely protected from CDT-catalyzed degradation (**Figure 2C**). Last, the integrity of the epithelial barrier function of confluently grown Caco-2 cells was analyzed. CDT-treatment clearly reduced TEER in the Caco-2 monolayer whereas this effect was delayed in the presence of α-defensin-5 (**Figure 2D**).

Treatment With α-Defensin-5 Protected Cells From the Combination of TcdA, TcdB, and CDT

Now, the medically relevant combination of all three *C. difficile* toxins together was examined. Especially in antibiotic-resistant hypervirulent *C. difficile* strains, the presence of all three toxins leads to a significant worsened outcome for infected patients. In the cell culture experiments the combination of all three toxins led to a very rapid rounding of Vero cells. The characteristic rounding was significantly delayed in the presence of α-defensin-5 and also for the combination, a clear time- and concentration-dependent inhibition became evident (**Figure 3A**). To confirm the results obtained so far and to directly visualize effects of the combination of TcdA, TcdB, and CDT in intact Caco-2 cells, fluorescence microscopy was performed. Unimpaired Caco-2 cells are characterized by a clear ring of cortical actin and homogeneously distributed Rac1. After treatment with the toxins, these characteristics were dramatically altered. In the presence of α-defensin-5, actin as well as Rac1 was almost entirely protected from toxin-induced modifications (**Figure 3B**).

Incubation of α-Defensin-5 With TcdA Resulted in Precipitation and With CDTb in Reduced Cytotoxicity and Pore Formation

Finally, the underlying molecular mode of inhibition was analyzed in more detail. For TcdA as well as for CDTa, no influence on the *in*

vitro-enzymatic activity in the presence of α-defensin-5 could be observed (**Figure 4A**). Based on previous experiments, the capability of α-defensin-5 to precipitate TcdA was investigated. When incubated without inhibitor, TcdA was nearly completely present in the supernatant fraction. In the presence of α-defensin-5, the effect was inverted and TcdA was mainly detectable in the pellet fraction (**Figure 4B**). For CDT, the underlying mechanism might be different and is most likely based on the impact of α-defensin-5 on the pore-forming activity of CDTb or more precisely on the inactivation of the cytotoxic CDTb-pore. In higher concentrations, CDTb is able to induce pores in the plasma membrane in the absence of the enzymatic component CDTa. The pore-formation leads to dramatic changes in cell morphology and cell viability. Both effects could efficiently be prevented by the addition of α-defensin-5 (**Figure 4C**). These findings were confirmed using the Ca^{2+}-imaging method in combination with living Caco-2 cells. Here, the increase in the Fura2 340/380 ratio, indicating the formation of CDTb-pores and the influx of Ca^{2+}-ions into the cytosol of Caco-2 cells, could be prevented in the presence of α-defensin-5 (**Figure 4D**).

DISCUSSION

For CDAD, as well as for many other important diseases that are caused by exotoxins that are released from bacteria in the human body, the efficient targeted inhibition of these toxins besides the application of antimicrobial drugs is of highest relevance because the toxins cause the disease. The optimal inhibitors should affect the invading bacteria but also the released exotoxins. Such properties have been reported for human α-defensins. The α-defensins belong to the group of AMPs and are distributed in large amounts in host defense cells and tissues. In contrast to other alpha-defensins, such as α-defensins-1–4, which are predominantly produced in neutrophilic granulocytes and are therefore also called human neutrophil-derived α-defensins (HNP)1–4, the here investigated α-defensin-5 is mainly produced by enteric Paneth cells (Lehrer et al., 1993). Paneth cells are specialized cells at the base of intestinal crypts, also known as crypts of Lieberkühn. As part of the local immune system in the small intestine, Paneth cells release α-defensin-5 (and -6) into the lumen of the crypts preventing local excessive colonization of microbes (Selsted and Ouellette, 1995). Like all defensins, α-defensin-5 contains six intramolecular cysteine residues which form an unalterable and specific pattern of disulfide-bridges (Selsted and Harwig, 1989). The defined arrangement of the intramolecular disulfide-bridges is accountable for a conserved backbone topology, that protects the small peptide from proteolysis and maintains the function of α-defensin-5 as broad-spectrum microbicide in the environment of the intestinal lumen (Alpha Defensin - an overview | ScienceDirect Topics). Therefore, microbicidal tissue concentrations between 0.5 and 2.5 mg/g can be achieved in the mucosa of the ileum (Ghosh et al., 2002). It became evident that in addition to their microbicidal activity, specific human defensins are able to inactivate and neutralize several bacterial toxins (Kim et al., 2005; Kim et al., 2006; Giesemann et al., 2008; Lehrer et al., 2009). Based on these previous findings, the protective role of α-defensin-5 against TcdA, TcdB, and CDT was investigated in this present study.

For TcdA, TcdB, and CDT, a time- and concentration-dependent inhibition by α-defensin-5 was observed. For all three toxins, the inhibition by α-defensin-5 could be quantified morphologically on Vero cells and biochemically on Caco-2 cells. By using fluorescence microscopy, the inhibitory potency of α-defensin-5 could be further strengthened. This fact could also be substantiated for the medically relevant combination of all three toxins together. However, the underlying inhibition mechanism seems to differ between the large clostridial glucosylating toxins TcdA and TcdB and the binary actin ADP-ribosylating toxin CDT. In the presence of the inhibitor we observed a clear precipitation of TcdA, which could be made visible in a sodium dodecyl sulfate polyacrylamide gel. At the same time, we could not detect any influence of α-defensin-5 on the enzymatic activity of TcdA, which is consistent with our earlier results for α-defensin-1 (Fischer et al., 2020) but in some contrast to the work of other groups. Giesemann et al. showed in an earlier study that both α-defensin-1 and α-defensin-5 can effectively inhibit TcdB, but not TcdA. In our present study, however, we clearly show inhibition of TcdA in the presence of α-defensin-5. In direct comparison, a broader concentration range of α-defensin-5 was tested in our study, and in addition, a five-fold less concentration of TcdA and recombinant instead of native TcdA was used. Giesemann et al. could show that at least for α-defensin-1, the inhibition of TcdB was mediated by negatively influencing the glucosyltransferase activity of TcdB whereas for α-defensin-5, less or almost no influence on the glycosyltransferase activity of the toxin was observed. This is in line with our findings of the present study, where also no influence of α-defensin-5 on the enzyme activity of TcdA was detected. Au contraire, we found, that binding and co-precipitation of TcdA is the underlying inhibitory mechanism of α-defensin-5. Extensive co-precipitation of TcdB with α-defensin-5 was also observed in the work of Giesemann et al. and in the present study we could show, that this is also the underlying mode of inhibition for TcdA. Presumably, native TcdA that was used by Giesemann et al. was more extensively bound by protein impurities that might have prevented successful interaction with α-defensin-5 (Giesemann et al., 2008).

For CDT, the mode of inhibition seems to be based on the inactivation of the CDTb-pore. Several binding/transport components of binary bacterial toxins form cation-selective channels to transport the enzymatically active subunits of such toxins into cells (Schmid et al., 1994). It was demonstrated that also CDTb forms pores in lipid bilayer membranes *in vitro* (Kronhardt et al., 2017). More recently, it was shown that CDTb forms di-heptamer like structures (Xu et al., 2020). Furthermore, when applied to cells, CDTb alone (in the absence of CDTa) is able to cause dramatic changes in cell morphology and cell viability (Kronhardt et al., 2017). These massive cell-damaging effects could be completely prevented by the addition of α-defensin-5. But also for CDT, we did not find any influence of the small peptide on the enzymatic activity, although this has already

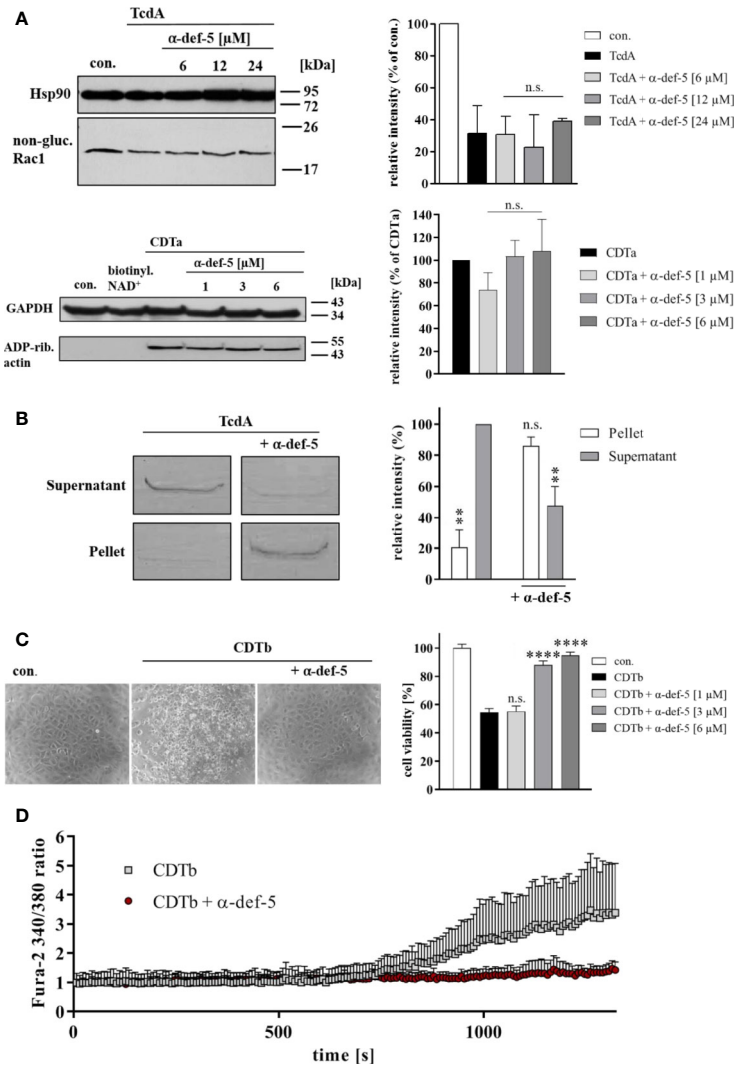

FIGURE 4 | α-Defensin-5 has no influence on the enzymatic activity of TcdA and CDTa but leads to precipitation of TcdA and inhibition of the cytotoxic pore-forming activity of CDTb. **(A)** Caco-2 lysate (40 μg) was incubated with TcdA (300 ng) and varying concentrations of α-defensin-5 (6, 12, 24 μM) for 1 h (left panel) at 37°C. Caco-2 lysate (40 μg) was incubated with CDTa (1 ng), 10 μM biotinylated NAD^+ and varying concentrations of α-defensin-5 (1, 3, 6 μM) for 30 min at 37°C. Next, samples were subjected to SDS-PAGE and Western Blotting. Non-glucosylated Rac1 was detected with a specific antibody, biotin-labeled, e.g., ADP-ribosylated actin was detected using streptavidin-peroxidase. Hsp90 and GAPDH were used to confirm equal protein loading. Values are given as mean ± SD (n = 2). Significance was determined using the one-way ANOVA test (n.s. = not significant). **(B)** TcdA (1 μg) was incubated with and without α-defensin-5 (6 μM) for 15 min at 37°C in serum-free medium. Afterward, samples were centrifuged and separated fractions were subjected to SDS-PAGE (left panel). Densitometric analyses from individual experiments are shown as bar graph (right panel). Values are given as mean ± SD (n = 2). Significance was determined using the one-way ANOVA test (n.s. = not significant, $^{**}p < 0.01$). **(C)** Vero cells were treated with CDTb (5.3 nM) in the absence of CDTa with or without increasing concentrations of α-defensin-5 (1, 3, 6 μM) for 4 h at 37°C. Representative images are shown in the left panel. After the incubation time, a MTS cell viability assay was performed. Values are given as mean ± SD (n=3). Significance was determined using the one-way ANOVA test (n.s. = not significant, $^{****}p < 0.0001$). **(D)** Caco-2 cells were seeded in an 8-well ibidi plate and pretreated with Fura-2AM (3 μM) for 45 min. Next, baseline was measured for 2 min, and the cells were then treated with CDTb (13 nM) in the presence or absence of α-defensin-5 (6 μM) as indicated.

been described for other toxins of the mono-ADP-ribosyltransferase family (Kim et al., 2006). Most likely, α-defensin-5 is not able to block existing CDTb pores like other known pore blockers such as chloroquine (Schmid et al., 1994) or other related compounds like fluphenazine (Bachmeyer et al., 2001; Bachmeyer et al., 2003). Based on our previous finding (Fischer et al., 2020), we assume the same underlying mode of inhibition for α-defensin-5 as for α-defensin-1, namely the prevention of the formation of new CDTb-pores by α-defensin-5. This conclusion could be drawn on the basis of analyzing cell morphology and viability as well as on the basis of calcium imaging. In these experiments, a clear increase in

intracellular Ca^{2+} was observable when Caco-2 cells were treated with CDTb in calcium containing medium. This effect was prevented in the presence of α-defensin-5 indicating the successful prevention of the formation of CDTb-pores. Interestingly, when Caco-2 cells were treated with CDTb in calcium-free medium, no increase in intracellular Ca^{2+} could be detected, suggesting that CDTb does not lead to the release of intracellular calcium per se (data not shown).

Taken together, α-defensin-5 is a specific inhibitor of *C. difficile* toxins TcdA, TcdB, and CDT. This human peptide might be an auspicious pharmacological inhibitor to treat/prevent CDAD, in particular after infection with hypervirulent, CDT-producing strains of *C. difficile*. Thereby, a beneficial role of α-defensin-5 might be a first line host defense mechanism against invading pathogens in combination with a newly discovered inhibitory potency against the produced protein toxins.

DATA AVAILABILITY STATEMENT

The raw data supporting the conclusions of this article will be made available by the authors, without undue reservation, to any qualified researcher.

AUTHOR CONTRIBUTIONS

SF designed, supervised, and analyzed experiments and wrote the manuscript. MK and ML performed experiments. PP and KA provided toxins, analyzed data, and proof-read the manuscript. HB wrote the manuscript and supervised the study.

FUNDING

The work in the Barth group was financially supported by the Deutsche Forschungsgemeinschaft project number 316249678- SFB 1279 (project C02). ML is a fellow of the Promotionsprogramm Experimentelle Medizin of the International Graduate School in Molecular Medicine in Ulm.

ACKNOWLEDGMENTS

We thank Prof. Manfred Frick and Dr. Giorgio Fois, Institute of General Physiology, Ulm for excellent iMic-support and Dr. Carsten Schwan, Institute of Experimental and Clinical Pharmacology and Toxicology, Freiburg for providing CDT-toxin.

REFERENCES

Aktories, K. (2011). Bacterial protein toxins that modify host regulatory GTPases. *Nat. Rev. Microbiol.* 9, 487–498. doi: 10.1038/nrmicro2592

Alpha Defensin - an overview | ScienceDirect Topics. Available at: https://www.sciencedirect.com/topics/neuroscience/alpha-defensin (Accessed March 19, 2020).

Bachmeyer, C., Benz, R., Barth, H., Aktories, K., Gilbert, M., and Popoff, M. R. (2001). Interaction of Clostridium botulinum C2 toxin with lipid bilayer membranes and Vero cells: inhibition of channel function by chloroquine and related compounds in vitro and intoxification in vivo. *FASEB J.* 15, 1658–1660. doi: 10.1096/fj.00-0671fje

Bachmeyer, C., Orlik, F., Barth, H., Aktories, K., and Benz, R. (2003). Mechanism of C2-toxin inhibition by Fluphenazine and related compounds: investigation of their binding kinetics to the C2II-channel using the current noise analysis. *J. Mol. Biol.* 333, 527–540. doi: 10.1016/j.jmb.2003.08.044

Carter, G. P., Rood, J.II, and Lyras, D. (2012). The role of toxin A and toxin B in the virulence of Clostridium difficile. *Trends Microbiol.* 20, 21–29. doi: 10.1016/j.tim.2011.11.003

Carter, G. P., Chakravorty, A., Nguyen, T. A. P., Mileto, S., Schreiber, F., Li, L., et al. (2015). Defining the roles of TcdA and TcdB in localized gastrointestinal disease, systemic organ damage, and the host response during Clostridium difficile infections. *mBio* 6, e00551–e00515. doi: 10.1128/mBio.00551-15

Chumbler, N. M., Farrow, M. A., Lapierre, L. A., Franklin, J. L., and Lacy, D. B. (2016). Clostridium difficile toxins TcdA and TcdB cause colonic tissue damage by distinct mechanisms. *Infect. Immun.* 84, 2871–2877. doi: 10.1128/IAI.00583-16

Debast, S. B., Bauer, M. P., Kuijper, E. J.European Society of Clinical Microbiology and Infectious Diseases (2014). European Society of Clinical Microbiology and Infectious Diseases: update of the treatment guidance document for Clostridium difficile infection. *Clin. Microbiol. Infect.* 20 (Suppl 2), 1–26. doi: 10.1111/1469-0691.12418

Egerer, M., Giesemann, T., Jank, T., Satchell, K. J. F., and Aktories, K. (2007). Autocatalytic cleavage of Clostridium difficile Toxins A and B depends on Cysteine Protease activity. *J. Biol. Chem.* 282, 25314–25321. doi: 10.1074/jbc.M703062200

Fischer, S., Popoff, M. R., and Barth, H. (2018). Human alpha-defensin-1 protects cells from intoxication with Clostridium perfringens iota toxin. *Pathog. Dis.* 76. doi: 10.1093/femspd/fty022

Fischer, S., Ückert, A. K., Landenberger, M., Papatheodorou, P., Hoffmann-Richter, C., Mittler, A.-K., et al. (2020). Human peptide α-defensin-1 interferes with Clostridioides difficile toxins TcdA, TcdB, and CDT. *FASEB J.* 34 (5), 6244–6261 doi: 10.1096/fj.201902816R

Ganz, T., and Lehrer, R.II (1994). Defensins. *Curr. Opin. Immunol.* 6, 584–589. doi: 10.1016/0952-7915(94)90145-7

Genth, H., Huelsenbeck, J., Hartmann, B., Hofmann, F., Just, I., and Gerhard, R. (2006). Cellular stability of Rho-GTPases glucosylated by Clostridium difficile toxin B. *FEBS Lett.* 580, 3565–3569. doi: 10.1016/j.febslet.2006.04.100

Ghosh, D., Porter, E., Shen, B., Lee, S. K., Wilk, D., Drazba, J., et al. (2002). Paneth cell trypsin is the processing enzyme for human defensin-5. *Nat. Immunol.* 3, 583. doi: 10.1038/ni797

Giesemann, T., Guttenberg, G., and Aktories, K. (2008). Human α-Defensins Inhibit Clostridium difficile Toxin B. *Gastroenterology* 134, 2049–2058. doi: 10.1053/j.gastro.2008.03.008

Goudarzi, M., Seyedjavadi, S. S., Goudarzi, H., Mehdizadeh Aghdam, E., and Nazeri, S. (2014). Clostridium difficile infection: epidemiology, pathogenesis, risk factors, and therapeutic options. *Scientifica.* 2014, 916826. doi: 10.1155/2014/916826

Gülke, I., Pfeifer, G., Liese, J., Fritz, M., Hofmann, F., Aktories, K., et al. (2001). Characterization of the enzymatic component of the ADP-Ribosyltransferase Toxin CDTa from Clostridium difficile. *Infect. Immun.* 69, 6004–6011. doi: 10.1128/IAI.69.10.6004-6011.2001

Jank, T., and Aktories, K. (2008). Structure and mode of action of clostridial glucosylating toxins: the ABCD model. *Trends Microbiol.* 16, 222–229. doi: 10.1016/j.tim.2008.01.011

Just, I., Selzer, J., von Eichel-Streiber, C., and Aktories, K. (1995a). The low molecular mass GTP-binding protein Rho is affected by toxin A from Clostridium difficile. *J. Clin. Invest.* 95, 1026–1031. doi: 10.1172/JCI117747

Just, I., Selzer, J., Wilm, M., Eichel-Streiber, C., von, Mann, M., and Aktories, K. (1995b). Glucosylation of Rho proteins by Clostridium difficile toxin B. *Nature* 375, 500. doi: 10.1038/375500a0

Just, I., Selzer, J., Hofmann, F., Green, G. A., and Aktories, K. (1996). Inactivation of Ras by Clostridium sordellii lethal toxin-catalyzed glucosylation. *J. Biol. Chem.* 271, 10149–10153. doi: 10.1074/jbc.271.17.10149

Kagan, B. L., Ganz, T., and Lehrer, R.II (1994). Defensins: a family of antimicrobial and cytotoxic peptides. *Toxicology* 87, 131–149. doi: 10.1016/0300-483x(94)90158-9

Kim, C., Gajendran, N., Mittrücker, H.-W., Weiwad, M., Song, Y.-H., Hurwitz, R., et al. (2005). Human α-defensins neutralize anthrax lethal toxin and protect against its fatal consequences. *PNAS* 102, 4830–4835. doi: 10.1073/pnas.0500508102

Kim, C., Slavinskaya, Z., Merrill, A. R., and Kaufmann, S. H. E. (2006). Human α-defensins neutralize toxins of the mono-ADP-ribosyltransferase family. *Biochem. J.* 399, 225–229. doi: 10.1042/BJ20060425

Kronhardt, A., Schwan, C., Maier, E., Popoff, M. R., and Benz, R. (2017). Clostridium difficile CDT Toxin forms two different types of channels in Lipid Bilayer membranes. *BAOJ Chem.* 3, 35.

Kuehne, S. A., Cartman, S. T., Heap, J. T., Kelly, M. L., Cockayne, A., and Minton, N. P. (2010). The role of toxin A and toxin B in Clostridium difficile infection. *Nature* 467, 711–713. doi: 10.1038/nature09397

Kuehne, S. A., Collery, M. M., Kelly, M. L., Cartman, S. T., Cockayne, A., and Minton, N. P. (2014). Importance of Toxin A, Toxin B, and CDT in virulence of an epidemic Clostridium difficile strain. *J. Infect. Dis.* 209, 83–86. doi: 10.1093/infdis/jit426

Kuijper, E. J., Coignard, B., Tüll, P.ESCMID Study Group for Clostridium difficile and EU Member States, and European Centre for Disease Prevention and Control (2006). Emergence of Clostridium difficile-associated disease in North America and Europe. *Clin. Microbiol. Infect.* 12 (Suppl 6), 2–18. doi: 10.1111/j.1469-0691.2006.01580.x

Kuijper, E. J., Barbut, F., Brazier, J. S., Kleinkauf, N., Eckmanns, T., Lambert, M. L., et al. (2008). Update of Clostridium difficile infection due to PCR ribotype 027 in Europ. *Euro. Surveill.* 13 (31), pii=18942. doi: 10.2807/ese.13.31.18942-en

Lehrer, R.II, Lichtenstein, A. K., and Ganz, T. (1993). Defensins: antimicrobial and cytotoxic peptides of mammalian cells. *Annu. Rev. Immunol.* 11, 105–128. doi: 10.1146/annurev.iy.11.040193.000541

Lehrer, R.II, Jung, G., Ruchala, P., Wang, W., Micewicz, E. D., Waring, A. J., et al. (2009). Human α-defensins inhibit Hemolysis mediated by cholesterol-dependent Cytolysins. *Infect. Immun.* 77, 4028–4040. doi: 10.1128/IAI.00232-09

Louie, T. J., Miller, M. A., Mullane, K. M., Weiss, K., Lentnek, A., Golan, Y., et al. (2011). Fidaxomicin versus Vancomycin for Clostridium difficile infection. *New Engl. J. Med.* 364, 422–431. doi: 10.1056/NEJMoa0910812

Papatheodorou, P., Zamboglou, C., Genisyuerek, S., Guttenberg, G., and Aktories, K. (2010). Clostridial glucosylating toxins enter cells via clathrin-mediated endocytosis. *PloS One* 5, e10673. doi: 10.1371/journal.pone.0010673

Papatheodorou, P., Barth, H., Minton, N., and Aktories, K. (2018). Cellular uptake and mode-of-action of Clostridium difficile toxins. *Adv. Exp. Med. Biol.* 1050, 77–96. doi: 10.1007/978-3-319-72799-8_6

Pépin, J., Valiquette, L., Alary, M.-E., Villemure, P., Pelletier, A., Forget, K., et al. (2004). Clostridium difficile-associated diarrhea in a region of Quebec from 1991 to 2003: a changing pattern of disease severity. *CMAJ* 171, 466–472. doi: 10.1503/cmaj.1041104

Pépin, J., Valiquette, L., and Cossette, B. (2005). Mortality attributable to nosocomial Clostridium difficile–associated disease during an epidemic caused by a hypervirulent strain in Quebec. *CMAJ* 173, 1037–1042. doi: 10.1503/cmaj.050978

Perelle, S., Gibert, M., Bourlioux, P., Corthier, G., and Popoff, M. R. (1997). Production of a complete binary toxin (actin-specific ADP-ribosyltransferase) by Clostridium difficile CD196. *Infect. Immun.* 65, 1402–1407. doi: 10.1128/IAI.65.4.1402-1407.1997

Rueden, C. T., Schindelin, J., Hiner, M. C., DeZonia, B. E., Walter, A. E., Arena, E. T., et al. (2017). ImageJ2: ImageJ for the next generation of scientific image data. *BMC Bioinf.* 18, 529. doi: 10.1186/s12859-017-1934-z

Schiavo, G., and van der Goot, F. G. (2001). The bacterial toxin toolkit. *Nat. Rev. Mol. Cell Biol.* 2, 530–537. doi: 10.1038/35080089

Schmid, A., Benz, R., Just, I., and Aktories, K. (1994). Interaction of Clostridium botulinum C2 toxin with lipid bilayer membranes. Formation of cation-selective channels and inhibition of channel function by chloroquine. *J. Biol. Chem.* 269, 16706–16711.

Schneider, C. A., Rasband, W. S., and Eliceiri, K. W. (2012). NIH Image to ImageJ: 25 years of image analysis. *Nat. Methods* 9, 671–675. doi: 10.1038/nmeth.2089

Schwan, C., Stecher, B., Tzivelekidis, T., van Ham, M., Rohde, M., Hardt, W.-D., et al. (2009). Clostridium difficile toxin CDT induces formation of microtubule-based protrusions and increases adherence of bacteria. *PloS Pathog.* 5, e1000626. doi: 10.1371/journal.ppat.1000626

Schwan, C., Nölke, T., Kruppke, A. S., Schubert, D. M., Lang, A. E., and Aktories, K. (2011). Cholesterol- and sphingolipid-rich microdomains are essential for microtubule-based membrane protrusions induced by Clostridium difficile transferase (CDT). *J. Biol. Chem.* 286, 29356–29365. doi: 10.1074/jbc.M111.261925

Selsted, M. E., and Harwig, S. S. (1989). Determination of the disulfide array in the human defensin HNP-2. A covalently cyclized peptide. *J. Biol. Chem.* 264, 4003–4007.

Selsted, M. E., and Ouellette, A. J. (1995). Defensins in granules of phagocytic and non-phagocytic cells. *Trends Cell Biol.* 5, 114–119. doi: 10.1016/S0962-8924(00)88961-8

Sheedlo, M. J., Anderson, D. M., Thomas, A. K., and Lacy, D. B. (2020). Structural elucidation of the Clostridioides difficile transferase toxin reveals a single-site binding mode for the enzyme. *PNAS* 117, 6139–6144. doi: 10.1073/pnas.1920555117

Spencer, R. C. (1998). Clinical impact and associated costs of Clostridium difficile-associated disease. *J. Antimicrob. Chemother.* 41, 5–12. doi: 10.1093/jac/41.suppl_3.5

Tart, S. B. (2013). The role of Vancomycin and Metronidazole for the treatment of Clostridium difficile–associated diarrhea. *J. Pharm. Pract.* 26, 488–490. doi: 10.1177/0897190013499525

Uptake and Trafficking of Protein Toxins | Holger Barth | Springer. Available at: https://www.springer.com/gp/book/9783319588919 (Accessed March 18, 2020).

van Kleef, E., Green, N., Goldenberg, S. D., Robotham, J. V., Cookson, B., Jit, M., et al. (2014). Excess length of stay and mortality due to Clostridium difficile infection: a multi-state modelling approach. *J. Hosp. Infect.* 88, 213–217. doi: 10.1016/j.jhin.2014.08.008

von Eichel-Streiber, C., Laufenberg-Feldmann, R., Sartingen, S., Schulze, J., and Sauerborn, M. (1992). Comparative sequence analysis of the Clostridium difficile toxins A and B. *Mol. Gen. Genet.* 233, 260–268. doi: 10.1007/bf00587587

Wilcox, M. H., Ahir, H., Coia, J. E., Dodgson, A., Hopkins, S., Llewelyn, M. J., et al. (2017). Impact of recurrent Clostridium difficile infection: hospitalization and patient quality of life. *J. Antimicrob. Chemother.* 72, 2647–2656. doi: 10.1093/jac/dkx174

Xu, X., Godoy-Ruiz, R., Adipietro, K. A., Peralta, C., Ben-Hail, D., Varney, K. M., et al. (2020). Structure of the cell-binding component of the Clostridium difficile binary toxin reveals a di-heptamer macromolecular assembly. *PNAS* 117, 1049–1058. doi: 10.1073/pnas.1919490117

Conflict of Interest: The authors declare that the research was conducted in the absence of any commercial or financial relationships that could be construed as a potential conflict of interest.

frontiers in Pharmacology

REVIEW
published: 18 August 2020
doi: 10.3389/fphar.2020.01276

Epilepsy-Related Voltage-Gated Sodium Channelopathies: A Review

Luis Felipe Santos Menezes[1], *Elias Ferreira Sabiá Júnior*[1], *Diogo Vieira Tibery*[1], *Lilian dos Anjos Carneiro*[2,3] *and Elisabeth Ferroni Schwartz*[1*]

[1] Laboratório de Neurofarmacologia, Departamento de Ciências Fisiológicas, Universidade de Brasília, Brasília, Brazil, [2] Faculdade de Medicina, Centro Universitário Euro Americano, Brasília, Brazil, [3] Faculdade de Medicina, Centro Universitário do Planalto Central, Brasília, Brazil

Epilepsy is a disease characterized by abnormal brain activity and a predisposition to generate epileptic seizures, leading to neurobiological, cognitive, psychological, social, and economic impacts for the patient. There are several known causes for epilepsy; one of them is the malfunction of ion channels, resulting from mutations. Voltage-gated sodium channels (NaV) play an essential role in the generation and propagation of action potential, and malfunction caused by mutations can induce irregular neuronal activity. That said, several genetic variations in NaV channels have been described and associated with epilepsy. These mutations can affect channel kinetics, modifying channel activation, inactivation, recovery from inactivation, and/or the current window. Among the NaV subtypes related to epilepsy, NaV1.1 is doubtless the most relevant, with more than 1500 mutations described. Truncation and missense mutations are the most observed alterations. In addition, several studies have already related mutated NaV channels with the electrophysiological functioning of the channel, aiming to correlate with the epilepsy phenotype. The present review provides an overview of studies on epilepsy-associated mutated human NaV1.1, NaV1.2, NaV1.3, NaV1.6, and NaV1.7.

Keywords: channelopathies, epilepsy, ion channel, mutation, sodium channel

OPEN ACCESS

Edited by:
Jean-Marc Sabatier, Aix-Marseille Université, France

Reviewed by:
Rikke Steensbjerre Møller, Filadelfia, Denmark
Roope Mannikko, University College London, United Kingdom
Theodore R. Cummins, Indiana University Bloomington, United States

****Correspondence:***
Elisabeth Ferroni Schwartz
efschwa@unb.br

Specialty section:
This article was submitted to Pharmacology of Ion Channels and Channelopathies, a section of the journal Frontiers in Pharmacology

Received: *21 April 2020*
Accepted: *31 July 2020*
Published: *18 August 2020*

Citation:
Menezes LFS, Sabiá Júnior EF, Tibery DV, Carneiro LdA and Schwartz EF (2020) Epilepsy-Related Voltage-Gated Sodium Channelopathies: A Review. Front. Pharmacol. 11:1276. doi: 10.3389/fphar.2020.01276

INTRODUCTION

Epilepsy is a disease known worldwide, affecting around 70 million people in the world (Thijs et al., 2019). It has been considered a disease and no longer a disorder or a family of disorders since 2014 by International League Against Epilepsy (ILAE) and the International Bureau for Epilepsy (IBE) (Falco-Walter et al., 2018). Epilepsy is conceptually defined as a disease in which an individual has at least two unprovoked or reflex seizures in a period greater than 24 h apart, one unprovoked or reflex seizure and a probability of having another seizure similar to the general recurrence risk after two unprovoked seizures (greater than or equal to 60%) over the next ten years or an epilepsy syndrome (Fisher et al., 2014).

When abnormal brain activity begins in one or more identified regions, epilepsy is called focal, whereas, when it occurs in both hemispheres with a wide distribution, it is called generalized. Finally, when it cannot be classified as either focal or generalized, it is called unknown (Devinsky et al., 2018).

Epilepsy can affect anyone, regardless of gender, age, and income levels (Saxena and Li, 2017). Understanding the etiology of epilepsy is crucial for clinical management of patients and for conducting neurobiological research that will direct future therapies (Thomas and Berkovic, 2014). The ILAE Task Force has defined six etiologic categories; they are not hierarchical and more than one might often apply (structural, genetic, infectious, metabolic, immune, and unknown) (Falco-Walter et al., 2018).

Among those genetically caused, it is possible to identify several epilepsy-related genes (Lindy et al., 2018). For example, voltage-gated potassium channel, voltage-gated calcium channel and voltage-gated chloride channel genes, GABA receptors, nicotinic acetylcholine receptors, polymerase (DNA) Gamma genes and voltage-gated sodium channel genes (Deng et al., 2014).

Voltage-gated sodium channels (NaV) can be found mainly in the central nervous system (CNS), peripheral nervous systems (PNS), skeletal, and cardiac muscles (Huang et al., 2017). NaVs are distributed throughout the body and play an important role in the generation and propagation of action potential (Wang et al., 2017b). Structurally, NaVs are composed by an α subunit organized in four homologous ligated domains (DI-DIV), each domain composed by six transmembrane segments (S1-S6), and one or more β subunits associated by non-covalent interactions or disulfide bond (Abdelsayed and Sokolov, 2013; Gilchrist et al., 2013; Catterall, 2017; Bouza and Isom, 2018; Jiang et al., 2020). The domains of an α subunit present a high degree of conservation with each other, presenting the region known as the voltage sensor domains (VSD) located in transmembranes S1-S4, especially S4 helix, which contains positively charged residues, and the pore-forming (PM) domain located in S5-S6 segments, structuring a four VSD around a central pore (Ahern et al., 2016).

The S4 helix of DI, DII, and DIII domains moves faster than the S4 helix of DIV during membrane depolarization, and this asynchronous movement is an essential feature in the steady activation voltage-dependent process, which provokes movement of S4-S5 intracellular links followed by the displacement of the S6 segments to initiate Na^+ influx (Goldschen-Ohm et al., 2013; Oelstrom et al., 2014). The movement of the S4 helix of DIV initiates the process of fast inactivation, since the movement of the voltage sensor in domain DIV is associated with the displacement of an intracellular loop between DIII and DIV within an IFM (isoleucine, phenylalanine, and methionine) motif that binds intracellular to PM and terminate Na^+ influx (Capes et al., 2013; Clairfeuille et al., 2019). A second type of reversible inactivation occurs after repetitive or prolonged stimulation and results in steady-state inactivation whose asymmetric movement of S6 segments collapses the pore (Payandeh et al., 2012; Zhang et al., 2012; Gamal El-Din et al., 2013; Silva and Goldstein, 2013; Ghovanloo et al., 2016). Consequently, electrophysiological changes such as increased current density, shifting steady-state activation, and inactivation to negative and positive values, respectively, enhanced persistent current, accelerated recovery from inactivation, and delayed fast inactivation can cause gain-of-function (GoF) in the channel. Also, decreased current density, positive shift in steady-state activation, negative shift in steady-state inactivation, and slower recovery from inactivation can cause loss-of-function (LoF) (Mantegazza et al., 2005; Liao et al., 2010; Lossin et al., 2012; Catterall, 2014b; Vanoye et al., 2014; Wagnon et al., 2017; Yang et al., 2018; Zaman et al., 2018; Wengert et al., 2019; Zhang S. et al., 2020).

Currently, there are nine different alpha subtypes of NaVs (NaV1.1-NaV1.9), and mutations in these channels can cause diseases known as channelopathies (Catterall et al., 2010). NaV1.1 (*SCN1A*), NaV1.2 (*SCN2A*), NaV1.3 (*SCN3A*), NaV1.6 (*SCN8A*) and NaV1.7 (*SCN9A*) are genes whose mutations are related to epilepsy. So far, there is no correlation of mutations in NaV1.4 (*SCN4A*), NaV1.5 (*SCN5A*), NaV1.8 (*SCN10A*), and NaV1.9 (SCN11A) with epilepsy, which is to be expected, since these channels are mainly expressed in skeletal muscles, cardiac tissues, dorsal root ganglia, trigeminal sensory neurons, nociceptive neurons of the dorsal root and trigeminal ganglia, respectively (Brunklaus et al., 2014). Both α and β subunits (*SCN1B*) have been reported as the cause of epilepsy phenotype (Meisler et al., 2010; Kaplan et al., 2016).

NaV channels rank amongst the 2% most conserved proteins in the human genome, with an extremely low rate of coding variation, accounting for nearly 5% of known epileptic encephalopathies (Petrovski et al., 2013; Mercimek-Mahmutoglu et al., 2015; Lek et al., 2016; Heyne et al., 2019). Pathogenic mutated residues are situated in the highly evolutionarily conserved portions of the channel: transmembrane segments, intracellular inactivation gate loop, and the proximal 2/3 of the C-terminal domain (Blanchard et al., 2015; Wagnon and Meisler, 2015). The final 1/3 portion of the C-terminal and cytoplasmic interdomain loops 1 and 2 are less conserved (Denis et al., 2019). The proximal 2/3 of the C-terminal are involved in the interaction of several binding sites for proteins and accessory molecules, like beta subunits β1 and β3, fibroblast growth factors (molecules implicated in neural development), calmodulin (regulatory protein in neuronal function and hyperexcitability) and G protein (Bähler and Rhoads, 2002; Spampanato, 2004; Wittmack et al., 2004; Laezza et al., 2009; Yang et al., 2010). Moreover, the C-terminal has been shown to interact with the inactivated channel via ionic interaction between its positively charged residues and negatively charged residues at the inactivation gate. A shift in any of the charges can brake electrostatic interaction and affect normal channel inactivation (Nguyen and Goldin, 2010; Shen et al., 2017; Johnson et al., 2018).

The N-terminal region seems to play a more important role on protein trafficking than on channel activity. This domain interacts with the light chain of microtubule-associated protein MAP1B, facilitating the traffic of the NaV channel to the neuronal cell surface (O'brien et al., 2012; Blanchard et al., 2015). In addition, mutation in the N-terminal leads to protein retention in the endoplasmic reticulum (Sharkey et al., 2009).

Newer genomic approaches, especially next generation sequencing (NGS), improve the rate and reduce the costs associated with genetic epilepsy diagnosis, since traditional

cytogenetic and microarray-based tests are lengthy, expensive, and diagnostic yield is incredibly low (Veeramah et al., 2013; Allen et al., 2016; Sands and Choi, 2017; Orsini et al., 2018). The use of gene panels and whole-exome sequencing (WES) provides a powerful tool to change the paradigm of genetic epilepsy diagnosis (Ng et al., 2010; Clark et al., 2018). These techniques have been widely used to elucidate suspected inherited neurological diseases in the last years, contributing to dramatically increase the number of patients diagnosed with genetic epilepsy. Both mendelian and *de novo* genetic epilepsy can be detected with these methods, but doubtless, *de novo* mutations are the most prevalent mutations related to epilepsy-related voltage-gated sodium channel mutations.

Gene therapy is promising as an effective approach to treat genetic diseases. Personalized epilepsy therapies are in development and have shown promising results, ranging from antisense oligonucleotides and small peptides to modulation of gene expression through epigenetics (Riban et al., 2009; Tan et al., 2017; Stoke Therapeutics, 2018; Perucca and Perucca, 2019). Even eating habits may be related to an improvement in the patient's clinical condition. Ketogenic diet has been described as an effective treatment in epilepsy (Gardella et al., 2018). Moreover, the combination of traditional antiepileptic drugs with new compounds displayed a synergic and improved efficacy, since these molecules do not compete for the same interaction site (Bialer et al., 2018). Each specific epilepsy-related NaV isoform will be presented and discussed in detail in the following sections.

NaV MUTATIONS

NaV1.1

The *SCN1A* gene encodes for the α subunit NaV1.1, and is allocated at the 2q24.3 chromosome between 165,984,641 and 166,149,161 base pairs, same gene cluster of *SCN2A-SCN3A* genes, being the most frequent target of mutation in genetic epilepsy syndromes (OMIM#182389) (Malo et al., 1991; Malo et al., 1994; Catterall et al., 2010). NaV1.1 is widely expressed in the CNS, predominant in inhibitory GABAergic interneurons, regulating neuronal excitability, and the reduction of its activity is one of the factors that cause epileptic diseases due to imbalance between inhibition and excitation (Yu et al., 2006; Verret et al., 2012; Tai et al., 2014; Rubinstein et al., 2015).

Epilepsy syndromes, such as generalized epilepsy with febrile seizures plus (GEFS+; Online Mendelian Inheritance in Man [OMIM] #604233), severe myoclonic epilepsy (SME) and SMEI, also known as Dravet syndrome (OMIM #607208), are associated with mutations in the *SCN1A* gene (Escayg and Goldin, 2010; Meng et al., 2015; Huang et al., 2017).

In the *SCN1A* mutation database (http://www.caae.org.cn/gzneurosci/scn1adatabase/data), among 1727 mutations described for the *SCN1A* gene, 1528 are related to epileptic diseases (**Table 1** and for the full description of mutations in the SCN1A gene, see **Supplementary Table S1**). Among the epilepsy-related mutations, 945 are related to severe myoclonic epilepsy of infancy (SMEI), 263 are related to severe myoclonic epilepsy (SME), 151 are related to severe myoclonic epilepsy borderline (SMEB), 18 are related to partial epilepsy (PE), 31 are related to partial epilepsy and febrile seizures plus (PEFS +), 8 are related to generalized epilepsy (GE), and 55 are related to generalized epilepsy with febrile seizures plus (GEFS +).

Mutations in the NaV1.1 channel are described in almost all regions of the protein and may cause GoF or LoF (Goldin and Escayg, 2010; Meng et al., 2015). Among the 52 mutations in *SCN1A* related to epilepsy with functional studies, 35 mutations (67.30%) exclusively display characteristics of LoF, 6 mutations (11.53%) display characteristics unique to GoF, and 11 mutations (21,15%) display characteristics of GoF+LoF, whereas, in GoF+LoF mutations, the main characteristic that gives GoF features is enhanced persistent current, present in 10 out of the 11 GoF+LoF mutations listed (**Tables 1** and **S1**).

Due to the role of the NaV1.1 channels in the regulation of electrical excitability by the inhibitory interneurons, prescription of AEDs non-selective sodium channel blockers (SCB) for SMEI or GEFS + syndromes is contraindicated, for it may aggravate crises due to the enhanced suppress status of the NaV1.1 channels (Catterall, 2014a; Shi et al., 2016; Knupp and Wirrell, 2018; Ziobro et al., 2018). The first-line drug-based therapy for *SCN1A* epilepsy diseases is the enhancement of postsynaptic GABAergic transmission with allosteric activation of $GABA_A$ receptors as target by Clobazam and/or an increase in GABA concentration in synaptic cleft resulting from increased GABA production and decreased GABA degradation as target by Valproic acid (Catterall, 2014a; Hammer et al., 2016; Knupp and Wirrell, 2018; Musto et al., 2020). Antisense nucleotides (ASO) therapy to increase mRNA of *SCN1A* for NaV1.1 channel expression in normal levels is a promising strategy for genetic disorders involving haploinsufficiency (Hsiao et al., 2016; Stoke Therapeutics, 2018). Drug-resistant Dravet syndrome cases may thrive on alternative therapeutic strategies based on ketogenic diets (Nabbout et al., 2011; Wu et al., 2018). A recent study with 20 patients with medically intractable Dravet syndrome caused by missense, non-sense, insertion, deletions and splicing mutations presents efficacy during three months of treatment in 17 patients, decreasing seizure frequency in more than 50% (Yan et al., 2018). Besisdes that, Epidiolex is an FDA approved CBD-based drug approved in June 2018 for the treatment of severe forms of epilepsy, as Dravet and Lennox-Gastaut syndromes (U.S. Food and Drug Administration [website]., 2018). Clinical trials using CBD in DS and LGS shown reduced frequency of seizures in monthly average (Lattanzi et al., 2020; Morano et al., 2020). Voltage-gated sodium channel are inhibit by CBD in low micromolar concentrations, IC_{50} between 1.9 and 3.8 μM, NaV1.4 and NaV1.1 being the most sensitive channels to CBD, 1.9 and 2.0 μM respectively, probably the mechanism of action is reducing channel availability due shift to more hyperpolarized potential in steady-state inactivation (Ghovanloo et al., 2019).

NaV1.2

NaV1.2 is encoded by the *SCN2A* gene (Wolff et al., 2017). It is located on chromosome 2q24.3 (Shi et al., 2009) and expressed in the CNS (Catterall, 2014a), especially in excitatory neurons (Syrbe et al., 2016) and glutamatergic neurons (Sanders et al.,

TABLE 1 | SCN1A-related epilepsies identified in clinical patients through WES and/or NGS.

Variant	Location	Mutation	Disease	Alteration on *biophysical properties* or/and Clinical report	Reference
Inherited mutation					
A27T	N-terminal	Missense	GEFS+ SMEB	Diffuse spikes, prevailing in posterior regions (EEG)	(Nicita et al., 2010)
L61P	N-terminal	Missense	DS	Febrile seizures	(Halvorsen et al., 2016)
F63L	N-terminal	Missense	DS	Severe developmental delay Spike and Waves in right fronto-temporal region with spreading (EEG)	(Nicita et al., 2010)
F90S	N-terminal	Missense	DS	Multifocal spikes, frontal-dominant spike-waves complex (EEG)	(Sun et al., 2008; Wang et al., 2012; Xu et al., 2014; Butler et al., 2017b)
S103G	N-terminal	Missense	SME DS	Ataxia Rare-spike wave complex (EEG)	(Fujiwara, 2003; Ebrahimi et al., 2010; Tonekaboni et al., 2013)
S106F	N-terminal	Missense	Focal epilepsy	Right temporal parietal occipital slow-wave and generalized spike-wave complex (EEG)	(Barba et al., 2014)
M145T	DI (S1)	Missense	Unidentified epilepsy	Decrease current density Shift steady-state inactivation to more positive values	(Mantegazza et al., 2005; Colosimo et al., 2007)
L193F	DI (S3)	Missense	GEFS+	Generalized tonic–clonic seizures	(Cui et al., 2011)
V244L	DI (S4-S5)	Missense	DS	Myoclonic seizures Generalized spikes or spike-and-wave complexes in the interictal (EEG)	(Morimoto et al., 2006)
R377Q	DI (S5-S6)	Missense	GEFS+	Generalized tonic-clonic seizures	(Zucca et al., 2008; Xu et al., 2015; Cetica et al., 2017; Lindy et al., 2018)
F412I	DI (S6)	Missense	SMEB GEFS+	Febrile seizure	(Ebrahimi et al., 2010; Tonekaboni et al., 2013)
K488EfsX6	DI-DII	FrameShift	DS	NR	(Yang et al., 2017)
R542Q	DI-DII	Missense	GEFS+ SME	NR	(Escayg et al., 2001; Weiss et al., 2003; Combi et al., 2009; Orrico et al., 2009; Wang et al., 2012; Lee et al., 2014; Lal et al., 2016)
R618C	DI-DII	Missense	PEFS+	Generalized tonic-clonic seizures Multifocal epilepsy and bilateral bursts of 3-4 Hz spike and wave (EEG)	(Brunklaus et al., 2015)
Y790C	DII (S1-S2)	Missense	GEFS+	Decreased current density Decreased of cell surface expression	(Annesi et al., 2003; Orrico et al., 2009; Bechi et al., 2015; Bennett et al., 2017)
R859H	DII (S4)	Missense	GEFS+	Shift steady state activation and inactivation to more negative values Enhanced Persistent current	(Volkers et al., 2011; Myers et al., 2017a; Lindy et al., 2018)
S1084C	DII-DIII	Missense	Juvenile myoclonic epilepsy DS	Paroxysmal generalised polyspike-and- wave complexes with myoclonic seizures (EEG)	(Jingami et al., 2014)
T1174S	DII-DIII	Missense	FHM FS	Shift steady state activation to more positive values Deceleration of recovery from fast inactivation Increase of persistent current	(Escayg et al., 2001; Gargus and Tournay, 2007; Yordanova et al., 2011; Rilstone et al., 2012; Cestèle et al., 2013; Lal et al., 2016)
V1353L	DIII (S5)	Missense	PEFS+ GEFS+	Non-functional channel	(Wallace et al., 2001; Lossin et al., 2003; Bennett et al., 2017)
A1429S	DIII (S5-S6)	Missense	Autossomal dominant nocturnal frontal lobe epilepsy	No definitive epileptic spikes (EEG)	(Sone et al., 2012)
R1596H	DIV (S2-S3)	Missense	GEFS+	Generalized spike-wave complexes (EEG) Normal imaging (MRI)	(Hoffman-Zacharska et al., 2015)
I1656M	DIV (S4)	Missense	GEFS+	Shift steady state activation to more positive values	(Lossin et al., 2003)
G1674S	DIV (S5)	Missense	FS+	Febrile seizure Hemiconvulsion	(Saitoh et al., 2015a)
***De novo* mutation**					
Q3X	N-terminal	Nonsense	DS	Generalized tonic clonic seizures	(Claes et al., 2003; Lim et al., 2011)
G58X	N-terminal	Nonsense	DS Focal Epilepsy	Autistic characteristics; Hyperactivity Periventricular nodular heterotopia (MRI)	(Barba et al., 2014)
Y65X	N-terminal	Nonsense	DS	Generalized tonic-clonic seizures	(Zucca et al., 2008)
E75D	N-terminal	Missense	DS	Slow-spike-wave complexes (EEG)	(Arafat et al., 2017)

(Continued)

TABLE 1 | Continued

Variant	Location	Mutation	Disease	Alteration on *biophysical properties* or/and Clinical report	Reference
L80_D81del	N-terminal	Inframe deletion	DS	Pharmacoresistant	(Usluer et al., 2016)
D81N	N-terminal	Missense	DS	Severe Motor and mental delay Multi-focal spike-waves (EEG)	(Usluer et al., 2016)
I91T	N-terminal	Missense	DS	Frontal-dominant spike-waves complex (EEG)	(Sun et al., 2008; Xu et al., 2014)
G96EfsX24	N-terminal	FrameShift	NR	Genetic generalized epilepsy with intellectual disability	(Fry et al., 2016)
R101Q	N-terminal	Missense	DS SMEB GEFS+ PEFS+	Psychomotor retardation	(Fukuma et al., 2004; Harkin et al., 2007; Marini et al., 2007; Depienne et al., 2008; Sun et al., 2010; Zuberi et al., 2011; Wang et al., 2012; Tonekaboni et al., 2013; Lee et al., 2014; Djémié et al., 2016)
A104V	N-terminal	Missense	DS	Epileptic discharges, slow spike and weave; sharp wave, sharp and slow wave complex (EEG)	(Kwong et al., 2012; Myers et al., 2017a)
R118S	N-terminal	Missense	DS	Generalized tonic-clonic seizures Severe mental retardation	(Zucca et al., 2008)
F144YfsX5	DI (S1)	Frameshift	SME DS	Moderate psychomotor retardation	(Fukuma et al., 2004; Zuberi et al., 2011; Wang et al., 2012; Villeneuve et al., 2014)
M145DfsX4	DI (S1)	Frameshift	PEFS+	Generalized tonic-clonic seizures without any provoked factors	(Yu et al., 2010)
G177E	DI (S2-S3)	Missense	SME DS	Non-functional channel	(Nabbout et al., 2003; Ohmori et al., 2006; Usluer et al., 2016)
L180X	DI (S2-S3)	Nonsense	DS	Focal spike wave (EEG)	(Liu et al., 2018)
W190X	DI (S3)	Nonsense	DS	Febrile, partial, generalized tonic-clonic and myo-clonic seizures Severe intellectual disability	(Marini et al., 2007; Kwong et al., 2012)
S213W	DI (S3-S4)	Missense	Epilepsy	Febrile and afebrile seizures Developmental delay	(Butler et al., 2017a)
R219SfsX57	DI (S4)	FrameShift	DS	Generalized tonic-clonic seizures	(Claes et al., 2001)
R222X	DI (S4)	Nonsense	DS SMEB	No measurable current	(Claes et al., 2001; Nabbout et al., 2003; Fukuma et al., 2004; Harkin et al., 2007; Depienne et al., 2008; Orrico et al., 2009; Zuberi et al., 2011; Wang et al., 2012; Xu et al., 2014; Esterhuizen et al., 2018)
I227S	DI (S4)	Missense	SME SMEB	Epileptiform discharges on both sides and spikes/ polyspikes during photic stimulation (EEG) Low current density (no detectable)	(Nabbout et al., 2003; Ohmori et al., 2006; Depienne et al., 2008; Mak et al., 2011; Wang et al., 2012; Lindy et al., 2018)
A239V	DI (S4-S5)	Missense	SME DS	Focal right fronto-temporal spikes with spreading (EEG) Severe developmental delay	(Iannetti et al., 2009; Nicita et al., 2010; Xu et al., 2014)
W280R	DI (S5-S6)	Missense	DS	Febrile seizures Status epilepticus Myoclonic Multifocal discharges (EEG)	(Nabbout et al., 2003; Wang et al., 2012; Liu et al., 2018)
P281L	DI (S5-S6)	Missense	DS	Moderate mental retardation	(Depienne et al., 2008; Gokben et al., 2017; Lindy et al., 2018)
E311X	DI (S5-S6)	Nonsense	DS	Haploinsufficiency	(Orrico et al., 2009)
G329A	DI (S5-S6)	Missense	GEFS+	Generalized tonic–clonic seizures	(Myers et al., 2017a)
G343E	DI (S5-S6)	Missense	SMEB SME DS	Spike-wave complex, Multifocal spikes (EEG)	(Fujiwara, 2003; Depienne et al., 2008; Zuberi et al., 2011)
D366E	DI (S5-S6)	Missense	DS	Generalized tonic-clonic seizures	(Zucca et al., 2008)
W384R	DI (S5-S6)	Missense	DS SMEB SME	Generalized tonic-clonic seizures Partial seizures	(Zuberi et al., 2011; Wang et al., 2012; Verbeek et al., 2013)
T391P	DI (S5-S6)	Missense	DS	Generalized tonic-conic seizures Partial Seizures	(Reyes et al., 2011)
R393H	DI (S5-S6)	Missense	DS SMEB	Generalized tonic-clonic seizures Myoclonus, Febrile seizures Developmental delay	(Claes et al., 2003; Marini et al., 2007; Sun et al., 2010; Zuberi et al., 2011; Lemke et al., 2012; Rilstone et al., 2012; Wang et al., 2012; Xu et al., 2014; Djémié et al., 2016; Haginoya et al., 2018)
V422L	DI (S6)	Missense	EE	Psychomotor developmental delay Theta activities with right predominance (EEG)	(Ohashi et al., 2014)

(Continued)

TABLE 1 | Continued

Variant	Location	Mutation	Disease	Alteration on *biophysical properties* or/and Clinical report	Reference
Y426N	DI-DII	Missense	DS	Decreased current density shift stead-state inactivation to more negative values Delayed recovery from inactivation	(Nabbout et al., 2003; Ohmori et al., 2006; Allen et al., 2016)
L433fsX16	DI-DII	FrameShift	Myoclonic astatic epilepsy	Generalized tonic-clonic seizures	(Ebach et al., 2005)
E435X	DI-DII	Nonsense	DS	Myoclonic seizures Atypical absence	(Fukuma et al., 2004; Wang et al., 2012)
Q554H	DI-DII	Missense	DS	Generalized tonic-clonic seizure Atonic and myoclonic seizures	(Skjei et al., 2015)
S662X	DI-DII	Nonsense	PEFS+	Generalized tonic-clonic seizures	(Yu et al., 2010)
W738X	DI-DII	Nonsense	SME	Febrile seizures Generalized tonic-clonic Severe intellectual disability	(Kwong et al., 2012; Xu et al., 2014)
T808S	DII (S2)	Missense	ICEGTC	Rare sharp waves in left temporal (EEG) Increase current density Delay recovery from inactivation	(Fujiwara, 2003; Rhodes et al., 2005)
S843X	DII (S3)	Nonsense	DS	Focal spike activity (EEG)	(Buoni et al., 2006)
R862G	DII (S4)	Missense	MMPSI	Multifocal epilepsy Hemiclonic Cardiac arrest Severe intellectual disability	(Carranza Rojo et al., 2011; Barba et al., 2014)
T932X	DII (S5-S6)	Nonsense	SME DS	Generalized tonic-clonic seizures Severe mental retardation	(Claes et al., 2003; Dhamija et al., 2014)
M934I	DII (S5-S6)	Missense	DS	Moderate psychomotor retardation	(Fukuma et al., 2004; Depienne et al., 2008; Wang et al., 2012)
H939Q	DII (S5-S6)	Missense	DS	Status epilepticus Generalized tonic-clonic seizures Complex partial seizures No measurable current	(Claes et al., 2003; Ohmori et al., 2006)
R946C	DII (S5-S6)	Missense	SME DS SMEB	Non- functional Channel	(Fukuma et al., 2004; Volkers et al., 2011; Zuberi et al., 2011; Wang et al., 2012; Lee et al., 2014; Xu et al., 2014; Lindy et al., 2018)
R946S	DII (S5-S6)	Missense	Severe idiopathic generalized epilepsy of infancy	Short generalized tonic-clonic seizures at night Seizure onset left temporo-parietal (EEG) Seizure onset left frontal Seizure onset right frontocentral,	(Ebach et al., 2005; Tiefes et al., 2019)
R946H	DII (S5-S6)	Missense	PEFS+ SMEB DS	Non-functional Channel	(Fukuma et al., 2004; Harkin et al., 2007; Depienne et al., 2008; Liao et al., 2010a; Verbeek et al., 2011; Volkers et al., 2011; Zuberi et al., 2011; Wang et al., 2012; Verbeek et al., 2013)
C959R	DII (S5-S6)	Missense	DS	Post trauma epilepsy Lateralized tonic-clonic seizures Severe mental retardation Non-functional Channel	(Claes et al., 2003; Ohmori et al., 2006)
V971L	DII (S6)	Missense	DS	Generalized and unilateral tonic-clonic seizures Myoclonic seizures Apneic spells	(Poryo et al., 2017)
V982L	DII (S6)	Missense	SMEB	Focal epilepsy	(Singh et al., 2009; Saitoh et al., 2012; Saitoh et al., 2015a; Saitoh et al., 2015b)
V983A	DII (S6)	Missense	ICEGTC	Multifocal spikes, high voltage slow-waves (EEG) Reduced current density Shift steady-state inactivation to more positive values Accelerated recovery from inactivation	(Fujiwara, 2003; Rhodes et al., 2005)
V983AfsX2	DII (S6)	FrameShift	DS	Enlarged extracerebral gap (MRI)	(Wang et al., 2017b)
L986F	DII (S6)	Missense	DS	Generalized tonic-clonic seizures Non-functional channel	(Claes et al., 2001; Lossin et al., 2003)
L991VfsX2	DII (S6)	FrameShift	DS	Febrile, partial, generalized tonic-clonic, myo-clonic seizures Moderate intellectual disability.	(Kwong et al., 2012)

(Continued)

TABLE 1 | Continued

Variant	Location	Mutation	Disease	Alteration on *biophysical properties* or/and Clinical report	Reference
N1011I	DII-DIII	Missense	ICEGTC	Rare sharp waves in lateral-temporal (EEG) Reduced current density Shift steady state inactivation to more negative values	(Fujiwara, 2003; Rhodes et al., 2005)
D1046MfsX9	DII-DIII	FrameShift	DS	Diffuse cerebral edema (Computed tomography)	(Myers et al., 2017b)
S1100KfsX8	DII-DIII	FrameShift	DS	Generalized clonic seizures Severe mental retardation	(Claes et al., 2001)
S1104X	DII-DIII	Missense	DS	Febrile seizures	(Depienne et al., 2008; Hernández Chávez et al., 2014)
E1153X	DII-DIII	Nonsense	DS	Focal epilepsy with frontal-lateral activity (EEG)	(Hernández Chávez et al., 2014)
E1176NfsX32	DII-DIII	FrameShift	DS	Severe intellectual disability Intractable seizures despite multiple anti-epileptic drugs	(Willemsen et al., 2012)
R1213X	DII-DIII	Nonsense	SME DS LGS	Rare spikes, multifocal spikes and spike-wave complex (EEG) Severe mental delay	(Fujiwara, 2003; Depienne et al., 2008; Zuberi et al., 2011; Wang et al., 2012; Allen et al., 2013; Xu et al., 2014; Lindy et al., 2018)
L1230P	DIII (S1)	Missense	DS	Focal spike-wave complex (EEG) Febrile seizures Myoclonic seizures	(Liu et al., 2018)
F1263L	DIII (S2)	Missense	SMEB	Rare spike-wave complex and poly spike-waves complex (EEG)	(Fujiwara, 2003)
R1636Q	DIV (S4)	Missense	DS LGS	Epileptic encephalopathy Myoclonic seizures	(Harkin et al., 2007; Butler et al., 2017b)
V1637E	DIV (S4)	Missense	DS	Episodes of status epilepticus triggered by fever	(Nishri et al., 2010; Zuberi et al., 2011)
F1671fsX8	DIV (S4-S5)	FrameShift	DS	Generalized tonic-clonic seizures Severe mental retardation	(Claes et al., 2001; Sugawara et al., 2002; Depienne et al., 2008; Riva et al., 2009)
A1685D	DIV (S5)	Missense	DS	Spike-wave complex (EEG) Non-functional channel	(Fujiwara, 2003) (Sugiura et al., 2012)
Y1694C	DIV (S5)	Missense	DS	Myoclonic seizures Atypical absence Severe psychomotor retardation	(Fukuma et al., 2004; Wang et al., 2012; Cetica et al., 2017)
L1717P	DIV (S5-S6)	Missense	SME	Generalized tonic clonic seizure	(Verbeek et al., 2013)
T1722A	DIV (S5-S6)	Missense	DS	Myoclonic, hemiclonic, focal seizures	(Wu et al., 2015)
C1741S	DIV (S5-S6)	Missense	TLE-MTS	Febrile status epilepticus	(Tiefes et al., 2019)
G1754R	DIV (S5-S6)	Missense	DS	Focal seizures Hemiconvulsions	(Petrelli et al., 2012)
S1768R	DIV (S6)	Missense	DS	Absences and tonic-clonic seizures	(Willemsen et al., 2012)
E1881X	C-terminal	Nonsense	DS SMEB	Febrile and generalized seizures	(Villeneuve et al., 2014)
Non genetic origin mutations reported*					
G177DfsX4	DI (S2-S3)	FrameShift	DS	Generalized tonic-clonic seizures	(Fujiwara, 2003)
V207G	DI (S3)	Missense	EE	Early-onset multifocal seizures	(Daoud et al., 2016)
D249E	DI (S4-S5)	Missense	DS	Generalized tonic seizures Absences; Mental retardation	(Le Gal et al., 2014)
N275K	DI (S5)	Missense	PEFS+	Hippocampal volume loss (MRI)	(Kim et al., 2014)
T363R	DI (S5-S6)	Missense	DS	Generalized tonic-clonic seizures	(Zuberi et al., 2011; Le Gal et al., 2014)
N416I	DI (S6)	Missense	DS	Focal spike-wave (EEG)	(Zhou et al., 2018)
S1631C	DIV (S3-S4)	Missense	DS	Multifocal spikes (EEG)	(Haginoya et al., 2018)

**Non genetic origin mutations reported: Mutations described through clinical diagnosis, but the mutation type (Mendelian or de novo) were not reported, mainly due to the lack of parents to perform genotyping and difficulty in contacting the family. Generalized epilepsy with febrile seizures plus (GEFS+); Febrile seizures (FS); Febrile seizures plus (FS+); Lennox-Gastaut syndrome (LGS); Dravet syndrome (DS); Borderline severe myoclonic epilepsy (SMEB); Severe myoclonic epilepsy (SME); Familial hemiplegic migraine (FHM); Partial epilepsy with antecedent FS (PEFS+); Intractable childhood epilepsy with generalized tonic–clonic seizures (ICEGTC); Intractable childhood epilepsy with generalized tonic-clonic seizures (ICE-GTC); Epileptic encephalopathy (EE); Malignant migrating partial seizures of infancy (MMPSI); Temporal lobe epilepsy (TLE); Mesial temporal sclerosis (MTS); Not Reported (NR); Domain (D); Segment (S); Electroencephalography (EEG); Magnetic resonance imaging (MRI).*

2018), unlike the NaV1.1 channel, which is highly expressed in the GABAergic interneurons (Catterall, 2014a).

More than 100 mutations have already been described for this gene, with approximately 300 patients studied yet (Reynolds et al., 2020) (**Table 2**). The most common diseases related with *SCN2A* mutation are West syndrome (WS; OMIM #308350), epilepsy of infancy with migrating focal seizures (EIMFS; OMIM #616645), and benign familial neonatal-infantile seizures (BFNIS; OMIM #607745) (Perucca and Perucca, 2019). Although epilepsy-related mutations are present throughout the channel, several hotspots such as the ion selectivity filter, the voltage-sensing domain, the intracellular N-terminal, and the C-terminal domain can be highlighted (Sanders et al., 2018).

NaV1.2 channels are expressed in the excitatory neurons; therefore, GoF mutations are related to epilepsy because it causes neuronal hyperexcitability. On the other hand, LoF mutations are related to autism and intellectual disability phenotype (Ben-Shalom et al., 2017). Nevertheless, some studies have already related loss of function to epilepsy, as described by Lossin and co-workers (2012) with *R1312T* mutation (Lossin et al., 2012).

TABLE 2 | SCN2A-related epilepsies identified in clinical patients through WES and/or NGS.

Variant	Location	Mutation	Disease	Alteration on *biophysical properties* or/ and Clinical report	Reference
Inherited mutation					
R19K	N-terminal	Missense	FS+	Febrile seizures Partial seizure with eye deviation	(Ito et al., 2004)
R36G	N-terminal	Missense	BFIS	Focal seizures Clonic seizures	(Wolff et al., 2017)
I172V	DI (S2)	Missense	FS	Fever-induced seizure susceptibility	(Saitoh et al., 2015a)
R188W	DI	Missense	FS+	Generalized tonic or tonic clonic seizures Partial seizures	(Ito et al., 2004)
A202V	DI	Missense	BFNS	Focal seizures Generalized tonic-clonic seizures	(Wolff et al., 2017)
V208E	DI	Missense	BFIS	NR	(Lemke et al., 2012)
R223Q	DI (S4)	Missense	BFNIS	Positive shifts of both activation and inactivation curves	(Berkovic et al., 2004; Scalmani et al., 2006; Zara et al., 2013)
D322N	DI (S5-S6)	Missense	DS	NR	(Shi et al., 2009)
F328V	DI (S5-S6)	Missense	SMEB	Status epilepticus Focal seizures Lesions in the right parietal, temporal and occipital lobes (MRI)	(Shi et al., 2009; Saitoh et al., 2015a)
Q383E	DI	Missense	BFNIS	Seizures in early infancy	(Syrbe et al., 2016)
E430Q	DI-DII	Missense	BFNIS	Focal spikes and bifrontal slow wave activity (EEG)	(Herlenius et al., 2007)
A467T	DI-DII	Missense	GEFS+	Loss of consciousness Clonic movements of all extremities High body temperature up to 40 ° Celsius	(Liu et al., 2018)
R524Q	DI-DII	Missense	FS	Febrile seizures	(Ito et al., 2004)
V892I	DII (S5)	Missense	BFNIS	NR	(Berkovic et al., 2004)
N1001K	DII-DIII	Missense	BFIS	Afebrile seizures Tonic body extension Right parietal–occipital sharp waves (EEG)	(Striano et al., 2006)
L1003I	DII-DIII	Missense	BFNIS	Generalized tonic-clonic seizures	(Berkovic et al., 2004)
R1319Q	DIII (S4)	Missense	BFNIS	Shift steady state activation and inactivation to more positive values	(Berkovic et al., 2004; Scalmani et al., 2006; Misra et al., 2008; Zara et al., 2013)
E1321K	DIII	Missense	BFNS	NR	(Grinton et al., 2015)
L1330F	DIII (S4–S5)	Missense	BFNIS	Shift steady state inactivation to more positive values	(Heron et al., 2002; Scalmani et al., 2006; Misra et al., 2008)
L1563V	DIV	Missense	BFNIS	Increase in neuronal excitability Accelerated recovery from fast inactivation	(Heron et al., 2002; Scalmani et al., 2006; Xu et al., 2007; Misra et al., 2008; Berecki et al., 2018)
Y1589C	DIV (S2-S3)	Missense	BFNIS	Increased persistent Na^+ current Delayed fast inactivation Acceleration of recovery	(Lauxmann et al., 2013)
I1596S	DIV (S3)	Missense	BFNIS	Central and posterior focal spikes (EEG)	(Herlenius et al., 2007)
K1641N	DIV	Missense	BFIS	Focal seizures with secondary generalization	(Zara et al., 2013)

(Continued)

TABLE 2 | Continued

Variant	Location	Mutation	Disease	Alteration on *biophysical properties* or/ and Clinical report	Reference
***De novo* mutation**					
R102X (Mutation expressed with wild type channel)	N-terminal	Nonsense	EE	Shift steady state inactivation to more negative values Decrease of available channel	(Kamiya, 2004; Ogiwara et al., 2009)
N132K	DI	Missense	EOEE	Tonic-clonic seizures	(Matalon et al., 2014)
M136I	DI	Missense	EIMFS	Focal seizures Spasms	(Carvill et al., 2013; Howell et al., 2015)
E169G	DI (S2)	Missense	EOEE	Multifocal spikes (EEG) Febrile seizure Myoclonic seizure Focal seizure	(Nakamura et al., 2013)
W191C	DI	Missense	EIMFS	Frequent multifocal spikes (EEG)	(Su et al., 2018)
F207S	DI	Missense	BNS	Tonic-clonic seizures Clonic seizures	(Wolff et al., 2017)
G211D	DI	Missense	WS	NR	(Kodera et al., 2013)
N212D	DI (S3-S4)	Missense	OS and WS	Eyelid myoclonic Spasms Hypsarrhythmia	(Nakamura et al., 2013)
R220G	DI	Missense	EE	Generalized tonic-clonic seizures Generalized spike and slow wave (EEG)	(Mercimek-Mahmutoglu et al., 2015)
T227I	DI	Missense	WS	Tonic seizures Apneic seizures Spasms	(Wolff et al., 2017)
T236S	DI (S4-S5)	Missense	OS	Focal seizure	(Nakamura et al., 2013)
A240S	DI	Missense	EIMFS	Focal seizures	(Howell et al., 2015)
M252V	DI (S5)	Missense	BFNIS	Increased persistent current Accelerated of recovery from fast inactivation Accelerated of recovery from slow inactivation	(Liao et al., 2010b)
V261M	DI (S5)	Missense	BFNIS	Enhanced persistent current Faster recovery from inactivation	(Liao et al., 2010b)
A263T	DI (S5)	Missense	EOEE	Multifocal spikes (EEG)	(Nakamura et al., 2013)
V423L	DI (S6)	Missense	OS	Change in slope of steady-state activation curve Enhanced persistent current	(Wolff et al., 2017)
E430G	DI-DII	Missense	OS	Generalized tonic-clonic seizures	(Matalon et al., 2014)
E717G.fs*30	DI-DII	Splice site	EE Cerebral and cerebellar atrophy	High amplitude sharp waves (EEG)	(Horvath et al., 2016)
G828V	DII	Missense	BNS	Focal seizures Clonic seizures Autonomic seizures Tonic-clonic seizures Multifocal spikes (EEG)	(Wolff et al., 2017)
R853Q	DII (S4)	Missense	WS	Reduced transient current amplitude and densityShift steady state inactivation to more negative values Decreased persistent current	(Samanta and Ramakrishnaiah, 2015; Wolff et al., 2017; Berecki et al., 2018; Mason et al., 2019)
R856L	DII	Missense (During embryogenesis)	EIMFS	Focal seizures	(Howell et al., 2015)
R856Q	DII	Missense	OS	Tonic seizures	(Wolff et al., 2017)
S863F	DII	Missense	BNS and Focal epilepsy	Generalized tonic-clonic seizures	(Wolff et al., 2017)
I873M	DII	Missense	EIEE	Abnormal electroretinogram	(Trump et al., 2016)
N876T	DII (S4-S5)	Missense	OS and WS	Spasms Focal seizure	(Nakamura et al., 2013)
L881P	DII	Missense	WS and LGS	Tonic seizures Tonic-clonic seizures Atypical absences	(Wolff et al., 2017)

(Continued)

TABLE 2 | Continued

Variant	Location	Mutation	Disease	Alteration on *biophysical properties* or/ and Clinical report	Reference
G882R	DII	Missense	EIMFS	Unilateral tonic-clonic	(Wolff et al., 2017)
G882E	DII	Missense	EIMFS	Focal seizures Autonomic seizures Hemiclonic seizures Myoclonic seizures Clonic seizures	(Wolff et al., 2017)
V887A	DII	Missense	OS	Spasms	(Wolff et al., 2017)
G899S	DII (S5)	Missense	Intractable infantile Childhood epilepsy	Tonic-clonic seizures and absences Shift steady-state activation to more positive values Increased slop factor	(Wolff et al., 2017)
K905N	DII	Missense	EIMFS	Focal seizures	(Carvill et al., 2013; Howell et al., 2015)
F928C	DII	Missense	EIMFS	Focal seizures	(Carvill et al., 2013; Howell et al., 2015)
H930Q	DII	Missense	MAE	Tonic-clonic seizures Atonic seizures Myoclonic-atonic seizures Tonic seizures Atypical absences	(Wolff et al., 2017)
N976K	DII	Missense	EE	Focal seizures	(Howell et al., 2015)
S987I	DII	Missense	EIEE	Focal and tonic seizures	(Trump et al., 2016)
G999L	DII-DIII	Missense	Infantile epilepsy	Diffuse slowing with high-amplitude bursts of activity (EEG) Generalized seizures with burst suppression	(Foster et al., 2017)
E999K	DII-DIII	Missense	EIEE	NR	(Trump et al., 2016)
E999V	DII-DIII	Missense	EIEE OS	NR	(Allen et al., 2016; Trump et al., 2016)
I1021Y.fs*16	DII-DIII	Frameshift	LGS	NR	(Carvill et al., 2013)
E1211K	DIII (S1)	Missense	WS	Shift steady-state activation and inactivation to more negative values Slower recovery from inactivation	(Ogiwara et al., 2009; Wong et al., 2015)
K1260E and K1260Q (Mosaic)	DIII	Missense	EIEE	NR	(Trump et al., 2016)
R1312T	DIII (S4)	Missense	DS	Reduced current density Shift steady-state activation and inactivation to more negative values Enhanced closed-state inactivation Slowed recovery from inactivation	(Shi et al., 2009; Lossin et al., 2012)
M1323V	DIII (S4-S5)	Missense	OS and WS	Multifocal spikes (EEG)	(Nakamura et al., 2013)
V1326D	DIII	Missense	EIMFS	Focal seizures	(Dhamija et al., 2013)
S1336Y	DIII (S4-S5)	Missense	OS and WS	Modified hypsarrhythmia	(Nakamura et al., 2013)
M1338T	DIII (S4-S5)	Missense	OS	Spasms Focal seizure Multifocal spikes (EEG)	(Nakamura et al., 2013)
L1342P	DIII	Missense	IOEE	Progressive brain atrophy Short tonic seizures Multifocal sharp wave activity (EEG)	(Hackenberg et al., 2014)
I1473M	DIII (S6)	Missense	SNEE	Shift steady-state inactivation to more negative values	(Ogiwara et al., 2009)
Q1479P	DIII	Missense	EIEE	NR	(Trump et al., 2016)
V1528Cfs*7	DIII-DIV	Frameshift	LGS	Tonic-clonic seizures Tonic seizures Status epilepticus	(Wolff et al., 2017)
Q1531K	DIII-DIV	Missense	BNS	Clonic seizures Generalized tonic-clonic seizures	(Wolff et al., 2017)
I1537S and M1538I	DIV	Missense	OS and WS	Clonic seizures Frequent seizure activity (EEG)	(Foster et al., 2017)
M1548V	DIV	Missense	OS and WS	Generalized tonic-clonic seizures	(Wolff et al., 2017)
G1593R	DIV	Missense	EIMFS	Focal seizures	(Howell et al., 2015)

(Continued)

TABLE 2 | Continued

Variant	Location	Mutation	Disease	Alteration on *biophysical properties* or/ and Clinical report	Reference
F1597L	DIV (S3)	Missense	EIMFS	Shift steady-state activation to more negative values accelerated recovery from fast inactivation	(Wolff et al., 2017)
D1598G	DIV (S3)	Missense	SME	Severe intellectual disability Developmental delay Seizures/ infantile spasms	(Need et al., 2012)
P1622S	DIV (S3-S4)	Missense	MAE	Shift steady-state inactivation to more negative values	(Wolff et al., 2017)
T1623N	DIV (S3-S4)	Missense	OS and WS	Multifocal spikes (EEG) Spasms Hypsarrhythmia	(Nakamura et al., 2013)
V1627M	DIV	Missense	EIMFS	Focal seizures Apnoeic seizures	(Wolff et al., 2017)
G1634V	DIV	Missense	OS	Focal seizures Spasms	(Howell et al., 2015)
I1640S	DIV	Missense	EE	Tonic seizures Focal seizues	(Wolff et al., 2017)
L1650P	DIV	Missense	EIEE	NR	(Trump et al., 2016)
A1652P	DIV	Missense	WS	Spasms	(Wolff et al., 2017)
S1656F	DIV	Missense	LGS	Generalized tonic-clonic seizures	(Wolff et al., 2017)
L1660T	DIV (S4-S5)	Missense	EE	Generalized tonic-clonic seizures	(Fukasawa et al., 2015)
L1660W	DIV	Missense	Acute encephalopathy	Tonic-clonic convulsions Frequent spikes and sharp waves in the right fronto-temporal regions (EEG) Cerebellar atrophy (MRI)	(Fukasawa et al., 2015)
Q1811E	C-terminal	Missense	OS	Generalized tonic-clonic seizures Focal seizures	(Wolff et al., 2017)
L1829F	C-terminal	Missense	EIEE	NR	(Trump et al., 2016)
H1853R	C-terminal	Missense	OS	Generalized tonic-clonic seizures Absence seizures	(Martin et al., 2014)
R1882L	C-terminal	Missense	Epilepsy	Generalized and irregular spike wave and polyspike wave activity (EEG) Focal and generalized tonic–clonic seizures with opisthotonus, bradycardia, and cyanosis	(Baasch et al., 2014)
R1882G	C-terminal	Missense	BIS	Shift steady-state inactivation to more positive values Increase current density and protein production	(Carvill et al., 2013; Schwarz et al., 2016; Wolff et al., 2017)
R1882Q	C-terminal	Missense	EIEE	Increased current density Enhanced persistent current	(Trump et al., 2016; Berecki et al., 2018; Mason et al., 2019)
D25Nβ1 **β1 subunit mutation***	β subunit	Substitution * human embryonic kidney 293 (HEK) cells co-expressing human Nav1.2 sodium channels and D25Nβ1	GEFS+	Inhibits the increment of functional expression of NaCh currents Abolishes the shift of the voltage dependence of activation and inactivation	(Baroni et al., 2018)
Chromosome 2q24.3 Portions of the *SCN2A* and *SCN3A* genes	Chromosome	Deletion (112-kb)	Mental retardation Infantile seizures	Anxiety disorders 'shiver-like' episodes	(Bartnik et al., 2011)
Chromosome q24.3q31.1 58 known genes including *SCN2A, SCN1A, SCN3A, SCN9A* and *SCN7A*	Chromosome	Deletion (10.29 - 10.58 Mb)	Severe epilepsy	Focal and generalized seizures Stereotypic and repetitive hand movements Slow background with high amplitude delta waves mixed with spikes and sharp waves on the temporo-occipital areas (EEG)	(Pescucci et al., 2007)
Non genetic origin mutations reported*					
V213D	DI (S4)	Missense	EOEE	Focal seizure Focal spikes (EEG)	(Nakamura et al., 2013)

(Continued)

TABLE 2 | Continued

Variant	Location	Mutation	Disease	Alteration on *biophysical properties* or/ and Clinical report	Reference
T218K	DI	Missense	EIMFS	Focal seizures Spasms	(Howell et al., 2015)
D649N	DI-DII	Missense	DS	NR	(Wang et al., 2012)
V752F	DI-DII	Missense	Absence epilepsy	Increased current density Shift steady-state activation and inactivation to more negative values	(Oliva et al., 2014)
M1128T	DII-DIII	Missense	AERRPS	Generalized convulsive seizure Slow background activity and rare multifocal spikes over the right temporal and bilateral frontopolar regions (EEG) Brain edema (Cranial computed tomography)	(Kobayashi et al., 2012)
G1522A	DIII-DIV	Missense	EE	Absence seizures Generalized spike and waves (EEG)	(Mercimek-Mahmutoglu et al., 2015)
R1629L	DIV (S4)	Missense	EOEE	Focal seizure Burst of spikes (EEG)	(Nakamura et al., 2013)
R1918H	C-terminus	Missense	GEFS+	Generalized tonic-clonic seizures	(Haug et al., 2001)
GAL879-881QQQ	DII (S4-S5) (rat brain)	Mutated channel in transgenic mice	Epilepsy	Delayed fast inactivation Increased persistent current when expressed in Xenopus oocytes	(Kearney et al., 2001)
R85Cβ1	Extracellular immunoglobulin-like domain (β1 subunit)	Substitution *Human embryonic kidney (HEK)-293T cells co-expressing human brain NaV1.2 alpha subunit and R85Cβ1	GEFS+	Fail to modulate fast inactivation kinetics Fail to modulated steady-state inactivation	(Xu et al., 2007)
R85Hβ1	Extracellular immunoglobulin-like domain (β1 subunit)	Substitution *Human embryonic kidney (HEK)-293T cells co-expressing human brain NaV1.2 alpha subunit and R85Hβ1	GEFS+	Fail to modulated fast inactivation kinetics	(Xu et al., 2007)
C121Wβ1 **β1 subunit mutation***	Ig-like domain (β1 subunit)	Substitution * Chinese hamster ovary (CHO) cells co-expressing human Nav1.2 sodium channels and C121Wβ1	GEFS+	Destabilization of steady-state inactivation potentials Disrupts the thermoprotective role of the β1 subunit on channel availability	(Egri et al., 2012; Abdelsayed and Sokolov, 2013)
Chromosome 2q24.3 **Involves the *SCN2A* and *SCN3A* genes**	Chromosome	Duplication (1.77 Mb)	EOEE	Multifocal spikes (EEG) Epileptic spasms	(Baumer et al., 2015)
Chromosome 2q24.3-q31.1 **47 genes involved including *SCN1A, SCN2A, SCN3A, SCN7A* and *SCN9A***	Chromosome	Deletion (10.4-Mb)	Severe epilepsy	Epileptic seizure with pale, atonic periods followed by a spasm-like out-throwing of both arms Predominantly right-sided epileptiform activity (EEG)	(Davidsson et al., 2008)

**Non genetic origin mutations reported: Mutations described through clinical diagnosis, but the mutation type (Mendelian or de novo) were not reported, mainly due to the lack of parents to perform genotyping and difficulty in contacting the family. Generalized epilepsy with febrile seizures plus (GEFS+); Benign familial neonatal-infantile seizures (BFNIS); Benign familial neonatal seizures (BFNS); Benign Familial Infantile Seizures (BFIS); Benign neonatal/infantile seizures (BNIS); Benign neonatal seizures (BNS); Benign infantile seizures (BIS); Febrile seizures (FS); Febrile seizures plus (FS+); Epilepsy of infancy with migrating focal seizures (EIMFS); Ohtahara syndrome (OS); West syndrome (WS); Lennox-Gastaut syndrome (LGS); Dravet syndrome (DS); Borderline severe myoclonic epilepsy (SMEB); Severe myoclonic epilepsy (SME); Early-onset epileptic encephalopathies (EOEE); Acute encephalitis with refractory, repetitive partial seizures (AERRPS); Early infantile epileptic encephalopathy (EIEE); myoclonic-atonic epilepsy; Infantile onset epileptic encephalopathy (IOEE); Sporadic neonatal epileptic encephalopathy (SNEE); Epileptic encephalopathy (EE); Not Reported (NR); Domain (D); Segment (S); Electroencephalography (EEG); Magnetic resonance imaging (MRI).*

Normally, LoF SCN2A gene mutations for epilepsy are related to late-onset epilepsy; however, the mechanism of action is unclear (Mason et al., 2019).

In some cases, NaV1.2 seizures are not controlled not even by various antiepileptic drugs, as with the patient described by Syrbe and colleagues (2016). The proband, even after being treated with oxcarbazepine (OXC), valproic acid, topiramate, sulthiame, phenytoin, among other drugs, kept on having seizures (Syrbe et al., 2016). Furthermore, the SCB drugs can assist the patient during the treatment as described by Gorman and King (2017). The patient had seizures controlled after administration of phenytoin (Gorman and King, 2017). In addition, Musto et al. (2020) cite benefits treatments using SCB such as carbamazepine, mexiletine, oxcarbazepine, phenytoin, lidocaine, and lamotrigine for patients with early onset epilepsies (Musto et al., 2020). Besides, Peters and colleagues studied a substance commercially used as an antianginal drug (human heart) called ranolazine that has been shown to affect NaV1.2 channels, reducing macroscopic currents and delaying the recovery of fast and slow inactivation of the NaV1.2 channel, consequently with more future studies ranolazine could be a efficacious therapy for epilepsy (Peters et al., 2013).

Drugs can be important to modulate channel kinetics for both GoF and LoF, but some precautions must be observed. For example, the degree of conservation between subtypes, such as NaV1.2 and other sodium channels as NaV1.5 and the excessive decrease in channel function or the excessive increase in function obtained by the drug (Sanders et al., 2018).

Organizations like the FamilieSCN2A Foundation (www.scn2a.org) might be essential in the search for new treatments. Understanding the genotype-phenotype of gain and loss of function is essential because science-patient relationship may be helpful in the search for new therapies (Sanders et al., 2018).

NaV1.3

SCN3A is a gene that encodes for type 3 voltage-gated Na^+ channel α subunit, the NaV1.3, located on human chromosome 2q24, in a cluster with *SCN1A* and *SCN2A* (Holland et al., 2008). NaV1.3 is expressed predominantly in the CNS during embryonic and neonatal development, being extremely low or sometimes undetectable in postnatal individuals. Subsequently, during infancy, it is gradually replaced by increased expression of the NaV1.1 isoform (Felts et al., 1997; Whitaker et al., 2000; Cheah et al., 2013; Zaman et al., 2018). On the other hand, studies regarding nervous system injury and neuropathic pain showed an increasing presence of NaV1.3 channels in affected tissues, suggesting a pivotal hole of these transmembrane proteins in these processes and diseases (Hains et al., 2003; Waxman and Hains, 2006; Black et al., 2008). For the reasons mentioned above, in the last decades, NaV1.3-associated pathogenesis has been restricted to pain. Recently, a genetic linkage between NaV1.3 mutated variants and epilepsy has been suggested, especially in cryptogenic epilepsy cases (OMIM#182391).

K354Q was the first described NaV1.3 epilepsy-related mutation that revealed harmful electrophysiological alterations (Holland et al., 2008; Estacion et al., 2010). In fact, mutations can change many functional characteristics of NaV1.3 affecting biophysical properties differently; however, these changes result predominantly in neuronal hyper-responsiveness (**Table 3**) (Cummins and Waxman, 1997; Chen et al., 2000; Cummins et al., 2001; Sun et al., 2007). Previous reports correlate heterozygous variants in *SCN3A* in association with moderate forms of epilepsy, while homozygosis is related with severe cognitive damage and premature mortality, resulting in a broad range of epileptic phenotypes (Estacion and Waxman, 2013; Vanoye et al., 2014; Lamar et al., 2017).

Different hereditary mutations on NaV1.3 have been reported to date in patients with epilepsy. In general, the biophysical characterization of these mutations reveals GoF, only one mutation (N302S) is related with LoF (Chen et al., 2015), but both GoF and LoF may lead to an increased seizure susceptibility (Lamar et al., 2017).

Moreover, several *de novo* mutations in *SCN3A* have been described in the last three years, related with severe infantile neurological dysfunctions and cognitive impairments. These mutations may alter the functionality of NaV1.3 channels, neurons organization, migration, and proliferation during the embryonic development (Smith et al., 2018). Epileptic encephalopathy and polymicrogyria are the main features related with these pathogenic variants, and, so far, polymicrogyria was not reported in other channelopathies, being an exclusive characteristic of *SCN3A* mutants (Inuzuka et al., 2019).

There is a lack of clinical data on *SCN3A*-related epilepsies, especially regarding treatment and the use of specific medication. However, *in vitro* studies reported that mutations related with GoF effect respond favorably to treatment using SCB, like phenytoin, carbamazepine, lacosamide, and topiramate (Sun et al., 2007; Sheets et al., 2008; Colombo et al., 2013; Zaman et al., 2018). The anticonvulsant valproic acid represents a novel and promising epigenetic therapeutic approach (Tan et al., 2017). The compound modulates the *SCN3A* gene through methylation, downregulating the expression of NaV1.3 and, consequently, decreasing biophysical alterations in the channel.

NaV1.6

The *SCN8A* gene encodes for type 8 voltage-gated Na^+ channel α subunit, the NaV1.6, located in chromosome 12q13.13. The first case of *SCN8A* pathogenic variant associated with epilepsy was reported eight years ago (Veeramah et al., 2012). Thereafter, due to advances in genome sequencing technology, especially the WES, the number of epilepsy diagnosis associated with NaV1.6 mutations has increased significantly (OMIM #600702), with more than 300 patients diagnosed with *SCN8A* epilepsy mutations and nearly 200 different putative spots of mutations described, totaling over 100 published reports (**Table 4**). A website developed especially to present *SCN8A* epilepsy and related diseases (www.scn8a.net) was created to provide information to families, clinicians, and researchers, gathering news and recent publications on the subject in a private forum for family interaction, to answer questions, strengthening the ties between the community and the researchers.

NaV1.6 is expressed since prenatal, during fetal development (Plummer et al., 1997). Shortly after birth, expression begins to increase, reaching maximum levels during the first years of life. This

TABLE 3 | SCN3A-related epilepsies identified in clinical patients through WES and/or NGS.

Variant	Location	Mutation	Disease	Alteration on *biophysical properties* or/and Clinical report	Reference
Inherited mutation					
K354Q	DI	Missense	CCE	Enhanced persistent current and current amplitude provokes by ramp protocol	(Holland et al., 2008; Estacion et al., 2010)
R357Q	DI (S5-S6)	Missense	Focal epilepsy	Reduced current density Enhanced current amplitude provokes by ramp voltage protocol	(Vanoye et al., 2014)
R621C	DI-DII	Missense	BECTS FS	Centro-temporal spikes (EEG)	(Zaman et al., 2018)
E1111K	DII-III	Missense	Focal epilepsy	Enhanced current amplitude provokes by ramp voltage protocol Enhanced persistent current	(Vanoye et al., 2014)
M1323V	DIII (S5-S6)	Missense	Focal epilepsy	Enhanced current amplitude provokes by ramp voltage protocol	(Vanoye et al., 2014)
C121Wβ1 **β1 subunit mutation***	Extracellular Ig loop	Substitution * Chinese hamster ovary (CHO) cells co-expressing human Nav1.3 sodium channels and C121Wβ1	GEFS+	Resistant to enter into close-state inactivation Shift steady state inacativation to more positive values	(Lucas et al., 2005)
Chromosome 2q24.3 Involves the *SCN1A,SCN2A*, and *SCN3A* genes	Chromosome	Duplication (1.57 Mb)	BFNS	NR	(Heron et al., 2010)
Chromosome 2q24.3 Involves the *SCN1A,SCN2A*, and *SCN3A* genes	Chromosome	Duplication (2.0 Mb)	Neonatal-infantile epilepsy	Facial flushing, head turning to the left, eye deviation, bilateral arm jerking movement	(Raymond et al., 2011)
Chromosome 2q23.3q24.3 Involves the *SCN2A* and *SCN3A* genes	Chromosome	Mosaic duplication (12 Mb)	DS BFNIS	Focal seizures with secondary generalization Atonic seizures (EEG)	(Vecchi et al., 2011)
***De novo* mutation**					
L247P	DI	Missense	Childhood focal epilepsy	Reduced current density associated with low protein expression	(Lamar et al., 2017)
I875T	DII (S4-S5)	Missense	EE	Enhanced persistente current Shift steady-state activation and inactivation to more negative values Generalized convulsion, infantile spasm	(Miyatake et al., 2018; Smith et al., 2018; Zaman et al., 2018)
P1333L	DIII	Missense	EIEE	Enhanced persistent current Increased current density Shift steady-state activation and inactivation to more negative values	(Trujillano et al., 2017; Zaman et al., 2018)
M1765I	DIV	Missense	Refractory epilepsy	Focal and generalized seizures Myoclonus and epileptic spasms	(Inuzuka et al., 2019)
V1769A	DIV (S6)	Missense	EIEE	Enhanced persistent current Shift steady-state activation to more negative values Shift steady-state inactivation to more positive values	(Zaman et al., 2018)
chromosome 2q24.3 Involves the *SCN1A,SCN2A*, and *SCN3A* genes	chromosome	Deletion (1.1 Mb)	WS	Typical hypsarrhythmic pattern (sleeping and awake)	(Chong et al., 2018)
Non genetic origin mutations reported*					
N302S	DI	Missense	GEFS+	Shift steady-state activation and inactivation to more positive values Slower recovery from inactivation with 500 ms duration pre pulse Faster recovery from inactivation with 20 ms duration pre pulse	(Chen et al., 2015)
D766N	DII (S2)	Missense	Focal epilepsy	Increased current amplitude by ramp voltage protocol	(Vanoye et al., 2014)

**Non genetic origin mutations reported: Mutations described through clinical diagnosis, but the mutation type (Mendelian or de novo) were not reported, mainly due to the lack of parents to perform genotyping and difficulty in contacting the family. Cryptogenic childhood epilepsy (CCE); Benign epilepsy with centro-temporal spikes (BECTS); Generalized epilepsy with febrile seizures plus (GEFS+); West syndrome (WS); Febrile seizures (FS); Benign familial neonatal-infantile seizures (BFNIS); Benign familial neonatal seizures (BFNS); Dravet syndrome (DS); Epileptic encephalopathy (EE); Early infantile epileptic encephalopathy (EIEE); Not Reported (NR); Domain (D); Segment (S); Electroencephalography (EEG).*

TABLE 4 | SCN8A-related epilepsies identified in clinical patients through WES and/or NGS.

Variant	Location	Mutation	Alteration on *biophysical properties* or/and Clinical report	Reference
Inherited mutation				
K101R	N-terminus	Missense	NR	(Butler et al., 2017b)
I137M	D1 (S1)	Missense	NR	(Johannesen et al., 2019)
T164M	DI (S2)	Missense	NR	(Butler et al., 2017a)
G269R	DI (S5)	Missense	Non-functional channel	(Wengert et al., 2019)
R530W	DI (S6)-DII (S1)	Missense	NR	(Olson et al., 2015)
N544 fs*39	DI (S6)-DII (S1)	Frameshift	NR	(Johannesen et al., 2019)
S702T	DI (S6)-DII (S1)	Missense	NR	(Jang et al., 2019)
G822R	DII (S3)	Missense	Non-functional channel	(Wengert et al., 2019)
V891M	DII (S5)	Missense	NR	(Johannesen et al., 2019)
L1290V	DIII (S3-S4)	Missense	NR	(Carvill et al., 2013)
L1331V	DIII (S5)	Missense	NR	(Larsen et al., 2015)
T1360N	DIII (S5-S6)	Missense	Shift steady-state inactivation to more negative values	(Wengert et al., 2019)
E1442K	DIII (S5-S6)	Missense	NR	(Liu et al., 2018)
I1464T	DIII (S6)-DIV (S1)	Missense	NR	(Johannesen et al., 2019)
G1476D	DIII (S6)-DIV (S1)	Missense	NR	(Han et al., 2017)
E1483K	DIII (S6)-DIV (S1)	Missense	NR	(Gardella et al., 2016)
I1583T	DIV (S3)	Missense	NR	(Berghuis et al., 2015)
V1598A	DIV (S3)	Missense	NR	(Wang et al., 2017a)
R1638C	DIV (S4)	Missense	Shift steady-state activation to more positive values	(Wengert et al., 2019)
V1758A	DIV (S6)	Missense	Shift steady-state activation to more positive values	(Zaman et al., 2019)
N1877S	C-Terminus	Missense	NR	(Butler et al., 2017b; Johannesen et al., 2019)
R1904C	C-Terminus	Missense	NR	(Schreiber et al., 2020)
***De novo* mutation**				
Exons 2-14	–	Deletion	NR	(Berghuis et al., 2015)
c.-8A > G UTR	5′ UTR	Eight base pairs change upstream of start codon	NR	(Johannesen et al., 2019)
c.4296A>G	DIII	Splice-site mutation	NR	(Denis et al., 2019)
M139I	D1 (S1)	Missense	Shift steady-state inactivation to more negative values Enhanced persistent current Slightly impaired fast channel inactivation	(Zaman et al., 2019)
I142V	D1 (S1)	Missense	NR	(Denis et al., 2019; Kim et al., 2019)
A205E	D1 (S1)	Missense	NR	(Lindy et al., 2018)
F210L	D1 (S1)	Missense	NR	(Mercimek-Mahmutoglu et al., 2015)
V211L	DI (S3)	Missense	NR	(Denis et al., 2019)
V211A	DI (S3)	Missense	NR	(Berkovic et al., 2018)
L213P	D1 (S3)	Missense	NR	(Denis et al., 2019)
G214D	DI (S3-S4)	Missense	NR	(Allen et al., 2013)
N215R	DI (S3-S4)	Missense	NR	(Larsen et al., 2015)
N215D	DI (S3-S4)	Missense	NR	(Deciphering Developmental Disorders Study, 2015)
V216D	DI (S3-S4)	Missense	NR	(Ohba et al., 2014)
R223G	D1 (S4)	Missense	Reduced current density Increased current amplitude provokes by ramp voltage protocol	(de Kovel et al., 2014; Berkovic et al., 2018; Denis et al., 2019)
I231T	D1 (S4)	Missense	NR	(Berkovic et al., 2018)
S232P	D1 (S4)	Missense	NR	(Wang et al., 2017a)
T239S	D1 (S4-S5)	Missense	NR	(Møller et al., 2016)
I240V	DI (S4-S5)	Missense	NR	(McNally et al., 2016)
L257V	DI (S5)	Missense	NR	(Schreiber et al., 2020)
F260S	DI (S5)	Missense	NR	(Larsen et al., 2015; Boerma et al., 2016)
C261F	DI (S5)	Missense	NR	(Rim et al., 2018; Kim et al., 2019)

(Continued)

TABLE 4 | Continued

Variant	Location	Mutation	Alteration on *biophysical properties* or/and Clinical report	Reference
L267S	DI (S5)	Missense	NR	(Malcolmson et al., 2016)
G317A	DI (S5-S6)	Missense	NR	(Denis et al., 2019)
F360A	DI (S5-S6)	Missense	NR	(Rolvien et al., 2017)
M367V	DI (S5-S6)	Missense	NR	(Lindy et al., 2018)
N374K	DI (S5-S6)	Missense	Shift steady-state activation to more negative values	(Johannesen et al., 2019; Zaman et al., 2019)
T386R	DI (S5-S6)	Missense	NR	(Lindy et al., 2018)
Y401H	DI (S6)	Missense	NR	(Gardella et al., 2018)
L405M	DI (S6)	Missense	NR	(Denis et al., 2019)
L407F	DI (S6)	Missense	NR	(Fung et al., 2015; Zhang et al., 2015)
A408T	DI (S6)	Missense	NR	(Trump et al., 2016; Denis et al., 2019)
V410L	DI (S6)	Missense	NR	(Larsen et al., 2015)
L483F	DI (S6) –DII (S1)	Missense	Slight shift steady-state activation to more negative values	(Zaman et al., 2019)
E587Ter	DI (S6)-DII (S1)	Nonsense	NR	(Schreiber et al., 2020)
I763V	DII (S1)	Missense	NR	(Butler et al., 2017b; Hewson et al., 2018; Lindy et al., 2018; Costain et al., 2019; Johannesen et al., 2019)
T767I	DII (S1)	Missense	Decreased current density Increased current amplitude provokes by voltage ramp protocol	(Estacion et al., 2014; Gardella et al., 2018; Lindy et al., 2018)
V791F	DII (S2)	Missense	NR	(Xie et al., 2019)
V842E	DII (S4)	Missense	NR	(Lindy et al., 2018)
S845F	DII (S4)	Missense	NR	(Lindy et al., 2018)
F846S	DII (S4)	Missense	NR	(Ohba et al., 2014)
L848W	DII (S4)	Missense	NR	(Denis et al., 2019)
R850Q	DII (S4)	Missense	Shift steady state inactivation to more negative values Increased persistent current Impaired inactivation	(Fung et al., 2015; Zhang et al., 2015; Lindy et al., 2018; Kim et al., 2019; Tsang et al., 2019; Pan and Cummins, 2020; Schreiber et al., 2020)
R850E	DII (S4)	Missense	NR	(Wang et al., 2017a)
R850L	DII (S4)	Missense	NR	(Gardella et al., 2018)
L864V	DII (S4-S5)	Missense	NR	(Gardella et al., 2018)
L875Q	DII (S5)	Missense	NR	(Allen et al., 2013)
A890T	DII (S5)	Missense	NR	(Fung et al., 2015; Larsen et al., 2015; Zhang et al., 2015)
V891M	DII (S5)	Missense	NR	(Wang et al., 2017a)
V960D	DII (S6)	Missense	NR	(Larsen et al., 2015)
L971V	DII (S6)	Missense	NR	(Kim et al., 2019)
S978R	DII (S6)-DIII (S1)	Missense	NR	(Kim et al., 2019)
S978G	DII (S6)-DIII (S1)	Missense	NR	(Parrini et al., 2017; Gardella et al., 2018)
N984K	DII (S6)-DIII (S1)	Missense	Shift steady-state activation to more negative values	(Blanchard et al., 2015; Boerma et al., 2016)
G1050S	DII (S6)-DIII (S1)	Missense	NR	(McMichael et al., 2015)
S1073N	DII (S6)-DIII (S1)	Missense	NR	(Lindy et al., 2018)
E1201K	DIII (S1)	Missense	NR	(Johannesen et al., 2019)
V1274M	DIII (S3)	Missense	NR	(Jang et al., 2019)
V1315M	DIII (S4-S5)	Missense	NR	(Trump et al., 2016; Bagnasco et al., 2018; Denis et al., 2019)
N1318S	DIII (S4-S5)	Missense	NR	(Johannesen et al., 2019; Lin et al., 2019)
A1319S	DIII (S4-S5)	Missense	NR	(Lindy et al., 2018)
A1319D	DIII (S4-S5)	Missense	NR	(Johannesen et al., 2019)
A1323S	DIII (S4-S5)	Missense	NR	(Trump et al., 2016)
A1323T	DIII (S4-S5)	Missense	NR	(Johannesen et al., 2019)
I1327V	DIII (S4-S5)	Missense	NR	(Vaher et al., 2013; Singh et al., 2015; Trump et al., 2016)
N1329D	DIII (S4-S5)	Missense	NR	(Butler et al., 2017b)

(Continued)

TABLE 4 | Continued

Variant	Location	Mutation	Alteration on *biophysical properties* or/and Clinical report	Reference
V1330M	DIII (S4-S5)	Missense	NR	(Schreiber et al., 2020)
L1332R	DIII (S5)	Missense	NR	(Butler et al., 2017b)
P1428_K1473del	DIII (S5-S6)	Missense	NR	(Larsen et al., 2015)
G1451S	DIII (S6)	Missense	Non-functional channel	(Blanchard et al., 2015; Denis et al., 2019)
N1466K	DIII (S6)-DIV (S1)	Missense	NR	(Ohba et al., 2014)
N1466T	DIII (S6)-DIV (S1)	Missense	NR	(Ohba et al., 2014)
Q1470K	DIII (S6)-DIV (S1)	Missense	NR	(Pons et al., 2018; Denis et al., 2019)
G1475R	DIII (S6)-DIV (S1)	Missense	Enhanced persistent current	(Hussain et al., 2016; Ortiz Madinaveitia et al., 2017; Parrini et al., 2017; Wang et al., 2017a; Gardella et al., 2018; Lindy et al., 2018; Xiao et al., 2018; Kim et al., 2019; Trivisano et al., 2019; Zaman et al., 2019; Ranza et al., 2020; Schreiber et al., 2020)
G1476S	DIII (S6)-DIV (S1)	Missense	NR	(Lindy et al., 2018)
I1479V	DIII (S6)-DIV (S1)	Missense	NR	(Larsen et al., 2015; Lindy et al., 2018; Schreiber et al., 2020)
E1483K	DIII (S6)-DIV (S1)	Missense	NR	(Johannesen et al., 2019)
A1491V	DIII (S6)-DIV (S1)	Missense	Shift steady-state activation to more negative values Increased current amplitude provokes by slow voltage ramp protocol	(Gardella et al., 2018; Lindy et al., 2018; Zaman et al., 2019)
M1494T	DIII (S6)-DIV (S1)	Missense	NR	(Kim et al., 2019)
K1498M	DIII (S6)-DIV (S1)	Missense	NR	(Gardella et al., 2018)
M1529V	DIV (S1)	Missense	NR	(Johannesen et al., 2019)
I1532F	DIV (S1)	Missense	NR	(Møller et al., 2016; Gardella et al., 2018)
M1536I	DIV (S1)	Missense	NR	(Lindy et al., 2018)
F1547V	DIV (S1-S2)	Missense	NR	(Gardella et al., 2018)
F1588L	DIV (S3)	Missense	NR	(Johannesen et al., 2019)
V1592L	DIV (S3)	Missense	NR	(Larsen et al., 2015; Ranza et al., 2020)
S1596C	DIV (S3)	Missense	NR	(Fung et al., 2015; Zhang et al., 2015; Boerma et al., 2016)
I1605R	DIV (S3-S4)	Missense	NR	(Larsen et al., 2015)
T1614A	DIV (S3-S4)	Missense	NR	(Johannesen et al., 2019)
R1617Q	DIV (S4)	Missense	Increased persistent current Increased peak current density Shift steady state activation to more negative values Shift steady-state inactivation to more positive values	(Rauch et al., 2012; Ohba et al., 2014; Dyment et al., 2015; Fung et al., 2015; Larsen et al., 2015; Zhang et al., 2015; Fung et al., 2017; Lindy et al., 2018; Johannesen et al., 2019; Schreiber et al., 2020)
R1620L	DIV (S4)	Missense	NR	(Rossi et al., 2017)
L1621W	DIV (S4)	Missense	NR	(Fung et al., 2015)
G1625R	DIV (S4)	Missense	NR	(Deciphering Developmental Disorders Study, 2015)
L1630P	DIV (S4)	Missense	NR	(Schreiber et al., 2020)
I1631N	DIV (S4)	Missense	NR	(Lindy et al., 2018)
M1645I	DIV (S4-S5)	Missense	NR	(Zhang et al., 2015)
A1650T	DIV (S4-S5)	Missense	NR	(Ohba et al., 2014; Larsen et al., 2015; Parrini et al., 2017; Gardella et al., 2018; Trivisano et al., 2019)
A1650V	DIV (S4-S5)	Missense	NR	(Lindy et al., 2018; Johannesen et al., 2019)
F1754S	DIV (S6)	Missense	NR	(Trump et al., 2016)
V1758A	DIV (S6)	Missense	Shift steady-state activation to more positive values	(Balciuniene et al., 2019; Johannesen et al., 2019; Zaman et al., 2019)
N1759T	DIV (S6)	Missense	NR	(Kim et al., 2019)
A1763G	DIV (S6)	Missense	NR	(Denis et al., 2019)
I1764M	DIV (S6)	Missense	NR	(Gardella et al., 2018)

(Continued)

TABLE 4 | Continued

Variant	Location	Mutation	Alteration on *biophysical properties* or/and Clinical report	Reference
N1768D	C-Terminus	Missense	Increased spontaneous firing Paroxysmal depolarizing-shift-like complexes, Increased firing frequency Increased persistent current	(Veeramah et al., 2012)
V1771I	C-Terminus	Missense	NR	(Johannesen et al., 2019)
Q1801E	C-Terminus	Missense	NR	(Larsen et al., 2015)
R1820X	C-Terminus	Nonsense	NR	(Møller et al., 2016; Johannesen et al., 2019)
R1831Q	C-Terminus	Missense	NR	(Liu et al., 2018)
R1831W	C-Terminus	Missense	NR	(Jang et al., 2019)
T1852I	C-Terminus	Missense	NR	(Lindy et al., 2018; Heyne et al., 2019)
L1865P	C-Terminus	Missense	NR	(Trump et al., 2016)
R1866Q	C-Terminus	Missense	NR	(Kothur et al., 2018; Johannesen et al., 2019)
E1870D	C-Terminus	Missense	NR	(Boerma et al., 2016)
R1872L	C-Terminus	Missense	Enhanced persistent current Increased peak current density Shift steady-state activation to more negative values Shift steady-state inactivation to more positive values	(Wagnon et al., 2016; Sprissler et al., 2017; Lindy et al., 2018; Zaman et al., 2019; Schreiber et al., 2020)
R1872Q	C-Terminus	Missense	Enhanced persistent current Increase peak current density Shift steady-state activation to more negative values Shift steady-state inactivation to more positive values	(Larsen et al., 2015; Horvath et al., 2016; Hussain et al., 2016; Arafat et al., 2017; Atanasoska et al., 2018; Lindy et al., 2018)
R1872W	C-Terminus	Missense	Enhanced persistent current Increased peak current density Shift steady-state activation to more negative values Shift steady-state inactivation to more positive values	(Ohba et al., 2014; Larsen et al., 2015; Takahashi et al., 2015; Gardella et al., 2018; Denis et al., 2019; Kim et al., 2019; Zaman et al., 2019)
N1877S	C-Terminus	Missense	NR	(Anand et al., 2016; Parrini et al., 2017; Wang et al., 2017a; Lindy et al., 2018; Costain et al., 2019; Epifanio et al., 2019; Jain et al., 2019; Ranza et al., 2020)
P1878S	C-Terminus	Missense	NR	(Lindy et al., 2018)
Non genetic origin mutations reported*				
R45Q	N-terminus	Missense	NR	(Encinas et al., 2019; Heyne et al., 2019)
A108fsXTer7	N-terminus	Truncated gene	NR	(Encinas et al., 2019)
T166I	DI (S2)	Missense	NR	(Encinas et al., 2019)
I202N	DI (S3)	Missense	NR	(Butler et al., 2017a)
V211L	DI (S3)	Missense	NR	(Encinas et al., 2019)
V211A	DI (S3)	Missense	NR	(Encinas et al., 2019)
R220H	D1 (S4)	Missense	NR	(Oates et al., 2018)
R223S	DI (S4)	Missense	NR	(Encinas et al., 2019)
T239A	DI (S4-S5)	Missense	NR	(Encinas et al., 2019)
I240V	DI (S4-S5)	Missense	NR	(Encinas et al., 2019)
I240L	DI (S4-S5)	Missense	NR	(Encinas et al., 2019)
L257V	DI (S5)	Missense	NR	(Encinas et al., 2019)
L267V	DI (S5)	Missense	NR	(Denis et al., 2019)
I268L	DI (S5)	Missense	NR	(Encinas et al., 2019)
F360A	DI (S5-S6)	Missense	NR	(Encinas et al., 2019)
M367V	DI (S5-S6)	Missense	NR	(Encinas et al., 2019)
R381Q	DI (S5-S6)	Missense	NR	(Encinas et al., 2019)
T386R	DI (S5-S6)	Missense	NR	(Encinas et al., 2019; Schreiber et al., 2020)
S399P	DI (S6)	Missense	NR	(Encinas et al., 2019; Heyne et al., 2019)
V410L	DI (S6)	Missense	NR	(Encinas et al., 2019)
Y414F	DI (S6)-DII (S1)	Missense	NR	(Butler et al., 2017a)
E416K	DI (S6)-DII (S1)	Missense	NR	(Encinas et al., 2019)
Q417P	DI (S6)-DII (S1)	Missense	NR	(Encinas et al., 2019)
R530Q	DI (S6)-DII (S1)	Missense	NR	(Encinas et al., 2019)
E587Ter	DI (S6)-DII (S1)	Nonsense	NR	(Encinas et al., 2019)

(Continued)

TABLE 4 | Continued

Variant	Location	Mutation	Alteration on *biophysical properties* or/and Clinical report	Reference
R598W	DI (S6)-DII (S1)	Missense	NR	(Encinas et al., 2019)
G692R	DI (S6)-DII (S1)	Missense	NR	(Encinas et al., 2019)
I763V	DII (S1)	Missense	NR	(Butler et al., 2017a; Encinas et al., 2019)
T767I	DII (S1)	Missense	Shift steady-state activation to more negative values	(Estacion et al., 2014)
L840P	DII (S3-S4)	Missense	NR	(Encinas et al., 2019)
L840F	DII (S3-S4)	Missense	NR	(Encinas et al., 2019)
S845F	DII (S4)	Missense	NR	(Encinas et al., 2019)
L864V	DII (S4-S5)	Missense	NR	(Trivisano et al., 2019)
I868T	DII (S4-S5)	Missense	NR	(Encinas et al., 2019)
A874T	DII (S4-S5)	Missense	NR	(Encinas et al., 2019)
V881A	DII (S5)	Missense	NR	(Encinas et al., 2019)
E936K	DII (S6)	Missense	NR	(Johannesen et al., 2019)
L969M	DII (S6)	Missense	NR	(Encinas et al., 2019)
S979F	DII (S6)-DIII (S1)	Missense	NR	(Encinas et al., 2019)
G1050S	DII (S6)-DIII (S1)	Missense	NR	(Encinas et al., 2019)
Y1241C	DIII (S2)	Missense	NR	(Encinas et al., 2019; Johannesen et al., 2019)
S1308P	DIII (S4)	Missense	NR	(Encinas et al., 2019)
V1315M	DIII (S4-S5)	Missense	NR	(Encinas et al., 2019)
L1320F	DIII (S4-S5)	Missense	NR	(Encinas et al., 2019; Schreiber et al., 2020)
A1323P	DIII (S4-S5)	Missense	NR	(Encinas et al., 2019)
I1327V	DIII (S4-S5)	Missense	NR	(Oates et al., 2018)
M1328T	DIII (S4-S5)	Missense	NR	(Encinas et al., 2019)
N1329D	DIII (S4-S5)	Missense	NR	(Butler et al., 2017a)
G1451S	DIII (S6)	Missense	NR	(Encinas et al., 2019)
G1461V	DIII (S6)	Missense	NR	(Encinas et al., 2019; Schreiber et al., 2020)
N1466K	DIII (S6)-DIV (S1)	Missense	NR	(Encinas et al., 2019)
F1467C	DIII (S6)-DIV (S1)	Missense	NR	(Encinas et al., 2019)
Q1470H	DIII (S6)-DIV (S1)	Missense	NR	(Trivisano et al., 2019)
I1479V	DIII (S6)-DIV (S1)	Missense	NR	(Encinas et al., 2019)
A1491V	DIII (S6)-DIV (S1)	Missense	Shift steady-state activation to more negative values	(Johannesen et al., 2018; Trivisano et al., 2019)
M1492V	DIII (S6)-DIV (S1)	Missense	NR	(Encinas et al., 2019; Ranza et al., 2020)
Q1501K	DIII (S6)-DIV (S1)	Missense	NR	(Encinas et al., 2019)
Splice donor c.4419+1A>G	DIII (S6)-DIV (S1)	Truncated gene	NR	(Encinas et al., 2019)
M1536I	DIV (S1)	Missense	NR	(Encinas et al., 2019)
V1592L	DIV (S3)	Missense	NR	(Encinas et al., 2019)
I1594L	DIV (S3)	Missense	NR	(Encinas et al., 2019)
S1596C	DIV (S3)	Missense	NR	(Encinas et al., 2019)
T1614A	DIV (S3-S4)	Missense	NR	(Encinas et al., 2019)
R1617Q	DIV (S4)	Missense	Enhanced persistent current Increased peak current density Shift steady-state activation to more negative values Shift steady-state inactivation to more positive values	(Encinas et al., 2019)
R1617P	DIV (S4)	Missense	NR	(Encinas et al., 2019)
G1625R	DIV (S4)	Missense	NR	(Encinas et al., 2019)
L1630P	DIV (S4)	Missense	NR	(Encinas et al., 2019)
F1642C	DIV (S4-S5)	Missense	NR	(Encinas et al., 2019)
A1650T	DIV (S4-S5)	Missense	NR	(Trivisano et al., 2019)
A1650V	DIV (S4-S5)	Missense	NR	(Encinas et al., 2019)

(Continued)

TABLE 4 | Continued

Variant	Location	Mutation	Alteration on *biophysical properties* or/and Clinical report	Reference
I1654N	DIV (S4-S5)	Missense	NR	(Johannesen et al., 2019)
N1759S	DIV (S6)	Missense	NR	(Encinas et al., 2019; Schreiber et al., 2020)
M1760I	DIV (S6)	Missense	Shift steady-state activation to more negative values Increase action potential firing frequency	(Liu et al., 2019)
N1768D	C-Terminus	Missense	Increased spontaneous firingParoxysmal depolarizing shift like complexes Increased firing frequency Enhanced persistent current	(Veeramah et al., 2012; Encinas et al., 2019)
K1807N	C-Terminus	Missense	NR	(Encinas et al., 2019)
R1831W	C-Terminus	Missense	NR	(Encinas et al., 2019)
D1833H	C-Terminus	Missense	NR	(Johannesen et al., 2019)
T1852I	C-Terminus	Missense	NR	(Encinas et al., 2019; Ranza et al., 2020)
R1872L	C-Terminus	Missense	Increased persistent current Increased peak current density Shift steady state activation to more negative values Shift steady inactivation to more positive values	(Encinas et al., 2019)
N1877S	C-Terminus	Missense	NR	(Johannesen et al., 2019; Schreiber et al., 2020)
R1904C	C-Terminus	Missense	NR	(Encinas et al., 2019)

**Non genetic origin mutations reported: Mutations described through clinical diagnosis, but the mutation type (Mendelian or de novo) were not reported, mainly due to the lack of parents to perform genotyping and difficulty in contacting the family. Not Reported (NR); Domain (D); Segment (S).*

channel is widely expressed in the nodes of Ranvier of myelinated axons and in the distal part of the axon initial segments (AIS), although they are also ubiquitously present throughout the central and peripheral nervous systems, in both excitatory and inhibitory neurons (Caldwell et al., 2000; Oliva et al., 2012). For these reasons, NaV1.6 is one of the most common subtype of voltage-gated sodium channels found in the central nervous system (Caldwell et al., 2000). In humans, the distal AIS is the specialized membrane region in neurons where action potentials are triggered. Overexpression of Nav1.6 in the AIS has been shown to cause an increase in spontaneous and repetitive firing (Hu et al., 2009; Sun et al., 2013), a possible explanation for why *SCN8A* mutations in epilepsy patients are predominantly GoF and affect the action potential threshold. On the other hand, the functional importance of Nav1.6 in inhibitory interneurons is not clear yet, but evidence indicates a role for Nav1.6 in establishing synaptic inhibition in the thalamic network (Makinson et al., 2017), supporting the LoF results caused by missense mutations in the mature protein. These attributes lead to different network effects in distinct nervous system circuits. Mutations in *SCN8A* are associated with early-infantile epileptic encephalopathy type 13 (EIEE13; OMIM #614558), a phenotypically heterogeneous early onset epilepsy, with seizure onset happening before 18 months of age (Hammer et al., 2016). Patients typically develop intellectual disability, developmental delay, and movement disorders (Ohba et al., 2014; Gardella et al., 2016; Johannesen et al., 2018). Co-occurrence of autism spectrum disorders, severe juvenile osteoporosis, bradyarrhythmia, cortical visual impairment, and gastrointestinal disorders have been reported in rare cases (Larsen et al., 2015; Hammer et al., 2016; Rolvien et al., 2017; Gardella et al., 2018). Sudden unexpected death in epilepsy (SUDEP) has also been linked to *SCN8A* mutations, described as the most common cause of death in epilepsy patients. Reports have suggested that patients with *SCN8A*-related epilepsy have increased risk of SUDEP, ranging from 1% to 10% (Hammer et al., 2016; Wang et al., 2017a; Gardella et al., 2018; Johannesen et al., 2018). One possible correlation of SUDEP with *SCN8A*-related epilepsy is the presence of NaV1.6 in heart muscles and tissues, being broadly expressed within ventricular myocytes (Maier et al., 2002). Single mutations may affect heart function, causing failure of the cardiorespiratory system and, consequently, death (Haufe et al., 2005; Noujaim et al., 2012). Most recently, few cases of *SCN8A*-related epilepsies with "milder" phenotype were associated with benign familial infantile seizures-5 (BFIS5; OMIM #617080) (Anand et al., 2016; Gardella et al., 2016; Han et al., 2017).

An increase in new described variants made some mutation patterns visible. Wagnon and co-workers observed numerous cases of the same epiletogenic mutation, and suggested that CpG dinucleotides are mutation hotspots that, through enzymatic processing and epigenetic methylation, can convert cytosine to thymine, such as arginine residues 1617 and 1872 (Wagnon and Meisler, 2015). The prominent number of new variant cases in Arg850 indicates this residue as a new hotspot, since the arginine codon holds a CpG dinucleotide. In addition to these mutation hotspots, residues I763, I1327, G1475, A1650, and N1877 do not present CpG dinucleotides in their codon; however, they can be considered recurrent mutations in view of its high repetition cases in literature (**Table 4**).

The mutation at position c.- 8A>G produces a pathogenic variant, despite not being inside the gene, or promoter regions,

transcriptional and translational sites. This mutation was detected in an untranslated region outside of the Kozak consensus sequence (Johannesen et al., 2019). Its role in *SCN8A*-related epilepsy is still unclear; however, it may change RNA stability, modulate transcriptional factors and promoters, modify the initiation of translation, or work as an enhancer or silencer in the splicing pattern. For all the reasons mentioned above, Nav1.6 variants are predominantly harmful, and the same mutation can lead to different phenotypes, hampering the correlation of genotypes with phenotypes (Blanchard et al., 2015).

SCN8A mutations can be both GoF and LoF, which will likely require different approaches and targets. Even in patients with the same SCN8A mutation, the response to the same drug treatment can differ. Surprisingly, most *SCN8A*-related epilepsies respond favorably to channel blockers. Phenytoin and lacosamide are SBCs widely used in SCN8A mutations with GoF effect, while carbamazepine exhibited positive seizure control in a patient with NaV 1.6 mutation and LoF effect. (Blanchard et al., 2015; Wagnon and Meisler, 2015; Hammer et al., 2016; Perucca and Perucca, 2019). Phenytoin demonstrated effectiveness in decreasing seizure episodes in several patients with *SCN8A*-related epilepsies, however, side effects during prolonged use are very common (Boerma et al., 2016; Braakman et al., 2017). A recent study of a DS model using zebrafish demonstrated the use of the channel blocking compound MV1312, which is 5–6 fold selectivity of NaV1.6 over NaV1.1–1.7, reduced burst movement phenotype and the number of epileptiform events, activity similar to that described with the use of a selective NaV1.1 activator AA43279 (Weuring et al., 2020). Selective Nav1.6 blockers may represent a new therapeutic strategy for DS patients. In addition, two precise and promising drugs have been described recently: XEN901 and GS967. XEN901 is an arylsulfonamide highly selective and potent NaV1.6 inhibitor that binds specifically in voltage sensor domain IV, avoiding recovery from inactivation. GS967 is a NaV1.6 modulator that inhibits the persistent sodium current and exhibits a protective effect (Baker et al., 2018; Bialer et al., 2018).

NaV1.7

The *SCN9A* gene encodes for the NaV1.7 channel, located in chromosome 2q24 (Yang et al., 2018). NaV1.7 is expressed preferably in the PNS, but it is also expressed in the CNS (Cen et al., 2017). Consequently, mutations in this channel are generally related to pain disorders (Young, 2007; Han et al., 2009; Doty, 2010; Rush et al., 2018); however, current studies have described a correlation between epilepsy and this channel (OMIM #603415).

Pain disorder mutations with GoF are related with diseases such as erythromelalgia (EMI), small-fiber neuropathy (SFN) and paroxysmal extreme pain disorder (PEPD), and mutations with LoF are related with congenital insensitivity to pain (CIP) (Cen et al., 2017). Epilepsy studies such as Zhang S. et al. (2020) showed mutations with GoF phenotype: W1150R, N641Y, and K655R mutations (**Table 5**). Being that, after treatment with OXC (120 μmol/L), N641Y and K655R reduced sodium current and decreased the opening time of the channel, while W1150R did not alter that (Zhang S. et al., 2020). However, in a study conducted by Yang et al. (2018), one of the patients presented generalized tonic-clonic

TABLE 5 | SCN9A-related epilepsies identified in clinical patients through WES and/or NGS.

Variant	Location	Mutation	Disease	Alteration on *biophysical properties* or/and Clinical report	Reference
Inherited mutation					
Q10R	N-terminal	Missense	GEFS+	Febrile and afebrile seizures Generalized tonic-clonic seizures	(Cen et al., 2017)
G327E	DI	Missense	Epilepsy	Generalized tonic-clonic seizure	(Yang et al., 2018)
N641Y	DI- DII	Missense	FS	Reduced electroconvulsive seizure thresholds (Knocking mice) Increased corneal kindling acquisition rates (Knocking mice) Increased current density Faster recovery from inactivation More susceptible to clonic and tonic seizures induced by electrical stimulation (mice) Enhanced persistent current	(Singh et al., 2009; Zhang S. et al., 2020)
I1901fs	C-terminal	Frameshift	Epilepsy	Generalized tonic-clonic seizure	(Yang et al., 2018)
Non genetic origin mutations reported*					
K655R	DI-DII	Missense	FS	Enhanced persistent current Faster recovery from inactivation	(Zhang S. et al., 2020)
W1150R	DII-DIII	Missense	FS	Increased current density Enhanced persistent current Focal seizures with secondary generalization High-potential spike activity, paroxysmal release, and d frequency power enhancement (EEG)	(Zhang S. et al., 2020)

seizure with fever, treated with sodium valproic acid, and a LoF mutation I1901fs was observed (Yang et al., 2018) (**Table 5**).

Variants of NaV1.7 have been related with febrile seizure or GEFS+ (Cen et al., 2017; Zhang S. et al., 2020) and even as asymptomatic (Singh et al., 2009). However, SCN9A can act as a putative modifier of NaV1.1 gene; consequently, it can elevate the severity of patients' phenotype (Guerrini et al., 2010; Parihar and Ganesh, 2013). Some NaV1.7 mutations could probably contribute to generate a genetic susceptibility to a known epilepsy disease called Dravet syndrome, in a multifactorial way, as a modifier gene (Singh et al., 2009; Doty, 2010; Mulley et al., 2013; Cen et al., 2017; Zhang T. et al., 2020). That said, some rare cases of DS found in patients can be understood (Mulley et al., 2013). For example, even parents with mild phenotype had children with severe cases (Guerrini et al., 2010).

CONCLUSION AND FUTURE PERSPECTIVES

The past two decades have enabled remarkable progress in understanding monogenic epilepsies. NaV-related epilepsies are diseases of phenotypic heterogeneity, since sodium channels are found in both the CNS and the PNS, but with different expression ranges. The lack of a clear genotype-phenotype correlation to help guide patient counseling and management by healthcare professionals makes it very complex, and often expensive, to determine a correct diagnosis. Consequently, identify the monogenic mutation in individual patients with epilepsy is important not only for diagnosis and prognosis, but also for a correct treatment approach (Mei et al., 2017; Reif et al., 2017).

Susceptibility to specific treatments may be different depending on the disease's features, diverging even in patients who share the same phenotype and/or mutation (Weber et al., 2014). The use of innovative tools that facilitate and prevent diagnostic delay in patients with epilepsy of unknown etiology onset is crucial. WES has proved to be a valuable tool to circumvent the lack of an accurate and fast diagnosis to epilepsies caused by monogenic mutation, and also cheapen and drastically anticipate diagnosis. This genetic diagnostic tool may reduce traditional investigation costs by 55 to 70%, besides avoiding further pre-surgical evaluation and epilepsy surgery (Kothur et al., 2018; Oates et al., 2018). In addition to the financial impact, it can anticipate diagnosis from nearly 3.5 years to 21 days, optimizing management and health care support (Oates et al., 2018).

Effective and safe drugs for the treatment of monogenic epilepsy are still an unmet clinical need. The drugs currently available in the pharmaceutical market are only palliative methods for a temporary control of the disease symptoms, and few patients will benefit from the existing pharmacotherapy, since a great number of patients treated with antiepileptic channel blockers showed no improvement in clinical conditions. Also, most treated patients exhibited manifold side effects, and the prolonged use of these medications proved to be harmful (Boerma et al., 2016; Braakman et al., 2017). Several examples of novel and promising candidate compounds to be used in personalized medicine, such as precision therapies, have been suggested. A previously study demonstrated that CBD at 1μM inhibit preferably resurgent currents than transient current in Nav1.6 WT and also inhibit peak resurgent current in Nav1.6 mutant N1768D, with less effect in current density and without alters voltage dependence of activation (Patel et al., 2016) Possibly the modulation of CBD over mutations in SCN8A that promotes a phenotype with increased resurgent currents would cause a reduction in the causative excitability of epileptic seizures. CBD also showed its ability to preferential inhibit resurgent currents in the NaV1.2 channel (Mason and Cummins, 2020). Due the role of Nav1.2 and Nav1.6 in excitatory neurons, preferentially inhibition in resurgent currents by CBD could possibly reduce the excitability in that subset of neurons and decrease the frequency of seizures by a change in threshold of activation and repetitive fire (Lewis and Raman, 2014). Peptides derived from scorpion and spider venom are well known modulator tools in neuroscience and showed specific capacity to regulate most NaV subtypes related with monogenic epilepsy, unlike the available promiscuous drugs that generally interact with any NaV channel isoform (Schiavon et al., 2006; Israel et al., 2018; Richards et al., 2018; Tibery et al., 2019; Zhang et al., 2019). Bioengineering tools, like antisense oligonucleotides capable to regulate NaV1.1 channels expression, and the peptide Hm1, that modulates the function of this subtype of sodium channel, are some innovative treatment examples (Richards et al., 2018; Stoke Therapeutics, 2018).

However, there is still a long path toward the development of efficacious treatments for NaV-related epilepsies. Recent studies offered a better understanding of the complexity of the phenotypic and genetic spectrum, which has only just begun to be elucidated. Biomolecular diagnostic tools will drastically reduce the developmental and cognitive effects caused by misdiagnosis and late diagnosis, and maybe, in the upcoming years, the treatment for inherited NaV-related epilepsies will be conducted ideally *in utero*, during the prenatal stage. Moreover, further functional studies, with greater cohorts of patients, represent an urgent medical need for a better understanding of the correlations between genotype and clinical symptoms, as well as the different NaV-related epilepsies mechanisms. These studies will improve clinical efficacy and promote safety diagnostic strategies, as well as develop prognosis prediction in the near future.

AUTHOR CONTRIBUTIONS

All authors made an intellectual and direct contribution for this article and approved it for publication.

FUNDING

This study was supported by the Conselho Nacional de Desenvolvimento Científico e Tecnológico (CNPq) [407625/2013-5] and the Fundação de Apoio à Pesquisa do Distrito Federal (FAPDF) [grants 193.001.202/2016 and 00193.0000109/2019-17].

ACKNOWLEDGMENTS

CNPq, CAPES, and the Molecular Biology postgraduate program of the University of Brasilia. LM received scholarships from CNPq and DT from CAPES. EFS was supported by CNPq.

SUPPLEMENTARY MATERIAL

The Supplementary Material for this article can be found online at: https://www.frontiersin.org/articles/10.3389/fphar.2020.01276/full#supplementary-material

REFERENCES

Abdelsayed, M., and Sokolov, S. (2013). Voltage-gated sodium channels. *Channels* 7, 146–152. doi: 10.4161/chan.24380

Ahern, C. A., Payandeh, J., Bosmans, F., and Chanda, B. (2016). The hitchhiker's guide to the voltage-gated sodium channel galaxy. *J. Gen. Physiol.* 147, 1–24. doi: 10.1085/jgp.201511492

Allen, A. S., Berkovic, S. F., Cossette, P., Delanty, N., Dlugos, D., Eichler, E. E., et al. (2013). De novo mutations in epileptic encephalopathies. *Nature* 501, 217–221. doi: 10.1038/nature12439

Allen, N. M., Conroy, J., Shahwan, A., Lynch, B., Correa, R. G., Pena, S. D. J., et al. (2016). Unexplained early onset epileptic encephalopathy: Exome screening and phenotype expansion. *Epilepsia* 57, e12–e17. doi: 10.1111/epi.13250

Anand, G., Collett-White, F., Orsini, A., Thomas, S., Jayapal, S., Trump, N., et al. (2016). Autosomal dominant SCN8A mutation with an unusually mild phenotype. *Eur. J. Paediatr. Neurol.* 20, 761–765. doi: 10.1016/j.ejpn.2016.04.015

Annesi, G., Gambardella, A., Carrideo, S., Incorpora, G., Labate, A., Pasqua, A. A., et al. (2003). Two Novel SCN1A Missense Mutations in Generalized Epilepsy with Febrile Seizures Plus. *Epilepsia* 44, 1257–1258. doi: 10.1046/j.1528-1157.2003.22503.x

Arafat, A., Jing, P., Ma, Y., Pu, M., Nan, G., Fang, H., et al. (2017). Unexplained Early Infantile Epileptic Encephalopathy in Han Chinese Children: Next-Generation Sequencing and Phenotype Enriching. *Sci. Rep.* 7:46227. doi: 10.1038/srep46227

Atanasoska, M., Vazharova, R., Ivanov, I., Balabanski, L., Andonova, S., Ivanov, S., et al. (2018). SCN8A p.Arg1872Gln mutation in early infantile epileptic encephalopathy type 13: Review and case report. *Biotechnol. Biotechnol. Equip.* 32, 1345–1351. doi: 10.1080/13102818.2018.1532815

Bähler, M., and Rhoads, A. (2002). Calmodulin signaling via the IQ motif. *FEBS Lett.* 513, 107–113. doi: 10.1016/S0014-5793(01)03239-2

Baasch, A. L., Hüning, I., Gilissen, C., Klepper, J., Veltman, J. A., Gillessen-Kaesbach, G., et al. (2014). Exome sequencing identifies a de novo SCN2A mutation in a patient with intractable seizures, severe intellectual disability, optic atrophy, muscular hypotonia, and brain abnormalities. *Epilepsia* 55, e25–e29. doi: 10.1111/epi.12554

Bagnasco, I., Dassi, P., Blé, R., and Vigliano, P. (2018). A relatively mild phenotype associated with mutation of SCN8A. *Seizure* 56, 47–49. doi: 10.1016/j.seizure.2018.01.021

Baker, E. M., Thompson, C. H., Hawkins, N. A., Wagnon, J. L., Wengert, E. R., Patel, M. K., et al. (2018). The novel sodium channel modulator GS-458967 (GS967) is an effective treatment in a mouse model of SCN8A encephalopathy. *Epilepsia* 59, 1166–1176. doi: 10.1111/epi.14196

Balciuniene, J., DeChene, E. T., Akgumus, G., Romasko, E. J., Cao, K., Dubbs, H. A., et al. (2019). Use of a Dynamic Genetic Testing Approach for Childhood-Onset Epilepsy. *JAMA Netw. Open* 2, e192129. doi: 10.1001/jamanetworkopen.2019.2129

Barba, C., Parrini, E., Coras, R., Galuppi, A., Craiu, D., Kluger, G., et al. (2014). Co-occurring malformations of cortical development and SCN1A gene mutations. *Epilepsia* 55, 1009–1019. doi: 10.1111/epi.12658

Baroni, D., Picco, C., and Moran, O. (2018). A mutation of SCN1B associated with GEFS+ causes functional and maturation defects of the voltage-dependent sodium channel. *Hum. Mutat.* 39, 1402–1415. doi: 10.1002/humu.23589

Bartnik, M., Chun-Hui Tsai, A., Xia, Z., Cheung, S., and Stankiewicz, P. (2011). Disruption of the SCN2A and SCN3A genes in a patient with mental retardation, neurobehavioral and psychiatric abnormalities, and a history of infantile seizures. *Clin. Genet.* 80, 191–195. doi: 10.1111/j.1399-0004.2010.01526.x

Baumer, F. M., Peters, J. M., El Achkar, C. M., and Pearl, P. L. (2015). SCN2A-Related Early-Onset Epileptic Encephalopathy Responsive to Phenobarbital. *J. Pediatr. Epilepsy* 05, 042–046. doi: 10.1055/s-0035-1567853

Bechi, G., Rusconi, R., Cestèle, S., Striano, P., Franceschetti, S., and Mantegazza, M. (2015). Rescuable folding defective NaV1.1 (SCN1A) mutants in epilepsy: Properties, occurrence, and novel rescuing strategy with peptides targeted to the endoplasmic reticulum. *Neurobiol. Dis.* 75, 100–114. doi: 10.1016/j.nbd.2014.12.028

Bennett, C. A., Petrovski, S., Oliver, K. L., and Berkovic, S. F. (2017). ExACtly zero or once. *Neurol. Genet.* 3, e163. doi: 10.1212/NXG.0000000000000163

Ben-Shalom, R., Keeshen, C. M., Berrios, K. N., An, J. Y., Sanders, S. J., and Bender, K. J. (2017). Opposing Effects on NaV1.2 Function Underlie Differences Between SCN2A Variants Observed in Individuals With Autism Spectrum Disorder or Infantile Seizures. *Biol. Psychiatry* 82, 224–232. doi: 10.1016/j.biopsych.2017.01.009

Berecki, G., Howell, K. B., Deerasooriya, Y. H., Cilio, M. R., Oliva, M. K., Kaplan, D., et al. (2018). Dynamic action potential clamp predicts functional separation in mild familial and severe de novo forms of SCN2A epilepsy. *Proc. Natl. Acad. Sci. U. S. A.* 115, E5516–E5525. doi: 10.1073/pnas.1800077115

Berghuis, B., de Kovel, C. G. F., van Iterson, L., Lamberts, R. J., Sander, J. W., Lindhout, D., et al. (2015). Complex SCN8A DNA-abnormalities in an individual with therapy resistant absence epilepsy. *Epilepsy Res.* 115, 141–144. doi: 10.1016/j.eplepsyres.2015.06.007

Berkovic, S. F., Heron, S. E., Giordano, L., Marini, C., Guerrini, R., Kaplan, R. E., et al. (2004). Benign Familial Neonatal-Infantile Seizures: Characterization of a New Sodium Channelopathy. *Ann. Neurol.* 55, 550–557. doi: 10.1002/ana.20029

Berkovic, S. F., Grinton, B., Dixon-Salazar, T., Laughlin, B. L., Lubbers, L., Milder, J., et al. (2018). De novo variants in the alternative exon 5 of SCN8A cause epileptic encephalopathy. *Genet. Med.* 20, 275–281. doi: 10.1038/gim.2017.100

Bialer, M., Johannessen, S. I. I., Koepp, M. J., Levy, R. H., Perucca, E., Tomson, T., et al. (2018). Progress report on new antiepileptic drugs: A summary of the Fourteenth Eilat Conference on New Antiepileptic Drugs and Devices (EILAT XIV). I. Drugs preclinical early clinical development. *Epilepsia* 59, 1811–1841. doi: 10.1111/epi.14557

Black, J. A., Nikolajsen, L., Kroner, K., Jensen, T. S., and Waxman, S. G. (2008). Multiple sodium channel isoforms and mitogen-activated protein kinases are present in painful human neuromas. *Ann. Neurol.* 64, 644–653. doi: 10.1002/ana.21527

Blanchard, M. G., Willemsen, M. H., Walker, J. B., Dib-Hajj, S. D., Waxman, S. G., Jongmans, M. C. J., et al. (2015). De novo gain-of-function and loss-of-function mutations of SCN8A in patients with intellectual disabilities and epilepsy. *J. Med. Genet.* 52, 330–337. doi: 10.1136/jmedgenet-2014-102813

Boerma, R. S., Braun, K. P., van de Broek, M. P. H., van Berkestijn, F. M. C., Swinkels, M. E., Hagebeuk, E. O., et al. (2016). Remarkable Phenytoin Sensitivity in 4 Children with SCN8A-related Epilepsy: A Molecular Neuropharmacological Approach. *Neurotherapeutics* 13, 192–197. doi: 10.1007/s13311-015-0372-8

Bouza, A. A., and Isom, L. L. (2018). "Voltage-Gated Sodium Channel b Subunits and Their Related Diseases," in *Handbook of experimental pharmacology* (Springer International Publishing), 423–450. doi: 10.1007/164_2017_48

Braakman, H. M., Verhoeven, J. S., Erasmus, C. E., Haaxma, C. A., Willemsen, M. H., and Schelhaas, H. J. (2017). Phenytoin as a last-resort treatment in SCN8A encephalopathy. *Epilepsia Open* 2, 343–344. doi: 10.1002/epi4.12059

Brunklaus, A., Ellis, R., Reavey, E., Semsarian, C., and Zuberi, S. M. (2014). Genotype phenotype associations across the voltage-gated sodium channel family. *J. Med. Genet.* 51, 650–658. doi: 10.1136/jmedgenet-2014-102608

Brunklaus, A., Ellis, R., Stewart, H., Aylett, S., Reavey, E., Jefferson, R., et al. (2015). Homozygous mutations in the SCN1A gene associated with genetic epilepsy

with febrile seizures plus and Dravet syndrome in 2 families. *Eur. J. Paediatr. Neurol.* 19, 484–488. doi: 10.1016/j.ejpn.2015.02.001

Buoni, S., Orrico, A., Galli, L., Zannolli, R., Burroni, L., Hayek, J., et al. (2006). SCN1delG) novel truncating mutation with benign outcome of severe myoclonic epilepsy of infancy. *Neurology* 66, 606–607. doi: 10.1212/01.WNL.0000198504.41315.B1

Butler, K. M., da Silva, C., Alexander, J. J., Hegde, M., and Escayg, A. (2017a). Diagnostic Yield From 339 Epilepsy Patients Screened on a Clinical Gene Panel. *Pediatr. Neurol.* 77, 61–66. doi: 10.1016/j.pediatrneurol.2017.09.003

Butler, K. M., da Silva, C., Shafir, Y., Weisfeld-Adams, J. D., Alexander, J. J., Hegde, M., et al. (2017b). De novo and inherited SCN8A epilepsy mutations detected by gene panel analysis. *Epilepsy Res.* 129, 17–25. doi: 10.1016/j.eplepsyres.2016.11.002

Caldwell, J. H., Schaller, K. L., Lasher, R. S., Peles, E., and Levinson, S. R. (2000). Sodium channel Nav1.6 is localized at nodes of Ranvier, dendrites, and synapses. *Proc. Natl. Acad. Sci.* 97, 5616–5620. doi: 10.1073/pnas.090034797

Capes, D. L., Goldschen-Ohm, M. P., Arcisio-Miranda, M., Bezanilla, F., and Chanda, B. (2013). Domain IV voltage-sensor movement is both sufficient and rate limiting for fast inactivation in sodium channels. *J. Gen. Physiol.* 142, 101–112. doi: 10.1085/jgp.201310998

Carranza Rojo, D., Hamiwka, L., McMahon, J. M., Dibbens, L. M., Arsov, T., Suls, A., et al. (2011). De novo SCN1A mutations in migrating partial seizures of infancy. *Neurology* 77, 380–383. doi: 10.1212/WNL.0b013e318227046d

Carvill, G. L., Heavin, S. B., Yendle, S. C., McMahon, J. M., O'Roak, B. J., Cook, J., et al. (2013). Targeted resequencing in epileptic encephalopathies identifies de novo mutations in CHD2 and SYNGAP1. *Nat. Genet.* 45, 825–830. doi: 10.1038/ng.2646

Catterall, W. A., Kalume, F., and Oakley, J. C. (2010). NaV1.1 channels and epilepsy. *J. Physiol.* 588, 1849–1859. doi: 10.1113/jphysiol.2010.187484

Catterall, W. A. (2014a). Sodium Channels, Inherited Epilepsy, and Antiepileptic Drugs. *Annu. Rev. Pharmacol. Toxicol.* 54, 317–338. doi: 10.1146/annurevpharmtox-011112-140232

Catterall, W. A. (2014b). Structure and function of voltage-gated sodium channels at atomic resolution. *Exp. Physiol.* 99, 35–51. doi: 10.1113/expphysiol.2013.071969

Catterall, W. A. (2017). Forty Years of Sodium Channels: Structure, Function, Pharmacology, and Epilepsy. *Neurochem. Res.* 42, 2495–2504. doi: 10.1007/s11064-017-2314-9

Cen, Z., Lou, Y., Guo, Y., Wang, J., and Feng, J. (2017). Q10R mutation in SCN9A gene is associated with generalized epilepsy with febrile seizures plus. *Seizure* 50, 186–188. doi: 10.1016/j.seizure.2017.06.023

Cheah, C. S., Westenbroek, R. E., Roden, W. H., Kalume, F., Oakley, J. C., Jansen, L. A., et al. (2013). Correlations in timing of sodium channel expression, epilepsy, and sudden death in Dravet syndrome. *Channels* 7, 468–472. doi: 10.4161/chan.26023

Chen, Y. H., Dale, T. J., Romanos, M. A., Whitaker, W. R. J., Xie, X. M., and Clare, J. J. (2000). Cloning, distribution and functional analysis of the type III sodium channel from human brain. *Eur. J. Neurosci.* 12, 4281–4289. doi: 10.1046/j.1460-9568.2000.01336.x

Cestèle, S., Labate, A., Rusconi, R., Tarantino, P., Mumoli, L., Franceschetti, S., et al. (2013). Divergent effects of the T1174S SCN1A mutation associated with seizures and hemiplegic migraine. *Epilepsia* 54, 927–935. doi: 10.1111/epi.12123

Cetica, V., Chiari, S., Mei, D., Parrini, E., Grisotto, L., Marini, C., et al. (2017). Clinical and genetic factors predicting Dravet syndrome in infants with SCN1A mutations. *Neurology* 88, 1037–1044. doi: 10.1212/WNL.0000000000003716

Chen, Y. J., Shi, Y. W., Xu, H. Q., Chen, M. L., Gao, M. M., Sun, W. W., et al. (2015). Electrophysiological Differences between the Same Pore Region Mutation in SCN1A and SCN3A. *Mol. Neurobiol.* 51, 1263–1270. doi: 10.1007/s12035-014-8802-x

Chong, P. F., Saitsu, H., Sakai, Y., Imagi, T., Nakamura, R., Matsukura, M., et al. (2018). Deletions of SCN2A and SCN3A genes in a patient with West syndrome and autistic spectrum disorder. *Seizure* 60, 91–93. doi: 10.1016/j.seizure.2018.06.012

Claes, L., Del-Favero, J., Ceulemans, B., Lagae, L., Van Broeckhoven, C., and De Jonghe, P. (2001). De novo mutations in the sodium-channel gene SCN1A cause severe myoclonic epilepsy of infancy. *Am. J. Hum. Genet.* 68, 1327–1332. doi: 10.1086/320609

Claes, L., Ceulemans, B., Audenaert, D., Smets, K., Löfgren, A., Del-Favero, J., et al. (2003). De novo SCN1A mutations are a major cause of severe myoclonic epilepsy of infancy. *Hum. Mutat.* 21, 615–621. doi: 10.1002/humu.10217

Clairfeuille, T., Cloake, A., Infield, D. T., Llongueras, J. P., Arthur, C. P., Li, Z. R., et al. (2019). Structural basis of a-scorpion toxin action on Nav channels. *Science* 363, 1–25. doi: 10.1126/science.aav8573

Clark, M. M., Stark, Z., Farnaes, L., Tan, T. Y., White, S. M., Dimmock, D., et al. (2018). Meta-analysis of the diagnostic and clinical utility of genome and exome sequencing and chromosomal microarray in children with suspected genetic diseases. *NPJ Genomic Med.* 3, 16. doi: 10.1038/s41525-018-0053-8

Colombo, E., Franceschetti, S., Avanzini, G., and Mantegazza, M. (2013). Phenytoin Inhibits the Persistent Sodium Current in Neocortical Neurons by Modifying Its Inactivation Properties. *PloS One* 8, e55329. doi: 10.1371/journal.pone.0055329

Colosimo, E., Gambardella, A., Mantegazza, M., Labate, A., Rusconi, R., Schiavon, E., et al. (2007). Electroclinical Features of a Family with Simple Febrile Seizures and Temporal Lobe Epilepsy Associated with SCN1A Loss-of-Function Mutation. *Epilepsia* 48, 1691–1696. doi: 10.1111/j.1528-1167.2007.01153.x

Combi, R., Grioni, D., Contri, M., Redaelli, S., Redaelli, F., Bassi, M. T., et al. (2009). Clinical and genetic familial study of a large cohort of Italian children with idiopathic epilepsy. *Brain Res. Bull.* 79, 89–96. doi: 10.1016/j.brainresbull.2009.01.008

Costain, G., Cordeiro, D., Matviychuk, D., and Mercimek-Andrews, S. (2019). Clinical Application of Targeted Next-Generation Sequencing Panels and Whole Exome Sequencing in Childhood Epilepsy. *Neuroscience* 418, 291–310. doi: 10.1016/j.neuroscience.2019.08.016

Cui, X., Zeng, F., Liu, Y., Zhang, J., Archacki, S., Zhan, T., et al. (2011). A novel SCN1A missense mutation causes generalized epilepsy with febrile seizures plus in a Chinese family. *Neurosci. Lett.* 503, 27–30. doi: 10.1016/j.neulet.2011.08.001

Cummins, T. R., and Waxman, S. G. (1997). Downregulation of tetrodotoxinresistant sodium currents and upregulation of a rapidly repriming tetrodotoxin-sensitive sodium current in small spinal sensory neurons after nerve injury. *J. Neurosci.* 17, 3503–3514. doi: 10.1523/jneurosci.17-10-03503.1997

Cummins, T. R., Aglieco, F., Renganathan, M., Herzog, R. I. I., Dib-Hajj, S. D., and Waxman, S. G. (2001). Nav1.3 sodium channels: Rapid repriming and slow closed-state inactivation display quantitative differences after expression in a mammalian cell line and in spinal sensory neurons. *J. Neurosci.* 21, 5952–5961. doi: 10.1523/jneurosci.21-16-05952.2001

Daoud, H., Luco, S. M., Li, R., Bareke, E., Beaulieu, C., Jarinova, O., et al. (2016). Next-generation sequencing for diagnosis of Rare diseases in the neonatal intensive care unit. *Cmaj* 188, E254–E260. doi: 10.1503/cmaj.150823

Davidsson, J., Collin, A., Olsson, M. E., Lundgren, J., and Soller, M. (2008). Deletion of the SCN gene cluster on 2q24.4 is associated with severe epilepsy: An array-based genotype–phenotype correlation and a comprehensive review of previously published cases. *Epilepsy Res.* 81, 69–79. doi: 10.1016/j.eplepsyres.2008.04.018

de Kovel, C. G. F., Meisler, M. H., Brilstra, E. H., van Berkestijn, F. M. C., van Lieshout, S., et al. (2014). Characterization of a de novo SCN8A mutation in a patient with epileptic encephalopathy. *Epilepsy Res.* 108, 1511–1518. doi: 10.1016/j.eplepsyres.2014.08.020

Deciphering Developmental Disorders Study (2015). Large-scale discovery of novel genetic causes of developmental disorders. *Nature* 519, 223–228. doi: 10.1038/nature14135

Deng, H., Xiu, X., and Song, Z. (2014). The molecular biology of genetic-based epilepsies. *Mol. Neurobiol.* 49, 352–367. doi: 10.1007/s12035-013-8523-6

Denis, J., Villeneuve, N., Cacciagli, P., Mignon-Ravix, C., Lacoste, C., Lefranc, J., et al. (2019). Clinical study of 19 patients with SCN8A-related epilepsy: Two modes of onset regarding EEG and seizures. *Epilepsia* 60, 845–856. doi: 10.1111/epi.14727

Depienne, C., Trouillard, O., Saint-Martin, C., Gourfinkel-An, I., Bouteiller, D., Carpentier, W., et al. (2008). Spectrum of SCN1A gene mutations associated with Dravet syndrome: analysis of 333 patients. *J. Med. Genet.* 46, 183–191. doi: 10.1136/jmg.2008.062323

Devinsky, O., Vezzani, A., Jette, N., De Curtis, M., and Perucca, P. (2018). Epilepsy. *Nat. Rev.* 3, 1–24. doi: 10.1038/nrdp.2018.24

Dhamija, R., Wirrell, E., Falcao, G., Kirmani, S., and Wong-Kisiel, L. C. (2013). Novel de novo SCN2A Mutation in a Child With Migrating Focal Seizures of Infancy. *Pediatr. Neurol.* 49, 486–488. doi: 10.1016/j.pediatrneurol.2013.07.004

Dhamija, R., Erickson, M. K., St Louis, E. K., Wirrell, E., and Kotagal, S. (2014). Sleep Abnormalities in Children With Dravet Syndrome. *Pediatr. Neurol.* 50, 474–478. doi: 10.1016/j.pediatrneurol.2014.01.017

Djémié, T., Weckhuysen, S., von Spiczak, S., Carvill, G. L., Jaehn, J., Anttonen, A.-K., et al. (2016). Pitfalls in genetic testing: the story of missed SCN1A mutations. *Mol. Genet. Genomic Med.* 4, 457–464. doi: 10.1002/mgg3.217

Doty, C. N. (2010). SCN9A: Another sodium channel excited to play a role in human epilepsies. *Clin. Genet.* 77, 326–328. doi: 10.1111/j.1399-0004.2009.01366_1.x

Dyment, D. A., Tétreault, M., Beaulieu, C. L., Hartley, T., Ferreira, P., Chardon, J. W., et al. (2015). Whole-exome sequencing broadens the phenotypic spectrum of rare pediatric epilepsy: A retrospective study. *Clin. Genet.* 88, 34–40. doi: 10.1111/cge.12464

Ebach, K., Joos, H., Doose, H., Stephani, U., Kurlemann, G., Fiedler, B., et al. (2005). SCN1A mutation analysis in myoclonic astatic epilepsy and severe idiopathic generalized epilepsy of infancy with generalized tonic-clonic seizures. *Neuropediatrics* 36, 210–213. doi: 10.1055/s-2005-865607

Ebrahimi, A., Houshmand, M., Tonekaboni, S. H., Fallah Mahboob Passand, M. S., Zainali, S., and Moghadasi, M. (2010). Two Novel Mutations in SCN1A Gene in Iranian Patients with Epilepsy. *Arch. Med. Res.* 41, 207–214. doi: 10.1016/j.arcmed.2010.04.007

Egri, C., Vilin, Y. Y., and Ruben, P. C. (2012). A thermoprotective role of the sodium channel β 1 subunit is lost with the β 1(C121W) mutation. *Epilepsia* 53, 494–505. doi: 10.1111/j.1528-1167.2011.03389.x

Encinas, A. C., Moore, I., (Ki), M., Watkins, J. C., and Hammer, M. F. (2019). Influence of age at seizure onset on the acquisition of neurodevelopmental skills in an SCN8A cohort. *Epilepsia* 60, 1711–1720. doi: 10.1111/epi.16288

Epifanio, R., Zanotta, N., Giorda, R., Bardoni, A., and Zucca, C. (2019). Novel epilepsy phenotype associated to a known SCN8A mutation. *Seizure* 67, 15–17. doi: 10.1016/j.seizure.2019.01.017

Escayg, A., Heils, A., MacDonald, B. T., Haug, K., Sander, T., and Meisler, M. H. (2001). A Novel SCN1A Mutation Associated with Generalized Epilepsy with Febrile Seizures Plus—and Prevalence of Variants in Patients with Epilepsy. *Am. J. Hum. Genet.* 68, 866–873. doi: 10.1086/319524

Escayg, A., and Goldin, A. L. (2010). Sodium channel SCN1A and epilepsy : Mutations and mechanisms. *Epilepsia* 51, 1650–1658. doi: 10.1111/j.1528-1167.2010.02640.x

Estacion, M., Gasser, A., Dib-Hajj, S. D., and Waxman, S. G. (2010). A sodium channel mutation linked to epilepsy increases ramp and persistent current of Nav1.3 and induces hyperexcitability in hippocampal neurons. *Exp. Neurol.* 224, 362–368. doi: 10.1016/j.expneurol.2010.04.012

Estacion, M., and Waxman, S. G. (2013). The response of NaV1.3 sodium channels to ramp stimuli: Multiple components and mechanisms. *J. Neurophysiol.* 109, 306–314. doi: 10.1152/jn.00438.2012

Estacion, M., O'Brien, J. E., Conravey, A., Hammer, M. F., Waxman, S. G., Dib-Hajj, S. D., et al. (2014). A novel de novo mutation of SCN8A (Nav1.6) with enhanced channel activation in a child with epileptic encephalopathy. *Neurobiol. Dis.* 69, 117–123. doi: 10.1016/j.nbd.2014.05.017

Esterhuizen, A.II, Mefford, H. C., Ramesar, R. S., Wang, S., Carvill, G. L., and Wilmshurst, J. M. (2018). Dravet syndrome in South African infants: Tools for an early diagnosis. *Seizure* 62, 99–105. doi: 10.1016/j.seizure.2018.09.010

Falco-Walter, J. J., Scheffer, I. E., and Fisher, R. S. (2018). The new definition and classification of seizures and epilepsy. *Epilepsy Res.* 139, 73–79. doi: 10.1016/j.eplepsyres.2017.11.015

Felts, P. A., Yokoyama, S., Dib-Hajj, S., Black, J. A., and Waxman, S. G. (1997). Sodium channel a-subunit mRNAs I, II, III, NaG, Na6 and hNE (PN1): different expression patterns in developing rat nervous system. *Mol. Brain Res.* 45, 71–82. doi: 10.1016/S0169-328X(96)00241-0

Fisher, R. S., Acevedo, C., Arzimanoglou, A., Bogacz, A., Cross, J. H., Elger, C. E., et al. (2014). ILAE Official Report: A practical clinical definition of epilepsy. *Epilepsia* 55, 475–482. doi: 10.1111/epi.12550

Foster, L. A., Johnson, M. R., MacDonald, J. T., Karachunski, P.II, Henry, T. R., Nascene, D. R., et al. (2017). Infantile Epileptic Encephalopathy Associated With SCN2A Mutation Responsive to Oral Mexiletine. *Pediatr. Neurol.* 66, 108–111. doi: 10.1016/j.pediatrneurol.2016.10.008

Fry, A. E., Rees, E., Thompson, R., Mantripragada, K., Blake, P., Jones, G., et al. (2016). Pathogenic copy number variants and SCN1A mutations in patients with intellectual disability and childhood-onset epilepsy. *BMC Med. Genet.* 17, 34. doi: 10.1186/s12881-016-0294-2

Fujiwara, T. (2003). Mutations of sodium channel alpha subunit type 1 (SCN1A) in intractable childhood epilepsies with frequent generalized tonic-clonic seizures. *Brain* 126, 531–546. doi: 10.1093/brain/awg053

Fukasawa, T., Kubota, T., Negoro, T., Saitoh, M., Mizuguchi, M., Ihara, Y., et al. (2015). A case of recurrent encephalopathy with SCN2A missense mutation. *Brain Dev.* 37, 631–634. doi: 10.1016/j.braindev.2014.10.001

Fukuma, G., Oguni, H., Shirasaka, Y., Watanabe, K., Miyajima, T., Yasumoto, S., et al. (2004). Mutations of Neuronal Voltage-gated Na+ Channel alpha1 Subunit Gene SCN1A in Core Severe Myoclonic Epilepsy in Infancy (SMEI) and in Borderline SMEI (SMEB). *Epilepsia* 45, 140–148. doi: 10.1111/j.0013-9580.2004.15103.x

Fung, L.-W. E., Kwok, S.-L. J., and Tsui, K.-W. S. (2015). SCN8A mutations in Chinese children with early onset epilepsy and intellectual disability. *Epilepsia* 56, 1319–1320. doi: 10.1111/epi.12925

Fung, C. W., Kwong, A. K. Y., and Wong, V. C. N. (2017). Gene panel analysis for nonsyndromic cryptogenic neonatal/infantile epileptic encephalopathy. *Epilepsia Open* 2, 236–243. doi: 10.1002/epi4.12055

Gamal El-Din, T. M., Martinez, G. Q., Payandeh, J., Scheuer, T., and Catterall, W. A. (2013). A gating charge interaction required for late slow inactivation of the bacterial sodium channel NavAb. *J. Gen. Physiol.* 142, 181–190. doi: 10.1085/jgp.201311012

Gardella, E., Becker, F., Møller, R. S., Schubert, J., Lemke, J. R., Larsen, L. H. G., et al. (2016). Benign infantile seizures and paroxysmal dyskinesia caused by an SCN8A mutation. *Ann. Neurol.* 79, 428–436. doi: 10.1002/ana.24580

Gardella, E., Marini, C., Trivisano, M., Fitzgerald, M. P., Alber, M., Howell, K. B., et al. (2018). The phenotype of SCN8A developmental and epileptic encephalopathy. *Neurology* 91, E1112–E1124. doi: 10.1212/WNL.0000000000006199

Gargus, J. J., and Tournay, A. (2007). Novel Mutation Confirms Seizure Locus SCN1A is Also Familial Hemiplegic Migraine Locus FHM3. *Pediatr. Neurol.* 37, 407–410. doi: 10.1016/j.pediatrneurol.2007.06.016

Ghovanloo, M. R., Aimar, K., Ghadiry-Tavi, R., Yu, A., and Ruben, P. C. (2016). Physiology and Pathophysiology of Sodium Channel Inactivation. *Curr. Top. Membr.* 78, 479–509. doi: 10.1016/bs.ctm.2016.04.001

Gokben, S., Onay, H., Yilmaz, S., Atik, T., Serdaroglu, G., Tekin, H., et al. (2017). Targeted next generation sequencing: the diagnostic value in early-onset epileptic encephalopathy. *Acta Neurol. Belg.* 117, 131–138. doi: 10.1007/s13760-016-0709-z

Gilchrist, J., Das, S., Van Petegem, F., and Bosmans, F. (2013). Crystallographic insights into sodium-channel modulation by the b4 subunit. *Proc. Natl. Acad. Sci.* 110, E5016–E5024. doi: 10.1073/pnas.1314557110

Goldin, A. L., and Escayg, A. (2010). Sodium channel SCN1A and epilepsy: mutations and mechanisms. *Epilepsia* 51:16. doi: 10.1111/j.1528-1167.2010.02640.x

Goldschen-Ohm, M. P., Capes, D. L., Oelstrom, K. M., and Chanda, B. (2013). Multiple pore conformations driven by asynchronous movements of voltage sensors in a eukaryotic sodium channel. *Nat. Commun.* 4, 1350. doi: 10.1038/ncomms2356

Gorman, K. M., and King, M. D. (2017). SCN2A p.Ala263Val Variant a Phenotype of Neonatal Seizures Followed by Paroxysmal Ataxia in Toddlers. *Pediatr. Neurol.* 67, 111–112. doi: 10.1016/j.pediatrneurol.2016.11.008

Grinton, B. E., Heron, S. E., Pelekanos, J. T., Zuberi, S. M., Kivity, S., Afawi, Z., et al. (2015). Familial neonatal seizures in 36 families: Clinical and genetic features correlate with outcome. *Epilepsia* 56, 1071–1080. doi: 10.1111/epi.13020

Guerrini, R., Cellini, E., Mei, D., Metitieri, T., Petrelli, C., Pucatti, D., et al. (2010). Variable epilepsy phenotypes associated with a familial intragenic deletion of the SCN1A gene. *Epilepsia* 51, 2474–2477. doi: 10.1111/j.1528-1167.2010.02790.x

Hackenberg, A., Baumer, A., Sticht, H., Schmitt, B., Kroell-Seger, J., Wille, D., et al. (2014). Infantile Epileptic Encephalopathy, Transient Choreoathetotic Movements, and Hypersomnia due to a De Novo Missense Mutation in the SCN2A Gene. *Neuropediatrics* 45, 261–264. doi: 10.1055/s-0034-1372302

Haginoya, K., Togashi, N., Kaneta, T., Hino-Fukuyo, N., Ishitobi, M., Kakisaka, Y., et al. (2018). [18F]fluorodeoxyglucose-positron emission tomography study of genetically confirmed patients with Dravet syndrome. *Epilepsy Res.* 147, 9–14. doi: 10.1016/j.eplepsyres.2018.08.008

Hains, B. C., Klein, J. P., Saab, C. Y., Craner, M. J., Black, J. A., and Waxman, S. G. (2003). Upregulation of sodium channel Nav1.3 and functional involvement in neuronal hyperexcitability associated with central neuropathic pain after spinal cord injury. *J. Neurosci.* 23, 8881–8892. doi: 10.1523/jneurosci.23-26-08881.2003

Halvorsen, M., Petrovski, S., Shellhaas, R., Tang, Y., Crandall, L., Goldstein, D., et al. (2016). Mosaic mutations in early-onset genetic diseases. *Genet. Med.* 18, 746–749. doi: 10.1038/gim.2015.155

Han, J. Y., Jang, J. H., Lee, I. G., Shin, S., and Park, J. (2017). A novel inherited mutation of SCN8a in a korean family with benign familial infantile epilepsy using diagnostic exome sequencing. *Ann. Clin. Lab. Sci.* 47, 747–753.

Han, C., Dib-Hajj, S. D., Lin, Z., Li, Y., Eastman, E. M., Tyrrell, L., et al. (2009). Early- and late-onset inherited erythromelalgia: genotypephenotype correlation. *Brain* 132, 1711–1722. doi: 10.1093/brain/awp078

Hammer, M. F., Wagnon, J. L., Mefford, H. C., Meisler, M. H., et al. (2016). "SCN8A-Related Epilepsy with Encephalopathy," in *GeneReviews® [Internet]*. Eds. M. P. Adam, H. H. Ardinger and R. A. Pagon (Seattle (WA): University of Washington).

Harkin, L. A., McMahon, J. M., Iona, X., Dibbens, L., Pelekanos, J. T., Zuberi, S. M., et al. (2007). The spectrum of SCN1A-related infantile epileptic encephalopathies. *Brain* 130, 843–852. doi: 10.1093/brain/awm002

Haug, K., Hallmann, K., Rebstock, J., Dullinger, J., Muth, S., Haverkamp, F., et al. (2001). The voltage-gated sodium channel gene SCN2A and idiopathic generalized epilepsy. *Epilepsy Res.* 47, 243–246. doi: 10.1016/S0920-1211(01)00312-6

Haufe, V., Camacho, J. A., Dumaine, R., Günther, B., Bollensdorff, C., von Banchet, G. S., et al. (2005). Expression pattern of neuronal and skeletal muscle voltage-gated Na+ channels in the developing mouse heart. *J. Physiol.* 564, 683–696. doi: 10.1113/jphysiol.2004.079681

Herlenius, E., Heron, S. E., Grinton, B. E., Keay, D., Scheffer, I. E., Mulley, J. C., et al. (2007). SCN2A mutations and benign familial neonatal-infantile seizures: The phenotypic spectrum. *Epilepsia* 48, 1138–1142. doi: 10.1111/j.1528-1167.2007.01049.x

Hernández Chávez, M., Mesa Latorre, T., Pedraza Herrera, M., and Troncoso Schifferli, M. (2014). ¿Crisis febriles complejas o síndrome de Dravet?: Descripción de 3 casos clínicos. *Rev. Chil. pediatría* 85, 588–593. doi: 10.4067/S0370-41062014000500010

Heron, S. E., Crossland, K. M., Andermann, E., Phillips, H. A., Hall, A. J., Bleasel, A., et al. (2002). Sodium-channel defects in benign familial neonatal-infantile seizures. *Lancet* 360, 851–852. doi: 10.1016/S0140-6736(02)09968-3

Heron, S. E., Scheffer, I. E., Grinton, B. E., Eyre, H., Oliver, K. L., Bain, S., et al. (2010). Familial neonatal seizures with intellectual disability caused by a microduplication of chromosome 2q24.3. *Epilepsia* 51, 1865–1869. doi: 10.1111/j.1528-1167.2010.02558.x

Hewson, S., Brunga, L., Ojeda, M. F., Imhof, E., Patel, J., Zak, M., et al. (2018). Prevalence of Genetic Disorders and GLUT1 Deficiency in a Ketogenic Diet Clinic. *Can. J. Neurol. Sci.* 45, 93–96. doi: 10.1017/cjn.2017.246

Heyne, H. O., Artomov, M., Battke, F., Bianchini, C., Smith, D. R., Liebmann, N., et al. (2019). Targeted gene sequencing in 6994 individuals with neurodevelopmental disorder with epilepsy. *Genet. Med.* 21, 2496–2503. doi: 10.1038/s41436-019-0531-0

Hoffman-Zacharska, D., Szczepanik, E., Terczynska, I., Goszczanska-Ciuchta, A., Zalewska-Miszkurka, Z., Tataj, R., et al. (2015). From focal epilepsy to dravet syndrome –heterogeneity of the phenotype due to SCN1A mutations of the p.Arg1596 amino acid residue in the nav1.1 subunit. *Neurol. Neurochir. Pol.* 49, 258–266. doi: 10.1016/j.pjnns.2015.06.006

Holland, K. D., Kearney, J. A., Glauser, T. A., Buck, G., Keddache, M., Blankston, J. R., et al. (2008). Mutation of sodium channel SCN3A in a patient with cryptogenic pediatric partial epilepsy. *Neurosci. Lett.* 433, 65–70. doi: 10.1016/j.neulet.2007.12.064

Horvath, G. A., Demos, M., Shyr, C., Matthews, A., Zhang, L., Race, S., et al. (2016). Secondary neurotransmitter deficiencies in epilepsy caused by voltage-gated sodium channelopathies: A potential treatment target? *Mol. Genet. Metab.* 117, 42–48. doi: 10.1016/j.ymgme.2015.11.008

Howell, K. B., McMahon, J. M., Carvill, G. L., Tambunan, D., Mackay, M. T., Rodriguez-Casero, V., et al. (2015). SCN2A encephalopathy. *Neurology* 85, 958–966. doi: 10.1212/WNL.0000000000001926

Hsiao, J., Yuan, T. Y., Tsai, M. S., Lu, C. Y., Lin, Y. C., Lee, M. L., et al. (2016). Upregulation of Haploinsufficient Gene Expression in the Brain by Targeting a Long Non-coding RNA Improves Seizure Phenotype in a Model of Dravet Syndrome. *EBioMedicine* 9, 257–277. doi: 10.1016/j.ebiom.2016.05.011

Hu, W., Tian, C., Li, T., Yang, M., Hou, H., and Shu, Y. (2009). Distinct contributions of Nav1.6 and Nav1.2 in action potential initiation and backpropagation. *Nat. Neurosci.* 12, 996–1002. doi: 10.1038/nn.2359

Huang, W., Liu, M., Yan, S. F., and Yan, N. (2017). Structure-based assessment of disease-related mutations in human voltage-gated sodium channels. *Protein Cell* 8, 401–438. doi: 10.1007/s13238-017-0372-z

Hussain, A., Seinfeld, S., and Morton, L. (2016). Genetic association with ictal cardiorespiratory phenomena: SCN8A case series. *J. Pediatr. Neurol.* 14, 151–155. doi: 10.1055/s-0036-1593744

Iannetti, P., Parisi, P., Spalice, A., Ruggieri, M., and Zara, F. (2009). Addition of verapamil in the treatment of severe myoclonic epilepsy in infancy. *Epilepsy Res.* 85, 89–95. doi: 10.1016/j.eplepsyres.2009.02.014

Inuzuka, L. M., Macedo-Souza, L.II, Della-Ripa, B., Cabral, K. S. S., Monteiro, F., Kitajima, J. P., et al. (2019). Neurodevelopmental disorder associated with de novo SCN3A pathogenic variants: two new cases and review of the literature. *Brain Dev.* 42, 211–216. doi: 10.1016/j.braindev.2019.09.004

Israel, M. R., Thongyoo, P., Deuis, J. R., Craik, D. J., Vetter, I., and Durek, T. (2018). The E15R Point Mutation in Scorpion Toxin Cn2 Uncouples Its Depressant and Excitatory Activities on Human Na V 1.6. *J. Med. Chem.* 61, 1730–1736. doi: 10.1021/acs.jmedchem.7b01609

Ito, M., Shirasaka, Y., Hirose, S., Sugawara, T., and Yamakawa, K. (2004). Seizure phenotypes of a family with missense mutations in SCN2A. *Pediatr. Neurol.* 31, 150–152. doi: 10.1016/j.pediatrneurol.2004.02.013

Jain, P., Gulati, P., Morrison-Levy, N., Yau, I., Alsowat, D., Otsubo, H., et al. (2019). "Breath holding spells" in a child with SCN8A-related epilepsy: Expanding the clinical spectrum. *Seizure* 65, 129–130. doi: 10.1016/j.seizure.2019.01.020

Jang, S. S., Kim, S. Y., Kim, H., Hwang, H., Chae, J. H., Kim, K. J., et al. (2019). Diagnostic Yield of Epilepsy Panel Testing in Patients With Seizure Onset Within the First Year of Life. *Front. Neurol.* 10, 988. doi: 10.3389/fneur.2019.00988

Jiang, D., Shi, H., Tonggu, L., Gamal El-Din, T. M., Lenaeus, M. J., Zhao, Y., et al. (2020). Structure of the Cardiac Sodium Channel. *Cell* 180, 122–134.e10. doi: 10.1016/j.cell.2019.11.041

Jingami, N., Matsumoto, R., Ito, H., Ishii, A., Ihara, Y., Hirose, S., et al. (2014). A novel SCN1A mutation in a cytoplasmic loop in intractable juvenile myoclonic epilepsy without febrile seizures. *Epileptic Disord.* 16, 227–231. doi: 10.1684/epd.2014.0657

Johannesen, K. M., Gardella, E., Scheffer, I., Howell, K., Smith, D. M., Helbig, I., et al. (2018). Early mortality in SCN8A -related epilepsies. *Epilepsy Res.* 143, 79–81. doi: 10.1016/j.eplepsyres.2018.04.008

Johannesen, K. M., Gardella, E., Encinas, A. C., Lehesjoki, A. E., Linnankivi, T., Petersen, M. B., et al. (2019). The spectrum of intermediate SCN8A-related epilepsy. *Epilepsia* 60, 830–844. doi: 10.1111/epi.14705

Johnson, C. N., Potet, F., Thompson, M. K., Kroncke, B. M., Glazer, A. M., Voehler, M. W., et al. (2018). A Mechanism of Calmodulin Modulation of the Human Cardiac Sodium Channel. *Structure* 26, 683–694.e3. doi: 10.1016/j.str.2018.03.005

Kamiya, K. (2004). A Nonsense Mutation of the Sodium Channel Gene SCN2A in a Patient with Intractable Epilepsy and Mental Decline. *J. Neurosci.* 24, 2690–2698. doi: 10.1523/JNEUROSCI.3089-03.2004

Kaplan, D. I. I., Isom, L. L., and Petrou, S. (2016). Role of sodium channels in epilepsy. *Cold Spring Harb. Perspect. Med.* 6:a022814. doi: 10.1101/cshperspect.a022814

Kearney, J., Plummer, N., Smith, M., Kapur, J., Cummins, T., Waxman, S., et al. (2001). A gain-of-function mutation in the sodium channel gene Scn2a results in seizures and behavioral abnormalities. *Neuroscience* 102, 307–317. doi: 10.1016/S0306-4522(00)00479-6

Kim, Y. O., Bellows, S., Mcmahon, J. M., Iona, X., Damiano, J., Dibbens, L., et al. (2014). Atypical multifocal Dravet syndrome lacks generalized seizures and

may show later cognitive decline. *Dev. Med. Child Neurol.* 56, 85–90. doi: 10.1111/dmcn.12322

Kim, H. J., Yang, D., Kim, S. H., Kim, B., Kim, H. D., Lee, J. S., et al. (2019). Genetic and clinical features of SCN8A developmental and epileptic encephalopathy. *Epilepsy Res.* 158, 106222. doi: 10.1016/j.eplepsyres.2019.106222

Knupp, K. G., and Wirrell, E. C. (2018). Treatment Strategies for Dravet Syndrome. *CNS Drugs* 32, 335–350. doi: 10.1007/s40263-018-0511-y

Kobayashi, K., Ohzono, H., Shinohara, M., Saitoh, M., Ohmori, I., Ohtsuka, Y., et al. (2012). Acute encephalopathy with a novel point mutation in the SCN2A gene. *Epilepsy Res.* 102, 109–112. doi: 10.1016/j.eplepsyres.2012.04.016

Kodera, H., Kato, M., Nord, A. S., Walsh, T., Lee, M., Yamanaka, G., et al. (2013). Targeted capture and sequencing for detection of mutations causing early onset epileptic encephalopathy. *Epilepsia* 54, 1262–1269. doi: 10.1111/epi.12203

Kothur, K., Holman, K., Farnsworth, E., Ho, G., Lorentzos, M., Troedson, C., et al. (2018). Diagnostic yield of targeted massively parallel sequencing in children with epileptic encephalopathy. *Seizure* 59, 132–140. doi: 10.1016/j.seizure.2018.05.005

Kwong, A. K. Y., Fung, C. W., Chan, S. Y., and Wong, V. C. N. (2012). Identification of SCN1A and PCDH19 mutations in Chinese children with Dravet syndrome. *PloS One* 7, e41802. doi: 10.1371/journal.pone.0041802

Laezza, F., Lampert, A., Kozel, M. A., Gerber, B. R., Rush, A. M., Nerbonne, J. M., et al. (2009). FGF14 N-terminal splice variants differentially modulate Nav1.2 and Nav1.6-encoded sodium channels. *Mol. Cell. Neurosci.* 42, 90–101. doi: 10.1016/j.mcn.2009.05.007

Lal, D., Reinthaler, E. M., Dejanovic, B., May, P., Thiele, H., Lehesjoki, A.-E., et al. (2016). Evaluation of Presumably Disease Causing SCN1A Variants in a Cohort of Common Epilepsy Syndromes. *PloS One* 11, e0150426. doi: 10.1371/journal.pone.0150426

Lamar, T., Vanoye, C. G., Calhoun, J., Wong, J. C., Dutton, S. B., Jorge, B. S., et al. (2017). SCN3A deficiency associated with increased seizure susceptibility. *Neurobiol. Dis.* 102, 38–48. doi: 10.1016/j.nbd.2017.02.006

Larsen, J., Carvill, G. L., Gardella, E., Kluger, G., Schmiedel, G., Barisic, N., et al. (2015). The phenotypic spectrum of SCN8A encephalopathy. *Neurology* 84, 480–489. doi: 10.1212/WNL.0000000000001211

Lattanzi, S., Brigo, F., Trinka, E., Zaccara, G., Striano, P., Del Giovane, C., et al. (2020). Adjunctive Cannabidiol in Patients with Dravet Syndrome: A Systematic Review and Meta-Analysis of Efficacy and Safety. *CNS Drugs* 34, 229–241. doi: 10.1007/s40263-020-00708-6

Lauxmann, S., Boutry-Kryza, N., Rivier, C., Mueller, S., Hedrich, U. B. S., Maljevic, S., et al. (2013). An SCN2A mutation in a family with infantile seizures from Madagascar reveals an increased subthreshold Na+ current. *Epilepsia* 54, e117–e121. doi: 10.1111/epi.12241

Lek, M., Karczewski, K. J., Minikel, E. V., Samocha, K. E., Banks, E., Fennell, T., et al. (2016). Analysis of protein-coding genetic variation in 60,706 humans. *Nature* 536, 285–291. doi: 10.1038/nature19057

Le Gal, F., Lebon, S., Ramelli, G. P., Datta, A. N., Mercati, D., Maier, O., et al. (2014). When is a child with status epilepticus likely to have Dravet syndrome? *Epilepsy Res.* 108, 740–747. doi: 10.1016/j.eplepsyres.2014.02.019

Lee, H.-F., Chi, C.-S., Tsai, C.-R., Chen, C.-H., and Wang, C.-C. (2014). Electroencephalographic features of patients with SCN1A-positive Dravet syndrome. *Brain Dev.* 37, 599–611. doi: 10.1016/j.braindev.2014.10.003

Lemke, J. R., Riesch, E., Scheurenbrand, T., Schubach, M., Wilhelm, C., Steiner, I., et al. (2012). Targeted next generation sequencing as a diagnostic tool in epileptic disorders. *Epilepsia* 53, 1387–1398. doi: 10.1111/j.1528-1167.2012.03516.x

Lewis, A. H., and Raman, I. M. (2014). Resurgent current of voltage-gated Na+ channels. *J. Physiol.* 592, 4825–4838. doi: 10.1113/jphysiol.2014.277582

Liao, W.-P., Shi, Y.-W., Long, Y.-S., Zeng, Y., Li, T., Yu, M.-J., et al. (2010a). Partial epilepsy with antecedent febrile seizures and seizure aggravation by antiepileptic drugs: Associated with loss of function of Nav1.1. *Epilepsia* 51, 1669–1678. doi: 10.1111/j.1528-1167.2010.02645.x

Liao, Y., Deprez, L., Maljevic, S., Pitsch, J., Claes, L., Hristova, D., et al. (2010b). Molecular correlates of age-dependent seizures in an inherited neonatal-infantile epilepsy. *Brain* 133, 1403–1414. doi: 10.1093/brain/awq057

Lim, B. C., Hwang, H., Chae, J. H., Choi, J.-E., Hwang, Y. S., Kang, S.-H., et al. (2011). SCN1A mutational analysis in Korean patients with Dravet syndrome. *Seizure* 20, 789–794. doi: 10.1016/j.seizure.2011.08.002

Lin, K. M., Su, G., Wang, F., Zhang, X., Wang, Y., Ren, J., et al. (2019). A de novo SCN8A heterozygous mutation in a child with epileptic encephalopathy: A case report. *BMC Pediatr.* 19, 400. doi: 10.1186/s12887-019-1796-9

Lindy, A. S., Stosser, M. B., Butler, E., Downtain-Pickersgill, C., Shanmugham, A., Retterer, K., et al. (2018). Diagnostic outcomes for genetic testing of 70 genes in 8565 patients with epilepsy and neurodevelopmental disorders. *Epilepsia* 59, 1062–1071. doi: 10.1111/epi.14074

Liu, J., Tong, L., Song, S., Niu, Y., Li, J., Wu, X., et al. (2018). Novel and de novo mutations in pediatric refractory epilepsy. *Mol. Brain* 11, 48. doi: 10.1186/s13041-018-0392-5

Liu, Y., Schubert, J., Sonnenberg, L., Helbig, K. L., Hoei-Hansen, C. E., Koko, M., et al. (2019). Neuronal mechanisms of mutations in SCN8A causing epilepsy or intellectual disability. *Brain* 142, 376–390. doi: 10.1093/brain/awy326

Lossin, C., Rhodes, T. H., Desai, R. R., Vanoye, C. G., Wang, D., Carniciu, S., et al. (2003). Epilepsy-Associated Dysfunction in the Voltage-Gated Neuronal Sodium Channel SCN1A. *J. Neurosci.* 23, 11289–11295. doi: 10.1523/jneurosci.23-36-11289.2003

Lossin, C., Shi, X., Rogawski, M. A., and Hirose, S. (2012). Compromised function in the Nav1.2 Dravet syndrome mutation R1312T. *Neurobiol. Dis.* 47, 378–384. doi: 10.1016/j.nbd.2012.05.017

Lucas, P. T., Meadows, L. S., Nicholls, J., and Ragsdale, D. S. (2005). An epilepsy mutation in the β1 subunit of the voltage-gated sodium channel results in reduced channel sensitivity to phenytoin. *Epilepsy Res.* 64, 77–84. doi: 10.1016/j.eplepsyres.2005.03.003

Maier, S. K. G., Westenbroek, R. E., Schenkman, K. A., Feigl, E. O., Scheuer, T., and Catterall, W. A. (2002). An unexpected role for brain-type sodium channels in coupling of cell surface depolarization to contraction in the heart. *Proc. Natl. Acad. Sci. U. S. A.* 99, 4073–4078. doi: 10.1073/pnas.261705699

Mak, C. M., Chan, K. Y. W., Yau, E. K. C., Chen, S. P. L., Siu, W. K., Law, C. Y., et al. (2011). Genetic diagnosis of severe myoclonic epilepsy of infancy (Dravet syndrome) with SCN1A mutations in the Hong Kong Chinese patients. *Hong Kong Med. J. = Xianggang yi xue za zhi* 17, 500–502.

Makinson, C. D., Tanaka, B. S., Sorokin, J. M., Wong, J. C., Christian, C. A., Goldin, A. L., et al. (2017). Regulation of Thalamic and Cortical Network Synchrony by Scn8a. *Neuron* 93, 1165–1179.e6. doi: 10.1016/j.neuron.2017.01.031

Malcolmson, J., Kleyner, R., Tegay, D., Adams, W., Ward, K., Coppinger, J., et al. (2016). SCN8A mutation in a child presenting with seizures and developmental delays. *Cold Spring Harb. Mol. Case Stud.* 2, a001073. doi: 10.1101/mcs.a001073

Malo, D., Schurr, E., Dorfman, J., Canfield, V., Levenson, R., and Gros, P. (1991). Three brain sodium channel a-subunit genes are clustered on the proximal segment of mouse chromosome 2. *Genomics* 10, 666–672. doi: 10.1016/0888-7543(91)90450-S

Malo, M. S., Blanchard, B. J., Andresen, J. M., Srivastava, K., Chen, X.-N., Li, X., et al. (1994). Localization of a putative human brain sodium channel gene (SCN1A) to chromosome band 2q24. *Cytogenet. Genome Res.* 67, 178–186. doi: 10.1159/000133818

Mantegazza, M., Gambardella, A., Rusconi, R., Schiavon, E., Annesi, F., Cassulini, R. R., et al. (2005). Identification of an Nav1.1 sodium channel (SCN1A) loss-of-function mutation associated with familial simple febrile seizures. *Proc. Natl. Acad. Sci. U. S. A.* 102, 18177–18182. doi: 10.1073/pnas.0506818102

Marini, C., Mei, D., Temudo, T., Ferrari, A. R., Buti, D., Dravet, C., et al. (2007). Idiopathic Epilepsies with Seizures Precipitated by Fever and SCN1A Abnormalities. *Epilepsia* 48, 1678–1685. doi: 10.1111/j.1528-1167.2007.01122.x

Martin, H. C., Kim, G. E., Pagnamenta, A. T., Murakami, Y., Carvill, G. L., Meyer, E., et al. (2014). Clinical whole-genome sequencing in severe early-onset epilepsy reveals new genes and improves molecular diagnosis. *Hum. Mol. Genet.* 23, 3200–3211. doi: 10.1093/hmg/ddu030

Mason, E. R., Wu, F., Patel, R. R., Xiao, Y., Cannon, S. C., and Cummins, T. R. (2019). Resurgent and gating pore currents induced by De Novo SCN2A epilepsy mutations. *eNeuro* 6, 1–17, ENEURO.0141–19.2019. doi: 10.1523/ENEURO.0141-19.2019

Mason, E. R., and Cummins, T. R. (2020). Differential inhibition of human Nav1.2 resurgent and persistent sodium currents by cannabidiol and GS967. *Int. J. Mol. Sci.* 21, 1–21. doi: 10.3390/ijms21072454

Matalon, D., Goldberg, E., Medne, L., and Marsh, E. D. (2014). Confirming an expanded spectrum of SCN2A mutations: a case series. *Epileptic Disord.* 16, 13–18. doi: 10.1684/epd.2014.0641

McMichael, G., Bainbridge, M. N., Haan, E., Corbett, M., Gardner, A., Thompson, S., et al. (2015). Whole-exome sequencing points to considerable genetic heterogeneity of cerebral palsy. *Mol. Psychiatry* 20, 176–182. doi: 10.1038/mp.2014.189

McNally, M. A., Johnson, J., Huisman, T. A., Poretti, A., Baranano, K. W., Baschat, A. A., et al. (2016). SCN8A Epileptic Encephalopathy: Detection of Fetal Seizures Guides Multidisciplinary Approach to Diagnosis and Treatment. *Pediatr. Neurol.* 64, 87–91. doi: 10.1016/j.pediatrneurol.2016.08.003

Mei, D., Parrini, E., Marini, C., and Guerrini, R. (2017). The Impact of Next-Generation Sequencing on the Diagnosis and Treatment of Epilepsy in Paediatric Patients. *Mol. Diagnosis Ther.* 21, 357–373. doi: 10.1007/s40291-017-0257-0

Meisler, M. H., O'Brien, J. E., and Sharkey, L. M. (2010). Sodium channel gene family: Epilepsy mutations, gene interactions and modifier effects. *J. Physiol.* 588, 1841–1848. doi: 10.1113/jphysiol.2010.188482

Meng, H., Xu, H. Q., Yu, L., Lin, G. W., He, N., Su, T., et al. (2015). The SCN1A Mutation Database: Updating Information and Analysis of the Relationships among Genotype, Functional Alteration, and Phenotype. *Hum. Mutat.* 36, 573–580. doi: 10.1002/humu.22782

Mercimek-Mahmutoglu, S., Patel, J., Cordeiro, D., Hewson, S., Callen, D., Donner, E. J., et al. (2015). Diagnostic yield of genetic testing in epileptic encephalopathy in childhood. *Epilepsia* 56, 707–716. doi: 10.1111/epi.12954

Misra, S. N., Kahlig, K. M., and George, A. L. (2008). Impaired Na V 1.2 function and reduced cell surface expression in benign familial neonatal-infantile seizures. *Epilepsia* 49, 1535–1545. doi: 10.1111/j.1528-1167.2008.01619.x

Miyatake, S., Kato, M., Sawaishi, Y., Saito, T., Nakashima, M., Mizuguchi, T., et al. (2018). Recurrent SCN3A p.Ile875Thr variant in patients with polymicrogyria. *Ann. Neurol.* 84, 159–161. doi: 10.1002/ana.25256

Møller, R. S., Larsen, L. H. G., Johannesen, K. M., Talvik, I., Talvik, T., Vaher, U., et al. (2016). Gene panel testing in epileptic encephalopathies and familial epilepsies. *Mol. Syndromol.* 7, 210–219. doi: 10.1159/000448369

Morano, A., Fanella, M., Albini, M., Cifelli, P., Palma, E., Giallonardo, A. T., et al. (2020). Cannabinoids in the treatment of epilepsy: Current status and future prospects. *Neuropsychiatr. Dis. Treat.* 16, 381–396. doi: 10.2147/NDT.S203782

Morimoto, M., Mazaki, E., Nishimura, A., Chiyonobu, T., Sawai, Y., Murakami, A., et al. (2006). SCN1A Mutation Mosaicism in a Family with Severe Myoclonic Epilepsy in Infancy. *Epilepsia* 47, 1732–1736. doi: 10.1111/j.1528-1167.2006.00645.x

Mulley, J. C., Hodgson, B., McMahon, J. M., Iona, X., Bellows, S., Mullen, S. A., et al. (2013). Role of the sodium channel SCN9A in genetic epilepsy with febrile seizures plus and Dravet syndrome. *Epilepsia* 54, e122–e126. doi: 10.1111/epi.12323

Musto, E., Gardella, E., and Møller, R. S. (2020). Recent advances in treatment of epilepsy-related sodium channelopathies. *Eur. J. Paediatr. Neurol.* 24, 123–128. doi: 10.1016/j.ejpn.2019.12.009

Myers, K. A., Burgess, R., Afawi, Z., Damiano, J. A., Berkovic, S. F., Hildebrand, M. S., et al. (2017a). De novo SCN1A pathogenic variants in the GEFS+ spectrum: Not always a familial syndrome. *Epilepsia* 58, e26–e30. doi: 10.1111/epi.13649

Myers, K. A., McMahon, J. M., Mandelstam, S. A., Mackay, M. T., Kalnins, R. M., Leventer, R. J., et al. (2017b). Fatal Cerebral Edema With Status Epilepticus in Children With Dravet Syndrome: Report of 5 Cases. *Pediatrics* 139, e20161933. doi: 10.1542/peds.2016-1933

Nabbout, R., Gennaro, E., Dalla Bernardina, B., Dulac, O., Madia, F., Bertini, E., et al. (2003). Spectrum of SCN1A mutations in severe myoclonic epilepsy of infancy. *Neurology* 60, 1961–1967. doi: 10.1212/01.WNL.0000069463.41870.2F

Nabbout, R., Copioli, C., Chipaux, M., Chemaly, N., Desguerre, I., Dulac, O., et al. (2011). Ketogenic diet also benefits Dravet syndrome patients receiving stiripentol: A prospective pilot study. *Epilepsia* 52, 54–57. doi: 10.1111/j.1528-1167.2011.03107.x

Nakamura, K., Kato, M., Osaka, H., Yamashita, S., Nakagawa, E., Haginoya, K., et al. (2013). Clinical spectrum of SCN2A mutations expanding to Ohtahara syndrome. *Neurology* 81, 992–998. doi: 10.1212/WNL.0b013e3182a43e57

Need, A. C., Shashi, V., Hitomi, Y., Schoch, K., Shianna, K. V., McDonald, M. T., et al. (2012). Clinical application of exome sequencing in undiagnosed genetic conditions. *J. Med. Genet.* 49, 353–361. doi: 10.1136/jmedgenet-2012-100819

Ng, S. B., Buckingham, K. J., Lee, C., Bigham, A. W., Tabor, H. K., Dent, K. M., et al. (2010). Exome sequencing identifies the cause of a mendelian disorder. *Nat. Genet.* 42, 30–35. doi: 10.1038/ng.499

Nguyen, H. M., and Goldin, A. L. (2010). Sodium channel carboxyl-terminal residue regulates fast inactivation. *J. Biol. Chem.* 285, 9077–9089. doi: 10.1074/jbc.M109.054940

Nicita, F., Spalice, A., Papetti, L., Ursitti, F., Parisi, P., Gennaro, E., et al. (2010). Genotype-phenotype correlations in a group of 15 SCN1A-mutated italian patients with GEFS+ spectrum (seizures plus, classical and borderline severe myoclonic epilepsy of infancy). *J. Child Neurol.* 25, 1369–1376. doi: 10.1177/0883073810365737

Nishri, D., Blumkin, L., Lev, D., Leshinsky-Silver, E., Abu-Rashid, M., Birch, R., et al. (2010). Hepatic coma culminating in severe brain damage in a child with a SCN1A mutation. *Eur. J. Paediatr. Neurol.* 14, 456–459. doi: 10.1016/j.ejpn.2010.03.002

Noujaim, S. F., Kaur, K., Milstein, M., Jones, J. M., Furspan, P., Jiang, D., et al. (2012). A null mutation of the neuronal sodium channel Na V 1.6 disrupts action potential propagation and excitation-contraction coupling in the mouse heart. *FASEB J.* 26, 63–72. doi: 10.1096/fj.10-179770

Oates, S., Tang, S., Rosch, R., Lear, R., Hughes, E. F., Williams, R. E., et al. (2018). Incorporating epilepsy genetics into clinical practice: A 360°evaluation. *NPJ Genomic Med.* 3, 13. doi: 10.1038/s41525-018-0052-9

O'Brien, J. E., Sharkey, L. M., Vallianatos, C. N., Han, C., Blossom, J. C., Yu, T., et al. (2012). Interaction of Voltage-gated Sodium Channel Na v 1.6 (SCN8A) with Microtubule-associated Protein Map1b. *J. Biol. Chem.* 287, 18459–18466. doi: 10.1074/jbc.M111.336024

Oelstrom, K., Goldschen-ohm, M. P., Holmgren, M., and Chanda, B. (2014). Evolutionarily conserved intracellular gate of voltage-dependent sodium channels. *Nat. Commun.* 5, 1–9. doi: 10.1038/ncomms4420

Ogiwara, I., Ito, K., Sawaishi, Y., Osaka, H., Mazaki, E., Inoue, I., et al. (2009). De novo mutations of voltage-gated sodium channel αiI gene SCN2A in intractable epilepsies. *Neurology* 73, 1046–1053. doi: 10.1212/WNL.0b013e3181b9cebc

Ohashi, T., Akasaka, N., Kobayashi, Y., Magara, S., Kawashima, H., Matsumoto, N., et al. (2014). Infantile epileptic encephalopathy with a hyperkinetic movement disorder and hand stereotypies associated with a novel SCN1A mutation. *Epileptic Disord.* 16, 208–212. doi: 10.1684/epd.2014.0649

Ohba, C., Kato, M., Takahashi, S., Lerman-Sagie, T., Lev, D., Terashima, H., et al. (2014). Early onset epileptic encephalopathy caused by de novo SCN8A mutations. *Epilepsia* 55, 994–1000. doi: 10.1111/epi.12668

Ohmori, I., Kahlig, K. M., Rhodes, T. H., Wang, D. W., and George, A. L. (2006). Nonfunctional SCN1A Is Common in Severe Myoclonic Epilepsy of Infancy. *Epilepsia* 47, 1636–1642. doi: 10.1111/j.1528-1167.2006.00643.x

Oliva, M., Berkovic, S. F., and Petrou, S. (2012). Sodium channels and the neurobiology of epilepsy. *Epilepsia* 53, 1849–1859. doi: 10.1111/j.1528-1167.2012.03631.x

Oliva, M. K., Mcgarr, T. C., Beyer, B. J., Gazina, E., Kaplan, D.II, Cordeiro, L., et al. (2014). Physiological and genetic analysis of multiple sodium channel variants in a model of genetic absence epilepsy. *Neurobiol. Dis.* 67, 180–190. doi: 10.1016/j.nbd.2014.03.007

Olson, H. E., Tambunan, D., LaCoursiere, C., Goldenberg, M., Pinsky, R., Martin, E., et al. (2015). Mutations in epilepsy and intellectual disability genes in patients with features of Rett syndrome. *Am. J. Med. Genet. Part A* 167, 2017–2025. doi: 10.1002/ajmg.a.37132

Orrico, A., Galli, L., Grosso, S., Buoni, S., Pianigiani, R., Balestri, P., et al. (2009). Mutational analysis of the SCN1A, SCN1B and GABRG2 genes in 150 Italian patients with idiopathic childhood epilepsies. *Clin. Genet.* 75, 579–581. doi: 10.1111/j.1399-0004.2009.01155.x

Orsini, A., Zara, F., and Striano, P. (2018). Recent advances in epilepsy genetics. *Neurosci. Lett.* 667, 4–9. doi: 10.1016/j.neulet.2017.05.014

Ortiz Madinaveitia, S., Serrano Madrid, M. L., Conejo Moreno, D., Sagarra Mur, D., Jiménez Corral, C., and Gutiérrez Álvarez, Á.M. (2017). Encefalopatía

epiléptica de inicio precoz en un paciente con mutación en SCN8A. *Rev. Neurol.* 65, 572. doi: 10.33588/rn.6512.2017426

Pan, Y., and Cummins, T. R. (2020). Distinct functional alterations in SCN8A epilepsy mutant channels. *J. Physiol.* 598, 381–401. doi: 10.1113/JP278952

Parrini, E., Marini, C., Mei, D., Galuppi, A., Cellini, E., Pucatti, D., et al. (2017). Diagnostic Targeted Resequencing in 349 Patients with Drug-Resistant Pediatric Epilepsies Identifies Causative Mutations in 30 Different Genes. *Hum. Mutat.* 38, 216–225. doi: 10.1002/humu.23149

Patel, R. R., Barbosa, C., Brustovetsky, T., Brustovetsky, N., and Cummins, T. R. (2016). Aberrant epilepsy-associated mutant Nav1.6 sodium channel activity can be targeted with cannabidiol. *Brain* 139, 2164–2181. doi: 10.1093/brain/aww129

Payandeh, J., Gamal El-Din, T. M., Scheuer, T., Zheng, N., and Catterall, W. A. (2012). Crystal structure of a voltage-gated sodium channel in two potentially inactivated states. *Nature* 486, 135–139. doi: 10.1038/nature11077

Perucca, P., and Perucca, E. (2019). Identifying mutations in epilepsy genes:Impact on treatment selection. *Epilepsy Res.* 152, 18–30. doi: 10.1016/j.eplepsyres.2019.03.001

Pescucci, C., Caselli, R., Grosso, S., Mencarelli, M. A., Mari, F., Farnetani, M. A., et al. (2007). 2q24–q31 Deletion: Report of a case and review of the literature. *Eur. J. Med. Genet.* 50, 21–32. doi: 10.1016/j.ejmg.2006.09.001

Peters, C. H., Sokolov, S., Rajamani, S., and Ruben, P. C. (2013). Effects of the antianginal drug, ranolazine, on the brain sodium channel NaV1.2 and its modulation by extracellular protons. *Br. J. Pharmacol.* 169, 704–716. doi: 10.1111/bph.12150

Petrelli, C., Passamonti, C., Cesaroni, E., Mei, D., Guerrini, R., Zamponi, N., et al. (2012). Early clinical features in Dravet syndrome patients with and without SCN1A mutations. *Epilepsy Res.* 99, 21–27. doi: 10.1016/j.eplepsyres.2011.10.010

Pons, L., Lesca, G., Sanlaville, D., Chatron, N., Labalme, A., Manel, V., et al. (2018). Neonatal tremor episodes and hyperekplexia-like presentation at onset in a child with SCN8A developmental and epileptic encephalopathy. *Epileptic Disord.* 20, 289–294. doi: 10.1684/epd.2018.0988

Petrovski, S., Wang, Q., Heinzen, E. L., Allen, A. S., and Goldstein, D. B. (2013). Genic Intolerance to Functional Variation and the Interpretation of Personal Genomes. *PloS Genet.* 9, 1–13. doi: 10.1371/journal.pgen.1003709

Plummer, N. W., McBurney, M. W., and Meisler, M. H. (1997). Alternative Splicing of the Sodium Channel SCN8A Predicts a Truncated Two-domain Protein in Fetal Brain and Non-neuronal Cells. *J. Biol. Chem.* 272, 24008–24015. doi: 10.1074/jbc.272.38.24008

Poryo, M., Clasen, O., Oehl-Jaschkowitz, B., Christmann, A., Gortner, L., and Meyer, S. (2017). Dravet syndrome: a new causative SCN1A mutation? *Clin. Case Rep.* 5, 613–615. doi: 10.1002/ccr3.787

Ranza, E., Z'Graggen, W., Lidgren, M., Beghetti, M., Guipponi, M., Antonarakis, S. E., et al. (2020). SCN8A heterozygous variants are associated with anoxic-epileptic seizures. *Am. J. Med. Genet. Part A.*. doi: 10.1002/ajmg.a.61513

Rauch, A., Wieczorek, D., Graf, E., Wieland, T., Endele, S., Schwarzmayr, T., et al. (2012). Range of genetic mutations associated with severe non-syndromic sporadic intellectual disability: an exome sequencing study. *Lancet* 380, 1674–1682. doi: 10.1016/S0140-6736(12)61480-9

Raymond, G., Wohler, E., Dinsmore, C., Cox, J., Johnston, M., Batista, D., et al. (2011). An interstitial duplication at 2q24.3 involving the SCN1A, SCN2A, SCN3A genes associated with infantile epilepsy. *Am. J. Med. Genet. Part A* 155, 920–923. doi: 10.1002/ajmg.a.33929

Reif, P. S., Tsai, M. H., Helbig, I., Rosenow, F., and Klein, K. M. (2017). Precision medicine in genetic epilepsies: break of dawn? *Expert Rev. Neurother.* 17, 381–392. doi: 10.1080/14737175.2017.1253476

Reyes, I. S., Hsieh, D. T., Laux, L. C., and Wilfong, A. A. (2011). Alleged Cases of Vaccine Encephalopathy Rediagnosed Years Later as Dravet Syndrome. *Pediatrics* 128. doi: 10.1542/peds.2010-0887

Reynolds, C., King, M. D., and Gorman, K. M. (2020). The phenotypic spectrum of SCN2A-related epilepsy. *Eur. J. Paediatr. Neurol.* 24, 117–122. doi: 10.1016/j.ejpn.2019.12.016

Rhodes, T. H., Vanoye, C. G., Ohmori, I., Ogiwara, I., Yamakawa, K., and George, A. L. (2005). Sodium channel dysfunction in intractable childhood epilepsy with generalized tonic-clonic seizures. *J. Physiol.* 569, 433–445. doi: 10.1113/jphysiol.2005.094326

Riban, V., Fitzsimons, H. L., and During, M. J. (2009). Gene therapy in epilepsy. *Epilepsia* 50, 24–32. doi: 10.1111/j.1528-1167.2008.01743.x

Richards, K. L., Milligan, C. J., Richardson, R. J., Jancovski, N., Grunnet, M., Jacobson, L. H., et al. (2018). Selective NaV1.1 activation rescues Dravet syndrome mice from seizures and premature death. *Proc. Natl. Acad. Sci. U.S. A.* 115, E8077–E8085. doi: 10.1073/pnas.1804764115

Rilstone, J. J., Coelho, F. M., Minassian, B. A., and Andrade, D. M. (2012). Dravet syndrome: Seizure control and gait in adults with different SCN1A mutations. *Epilepsia* 53, 1421–1428. doi: 10.1111/j.1528-1167.2012.03583.x

Rim, J. H., Kim, S. H., Hwang, I. S., Kwon, S. S., Kim, J., Kim, H. W., et al. (2018). Efficient strategy for the molecular diagnosis of intractable early-onset epilepsy using targeted gene sequencing. *BMC Med. Genomics* 11, 6. doi: 10.1186/s12920-018-0320-7

Riva, D., Vago, C., Pantaleoni, C., Bulgheroni, S., Mantegazza, M., and Franceschetti, S. (2009). Progressive neurocognitive decline in two children with Dravet syndrome, de novo SCN1A truncations and different epileptic phenotypes. *Am. J. Med. Genet. Part A* 149A, 2339–2345. doi: 10.1002/ajmg.a.33029

Rolvien, T., Butscheidt, S., Jeschke, A., Neu, A., Denecke, J., Kubisch, C., et al. (2017). Severe bone loss and multiple fractures in SCN8A-related epileptic encephalopathy. *Bone* 103, 136–143. doi: 10.1016/j.bone.2017.06.025

Rossi, M., El-Khechen, D., Black, M. H., Farwell Hagman, K. D., Tang, S., and Powis, Z. (2017). Outcomes of Diagnostic Exome Sequencing in Patients With Diagnosed or Suspected Autism Spectrum Disorders. *Pediatr. Neurol.* 70, 34–43.e2. doi: 10.1016/j.pediatrneurol.2017.01.033

Rubinstein, M., Westenbroek, R. E., Yu, F. H., Jones, C. J., Scheuer, T., and Catterall, W. A. (2015). Genetic background modulates impaired excitability of inhibitory neurons in a mouse model of Dravet syndrome. *Neurobiol. Dis.* 73, 106–117. doi: 10.1016/j.nbd.2014.09.017

Rush, A. M., Dib-Hajj, S. D., Liu, S., Cummins, T. R., Black, J. A., and Waxman, S. G. (2018). "A Single Sodium Channel Mutation Produces Hyperor Hypoexcitability In Different Types Of Neurons," in *Chasing Men on Fire* (PNAS: The MIT Press), 89–101. doi: 10.7551/mitpress/10310.003.0014

Saitoh, M., Shinohara, M., Hoshino, H., Kubota, M., Amemiya, K., Takanashi, J., et al. (2012). Mutations of the SCN1A gene in acute encephalopathy. *Epilepsia* 53, 558–564. doi: 10.1111/j.1528-1167.2011.03402.x

Saitoh, M., Ishii, A., Ihara, Y., Hoshino, A., Terashima, H., Kubota, M., et al. (2015a). Missense mutations in sodium channel SCN1A and SCN2A predispose children to encephalopathy with severe febrile seizures. *Epilepsy Res.* 117, 1–6. doi: 10.1016/j.eplepsyres.2015.08.001

Saitoh, M., Shinohara, M., Ishii, A., Ihara, Y., Hirose, S., Shiomi, M., et al. (2015b). Clinical and genetic features of acute encephalopathy in children taking theophylline. *Brain Dev.* 37, 463–470. doi: 10.1016/j.braindev.2014.07.010

Samanta, D., and Ramakrishnaiah, R. (2015). De novo R853Q mutation of SCN2A gene and West syndrome. *Acta Neurol. Belg.* 115, 773–776. doi: 10.1007/s13760-015-0454-8

Sanders, S. J., Campbell, A. J., Cottrell, J. R., Moller, R. S., Wagner, F. F., Auldridge, A. L., et al. (2018). Progress in Understanding and Treating SCN2A –Mediated Disorders. *Trends Neurosci.* 41, 442–456. doi: 10.1016/j.tins.2018.03.011

Sands, T. T., and Choi, H. (2017). Genetic Testing in Pediatric Epilepsy. *Curr. Neurol. Neurosci. Rep.* 17, 1–11. doi: 10.1007/s11910-017-0753-y

Saxena, S., and Li, S. (2017). Defeating epilepsy: A global public health commitment. *Epilepsia Open* 2, 153–155. doi: 10.1002/epi4.12010

Scalmani, P., Rusconi, R., Armatura, E., Zara, F., Avanzini, G., Franceschetti, S., et al. (2006). Effects in neocortical neurons of mutations of the Nav1.2 Na+ channel causing benign familial neonatal-infantile seizures. *J. Neurosci.* 26, 10100–10109. doi: 10.1523/JNEUROSCI.2476-06.2006

Schreiber, J. M., Tochen, L., Brown, M., Evans, S., Ball, L. J., Bumbut, A., et al. (2020). A multi-disciplinary clinic for SCN8A-related epilepsy. *Epilepsy Res.* 159, 106261. doi: 10.1016/j.eplepsyres.2019.106261

Schwarz, N., Hahn, A., Bast, T., Müller, S., Löffler, H., Maljevic, S., et al. (2016). Mutations in the sodium channel gene SCN2A cause neonatal epilepsy with late-onset episodic ataxia. *J. Neurol.* 263, 334–343. doi: 10.1007/s00415-015-7984-0

Schiavon, E., Sacco, T., Cassulini, R. R., Gurrola, G., Tempia, F., Possani, L. D., et al. (2006). Resurgent Current and Voltage Sensor Trapping Enhanced Activation by a b-Scorpion Toxin Solely in Na v 1.6 Channel. *J. Biol. Chem.* 281, 20326–20337. doi: 10.1074/jbc.M600565200

Sharkey, L. M., Jones, J. M., Hedera, P., and Meisler, M. H. (2009). Evaluation of SCN8A as a candidate gene for autosomal dominant essential tremor. *Park. Relat. Disord.* 15, 321–323. doi: 10.1016/j.parkreldis.2008.06.010

Sheets, P. L., Heers, C., Stoehr, T., and Cummins, T. R. (2008). Differential block of sensory neuronal voltage-gated sodium channels by lacosamide [(2R)-2-(acetylamino)-N-benzyl-3-methoxypropanamide], lidocaine, and carbamazepine. *J. Pharmacol. Exp. Ther.* 326, 89–99. doi: 10.1124/jpet.107.133413

Shen, H., Zhou, Q., Pan, X., Li, Z., Wu, J., and Yan, N. (2017). Structure of a eukaryotic voltage-gated sodium channel at near-atomic resolution. *Science* 355, 1–12. doi: 10.1126/science.aal4326

Shi, X., Yasumoto, S., Nakagawa, E., Fukasawa, T., Uchiya, S., and Hirose, S. (2009). Missense mutation of the sodium channel gene SCN2A causes Dravet syndrome. *Brain Dev.* 31, 758–762. doi: 10.1016/j.braindev.2009.08.009

Shi, X. Y., Tomonoh, Y., Wang, W. Z., Ishii, A., Higurashi, N., Kurahashi, H., et al. (2016). Efficacy of antiepileptic drugs for the treatment of Dravet syndrome with different genotypes. *Brain Dev.* 38, 40–46. doi: 10.1016/j.braindev.2015.06.008

Silva, J. R., and Goldstein, S. A. N. (2013). Voltage-sensor movements describe slow inactivation of voltage-gated sodium channels I: Wild-type skeletal muscle NAv1.4. *J. Gen. Physiol.* 141, 309–321. doi: 10.1085/jgp.201210909

Singh, N. A., Pappas, C., Dahle, E. J., Claes, L. R. F., Pruess, T. H., De Jonghe, P., et al. (2009). A Role of SCN9A in Human Epilepsies, As a Cause of Febrile Seizures and As a Potential Modifier of Dravet Syndrome. *PloS Genet.* 5, e1000649. doi: 10.1371/journal.pgen.1000649

Singh, R., Jayapal, S., Goyal, S., Jungbluth, H., and Lascelles, K. (2015). Early-onset movement disorder and epileptic encephalopathy due to de novo dominant SCN8A mutation. *Seizure* 26, 69–71. doi: 10.1016/j.seizure.2015.01.017

Skjei, K. L., Church, E. W., Harding, B. N., Santi, M., Holland-Bouley, K. D., Clancy, R. R., et al. (2015). Clinical and histopathological outcomes in patients with SCN1A mutations undergoing surgery for epilepsy. *J. Neurosurg. Pediatr.* 16, 668–674. doi: 10.3171/2015.5.PEDS14551

Smith, R. S., Kenny, C. J., Ganesh, V., Jang, A., Borges-Monroy, R., Partlow, J. N., et al. (2018). Sodium Channel SCN3A (NaV1.3) Regulation of Human Cerebral Cortical Folding and Oral Motor Development. *Neuron* 99, 905–913.e7. doi: 10.1016/j.neuron.2018.07.052

Spampanato, J. (2004). A Novel Epilepsy Mutation in the Sodium Channel SCN1A Identifies a Cytoplasmic Domain for Subunit Interaction. *J. Neurosci.* 24, 10022–10034. doi: 10.1523/JNEUROSCI.2034-04.2004

Sone, D., Sugawara, T., Sakakibara, E., Tomioka, Y., Taniguchi, G., Murata, Y., et al. (2012). A case of autosomal dominant nocturnal frontal lobe epilepsy (ADNFLE) coexisting with pervasive developmental disorder harboring SCN1A mutation in addition to CHRNB2 mutation. *Epilepsy Behav.* 25, 192–195. doi: 10.1016/j.yebeh.2012.07.027

Stoke Therapeutics (2018). *Stoke Therapeutics Presents Data Showing Single Dose of ASO Therapy Restores Normal Protein Levels in Animal Model of Genetic Epilepsy*. Available at: https://www.stoketherapeutics.com/press-releases/stoketherapeutics-presents-data-showing-single-dose-of-aso-therapy-restoresnormal-protein-levels-in-animal-model-of-genetic-epilepsy/ (Accessed December 2, 2020).

Sprissler, R. S., Wagnon, J. L., Bunton-Stasyshyn, R. K., Meisler, M. H., and Hammer, M. F. (2017). Altered gene expression profile in a mouse model of SCN8A encephalopathy. *Exp. Neurol.* 288, 134–141. doi: 10.1016/j.expneurol.2016.11.002

Striano, P., Bordo, L., Lispi, M. L., Specchio, N., Minetti, C., Vigevano, F., et al. (2006). A novel SCN2A mutation in family with benign familial infantile seizures. *Epilepsia* 47, 218–220. doi: 10.1111/j.1528-1167.2006.00392.x

Su, D. J., Lu, J. F., Lin, L. J., Liang, J. S., and Hung, K. L. (2018). SCN2A mutation in an infant presenting with migrating focal seizures and infantile spasm responsive to a ketogenic diet. *Brain Dev.* 40, 724–727. doi: 10.1016/j.braindev.2018.03.005

Sugawara, T., Mazaki-Miyazaki, E., Fukushima, K., Shimomura, J., Fujiwara, T., Hamano, S., et al. (2002). Frequent mutations of SCN1A in severe myoclonic epilepsy in infancy. *Neurology* 58, 1122–1124. doi: 10.1212/WNL.58.7.1122

Sugiura, Y., Ogiwara, I., Hoshi, A., Yamakawa, K., and Ugawa, Y. (2012). Different degrees of loss of function between GEFS+ and SMEI Na v1.1 missense mutants at the same residue induced by rescuable folding defects. *Epilepsia* 53, 111–114. doi: 10.1111/j.1528-1167.2012.03467.x

Sun, G., Werkman, T. R., Battefeld, A., Clare, J. J., and Wadman, W. J. (2007). Carbamazepine and Topiramate Modulation of Transient and Persistent Sodium Currents Studied in HEK293 Cells Expressing the Na v 1.3?? *Subunit. Epilepsia* 48, 774–782. doi: 10.1111/j.1528-1167.2007.01001.x

Sun, H., Zhang, Y., Liang, J., Liu, X., Ma, X., Qin, J., et al. (2008). Seven novel SCN1A mutations in Chinese patients with severe myoclonic epilepsy of infancy. *Epilepsia* 49, 1104–1107. doi: 10.1111/j.1528-1167.2008.01549_2.x

Sun, H., Zhang, Y., Liu, X., Ma, X., Yang, Z., Qin, J., et al. (2010). Analysis of SCN1A mutation and parental origin in patients with Dravet syndrome. *J. Hum. Genet.* 55, 421–427. doi: 10.1038/jhg.2010.39

Sun, W., Wagnon, J. L., Mahaffey, C. L., Briese, M., Ule, J., and Frankel, W. N. (2013). Aberrant sodium channel activity in the complex seizure disorder of Celf4 mutant mice. *J. Physiol.* 591, 241–255. doi: 10.1113/jphysiol.2012.240168

Syrbe, S., Zhorov, B. S., Bertsche, A., Bernhard, M. K., Hornemann, F., Mütze, U., et al. (2016). Phenotypic Variability from Benign Infantile Epilepsy to Ohtahara Syndrome Associated with a Novel Mutation in *SCN2A*. *Mol. Syndromol.* 7, 182–188. doi: 10.1159/000447526

Tai, C., Abe, Y., Westenbroek, R. E., Scheuer, T., and Catterall, W. A. (2014). Impaired excitability of somatostatin- and parvalbumin-expressing cortical interneurons in a mouse model of Dravet syndrome. *Proc. Natl. Acad. Sci. U. S. A.* 111, 3139–3148. doi: 10.1073/pnas.1411131111

Takahashi, S., Yamamoto, S., Okayama, A., Araki, A., Saitsu, H., Matsumoto, N., et al. (2015). Electroclinical features of epileptic encephalopathy caused by SCN8A mutation. *Pediatr. Int.* 57, 758–762. doi: 10.1111/ped.12622

Tan, N.-N., Tang, H.-L., Lin, G.-W., Chen, Y.-H., Lu, P., Li, H.-J., et al. (2017). Epigenetic Downregulation of Scn3a Expression by Valproate: a Possible Role in Its Anticonvulsant Activity. *Mol. Neurobiol.* 54, 2831–2842. doi: 10.1007/s12035-016-9871-9

Thijs, R. D., Surges, R., O'Brien, T. J., and Sander, J. W. (2019). Epilepsy in adults. *Lancet* 393, 689–701. doi: 10.1016/S0140-6736(18)32596-0

Thomas, R. H., and Berkovic, S. F. (2014). The hidden genetics of epilepsy – A clinically important new paradigm. *Nat. Rev. Neurol.* 10, 283–292. doi: 10.1038/nrneurol.2014.62

Tibery, D. V., Campos, L. A., Mourão, C. B. F., Peigneur, S., Tytgat, J., Schwartz, E. F., et al. (2019). Electrophysiological characterization of Tityus obscurus b toxin 1 (To1) on Na+-channel isoforms. *Biochim. Biophys. Acta - Biomembr.* 1861, 142–150. doi: 10.1016/j.bbamem.2018.08.005

Tiefes, A. M., Hartlieb, T., Tacke, M., von Stülpnagel-Steinbeis, C., Larsen, L. H. G., Hao, Q., et al. (2019). Mesial Temporal Sclerosis in SCN1A -Related Epilepsy: Two Long-Term EEG Case Studies. *Clin. EEG Neurosci.* 50, 267–272. doi: 10.1177/1550059418794347

Tonekaboni, S. H., Ebrahimi, A., Bakhshandeh Bali, M. K., Taheri Otaghsara, S. M., Houshmand, M., Nasehi, M. M., et al. (2013). Sodium channel gene mutations in Children with GEFS+ and Dravet syndrome: A cross sectional study. *Iran. J. Child Neurol.* 7, 31–36. doi: 10.22037/ijcn.v7i2.4074

Trivisano, M., Pavia, G. C., Ferretti, A., Fusco, L., Vigevano, F., and Specchio, N. (2019). Generalized tonic seizures with autonomic signs are the hallmark of SCN8A developmental and epileptic encephalopathy. *Epilepsy Behav.* 96, 219–223. doi: 10.1016/j.yebeh.2019.03.043

Trujillano, D., Bertoli-Avella, A. M., Kumar Kandaswamy, K., Weiss, M. E., Köster, J., Marais, A., et al. (2017). Clinical exome sequencing: Results from 2819 samples reflecting 1000 families. *Eur. J. Hum. Genet.* 25, 176–182. doi: 10.1038/ejhg.2016.146

Trump, N., McTague, A., Brittain, H., Papandreou, A., Meyer, E., Ngoh, A., et al. (2016). Improving diagnosis and broadening the phenotypes in early-onset seizure and severe developmental delay disorders through gene panel analysis. *J. Med. Genet.* 53, 310–317. doi: 10.1136/jmedgenet-2015-103263

Tsang, M. H.-Y., Leung, G. K.-C., Ho, A. C.-C., Yeung, K.-S., Mak, C. C.-Y., Pei, S. L.-C., et al. (2019). Exome sequencing identifies molecular diagnosis in children with drug-resistant epilepsy. *Epilepsia Open* 4, 63–72. doi: 10.1002/epi4.12282

U.S. Food and Drug Administration [website] (2018). *FDA Approves First Drug Comprised of an Active Ingredient Derived from Marijuana to Treat Rare, Severe Forms of Epilepsy*. Available at: https://www.fda.gov/news-events/pressannouncements/fda-approves-first-drug-comprised-active-ingredientderived-marijuana-treat-rare-severe-forms (Accessed March 7, 2020).

Usluer, S., Salar, S., Arslan, M., Yiş, U., Kara, B., Tektürk, P., et al. (2016). SCN1A gene sequencing in 46 Turkish epilepsy patients disclosed 12 novel mutations. *Seizure* 39, 34–43. doi: 10.1016/j.seizure.2016.05.008

Vaher, U., Nõukas, M., Nikopensius, T., Kals, M., Annilo, T., Nelis, M., et al. (2013). De Novo SCN8A Mutation Identified by Whole-Exome Sequencing in a Boy With Neonatal Epileptic Encephalopathy, Multiple Congenital Anomalies, and Movement Disorders. *J. Child Neurol.* 29, NP202–NP206. doi: 10.1177/0883073813511300

Vanoye, C. G., Gurnett, C. A., Holland, K. D., George, A. L., and Kearney, J. A. (2014). Novel SCN3A variants associated with focal epilepsy in children. *Neurobiol. Dis.* 62, 313–322. doi: 10.1016/j.nbd.2013.10.015

Vecchi, M., Cassina, M., Casarin, A., Rigon, C., Drigo, P., De Palma, L., et al. (2011). Infantile epilepsy associated with mosaic 2q24 duplication including SCN2A and SCN3A. *Seizure* 20, 813–816. doi: 10.1016/j.seizure.2011.07.008

Veeramah, K. R., O'Brien, J. E., Meisler, M. H., Cheng, X., Dib-Hajj, S. D., Waxman, S. G., et al. (2012). De novo pathogenic SCN8A mutation identified by whole-genome sequencing of a family quartet affected by infantile epileptic encephalopathy and SUDEP. *Am. J. Hum. Genet.* 90, 502–510. doi: 10.1016/j.ajhg.2012.01.006

Veeramah, K. R., Johnstone, L., Karafet, T. M., Wolf, D., Sprissler, R., Salogiannis, J., et al. (2013). Exome sequencing reveals new causal mutations in children with epileptic encephalopathies. *Epilepsia* 54, 1270–1281. doi: 10.1111/epi.12201

Verbeek, N. E., van Kempen, M., Gunning, W. B., Renier, W. O., Westland, B., Lindhout, D., et al. (2011). Adults with a history of possible Dravet syndrome: An illustration of the importance of analysis of the SCN1A gene. *Epilepsia* 52, e23–e25. doi: 10.1111/j.1528-1167.2011.02982.x

Verbeek, N. E., van der Maas, N. A. T., Jansen, F. E., van Kempen, M. J. A., Lindhout, D., and Brilstra, E. H. (2013). Prevalence of SCN1A-Related Dravet Syndrome among Children Reported with Seizures following Vaccination: A Population-Based Ten-Year Cohort Study. *PloS One* 8, e65758. doi: 10.1371/journal.pone.0065758

Verret, L., Mann, E. O., Hang, G. B., Barth, A. M. I. I., Cobos, I., Ho, K., et al. (2012). Inhibitory interneuron deficit links altered network activity and cognitive dysfunction in alzheimer model. *Cell* 149, 708–721. doi: 10.1016/j.cell.2012.02.046

Villeneuve, N., Laguitton, V., Viellard, M., Lépine, A., Chabrol, B., Dravet, C., et al. (2014). Cognitive and adaptive evaluation of 21 consecutive patients with Dravet syndrome. *Epilepsy Behav.* 31, 143–148. doi: 10.1016/j.yebeh.2013.11.021

Volkers, L., Kahlig, K. M., Verbeek, N. E., Das, J. H. G., van Kempen, M. J. A., Stroink, H., et al. (2011). Na v1.1 dysfunction in genetic epilepsy with febrile seizures-plus or Dravet syndrome. *Eur. J. Neurosci.* 34, 1268–1275. doi: 10.1111/j.1460-9568.2011.07826.x

Wagnon, J. L., and Meisler, M. H. (2015). Recurrent and non-recurrent mutations of SCN8A in epileptic encephalopathy. *Front. Neurol.* 6, 104. doi: 10.3389/fneur.2015.00104

Wagnon, J. L., Barker, B. S., Hounshell, J. A., Haaxma, C. A., Shealy, A., Moss, T., et al. (2016). Pathogenic mechanism of recurrent mutations of SCN8A in epileptic encephalopathy. *Ann. Clin. Transl. Neurol.* 3, 114–123. doi: 10.1002/acn3.276

Wagnon, J. L., Barker, B. S., Ottolini, M., Park, Y., Volkheimer, A., Valdez, P., et al. (2017). Loss-of-function variants of SCN8A in intellectual disability without seizures. *Neurol. Genet.* 3, e170. doi: 10.1212/NXG.0000000000000170

Wallace, R. H., Scheffer, I. E., Barnett, S., Richards, M., Dibbens, L., Desai, R. R., et al. (2001). Neuronal sodium-channel β1-subunit mutations in generalized epilepsy with febrile seizures plus. *Am. J. Hum. Genet.* 68, 859–865. doi: 10.1086/319516

Wang, J. W., Shi, X. Y., Kurahashi, H., Hwang, S. K., Ishii, A., Higurashi, N., et al. (2012). Prevalence of SCN1A mutations in children with suspected Dravet syndrome and intractable childhood epilepsy. *Epilepsy Res.* 102, 195–200. doi: 10.1016/j.eplepsyres.2012.06.006

Wang, J., Gao, H., Bao, X., Zhang, Q., Li, J., Wei, L., et al. (2017a). SCN8A mutations in Chinese patients with early onset epileptic encephalopathy and benign infantile seizures. *BMC Med. Genet.* 18, 104. doi: 10.1186/s12881-017-0460-1

Wang, Y., Du, X., Bin, R., Yu, S., Xia, Z., Zheng, G., et al. (2017b). Genetic Variants Identified from Epilepsy of Unknown Etiology in Chinese Children by Targeted Exome Sequencing. *Sci. Rep.* 7, 40319. doi: 10.1038/srep40319

Waxman, S. G., and Hains, B. C. (2006). Fire and phantoms after spinal cord injury: Na+ channels and central pain. *Trends Neurosci.* 29, 207–215. doi: 10.1016/j.tins.2006.02.003

Weber, Y. G., Nies, A. T., Schwab, M., and Lerche, H. (2014). Genetic Biomarkers in Epilepsy. *Neurotherapeutics* 11, 324–333. doi: 10.1007/s13311-014-0262-5

Weiss, L. A., Escayg, A., Kearney, J. A., Trudeau, M., MacDonald, B. T., Mori, M., et al. (2003). Sodium channels SCN1A, SCN2A and SCN3A in familial autism. *Mol. Psychiatry* 8, 186–194. doi: 10.1038/sj.mp.4001241

Wengert, E. R., Tronhjem, C. E., Wagnon, J. L., Johannesen, K. M., Petit, H., Krey, I., et al. (2019). Biallelic inherited SCN8A variants, a rare cause of SCN8A -related developmental and epileptic encephalopathy. *Epilepsia* 60, 2277–2285. doi: 10.1111/epi.16371

Weuring, W. J., Singh, S., Volkers, L., Rook, M. B., Van't Slot, R. H., Bosma, M., et al. (2020). NaV1.1 and NaV1.6 selective compounds reduce the behavior phenotype and epileptiform activity in a novel zebrafish model for Dravet syndrome. *PloS One* 15, 1–17. doi: 10.1371/journal.pone.0219106

Whitaker, W. R. J., Clare, J. J., Powell, A. J., Chen, Y. H., Faull, R. L. M., and Emson, P. C. (2000). Distribution of voltage-gated sodium channel?-subunit and?-subunit mRNAs in human hippocampal formation, cortex, and cerebellum. *J. Comp. Neurol.* 422, 123–139. doi: 10.1002/(SICI)1096-9861(20000619)422:1<123::AID-CNE8>3.0.CO;2-X

Willemsen, M. H., Rensen, J. H. M., van Schrojenstein-Lantman de Valk, H. M. J., Hamel, B. C. J., and Kleefstra, T. (2012). Adult Phenotypes in Angelman- and Rett-Like Syndromes. *Mol. Syndromol.* 2, 217–234. doi: 10.1159/000335661

Wittmack, E. K., Rush, A. M., Craner, M. J., Goldfarb, M., Waxman, S. G., and Dib-Hajj, S. D. (2004). Fibroblast growth factor homologous factor 2B: Association with Na v1.6 and selective colocalization at nodes of Ranvier of dorsal root axons. *J. Neurosci.* 24, 6765–6775. doi: 10.1523/JNEUROSCI.1628-04.2004

Wolff, M., Johannesen, K. M., Hedrich, U. B. S., Masnada, S., Rubboli, G., Gardella, E., et al. (2017). Genetic and phenotypic heterogeneity suggest therapeutic implications in SCN2A-related disorders. *Brain* 140, 1316–1336. doi: 10.1093/brain/awx054

Wong, V. C. N., Fung, C. W., and Kwong, A. K. Y. (2015). SCN2A mutation in a Chinese boy with infantile spasm - response to Modified Atkins Diet. *Brain Dev.* 37, 729–732. doi: 10.1016/j.braindev.2014.10.008

Wu, Y. W., Sullivan, J., McDaniel, S. S., Meisler, M. H., Walsh, E. M., Li, S. X., et al. (2015). Incidence of dravet syndrome in a US population. *Pediatrics* 136, e1310–e1315. doi: 10.1542/peds.2015-1807

Wu, Q., Wang, H., Fan, Y. Y., Zhang, J. M., Liu, X. Y., Fang, X. Y., et al. (2018). Ketogenic diet effects on 52 children with pharmacoresistant epileptic encephalopathy: A clinical prospective study. *Brain Behav.* 8, 1–8. doi: 10.1002/brb3.973

Xiao, Y., Xiong, J., Mao, D., Liu, L., Li, J., Li, X., et al. (2018). Early-onset epileptic encephalopathy with de novo SCN8A mutation. *Epilepsy Res.* 139, 9–13. doi: 10.1016/j.eplepsyres.2017.10.017

Xie, H., Su, W., Pei, J., Zhang, Y., Gao, K., Li, J., et al. (2019). De novo SCN1A, SCN8A, and CLCN2 mutations in childhood absence epilepsy. *Epilepsy Res.* 154, 55–61. doi: 10.1016/j.eplepsyres.2019.04.005

Xu, R., Thomas, E. A., Gazina, E. V., Richards, K. L., Quick, M., Wallace, R. H., et al. (2007). Generalized epilepsy with febrile seizures plus-associated sodium channel β1 subunit mutations severely reduce beta subunit-mediated modulation of sodium channel function. *Neuroscience* 148, 164–174. doi: 10.1016/j.neuroscience.2007.05.038

Xu, X., Zhang, Y., Sun, H., Liu, X., Yang, X., Xiong, H., et al. (2014). Early clinical features and diagnosis of Dravet syndrome in 138 Chinese patients with SCN1A mutations. *Brain Dev.* 36, 676–681. doi: 10.1016/j.braindev.2013.10.004

Xu, X., Yang, X., Wu, Q., Liu, A., Yang, X., Ye, A. Y., et al. (2015). Amplicon Resequencing Identified Parental Mosaicism for Approximately 10% of " de novo " SCN1A Mutations in Children with Dravet Syndrome. *Hum. Mutat.* 36, 861–872. doi: 10.1002/humu.22819

Yan, N., Xin-Hua, W., Lin-Mei, Z., Yi-Ming, C., Wen-Hui, L., Yuan-Feng, Z., et al. (2018). Prospective study of the efficacy of a ketogenic diet in 20 patients with Dravet syndrome. *Seizure* 60, 144–148. doi: 10.1016/j.seizure.2018.06.023

Yang, Y.-C., Huang, C.-S., and Kuo, C.-C. (2010). Lidocaine, Carbamazepine, and Imipramine Have Partially Overlapping Binding Sites and Additive Inhibitory Effect on Neuronal Na+ Channels. *Anesthesiology* 113, 160–174. doi: 10.1097/ALN.0b013e3181dc1dd6

Yang, X., Liu, A., Xu, X., Yang, X., Zeng, Q., Ye, A. Y., et al. (2017). Genomic mosaicism in paternal sperm and multiple parental tissues in a Dravet syndrome cohort. *Sci. Rep.* 7, 15677. doi: 10.1038/s41598-017-15814-7

Yang, C., Hua, Y., Zhang, W., Xu, J., Xu, L., Gao, F., et al. (2018). Variable epilepsy phenotypes associated with heterozygous mutation in the SCN9A gene: report of two cases. *Neurol. Sci.* 39, 1113–1115. doi: 10.1007/s10072-018-3300-y

Yordanova, I., Todorov, T., Dimova, P., Hristova, D., Tincheva, R., Litvinenko, I., et al. (2011). One novel Dravet syndrome causing mutation and one recurrent MAE causing mutation in SCN1A gene. *Neurosci. Lett.* 494, 180–183. doi: 10.1016/j.neulet.2011.03.008

Young, F. (2007). When adaptive processes go awry: gain-of-function in SCN9A. *Clin. Genet.* 73, 34–36. doi: 10.1111/j.1399-0004.2007.00922.x

Yu, F. H., Mantegazza, M., Westenbroek, R. E., Robbins, C. A., Kalume, F., Burton, K. A., et al. (2006). Reduced sodium current in GABAergic interneurons in a mouse model of severe myoclonic epilepsy in infancy. *Nat. Neurosci.* 9, 1142–1149. doi: 10.1038/nn1754

Yu, M.-J., Shi, Y.-W., Gao, M.-M., Deng, W.-Y., Liu, X.-R., Chen, L., et al. (2010). Milder phenotype with SCN1A truncation mutation other than SMEI. *Seizure* 19, 443–445. doi: 10.1016/j.seizure.2010.06.010

Zaman, T., Helbig, I., Božović, I. B., DeBrosse, S. D., Bergqvist, A. C., Wallis, K., et al. (2018). Mutations in SCN3A cause early infantile epileptic encephalopathy. *Ann. Neurol.* 83, 703–717. doi: 10.1002/ana.25188

Zaman, T., Abou Tayoun, A., and Goldberg, E. M. (2019). A single-center SCN8A-related epilepsy cohort: clinical, genetic, and physiologic characterization. *Ann. Clin. Transl. Neurol.* 6. doi: 10.1002/acn3.50839. acn3.50839.

Zara, F., Specchio, N., Striano, P., Robbiano, A., Gennaro, E., Paravidino, R., et al. (2013). Genetic testing in benign familial epilepsies of the first year of life: Clinical and diagnostic significance. *Epilepsia* 54, 425–436. doi: 10.1111/epi.12089

Zhang, X., Ren, W., Decaen, P., Yan, C., Tao, X., Tang, L., et al. (2012). Crystal structure of an orthologue of the NaChBac voltage-gated sodium channel. *Nature* 486, 130–135. doi: 10.1038/nature11054

Zhang, Y., Kong, W., Gao, Y., Liu, X., Gao, K., Xie, H., et al. (2015). Gene Mutation Analysis in 253 Chinese Children with Unexplained Epilepsy and Intellectual/Developmental Disabilities. *PloS One* 10, e0141782. doi: 10.1371/journal.pone.0141782

Zhang, S., Zhang, Z., Shen, Y., Zhu, Y., Du, K., Guo, J., et al. (2020). SCN9A Epileptic Encephalopathy Mutations Display a Gain-of-function Phenotype and Distinct Sensitivity to Oxcarbazepine. *Neurosci. Bull.* 36, 11–24. doi: 10.1007/s12264-019-00413-5

Zhang, F., Wu, Y., Zou, X., Tang, Q., Zhao, F., and Cao, Z. (2019). BmK AEP, an Anti-Epileptic Peptide Distinctly Affects the Gating of Brain Subtypes of Voltage-Gated Sodium Channels. *Int. J. Mol. Sci.* 20, 729. doi: 10.3390/ijms20030729

Zhang, T., Chen, M., Zhu, A., Zhang, X., and Fang, T. (2020). Novel mutation of SCN9A gene causing generalized epilepsy with febrile seizures plus in a Chinese family. *Neurol. Sci.* 41, 1913–1917. doi: 10.1007/s10072-020-04284-x

Zhou, P., He, N., Zhang, J. W., Lin, Z. J., Wang, J., Yan, L. M., et al. (2018). Novel mutations and phenotypes of epilepsy-associated genes in epileptic encephalopathies. *Genes Brain Behav.* 17, e12456. doi: 10.1111/gbb.12456

Ziobro, J., Eschbach, K., Sullivan, J. E., and Knupp, K. G. (2018). Current Treatment Strategies and Future Treatment Options for Dravet Syndrome. *Curr. Treat. Options Neurol.* 20, 1–15. doi: 10.1007/s11940-018-0537-y

Zuberi, S. M., Brunklaus, A., Birch, R., Reavey, E., Duncan, J., and Forbes, G. H. (2011). Genotype-phenotype associations in SCN1A-related epilepsies. *Neurology* 76, 594–600. doi: 10.1212/WNL.0b013e31820c309b

Zucca, C., Redaelli, F., Epifanio, R., Zanotta, N., Romeo, A., Lodi, M., et al. (2008). Cryptogenic Epileptic Syndromes Related to SCN1A. *Arch. Neurol.* 65, 489. doi: 10.1001/archneur.65.4.489

Conflict of Interest: The authors declare that the research was conducted in the absence of any commercial or financial relationships that could be construed as a potential conflict of interest.

frontiers in Pharmacology

ORIGINAL RESEARCH
published: 08 September 2020
doi: 10.3389/fphar.2020.526129

Recombinant Ricin Toxin Binding Subunit B (RTB) Stimulates Production of TNF-α by Mouse Macrophages Through Activation of TLR4 Signaling Pathway

Na Xu[1,2†], Kaikai Yu[1†], Haotian Yu[1†], Jianxu Zhang[1], Yang Yang[3], Mingxin Dong[1], Yan Wang[1], Ying Chang[1,2], Yucheng Sun[1], Yanguang Hou[1], Chengbiao Sun[1], Jiayu Wan[1] and Wensen Liu[1*]*

[1] Institute of Military Veterinary Medicine, Academy of Military Medical Sciences, Zoonosis Prevention and Control Key Laboratory, Changchun, China, [2] Jilin Medical University, Jilin, China, [3] Institute of Translational Medicine, First Hospital of Jilin University, Changchun, China

OPEN ACCESS

Edited by:
Jean-Marc Sabatier,
Aix-Marseille Université, France

Reviewed by:
Hai Minh Nguyen,
University of California, Davis, United States
Elena Conte,
University of Bari Aldo Moro, Italy

***Correspondence:**
Wensen Liu
liuws85952@163.com
Jiayu Wan
wanjiayu@hotmail.com

[†]These authors have contributed equally to this work

Specialty section:
This article was submitted to Pharmacology of Ion Channels and Channelopathies, a section of the journal Frontiers in Pharmacology

Received: 12 January 2020
Accepted: 19 August 2020
Published: 08 September 2020

Citation:
Xu N, Yu K, Yu H, Zhang J, Yang Y, Dong M, Wang Y, Chang Y, Sun Y, Hou Y, Sun C, Wan J and Liu W (2020) Recombinant Ricin Toxin Binding Subunit B (RTB) Stimulates Production of TNF-α by Mouse Macrophages Through Activation of TLR4 Signaling Pathway. Front. Pharmacol. 11:526129. doi: 10.3389/fphar.2020.526129

Ricin toxin binding subunit B (RTB) is a galactose-binding lectin protein derived from the beans of the castor oil plant (*Ricinus communis*). Our previous studies have reported a direct immunomodulatory effect of recombinant RTB, which stimulates RAW264.7 cells to produce cytokines including TNF-α. However, the role of RTB in innate immune response and its specific mechanism have not been reported in detail. In this work, the results showed that RTB treatment of macrophages significantly increased TLR4 protein levels. RTB also activated TLR4 downstream events, including MyD88, IRAK, and TRAF6, resulting in macrophage activation and TNF-α production. This process is reflected in the increase of IκB phosphorylation. TLR4 knockdown macrophages treated with RTB exhibited greatly reduced IκB phosphorylation and TNF-α secretion. Moreover, treatment with MyD88 inhibitor also suppressed TNF-α production. The docking of RT and TLR4 was simulated by computer, and the contact residues were concentrated on RTB. Our results suggest that recombinant RTB can activate mouse macrophages to secrete TNF-α through activation of NF-κB *via* the TLR4 signaling pathways.

Keywords: ricin toxin binding subunit B, macrophage, TLR4, cytokine, signaling pathway

INTRODUCTION

Ricin is a plant toxin extracted from castor bean (*Ricinus communis*), which belongs to type II ribosome-inactivating proteins. The ricin holotoxin consists of a toxic moiety A chain (RTA) and a lectin moiety B chain (RTB) linked *via* a disulfide bond. (Lord and Spooner, 2011). The A-chain has N-glycosidase enzymatic activity and causes protein synthesis arrest in mammalian cells. The B-chain is a galactose-binding lectin protein that binds to galactosyl moieties on the eukaryotic cell membrane (Stirpe and Barbieri, 1986; Lord et al., 2003). Our previous studies reported that recombinant RTB is an immunomodulatory stimulus that stimulates the RAW264.7 mouse macrophage cell line to produce inducible NOS (iNOS), tumor necrosis factor–α (TNF-α) and

interleukin 6 (IL-6) *via* signaling pathways that may involve protein tyrosine kinase, NF-κB, and JAK-STAT activation (Liu et al., 2013; Xu et al., 2013). However, the role of RTB in innate immune response and its specific mechanism have not been understood very well.

Macrophages are important immune cells, which play an important role in anti-infection, anti-tumor and immune regulation as the first line of defense of innate immunity. Activated macrophages release many types of cell factors to remove pathogens (Akira et al., 2006; Mogensen, 2009). When pathogens invade the body, a series of intracellular signal transduction pathways are activated by various pattern recognition receptors (PRRs) expressed on macrophages. Toll-like receptor (TLR), a member of the PRR family which involved in stimulating innate immune response (Horng et al., 2002). When TLRs are activated, they require adaptor molecules, including myeloid differentiation primary response protein 88 (MyD88), TIR-domain-containing adaptor-inducing interferon-β (TRIF), IL-1R–associated kinases (IRAKs), and TNF receptor associated factor 6 (TRAF6) (Motshwene et al. 2009; Pålsson-McDermott and O'Neill, 2009; Lin et al., 2010). MyD88 is recruited by TLR4, and TNF-α is secreted following LPS mediates the activation of MyD88-dependent pathway by stimulating TLR4 (Park et al., 2010).

Since RTB has been shown to induce TNF-α production by RAW264.7 cells, we investigated whether TLR4 signaling pathway plays a key role in RTB-mediated TNF-a secretion.

MATERIALS AND METHODS

Protein

RTB was cloned and expressed in Escherichia coli as described in our previous reaserch with a slight modification (5). The protein was purified using a nickel column (Ni-NTA; General Electric Corp., Boston, MA, US). Endotoxin was removed using Detoxi-Gel™ Endotoxin Removing Gel (Invitrogen, Frederic, MD, USA). The endotoxin contamination in the RTB was <0.03 pg/μg to exclude the possibility of LPS contamination.

Cell Culturing

RAW264.7 cells were incubated in RPMI-1640 medium (Gibco, Carlsbad, CA, USA), containing 10% fetal calf serum (FCS) (Hyclone, Logan, UT, USA), 100 U/mL of penicillin, and 100 U/mL of streptomycin at 37°C in a humidified atmosphere containing 5% CO_2 and 95% air.

Cell Viability Assay

RAW264.7 cells were plated into 96-well plates at 5×10^4 cells/well and cultured for 24 h. After addition of various concentrations of RTB (12.5, 25, 50, and 100 μg/mL), the cells were incubated with 10 μL of Alamar Blue cell viability reagent (Invitrogen, Frederic, MD, USA) in medium for 24 h at 37°C. The absorbance was measured at wavelengths of 570 and 610 nm.

RNA Interference

RAW264.7 cells were transfected with psiRNA-mTLR4 to knockdown the TLR4 gene and with empty plasmid psiRNA-LucGL3 as control. Zeocin selection was used to collect the stably transfected RAW264.7 cells. The expression of TLR4 was examined by RT-PCR and western blotting.

Western Blot Analysis

RAW264.7 cells were pretreated with or without RTB for the indicated time period, lysed with 100 μL of RIPA lysis buffer (Beyotime Institute of Biotechnology, Jiangsu, China) in the presence of protease inhibitor. Protein samples were separated by 10% SDS-PAGE and transferred to polyvinylidene difluoride (PVDF) membranes (Merck-Millipore, Darmstadt, Germany). The PVDF membranes were blocked with 5% non-fat milk (BD Biosciences, Franklin Lakes, NJ, USA) for 1 h at room temperature and then incubated with TLR4, MyD88, IRAK, TRAF6, or pIκB antibody (Cell Signaling Technology, Danvers, MA, USA) followed by appropriate secondary antibodies. Immunodetection was performed using ECL reagents (GE Healthcare).

Cytokine Assays

To evaluation the TNF-a secretion induced by RTB, RAW264.7 cells or TLR4- siRNA treated RAW264.7 cells were plated into 24-well plates, stimulated with RTB (50 μg/mL), the MyD88 inhibitor Pepinh-MYD (25 mM) (InvivoGen, San Diego, CA, USA) or TAK-242 (50 nM) (MedChemExpress, Monmouth Junction, NJ, USA) for 24 h. Cytokine production in the supernatants was measured *via* ELISA, according to the manufacturers' instructions (Biolegend, San Diego, CA, USA).

Flow Cytometry

RAW264.7 cells were stimulated with or without RTB, and incubated with PE-conjugated anti-mouse TLR4 (Ebioscience, San Diego, CA, USA) for 30 min at 4°C. PE-labeled IgG antibody was used as control. Flow cytometry analysis was performed using a CytoFLEX (BECKMAN COULTER) flow cytometer.

Computer Simulation of Molecular Docking

The amino acid sequences of TLR4 and RT were obtained from the NCBI database (https://www.ncbi.nlm.nih.gov). Protein modeling was performed using the Swiss-Model (swissmodel.expasy.org) online service *via* the TLR4 and RT amino acid sequences. An appropriate template was selected to model the 3D structure of the protein according to the sequence alignment. Then the protein structure was optimized by Discovery Studio 4.5 (Acclery, Inc.). The Discovery Studio Client was used to visualize the protein structure model, and the ZDOCK algorithm was used to simulate the intermolecular docking. The results of molecular docking were optimized and analyzed by using RDOCK.

Abbreviations: RTB, Ricin toxin binding subunit B; RIP, Ribosome-inactivating protein; RTA, Ricin toxin binding subunit A; iNOS, Inducible NOS; TNF, Tumor necrosis factor; IL, Interleukin; DCs, Dendritic cells; PRRs, Pattern-recognition receptors; TLRs, Toll-like receptors; MyD88, Primary response protein 88; TRIF, TIR-domain-containing adaptor inducing interferon-β; IRAKs, IL-1R associated kinases; TRAF6, Tumor-necrosis factor receptor associated factor;6 FCS, Fetal calf serum; PVDF, Polyvinylidene difluoride.

Statistical Analysis

One-way ANOVA followed by a *post hoc* comparison using the least significant difference (LSD) and independent t-test were performed for data comparison using SPSS 11.0 statistical software(IBM, Armonk, NY, USA). All graphical illustrations were generated in Graph Pad Prism 6. Significance was indicated as follows: *$p \leq 0.05$; **$p \leq 0.01$; ***$p \leq 0.001$.

RESULTS

Cell Viability Assay

Alamar Blue assay was used to measure cell viability and cytotoxicity. The results showed that RTB was not toxic to RAW264.7 cells at concentrations of 12.5–100 μg/mL (**Figure 1**). Based on this result, 50 μg/mL was used in subsequent experiments.

The Effects of RTB on TLR4 Expression in RAW264.7 Cells

To study whether TNF-α production by RAW264.7 cells induced by RTB is related to the TLR4 signaling pathway, we first determined the expression of TLR4. Enhanced protein expression induced by RTB was observed. The maximum expression of TLR4 was observed at 3 h and then decreased gradually up to 6 h (**Figure 2**).

RTB Activates the TLR4 Signaling Pathway in RAW264.7 Cells

To determine whether RTB activates the TLR4 signaling pathway, we examined whether downstream signaling molecules MyD88, IRAK, and TRAF6 were stimulated by RTB. As shown in **Figure 3**, RTB-treated macrophages showed increases in the expression of MyD88, IRAK, and TRAF6. MyD88, IRAK, and TRAF6 protein expression all showed a similar result to TLR4, reaching their maximum level at 3 h and then decreasing gradually up to 6 h.

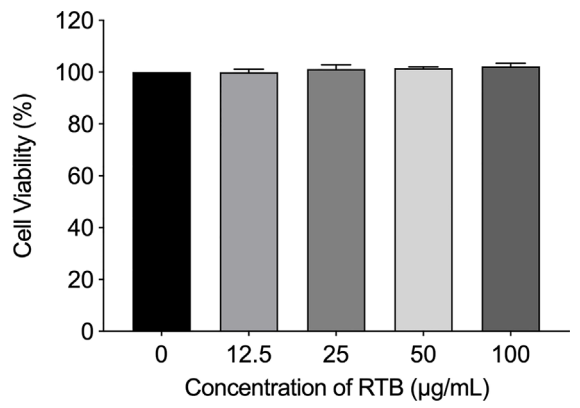

FIGURE 1 | Effects of RTB on cell viability. Cells were treated with various concentrations of RTB for 24 h. Cell proliferation was analyzed by Alamar Blue assay. Cell viability without RTB treatment (control) was taken as 100%. Data represent the mean ± SD from three representative experiments.

TLR4-Dependent TNF-α Production Following RTB Stimulation

We further determined whether TNF-α secretion was induced through RTB-activated TLR4 signaling pathways. We examined the effect of treatment with a TLR4 siRNA or MyD88 inhibitor on the RTB-activated induction of TNF-α in RAW264.7 cells. A TLR4 knockdown RAW264.7 cell line was created by stable transfection with psiRNA-mTLR4 (**Figure 4A**). TNF-α expression was significantly reduced in TLR4- siRNA or MyD88 inhibitor treated macrophages (**Figures 4B–D**).

TLR4-Dependent Activation of NF-κB Following RTB Stimulation

To further explore whether TLR4 is involved in RTB-induced macrophage activation, IκB activation was measured to identify signaling changes. As shown in **Figure 5**, the expression of phosphorylated IκB was up-regulated within 3 h of RTB stimulation. In contrast, expression of phosphorylated IκB in TLR4- siRNA treated macrophages was substantially reduced.

Computer Simulation of the Interface of RT and TLR4

Model and optimize the structural models of RT (ID: 2vlc) and TLR4 (ID: 3vq1) through the Swiss-Model online server. The Dock and Analyze Protein Complexes tool panel in Discovery Studio was used to dock proteins with the Dock Proteins (ZDOCK) protocol and display. Then, the ZRANK analysis tool was used to determine the complex structure of RT and TLR4, and the conformation of the complex was optimized by the RDOCK algorithm, and the optimal docking structure of RT and TLR4 was determined. The binding interface and area of RT and TLR4 are shown in **Figure 6** and **Table 1**.

In previous studies, we have verified the interaction between RT and TLR4 through immunoprecipitation (Dong et al., 2019), which supports the molecular docking model of RT and TLR4 in this section.

DISCUSSION

RTB is a glycoprotein that delivers RTA to the cytoplasm of host cells *via* glycoproteins and glycolipids located at the cell surface (Olsnes et al., 1975; Hartley and Lord, 2004). Similar to the effects of other bacterial and plant AB toxins on the immune response, we found that recombinant RTB possesses several immunostimulatory functions (Liu et al., 2013; Xu et al., 2013). In this study, we identified a novel TLR4 activator, RTB. We showed that recombinant RTB induced TNF-α production and NF-κB activation in a TLR4-dependent manner in RAW264.7 macrophages.

TLR4 is commonly expressed on macrophages, dendritic cells and other cells. TLR4 signaling pathways are known to play important roles in immune cell activation (Kawai and Akira, 2010; Gay et al., 2014). In previous studies, we have verified the interaction between RT and TLR4 through immunoprecipitation (Dong et al., 2019). In this study, when RAW264.7 cells were treated with RTB, it was observed that recombinant RTB

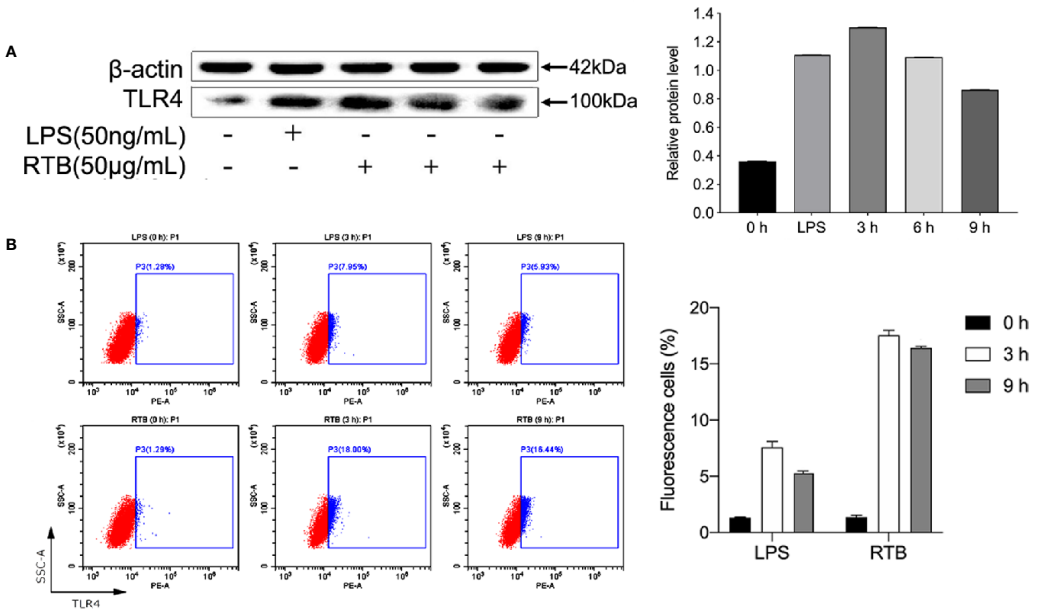

FIGURE 2 | The analysis of TLR4 expression on RTB-treated RAW264.7 cells. **(A)** Expression levels of TLR4 were detected by western blotting. Cells were treated with RTB (50 μg/mL) for 3, 6, or 9 h or LPS (50 ng/mL) for 6 h. Whole cell lysates were prepared and TLR4 protein expression checked by western blotting using a specific antibody against TLR4 or β-actin. Relative protein level represents the relative ratio of expression of each protein versus actin. **(B)** TLR4 expression on RAW264.7 cells were analysed by flow cytometry. Cells were treated with RTB (50 μg/mL) for 3 or 9 h or LPS (50 ng/mL) for 3 h. TLR4 expressions were examined by flow cytometry. Representative results from one of three experiments with similar results are shown. Data represent the mean ± SD from three representative experiments.

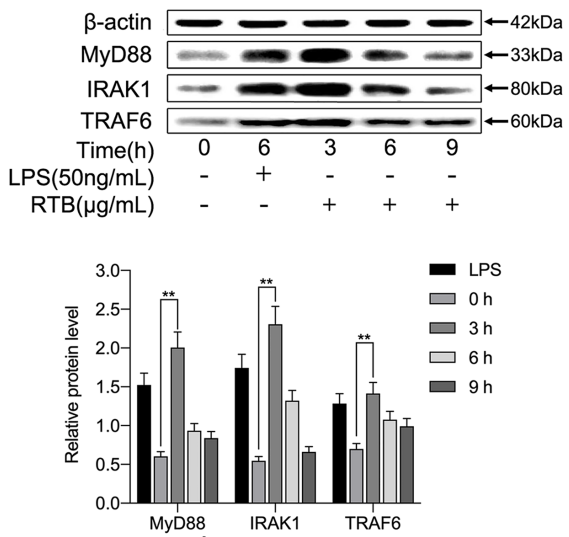

FIGURE 3 | Effect of RTB on the expression of TLR4-signaling pathway components in RAW264.7 cells. RAW264.7 cells were treated with RTB (50 μg/mL) for 3, 6, or 9 h or LPS (50 ng/mL) for 6 h. Expression levels of MyD88, IRAK1, and TRAF6 were determined by western blotting. Relative protein level represents the relative expression of each protein versus actin. Representative results from one of three experiments with similar results are shown. Data represent the mean ± SD of three replicates. Significance was indicated as follows: $p \leq 0.01$ (**).

stimulated expression of the TLR4 protein. We further studied the immunomodulatory effect of RTB on TLR4 signaling pathway to clarify its mechanism. First, the Alamar Blue analysis method was used to identify that RTB was not toxic to cells. The expression of TLR4 induced by RTB was enhanced by western blot. The maximum expression of TLR4 was observed at 3 h and gradually decreased until 6 h. To determine whether RTB activates the TLR4 signaling pathway, we examined whether downstream signaling molecules MyD88, IRAK, and TRAF6 were stimulated by RTB. RTB-treated macrophages showed increases in the expression of MyD88, IRAK, and TRAF6. MyD88, IRAK, and TRAF6 protein expression all showed a similar result to TLR4, reaching their maximum level at 3 h and then decreasing gradually up to 6 h. These data indicated that TLR4 might mediate the biological effects of RTB on macrophages. TNF-α is produced in response to LPS through a TLR4/MyD88-dependent pathway (Park et al., 2010). We found that RTB-induced TNF-α secretion was inhibited by treating macrophages with the MyD88 inhibitor Pepinh-MYD and TAK-242, and inhibition of TNF-α secretion was observed in TLR4-/- mouse macrophages. Furthermore, the docking of RT and TLR4 was simulated by computer and the contact residues were concentrated on RTB. The simulation results found that the surface contact residues of TLR4 and RT were concentrated on the B subunit. These data suggest that RTB stimulates TNF-α production by RAW264.7 cells *via* the TLR4 signaling pathway and that TLR4 might act as an RTB receptor.

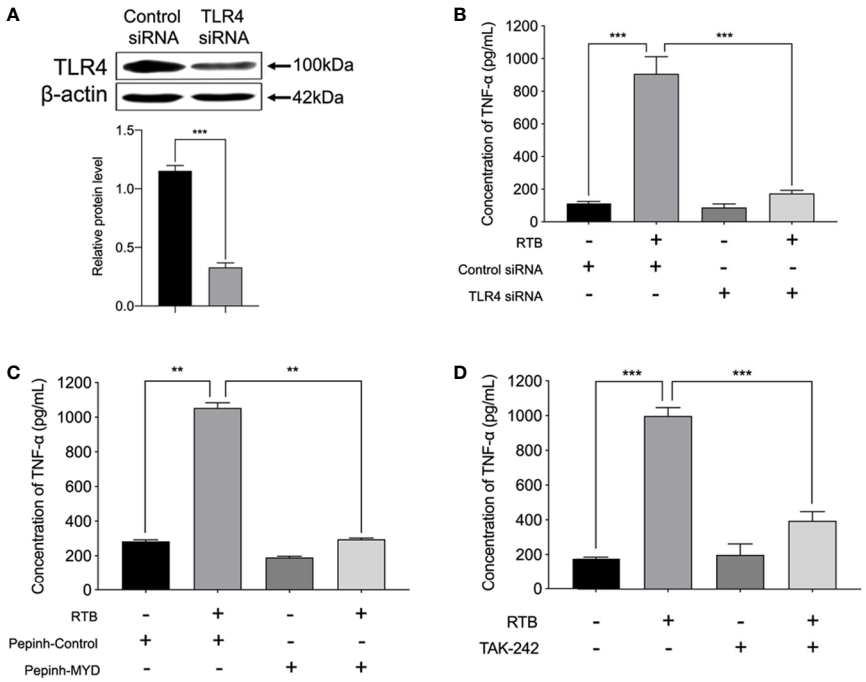

FIGURE 4 | TNF-α production in Raw264.7 cells treated with RTB. **(A)** Cells were stably transfected with control siRNA or siRNA specific for TLR4.Western blotting analysis of TLR4 in cell lysates. **(B)** TNF-α production in stably-transfected RAW264.7 cells treated with RTB. TLR4 siRNA stably-transfected RAW264.7 cells were treated with RTB (50 μg/mL) for 24 h. TNF-α production was measured by ELISA. Data are presented as mean ± SD of three replicates. Shown are representative results from one of three experiments with similar results. **(C)** Raw264.7 cells were treated with or without the MyD88 inhibitor Pepinh-MYD (25 mM) and incubated for 24 h and then stimulated with RTB (50 μg/mL) for 24 h. TNF-α production was measured by ELISA. Data are presented as mean ± SD of three replicates. Representative results from one of three experiments with similar results are shown. **(D)** Raw264.7 cells were treated with or without another MyD88 inhibitor TAK-242 (50 nM) and incubated for 24 h and then stimulated with RTB (50 μg/mL) for 24 h. TNF-α production was measured by ELISA. Data are presented as mean ± SD of three replicates. Representative results from one of three experiments with similar results are shown. Significance was indicated as follows: $^{**}p \leq 0.01$; $^{***}p \leq 0.001$.

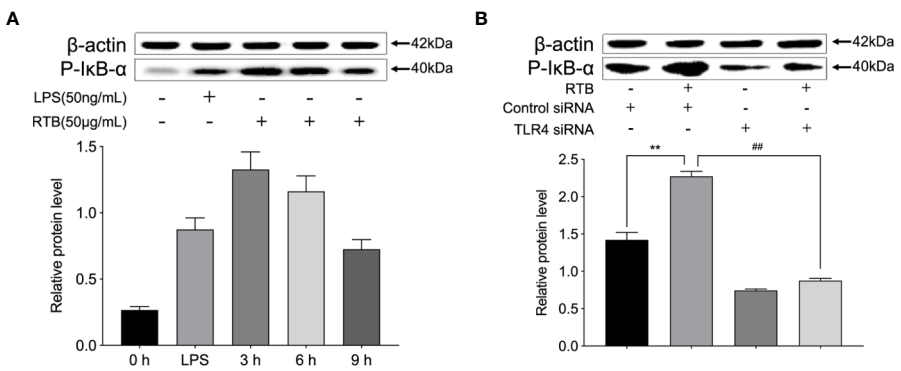

FIGURE 5 | pIκB expression in Raw264.7 cells treated with RTB. **(A)** Raw264.7 cells were treated with RTB (50 μg/mL) for 3, 6, or 9 h or LPS (50 ng/mL) for 6 h. Levels of pIκB were determined by western blotting. The relative protein levels are expressed as the relative ratios versus actin. Representative results from one of three experiments with similar results are shown. Values are the mean ± SD of three replicates. **(B)** TLR4 stably transfected RAW264.7 cells were stimulated with RTB (50 μg/mL), and pIκB levels were determined by western blotting. Representative results from one of three experiments with similar results are shown. Values are the mean ± SD of three replicates. $^{**}p < 0.01$ compared to control siRNA group. $^{\#\#}p < 0.01$ compared to control siRNA treated with RTB.

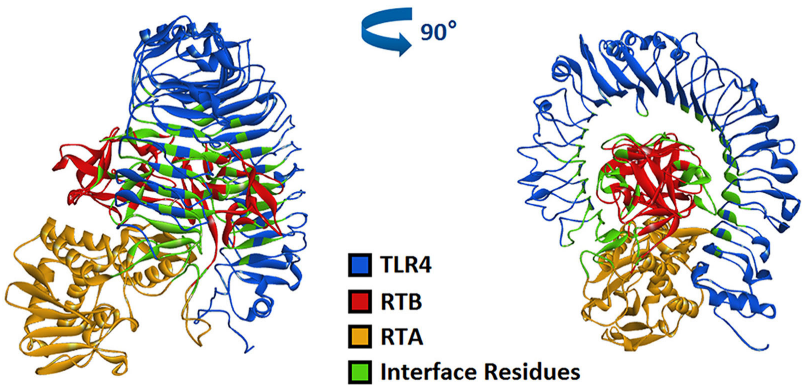

FIGURE 6 | Computerized simulation to reveal the complex of TLR4 bound by RT. RT formed a contact interface with residues mainly in RTB domain.

TABLE 1 | The binding interface and area of RT and TLR4.

From	To	RT Domain	Distance	Category
TLR4:LYS475:NZ	RT:ASP336:OD2	RTB	3.06226	Hydrogen bond; electrostatic
TLR4:LYS354:NZ	RT:ASP500:OD2	RTB	3.16169	Hydrogen bond; electrostatic
TLR4:ARG74:NH1	RT:GLU30:OE2	RTA	4.81973	Electrostatic
TLR4:ARG416:NH2	RT:GLU128:OE2	RTA	4.74054	Electrostatic
TLR4:ARG512:NH1	RT:GLU134:OE1	RTA	3.78613	Electrostatic
TLR4:LYS533:NZ	RT:ASP41:OD2	RTA	5.13394	Electrostatic
TLR4:LYS475:NZ	RT:TRP351	RTB	4.49247	Electrostatic
TLR4:TYR37:OH	RT:PRO297:O	RTB	3.38661	Hydrogen bond
TLR4:ARG86:NH1	RT:SER543:O	RTB	3.34691	Hydrogen bond
TLR4:SER104:OG	RT:SER418:OG	RTB	2.51362	Hydrogen bond
TLR4:ARG337:NE	RT:SER520:OG	RTB	3.36619	Hydrogen bond
TLR4:ARG337:NH1	RT:SER520:OG	RTB	3.32147	Hydrogen bond
TLR4:TYR454:OH	RT:LYS354:O	RTB	2.64150	Hydrogen bond
TLR4:LYS503:NZ	RT:LYS354:O	RTB	3.21736	Hydrogen bond
TLR4:SER545:OG	RT:ASN374:OD1	RTB	3.38933	Hydrogen bond
TLR4:SER300:N	RT:SER54:OG	RTA	3.17882	Hydrogen bond
TLR4:TRP351:NE1	RT:GLN428:OE1	RTB	2.27258	Hydrogen bond
TLR4:ASN356:ND2	RT:ASP500:OD2	RTB	2.42735	Hydrogen bond
TLR4:THR357:N	RT:SER526:OG	RTB	2.84165	Hydrogen bond
TLR4:THR357:OG1	RT:ASN524:OD1	RTB	2.33051	Hydrogen bond
TLR4:ASN427:ND2	RT:ASP377:OD1	RTB	3.00993	Hydrogen bond
TLR4:TYR439:OH	RT:ASP83:OD2	RTA	2.43764	Hydrogen bond
TLR4:ARG512:NE	RT:GLU134:OE1	RTA	2.71612	Hydrogen bond
TLR4:ARG512:NH1	RT:GLY110:O	RTA	2.90917	Hydrogen bond
TLR4:LYS533:NZ	RT:MET40:SD	RTA	2.99009	Hydrogen bond
TLR4:ARG86:CD	RT:SER543:O	RTB	2.85600	Hydrogen bond
TLR4:HIS424:CD2	RT:ASP339:OD2	RTB	2.86625	Hydrogen bond
TLR4:HIS527:CE1	RT:SER355:O	RTB	3.43343	Hydrogen bond
TLR4:TYR449:OH	RT:TRP351	RTB	4.13152	Hydrogen bond
TLR4:SER509:OG	RT:TYR183	RTA	3.55468	Hydrogen bond
TLR4:ILE511:CG2	RT:HIS158	RTA	3.33491	Hydrophobic
TLR4:LEU539:CD2	RT:PHE62	RTA	3.53391	Hydrophobic
TLR4:PRO33	RT:PRO297	RTA	3.93392	Hydrophobic
TLR4:MET40	RT:LEU541	RTB	5.33807	Hydrophobic
TLR4:LYS263	RT:LEU519	RTB	4.69888	Hydrophobic
TLR4:ALA71	RT:PRO27	RTA	4.23869	Hydrophobic
TLR4:ARG74	RT:ILE29	RTA	5.19910	Hydrophobic
TLR4:TRP81	RT:ILE413	RTB	4.82280	Hydrophobic
TLR4:HIS429	RT:PRO352	RTB	5.47002	Hydrophobic
TLR4:TRP407	RT:VAL31	RTA	5.11514	Hydrophobic
TLR4:TYR542	RT:VAL133	RTA	4.98381	Hydrophobic

TLR4 recruits MyD88 through the TIR domain. MyD88 then activates IRAK and TRAF6, which activates MAPK and various transcription factors such as NF-κB (Putra et al., 2014; Yanagibashi et al., 2015; Sakai et al., 2017). IκB-α is an inhibitory protein bound to dimers of NF-κB that retains NF-κB dimers in the cytoplasm. The NF-κB pathway is activated by increasing the level of IκB-α phosphorylation, which causes the release of NF-κB and the expression of cytokine genes, such as TNF-α, IL-1, and IL-6 (Yamamoto and Gaynor, 2004; Kuan et al., 2012; Karin and Delhase, 2012). Our previous studies reported that NF-κB pathways may be involved in RTB-induced TNF-α production. In accordance with our previous study, IκB phosphorylation was altered in RTB-treated macrophages; this effect could be reversed in TLR4- siRNA treated macrophages after RTB treatment. These data suggest that NF-κB is an important signaling pathway in RTB-treated RAW264.7 cells.

The present study demonstrates the mechanism of RTB and TLR4, the induction of TNF-α production by RTB, and the correlation between TNF-α production and activation of the TLR4-dependent pathway induced by RTB stimulation. RTB stimulated macrophages through TLR4-dependent NF-κB activation. These signaling pathways may be responsible for TNF-α production. These data suggest that RTB activates macrophages to trigger TNF-α production through interaction with TLR4-mediated pathways.

DATA AVAILABILITY STATEMENT

The datasets generated for this study are available on request to the corresponding authors.

AUTHOR CONTRIBUTIONS

Conceptualization: NX and WL. Methodology: MD. Software: HY. Validation: YW and MD. Resources: YW. Data curation: YW. Writing (original draft preparation): NX and HY. Writing (review and editing): WL. Project administration: NX. Funding acquisition: NX. All authors contributed to the article and approved the submitted version.

FUNDING

This work was supported by the National Science and Technology Major Project(no.2018ZX10101003-005), National Natural Sciences Foundation of China (no. 81773630), and Project Agreement for Science & Technology Development, Jilin Province (no. 20180201004 YY).

REFERENCES

Akira, S., Uematsu, S., and Takeuchi, O. (2006). Pathogen recognition and innate immunity. *Cell* 124 (4), 783–801. doi: 10.1016/j.cell.2006.02.015

Dong, M., Yu, H., Wang, Y., Sun, C., Chang, Y., Yin, Q., et al. (2019). Critical Role of Toll-Like Receptor 4 (TLR4) in Ricin Toxin-Induced Inflammatory Responses in Macrophages. *Toxicol. Lett.* 321, 54–60. doi: 10.1016/j.toxlet.2019.12.021

Gay, N. J., Symmons, M. F., Gangloff, M., and Bryant, C. E. (2014). Assembly and localization of Toll-like receptor signalling complexes. *Nat. Rev. Immunol.* 14 (8), 546–558. doi: 10.1038/nri3713

Hartley, M. R., and Lord, J. M. (2004). Cytotoxic ribosome-inactivating lectins from plants. *Biochim. Biophys. Acta* 1701 (1-2), 1–14. doi: 10.1016/j.bbapap.2004.06.004

Horng, T., Barton, G. M., Flavell, R. A., and Medzhitov, R. (2002). The adaptor molecule TIRAP provides signalling specificity for Toll-like receptors. *Nature* 420 (6913), 329–333. doi: 10.1038/nature01180

Karin, M., and Delhase, M. (2012). The IKB kinase (IKK) and NF-KB: key elements of proinflammatory signaling. *Semin. Immunol.* 14 (1), 114–120. doi: 10.1006/smim.2000.0210

Kawai, T., and Akira, S. (2010). The role of pattern-recognition receptors in innate immunity: update on Toll-like receptors. *Nat. Immunol.* 11 (5), 373–384. doi: 10.1038/ni.1863

Kuan, Y. C., Lee, W. T., Hung, C. L., Yang, C., and Sheu, F. (2012). Investigating the function of a novel protein from A noectochilus formosanus which induced macrophage differentiation through TLR4-mediated NF-κB activation. *Int. Immunopharmacol.* 14 (1), 114–120. doi: 10.1016/j.intimp.2012.06.014

Lin, S. C., Lo, Y. C., and Wu, H. (2010). Helical assembly in the MyD88-IRAK4-IRAK2 complex in TLR/IL-1R signaling. *Nature* 465 (7300), 885–890. doi: 10.1038/nature09121

Liu, W., Xu, N., Yuan, H., Li, S., Liu, L., Pu, Z., et al. (2013). Immunomodulatory Activity of Recombinant Ricin Toxin Binding Subunit B (RTB). *Int. J. Mol. Sci.* 14 (6), 12401–12410. doi: 10.3390/ijms140612401

Lord, J. M., and Spooner, R. A. (2011). Ricin trafficking in plant and mammalian cells. *Toxins (Basel)* 3 (7), 787–801. doi: 10.3390/toxins3070787

Lord, M. J., Jolliffe, N. A., Marsden, C. J., Pateman, C. S., Smith, D. C., Spooner, R. A., et al. (2003). Ricin: mechanisms of cytotoxicity. *Toxicol. Rev.* 22 (1), 53–64. doi: 10.2165/00139709-200322010-00006

Mogensen, T. H. (2009). Pathogen recognition and inflammatory signaling in innate immune defenses. *Clin. Microbiol. Rev.* 22 (2), 240–273. doi: 10.1128/CMR.00046-08

Motshwene, P. G., Moncrieffe, M. C., Grossmann, J. G., Kao, C., Ayaluru, M., Sandercock, A. M., et al. (2009). An oligomeric signaling platform formed by Toll-like receptor signal transducers MyD88 and IRAK-4. *J. Biol. Chem.* 284, 25404–25411. doi: 10.1074/jbc.M109.022392

Olsnes, S., Fernandez-Puentes, C., Carrasco, L., and Vazquez, D. (1975). Ribosome inactivation by the toxic lectins abrin and ricin Kinetics of the enzymic activity of the toxin A-chains. *Eur. J. Biochem.* 60 (1), 281–288. doi: 10.1111/j.1432-1033.1975.tb21001.x

Pålsson-McDermott, E. M., and O'Neill, L. A. (2009). Signal transduction by the lipopolysaccharide receptor Toll-like receptor-4. *Immunology* 284 (37), 25404–25411. doi: 10.1111/j.1365-2567.2004.01976.x

Park, H. J., Hong, J. H., Kwon, H. J., Kim, Y., Lee, K. H., Kim, J. B., et al. (2010). TLR4-Mediated activation of mouse macrophages by Korean mistletoe lectin-C (KML-C). *Biochem. Biophys. Res. Commun.* 396 (3), 721–725. doi: 10.1016/j.bbrc.2010.04.169

Putra, A. B., Nishi, K., Shiraishi, R., Doi, M., and Sugahara, T. (2014). Jellyfish collagen stimulates production of TNF-α and IL-6 by J774.1 cells through activation of NF-κB and JNK via TLR4 signaling pathway. *Mol. Immunol.* 58 (1), 32–37. doi: 10.1016/j.molimm.2013.11.003

Sakai, J., Cammarota, E., Wright, J. A., Cicuta, P., Gottschalk, R. A., Li, N., et al. (2017). Lipopolysaccharide-induced NF-κB nuclear translocation is priarily dependent on MyD88, but TNF-α expression requires TRIF and MyD88. *Sci. Rep.* 7 (1), 1428. doi: 10.1038/s41598-017-01600-y

Stirpe, F., and Barbieri, L. (1986). Ribosome-inactivating proteins up to date. *FEBS Lett.* 195 (1-2), 1–8. doi: 10.1016/0014-5793(86)80118-1 20.

Xu, N., Yuan, H., Liu, W., Li, S., Liu, Y., Wan, J., et al. (2013). Activation of RAW264.7 mouse macrophage cells in vitro through treatment with recombinant ricin toxin-bindingsubunit B: Involvement of protein tyrosine, NF-κB and JAK-STAT kinase signaling pathways. *Int. J. Mol. Med.* 32 (3), 729–735. doi: 10.3892/ijmm.2013.1426

Yamamoto, Y., and Gaynor, R. B. (2004). IkappaB kinases: key regulators of the NF-kappaB pathway. *Trends Biochem. Sci.* 29 (2), 72–79. doi: 10.1016/j.tibs.2003.12.003

Yanagibashi, T., Nagai, Y., Watanabe, Y., Ikutani, M., Hirai, Y., and Takatsu, K. (2015). Differential requirements of MyD88 and TRIF pathways in TLR4-mediated immune responses inmurine B cells. *Immunol. Lett.* 163 (1), 22–31. doi: 10.1016/j.imlet.2014.11.012

Conflict of Interest: The authors declare that the research was conducted in the absence of any commercial or financial relationships that could be construed as a potential conflict of interest.

frontiers in Pharmacology

ORIGINAL RESEARCH
published: 07 October 2020
doi: 10.3389/fphar.2020.545555

Incidence Rate of Hypersensitivity Reactions to Bee-Venom Acupuncture

Eun-Jung Lee[1], *Yo-Chan Ahn*[2], *Young-Il Kim*[3], *Min-Seok Oh*[1], *Yang-Chun Park*[4] *and Chang-Gue Son*[5]*

[1] Department of Korean Rehabilitation Medicine, College of Korean Medicine, Daejeon University, Daejeon, South Korea, [2] Department of Health Service Management, Daejeon University, Daejeon, South Korea, [3] Department of Acupuncture and Moxibustion Medicine, College of Korean Medicine, Daejeon University, Daejeon, South Korea, [4] Division of Respiratory System, Department of Internal Medicine, College of Korean Medicine, Daejeon University, Daejeon, South Korea, [5] Department of Gastrobilliary System, Dunsan Hospital of Daejeon University, Daejeon, South Korea

OPEN ACCESS

Edited by:
Jean-Marc Sabatier, Aix-Marseille Université, France

Reviewed by:
Nathalie K. Zgheib, American University of Beirut, Lebanon
Wojciech Francuzik, Charité–Universitätsmedizin Berlin, Germany

***Correspondence:**
Chang-Gue Son
ckson@dju.ac.kr

Specialty section:
This article was submitted to Translational Pharmacology, a section of the journal Frontiers in Pharmacology

Received: *25 March 2020*
Accepted: *11 September 2020*
Published: *07 October 2020*

Citation:
Lee E-J, Ahn Y-C, Kim Y-I, Oh M-S, Park Y-C and Son C-G (2020) Incidence Rate of Hypersensitivity Reactions to Bee-Venom Acupuncture. Front. Pharmacol. 11:545555. doi: 10.3389/fphar.2020.545555

Introduction: Bee-venom acupuncture (BVA) has been widely applied to various disorders including pain-related diseases; however, patients are often warned of adverse reactions such as anaphylaxis. This study aimed to estimate the risk of hypersensitivity reactions to BVA and to determine their clinical features.

Methods: We retrospectively surveyed the medical records of patients treated by BVA between January 2010 and April 2019 in Dunsan Hospital of Daejeon University, and all cases of allergic reactions and their clinical symptoms were analyzed.

Results: A total of 8,580 patients (males 4,081 and females 4,499) were treated with BVA which amounts to a total of 60,654 treatments (average 7.1 ± 14.8 times). A total of fifteen patients (7 males and 8 females) reported an allergic reaction (0.175%, 95% CI, 0.086–0.263) of type 1 hypersensitivity, indicating a rate of allergic reaction in 0.025% (95% CI, 0.012–0.037) of the total BVA treatments. The average number of BVA treatments in those patients was 6.9 ± 6.5 (males: 4.1 ± 3.4 and females: 9.3 ± 7.9). Among the cases of hypersensitivity reactions, 4 involved anaphylactic shock; therefore, the incidence rate of anaphylaxis was 0.047% (95% CI, 0.001–0.092) for the 8,580 subjects and 0.007% (95% CI, 0.000–0.013) for the 60,654 treatments. All grade 1 cases were recovered within 1 day, whereas others took up to 30 days for complete recovery.

Conclusion: Our results may emphasize paying attention to unforeseeable risks of anaphylaxis after bee-venom acupuncture. This study could be essential reference data for the guidelines of appropriate use of bee-venom acupuncture and bee-venom-derived interventions in clinical applications.

Keywords: bee venom, adverse drug reaction, hypersensitivity, anaphylaxis, side effect, acupuncture

INTRODUCTION

Recently, venoms have received a lot of attention as an intervention for diseases. Among these, bee-venom is most commonly used as painkillers and anti-inflammatory drugs (Seo et al., 2017; Memariani et al., 2019). Furthermore, bee-venom is an effective therapeutic for other challenging disorders, including incurable skin disease, cancer, and Parkinson's disease (Hartmann et al., 2016; Gu et al., 2018; Aufschnaiter et al., 2020). Despite these potential applications, however, the clinical use of bee-venom is limited due to allergic reactions, including life-threatening responses such as anaphylaxis.

In general, adverse drug reactions (ADRs) are one of the major reasons why the drugs were withdrawn from the post marketing phase (Demoly et al., 2008; Onakpoya et al., 2019). Drug hypersensitivity reactions account for 15% of ADRs (Pichler and Hausmann, 2016). Drug-induced anaphylaxis is the most serious and life-threatening hypersensitivity reaction (Turner et al., 2017) and many drugs that trigger anaphylaxis involving antibiotics, radiocontrast agents, and nonsteroidal anti-inflammatory drugs (NSAIDs) are frequently problematic in clinic (Wood et al., 2014; Giavina-Bianchi et al., 2018). Regarding NSAIDs-related incidence rate of hypersensitivity and anaphylaxis, one US clinical study reported as 0.30 and 0.02%, respectively (Blumenthal et al., 2017). Another study presented incidence rates of 0.48% for hypersensitivity reactions and 0.01% for anaphylaxis from 9,528 MRI examinations with contrast-agent (Li et al., 2006).

Bee-venom acupuncture (BVA) is a common therapeutic used worldwide, especially in Korean and Chinese clinics. Since one death by BVA anaphylactic shock was reported, the safety of bee-venom has been an important issue in Korea (Jung et al., 2012b). Two studies demonstrated partially BVA-related hypersensitivity reactions using data from clinical trials or hospital records (Park et al., 2015; Kim et al., 2016); however, further studies are still required to provide better clinical guidance for safe use of BVA. The present study aimed to estimate the risk size of hypersensitivity reactions by BVA and to determine their clinical features.

MATERIALS AND METHODS

Study Design

This study was a retrospective analysis. The data source was the electronic medical records (EMRs) of 66,614 subjects who had visited the pain-spine center and rehabilitation center in Dunsan Hospital of Daejeon University, South Korea, from January 2010 to March 2019. This process was conducted *via* integrated hospital information system (IHIS) that analyzed the order communication system (OCS) and EMR. We first selected only subjects treated with BVA and then searched the cases with hypersensitivity after BVA treatment. We analyzed the incidence rate of hypersensitivity reactions and anaphylactic shock along with their clinical features. The inclusion criteria for the selection of patients and the incidence of a hypersensitivity reaction were as follows: 1) subjects who had been treated with BVA at least once, as recorded in their EMRs; or 2) subjects who complained of a BVA-related systemic allergic reaction with/without the prescription of anti-allergic drugs such as antihistamines, adrenaline, or adrenal cortex hormones. Strategy to identify the hypersensitivity cases was based on the guideline for BVA treatment, which all the cases of BVA allergic reaction should be referred to one conventional doctor in same hospital. We carefully reviewed the full medical records for all the suspected cases.

BVA

The bee-venom source for BVA used in two centers was produced by Green Myeongpum Pharm Company (Namyangju, Korea). This bee-venom source was validated for its main active compound (over 99.9% melittin) and allergen-free purification (phospholipase A2, apamin, hyaluronidase, and histamine) and was then diluted to 10% with normal saline by Jaseng Namyangju Industrial Institute (Namyangju, Korea) or Kirin Korean Medicine Industrial Institute (Wonju, Korea). BVA treatment was conducted with an injection of bee-venom solution (range, 1.0 to 2.0 mL) at a specific acupoint of skin or muscle with interval of 3 or 4 days.

Ethics Statement

This study was approved by the Institutional Review Board for Human Research of Daejeon University Dunsan Hospital (approval number: DJDSKH-18-E-08-2). We have obtained verbal consent from every subject identified as having a hypersensitivity reaction.

Data Source Extraction and Analysis

We extracted general information on the subjects treated with BVA including gender, age, frequency of BVA prescriptions and the main health complaint (according to the International Classification of Diseases-10; ICD 10) and cases of hypersensitivity reaction including its primary symptoms, the recovery period, and the presence of a family history of allergy-related illness. We, thus, calculated the incidence rate of hypersensitivity reactions and anaphylactic shock, with the number of subjects and times of BVA treatment. The type of hypersensitivity reaction was classified according to immune mechanisms and clinical symptoms (Dispenza, 2019). The severity of the allergic symptoms was assessed in three categories proposed by Brown SG (Brown, 2004), which was established by slight modification from Muller's four classifications (Mueller, 1966), while the definition of anaphylaxis followed the 2010 World Allergy Organization guideline (Simons et al., 2011) as shown in **Supplementary Table 1**. For every subject identified as having a hypersensitivity reaction, we conducted a telephone survey to clarify the consequences and other medical events since they stopped BVA treatment.

Statistical Analysis

Categorical variables were expressed as frequency and percentages, and averages were expressed as the means ± standard deviation

Abbreviations: ADR, Adverse drug reaction; BVA, Bee-venom acupuncture; EMR, Electronic medical record; ICD-10; International classification of diseases-10, NSAID, Nonsteroidal anti-inflammatory drug.

(SD). The incidence rate was given as a percentage within the 95% confidence interval. The comparison between male and female was analyzed using chi-squared test or Fisher exact test. Statistical analyses were performed with the SPSS statistical software package version 18.0 (SPSS Inc., Chicago, IL, USA).

RESULTS

Characteristics of Subjects

From EMR analysis, 8,580 subjects (4,081 males and 4,499 females) met our study criteria. The total number of BVA prescriptions was 60,654, accounting for an average of 7.1 ± 14.8 BVA treatments per subject (males: 7.0 ± 11.8 vs. females: 7.1 ± 17.1, $p > 0.05$). The median age of the subjects was 53 years (range, 13–98 years). Most subjects (93%) had complaints of the musculoskeletal system and connective tissue or injury-related pain. The number of subjects were counted without duplication, no matter how many times they visited hospitals as an inpatient or outpatient (**Table 1**).

Incidence Rates of Hypersensitivity Reaction and Anaphylaxis

Fifteen subjects (seven males and eight females) showed hypersensitivity reactions to BVA, with an incidence rate of 0.175% (95% CI: 0.086–0.263%) from 8,580 subjects and 0.025% (95% CI: 0.012–0.037%) from 60,654 treatments. Among those, four cases were anaphylactic shock, corresponding to 0.047% (95% CI: 0.001–0.092) of subjects and 0.007% (95% CI: 0.000–0.013) of treatments, respectively. No significant difference by gender was observed for total hypersensitivity. The anaphylactic shock was more frequent in female than male for both subjects (0.067% in female vs. 0.025% in male) and treatments (0.003% in female vs. 0.009% in male), but no statistical significance was observed ($p > 0.05$, **Table 2**).

TABLE 1 | Characteristics of subjects.

Subjects	Male/Female (%)	Total
Number of subjects (%)	4,081 (47.6)/4,499 (52.4)	8,580 (100)
Median age (year, range)	49 (13 to 88)/53 (13 to 98)	53 (13 to 98)
Number of BVA treatments (%)	28,626 (47.6)/32,028 (52.4)	60,654 (100)
Mean N. of BVA treatments	7.0 ± 11.8/7.1 ± 17.1	7.1 ± 14.8
Main complains (ICD-10)		**N. of subjects (%)**
M00-M99: Diseases of the musculoskeletal system and connective tissue		4,724 (50.2)
S00-T98: Injury, poisoning and certain other consequences of external causes		4,027 (42.8)
G00-G99: Diseases of the nervous system		449 (4.8)
R00-R99: Symptoms, signs and abnormal clinical and laboratory findings, NEC		95 (1.0)
Others		110 (1.8)
Total subjects*		9,405 (100)

**Duplication was permitted to be counted in case one patient received BVA treatment as an inpatient and an outpatient. Therefore, this number is larger than number for analysis (8,580 subjects).*

Clinical Features of Hypersensitivity Reaction and Anaphylaxis

Regarding the severity of the symptom, 6 cases were grade 1, while 7 and 2 cases were belonged to grade 2 and 3, respectively (**Table 2**). All cases of hypersensitivities appeared immediately or within one hour after BVA treatment, which is the typical feature of type 1 hypersensitivity. They completely recovered, although one subject was hospitalized. Skin symptoms such as generalized itchiness and urticaria were the most common (80%), followed by respiratory symptoms (46.7%), cardiovascular and neurological symptoms (26.7%), and gastrointestinal symptoms (20%). Twelve out of 15 cases occurred after several BVA treatments, while three cases showed the hypersensitivity reactions on the first exposure in our hospital (**Table 3**).

DISCUSSION

In this study, we investigated the clinical question: what is the risk size of BVA-derived hypersensitivity reactions, including anaphylactic shock and its clinical features. Most of the subjects had disorders related to the musculoskeletal system and joints, on which bee-venom and its main components may have a therapeutic effect as a painkiller or chondroprotective agent (Jeong et al., 2015). The incidence rate of hypersensitivity reactions in our study (0.175% from 8,580 subjects and 0.025% from 60,654 treatments) was slightly lower than results from another retrospective study, which showed a 0.23% incidence rate of BVA-induced hypersensitivity reactions (Kim et al., 2016). Drug-induced hypersensitivities can be broadly classified into four types by immune mechanisms (Dispenza, 2019). BV-induced allergic reaction is known mainly to be of type 1 hypersensitivity which is mediated by IgE (Kwon et al., 2009).

In our results, all cases with hypersensitivities appeared immediately or within one hour after BVA treatment,

TABLE 2 | Incidence rate of hypersensitivity reaction and anaphylactic shock.

Hypersensitivity reaction	Incidence rate (95% CI)
By subjects (15 of 8,580)	0.175% (0.086–0.263)
Male (7 of 4,081)	0.172% (0.045–0.298)
Female (8 of 4,499)	0.178% (0.055–0.301)
By treatments (15 of 60,654)	0.025% (0.012–0.037)
Male (7 of 28,626)	0.024% (0.006–0.043)
Female (8 of 32,028)	0.025% (0.008–0.042)
Anaphylaxis shock	**Incidence rate (95% CI)**
By subjects (4 of 8,580)	0.047% (0.001–0.092)
Male (1 of 4,081)	0.025% (-0.024–0.073)
Female (3 of 4,49	0.067% (-0.009–0.142)
By treatments (4 of 60,654)	0.007% (0.000–0.013)
Male (1 of 28,626)	0.003% (-0.003–0.010)
Female (3 of 32,028)	0.009% (-0.001–0.020)
Severity of symptom	**Frequency (%)**
Grade 1 (Mild)	6 (male 4, female 2), 40.0%
Grade 2 (Moderate)	7 (male 3, female 4), 46.7%
Grade 3 (Severe)	2 (male 0, female 2), 13.3%

TABLE 3 | Characteristics of 15 allergic reaction cases with bee-venom acupuncture.

Case (sex/age)	Chief complaints (allergy disorders*)	Family history of allergy	No. BVA treatment† (Interval‡)	Allergic reaction		
				Main symptoms	Type (Grade)§	Outcome (follow-up)#
P1 (M/36)	Cervical sprain	Fish allergy (mother)	1 (0 d)	Urticaria	Type1 (G 1)	Recovered (1d, itch)
P2 (M/38)	Cervical sprain	None	2 (14 d)	Urticaria	Type1 (G 1)	Recovered (1d, itch)
P3 (M/44)	Cervical sprain	Asthma (brother)	4 (3 d)	Urticaria	Type1 (G 1)	Recovered (1d, itch)
P4 (M/48)	Lumbar HNP	None	3 (7 d)	Urticaria	Type1 (G 1)	Recovered (1d, itch)
P5 (F/53)	Cervical HNP (aspirin allergy)	None	1 (0 d)	Urticaria	Type1 (G 1)	Recovered (1 d, itch)
P6 (F/56)	Cervical sprain	None	1 (0 d)	Urticaria	Type1 (G 1)	Recovered (1 d, itch)
P7 (M/32)	Knee contusion (allergic rhinitis)	Allergic rhinitis (brother)	2 (8 d)	Dizziness, throat tightness, weakness, anxiety	Type1 (G 2)	Recovered (1d, dizziness)
P8 (M/64)	Sprain of knee	None	11 (22 d)	Urticaria, constriction in chest, weakness	Type1 (G 2)	Recovered (30 d, weakness)
P9 (F/32)	Cervical sprain	None	14 (64 d)	Urticaria, localized edema, throat tightness	Type1 (G 2)	Recovered (2 d, itch)
P10 (F/42)	Cervical sprain (allergic rhinitis)	None	22 (7 d)	Headache, dizziness, numbness, abdominal pain, generalized pain	Type1 (G 2)	Recovered (21 d, dizziness)
P11 (F/42)	Frozen shoulder (contrast agent allergy)	None	15 (4 d)	Urticaria, erythema, throat swelling	Type1 (G 2)	Recovered (3 d, throat swelling)
P12 (M/70)	Lumbar stenosis (asthma)	None	6 (362 d)	Urticaria, pain, chilling, cold sweat, nausea, vomiting, anxiety, dyspnea	Type1 (G 2)	Recovered (30 d, anxiety)
P13 (F/62)	Lumbar HNP	None	13 (231 d)	Urticaria, paresthesia, throat tightness, dyspnea	Type1 (G 2)	Recovered (2 d, weakness)
P14 (F/59)	Spinal stenosis	None	2 (391 d)	Urticaria, throat tightness, chest pain, nausea, vomiting, dizziness, dyspnea, hypotension, loss of consciousness	Type1 (G 3)	Recovered (14 d, dizziness, weakness)
P15 (F/60)	Cervical HNP (allergic rhinitis)	Allergic rhinitis (son)	6 (129 d)	Weakness, paresthesia, throat tightness, dyspnea, lip edema, hypotension, loss of consciousness	Type1 (G 3)	Recovered (3 d, lip edema)

**Presence of allergy disorders in an ordinary day. †Number of BVA treatments by the day of an allergic reaction. ‡Duration between two time points (the last BVA-treatment and the next previous BVA administration). §Severity of allergic reactions according to the grading system. Grade 1, 2, and 3 refer to 'mild', 'moderate', and 'severe' for classification of symptom's severity. #The time point when the last symptom(s) disappeared.*

indicating the typical feature of type 1 hypersensitivity. Their clinical severities were 40.0%, 46.7%, and 13.3% for grade 1 to grade 3, respectively (**Table 2**). In general, anaphylaxis is the most severe systemic hypersensitivity reaction. In the United States, 1.6–5.1% of the population are estimated to have experienced anaphylaxis, and 1% of hospitalizations for anaphylaxis showed fatal results (Ma et al., 2014; Wood et al., 2014). The contrast agents for MRI examination are well known to show a high rate of anaphylactic reactions. Our data showed four cases of anaphylaxis due to BVA, corresponding to 0.047% of subjects and 0.007% of treatments (**Table 2**), which is very similar to the overall incidence rates of MRI contrast agents. One Korean group analyzed MRI contrast agent-related adverse reactions according to both patients (84,367 patients) and doses (141,623 total doses) as we did, presenting 0.121% (patients) and 0.079% (doses) for hypersensitivity and 0.01% (patients) and 0.008% (doses) for anaphylaxis (Jung et al, 2012a). Although our study and other studies showed the two kinds of the incidence rate of hypersensitivity reactions and anaphylaxis (patients vs. treatments), treatment-derived rates would be underestimated due to the repeated BVA treatments likely 5 to 10 BVA sessions per patient. Accordingly, we have to notice that the patient-derived rates reflect further practically the risk sizes comparing with the treatment-derived rates.

In general, the occurrence of drug-related adverse reactions, including anaphylaxis, depends on the three main factors: the drug properties themselves, the genetic backgrounds of subjects and environmental factors such as the coadministration of drugs, alcohol or food, underlying disorders, gender, age, or even psychiatric status (Merle et al., 2005; Nguyen et al., 2006; Zhang et al., 2009; Liao et al., 2019). In its original state, bee venom is a complex mixture of proteins (phospholipase A2, phospholipase B, and hyaluronidase), peptides (mainly melittin) and low-molecular-mass components such as histamine (Wehbe et al., 2019), while the bee-venom which was used in this study is composed of 99.9% melittin with removal of major toxic/allergic proteins. One previous study in Korea (using a diluted BV material without allergen-purification studied from 1998 to

2000) presented a 4-fold higher anaphylaxis incidence rate (0.03% of 32,000 treatments) compared to the present results (Hwang and Lee, 2000). Females are known to be more susceptible to ADRs, including anaphylaxis (Jensen-Jarolim and Untersmayr, 2008). In our results, the incidence rate of anaphylaxis (but not total hypersensitivity) was 3-fold higher in females than in males, as shown in the above MRI contrast agents (1.5-fold) (Jung et al., 2012a) and BVA (2.4-fold in Kim's study, 2.7-fold in Hwang's study) (Hwang and Lee, 2000; Kim et al., 2016). Previous clinical studies have reported a positive relationship between immune disorders and hypersensitivity reactions, likely a 1.7-fold higher incidence of adverse reactions to NSAIDs in subjects with autoimmune diseases (Blumenthal et al., 2017). Our study found that 40% of cases (6 out of 15 with hypersensitivity reactions) had underlying allergic diseases, but we cannot identify the exact correlation due to the lack of information for all subjects underwent BVA treatment. As in other studies, age did not affect the incidence of hypersensitivity or anaphylactic reactions in our study. Regarding the main symptoms of hypersensitivity reactions and their frequency, skin symptoms such as generalized itchiness and urticaria were the most common (12 cases, 80%) and disappeared within one or two days.

The subjects with a higher grade of severity (2 or 3 grade) complained of respiratory, gastrointestinal, cardiovascular, and neurological symptoms such as dyspnea, nausea, vomiting, abdominal pain, hypotension, or loss of consciousness, respectively. Although one patient was hospitalized for three days, and weakness and anxiety in two subjects were likely to last up to 30 days, all patients completely recovered (**Table 3**). The two severe cases with hypotension and loss of consciousness were treated with epinephrine and dexamethasone, while 13 cases (mild and moderate) were treated with antihistamine only or as a combination with dexamethasone according to international management guidelines for anaphylaxis. The average number of BVA treatments was 7.1 ± 14.8 in a total 8,580 subjects (**Table 1**), and 15 cases had the 6.9 ± 6.5 treatments (males 4.1 ± 3.4 and females 9.3 ± 7.9) before occurrence of the adverse reactions (**Table 3**, but the average number of treatments was not shown in table). Twelve cases of hypersensitivity reactions happened after several BVA treatments, while three cases showed it immediately on the first exposure in our hospital. However, these three subjects (P1, P5 and P6 in **Table 3**) had had BVA treatments in other clinics before visiting our hospital and two (P1 and P6) had experiences of mild allergic reactions (reconfirmed by phone call). In general, anaphylaxis is caused by IgE-mediated immunological release of chemical mediators; thus, repeated exposure to allergens can boost the production of IgE (Okano et al., 1999). One study reported that half of the bee-venom anaphylaxis-related deaths did not show allergic reactions to bee-venom exposure in the past (Golden, 2007). Interestingly, all anaphylaxis cases had long duration (between 129 ~ 391 days) between two time points, the last BVA treatment and the next previous BVA administration (**Table 3**). Currently, we cannot explain the reasons for our results; however, we have to pay attention to melittin itself, the core component of BV. Although the bee-venom used in present study was prepared by removing major allergens, melittin was known to induce minor allergic reaction (Jarisch et al., 1979). Melittin also can form a complex with phospholipase A2 (PLA2, the second most abundant compound), which consequentially cleaves cellular membrane phospholipids and then leads to inflammatory reaction (Mingarro et al., 1995). Accordingly, the repeated exposure of melittin of BVA could evoke the allergic reactions including anaphylactic shock in certain subjects. This might be supported by our result, which high grades (2 or 3) of hypersensitivity reactions occurred with greater number of BVA treatments (10.1 ± 6.7 times) compared to grade 1 (2.0 ± 1.3 times).

Skin tests are generally adapted for the prediction of a drug hypersensitivity (Brockow et al., 2002). At present, we recommend skin tests for every patient requiring BVA treatment, one before the first treatment and another after the 2-week interval period. However, it should be noted that all hypersensitive persons cannot be identified only through the skin test. High levels of serum IgE and tryptase are good indicators for type 1 hypersensitivity, including anaphylaxis (Rueff et al., 2009). In addition, the determination of the baseline serum tryptase levels in patients who underwent anaphylaxis to BVA could be helpful to rule out an unspecific mast cell activation disorder (Vitte, 2015). We however didn't conduct those tests in present study. This would be the limitation of our present study along with a retrospective study.

Taken together, we can expect that the BVA-related risks of a hypersensitivity reaction and anaphylaxis are approximately 0.175 and 0.025% of subjects, and 0.025 and 0.007% of treatments. This risk of anaphylaxis shouldn't be ignored, moreover requires to pay careful attention in clinical application of BVA due to the possibility of fatal outcome. This study would be a useful reference for the safe clinical application of bee-venom-derived interventions and their pharmaceutical development in the future.

DATA AVAILABILITY STATEMENT

The raw data supporting the conclusions of this article will be made available by the authors, without undue reservation, to any qualified researcher.

ETHICS STATEMENT

The studies involving human participants were reviewed and approved by Institutional Review Board for Human Research in Dunsan Hospital of Daejeon University (approval number: DJDSKH-18-E-08-2). Written informed consent for participation was not provided by the participants' legal guardians/next of kin because the institute proved the no-

requirement of the written consent; however, we have obtained verbal consent from every subject identified as having a hypersensitivity reaction.

AUTHOR CONTRIBUTIONS

E-JL participated mainly in the design of the experiments and manuscript preparation. Y-CA, Y-CP, M-SO, and Y-IK contributed to the data collection and manuscript preparation including revision process. C-GS supervised whole processes of experiments and manuscript preparation. All authors contributed to the article and approved the submitted version.

FUNDING

This study was supported by the Ministry of Education, Science and Technology (NRF-2018R1A6A1A03025221) and the Ministry of Health and Welfare of South Korea (grant number: HI15C0006).

SUPPLEMENTARY MATERIAL

The Supplementary Material for this article can be found online at: https://www.frontiersin.org/articles/10.3389/fphar.2020.545555/full#supplementary-material

REFERENCES

Aufschnaiter, A., Kohler, V., Khalifa, S., Abd El-Wahed, A., Du, M., El-Seedi, H., et al. (2020). Apitoxin and Its Components against Cancer, Neurodegeneration and Rheumatoid Arthritis: Limitations and Possibilities. *Toxins (Basel)* 12 (2), E66. doi: 10.3390/toxins12020066

Blumenthal, K. G., Lai, K. H., Huang, M., Wallace, Z. S., Wickner, P. G., and Zhou, L. (2017). Adverse and Hypersensitivity Reactions to Prescription Nonsteroidal Anti-Inflammatory Agents in a Large Health Care System. *J. Allergy Clin. Immunol. Pract.* 5 (3), 737–743. doi: 10.1016/j.jaip.2016.12.006

Brockow, K., Romano, A., Blanca, M., Ring, J., Pichler, W., and Demoly, P. (2002). General considerations for skin test procedures in the diagnosis of drug hypersensitivity. *Allergy* 57 (1), 45–51. doi: 10.1046/j.0105-4538.2001.00001.x-i8

Brown, S. G. (2004). Clinical features and severity grading of anaphylaxis. *J. Allergy Clin. Immunol.* 114 (2), 371–376. doi: 10.1016/j.jaci.2004.04.029

Demoly, P., Pichler, W., Pirmohamed, M., and Romano, A. (2008). Important questions in Allergy: 1 - drug allergy/hypersensitivity. *Allergy* 63 (5), 616–619. doi: 10.1111/j.1398-9995.2008.01693.x

Dispenza, M. C. (2019). Classification of hypersensitivity reactions. *Allergy Asthma Proc.* 40, 470–473. doi: 10.2500/aap.2019.40.4274

Giavina-Bianchi, P., Aun, M. V., and Kalil, J. (2018). Drug-induced anaphylaxis: is it an epidemic? *Curr. Opin. Allergy Clin. Immunol.* 18 (1), 59–65. doi: 10.1097/ACI.0000000000000411

Golden, D. B. (2007). Insect sting anaphylaxis. *Immunol. Allergy Clin. North Am.* 27 (2), 261–272. doi: 10.1016/j.iac.2007.03.008

Gu, H. M., Kim, W. H., An, H. J., Kim, J. Y., Gwon, M. G., Han, S. M., et al. (2018). Therapeutic effects of bee venom on experimental atopic dermatitis. *Mol. Med. Rep.* 18 (4), 3711–3718. doi: 10.3892/mmr.2018.9398

Hartmann, A., Müllner, J., Meier, N., Hesekamp, H., van Meerbeeck, P., Habert, M. O., et al. (2016). Bee Venom for the Treatment of Parkinson Disease - A Randomized Controlled Clinical Trial. *PloS One* 11 (9), e0162937. doi: 10.1371/journal

Hwang, Y., and Lee, B. (2000). Clinical study of anaphylaxis on bee venom acupuncture. *J. Kor. Acup. Mox. Society* 17 (4), 149–159.

Jarisch, R., Yman, L., Boltz, A., Sandor, I., and Janitsch, A. (1979). IgE antibodies to bee venom, phospholipase A, melittin and wasp venom. *Clin. Allergy* 9 (5), 535–341. doi: 10.1111/j.1365-2222.1979.tb02518.x

Jensen-Jarolim, E., and Untersmayr, E. (2008). Gender-medicine aspects in allergology. *Allergy* 63 (5), 610–615. doi: 10.1111/j.1398-9995.2008.01645.x

Jeong, Y. J., Shin, J. M., Bae, Y. S., Cho, H. J., Park, K. K., Choe, J. Y., et al. (2015). Melittin has a chondroprotective effect by inhibiting MMP-1 and MMP-8 expressions via blocking NF-κB and AP-1 signaling pathway in chondrocytes. *Int. Immunopharmacol.* 25 (2), 400–405. doi: 10.1016/j.intimp.2015.02.021

Jung, J. W., Jeon, E. J., Kim, J. W., Choi, J. C., Shin, J. W., Kim, J. Y., et al. (2012a). A Fatal Case of Intravascular Coagulation After Bee Sting Acupuncture. *Allergy Asthma Immunol. Res.* 4 (2), 107–109. doi: 10.4168/aair.2012.4.2.107

Jung, J. W., Kang, H. R., Kim, M. H., Lee, W., Min, K. U., Han, M. H., et al. (2012b). Immediate hypersensitivity reaction to gadolinium-based MR contrast media. *Radiology* 264 (2), 414–422. doi: 10.1148/radiol.12112025

Kim, M. R., Shin, J. S., Lee, J. H., Lee, Y. J., Ahn, Y. J., Park, K. B., et al. (2016). Safety of Acupuncture and Pharmacopuncture in 80,523 Musculoskeletal Disorder Patients, A Retrospective Review of Internal Safety Inspection and Electronic Medical Records. *Med. (Baltimore)* 95 (18), e3635. doi: 10.1097/MD.0000000000003635

Kwon, K. R., Kang, K. S., Lee, K. H., Lim, C. S., Jeong, H. S., and Kwon, H. Y. (2009). Clinical observation of anaphylaxis after treated with Sweet BV. *J. Pharmacopuncture* 12 (2), 85–90. doi: 10.3831/KPI.2009.12.2.085

Li, A., Wong, C. S., Wong, M. K., Lee, C. M., and Au Yeung, M. C. (2006). Acute adverse reactions to magnetic resonance contrast media – gadolinium chelates. *Br. J. Radiol.* 79 (941), 368–3671. doi: 10.1259/bjr/88469693

Liao, P. J., Mao, C. T., Chen, T. L., Deng, S. T., and Hsu, K. H. (2019). Factors associated with adverse drug reaction occurrence and prognosis, and their economic impacts in older inpatients in Taiwan: a nested case–control study. *BMJ Open* 9 (5), e026771. doi: 10.1136/bmjopen-2018-026771

Ma, L., Danoff, T. M., and Borish, L. (2014). Case fatality and population mortality associated with anaphylaxis in the United States. *J. Allergy Clin. Immunol.* 133 (3), 1075–1083. doi: 10.1016/j.jaci.2013.10.029

Memariani, H., Memariani, M., Shahidi-Dadras, M., Nasiri, S., Akhavan, M. M., and Moravvej, H. (2019). Melittin: from honeybees to superbugs. *Appl. Microbiol. Biotechnol.* 103 (8), 3265–3276. doi: 10.1007/s00253-019-09698-y

Merle, L., Laroche, M. L., Dantoine, T., and Charmes, J. P. (2005). Predicting and preventing adverse drug reactions in the very old. *Drugs Aging* 22 (5), 375–392. doi: 10.2165/00002512-200522050-00003

Mingarro, I., Pérez-Payá, E., Pinilla, C., Appel, J. R., Houghten, R. A., and Blondelle, S. E. (1995). Activation of bee venom phospholipase A2 through a peptide-enzyme complex. *FEBS Lett.* 372 (1), 131–134. doi: 10.1016/0014-5793(95)00964-B

Mueller, H. L. (1966). Diagnosis and treatment of insect sensitivity. *J. Asthma Res.* 3 (4), 331–333. doi: 10.3109/02770906609106941

Nguyen, J. K., Fouts, M. M., Kotabe, S. E., and Lo, E. (2006). Polypharmacy as a risk factor for adverse drug reactions in geriatric nursing home residents. *Am. J. Geriatr. Pharmacother.* 4 (1), 36–41. doi: 10.1016/j.amjopharm.2006.03.002

Okano, M., Nishizaki, K., Satoskar, A. R., Yoshino, T., Masuda, Y., and Harn, D. A. Jr (1999). Involvement of carbohydrate on phospholipase A2, a bee-venom allergen, in vivo antigen-specific IgE synthesis in mice. *Allergy* 54 (8), 811–818. doi: 10.1034/j.1398-9995.1999.00096.x

Onakpoya, I. J., Heneghan, C. J., and Aronson, J. K. (2019). Post-marketing withdrawal of 462 medicinal products because of adverse drug reactions: a systematic review of the world literature. *BMC Med.* 17 (1), 56. doi: 10.1186/s12916-019-1294-9

Park, J. H., Yim, B. K., Lee, J. H., Lee, S., and Kim, T. H. (2015). Risk associated with bee venom therapy: a systematic review and meta-analysis. *PloS One* 10 (5), e0126971. doi: 10.1371/journal.pone.0126971

Pichler, W. J., and Hausmann, O. (2016). Classification of Drug Hypersensitivity into Allergic, p-i, and Pseudo-Allergic Forms. *Int. Arch. Allergy Immunol.* 171 (3-4), 166–179. doi: 10.1159/000453265

Rueff, F., Przybilla, B., Bilo, M. B., Muller, U., Scheipl, F., Aberer, W., et al. (2009). Predictors of severe systemic anaphylactic reactions in patients with Hymenoptera venom allergy: importance of baseline serum tryptase-a study

of the European Academy of Allergology and Clinical Immunology Interest Group on Insect Venom Hypersensitivity. *J. Allergy Clin. Immunol.* 124 (5), 1047–1054. doi: 10.1016/j.jaci.2009.08.027

Seo, B. K., Han, K., Kwon, O., Jo, D. J., and Lee, J. H. (2017). Efficacy of Bee Venom Acupuncture for Chronic Low Back Pain: A Randomized, Double-Blinded, Sham-Controlled Trial. *Toxins (Basel)* 9 (11), E361. doi: 10.3390/toxins9110361

Simons, F. E., Ardusso, L. R., Bilò, M. B., El-Gamal, Y. M., Ledford, D. K., Ring, J., et al. (2011). World Allergy Organization. World Allergy organization anaphylaxis guidelines: summary. *J. Allergy Clin. Immunol.* 127 (3), 587–593. doi: 10.1016/j.jaci.2011.01.038

Turner, P. J., Jerschow, E., Umasunthar, T., Lin, R., Campbell, D. E., and Boyle, R. J. (2017). Fatal Anaphylaxis: Mortality Rate and Risk Factors. *J. Allergy Clin. Immunol. Pract.* 5 (5), 1169–1178. doi: 10.1016/j.jaip.2017.06.031

Vitte, J. (2015). Human mast cell tryptase in biology and medicine. *Mol. Immunol.* 63, 18–24. doi: 10.1016/j.molimm.2014.04.001

Wehbe, R., Frangieh, J., Rima, M., El Obeid, D., Sabatier, J. M., and Fajloun, Z. (2019). Bee Venom: Overview of Main Compounds and Bioactivities for Therapeutic Interests. *Molecules* 24 (16), E2997. doi: 10.3390/molecules 24162997

Wood, R. A., Camargo, C. A., Lieberman, P., Sampson, H. A., Schwartz, L. B., Zitt, M., et al. (2014). Anaphylaxis in America: the prevalence and characteristics of anaphylaxis in the United States. *J. Allergy Clin. Immunol.* 133 (2), 461– 467. doi: 10.1016/j.jaci.2013.08.016

Zhang, M., Holman, C. D., Price, S. D., Sanfilippo, F. M., Preen, D. B., and Bulsara, M. K. (2009). Comorbidity and repeat admission to hospital for adverse drug reactions in older adults: retrospective cohort study. *BMJ* 338, a2752. doi: 10.1136/bmj.a2752

Conflict of Interest: The authors declare that the research was conducted in the absence of any commercial or financial relationships that could be construed as a potential conflict of interest.

frontiers in Pharmacology

HYPOTHESIS AND THEORY
published: 14 December 2020
doi: 10.3389/fphar.2020.574925

How the Toxin got its Toxicity

Timothy N. W. Jackson[1]* *and Ivan Koludarov*[2]*

[1]Australian Venom Research Unit, Department of Pharmacology and Therapeutics, University of Melbourne, Melbourne, Australia, [2]Animal Venomics Group, Justus Leibig University, Giessen, Germany

Venom systems are functional and ecological traits, typically used by one organism to subdue or deter another. A predominant subset of their constituent molecules—"toxins"—share this ecological function and are therefore molecules that mediate interactions between organisms. Such molecules have been referred to as "exochemicals." There has been debate within the field of toxinology concerning the evolutionary pathways leading to the "recruitment" of a gene product for a toxic role within venom. We review these discussions and the evidence interpreted in support of alternate pathways, along with many of the most popular models describing the origin of novel molecular functions in general. We note that such functions may arise with or without gene duplication occurring and are often the consequence of a gene product encountering a novel "environment," i.e., a range of novel partners for molecular interaction. After stressing the distinction between "activity" and "function," we describe in detail the results of a recent study which reconstructed the evolutionary history of a multigene family that has been recruited as a toxin and argue that these results indicate that a pluralistic approach to understanding the origin of novel functions is advantageous. This leads us to recommend that an expansive approach be taken to the definition of "neofunctionalization"—simply the origins of a novel molecular function by any process—and "recruitment"—the "weaponization" of a molecule via the acquisition of a toxic function in venom, by any process. Recruitment does not occur at the molecular level or even at the level of gene expression, but only when a confluence of factors results in the ecological deployment of a physiologically active molecule as a toxin. Subsequent to recruitment, the evolutionary regime of a gene family may shift into a more dynamic form of "birth-and-death." Thus, recruitment leads to a form of "downwards causation," in which a change at the ecological level at which whole organisms interact leads to a change in patterns of evolution at the genomic level.

Keywords: toxin, venom, evolution, molecule, function, genomics, duplication, gene expression

OPEN ACCESS

Edited by:
Yuri N. Utkin, Institute of Bioorganic Chemistry (RAS), Russia

Reviewed by:
Yehu Moran, Hebrew University of Jerusalem, Israel
Kevin Arbuckle, Swansea University, United Kingdom

***Correspondence:**
Timothy N. W. Jackson
timothy.jackson@unimelb.edu.au
Ivan Koludarov
jcoludar@gmail.com

Specialty section:
This article was submitted to Pharmacology of Ion Channels and Channelopathies, a section of the journal Frontiers in Pharmacology

Received: *22 June 2020*
Accepted: *20 October 2020*
Published: *14 December 2020*

Citation:
Jackson TNW and Koludarov I (2020) How the Toxin got its Toxicity. Front. Pharmacol. 11:574925. doi: 10.3389/fphar.2020.574925

INTRODUCTION

Venom Systems are Functional Ecological Traits

Venom systems are functional and ecological traits, used by one organism to subdue, deter, or surreptitiously feed upon, another (Jackson et al., 2019). A venom system is composed of a secretion—the venom itself—the tissue that produces that secretion (e.g., a "venom gland"), and a delivery mechanism (e.g., fangs or a stinger) that inoculates the secretion to the target organism. The functional constituents of the venom itself are physiologically active molecules, largely proteins and peptides, known as "toxins." As these toxins have been designed (by natural selection) to function outside the body of the producing organism, they have been referred to as "exochemicals,"

and their function has been described as "exophysiological." That exochemicals are related to endophysiological counterparts has long been understood, but the evolutionary pathways through which a typical enzyme or peptide with a regulatory function within the body of the producing organism becomes a weaponised, exophysiological "toxin," remain only partially understood.

Recruitment vs. Restriction

The dominant view in evolutionary toxinology has reflected the dominant view in molecular evolution more broadly. What is referred to as "recruitment" in toxinology is a coarse-grained description of the acquisition of a novel function at the molecular level that mirrors Ohno's influential "neofunctionalization (NF)" model, in which "random" (unselected) gene duplication results in a functionally redundant copy or copies (Ohno, 1970). This redundancy relaxes constraints on the gene network by rendering the accumulation of mutations by any one copy functionally neutral, thereby facilitating exploration of sequence space. When this random walk results in the discovery of a "good trick," positive selection fixes the mutation and NF has occurred. In the toxinological literature, this has been described as the duplication of a gene with a "physiological" function conferring the possibility of "recruitment to the venom gland" and "weaponization"—the acquisition of a toxic function within venom (e.g., Fry and Wüster, 2004; Lynch, 2007). Though this model has been widely accepted in toxinology for much of the twenty first century, it has also been criticised on the basis of a lack of experimental evidence. In 2014, Hargreaves et al. suggested that subfunctionalisation, in which duplication of a multifunctional parent gene enables the segregation of functions among daughter genes, is a more likely process for the origins of toxin genes (Hargreaves et al., 2014). They termed this process "restriction" (rather than recruitment), suggesting that following the acquisition of a novel, toxic function, a gene which was previously widely expressed would have its expression restricted to the venom gland (to avoid auto-toxicity), rather than recruited to it.

In order to compare and contrast "restriction" and "recruitment," as well as other models of the acquisition of toxic function, it is necessary to both review the diversity of models that have been proposed within the molecular evolution literature, and to consider what sort of evidence would be required to differentiate them empirically. In this article, we briefly review these models and then consider their applicability to toxin evolution based on evidence from a number of studies. We also consider the appropriate definition of "function" in a biological context and distinguish the origins of a novel function from the origins of mere activities. We then discuss in detail data arising from our reconstruction of the evolutionary history of the multigene family phospholipase a2g2, which is a major component of the venoms of viperid snakes. We consider the applicability of a range of gene evolution models to this data. Finally, we suggest that the terms "NF" and "recruitment" be considered general terms—the former for the origins of novel molecular functions and the latter for the "weaponization" of molecules as toxins in venom systems, regardless of the precise sequence of events that facilitated the origin of this novel toxic function.

REVIEW OF MODELS

Ohno's Dilemma; Neofunctionalization, Subfunctionalization and Moonlighting

Despite the continued influence of Ohno's model, a vibrant literature on gene duplication has subsequently produced many other models, a number of which are reviewed in (Innan and Kondrashov, 2010), which either expand upon or contradict the basic NF framework. A number of these attempt to account for what has been dubbed "Ohno's Dilemma" (Bergthorsson et al., 2007)—how do duplicate genes survive long enough under neutral conditions to acquire the necessary changes of sequence or expression regulation that result in functional divergence? Several possible fates for duplicates are frequently discussed. One likely outcome is that duplicates are pseudogenised, either by further random events or as a direct result of selection stabilizing gene dosage (Bergthorsson et al., 2007; Birchler and Veitia, 2012).

Two models are most widely invoked to describe the fate of duplicates that survive and go on to fulfil functional roles—"subfunctionalization" (SF) and "NF" (Force et al., 1999; Conant and Wolfe, 2008; see **Figure 1** for illustrations of common models of gene evolution). In the former the parent gene performed multiple functions, which are subsequently distributed between the duplicates, each of which may acquire function-impairing "degenerate" mutations resulting in the necessary maintenance of both copies to fulfil the functional role of the parent gene. In the latter, a novel function is discovered during the period of relaxed constraint immediately following duplication.

Both NF and SF give pride-of-place to gene duplication as a facilitator of functional change and thus it may appear as though duplication must precede the origin of novel functions. However, it should also be noted that novel functions may emerge as the result of changes of tissue-specific expression patterns in the absence of duplication, a process known as "gene sharing" (Wistow and Piatigorsky, 1987) or "moonlighting" (Copley, 2014). Following this period of functional sharing, duplication may facilitate the emergence of distinct proteins capable of subdividing the shared function between them (Force et al., 1999) and specializing for one of the ancestral functions (Hughes, 1994). Even in SF, which does not directly describe the origins of a "novel function" (since the gene in question is already pleiotropic during the period described by the model), the secondary function is "novel" (i.e., originates later in the evolutionary history of the gene) relative to the "original" function. Thus, in these scenarios acquisition of a novel function occurs prior to duplication (Piatigorsky and Wistow, 1991). It should be noted, however, that most models to do not appear to take into account the role that widespread pleiotropy and redundancy (which results in many mutations being functionally neutral) must play in the origins of novel molecular functions (Wang et al., 2010). These processes,

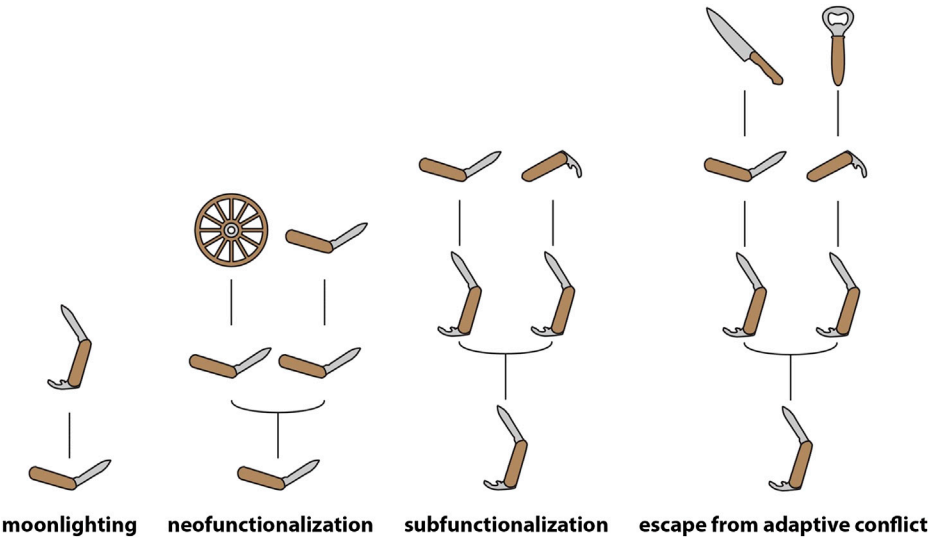

FIGURE 1 | Models of gene evolution. Schematic representation of the most prominent models of gene evolution, with genes and their functions being represented as human tools. Note that moonlighting occurs in the absence of any duplication, with the product of a single gene fulfilling multiple functional roles—pleiotropy of this kind is likely extremely widespread (Paaby and Rockman, 2013), and though genes are depicted as having single functions at the base of the moonlighting and neofunctionalization models in this figure, this should be understood as purely illustrative.

which are intimately involved in the evolution of complexity, must surely complicate analyses of the emergence of such functions. Toxin genes may represent a special case here, in that their toxicity may prevent them from fulfilling multiple functional roles in a phenotype (however, see Casewell et al., 2012). Detailed discussion of these factors is beyond the scope of the present article, but their potential importance should be kept in mind when models are discussed.

Dosage Balance

The "classic" models have been further nuanced by the recognition of distinct forms of SF and NF. "Escape from adaptive conflict" (EAC), in which a novel specialized function emerges following the partitioning of the ancestral function (Innan and Kondrashov, 2010), may be considered an extension of "SF," though the difference between EAC and "specialization," which was described by Hughes (1994), *prior* to Force et al. (1999) proposal of SF, appears minimal. The NF paradigm, on the other hand, has been extended by models in which duplication is intrinsically advantageous and thus may be positively selected. In these latter models, the initial benefit of duplication may be the consequence of increased gene dosage, increased robustness (protection against deleterious point mutations), or the "spontaneous origin" of a novel "function" (though "activity" or "propensity" would be more appropriate terms for such spontaneous novelties, cf. Innan and Kondrashov, 2010; see below for further discussion). In all such cases, the consequent accumulation of redundant copies in gene family networks may generate a hotspot for functional novelty. As recognized by Ohno (1970) and supported by much subsequent research, gene duplication often results in an increase in the dosage of the product encoded by the multiplied genes (e.g., Conant et al., 2014; Margres et al., 2017). In light of this, much of the recent literature on gene duplication centers on the importance of gene dosage in determining the fate of duplicates. A key observation in this regard is the divergent fates of duplicates that originate in whole genome duplication (WGD) events and those that are locally (segmentally) duplicated (LD) (Birchler and Veitia, 2012; Conant et al., 2014). In the case of WGD, preserved duplicates are typically those with numerous interaction partners with which they must maintain precise stoichiometric balance—if one half of a pair is lost, a dosage imbalance may occur. Conversely, duplicates preserved after LD tend to be genes with few interaction partners—they can persist in the genome because their origin does not cause a dosage imbalance. Such genes are "dosage-insensitive." Expression levels of many genes may vary considerably within a population—while heritable, much of this variation is stochastic and may be neutral or nearly neutral. On the other hand, it may be a cryptic contributor to diseases (Cheung et al., 2003) and also represents some of the "standing variation" which may facilitate the evolution of complex traits, including venoms (see below).

Selection for Increased Dosage

In certain circumstances, an increase in gene dosage may be directly selected for, a possibility highlighted by models such as "concerted evolution" (CE) and "innovation-amplification-diversification" (IAD) (**Figure 2**). Since the 1970s, CE has been a popular model for explaining the evolution of multigene families with members that share highly similar sequences in regions that encode the mature product (Nei and

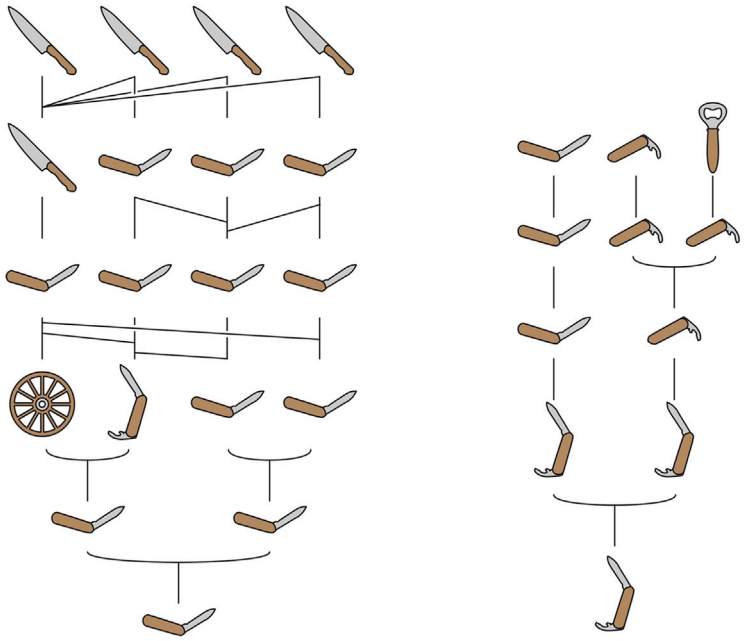

FIGURE 2 | Schematic representation of "concerted evolution" and "innovation-amplification-diversification" using human tools. Note that gene conversion/unequal crossover in concerted evolution result in each gene within a homogenized tandem array having multiple ancestors in the previous generation.

Rooney, 2005). In this model, mutations acquired by one member are either shared with other members or reversed, due to gene conversion or unequal crossing over among all members of the family. Thus, an array of highly similar genes is maintained within the genome of a single species, facilitating the expression of a large quantity of the product of these genes. The canonical example of CE is ribosomal RNA. The model was originally proposed to explain the curious fact that the ribosomal RNA genes of *Xenopus laevis* and *X. muelleri* exist in tandem arrays of as many as 450 copies which differ very little within each species but diverge by up to 10% between the two (Brown et al., 1972).

IAD is a model that combines elements of CE with the SF and NF model. In this model, the parent gene possesses a "weak secondary activity" (as in SF) that results in selection for increased gene dosage (Näsvall et al., 2012). This selection pressure either drives gene duplication or results in the preservation of "random" duplicates, resulting in a redundant array that enables specialisation for either the parent or secondary function, or the origin of entirely novel functions (as in NF). Pluralistic models like IAD have become increasingly popular as the combination of genomic sequences and gene expression data has revealed the complexity involved in the evolution of novel functions.

Layers of Evidence; Activity vs. Function

Indeed, differentiating between the various models described above requires multiple layers of evidence. It is not enough to show that duplication has occurred in a gene family and associate it with the diverse functions within that family, it is necessary to pinpoint the timing of the duplication events in relation to the origins of the novel functions. Without knowing whether a function emerged prior or subsequent to duplication, for example, it is impossible to differentiate between SF and NF. Furthermore, reconstructing the evolutionary history of gene expression patterns is necessary. This is because novel functions may emerge as the result of changes in expression and thus the "environment" of the gene product, which is composed of the other gene products available to interact with (Jackson et al., 2019). Such a shift in environment may be more significant in some cases than a change at the level of gene sequence. This point is particularly relevant for the acquisition of a novel toxic function (e.g., a role in venom) because toxins are "exochemical," meaning that they find their interaction partners (targets) in the bodies of other organisms.

It is also important to stress the distinction between activity and function. A change in gene sequence or even expression site may confer a novel activity to a gene product, but in biology a novel function should only be recognised when that shift makes a contribution to the ecology of the organism (Jackson and Fry, 2016). A change in activity detectable in the laboratory may therefore be little more than an epiphenomenal property of a gene product, and not a true function. This is once again of particular relevance when considering the origins of toxic functions. As discussed above, venom is a functional and intrinsically ecological trait. Toxins, as the active components of venoms, possess an equally ecological function—they are, along with other components of an organism's "exophysiology" (e.g., pheromones), molecules

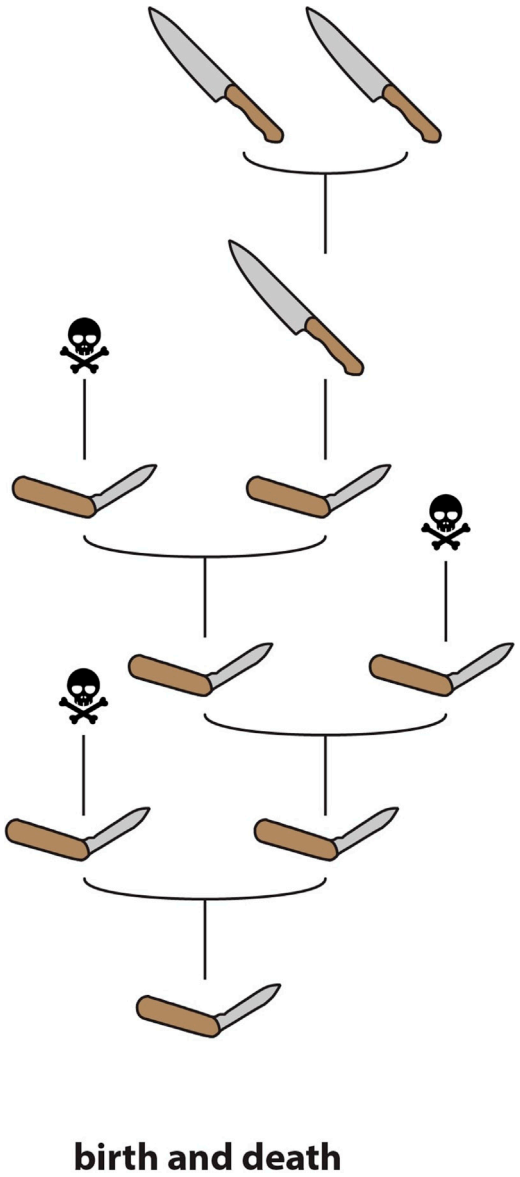

FIGURE 3 | Schematic representation of "birth-and-death" molecular evolution. Genes are continuously duplicated; some go on to develop novel functions whereas others are pseudogenized ("death").

that mediate interactions between organisms. We recognise that it may be exceptionally difficult to experimentally demonstrate a functional role for a putative "toxin" in the ecology of a venomous animal; however, we make the aforementioned distinction between activity and function due to its theoretical significance in evolutionary biology. When "layers of evidence" are combined—from *in vitro* activities to the presence of specialised anatomical structures for venom delivery to observations consistent with the ecological deployment of venom—it may be entirely reasonable to infer the functional role of a given gene product.

EVIDENCE FOR GENE EVOLUTION MODELS WITHIN TOXINOLOGY

Redundancy and "Birth-and-Death"

The idea that redundancy facilitates the evolution of novelty did not originate with Ohno but, in the context of biological evolution, goes back at least to Darwin, who noted that:

"...two distinct organs, or the same organ under two very different forms, may simultaneously perform in the same individual the same function, and this is an extremely important means of transition...." (Darwin, 1859)

The fact that duplication and redundancy are central to the evolution of novel functions within toxin multigene families has long been recognised (Nakashima et al., 1993; Duda and Palumbi, 1999) and is supported by a considerable body of evidence. However, it is one thing to note that toxins are typically members of multigene families, and that redundancy within these tandem arrays facilitates the evolution of new or more specialised toxic activities (i.e., to describe the evolution of these gene families as conforming to a process of "birth-and-death"—Nei and Rooney, 2005; **Figure 3**), and another thing to assert that "NF" (in the sense of Ohno, 1970) is involved in the *initial acquisition of a functional role in venom*. Garnering evidence in support of this latter assertion is considerably more challenging.

The inference that toxin genes are "recruited" from non-toxin endophysiological precursors (often referred to simply as "body" genes) has been drawn from the fact that toxin genes are typically members of widely expressed gene families. In a seminal study that is frequently referenced to support the assertion that toxin genes are "recruited" following duplication of genes encoding "body proteins," information concerning the expression patterns and functions of homologues of toxin genes was compiled from the literature (Fry, 2005). Another study widely cited in support of the "recruitment hypothesis" (Lynch, 2007) references an earlier study demonstrating that the type-1 phospholipase a2 genes that encode toxins in the venoms of snakes in the family Elapidae are closely related to genes primarily expressed in the pancreas (Fujimi et al., 2002). In both Fry (2005) and Lynch (2007), the placement of toxin genes within families that include non-toxin homologues, along with the fact that "birth-and-death" is occurring within these families, is used to support the conjecture that gene duplication is required for toxin recruitment, however, no specific evidence in support of this hypothesis is provided.

Among the best evidence for the classic recruitment hypothesis is provided in a series of studies investigating the acquisition of a novel function in the venom of Australian elapid snakes by the activated form of the coagulation factor X (fXa) (Reza et al., 2005; Reza et al., 2006; Kwong et al., 2009). These studies identified multiple copies of the gene in two species of elapid, with different tissue-specific sites of expression. In *Tropidechis carinatus*, the ancestral coagulation factor-encoding gene was expressed in the liver, whereas a derived form, with modifications enhancing its toxic function, was expressed in the venom gland (Reza et al., 2005; Reza et al., 2007). Three distinct forms were sequenced for *Pseudonaja*

textilis, two expressed in the liver and one in the venom gland. One of the liver-expressed forms was expressed at extremely low levels and was structurally intermediate between the ancestral gene (encoding the coagulation factor) and the derived toxin form (Reza et al., 2006). This was interpreted as evidence of duplication of the gene expressed in the liver, with subsequent recruitment to the venom gland via mutations in the regulatory regions of the genes, which were described in subsequent papers (Reza et al., 2006; Kwong et al., 2009). Another example of "NF" (*sensu* Ohno) in a venom system is the recruitment of a specialised form of insulin as a toxin in the venom of the piscivorous cone snails *Conus geographus* and *C. tulipa* (Safavi-Hemami et al., 2015). These weaponised insulins are exhibit a structure that is convergent with vertebrate insulins (and thus divergent from the endophysiological mollusc insulin they are descended from) and remarkably similar to the endogenous insulins of fish. This example furnishes evidence not only of NF in the evolution of a novel, toxic form of a protein species, but also of the taxon-specific targeting of the toxin, making it a striking example of the opportunity presented by venom systems as models linking molecular evolutionary pathways to ecology.

As mentioned previously, Hargreaves et al. (2014) took exception to the general acceptance of the "recruitment hypothesis" in the toxinological literature despite lack of widespread evidence in support of it. Hargreaves et al. used the fact that toxin gene homologues are often widely expressed in various bodily tissues, including in the oral glands, to argue for an alternate model—termed "restriction"—in which widely expressed genes are restricted to the venom gland after acquiring a toxic function. They further suggested that restriction should be considered a form of SF, rather than NF.

No "One Size Fits All" Model of Toxin Evolution

In fact, many different models have been applied to explain observed patterns of toxin evolution, suggesting that there is no "one size fits all" model. "Birth-and-death" does seem to be a very common process in toxin multigene families, but CE in which all members of a tandem array of toxins possess identical or near-identical sequences (e.g., Moran et al., 2008) has also been observed. Indeed, both processes may occur in the same system simultaneously, as recently demonstrated within the toxin gene family Nv1 of the anemone *Nematostella vectensis* (Sachkova et al., 2019). Contrary to the reasonable intuition that a toxic gene product must be specialised for delivery to other organisms due to the risk of auto-toxicity, moonlighting may also be relatively common, and examples have been described in platypus (Wong and Belov, 2012), parasitoid wasp (Martinson et al., 2017) and snake (Vonk et al., 2013) venom systems. Unlike "birth-and-death" and CE, evidence of moonlighting is directly relevant to the origins of a toxic function within a gene family.

More recently, multiple studies have provided evidence that selection for increased dosage may play an important role in the evolution of toxin gene families and the accumulation of duplicate genes which subsequently form redundant arrays which enable the accumulation of mutations and thus functional diversification (Margres et al., 2017; Sachkova et al., 2019; Giorgianni et al., 2020) At least one of these studies has explicitly interpreted their evidence as an example of "IAD," although they highlight the similarity of this model with "EAC" and suggest that either of these models may account for the pattern they observe (Giorgianni et al., 2020). This same study also interpreted their evidence as support of the "recruitment hypothesis," because the non-toxin gene most closely related to those that encode toxins is not expressed in the venom gland. However, it should be noted that both IAD and EAC posit an ancestral gene with (at least) dual functions (Innan and Kondrashov, 2010; Näsvall et al., 2012). If these models explain the origins of a toxic function, it is necessary that that function be one of the ancestral functions, i.e., that it is present *prior* to duplication. This seems to contradict the spirit of the "recruitment hypothesis" which states that toxin genes are recruited into the venom arsenal (i.e., acquire their toxic function) subsequent to the duplication of a gene encoding a "bodily protein."

Genomic Data Provide Additional Insight

The use of genomic sequences has enabled reconstruction of the evolutionary history of gene families at an unprecedented level of detail. Unsurprisingly, these data have shed light on the molecular evolutionary processes involved in the origins of toxin genes. Analysis of the genome of the non-venomous Burmese python (*Python bivittatus*) indicated that venom gene homologues are expressed in a wide variety of tissues, including in many cases the rictal gland (Reyes-Velasco et al., 2014). The rictal gland is part of the same dental/labial gland complex as the venom gland (Jackson et al., 2017) and in species of snake that possess both a venom gland and a rictal gland (often only one or the other is present), the two glands exhibit markedly similar gene expression profiles (Fry et al., 2013). Given the complexity involved in deconvoluting the plethora of transitional forms of oral gland and "venom system" development in snakes, it is impossible to say whether or not the common ancestor of all snakes was likely "venomous"—i.e., used its toxic oral secretions in prey subjugation (Jackson et al., 2017).

Regardless, expression of toxin homologues (and indeed toxic proteins) in oral glands is widespread in non-venomous vertebrates, for example leopard geckos (Hargreaves et al., 2014) and mice (Hiramatsu et al., 1980). Reyes-Velasco et al. (2014) used this evidence from the python genome to formulate their "stepwise intermediate nearly neutral evolutionary recruitment" (SINNER) model of venom evolution, in which toxin precursor genes which are constitutively expressed at low levels in the oral glands have their expression elevated specifically in the oral gland (presumably via selection for a toxic function, though this is not specified), and then reduced in other tissues to avoid auto-toxicity (a process presumably selected for following specialisation for the toxic function). The model does not explicitly invoke a role for gene duplication in the origin of the novel function, but it is suggested that duplication would remove constraints and thus facilitate specialisation for a toxic function. The model is therefore very similar to IAD and EAC, in which duplication following a period of "gene sharing"

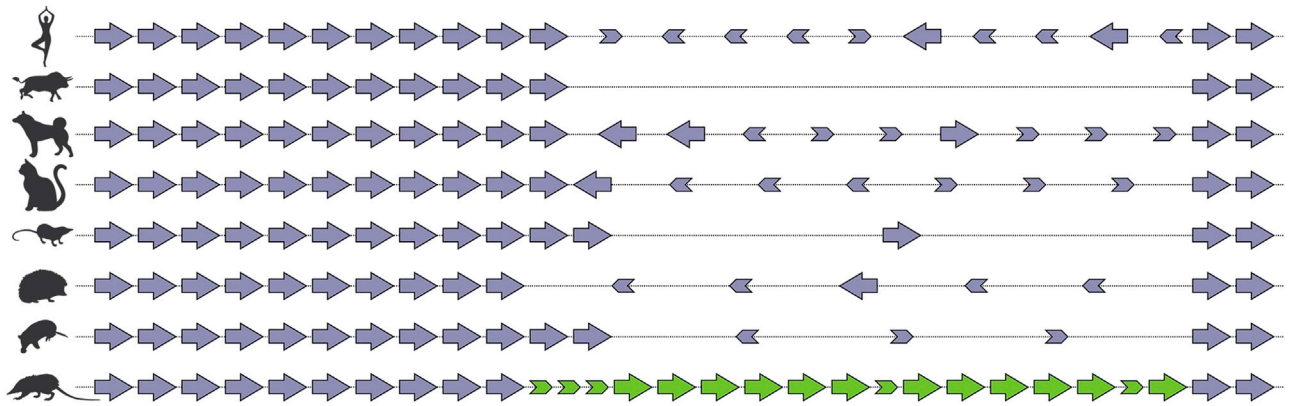

FIGURE 4 | Schematic representation of tissue kallikrein gene cluster in selected species of mammals after (Casewell et al., 2019). *Solenodon* venom genes are colored green, "physiological" genes are colored violet. Note that all expansion occurs within the same region of the cluster, and that much "exonic debris" remains after the partial deletion of genes, a characteristic sign of "birth-and-death"

(i.e., moonlighting) enables increased gene expression (in IAD) and specialisation. SINNER is therefore another name for a sequence of events which already has several very similar formulations – "specialisation," EAC, and IAD (Hughes, 1994; Innan and Kondrashov, 2010; Näsvall et al., 2012).

There are many examples, from across the animal kingdom, of toxin genes which have been recruited from multigene families (Fry et al., 2009). This suggests that an ancestral propensity to duplicate may be a property that "exapts" (Gould and Vrba, 1982) a locus for recruitment to a venom system. The recent sequencing of the genome of the venomous mammal *Solenodon paradoxus* has provided vivid evidence of the consequences of weaponization for a gene family which ancestrally undergoes evolution by birth-and-death (Casewell et al., 2019). Comparison of the *S. paradoxus* genome with that of other mammals revealed that birth-and-death was a widely occurring process, with the same locus within the kallikrein cluster showing evidence of it in the majority of the fifteen mammalian taxa investigated. Despite all lineages sharing 10 of the 15 KLK genes, there were numerous lineage-specific gain and loss events at this locus, as well as a smattering of "exonic debris"—the remnants of genes in the process of being expunged from the genome. In *S. paradoxus* however, which utilises kallikreins in its venom, there was an accumulation of copies that far outstripped that observed in any other taxon (**Figure 4**). This suggests that recruitment into venom creates a selection pressure for the accumulation of duplicate copies at a locus with an ancestral propensity for duplication.

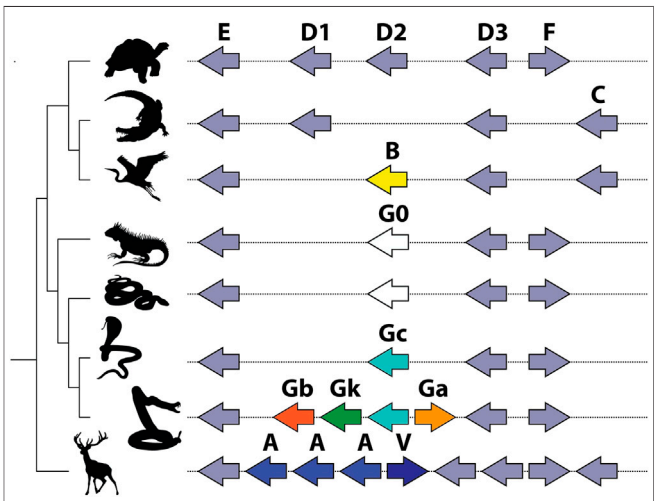

FIGURE 5 | Schematic representation of Pla2g2 gene cluster in vertebrate lineages after (Koludarov et al., 2019). Note that all expansion within the cluster takes place at the same location, and all novel clades (g2B in birds; g2G in squamates; and g2A and g2V in mammals) are descended from the same subclade (g2D).

RECONSTRUCTING THE EVOLUTIONARY HISTORY OF A MULTIGENE FAMILY

Phospholipase a2g2

The most comprehensive reconstruction of the evolutionary history of a toxin multigene family to-date was performed on the phospholipase a2 group 2 family, which is an important component of the venom of viperid snakes. To analyze a dataset comprising 110 genomic sequences from 93 species from across the animal kingdom, the study utilized a comparative approach combining manual genomic annotation, phylogenetics, selection rate estimates, and analysis of synteny. The following is a detailed discussion of the results of this study that pertain to the origins of a toxic function in venom for members of the gene family. Please refer to the original study (Koludarov et al., 2019) for additional details.

The Pla2g2 family is located in a remarkably syntenic genomic region, which facilitated the comparative approach of the study. All lineage-specific innovations within the cluster stem from the same locus, ancestrally associated with Pla2g2 subclade D (**Figure 5**). Mammals (Pla2g2A and g2V), birds (Pla2g2B),

and squamate reptiles all exhibit lineage-specific derivations arising from within the D subclade. Subclade G of Pla2g2 is the lineage unique to squamate reptiles (lizards and snakes). The plesiomorphic form of this gene (given the name "Pla2g2G0") was present in a single copy in the genomes of all squamates surveyed other than members of the Caenophidia ("advanced snakes"). In the caenophidian snakes (Elapidae, Viperidae and various non-front-fanged families formerly grouped in Colubridae), the gene is structurally derived (and given the name "Pla2g2Gc"). This gene (hereafter "g2Gc") was present as a single copy in the genomes of all non-viperid caenophidians. In viperids, the G subclade has expanded considerably in association with its "recruitment" for a toxic function in venom and viperid genomes contain unique toxin-encoding forms such as "Gck" (a transitional form between Gc and Gk) "Gk", "Ga", and "Gb" (Dowell et al., 2016).

Pla2g2 in Snake Venom

The MRCA of the advanced snakes may have been venomous (Jackson et al., 2017) and thus the potential exists at that early stage for positive selection acting upon genes encoding orally secreted toxins. It is unclear, however, whether g2Gc was in fact utilized as a venom toxin by early caenophidian snakes and whether this function may have provided the selection pressure leading to the fixation of this form in the (inferred) MRCA. However, the ancestral membrane-degrading activity of Pla2g2 gene products (Six and Dennis, 2000) exapts them for utilization as toxins or as antimicrobial components of innate immunity—note that these are not mutually exclusive as immune components are frequently co-opted for use as toxins (e.g., Whittington et al., 2008; Georgieva et al., 2011; Wong and Belov, 2012). Not all genes within the Gc group have been functionally characterized at this stage and data concerning their expression in various tissues is limited; these data are important in resolving the evolutionary pathways leading to the deployment of this gene family in the venom of viperid snakes. Regardless, Gck is selectively expressed in the venom gland of extant crotaline viperid snakes (Aird et al., 2017; Dowell et al., 2018). The homologous gene (Gc) is not expressed in the venom gland or accessory gland of the elapid snake O. hannah (despite being 94% similar in sequence to the viperid form), indicating that it is not utilized as a toxin by this species; it is also expressed at extremely low levels in pooled tissues, which may be indicative of its incipient toxicity (Vonk et al., 2013). While elapid snakes do utilize phospholipases as toxins, all known elapid Pla2 venom toxins are members of group 1, which is unrelated to group 2 (Fujimi et al., 2002).

Toxic Function may Arise Prior to Duplication

In viperid snakes the plesiotypic form Gc, along with transitional and highly derived toxin forms, is expressed in the venom gland (Aird et al., 2017; Dowell et al., 2018). Thus, we infer that that the novel toxic function arose prior to duplication, possibly via co-option facilitated by a shift in tissue-specific expression patterns which resulted in its expression in the venom gland. Stochastic gene expression of this kind has been linked to the phenotypic diversity from which the origins of novel adaptations may arise (True and Carroll, 2002; Kaern et al., 2005; Woods, 2014). At present, our ability to pinpoint the origin of the toxin function in Viperidae is limited as we lack necessary transitional forms within that family. Duplication of the gene occurred sometime between the split of viperid snakes from the main stem of Colubroidea and the origin of the MRCA of extant Viperidae, which possessed additional copies. Thus, we infer that expansion at the locus occurred subsequent to the acquisition of the toxic function, similar to the pattern observed for *Solenodon paradoxus* (**Figure 6**).

The alternative possibility is that duplication occurred prior to "recruitment" to the venom system, giving rise to the new gene g2Ga. The protein encoded by this new gene, possessing by chance a greater toxicity than that of its parent gene (g2Gc), would have been selected for venom gland-specific expression and the parent gene was co-expressed due to the co-regulation of neighboring genes. This interpretation is complicated by the fact that g2Gc, which is initially a passively co-expressed (unselected) gene in the venom system according to this scenario, later evolves (in a Crotalinae-specific derivation) into the myotoxic g2Gk (a.k.a. "Lys49 Pla2s") (**Figure 6**). Thus, instead of one, this alternate hypothesis requires as many as three "recruitment" events—one (of g2Ga) for the initial addition to the venom arsenal, a second one associated with the mutation of g2Gc into g2Gk and a third one in which g2Gb (which originates from a duplication of g2Ga which may pre- or post-date recruitment in this scenario) becoming a basic subunit of neurotoxic dimeric Pla2g2. In either case, changes in gene expression, which are untraceable at this level of analysis (and possibly lost to the sands of time) are crucially important in the initial acquisition of the novel, toxic function. Given the presence of additional "random" (unselected) steps in the latter scenario (duplication precedes novel function), we prefer the former (novel function precedes duplication—see below for a more detailed discussion). However, additional research is required to definitively differentiate between these hypotheses.

The Role of Venom Delivery Systems in Recruitment

Viperid snakes diverged early from the main stem of the caenophidian lineage (which includes elapid snakes; the front-fanged lamprophiids *Atractaspis* and *Homoroselaps*; and many non-front-fanged venomous species) and the most striking synapomorphy of the family (Viperidae) is the possession of large, hollow fangs which are the sole tooth located on a mobile maxillary bone (Fry et al., 2012). These fangs, like those of other front-fanged snakes, are connected to the venom gland by an enclosed duct, and the gland itself is surrounded by compressor musculature which contracts during venom delivery. Together these anatomical components form a "high-pressure" venom delivery system, and viperids were the first lineage of snakes in which such a system evolved. That members of the Gc group of Pla2g2 apparently only became specialized for use as venom toxins after the divergence of Viperidae from other advanced

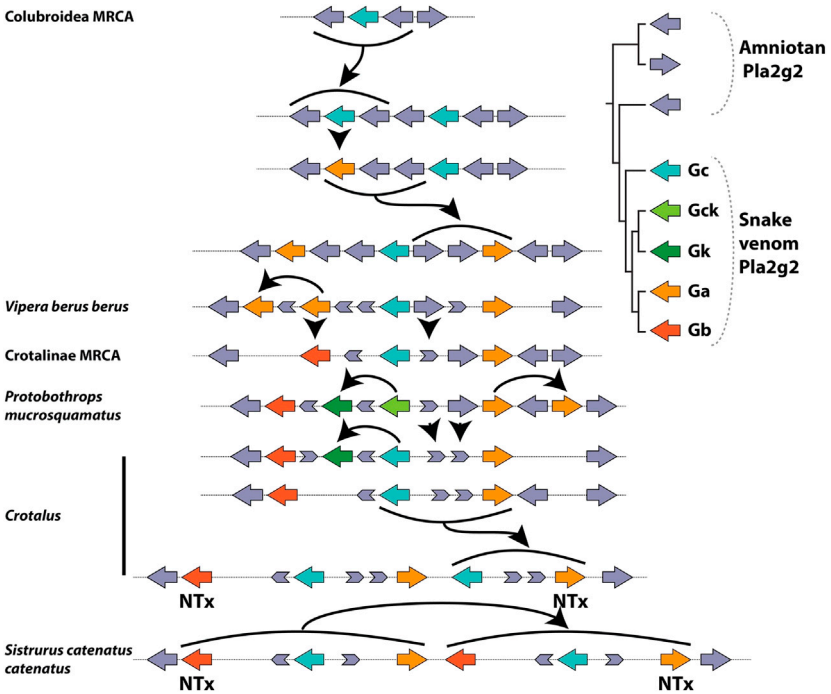

FIGURE 6 | Lineage-specific expansion and diversification of the Pla2g2 subfamily in viperid snakes after (Koludarov et al., 2019). Note the presence of multiple fragments of "exonic debris" (mainly from g2E and g2D) that make possible the reconstruction of the evolutionary history, including all duplication events, of this genomic region in viperid snakes. Arrows indicate birth and death events. A number of the duplication events (bold arrows) do not involve single genes (unlike g2A of mammals) but rather small groups which are duplicated as units ("cassettes"), typically composed of a g2G gene flanked by parts of g2E and g2D.

snakes suggests that the acquisition of this function may have been associated with the evolution of a delivery system capable of inoculating the toxin directly into the muscle tissue of potential prey organisms.

This hypothesis is consistent with the subsequent diversification of the subfamily in viperid snakes, including the evolution of specialized myotoxic and presynaptically neurotoxic forms. Myotoxic Pla2 are likely to be more effective as toxins if delivered intramuscularly—a feat that non-front-fanged snakes, and even many front-fanged elapid snakes, are unlikely to be capable of. It should be noted, however, that myotoxic phospholipases have been independently recruited (from group 1 Pla2) as toxins in elapid snakes. These toxins are particularly enriched in the venoms of large species capable of exerting considerable bite force (e.g., *Pseudechis australis*—Georgieva et al., 2011) and in species which feed on prey items that lack a layer of subcutaneous fat (e.g., some hydrophiine sea snakes—Gopalakrishnakone et al., 1997; Phillips, 2002). It is plausible, therefore, that the ability to inoculate venom intramuscularly has played a role in the recruitment or enrichment of myotoxic Pla2g1 in elapid snakes—co-evolution of toxins and associated delivery anatomy is a reasonable expectation, and has been reported previously in toxicoferan reptiles (e.g.,—Fry et al., 2012) and cnidarians (Surm et al., 2019). As far as the present case of Pla2g2 in viperid snake evolution is concerned, additional investigation of snake bite force mechanics and feeding ecology is required to test these conjectures.

Expansion of the Locus Following Recruitment

Subsequent to the acquisition of the toxic function, a series of duplication events expanded this lineage in viperid snakes, the first of which gave rise to two new isoforms—the g2Ga (acidic) and g2Gb (basic) venom Pla2s (**Figure 6**). These forms are more highly expressed in viper venom glands than the plesiotypic g2Gc form (Aird et al., 2017). Pla2g2G venom genes were duplicated in multiple lineages to produce genes that became subunits of heterodimeric neurotoxins in several *Crotalus* and *Sistrurus* species (French et al., 2004; Doley et al., 2010). As revealed by the arrangement and orientation of genes and exonic debris, these neurotoxins arose via independent duplications in each of these two genera (**Figure 6**; cf. Dowell et al., 2016), an example of convergent evolution made possible by the fact that a single point mutation is all that is required to "unlock cascading exaptations," leading to the derivation of this potent toxin (Whittington et al., 2018). In parallel, g2Gc (the plesiotypic form) mutated (again in the absence of duplication) into g2Gck in Crotalinae (pit vipers), and an additional duplication of this form became the non-catalytic myotoxin (g2Gk) (**Figure 6**). In tandem with the evolution of these derived forms, the plesiotypical Gc and Gck appear to have had their expression suppressed, despite still being

present in the genomes of many viperid snakes (Aird et al., 2017; Dowell et al., 2016; Dowell et al., 2018).

An Ancestral Propensity for Duplication

The data described above concerning Pla2g2Gc suggest that duplication need not have been a prerequisite for the acquisition of a novel exophysiological function by this gene's product in viperid snake venom. Although duplication may not have been proximally involved in the acquisition of the toxic function, the gene was part of a gene cluster, which is an important factor influencing its evolutionary trajectory and is consistent with the recruitment of many other toxins from multigene families (Fry et al., 2009). This is both because the locus clearly possesses an ancestral propensity for duplication, and because the gene's function may have been shared with the sister genes (in case of the g2G ancestor, presumably g2D or even g2E/F/C). This redundancy probably decreased the evolutionary constraints on each gene. Importantly, all of the novel clades of Pla2g2 in distinct animal lineages originate from the same locus (ancestrally occupied by Pla2g2D—Koludarov et al., 2019), highlighting the influence of genomic context on duplication propensity and hence functional diversification (Jackson et al., 2019). It should be noted, however, that the original expansion events leading to the formation of the Pla2g2 cluster are ancient (>300 mya—Koludarov et al., 2019) and the general trend subsequent to this expansion appears to be toward reduction through gene loss, rather than further multiplication.

The pattern observed, in which both the emergence of novel functions and subsequent gene family expansion take place at the same locus in distantly related taxa, suggests that such loci have a deep ancestral propensity for mutation and duplication. The propensity for duplication is likely conferred by genomic structure, as particular arrangements of genetic material facilitate duplication (Reams and Roth, 2015). This propensity, however, may typically be constrained. The alternative, still advocated by some biologists (c.f. Dunn and Munro, 2016), is that duplications occur randomly throughout the genome and that regions only differ in copy number variation (CNV) due to the differential preservation of duplicates. This seems implausible for two reasons: 1) because exonic/intronic debris is typically evident following deletion (unless the deletions are extremely ancient events)—this debris was not detected throughout the genomes in the present study but only, *ex hypothesi*, in isolated regions in particular genomes (i.e., those in which birth-and-death is taking place); and 2) because down-regulation ("dosage sharing") or silencing with methylation may facilitate the long-term preservation of segmental duplications in genomes despite the predictions of the dosage balance hypothesis (Assis and Bachtrog, 2015; Lan and Pritchard, 2016; Guschanski et al., 2017). Another alternative is that individuals in which deleterious duplications occur are strongly selected against and thus no evidence of these duplications persists in sequenced genomes, but this also seems an unnecessarily extreme speculation as it requires that such duplications be invariably lethal or render organisms sterile—i.e., individuals in which duplication takes place must produce no offspring. We note that it is far from novel to interpret patterns of duplication as non-random (e.g., Bailey et al., 2002), indeed we feel that this should be considered the null hypothesis in the absence of the evidence described above.

GENE DUPLICATION AND THE EVOLUTION OF TOXIC FUNCTIONS

Recruitment in the Absence of Duplication

Several studies have downplayed the role of gene duplication in the acquisition of a toxic function by certain gene families in certain venomous lineages. In the platypus, for example, a majority of toxin-encoding genes do not exhibit lineage-specific expansions (Wong and Belov, 2012), rather toxins appear to have been recruited from gene families with pre-existing CNV, and no expansion has taken place subsequent to recruitment. In parasitoid wasps, duplication appears to have played even less of a role, with the predominant mode of venom diversification within and among lineages being shifts in cis-regulated gene expression in the absence of either gene duplication associated with acquisition of a toxin function, or gene deletion associated with its loss (Martinson et al., 2017).

The Evolution of Novel Functions is Facilitated by Changes in a Gene Product's Ecology

A protein's function is fundamentally relational, i.e., defined interdependently as the consequence of interaction between one protein and another (Guttinger, 2018). We suggest that the emergence of novel functions becomes possible when a gene product's context changes and it is exposed to a novel suite of interaction partners. This change of context is analogous to the changing ecology of an organism invading a new environment and the dynamic evolution that this may facilitate is therefore analogous to speciation via adaptive radiation (Jackson et al., 2019). A change of context may occur in multiple ways for a gene product, with or without gene duplication: following a stochastic change in expression pattern that sees a gene being expressed in a novel tissue, i.e., a tissue in which the gene product in question is not typically expressed (Kaern et al., 2005; Woods, 2014); following a structural change that modifies a protein's interactive propensity (i.e., exposes it to a novel context in terms of potential partners for interaction); or following the evolution of a "delivery system" (e.g., long hollow fangs) capable of delivering the gene product into a novel context (e.g., muscle tissue of prey animals). Such changes of context may lead to the discovery of a "good trick" (Dennett, 1995) by fortuitously facilitating an interaction with a positive impact on fitness. It is at this point that a genuinely novel function emerges. If both functions (ancestral and derived) persist for the same gene, this may create pressure for duplication, as the multiple functions of the protein require segregation into discrete genes, a situation similar to that described in the "specialization," "SF," and "EAC" models (Hughes, 1994; Force et al., 1999; Innan and Kondrashov, 2010).

NEOFUNCTIONALIZATION AND RECRUITMENT, *SENSU LATO*

Models and Pluralism

The precise sequence of events leading to the recruitment of Pla2g2Gc as a toxin cannot be definitively determined based on available data, however, it may superficially appear as though the single model the events described above most closely resemble is "SF" (Force et al., 1999). However, additional processes (e.g., "moonlighting" and "NF") not described by that model also appear to have contributed to the origins of functional novelty within this gene family, and periods of "degeneration" (a feature of the SF hypothesis) may or may not have occurred (see below for further discussion). The "specialisation" model (Hughes, 1994) may describe the data even more closely, since recruitment as a toxin likely involved specialization for a novel function following an initially pleiotropic period. However, as with SF, this model does not describe a subsequent period of classic NF, which is observable within the viperid-specific toxin forms of Pla2g2. Perhaps then "IAD" (Näsvall et al., 2012) is the explanatory model that fits data most accurately. IAD, as described above, is a model that subsumes several other popular models into its narrative, and we suggest that any sufficiently fine-grained reconstruction of the evolutionary history of a gene family will require such a pluralistic approach. This raises the question of whether or not any single, relatively simplistic, model can ever adequately describe the emerge of novel functions.

Conant et al. (2014) suggested that a "pluralistic framework" incorporating multiple models may be the most appropriate way to understand the fate of duplicate genes and our analysis corroborates this assertion. The following paragraphs conjecturally describe events that may occur in episodes of "NF" (or "recruitment"). The term NF is used here to describe the emergence of novel functions at the molecular level, and not merely that emergence via Ohno's model, and "recruitment" is used to mean the acquisition of a toxic function in venom, without or without duplication. This discussion should not be thought of as an attempt to define a new formal model, but rather to show how each of the previously proposed models may capture only part of the truth. Additional processes not described here likely occur in other cases.

Innovation

The initial acquisition of a novel activity may occur: 1) when noisy expression patterns (Kaern et al., 2005; Woods, 2014) instigate a moonlighting scenario—a single copy gene fulfilling multiple functions by virtue of expression in multiple locations (Copley, 2014); or 2) when structural change facilitates interaction with novel partners, while maintaining the ancestral function. Note that in a moonlighting scenario there may be the acquisition of a "weak secondary function" (the "innovation" phase of IAD) in the absence of any structural change to the gene. The novel activity may then expose the gene to a distinct selection regime, which is the point at which activity becomes function. Selection may then facilitate the accumulation and fixation of further mutations. When a novel function is acquired by a single copy gene, this may create pressure for the creation of duplicate copies such that the multiple functions can be segregated between those copies, which may then specialize. Such a scenario, along with those in which duplication is positively selected due to the benefits of increased gene dosage or robustness (Innan and Kondrashov, 2010), may result in selection driving an increased duplication rate. An additional hypothesis describing positive selection on accumulation of duplicate genes suggests that this may occur when duplication results in the spontaneous origin of a novel "function," however, this might be better referred to as a novel "propensity." Again, it is debatable whether a trait qualifies as functional *prior* to making a contribution to organismal fitness (i.e., prior to selection) (Jackson and Fry, 2016; cf. ; Innan and Kondrashov, 2010).

Amplification and Exochemical Escape

Certain novel functions lead to selection for increased expression of a gene product, which also contributes to the fixation of duplicate copies (Margres et al., 2017). This corresponds to the "amplification" phase of IAD, in which selection for the "weak secondary function" drives the accumulation of duplicates (Näsvall et al., 2012). Notably, in exochemical systems, since the interaction partners of gene products originate outside the body of the producing organism and the products are secreted extracellularly, the likelihood of a deleterious impact of mutations on fitness is decreased (allowing for their accumulation) and there are no (internal) stoichiometric constraints on dosage. Thus, products of duplicate genes in exochemical systems may escape both negative selection and down-regulation or silencing, thereby having the opportunity of diversifying and rapidly contributing to organismal fitness.

In contrast to the model proposed by Lan and Pritchard (2016) in which coregulation of tandem duplications delays sub- and neo-functionalization, this removal of constraint may facilitate rapid evolutionary divergence prior to genomic separation of duplicate genes. This phenomenon may be termed "exochemical escape," where "escape" refers to the evasion of dosage balance constraints and thereby the solution to "Ohno's dilemma" (Bergthorsson et al., 2007). A lack of dosage constraint on exochemical/extracellular proteins may also explain the lack of concordance between the evolution of these systems and the broader trend in conservation or deletion of duplicates following whole-genome duplications versus segmental duplications (Conant et al., 2014)—in exochemical systems, segmentally duplicated genes may persist even when they have many interaction partners and are involved in the formation of protein complexes.

Diversification

Subsequent to initial duplication, specialization (a.k.a. "EAC"—Hughes, 1994; Innan and Kondrashov, 2010; also "diversification" in the IAD model) may occur, in which one copy of the gene maintains the original function and the other specializes for its exochemical role, e.g., a role in venom in viperid snakes. This specialization may result in selection for tissue-specific patterns of expression—although it has been suggested that the expression of tandem duplicates is likely to be co-

regulated until one copy undergoes chromosomal displacement (Lan and Pritchard, 2016), available expression data clearly indicate that Pla2g2G are highly tissue-specific in their expression and that neighboring genes (Pla2g2E and Pla2g2D) are not expressed in the venom gland (Vonk et al., 2013; Dowell et al., 2016; Aird et al., 2017).

More is Better

This specialization may lead to increased selection on dosage, driving the accumulation of duplicate genes now specifically expressed within the exochemical system (further "amplification," following "diversification"). This is particularly likely for systems in which more gene product is "better," either leading to a more toxic venom (Margres et al., 2017) or more effective response to infection (e.g., mammalian g2A). At this point, classic Ohno-style redundancy occurs, as multiple gene copies represent both a larger target for mutational change (and thus a network for exploring phenotype space) and each becomes less constrained by purifying selection (Aird et al., 2017). This in turn leads to NF, in Ohno's sense of the term, in which specific gene copies evolve interactions with novel partners.

Co-Option Leads to Neofunctionalization

The aforementioned sequence describes a sequence (and a hypothesis in need of further testing) that loosely subsumes moonlighting, specialization/SF and NF into a single temporal series. It is similar to IAD but includes additional rounds of amplification following specialization for an exochemical role. As with the first round of amplification, the accumulation of duplicates facilitates classic NF via redundancy. Models in which duplication is central to the evolution of functional novelty have dominated discussion in recent years, but the co-option of single copy genes is likely also widespread (True and Carroll, 2002; Martinson et al., 2017) and may be the first step on the pathway toward "NF." Assertions that functional novelty may often precede duplication are nothing new. Indeed, they date back at least to the work of Serebrovsky (1938, referenced in Taylor and Raes, 2004), who discussed the pleiotropic effects of a single gene being distributed between daughter genes following duplication (see also Piatigorsky and Wistow, 1991). More recently, Hughes explicitly states that a period of gene sharing precedes duplication-facilitated specialization (Hughes, 1994). Whether these models, or that which we have outlined in the previous paragraph, should be considered "SF" (Force et al., 1999) is perhaps a moot point. The formal SF model includes "degeneration" (of regulatory elements or functional structures) following duplication. While this may occur, the significant consequence of duplication, particularly in terms of venom toxins, appears to be "EAC" (Hughes, 1994; Des Marais and Rausher, 2008), which in turn leads to NF proper (Ohno, 1970). This pattern conforms with the analyses of Assis and Bachtrog (Assis and Bachtrog, 2015), who demonstrated that SF was rare in comparison to conservation, specialization, or NF, and indicated that SF may be merely a stage in the evolutionary series leading toward NF.

Models are Maps, not Territory

In any case, formal models are rarely more than schematics, and there is little reason to expect real world sequences of events to conform to them precisely. Thus, while we do not believe we have reconstructed a history that conforms to rigorously defined "SF," clearly that history resembles this model, just as it resembles elements of several others. Hargreaves et al. (Hargreaves et al., 2014) previously argued that venom toxins likely acquire their toxic functions via SF rather than NF. In this they were making a point of difference with much of the molecular evolutionary work done in the field of toxinology (e.g., Reza et al., 2005; Lynch, 2007; Fry et al., 2012), in which it had been previously well accepted that Ohno-style NF was the dominant process of protein "weaponization." Indeed, as more research is conducted on the genomes of venomous organisms, it is becoming increasingly evident that even for toxin evolution there can be no one size fits all explanation. For example, in the king cobra genome, evidence of moonlighting was reported for some toxin genes alongside considerable evidence of toxin-specific gene family expansion, which appeared to confirm the classic NF model's applicability to toxin evolution (Vonk et al., 2013). A similar pattern of gene family expansion was observed in the genome of the anemone *Actinia tenebrosa* (Surm et al., 2019) and has been observed in a huge number of studies of various venom taxa, a comprehensive review of which is beyond the scope of the present article. The platypus genome, on the other hand, revealed a pattern in which toxin genes are recruited from families with ancestral CNV, and no evidence of lineage-specific (i.e., associated with the toxin function) expansion was uncovered for most of these families (Wong and Belov, 2012). In parasitoid wasps, yet another pattern was observed in which duplication appears to play almost no role; rather, acquisition and loss of toxic function was facilitated by changes in cis-regulated gene expression (Martinson et al., 2017).

Neofunctionalization = "Origin of a Novel Function"

In our study, as described above, we have detected a pattern that suggests that both co-option facilitated by changes in gene expression and lineage-specific gene family expansion are important in toxin evolution. We therefore agree (with Hargreaves et al., 2014 and others) that Ohno's model does not account for all the details, but feel that it describes an important part of the process characteristic of certain venom toxin families, namely the expansion of these families via duplication and the attendant positively selected evolution of multiple novel functions. We further recommend that the term "NF" not be too narrowly defined, as it, etymologically, merely refers to the origin of novel functions. Ohno's initial coinage was a catchy one and we would like the usage of this term to be legitimate, despite the fact that in its narrow definition is does not capture all the details. Those that have read Ohno's monumental publication of 1970 (Ohno, 1970), know that his thought was expansive and that he described processes akin to SF working alongside the NF for which he is remembered. In this sense he was like Darwin, whose thoughts on evolution extended beyond Natural Selection and the conceptual tools of what

became, in the 20th Century, Neo-Darwinism. Thus "Darwinism" is more expansive than "Neo-Darwinism" and "NF" may be legitimately considered more expansive than its formal definition suggests.

This "highway to NF" that we conjecture has shaped the evolution of certain branches of the Pla2g2 family may be unique to rapidly evolving exochemical systems or may be more widespread. In other cases of multiplication within the Pla2g2 family, however, diversification takes place much more sedately. This is evidenced by the fact that plesiotypical D-clade proteins in turtles and alligators are more similar to each other and even to EFC-clade proteins than they are to the divergent forms of mammals, birds or squamates (Koludarov et al., 2019). Thus, sequence divergence and the antiquity of the duplication event are not tightly correlated in this gene family—the functional role of the gene in question dictates the dynamism of its evolution.

Functions Exist at the Organismal Level

At this point it is necessary to reiterate a fact often overlooked by studies investigating the origins of novel functions at the molecular level—functions exist at the organismal level. There is an implicit assumption (perhaps transmitted from physics) that causal pathways must flow from small things like genes "upwards" to large things like organisms. Such an assumption has no place in evolutionary biology, in which selection pressures which originate at the level of organisms interacting with their environment shape the evolution of lineages. In biology, a "function" is the purpose of trait that justifies its existence via its contribution to the fitness of the organism that possesses it (Jackson and Fry, 2016). In order for a gene product to acquire a novel function as a venom toxin, there must be a confluence of factors – an appropriate activity, an appropriate site and level of expression, and a delivery mechanism capable of inoculating the toxin. Note that the requirements of the delivery system are dictated by the activity and available concentration of the toxin—venom systems are integrated, and the evolutionary dynamics of their components reflects this complexity. In the case of Pla2g2G, the "recruited" gene occurs at a locus with an ancestral propensity for duplication. This is likely the case for many toxins, as being part of a multifunctional multigene family presents obvious advantages for both the derivation of new activities in general, and new toxic activities specifically. Thus, such multigene families are exapted for recruitment into venom systems. However, the evidence garnered from the reconstruction of this gene family's evolutionary history indicates that the duplication rate at that locus was dramatically elevated *subsequent to the acquisition of the toxic function*. The same pattern was observed for kallikrein genes in the genome of *Solenodon paradoxus* (Casewell et al., 2019). Thus, these studies provide a nice example of the kind of "downwards causation" that is likely ubiquitous in evolutionary biology (Noble, 2013; Ellis, 2015; Noble et al., 2019), in which the state and behavior of the organism as a whole influence the state of its constituent molecules just as much as the opposite.

CONCLUSION

There are many models of the evolution of novel functions at the molecular level and each of them may describe a possible process that occurs in nature. It is unlikely, however, that any of them captures the full range of possible pathways through which novelty emerges, or even tells the full story of any particular pathway. This is to be expected—at their best, models are akin to accurate maps, and maps are always coarse-grained representations of the realities they describe. In this article we have reviewed a number of these models and data that has been interpreted as evidence of their involvement in the acquisition, by proteins, of toxic functions in venom. We prefer to call the acquisition of such a function "recruitment," regardless of the specific pathway(s) involved, because this term captures the fact that a toxin is a "weaponized molecule."

This broad usage of the term "recruitment" should be understood as distinct from its narrower usage to describe a hypothesis in which the origin of a toxic function occurs subsequent to "duplication of a bodily protein." This process may occur, but it is certainly not the only way in which a toxic function emerges. Neither is expression of a potentially toxic molecule in an oral gland (or any secretory tissue associated with a venom system) sufficient for recruitment to occur. It is likely that the oral glands of all vertebrates secrete a plethora of molecules (e.g., enzymes involved in pre-digestion, as well as antimicrobial peptides) that could potentially be deployed as venom toxins. Despite this, the majority of vertebrates are clearly non-venomous. This is because a venom toxin is a component of an integrated system which includes a delivery mechanism and which serves an ecological function. In the absence of this ecological function—active delivery of the secretion to a target organism to facilitate feeding, defense or (in this case of "venomous" parasites) surreptitious feeding—the potential toxicity of many secretory molecules remains untapped.

While there has been debate about whether "recruitment" or "restriction" (NF or SF) is the primary route through which the evolution of a toxic function occurs (Hargreaves et al., 2014), this debate misses the aforementioned point—neither of these processes is sufficient unto itself for the acquisition of such a function. Indeed, both of them are likely involved in recruitment (*sensu lato*), either in separate cases or as distinct stages within a single process. Certainly, there can be no doubt that NF as described by Ohno (1970) is an active process in toxin multigene families, in which redundancy conferred by the accumulation of duplicates in tandem arrays facilitates the origin of novel activities. These novel activities may become novel functions as attacking new targets within the physiology of an envenomed organism is an important process that contributes to the evolutionary success of venoms (Casewell et al., 2019). However, NF (or birth-and-death) within a toxin multigene family is not evidence that the same process was involved in the initial acquisition of a toxic function in venom by members of the family. In any case, the redundancy among models of gene evolution—several of which are either the same or

subsume one-another—suggests that arguing over which is the "primary" model involved in toxin evolution may be unproductive.

As well as recommending an expansive definition for "recruitment," we suggest that "NF" is a suitable term for the origin of novel molecular functions in general. In this, we argue simply that the etymology is appropriate, and that simpler terminology is often preferable to a proliferation of models with increasingly elaborate acronyms that only confuse the issue. Genomic data, particularly when combined with expression data, now present an extremely rich source of information about molecular evolution. When a comparative approach is employed, these data facilitate the reconstruction of evolutionary histories at an unprecedented level of detail. As evolutionary toxinology marches further into the genomic era, we expect further evidence that myriad variations on a theme exist in nature, and that each case, when reconstructed to a sufficiently fine-grained degree, is unique unto itself. In evolution whatever can happen, will happen.

DATA AVAILABILITY STATEMENT

The data analyzed in this study is subject to the following licenses/restrictions: Data can be made available on request. Requests to access these datasets should be directed to jcoludar@gmail.com.

AUTHOR CONTRIBUTIONS

TJ conceived and wrote the bulk of the manuscript. IK contributing conception, writing and editing of the manuscript and made the figures.

FUNDING

IK was funded by the German Research Foundation (DFG), grant RE3454/6-1. TJ was supported by a grant from the National Health and Medical Research Council (NHMRC) to the Australian Venom Research Unit.

REFERENCES

Aird, S. D., Arora, J., Barua, A., Qiu, L., Terada, K., and Mikheyev, A. S. (2017). Population genomic analysis of a pitviper reveals microevolutionary forces underlying venom chemistry. *Genome Biol. Evol.* 9, 2640–2649. doi:10.1093/gbe/evx199

Assis, R. and Bachtrog, D. (2015). Rapid divergence and diversification of mammalian duplicate gene functions. *BMC Evol. Biol.* 15, 138. doi:10.1186/s12862-015-0426-x

Bailey, J. A., Gu, Z., Clark, R. A., Reinert, K., Samonte, R. V., Schwartz, S., et al. (2002). Recent segmental duplications in the human genome. *Science* 297, 1003–1007. doi:10.1126/science.1072047

Bergthorsson, U., Andersson, D. I., and Roth, J. R. (2007). Ohno's dilemma: Evolution of new genes under continuous selection. *Proc. Natl. Acad. Sci. U.S.A.* 104, 17004–17009. doi:10.1073/pnas.0707158104

Birchler, J. A. and Veitia, R. A. (2012). Gene balance hypothesis: connecting issues of dosage sensitivity across biological disciplines. *Proc. Natl. Acad. Sci. U.S.A.* 109, 14746–14753. doi:10.1073/pnas.1207726109

Brown, D. D., Wensink, P. C., and Jordan, E. (1972). A comparison of the ribosomal DNA's of Xenopus laevis and Xenopus mulleri: the evolution of tandem genes. *J. Mol. Biol.* 63, 57–73. doi:10.1016/0022-2836(72)90521-9

Casewell, N. R., Huttley, G. A., and Wüster, W. (2012). Dynamic evolution of venom proteins in squamate reptiles. *Nat. Commun.* 3, 1066. doi:10.1038/ncomms2065

Casewell, N. R., Petras, D., Card, D. C., Suranse, V., Mychajliw, A. M., Richards, D., et al. (2019). Solenodon genome reveals convergent evolution of venom in eulipotyphlan mammals. *Proc. Natl. Acad. Sci. U.S.A.* 116, 25745–25755. doi:10.1073/pnas.1906117116

Cheung, V. G., Conlin, L. K., Weber, T. M., Arcaro, M., Jen, K.-Y., Morley, M., et al. (2003). Natural variation in human gene expression assessed in lymphoblastoid cells. *Nat. Genet.* 33, 422–425. doi:10.1038/ng1094

Conant, G. C., Birchler, J. A., and Pires, J. C. (2014). Dosage, duplication, and diploidization: clarifying the interplay of multiple models for duplicate gene evolution over time. *Curr. Opin. Plant Biol.* 19, 91–98. doi:10.1016/j.pbi.2014.05.008

Conant, G. C. and Wolfe, K. H. (2008). Turning a hobby into a job: how duplicated genes find new functions. *Nat. Rev. Genet.* 9, 938–950. doi:10.1038/nrg2482

Copley, S. D. (2014). An evolutionary perspective on protein moonlighting. *Biochem. Soc. Trans.* 42, 1684–1691. doi:10.1042/bst20140245

Darwin, C. (1859). *On the Origin of Species*. London, UK: John Murrary, 502.

Dennett, D. (1995). *Darwin's Dangerous Idea*. New York, NY: Simon & Schuster.

Des Marais, D. L. and Rausher, M. D. (2008). Escape from adaptive conflict after duplication in an anthocyanin pathway gene. *Nature* 454, 762–765. doi:10.1038/nature07092

Doley, R., Zhou, X., and Kini, R. M. (2010). "Snake venom phospholipase A2 enzymes," in Handbook of venoms and toxins of reptiles. Editor S. P. Mackessy (Boca Raton, FL: CRC Press), 173–205.

Dowell, N. L., Giorgianni, M. W., Griffin, S., Kassner, V. A., Selegue, J. E., Sanchez, E. E., et al. (2018). Extremely divergent haplotypes in two toxin gene complexes Encode alternative venom types within rattlesnake species. *Curr. Biol.* 28, 1016–1026. doi:10.1016/j.cub.2018.02.031

Dowell, N. L., Giorgianni, M. W., Kassner, V. A., Selegue, J. E., Sanchez, E. E., and Carroll, S. B. (2016). The deep origin and recent loss of venom toxin genes in rattlesnakes. *Curr. Biol.* 26, 2434–2445. doi:10.1016/j.cub.2016.07.038

Duda, T. F. and Palumbi, S. R. (1999). Molecular genetics of ecological diversification: duplication and rapid evolution of toxin genes of the venomous gastropod Conus. *Proc. Natl. Acad. Sci. U.S.A.* 96, 6820–6823. doi:10.1073/pnas.96.12.6820

Dunn, C. W. and Munro, C. (2016). Comparative genomics and the diversity of life. *Zool. Scripta* 45, 5–13. doi:10.1111/zsc.12211

Ellis, G. (2015). "Recognising top-down causation,"in *Questioning the foundations of physics: which of our fundamental assumptions are wrong?* Editors A. Aguirre, B. Foster, and Z. Merali (Cham, Switzerland: Springer International Publishing), 17–44.

Force, A., Lynch, M., Pickett, F. B., Amores, A., Yan, Y. L., and Postlethwait, J. (1999). Preservation of duplicate genes by complementary, degenerative mutations. *Genetics* 151, 1531–1545.

French, W. J., Hayes, W. K., Bush, S. P., Cardwell, M. D., Bader, J. O., and Rael, E. D. (2004). Mojave toxin in venom of Crotalus helleri (Southern Pacific Rattlesnake): molecular and geographic characterization. *Toxicon* 44, 781–791.

Fry, B. G., Casewell, N. R., Wüster, W., Vidal, N., Young, B., and Jackson, T. N. W. (2012). The structural and functional diversification of the Toxicofera reptile venom system. *Toxicon* 60, 434–448. doi:10.1016/j.toxicon.2012.02.013

Fry, B. G. (2005). From genome to "venome": molecular origin and evolution of the snake venom proteome inferred from phylogenetic analysis of toxin sequences and related body proteins. *Genome Res.* 15, 403–420. doi:10.1101/gr.3228405

Fry, B. G., Roelants, K., Champagne, D. E., Scheib, H., Tyndall, J. D. A., King, G. F., et al. (2009). The toxicogenomic multiverse: convergent recruitment of proteins into animal venoms. *Annu. Rev. Genom. Hum. Genet.* 10, 483–511. doi:10.1146/annurev.genom.9.081307.164356

Fry, B. G., Undheim, E. A. B., Ali, S. A., Jackson, T. N. W., Debono, J., Scheib, H., et al. (2013). Squeezers and leaf-cutters: differential diversification and

degeneration of the venom system in toxicoferan reptiles. *Mol. Cell. Proteomics.* 12, 1881–1899.

Fry, B. G. and Wüster, W. (2004). Assembling an arsenal: origin and Evolution of the snake venom proteome inferred from phylogenetic analysis of toxin sequences. *Mol. Biol. Evol.* 21, 870–883. doi:10.1093/molbev/msh091

Fujimi, T. J., Kariya, Y., Tsuchiya, T., and Tamiya, T. (2002). Nucleotide sequence of phospholipase A 2 gene expressed in snake pancreas reveals the molecular evolution of toxic phospholipase A 2 genes. *Gene* 292, 225–231. doi:10.1016/s0378-1119(02)00682-0

Georgieva, D., Seifert, J., Öhler, M., Von Bergen, M., Spencer, P., Arni, R. K., et al. (2011). Pseudechis australisVenomics: adaptation for a defense against microbial pathogens and recruitment of body transferrin. *J. Proteome Res.* 10, 2440–2464. doi:10.1021/pr101248e

Giorgianni, M. W., Dowell, N. L., Griffin, S., Kassner, V. A., Selegue, J. E., and Carroll, S. B. (2020). The origin and diversification of a novel protein family in venomous snakes. *Proc. Natl. Acad. Sci. U.S.A.* 117, 10911–10920. doi:10.1073/pnas.1920011117

Gopalakrishnakone, P., Ponraj, D., and Thwin, M. M. (1997). "Myotoxic phospholipases from snake venoms: general myoglobinuric and local myonecrotic toxins,"in *Venom phospholipase a2 enzymes: structure, function and mechanism*. Editors R. M. Kini (Chichester, UK: John Wiley & Sons), 287–320.

Gould, S. J. and Vrba, E. S. (1982). Exaptation-a missing term in the science of form. *Paleobiology* 8, 4–15. doi:10.1017/s0094837300004310

Guschanski, K., Warnefors, M., and Kaessmann, H. (2017). The evolution of duplicate gene expression in mammalian organs. *Genome Res.* 27, 1461–1474. doi:10.1101/gr.215566.116

Guttinger, S. (2018). "A process ontology for macromolecular biology,"in *Everything flows: towards a processual philosophy of biology*. Editors D. J. Nicholson and J. Dupré (Oxford, UK: Oxford University Press).

Hargreaves, A. D., Swain, M. T., Hegarty, M. J., Logan, D. W., and Mulley, J. F. (2014). Restriction and recruitment-gene duplication and the origin and Evolution of snake venom toxins. *Genome Biol. Evol.* 6, 2088–2095. doi:10.1093/gbe/evu166

Hiramatsu, M., Hatakeyama, K., and Minami, N. (1980). Male mouse submaxillary gland secretes highly toxic proteins. *Experientia* 36, 940–942. doi:10.1007/bf01953804

Hughes, A. L. (1994). The evolution of functionally novel proteins after gene duplication. *Proc. Roy. Soc. Lond. B*, 119–124.

Innan, H. and Kondrashov, F. (2010). The evolution of gene duplications: classifying and distinguishing between models. *Nat. Rev. Genet.* 11, 97–108. doi:10.1038/nrg2689

Jackson, T. and Fry, B. (2016). A tricky trait: applying the fruits of the "function debate" in the philosophy of biology to the "venom debate" in the science of toxinology. *Toxins* 8, 263. doi:10.3390/toxins8090263

Jackson, T. N. W., Jouanne, H., and Vidal, N. (2019). Snake venom in context: neglected clades and concepts. *Front. Ecol. Evol.* 7, 332. doi:10.3389/fevo.2019.00332

Jackson, T. N. W., Young, B., Underwood, G., Mccarthy, C. J., Kochva, E., Vidal, N., et al. (2017). Endless forms most beautiful: the evolution of ophidian oral glands, including the venom system, and the use of appropriate terminology for homologous structures. *Zoomorphology* 136, 107–130. doi:10.1007/s00435-016-0332-9

Kaern, M., Elston, T. C., Blake, W. J., and Collins, J. J. (2005). Stochasticity in gene expression: from theories to phenotypes. *Nat. Rev. Genet.* 6, 451–464. doi:10.1038/nrg1615

Koludarov, I., Jackson, T. N., Pozzi, A., and Mikheyev, A. S. (2019). Family saga: reconstructing the evolutionary history of a functionally diverse gene family reveals complexity at the genetic origins of novelty. *bioRxiv*, 583344. doi:10.1101/583344

Kwong, S., Woods, A. E., Mirtschin, P. J., Ge, R., and Kini, R. (2009). The recruitment of blood coagulation factor X into snake venom gland as a toxin. *Thromb. Haemostasis* 102, 469–478. doi:10.1160/th09-03-0162

Lan, X. and Pritchard, J. K. (2016). Coregulation of tandem duplicate genes slows evolution of subfunctionalization in mammals. *Science* 352, 1009–1013. doi:10.1126/science.aad8411

Lynch, V. J. (2007). Inventing an arsenal: adaptive evolution and neofunctionalization of snake venom phospholipase A2 genes. *BMC Evol. Biol.* 7, 2. doi:10.1186/1471-2148-7-2

Margres, M. J., Bigelow, A. T., Lemmon, E. M., Lemmon, A. R., and Rokyta, D. R. (2017). Selection to increase expression, not sequence diversity, precedes gene family origin and expansion in rattlesnake venom. *Genetics* 206, 1569–1580. doi:10.1534/genetics.117.202655

Martinson, E. O., MrinaliniKelkar, Y. D., Chang, C.-H., and Werren, J. H. (2017). The Evolution of venom by Co-option of single-copy genes. *Curr. Biol.* 27, 2007–2013.e8. doi:10.1016/j.cub.2017.05.032

Moran, Y., Weinberger, H., Sullivan, J. C., Reitzel, A. M., Finnerty, J. R., and Gurevitz, M. (2008). Concerted Evolution of sea anemone neurotoxin genes is revealed through analysis of the Nematostella vectensis genome. *Mol. Biol. Evol.* 25, 737–747. doi:10.1093/molbev/msn021

Nakashima, K., Ogawa, T., Oda, N., Hattori, M., Sakaki, Y., Kihara, H., et al. (1993). Accelerated evolution of Trimeresurus flavoviridis venom gland phospholipase A2 isozymes. *Proc. Natl. Acad. Sci. U.S.A.* 90, 5964–5968. doi:10.1073/pnas.90.13.5964

Näsvall, J., Sun, L., Roth, J. R., and Andersson, D. I. (2012). Real-time Evolution of new genes by innovation, amplification, and divergence. *Science* 338, 384–387. doi:10.1126/science.1226521

Nei, M. and Rooney, A. P. (2005). Concerted and birth-and-death Evolution of multigene families. *Annu. Rev. Genet.* 39, 121–152. doi:10.1146/annurev.genet.39.073003.112240

Noble, D. (2013). A biological relativity view of the relationships between genomes and phenotypes. *Prog. Biophys. Mol. Biol.* 111, 59–65. doi:10.1016/j.pbiomolbio.2012.09.004

Noble, R., Tasaki, K., Noble, P. J., and Noble, D. (2019). Biological relativity requires circular causality but not symmetry of causation: so, where, what and when are the boundaries?. *Front. Physiol.* 10, 827. doi:10.3389/fphys.2019.00827

Ohno, S. (1970). *Evolution by gene duplication*. Berlin, Germany: Springer.

Paaby, A. B. and Rockman, M. V. (2013). The many faces of pleiotropy. *Trends Genet.* 29, 66–73. doi:10.1016/j.tig.2012.10.010

Phillips, C. M. (2002). Sea snake envenomation. *Dermatol. Ther.* 15, 58–61. doi:10.1046/j.1529-8019.2002.01504.x

Piatigorsky, J. and Wistow, G. (1991). The recruitment of crystallins: new functions precede gene duplication. *Science* 252, 1078–1079. doi:10.1126/science.252.5009.1078

Reams, A. B. and Roth, J. R. (2015). Mechanisms of gene duplication and amplification. *Cold Spring Harbor Perspect. Biol.* 7, a016592. doi:10.1101/cshperspect.a016592

Reyes-Velasco, J., Card, D. C., Andrew, A. L., Shaney, K. J., Adams, R. H., Schield, D. R., et al. (2014). Expression of venom gene homologs in diverse Python tissues suggests a new model for the Evolution of snake venom. *Mol. Biol. Evol.* 32, 173–183. doi:10.1093/molbev/msu294

Reza, M. A., Minh Le, T. N., Swarup, S., and Manjunatha Kini, R. (2006). Molecular evolution caught in action: gene duplication and evolution of molecular isoforms of prothrombin activators in Pseudonaja textilis (brown snake). *J. Thromb. Haemostasis* 4, 1346–1353. doi:10.1111/j.1538-7836.2006.01969.x

Reza, M. A., Swarup, S., and Kini, R. M. (2005). Gene structures of trocarin D and coagulation factor X, two functionally diverse prothrombin activators from Australian rough scaled snake. *Pathophysiol. Haemostasis Thrombosis* 34, 205–208. doi:10.1159/000092425

Reza, M. A., Swarup, S., and Kini, R. M. (2007). Structure of two genes encoding parallel prothrombin activators in Tropidechis carinatus snake: gene duplication and recruitment of factor X gene to the venom gland. *J. Thromb. Haemostasis* 5, 117–126. doi:10.1111/j.1538-7836.2006.02266.x

Sachkova, M. Y., Singer, S. A., Macrander, J., Reitzel, A. M., Peigneur, S., Tytgat, J., et al. (2019). The birth and death of toxins with distinct functions: a case study in the sea anemone Nematostella. *Mol. Biol. Evol.* 36, 2001–2012. doi:10.1093/molbev/msz132

Safavi-Hemami, H., Gajewiak, J., Karanth, S., Robinson, S. D., Ueberheide, B., Douglass, A. D., et al. (2015). Specialized insulin is used for chemical warfare by fish-hunting cone snails. *Proc. Natl. Acad. Sci. U.S.A.* 112, 1743–1748. doi:10.1073/pnas.1423857112

Six, D. A. and Dennis, E. A. (2000). The expanding superfamily of phospholipase A2 enzymes: classification and characterization. *Biochim. Biophys. Acta Mol. Cell Biol. Lipids* 1488, 1–19. doi:10.1016/s1388-1981(00)00105-0

Surm, J. M., Smith, H. L., Madio, B., Undheim, E. A. B., King, G. F., Hamilton, B. R., et al. (2019). A process of convergent amplification and tissue-specific expression dominates the evolution of toxin and toxin-like genes in sea anemones. *Mol. Ecol.* 28, 2272–2289. doi:10.1111/mec.15084

Taylor, J. S. and Raes, J. (2004). Duplication and divergence: the evolution of new genes and old ideas. *Annu. Rev. Genet.* 38, 615–643. doi:10.1146/annurev.genet.38.072902.092831

True, J. R. and Carroll, S. B. (2002). Gene Co-option in physiological and morphological Evolution. *Annu. Rev. Cell Dev. Biol.* 18, 53–80. doi:10.1146/annurev.cellbio.18.020402.140619

Vonk, F. J., Casewell, N. R., Henkel, C. V., Heimberg, A. M., Jansen, H. J., Mccleary, R. J. R., et al. (2013). The king cobra genome reveals dynamic gene evolution and adaptation in the snake venom system. *Proc. Natl. Acad. Sci. U.S.A.* 110, 20651–20656. doi:10.1073/pnas.1314702110

Wang, Z., Liao, B.-Y., and Zhang, J. (2010). Genomic patterns of pleiotropy and the evolution of complexity. *Proc. Natl. Acad. Sci. U.S.A.* 107, 18034–18039. doi:10.1073/pnas.1004666107

Whittington, A. C., Mason, A. J., and Rokyta, D. R. (2018). A single mutation unlocks cascading exaptations in the origin of a potent pitviper neurotoxin. *Mol. Biol. Evol.* 35, 887–898. doi:10.1093/molbev/msx334

Whittington, C. M., Papenfuss, A. T., Bansal, P., Torres, A. M., Wong, E. S. W., Deakin, J. E., et al. (2008). Defensins and the convergent evolution of platypus and reptile venom genes. *Genome Research* 18, 986–994. doi:10.1101/gr.7149808

Wistow, G. and Piatigorsky, J. (1987). Recruitment of enzymes as lens structural proteins. *Science* 236, 1554–1556. doi:10.1126/science.3589669

Wong, E. S. W. and Belov, K. (2012). Venom evolution through gene duplications. *Gene* 496, 1–7. doi:10.1016/j.gene.2012.01.009

Woods, H. A. (2014). Mosaic physiology from developmental noise: within-organism physiological diversity as an alternative to phenotypic plasticity and phenotypic flexibility. *J. Exp. Biol.* 217, 35–45. doi:10.1242/jeb.089698

Conflict of Interest: The authors declare that the research was conducted in the absence of any commercial or financial relationships that could be construed as a potential conflict of interest.

frontiers in Pharmacology

ORIGINAL RESEARCH
published: 13 January 2021
doi: 10.3389/fphar.2020.563858

A Novel Insecticidal Spider Peptide that Affects the Mammalian Voltage-Gated Ion Channel hKv1.5

*Diana Alvarado[1], Samuel Cardoso-Arenas[1], Ligia-Luz Corrales-García[1,2], Herlinda Clement[1], Iván Arenas[1], Pavel Andrei Montero-Dominguez[1], Timoteo Olamendi-Portugal[1], Fernando Zamudio[1], Agota Csoti[3], Jesús Borrego[1], Gyorgy Panyi[3], Ferenc Papp[3] and Gerardo Corzo[1]**

[1]*Departamento de Medicina Molecular y Bioprocesos, Instituto de Biotecnología, Universidad Nacional Autónoma de México, Cuernavaca, México,* [2]*Departamento de Alimentos, Facultad de Ciencias Farmacéuticas y Alimentarias, Universidad de Antioquia, Medellín, Colombia,* [3]*Department of Biophysics and Cell Biology, Faculty of Medicine, University of Debrecen, Debrecen, Hungary*

OPEN ACCESS

Edited by:
Jean-Marc Sabatier, Aix-Marseille Université, France

Reviewed by:
Volker Herzig, University of the Sunshine Coast, Australia
Luiza Gremski, Federal University of Paraná, Brazil

***Correspondence:**
Gerardo Corzo
corzo@ibt.unam.mx

Specialty section:
This article was submitted to Pharmacology of Ion Channels and Channelopathies, a section of the journal Frontiers in Pharmacology

Received: *19 May 2020*
Accepted: *26 October 2020*
Published: *13 January 2021*

Citation:
Alvarado D, Cardoso-Arenas S, Corrales-García L-L, Clement H, Arenas I, Montero-Dominguez PA, Olamendi-Portugal T, Zamudio F, Csoti A, Borrego J, Panyi G, Papp F and Corzo G (2021) A Novel Insecticidal Spider Peptide that Affects the Mammalian Voltage-Gated Ion Channel hKv1.5. Front. Pharmacol. 11:563858. doi: 10.3389/fphar.2020.563858

Spider venoms include various peptide toxins that modify the ion currents, mainly of excitable insect cells. Consequently, scientific research on spider venoms has revealed a broad range of peptide toxins with different pharmacological properties, even for mammal species. In this work, thirty animal venoms were screened against $hK_v1.5$, a potential target for atrial fibrillation therapy. The whole venom of the spider *Oculicosa supermirabilis*, which is also insecticidal to house crickets, caused voltage-gated potassium ion channel modulation in $hK_v1.5$. Therefore, a peptide from the spider *O. supermirabilis* venom, named Osu1, was identified through HPLC reverse-phase fractionation. Osu1 displayed similar biological properties as the whole venom; so, the primary sequence of Osu1 was elucidated by both of N-terminal degradation and endoproteolytic cleavage. Based on its primary structure, a gene that codifies for Osu1 was constructed *de novo* from protein to DNA by reverse translation. A recombinant Osu1 was expressed using a pQE30 vector inside the *E. coli* SHuffle expression system. recombinant Osu1 had voltage-gated potassium ion channel modulation of human $hK_v1.5$, and it was also as insecticidal as the native toxin. Due to its novel primary structure, and hypothesized disulfide pairing motif, Osu1 may represent a new family of spider toxins.

Keywords: atrial fibrillation, Kv1.5, *Oculicosa supermirabilis*, recombinant expression, spider venom

INTRODUCTION

Spider venoms are a heterogeneous mixture of molecules that range from enzymes to toxic peptides and small organic components (Pineda et al., 2014). Among the toxic peptides, there are disulfide-rich neurotoxins harmful to insects, and perhaps due to molecular serendipity, some of them are also toxic to mammals, which affect cell receptors, especially ion channels. So, most of the spider neurotoxins could be considered, from the molecular perspective, as precious and unique molecules to help us to understand some of the ion channels' mechanisms that are important for physiological purposes (Nicholson and Graudins, 2002). Also, it is well known that spider peptide toxins tend to be promiscuous concerning their selectivity for ion channels. Still, some could be specific and exclusive to unveil relevant domains of the ion channel structures (Corzo and Escoubas, 2003). For example, the spider δ-atracotoxins (δ-ACTXs), that belong to the NaSpTx spider family 4, are disulfide-rich

neurotoxins that modify the voltage-gated sodium channels (Na_v), both in insects and in mammals. Those neurotoxins bind to domain IV in the S3/S4 loop, also identified as neurotoxin receptor site-3 (Clairfeuille et al., 2019), decreasing the fast inactivation of Na_vs (Gunning et al., 2003). Since δ-ACTXs have this dual effect on both mammals and insects, they have facilitated our understanding of some of the molecular interactions with Na_v (Borrego et al., 2020). Thus, the search for new spider peptide structures that could contribute to ion channel physiology knowledge should be granted and embraced. In this tenor, the advent of transcriptomics and proteomics for studying spider venom glands and venoms, respectively, have exponentially uncovered a significant number of primary structures from spider venoms (Zhang et al., 2010; Quintero-Hernandez et al., 2011; Jiang et al., 2013; Oldrati et al., 2017; Langenegger et al., 2019). Nevertheless, understanding the mechanism of action of most spider structures already found has been hampered mainly because of insufficient infrastructure in both material and academic to obtain enough quantities of such spider peptides by natural, synthetic, or recombinant means (Quintero-Hernandez et al., 2011). Also, it has been limited because of the low capacity of most research labs to test a wide range of a growing number of ion channels and their subtypes compared to the known motifs in spiders to discern their correct cellular or molecular targets.

In this work, we look for spider peptides that target the voltage-gated potassium channels (K_v), specifically the $hK_v1.5$ potassium channel, in which ion currents are also referred to IKur, and they are the main ion currents in the repolarization of the atrial action potential (AP). IKur has been observed in human atrial myocytes, but it is absent in the human ventricle (Fedida et al., 1993). Several researchers have concluded that the blockage of IKur could prolong the duration of AP of atrial fibrillation (AF) in patients (Brunner et al., 2003; Guo et al., 2016), and stop fibrillation, indicating that $hK_v1.5$ is potentially a selective target and safe strategy for AF therapy (Lip and Tse, 2007; Ehrlich et al., 2008; Ford and Milnes, 2008; Ehrlich and Nattel, 2009; Ravens, 2010). Therefore, one of our research goals is to discover selective $hK_v1.5$ peptide inhibitors and test them in an AF model. At present, all of the known $hK_v1.5$ blockers are small molecules (Gutman et al., 2005; Wettwer and Terlau, 2014; Bajaj and Han, 2019). However, they are usually not as selective as large molecules, e.g., peptides, which have a much larger interacting surface with ion channels than the small molecules, and the larger the interaction, the higher the selectivity and the lower the risk of side effects (Corzo et al., 2008; Ali et al., 2019). Perhaps one of the main reasons for the absence of $hK_v1.5$ peptide inhibitors is because this subtype of ion channel does have a positively charged Arg residue in its selectivity pore, unlike other K_v ion channels (Zhu et al., 2005), which prevents the potential blocking peptides from binding to hK_v channels. So, here we report the primary structure of a spider toxin, named Osu1, that affects $hK_v1.5$, and it seems to be one of the first electric-current modifier peptides of this ion channel. One of the peculiarities of Osu1, according to our results, is that it does not bind to the selectivity pore, but the voltage-sensing domain; so, it does not block the pore of $hK_v1.5$ but prevents its opening at physiological membrane potentials. Nevertheless, the result would be the same; if there is no K^+ ion flow through $hK_v1.5$, i.e., no IKur current, and if there is no repolarizing outward IKur current during the atrial AP of an AF patient, the duration of AP would be prolonged, and fibrillation will be abolished (Guo et al., 2016). Besides the effects of Osu1 on $hK_v1.5$, it is also insecticidal, and according to its amino acid sequence, it could be placed in a new spider toxin family; that is, none of the already proposed spider toxin families (Klint et al., 2012) has a primary structure similar to Osu1. Furthermore, most of the spider peptides with significant identity (90–95%) to Osu1 have been found just as transcripts, and only a spider peptide toxin with 48% identity to Osu1, ω-agatoxin-IA, has biochemical properties already reported (Santos et al., 1992). Finally, based on software that predicts three-dimensional protein structures, Osu1 may have a different disulfide-pairing motif than the known spider peptides.

MATERIAL AND METHODS

Strains, Vectors, and Enzymes

Bacterial strains: *E. coli* XL1-Blue (cloning) (*gyrA96 recA1 hsdR17 endA1 thi-1 relA1 supE44 lac* [F′ *proAB* Tn*10* (Tetr) *lacI*^{q}ZΔ*M15*]) (Agilent, United States); and *E. coli* SHuffle®T7 (Expression) (*pro*, F′ *lac*, *lacI*^{q} *araD139* Δ*(ara-leu)7697 lacZ::T7 fhuA2 gene1* Δ*(phoA)PvuII ahpC* phoR galE (or U)* Δ*trxB rpsL150*(Str^R *galK* λ*att*:pNEB3-r1-*cDsbC* (Spec^R, *lacI*^{q})) Δ*(malF)3* Δ*gor*) (New England BioLabs, Ipswich, MA, United States), respectively. Plasmid pQE30 (Qiagen, CA, United States) was used for cloning the Osu1 gene, and production of the 6His-tagged recombinant Osu1 (rOsu1). The enzymes were from New England Biolabs (NEB, Ipswich, MA, United States) (Taq-Polymerases, Vent-Polymerase, restriction enzymes), T4 Ligase from Fermentas (Carlsbad, CA, United States).

Isolation and Chemical Characterization of Osu1

The venom from the spider *Oculicosa supermirabilis* was extracted by electrical stimulation. The spiders were field-collected in the Kazakhstan Republic (Fauna Ltd.). At the Institute of Zoology in Almaty, Kazakhstan, the spiders were identified. This species is found in Kazakhstan, Uzbekistan, and Turkmenistan (Logunov and Gromov, 2011). The raw venom (the venom of more than 200 individuals, females, and males were milked and pooled, to yield 2 mg) was dissolved in water with 0.1% of trifluoracetic acid (TFA) and then centrifuged to remove all the insoluble material (14,000 *g* for 5 min). The liquid phase was injected directly for fractioning using High-Performance Liquid Chromatography (HPLC). The venom mixture was separated using a reverse-phase analytical C_{18} column ($5C_{18}$MS, 4.6 × 250 mm, Vydac, United States) equilibrated in 0.1% TFA, and eluted with 0–60% acetonitrile in 0.1% TFA in a linear gradient, run for 60 min (1 ml/min) (Corzo et al., 2001). The elution fractions were monitored at 280 nm, collected in 1.5 ml vials, and dehydrated under a high vacuum. The dried samples were used first to conduct

electrophysiological assays. Those fractions capable of affecting $hK_v1.5$ channels were subjected to another purification process using a C_{18} reverse-phase column (4.6 × 250 mm, Vydac, United States) equilibrated in 0.1% TFA, and eluted with 20–60% acetonitrile in 0.1%TFA in a linear gradient, and run for 40 min (1 ml/min). The new fractionated components were again subjected to electrophysiological assays. It was analyzed by mass spectrometry using a Thermo Scientific LCQ Fleet ion trap mass spectrometer (San Jose, CA, United States) with a Surveyor MS syringe pump delivery system. The pure peptide was also subjected to Edman degradation using an LF3000 Protein Sequencer (Beckman, CA, United States), and endoproteolytic digestions to determine its primary structure, as reported previously by our group (Corzo et al., 2008).

Osu1 Gene Construction

- The primary structure of the peptide Osu1 was used to do a reverse translation and thus generate a DNA sequence (https://www.bioinformatics.org/sms2/rev_trans.html). Afterward, the obtained sequence was analyzed and adjusted, complying with the preferential codon usage of *E. coli* (http://www.kazusa.or.jp/codon). Then, we designed four overlapping synthetic oligonucleotides (**Supplementary Table S1**) to construct the Osu1 gene. Additionally, the recognition strings for *Bam*HI (GGATCC) and Factor Xa protease (ATCGAGGGAAGG) were added at the beginning of oligonucleotide Osu1-Up1. Two stop codons (TAATAG) and the restriction sequence for *Pst*I (CTGCAG) were added to the end of oligonucleotide Osu1-Lw4.
- The Osu1 gene was constructed *in vitro* using the "overlapping oligonucleotide extension" following the Polymerase Chain Reaction (PCR). In a few words, Osu1-Lw2 plus Osu1-Up3 oligonucleotides (17 bp overlap) were mixed in 0.1 pmol/μl final concentration each, with the other components in the reaction mixture including Vent polymerase for PCR, and then amplified in eight cycles under the following conditions: 94°C/30 s, 58°C/30 s, and 72°C/30 s. After the eighth cycle, oligonucleotides Osu1-Up1 plus Osu1-Lw4 were added to the reaction mixture (0.4 pmol/μl final concentration each) and followed by 25 amplification cycles with the following conditions: 94°C/30 s, 60°C/40 s, and 72°C/30 s. A final elongation step was carried out at 72°C/10 min. The PCR product was run on 1% agarose gels containing GelRed® (Biotium, Fremont, CA, United States) and envisioned under ultraviolet (UV) light (DNA marker from NEB, Ipswich, MA, United States). Afterward, the amplification product was purified from the agarose gel with the High Pure Plasmid Isolation kit (Roche, Basel, Switzerland).

The assembled and purified gene was digested with *Bam*HI and *Pst*I enzymes (NEB). The gen was run and extracted from agarose gel, then ligated (T4 ligase, Fermentas) to the pQE30 expression plasmid, previously restricted by the same enzymes. The new recombinant plasmid (pQE30/Osu1) was used to transform *E. coli* XL1-Blue cells by heat shock. The plasmid's antibiotic selection system enabled us to pick some colonies to be tested using PCR (pQE-Fwd (5′-GAGCGGATAACAATTATA A-3′) and pQE-Rev (5′-GGTCATTACTGGATCTAT-3′). Four colonies with the predicted amplification band were subjected to plasmid purification and then sequenced at the Institute of Biotechnology, UNAM, Mexico.

Expression Screening

The recombinant plasmid pQE30/Osu1, sequence confirmed, was used to transform *E. coli* SHuffle cells for testing expression. Briefly, the transformation procedure was as follows: 50 ng of pQE30/Osu1 plasmid was blended with 100 μl of competent *E.* coli/SHuffle cells and maintained in ice for 30 min, then heated the mix for 1 min at 42°C, followed by cooling in ice for 5 min. Afterward, we added 220 μl of Super Optimal broth with Catabolite repression (SOC) medium, and the mix was kept for 60 min at 37°C. After incubation, 50 μl of the mixture were spread over Petri dishes containing (Luria-Bertani) LB agar-media with ampicillin (100 μg/ml) (Sigma, St. Louis, MO, United States). Grown colonies that harbored the pQE30/Osu1 vector were used to screen their expression. Colonies individually were selected, and seeding each in 3 ml of LB broth, including ampicillin plus 1 mM isopropyl ß-D-thiogalactoside (IPTG, Sigma, St. Louis, MO, United States). Then they were incubated overnight in a shaker at 250 rpm and 37°C. Expression was tested qualitatively by SDS-PAGE. Lastly, a positive clone was selected to evaluate the expression of Osu1.

Expression of Recombinant Osu1

rOsu1 was produced in the *E. coli* SHuffle strain. LB broth was used to cultivate cells until an optical density (OD_{600}) of 0.6. At that point, 0.5 mM of IPTG was added to induce the peptide expression. Induced cells were maintained for 8 h at 25°C and then collected by centrifugation (5,500 *g*, 20 min, 4°C). Using a mechanical system (One-Shot Cell Disruptor from Constant Systems, Northants, United Kingdom), the cells were burst down. The disrupted cells were subjected to centrifugation (10,000 *g*, 20 min, 4°C) to separate inclusion bodies, which were solubilized using guanidine hydrochloride (GdHCl) 6M, Tris HCl 50 mM, pH 8. Employing Ni-NTA agarose (Qiagen, CA, United States), we purify the recombinant peptides from the dissolved inclusion bodies. Afterward, the peptide was reduced using dithiothreitol (DTT) (Sigma-Aldrich, Ontario, Canada) for 1 h at 37°C. The product was subjected to analytical RP-HPLC (C_{18} column 4.6 × 250 mm, Vydac, United States) using 20–60% acetonitrile in 0.1% TFA in a linear gradient, and run for 40 min (1 ml/min). The obtained reduced fractions were folded *in vitro*. Briefly, the reduced peptide (50 μg/ml) was added to a refolding buffer (0.1 M Tris, pH 8, 2 M GdHCl, 1 mM GSSG, and 10 mM GSH). The mixture was allowed to oxidize for 4 days at 4°C. After that, it was driven to pH 2 by TFA addition. The folded peptide was cleaned by analytical RP-HPLC (C_{18} column 4.6 × 250 mm, Vydac, United States) using the gradient previously mentioned.

In vivo Biological Activity

Fractions obtained from RP-HPLC were tested in mice (strain CD-1, 17–21 g) by intracranial (ic) injection and in house-crickets (*Acheta domesticus,* 0.1–0.16 g) by lateroventral

thoracic injection (lv). Osu1 was not toxic to mice up to 5 μg/mouse. The median paralyzing dose (PD_{50}) in crickets was defined as the amount of peptide that produces the paralysis of 50% of the population of crickets experimentally evaluated. The median lethal dose (LD_{50}) in crickets was defined as the amount of peptide that produces the death of 50% of the treated population. The PD_{50} and LD_{50} were determined using the Dixon method (Dixon, 1965). In brief, one cricket each time was dosed with established doses within regular periods. If the first cricket was paralyzed at least 1 min within the first 10 min after the inoculation, the next cricket was injected with a lower dose. Similarly, if the first cricket was death after 30 min following the injection, the next cricket was inoculated with a lower dose. This progression proceeded until required insects were dosed for calculating either the PD_{50} or the LD_{50}. The mean and the confidence intervals of either the PD_{50} or the LD_{50} were determined, according to Dixon (1965). Experiments with animals were earlier accepted by the Bioethics Committee of the Biotechnology Institute (project No. A1-S-8005) and conducted complying with proper regulations.

Electrophysiology

Murine erythroleukemia (MEL) cells stably expressing $hK_v1.5$ channels were maintained following usual conditions, as described before (Grissmer et al., 1994) and were a gift from Dr. Heike Wulff. According to standard protocols, voltage-clamped cells were used to measure the whole-cell currents (Corzo et al., 2008). A Multiclamp 700B amplifier attached to a personal computer (1322A data acquisition hardware, Molecular Devices, Sunnyvale, CA) was employed. A series resistance compensation up to 70% was used to achieve good voltage-clamp conditions and minimize voltage errors. Leitz Fluovert (Leica, Wetzlar, Germany) or Nikon TE2000-U fluorescence microscopes were used to observing cells. Pipettes were pulled from GC 150 F-15 borosilicate glass capillaries Harvard Apparatus (Kent, United Kingdom) in five stages, which resulted in electrodes with 3–5 MOhm resistance in the bath. The composition of the bath solution was 5 mM KCl, 145 mM NaCl, 2.5 mM $CaCl_2$, 1 mM $MgCl_2$, 10 mM HEPES, 5.5 mM glucose, 0.1 mg/ml bovine serum albumin (Sigma-Aldrich), and, pH 7.35. From a holding potential of −100 mV, voltage steps to +50 mV were applied for ionic current measurements every 15 s. The pClamp10 software package (Molecular Devices) was used for data acquisition and analysis. Whole-cell current traces were adjusted for ohmic leakage, before analysis and were digitally filtered (three-point boxcar smoothing). The current activation kinetics were characterized by implementing a single-exponential function (f(t) = A*Exp(−t/tau)+C).

Secondary Structure of Recombinant Osu1

The secondary structure of rOsu1 was evaluated by circular dichroism (CD). The measurement was carried out on a Jasco model J-720 spectropolarimeter (Jasco, Tokyo, Japan), from 250 to 190 nm in an aqueous solution of 60% trifluoroethanol (TFE), at room temperature, with a 1-mm pathlength cell. Data were collected at 1 nm with a scan rate of 20 nm/min, and a time constant of 0.5 s. The concentration of rOsu1was 60 μM. Data was the average of three separate recordings and analyzed by the software Bestsel (http://bestsel.elte.hu/index.php) (Micsonai et al., 2018). A recombinant scorpion neurotoxin (rCssII), previously characterized by NMR and CD, and also a three-finger toxin, was used as comparative controls under the same extent conditions.

Structural Model of Osu1

The amino acid sequence of Osu1 was used to generate a three-dimensional structure through different modeling programs. These programs are based on different 3D structure prediction techniques, such as I-Tasser (Yang and Zhang, 2015), Swiss-Model (Waterhouse et al., 2018), Robetta (Kim et al., 2004) and Modeller (Webb and Sali, 2016). For Modeller, a sequence alignment between Osu1 and the template, OtTx1a (PDB ID: 2n86), was calculated to guide the modeling, using the T-Coffee homology extension (PSI-coffee) algorithm (Di Tommaso et al., 2011). The NMR structure of the spider toxin OtTx1a (PDB ID: 2n86) was used as a template according to the best parameters found by LOMETS (Local Meta-Threading Server) (Wu and Zhang, 2007). A total of 10,000 models were generated by Modeller, selecting the most representative model using the root mean square deviation (RMSD), DOPE score, and main chain quality through PROCHECK (Dunbrack, 2004). From the set of structures generated by I-Tasser, Swiss-Model, and Robetta, only the models with full Cys oxidation were selected for the final analysis. The final figures were prepared with VMD (Humphrey et al., 1996; Dunbrack, 2004) and ESPrit3.0 (Gouet et al., 1999).

Statistical Analysis

The SPSS statistical software was used for statistical analysis (SPSS Inc., Chicago, IL, United States). The mean ± standard error of the mean (SEM) and 95% confidence intervals were used to express the data. Student paired *t-test*, analysis of variance (ANOVA), or Tukey's test (for multiple comparisons) were used to determine the statistical significance. $p < 0.05$ was considered significant.

RESULTS

Toxin Purification and Sequencing

After an initial screening of some arachnid venoms (data not shown), the venom of *Oculicosa supermirabilis* showed activity over $hK_v1.5$. Fractionation of crude venom by reversed-phase HPLC resulted in more than 60 fractions that were manually collected and assayed for biological activity toward $hK_v1.5$, mice, and crickets (**Figure 1**). Although fractions #59, #61 and #67 were toxic to insects, only fraction #59 presented activity affecting the $hK_v1.5$ (**Figure 2**). The before-mentioned fraction was analyzed by mass spectrometry, and it was further purified again by reversed-phase chromatography. As confirmed by analytical chromatography and mass spectrometry, the fraction #59 was obtained at a high purity level and was named Osu1. It represented a concentration of *ca* 60 μg per mg of the dry crude venom of *O. supermirabilis*. The data obtained from

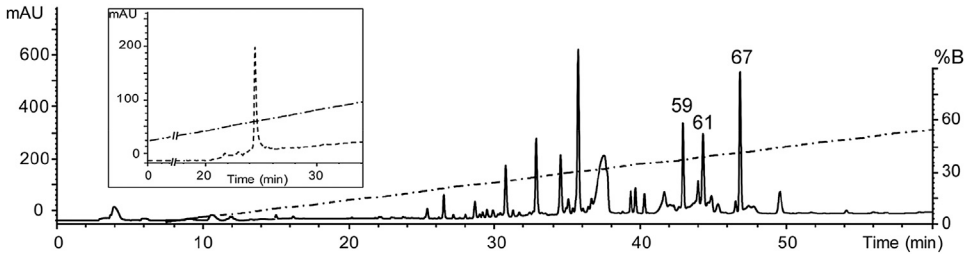

FIGURE 1 | Reverse-phase HPLC chromatogram of the venom of *O. supermirabilis*. The soluble venom of *O. supermirabilis* (obtained from 2 mg crude soluble venom) was fractionated using a reverse-phase analytical C_{18} column ($5C_{18}$MS, 4.6 × 250 mm) equilibrated in 0.1% TFA, and eluted with a linear gradient of acetonitrile (solution B) starting after 5 min from 0 to 60% in 0.1% TFA, run for 60 min at a flow rate of 1 ml/min. The fraction peak #59 in the figure was the fraction that gave positive results in modifying currents in $hK_v1.5$, and was further purified to homogeneity (Inside figure) starting after 5 min from 20 to 60% CH_3CN during 40 min at a flow rate of 1 ml/min.

automated direct Edman sequencing of the reduced-alkylated fraction #59, and later from endoproteolytic cleavages followed of digested peptide purification, and again N-terminal Edman degradation of such peptide fractions allowed the complete determination of the primary structure of Osu1.

Briefly, direct Edman degradation of the alkylated fraction #59 provided an unambiguous sequence up to amino acid at position 44 (**Table 1**). Some of the remaining alkylated fraction #59 was enzymatically cleaved by Lys-C, and peptide fractions were collected by RP-HPLC (**Supplementary Figure S1**). The N-terminal direct sequencing of the alkylated fraction #59 and three of such Lys-C digested peptide fragments allowed the identification of 63 residues of the Osu1 primary structure. Additionally, because of a difference of practically 128 atomic mass units, a Lys residue was placed at position 53 (**Table 1**, bold), which was also supported by similar amino acid sequence identities found in spider peptide precursors from the venom gland transcriptome of *Lycosa singoriensis* spider (**Table 2**).

The amino acid sequence agreed on the data gathered from mass spectrometry (**Table 1**). The estimated theoretical molecular weight of Osu1, assuming pairing the eight cysteine residues into four disulfide bridges, and a free C-terminal carboxylic acid, was 7,477.7 Da. The −0.3 Da mass variation among the calculated and measured molecular mass of Osu1 (7,477.4 Da) may be within the mass spectrometric equipment error. Also, we indirectly speculate that the C-terminal of Osu1 is not amidated based on the transcripts (B6DD30.1 and B6DD33.1) found by Zhang et al. (2010) given that it has not an endoproteolytic amidation signal (**Table 2**). The amino acid sequence of Osu1 has some identities with toxins from spiders of the same family (Lycosidae), and with others in the same evolutionary clade (Agelenidae and Pisauridae). An automated database search and multiple alignment computations showed that Osu1 had marked identities with peptides from the venom from *Lycosa singoriensis, Cupiennius salei, Dolomedes mizhoanus*, and *Agelenopsis aperta* (**Table 2**). Most of those toxins have only been registered at the transcriptomic level, and there is no expression evidence within their venom, except for ω-agatoxin-1A, which seems to form heterodimeric structure. However, its three-dimensional structure has not been solved yet (Santos et al., 1992).

Construction of Osu1

The synthetic oligonucleotides, Osu1-Up1, Osu1-Lw2, Osu1-Up3, and Osu1-Lw4 (**Supplementary Table S1**), were conveniently assembled using the overlapping oligonucleotide extension, as specified previously in the *Material and Methods* section. The obtained synthetic gene Osu1 was indeed cloned to produce the recombinant plasmid pQE30/Osu1, which was verified by DNA sequencing to confirm the reading frame and the conservation of restriction sites. *E. coli* SHuffle colonies were transfected with the sequenced construct. Some of those colonies could express the peptide Osu1 fused to a His-Tag, as proved by the expression screening of various colonies withholding the plasmid pQE30/Osu1. The expressed protein was confirmed by SDS-PAGE and a band with an apparent molecular weight in the 5–15 kDa region. Then, we picked one of those colonies to overexpress Osu1.

Recombinant Expression and Purification Osu1 (rOsu1)

The rOsu1 includes an extra N-terminal sequence of 16 amino acids (MRSGHHHHHHGSIEGR) plus the following Osu1 mature peptide (**Table 1**). The rOsu1 was expressed using the *E. coli* Shuffle strain (**Figures 3A**). The expressed proteins were found in inclusion bodies, and they were dissolved utilizing chaotropic agents and purified employing nickel affinity chromatography (NiNTA). SDS-PAGE confirmed the existence of rOsu1; that is, the rOsu1 band was observed between the molecular weight markers of 10 and 15 kDa, which were also observed after the purification of inclusion bodies using the NiNTA column (**Figures 3B**). The rOsu1 position above 10 kDa under SDS-PAGE obeys mainly to its charge:mass ratio, this unpredictive position under SDS-PAGE has been observed in other recombinant peptides with a high content of basic amino acids (Estrada et al., 2007; de la Rosa et al., 2018). For folding, the cystines of rOsu1 were reduced with DTT and folded *in vitro* in the presence of the GSH/GSSG par redox. After the *in vitro* folding and HPLC purification (**Figure 4**), the experimental molecular masses of rOsu1 was obtained (9,331.6 Da), and it was in good agreement according to their expected theoretical molecular mass (9,331.7 Da). The expression

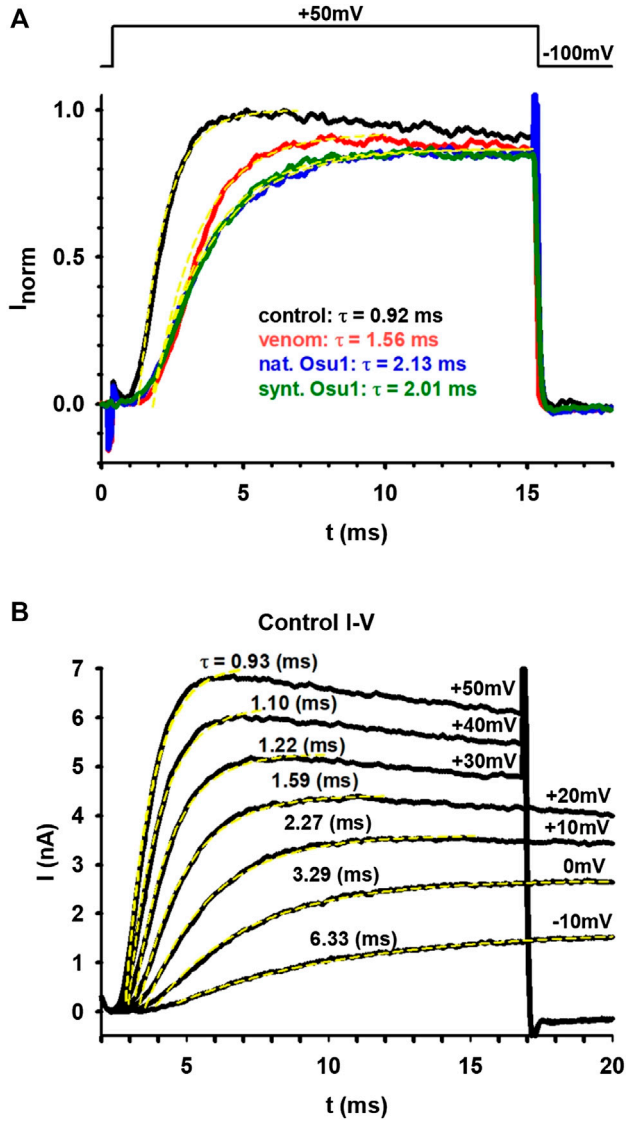

FIGURE 2 | *Oculicosa supermirabilis* venom and fraction #59 modifies $hK_v1.5$ currents expressed in MEL cells. **(A)** shows the current traces recorded under normal conditions (black), in the presence of complete venom (10 µg/ml; red), with fraction #59 or Osu1 (6.5 µg/ml, ~0.9 µM; blue) and recombinant rOsu1 (3 µM; green). The voltage protocol is shown above the figure. The current traces were fitted with a single-exponential function (yellow dashed lines), and the tau values for each trace are indicated with the appropriate color coding. **(B)** displays I-V curves where the ionic currents were recorded under normal conditions and were evoked from −100 mV holding potential to different depolarizing potentials: from −10 mV up to +50 mV. The appropriate membrane potential values are indicated next to the traces along with the tau values coming from a single-exponential fitting.

yield of rOsu1 was calculated *ca* of 0.4 mg of folded peptide/L. The extra N-terminal poly His-tag sequence in the rOsu1 could not be removed because peptide degradation was observed due to non-specific cleavage by FXa (**Supplementary Figure S2**). Even though the difference between the chromatographic retention time of rOsu1 and the native Osu1, was 0.7 min under similar reverse-phase chromatographic conditions. That is, the chromatographic retention time of rOsu is shorter than the native Osu1because the poly His-tag in rOsu1 makes it a little bit more hydrophilic than its native counterpart (**Supplementary Figure S3**). Similar retention time differences have been observed between recombinant peptides and native ones (Estrada et al., 2007).

In vivo Biological Activity

The PD_{50} and LD_{50} in house-crickets were calculated using the folded rOsu1 peptide (**Table 3**). For house crickets, the PD_{50} and LD_{50} of rOsu1 decreased 5.4 and less than 5.3-fold, respectively, compared to the native peptide. Presumably, the extra N-terminal residues of rOsu1 could explain the difference between PD_{50} and LD_{50}, compared to the native toxin. These N-terminal residues may interfere in the *in vivo* activity (Estrada et al., 2007). Also, some incorrectly folded rOsu1 may hamper the insecticidal activity compared to the correctly folded rOsu1. However, the rOsu1 has a similar biological effect as the native peptide, indicating a substantial proportion of the recombinant peptide's correct folding. The biological activity toward insects was similar to other spider peptide toxins (Pineda et al., 2018).

Electrophysiology

We tested 30 different animal venoms on the $hK_v1.5$ ion channel (see **Supplementary Table S2**). Five of these showed an effect on the ion current flowing through $hK_v1.5$. Of these five, one, the venom of *O. supermirabilis* was further investigated, and the peptide responsible for the effect was determined. First, the whole venom of *O. supermirabilis* was tested on MEL cells, stably expressing $hK_v1.5$ channels. Panel A of **Figure 2** shows the current traces recorded on MEL cells under control conditions, in the absence of the venom (black), and in the presence of complete venom (10 µg/ml; red). Besides decreasing the current amplitude, we noticed that the kinetics of the ionic current changed and slowed down, indicating that this was not a simple pore inhibition. It is more likely that one of the venom's peptides is bound to the voltage sensor of the $hK_v1.5$ ion channel, thereby altering the gating kinetics of the channel. Therefore, the activation kinetics of ion currents in the presence and absence of venom were determined. Using a single exponential function, we fitted the rising part of the current, and the tau parameter of the fitting proved that the venom's presence slows down the current activation kinetics. After fractionation of the venom, the effect of each fraction on the $hK_v1.5$ currents, was tested. Only one fraction showed an effect, the #59, which we named Osu1. We performed the same experiment with Osu1 (6.5 µg/ml, ~0.9 µM) as we did with the whole venom described above. Panel A of **Figure 2** shows the results with blue: slower activation kinetics, similarly to the venom-experiment. We also tested the recombinant rOsu1 on $hK_v1.5$ currents at a concentration of 3 µM, which gave a very similar result to the native Osu1 (see the current trace in **Figure 2** in green). The average tau parameters in the presence, and the absence, of rOsu1 were 2.02 ± 0.08 ms and 0.98 ± 0.04 (n = 3), respectively. Comparing them with a paired t-test, the difference is significant (p = 0.014), indicating that rOsu1 slows down the $hK_v1.5$ current activation kinetics significantly. Based on our

TABLE 1 | Amino acid sequencing and molecular masses of endoproteolytic fractions from Osu1.

Peptide	Amino acid sequence	MW(Da) The	MW(Da) Exp
Fraction #59	RLALPPGAVCNGHKSDCQCFGAKYKCSCPFFWRFRKSAECHCKK	--	7,477.4[a,b] (7,941.4)
	---------->		
	Direct Edman		
	C---------->K	1,476.7	1,476.2[a] (1,590.2)
	G------>K	932.1	931.2[c] (931.2)
	R--------->D	1,451.5	1,450.7[a] (1,507.7)
	Lys-C		
Osu1	RLALPPGAVCNGHKSDCQCFGAKYKCSCPFFWRFRKSAECHCKKGWAWTAIK**K**RSCHNRYQWSD	7,477.7	7,477.4[a,b] (7,941.4)

[a]*Molecular mass after subtraction of –57 Da (Cysteine carbamidomethylation by iodoacetamine) to the molecular masses of the alkylated fractions containing Cys (HPLC separation and molecular masses of alkylated fractions are shown in* ***Supplementary Figure S1****).*
[b]*A subtraction of an extra –8 Da to the alkylated Osu1 was performed assuming four disulfide bridges.*
[c]*Non-alkylated peptide fragment. The experimental molecular masses in parenthesis are shown in* ***Supplementary Figure S1****.*

TABLE 2 | Alignment of amino acid sequences of Osu1.

Peptide	Sequence	Identity (%)	Access
	1 10 20 30 40 50 60		
Osu1	RLALPPGAV**C**NGHKSD**C**Q**C**FGAKYK**C**S**C**PFFWRFRKSAE**C**H**C**KKGWAWTAI**K**KRS**C**HNRYQWSD	100	[a]C0HLR8
Ls1b	RMALPPGAV**C**NGHKSD**C**Q**C**FGAKYK**C**S**C**PFLWRFRRSAE**C**H**C**KKGWAWTAI**K**KRS**C**HNRYQWSG	95	B6DD30.1
Ls1e	RMALPPGAV**C**IGHKSD**C**Q**C**FGAKYK**C**S**C**PFLWRFRRSAK**C**H**C**RKGWAWTAI**K**KRS**C**HNRYQWSG	90	B6DD33.1
A0A4Y5UGQ5_CUPSA	RFMLRVGAV**C**DGNKSD**C**Q**C**LGKWIK**C**G**C**PFLWPMR-SGP**C**H**C**TKGRRYTYN**K**KLS**C**SNRYLWAS	57	QDC23149.1
S5MYD7_9ARAC	RKSLPEGAE**C**DGDGSD**C**Q**C**YGKWHK**C**G**C**PFFWKMR-GLK**C**H**C**TWGMKHT**C**ITKLS**C**PNRGEWGL	53	AGR53464.1
ω-agatoxin-1A	AKALPPGSV**C**DGNESD**C**K**C**YGKWHK**C**R**C**PWKWHFTGEGP**C**T**C**EKGMKHT**C**ITKLH**C**PNKAEWGL	48	P15969.2
	* *: * *. ***:* * ** **: * : * * * * .* * *: *		

[a]*The protein sequence data reported in this paper will appear in the UniProt Knowledgebase under the accession number C0HLR8. Asterisks represent conserved amino acids. U2-lycotoxin-Ls1b and U2-lycotoxin-Ls1e are from* Lycosa singoriensis; *A0A4Y5UGQ5_CUPSA is from* Cupiennius salei; *S5MYD7_9ARAC is from* Dolomedes mizhoanus; *ω-agatoxin-1A is from* Agelenopsis aperta.

measurements, rOsu1 binds to $hK_v1.5$ in a non-reversible manner (**Supplementary Figure S4**). Panel B of **Figure 2** displays part of the I-V curve. The ionic currents were measured under controlled conditions and were elicited from −100 mV holding potential to different depolarizing potentials: from −10 mV up to +50 mV. The appropriate membrane potential values were indicated next to the traces and the tau values coming from a single-exponential fitting. Panel B also compares the tau values seen in panel A measured in the venom's presence of Osu1 (natural or recombinant) with the tau values measured under different membrane potentials. So, the tau values obtained in panel A were compared to those of panel B; in this way, we observe some of the effects caused by venom and Osu1 (natural or recombinant). We can conclude that the whole venom caused a shift of about 20–30 mV, while Osu1 (both natural and synthetic/recombinant) affected a variation roughly 30–40 mV.

Secondary Structure and Proposed Structural Model

The CD values for the rOsu1 had a minimum and maximum spectrum around 206 and 192 nm, respectively, which represents antiparallel β-sheets (Little et al., 1998). Additionally, α-helix structures were also apparent by another observed minimum at 220 nm (**Figure 5**). The CD spectrum was evaluated using the deconvolution software from Bestsel (Micsonai et al., 2018), in order to predict the percentages of the secondary structure of rOsu1. The predicted values were 13.6, 23.9, 16.1, 46.4% of α-helix, β-antiparallel, β-turns and random coil, respectively. Taking in account such data, and because the comparison with native Osu1 was not possible because of the low amounts remaining from the crude venom, we decide to compare the rOsu1 secondary structure with that of an α/β motif, which is represented by rCssII, a

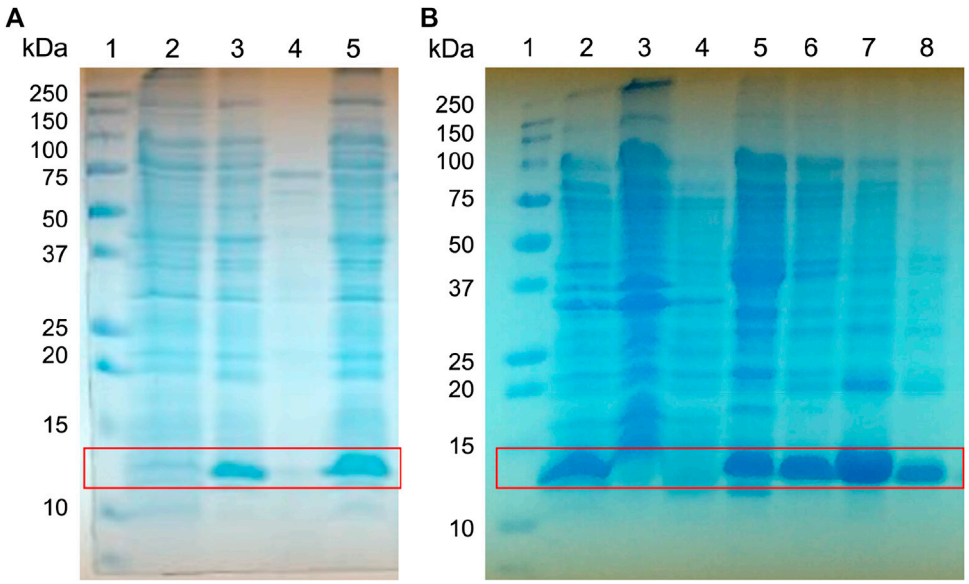

FIGURE 3 | Expression screening of the fusion protein His-Tag-Osu1. Whole-cell lysates were analyzed by reducing **(A)** 15% SDS-PAGE, for the screening of His-Tag-Osu1 expression, identifying the recombinant protein. 1) Molecular weight markers. 2. Non-induced cells. 3. Induced cells. 4. Soluble fraction. 5. Inclusion bodies lysates; and by **(B)** 15% Gel SDS-PAGE, for purification of inclusion bodies using a NiNTA column. 1. Molecular weight marker. 2. Inclusion bodies lysate. 3. Recirculating. 4. First wash with GdHCl 6M, Tris HCl pH 8, 50 mM. 5. Second wash with GdHCl 6 M, Imidazole 40 mM, Tris HCl pH 8, 50 mM. 6–8. Elutions with GdHCl 6M, Imidazole 400 mM, Tris HCl pH 8, 50 mM.

recombinant neurotoxin from the venom of the scorpion *Centruroides suffusus suffusus* (Estrada et al., 2007; Saucedo et al., 2012). The rCssII also contains an N-terminal poly His-tag, four disulfide bridges, representing a structure with α-helix and β-antiparallel secondary structures. The rCssII had similar CD spectrum as rOsu1; so rOsu1 most likely contain both secondary structures (α-helix and β-antiparallel). Moreover, the CD spectrum of rOsu1 was compared to the CD spectrum of a short "three-finger" recombinant (also with poly His-tag) neurotoxin named ScNtx. Short three-finger toxins are from elapid venoms, and they also contain four disulfides bridged peptides, but its secondary structure is mainly antiparallel (de la Rosa et al., 2018). The CD spectrum of the short "three-finger" neurotoxin differs from that of the rOsu1 and rCssII, suggesting that indeed the secondary structure of rOsu1 and rCssII are not completely β-antiparallel.

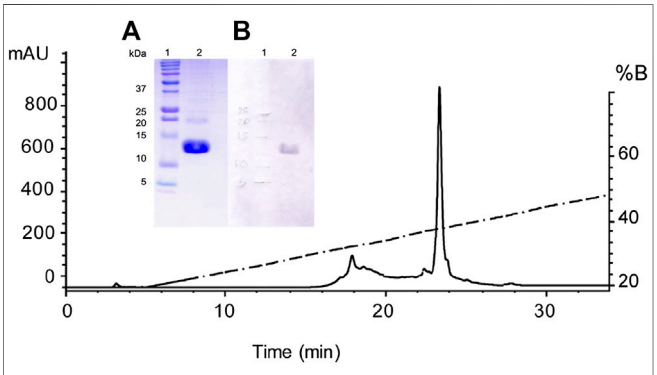

FIGURE 4 | Purification of the recombinant Osu1 by RP-HPLC. Chromatographic separation of the Ni-NTA eluate by RP-HPLC using an analytical C_{18} column and a gradient of aqueous acetonitrile containing 0.1% TFA, starting after 5 min from 20 to 60% CH_3CN during 40 min at a flow rate of 1 ml/min. Inside figure; **(A)** A 15% SDS-PAGE showing in lane 1 the molecular weight markers in kDa, and in lane 2, the pure recombinant Osu1 from the HPLC chromatogram obtained at the retention time of 23.5 min; and **(B)** A Western-blot showing in lane 1 the molecular weight markers in kDa, and in lane 2, the pure recombinant Osu1 from the HPLC chromatogram obtained at the retention time of 23.5 min developed using an anti-His antibody.

Four *in silico* models were created to propose a three-dimensional structure of Osu1 (**Supplementary Figure S5**). Interestingly, three out of the four protein model programs used (I-Tasser, Modeller, and Swiss-Model) gave similar disulfide bond patterns (residues Cys28-Cys40, Cys10-Cys26, Cys19-Cys42, and Cys17-Cys56). The modeling of proteins located in the "twilight zone" (20–35% protein identity, according to Doolittle, 1986), such as Osu1 concerning OtTx1a (27%), is considered a difficult problem to solve (Doolittle, 1986; Peng and Xu, 2010). Even though, the correct oxidation of all Cys, the same disulfide bond arrangement, and the similar 3D structure (double

TABLE 3 | Paralytic and lethal activity of Osu1 and rOsu1.

Peptide	PD_{50} crickets		LD_{50} crickets	
	(μg/g)	(pmol/g)	(μg/g)	(pmol/g)
Control (H_20)	—		—	
Native Osu1	0.05 (0.01–0.08)	6.6 (1.3–10.6)	<0.1	<13.3
rOsu1	0.27 (0.23–0.27)	36.1 (30.7–36.1)	0.53 (0.49–0.54)	70.8 (65.5–72.2)

95% confidence intervals (CI) are shown in parentheses.

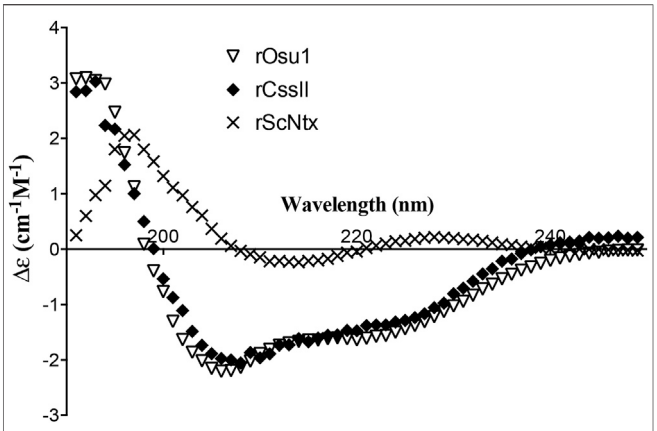

FIGURE 5 | Circular dichroism of recombinant neurotoxins. rOsu1, a recombinant neurotoxin from the venom of the spider *Oculicosa supermirabilis* (This work). rCssII, a recombinant neurotoxin from the venom of the scorpion *Centruroides suffusus suffusus* (Estrada et al., 2007). ScNtx a consensus short "three-finger" recombinant neurotoxin from elapid venom (de la Rosa et al., 2018).

antiparallel strand) presented by those three modeling programs allow us to propose a 3D structure for Osu1. Interestingly, even though the structure of OtTx1a, used as a template, has an ICK-type disulfide bridge arrangement, the *in silico* Osu1 structure generated with such protein structure programs did not inherit the three-dimensional arrangements of the template. Also, three models (Modeller, Swiss-Model and Robetta) predicted an β-antiparallel and an α-helix secondary structures. According to the CD spectrum of rOsu1, a small α-helix of 10–11 residues may be formed; that is 13.6% of α-helix in the 80 residues of rOsu1. The three models predict an α-helix between positions Cys42 to Cys56. From such three rOsu1 models, the one created by Modeller (**Figure 6**) was selected to represent the possible structure of Osu1. That model harmonizes with the CD spectrum, has the lowest RMSD value (3.8 Å) of the main chain (N, C, CA, and O). It holds the best percentages of structural quality for the phi and psi angles of 90.9% in the most favorable regions of the Ramachandran plot, giving confidence to such *in silico* model when compared to the other Osu1 models created by I-Tasser or Swiss-Model regarding the template OtTx1a (see **Supplementary Table S3** and **Supplementary Figure S6**). Since the structure created with Modeller, as well as the structures generated with I-Tasser and Swiss-Model, presented the disulfide arrangement Cys28-Cys40, Cys10-Cys26, Cys19-Cys42, and Cys17-Cys56 (**Figure 6**, top), which is not common in spider peptides motifs (Klint et al., 2012; Langenegger et al., 2019). The mentioned results allow us to speculate that Osu1 represents a new family of spider toxins (**Figure 7**). According to Klint et al. (2012), the disulfide pairing of OtTx1a seems to belong to the NaSpTx family #6 (**Figure 7**), but Osu1 certainly did not fix in the same spider toxin family. Here our intention is not to propose Osu1 as new Na_v spider toxin, but to use the Klint et al. spiders' toxin classification to show the novel amino acid sequence between Cys residues, and the possible disulfide-pairing motif of Osu1 (**Figure 7**). That is, Klint et al. (2012) classified most of the spider amino acid sequences and possible disulfide bridges for Na_v spider peptide toxins. In addition, in their classification, they also included specific spider peptide sequences for K_v, Ca_v, and TRP ion channels as well as spider peptide sequences without specific targets. Osu1 does not fix in any of the spider toxin families proposed. So, the speculation that Osu1 may represent a new family of spider peptide toxins based on its possible disulfide bond motif (based on

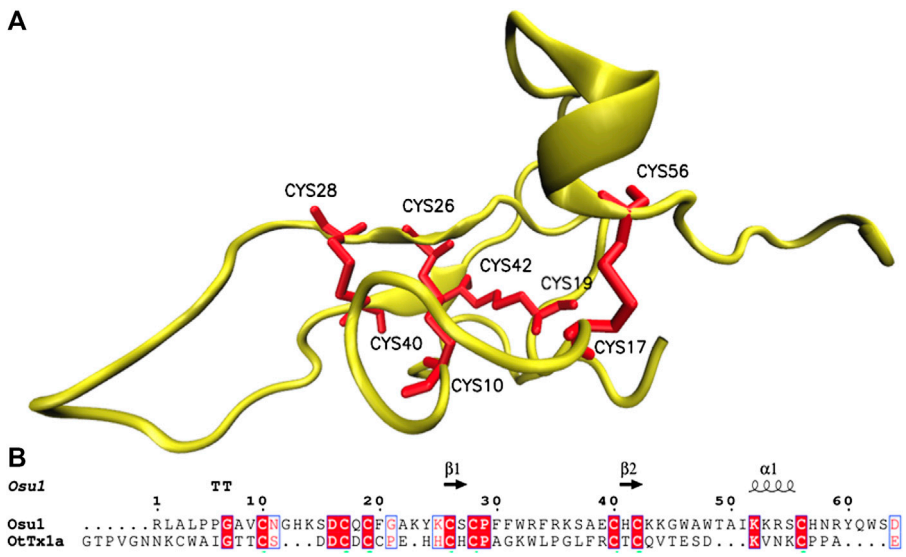

FIGURE 6 | Structural model of Osu1. The structure was generated using Modeller, based on the solved structure of OtTx1a (PDB: 2n86), and it presents a disulfide pairing of Cys28-Cys40, Cys10-Cys26, Cys19-Cys42, and Cys17-Cys56. The protein alignment between Osu1 and OtTx1a showing residues involve in secondary structure is shown below (T means β-turns and the arrows correspond to the antiparallel β-structure).

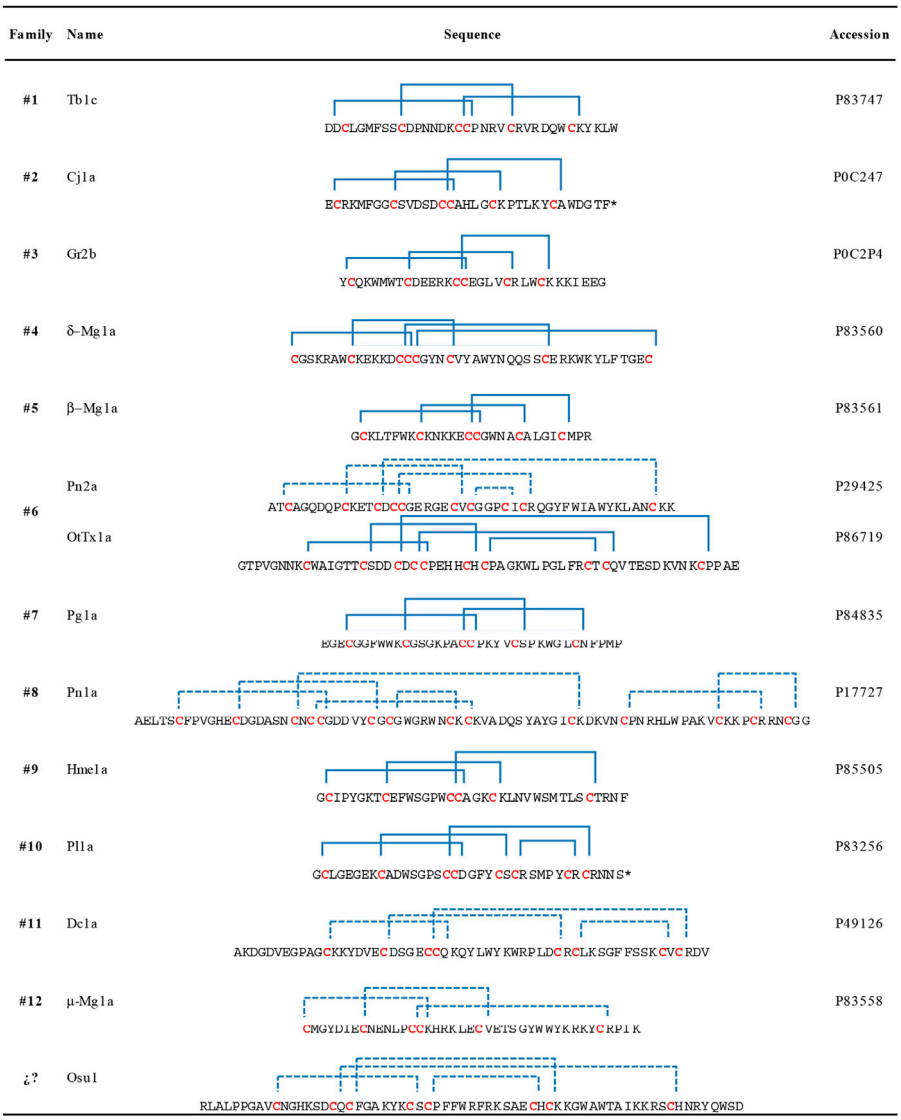

FIGURE 7 | Amino acid sequences and disulfide pairing of a representative member of the proposed families of spider sodium channel toxins, according to Klint et al. (2012) including the proposed primary structure and possible disulfide pairing in Osu1 as a new member of spider toxins. A primary structure of a representative member of each family is shown. Disulfide bridges are colored blue, and blue dotted lines represent predicted disulfide bond connectivities that have not been experimentally validated. Asterisks at the C-terminal mean C-amidation. Here our intention is not to propose Osu1 as new Na_v spider toxin, but to use the Klint *et al.* spiders' toxin classification to show the novelty of the amino acid sequence between Cys residues, and the possible disulfide-pairing motif of Osu1. Toxin names are based on the rational nomenclature devised for spider-venom peptides (King et al., 2008).

bioinformatics model), and three-dimensional structure must be confirmed by experimental techniques such as NMR or X-Ray crystallography.

DISCUSSION

To our knowledge, this is the first study examining the venom of the spider *Oculicosa supermirabilis*. A database search was performed to find out toxins of peptide nature similar to Osu1. So, transcriptomic and proteomic reports of spiders belonging to the phylogenetically distant families, such as Sparassidae, Theraphosidae, Viridasiidae, and Theridiidae, have described spider peptides precursors with some degree of identity to Osu1. However, still, none have been detected in such spider venoms by mass spectrometry or N-terminal peptide sequencing (Oldrati et al., 2017). Nonetheless, only peptide toxins with high identities (90–95%) to Osu1 were found in the spider gland transcriptomes, mainly from the Lycosidae and Pisauridae families (Zhang et al., 2010; Jiang et al., 2013). According to this, *O. supermirabilis* belongs to the Lycosidae family but has been phylogenetically related to the Pisauridae family (Zhang et al., 2010; Jiang et al., 2013).

Besides the novelty of its primary structure, Osu1 can modify the ion currents of the $hK_v1.5$ in contrast to other K_v peptide inhibitors. To our best knowledge, Osu1 is the first peptide that modifies and inhibits the ion current flowing through $hK_v1.5$ at a given membrane potential. Based on our results, Osu1 does not bind to the $hK_v1.5$ pore, but most likely, it adheres to the VSD of the $hK_v1.5$. Consequently, Osu1 could not be considered a pore blocker, since it prevents $hK_v1.5$ from opening at given membrane potential. Because of the limited amounts of natural and rOsu1 peptide to conduct the electrophysiological assays, we performed the measurements in a limited way. So, we could not determine a dose-response curve or selectivity measurements over other ion channels.

On the other hand, from the insecticidal perspective, the Osu1 showed paralysis/death effects on crickets, and phenotypically, it induced an excitatory slow-onset impact on them, leading to irreversible spastic paralysis. According to Johnson et al. (1998), this type of effect suggests that the molecular target is likely to be an ion channel found in the CNS. The insecticidal activity of Osu1 is in the range of some spider neurotoxins that affect insects' Na_v channels, such as μ-agatoxin-Aa1a from the spider *Agelenopsis aperta* (LD_{50} of 75.0 pmol/g over *Musca domestica*) (Skinner et al., 1989) and μ-diguetoxin-Dc1a from the spider *Diguetia canities* (PD_{50} 231.0 pmol/g and LD_{50} 13.0 pmol/g, over *Lucilia cuprina*) (Bende et al., 2014). Additionally, the insecticidal activity of Osu1 is in the range of some spider neurotoxins that affect insects' Ca_v channels, such as ω-hexatoxin-Hv1e from the spider *Hadronyche versuta* (LD_{50} of 103 pmol/g over *Acheta domesticus*) (Wang et al., 2001). In contrast to its insecticidal activity, Osu1 was not active in mice when injected intracranially at 0.5 μg/g or 66 pmol/g mouse, compared to spider peptides toxic to mammals such κ-theraphotoxin-Hs1a, a non-selective K_v toxin, from the spider *Haplopelma schmidti*, which has an LD_{50} of 0.25 μg/g or 41.5 pmol/g *Mus musculus* after intracranial injection (Liang, 2004). Moreover, the Osu1 activity is not significant compared to the toxic μ-ctenitoxin-Pn1a from the spider *Phoneutria nigriventer*, which has an LD_{50} of 0.047 μg/g or 5.5 pmol/g *Mus musculus* after intracerebroventricular injection (Diniz et al., 1990). Since Osu1 also showed a modulating effect on the $hK_v1.5$ channel's opening, this peptide toxin could be considered as promiscuous, like many other spider toxins with dual or multiple activities toward different receptors. That is, although potassium channels are common targets for various animal peptide toxins, few of such peptide toxins are also paralytic/lethal to insects affecting Na_v and/or Ca_v ion channels.

Concerning the structure of Osu1, although it is deserving of remembering that any molecular model is uncertain, structural model algorithms have undergone significant development in the last few years to the point that they can predict full structures based just on primary structures. So, the proposed cysteine pattern here (Cys28-Cys40, Cys10-Cys26, Cys19-Cys42, and Cys17-Cys56) in Osu1 does not belong to any of the known disulfide arrangements in spider toxins, such as the inhibitor cystine knot (ICK), disulfide-directed β-hairpin motif (DDH), Kunitz-type, Colipase or MIT1-like, or helical arthropod-neuropeptide-derived motifs (Langenegger et al., 2019). Remarkably, the cysteine arrangement without two cysteine residues in a row is also quite uncommon for large spiders' peptide toxins. Only in few spider venoms have been reported, such as the ω-agatoxin-IA, a heterodimeric protein with five disulfide bridges which inhibits insect voltage-sensitive Ca^{2+} channels (Pocock and Nicholls, 1992). The sequence identity of ω-agatoxin-IA compared to Osu1 is just 48%. Indeed, the position of cysteine residues in Osu1 resembles in some way to the insecticidal spider toxins from theraphosids such as *Brachypelma, Lasiodora, Grammostola, Chilobrachys, Aphonopelma*, and *Haplopelma* among others, which disulfide connections are considered as disulfide-directed β-hairpin (DDH) motifs. However, such spider toxins are far shorter (*ca* 40 mer) and contain only three disulfide bridges.

Accordingly, Osu1 may be considered a member of a new spider peptide family since its primary structure (XnCX6CX1CX6CX1CX11CX1CX13CXn) and disulfide bridge patterns seem to differ significantly from those primary structures of the families previously proposed (Klint et al., 2012) (**Figure 7**).

CONCLUDING REMARKS

Osu1 seems to represent a new type of spider toxins based on its primary structures, possible cysteine-bond motif, and modulating effect on $hK_v1.5$. Osu1 is insecticidal and might be considered non-toxic to vertebrates. Given that Osu1 can be synthesized by recombinant means and folded correctly, this peptide could be crucial for studying AF and its implications in heart failure, strokes, and other heart-related complications.

DATA AVAILABILITY STATEMENT

The protein sequence data reported can be found in the UniProt Knowledgebase under the accession number C0HLR8.

ETHICS STATEMENT

All animal experiments were previously approved by the Bioethics Committee of the Biotechnology Institute (project No. A1-S-8005) and carried out following appropriate regulations.

AUTHOR CONTRIBUTIONS

SC-A and IA performed the native Osu1 purification; TO-P, FZ, and GC elucidated the primary structure of Osu1; LC-G designed and cloned the Osu1; DA, HC, and LC-G expressed the Osu1; DA and HC performed the biological activity in crickets and mice; FP,

AC, and JB performed the electrophysiological experiments; DA and PM-G performed the Osu1 structural models; FP, GP, and GC financed, reviewed and wrote the manuscript.

FUNDING

This work received funding from the Dirección General de Asuntos del Personal Académico (DGAPA-UNAM) grant number IN203118 awarded to GC, and from FORDECYT "Venenos y Antivenenos" grant number 303045. The following grants also supported OTKA Bridging Fund 1G3DBKB0BFPF247 (FP); OTKA K119417 (GP); EFOP-3.6.1-16-2016-00022, Ministry of Human Capacities, Hungary (GP); GINOP-2.3.2-15-2016- 00015 (GP). DA and SC-A are MSc students from Programa de Maestría en Ciencias Bioquímicas. PM-D and JB are PhD students from Programa de Doctorado en Ciencias Bioquímicas and Ciencias Biomédicas, both at the Universidad Nacional Autónoma de México (UNAM). All four postgraduate students are supported by CONACyT-México (Fellowship CVUs No. 925354, No. 884453, No. 775900 and No. 487264/415092, respectively).

ACKNOWLEDGMENTS

We acknowledge Paul Gaytán, M.C. Eugenio López-Bustos, and Q.I. Santiago Becerra from Unidad de Síntesis y Secuenciación de ADN at Instituto de Biotecnología.

SUPPLEMENTARY MATERIAL

The Supplementary Material for this article can be found online at: https://www.frontiersin.org/articles/10.3389/fphar.2020.563858/full#supplementary-material.

REFERENCES

Ali, A. M., Atmaj, J., Van Oosterwijk, N., Groves, M. R., and Dömling, A. (2019). Stapled peptides inhibitors: a new window for target drug discovery. *Comput. Struct. Biotechnol. J.* 17, 263–281. doi:10.1016/j.csbj.2019.01.012

Bajaj, S. and Han, J. (2019). Venom-derived peptide modulators of cation-selective channels: friend, foe or frenemy. *Front. Pharmacol.* 10, 58. doi:10.3389/fphar.2019.00058

Bende, N. S., Dziemborowicz, S., Mobli, M., Herzig, V., Gilchrist, J., and Wagner, J., et al. (2014). A distinct sodium channel voltage-sensor locus determines insect selectivity of the spider toxin Dc1a. *Nat. Commun.* 5, 4350. doi:10.1038/ncomms5350

Borrego, J., Clement, H., Corrales-García, L.-L., Arenas, I., and Corzo, G. (2020). Key amino acid residues involved in mammalian and insecticidal activities of Magi4 and Hv1b, cysteine-rich spider peptides from the delta-atracotoxin family. *Amino Acids* 52 (3), 465–475. doi:10.1007/s00726-020-02825-4

Brunner, M., Kodirov, S. A., Mitchell, G. F., Buckett, P. D., Shibata, K., and Folco, E. J.E. J., et al. (2003). *In vivo* gene transfer of Kv1.5 normalizes action potential duration and shortens QT interval in mice with long QT phenotype. *Am. J. Physiol. Heart Circ. Physiol.* 285 (1), H194–H203. doi:10.1152/ajpheart.00971.2002

Clairfeuille, T., Cloake, A., Infield, D. T., Llongueras, J. P., Arthur, C. P., and Li, Z. R.Z. R., et al. (2019). Structural basis of alpha-scorpion toxin action on Nav channels. *Science* 363 (6433), aav8573. doi:10.1126/science.aav8573

Corzo, G., Adachi-Akahane, S., Nagao, T., Kusui, Y., and Nakajima, T. (2001). Novel peptides from assassin bugs (Hemiptera: reduviidae): isolation, chemical and biological characterization. *FEBS Lett.* 499 (3), 256–261. doi:10.1016/S0014-5793(01)02558-3

Corzo, G. and Escoubas, P. (2003). Pharmacologically active spider peptide toxins. *Cell. Mol. Life Sci.* 60, 2409–2426. doi:10.1007/s00018-003-3108-6

Corzo, G., Papp, F., Varga, Z., Barraza, O., Espino-Solis, P. G., and Rodríguez de la Vega, R. C.R. C., et al. (2008). A selective blocker of Kv1.2 and Kv1.3 potassium channels from the venom of the scorpion Centruroides suffusus suffusus. *Biochem. Pharmacol.* 76 (9), 1142–1154. doi:10.1016/j.bcp.2008.08.018

de la Rosa, G., Corrales-García, L. L., Rodriguez-Ruiz, X., López-Vera, E., and Corzo, G. (2018). Short-chain consensus alpha-neurotoxin: a synthetic 60-mer peptide with generic traits and enhanced immunogenic properties. *Amino Acids* 50 (7), 885–895. doi:10.1007/s00726-018-2556-0

Di Tommaso, P., Moretti, S., Xenarios, I., Orobitg, M., Montanyola, A., Chang, J. M., et al. (2011). T-Coffee: a web server for the multiple sequence alignment of protein and RNA sequences using structural information and homology extension. *Nucleic Acids Res.* 39 (Web Server issue), W13–W17. doi:10.1093/nar/gkr245

Dixon, W. J. (1965). The Up-and-Down method for small samples. *J. Am. Stat. Assoc.* 60, 967–978. doi:10.2307/228339810.1080/01621459.1965.10480843

Doolittle, R. F. (1986). *Of URFS and ORFS: a primer on how to analyze derived amino acid sequences*. Mill Valley, CA: University Science Books.

Dunbrack, R. L. (2004). "Procheck,"in *Dictionary of bioinformatics and computational biology*. Editors J. M. Hancock and M. J. Zvelebil (Hoboken, NJ: Wiley).

Ehrlich, J. R., Biliczki, P., Hohnloser, S. H., and Nattel, S. (2008). Atrial-selective approaches for the treatment of atrial fibrillation. *J. Am. Coll. Cardiol.* 51 (8), 787–792. doi:10.1016/j.jacc.2007.08.067

Ehrlich, J. R. and Nattel, S. (2009). Novel approaches for pharmacological management of atrial fibrillation. *Drugs* 69 (7), 757–774. doi:10.2165/00003495-200969070-00001

Estrada, G., Garcia, B. I., Schiavon, E., Ortiz, E., Cestele, S., and Wanke, E., et al. (2007). Four disulfide-bridged scorpion beta neurotoxin cssII: heterologous expression and proper folding *in vitro*. *Biochim. Biophys. Acta* 1770 (8), 1161–1168. doi:10.1016/j.bbagen.2007.04.006

Fedida, D., Wible, B., Wang, Z., Fermini, B., Faust, F., Nattel, S., et al. (1993). Identity of a novel delayed rectifier current from human heart with a cloned K+ channel current. *Circ. Res. Res* 73 (1), 210–216. doi:10.1161/01.res.73.1.210

Ford, J. W. and Milnes, J. T. (2008). New drugs targeting the cardiac ultra-rapid delayed-rectifier current (I Kur): rationale, pharmacology and evidence for potential therapeutic value. *J. Cardiovasc. Pharmacol.* 52 (2), 105–120. doi:10.1097/FJC.0b013e3181719b0c

Gouet, P., Courcelle, E., Stuart, D.I., and Metoz, F. (1999). ESPript: analysis of multiple sequence alignments in PostScript. *Bioinformatics* 15 (4), 305–308. doi:10.1093/bioinformatics/15.4.305

Grissmer, S., Nguyen, A. N., Aiyar, J., Hanson, D. C., Mather, R. J., Gutman, G. A., et al. (1994). Pharmacological characterization of five cloned voltage-gated K+ channels, types Kv1. 1, 1.2, 1.3, 1.5, and 3.1, stably expressed in mammalian cell lines. *Mol. Pharmacol.* 45 (6), 1227–1234.

Gunning, S. J., Chong, Y., Khalife, A. A., Hains, P. G., Broady, K. W., and Nicholson, G. M. (2003). Isolation of δ-missulenatoxin-Mb1a, the major vertebrate-active spider δ-toxin from the venom of Missulena bradleyi (Actinopodidae). *Fed. Eur. Biochem. Soc. Lett.* 554 (1–2), 211–218. doi:10.1016/s0014-5793(03)01175-x

Guo, X., Chen, W., Sun, H., and You, Q. (2016). Kv1.5 inhibitors for treatment of atrial fibrillation: a tradeoff between selectivity and non-selectivity. *Curr. Top. Med. Chem.* 16 (16), 1843–1854. doi:10.2174/1568026616666160315142647

Gutman, G. A., Chandy, K. G., Grissmer, S., Lazdunski, M., McKinnon, D., Pardo, L. A., et al. (2005). International Union of Pharmacology. LIII. Nomenclature and molecular relationships of voltage-gated potassium channels. *Pharmacol. Rev.* 57 (4), 473–38. doi:10.1124/pr.57.4.10

Humphrey, W., Dalke, A., and Schulten, K. (1996). VMD: visual molecular dynamics. *J. Mol. Graph.* 14 (1), 33–38, 27-8. doi:10.1016/0263-7855(96)00018-5

Jiang, L., Liu, C., Duan, Z., Deng, M., Tang, X., and Liang, S. (2013). Transcriptome analysis of venom glands from a single fishing spider Dolomedes mizhoanus. *Toxicon* 73, 23–32. doi:10.1016/j.toxicon.2013.07.005

Johnson, J. H., Bloomquist, J. R., Krapcho, K. J., Kral, R. M. J., Trovato, R., Eppler, K. G., et al. (1998). Novel insecticidal peptides from Tegenaria agrestis spider venom may have a direct effect on the insect central nervous system. *Arch. Insect. Biochem. Physiol.* 38, 19–31. doi:10.1002/(SICI)1520-6327(1998)38:1<19::AID-ARCH3>3.0.CO;2-Q

Kim, D. E., Chivian, D., and Baker, D. (2004). Protein structure prediction and analysis using the Robetta server. *Nucleic Acids Res.* 32 (Web Server issue), W526–W531. doi:10.1093/nar/gkh468

King, G. F., Gentz, M. C., Escoubas, P., and Nicholson, G. M. (2008). A rational nomenclature for naming peptide toxins from spiders and other venomous animals. *Toxicon* 52 (2), 264–276. doi:10.1016/j.toxicon.2008.05.020

Klint, J. K., Senff, S., Rupasinghe, D. B., Er, S. Y., Herzig, V., Nicholson, G. M., et al. (2012). Spider-venom peptides that target voltage-gated sodium channels: pharmacological tools and potential therapeutic leads. *Toxins* 60 (4), 478–491. doi:10.1016/j.toxicon.2012.04.337

Langenegger, N., Nentwig, W., and Kuhn-Nentwig, L. (2019). Spider venom: components, modes of action, and novel strategies in transcriptomic and proteomic analyses. *Toxins (Basel)* 11 (10), 611. doi:10.3390/toxins11100611

Liang, S. (2004). An overview of peptide toxins from the venom of the Chinese bird spider Selenocosmia huwena Wang [=Ornithoctonus huwena (Wang)]. *Toxicon* 43 (5), 575–585. doi:10.1016/j.toxicon.2004.02.005

Lip, G. Y. and Tse, H. F. (2007). Management of atrial fibrillation. *Lancet* 370 (9587), 604–618. doi:10.1016/S0140-6736(07)61300-2

Little, M. J., Wilson, H., Zappia, C., Cestèle, S., Tyler, M. I., Martin-Eauclaire, M.-F., et al. (1998). δ-Atracotoxins from Australian funnel-web spiders compete with scorpion α-toxin binding on both rat brain and insect sodium channels.*Fed. Eur. Biochem. Soc. Lett.* 439, 246–252. doi:10.1016/S0014-5793(98)01378-7

Logunov, D. V. and Gromov, A. V. (2011). Notes on the distribution of Oculicosa supermirabilis (araneae, Lycosidae). *Arachnol. Mittl.* 42, 48–51. doi:10.5431/aramit4208

Micsonai, A., Wien, F., Bulyaki, E., Kun, J., Moussong, E., Lee, Y. H., et al. (2018). BeStSel: a web server for accurate protein secondary structure prediction and fold recognition from the circular dichroism spectra. *Nucleic Acids Res.* 46 (W1), W315–W322. doi:10.1093/nar/gky497

Nicholson, G. M. and Graudins, A. (2002). Spiders of medical importance in the Asia-Pacific: atracotoxin, latrotoxin and related spider neurotoxins. *Clin. Exp. Pharmacol. Physiol.* 29, 785–794. doi:10.1046/j.1440-1681.2002.03741.x

Oldrati, V., Koua, D., Allard, P. M., Hulo, N., Arrell, M., Nentwig, W., et al. (2017). Peptidomic and transcriptomic profiling of four distinct spider venoms. *PLoS One* 12 (3), e0172966. doi:10.1371/journal.pone.0172966

Peng, J. and Xu, J. (2010). Low-homology protein threading. *Bioinformatics* 26 (12), i294–i300. doi:10.1093/bioinformatics/btq192

Pineda, S. S., Chaumeil, P. A., Kunert, A., Kaas, Q., Thang, M. W. C., Le, L., et al. (2018). ArachnoServer 3.0: an online resource for automated discovery, analysis and annotation of spider toxins. *Future Medicinal Chemistry* 34 (6), 1074–1076. doi:10.1093/bioinformatics/btx661

Pineda, S. S., Undheim, E. A., Rupasinghe, D. B., Ikonomopoulou, M. P., and King, G. F. (2014). Spider venomics: implications for drug discovery. *Future Med. Chem.* 6 (15), 1699–1714. doi:10.4155/fmc.14.103

Pocock, J. M. and Nicholls, D. G. (1992). A toxin (Aga-GI) from the venom of the spider Agelenopsis aperta inhibits the mammalian presynaptic Ca2+ channel coupled to glutamate exocytosis. *Eur. J. Pharmacol.* 226 (4), 343–350. doi:10.1016/0922-4106(92)90052-w

Quintero-Hernandez, V., Ortiz, E., Rendon-Anaya, M., Schwartz, E. F., Becerril, B., Corzo, G., et al. (2011). Scorpion and spider venom peptides: gene cloning and peptide expression. *Pharmacology & Therapeutics* 58 (8), 644–663. doi:10.1016/j.toxicon.2011.09.015

Ravens, U. (2010). Antiarrhythmic therapy in atrial fibrillation. *Pharmacol. Ther.* 128 (1), 129–5. doi:10.1016/j.pharmthera.2010.06.004

Santos, A. D., Imperial, J. S., Chaudhary, T., Beavis, R. C., Chait, B. T., and Hunsperger, J. P., et al. (1992). Heterodimeric structure of the spider toxin omega-agatoxin IA revealed by precursor analysis and mass spectrometry. *J. Biol. Chem.* 267, 20701–20705.

Saucedo, A. L., del Rio-Portilla, F., Picco, C., Estrada, G., Prestipino, G., and Possani, L. D., et al. (2012). Solution structure of native and recombinant expressed toxin CssII from the venom of the scorpion Centruroides suffusus suffusus, and their effects on Nav1.5 sodium channels. *Biochim. Biophys. Acta* 1824 (3), 478–5. doi:10.1016/j.bbapap.2012.01.003

Skinner, W. S., Adams, M. E., Quistad, G. B., Kataoka, H., Cesarin, B. J., and Enderlin, F. E., et al. (1989). Purification and characterization of two classes of neurotoxins from the funnel web spider, *Agelenopsis aperta*. *J. Biol. Chem.* 264 (4), 2150–21505.

Wang, X. H., Connor, M., Wilson, D., Wilson, H. I., Nicholson, G. M., and Smith, R., et al. (2001). Discovery and structure of a potent and highly specific blocker of insect calcium channels. *J. Biol. Chem.* 276 (43), 40306–40312. doi:10.1074/jbc.M105206200

Waterhouse, A., Bertoni, M., Bienert, S., Studer, G., Tauriello, G., Gumienny, R., et al. (2018). SWISS-MODEL: homology modelling of protein structures and complexes. *Nucleic Acids Res* 46 (W1), W296–W303. doi:10.1093/nar/gky427

Webb, B. and Sali, A. (2016). Comparative pProtein sStructure mModeling uUsing MODELLER. *Curr. Protoc. Protein Sci.* 86, 2.9.1–2.9.37. doi:10.1002/cpps.20

Wettwer, E. and Terlau, H. (2014). Pharmacology of voltage-gated potassium channel Kv1.5--impact on cardiac excitability. *Curr. Opin. Pharmacol.* 15, 115–121. doi:10.1016/j.coph.2014.02.001

Wu, S. and Zhang, Y. (2007). LOMETS: a local meta-threading-server for protein structure prediction. *Nucleic Acids Res.* 35 (10), 3375–3382. doi:10.1093/nar/gkm251

Yang, J. and Zhang, Y. (2015). I-TASSER server: new development for protein structure and function predictions. *Nucleic Acids Res.* 43 (W1), W174–W181. doi:10.1093/nar/gkv342

Zhang, Y., Chen, J., Tang, X., Wang, F., Jiang, L., Xiong, X., et al. (2010). Transcriptome analysis of the venom glands of the Chinese wolf spider Lycosa singoriensis. *Zoology (Jena)* 113 (1), 10–18. doi:10.1016/j.zool.2009.04.001

Zhu, J., Gomez, B., Watanabe, I., and Thornhill, W. B. (2005). Amino acids in the pore region of Kv1 potassium channels dictate cell-surface protein levels: a possible trafficking code in the Kv1 subfamily. *Biochem. J.* 388 (Pt 1), 355–362. doi:10.1042/BJ20041447

Conflict of Interest: The authors declare that the research was conducted in the absence of any commercial or financial relationships that could be construed as a potential conflict of interest.

The reviewer EU declared a past co-authorship with one of the authors GP to the handling editor.

frontiers in Pharmacology

ORIGINAL RESEARCH
published: 28 January 2021
doi: 10.3389/fphar.2020.633679

Spider Venom Peptide Pn3a Inhibition of Primary Afferent High Voltage-Activated Calcium Channels

Jeffrey R. McArthur[1]†, Nehan R. Munasinghe[2]†, Rocio K. Finol-Urdaneta[1,3], David J. Adams[1] and Macdonald J. Christie[2]*

[1]Illawarra Health and Medical Research Institute (IHMRI), University of Wollongong, Wollongong, NSW, Australia, [2]Discipline of Pharmacology, University of Sydney, Sydney, NSW, Australia, [3]Electrophysiology Facility for Cell Phenotyping and Drug Discovery, IHMRI, Wollongong, NSW, Australia

Despite potently inhibiting the nociceptive voltage-gated sodium (Na_v) channel, $Na_v1.7$, μ-theraphotoxin Pn3a is antinociceptive only upon co-administration with sub-therapeutic opioid agonists, or by itself at doses >3,000-fold greater than its $Na_v1.7$ IC_{50} by a yet undefined mechanism. Na_v channels are structurally related to voltage-gated calcium (Ca_v) channels, Ca_v1 and Ca_v2. These channels mediate the high voltage-activated (HVA) calcium currents (I_{Ca}) that orchestrate synaptic transmission in nociceptive dorsal root ganglion (DRG) neurons and are fine-tuned by opioid receptor (OR) activity. Using whole-cell patch clamp recording, we found that Pn3a (10 μM) inhibits ~55% of rat DRG neuron HVA-I_{Ca} and 60–80% of $Ca_v1.2$, $Ca_v1.3$, $Ca_v2.1$, and $Ca_v2.2$ mediated currents in HEK293 cells, with no inhibition of $Ca_v2.3$. As a major DRG I_{Ca} component, $Ca_v2.2$ inhibition by Pn3a (IC_{50} = 3.71 ± 0.21 μM) arises from an 18 mV hyperpolarizing shift in the voltage dependence of inactivation. We observed that co-application of Pn3a and μ-OR agonist DAMGO results in enhanced HVA-I_{Ca} inhibition in DRG neurons whereas co-application of Pn3a with the OR antagonist naloxone does not, underscoring HVA channels as shared targets of Pn3a and opioids. We provide evidence that Pn3a inhibits native and recombinant HVA Ca_vs at previously reportedly antinociceptive concentrations in animal pain models. We show additive modulation of DRG HVA-I_{Ca} by sequential application of low Pn3a doses and sub-therapeutic opioids ligands. We propose Pn3a's antinociceptive effects result, at least in part, from direct inhibition of HVA-I_{Ca} at high Pn3a doses, or through additive inhibition by low Pn3a and mild OR activation.

Keywords: antinociceptive, calcium channel, dorsal root ganglion, high-voltage activated, opioids, pain, spider venom-derived peptide

OPEN ACCESS

Edited by:
Jean-Marc Sabatier, Aix-Marseille Université, France

Reviewed by:
Victor Ruiz-Velasco, Pennsylvania State University, United States
Rajesh Khanna, University of Arizona, United States

***Correspondence:**
Jeffrey R. McArthur
jeffreym@uow.edu.au

†*These authors share first authorship*

Specialty section:
This article was submitted to Pharmacology of Ion Channels and Channelopathies, a section of the journal Frontiers in Pharmacology

Received: *25 November 2020*
Accepted: *30 December 2020*
Published: *28 January 2021*

Citation:
McArthur JR, Munasinghe NR, Finol-Urdaneta RK, Adams DJ and Christie MJ (2021) Spider Venom Peptide Pn3a Inhibition of Primary Afferent High Voltage-Activated Calcium Channels. Front. Pharmacol. 11:633679. doi: 10.3389/fphar.2020.633679

INTRODUCTION

Physiological pain (acute, nociceptive) functions as early warning to protect the organism from injury. In contrast, pathological pain (chronic, neuropathic) originates from maladaptive operation of the nervous system. The sensory nervous system (primary afferent neurons, spinal interneurons, ascending tracts, and supraspinal areas) mediates pain signaling to the brain. Upon damage, nociceptors become sensitized/activated leading to opening of excitatory voltage-gated sodium (Na_v) and calcium (Ca_v) channels causing the subsequent firing of action potentials along sensory axons to the spinal cord. Induction and maintenance of central

sensitization depend on peripheral nociceptors regarded as important targets for analgesics, with most efforts dedicated to the development of peripheral $Na_v1.7$, $Na_v1.8$, and $Na_v1.9$ modulators as potential therapeutics.

Loss-of-function mutation of the *SCN9A* gene that codes for $Na_v1.7$ leads to congenital insensitivity to pain (Cox et al., 2006), whereas *SCN9A* gain-of-function mutations causes paroxysmal extreme pain disorder and primary erythromelalgia (Dib-Hajj et al., 2008). These observations lead to increased interest in discovery of a highly selective and potent inhibitors of $Na_v1.7$ to reduce the side effects seen in pan Na_v channel inhibitors. However, $Na_v1.7$ inhibitors have for the most part failed to reproduce the pain-free state observed in chronic insensitivity to pain (CIP) (Eagles et al., 2020). Subsequently it was shown that genetic deletion of *SCN9A* in both mice and humans, that the absence of functional $Na_v1.7$ but not $Na_v1.8$, increases endogenous opioid receptor (OR) analgesia via upregulation of the enkephalin precursor *Penk* mRNA, which could be inhibited by the OR antagonist, naloxone (Minett et al., 2015). μ-Theraphotoxin Pn3a (μ-TRTX-Pn3a), a three disulphide bridged, 35 amino acid peptide isolated from the venom of the South American tarantula *Pamphobeteus nigricolour*, is a selective and potent $Na_v1.7$ channel inhibitor (Deuis et al., 2017). Yet, despite Pn3a's high potency against $Na_v1.7$-mediated currents, administration of 3 mg/kg of the peptide fails to produce analgesia in various animal pain models (Deuis et al., 2017). Nevertheless, local (3 μM) or systemic treatment (3 mg/kg) Pn3a administration causes antinociceptive behavior in mouse models of acute postsurgical pain. Interestingly, co-administration of Pn3a (1 mg/kg) with sub-therapeutic doses of opioids results in significant analgesia/anti-allodynia advocating for synergistic analgesic effects in rodent models of pain (Deuis et al., 2017; Mueller et al., 2019). In these reports, opioid receptor (OR) modulators naloxone and oxycodone did not alter $Na_v1.7$ currents, nor Pn3a affected μ-/δ-/κ- OR mediated signaling (Mueller et al., 2019). Thus, the mechanisms behind the observed antinociceptive effects seemed unclear.

Animal toxins interacting with voltage-gated ion channels (VGICs) typically fall into two groups: pore blocking toxins, which sterically and electrostatically inhibit ion permeation (Hui et al., 2002; Finol-Urdaneta et al., 2020), and gating modifiers, that interact with the voltage sensor domain (Swartz and MacKinnon, 1995), such as Pn3a (Mueller et al., 2020). Recently, more detailed characterization of toxins and drugs once thought "selective" for a particular ion channel have proven active against others. Pore blocking Na_v channel toxins cross-react with other targets, include tetrodotoxin (Na_v/Ca_v), saxitoxin ($Na_v/K_v/Ca_v$) and μ-conotoxin PIIIA ($Na_v/K_v/Na_vBac$) (McArthur et al., 2011; Leipold et al., 2017; Finol-Urdaneta et al., 2019); whereas voltage-sensing domain (VSD) gating modifier toxins like ProTxI ($Na_v/K_v/Ca_v$/TRPA1) (Middleton et al., 2002; Bosmans et al., 2008; Bladen et al., 2014; Gui et al., 2014), ProTxII (Na_v/Ca_v) (Middleton et al., 2002; Bladen et al., 2014), kurtoxin (Na_v/Ca_v) (Chuang et al., 1998), Hanatoxin ($K_v/Na_v/Ca_v$) (Swartz and MacKinnon, 1995; Li-Smerin and Swartz, 1998; Bosmans et al., 2008), and JZTX-I (Na_v/K_v) (Xiao et al., 2005; Yuan et al., 2007). Furthermore, small molecule compounds modulating VSDs include capsaicin, and capsazepine (TRPV1/K_v/Ca_v) (Kuenzi and Dale, 1996; Caterina et al., 1997; McArthur et al., 2019) to name a few.

Given the structural conservation between Na_vs and Ca_vs, the actions of Pn3a over native and recombinant Ca_v channels were investigated. Whole-cell patch clamp recording was used to assess Pn3a's effects on high voltage-activated (HVA) calcium currents (I_{Ca}) in rat DRG neurons and heterologously expressed Ca_v channels in HEK293 cells. Our results show that Pn3a inhibits HVA I_{Ca} in isolated rat DRG neurons at concentrations reported to produce analgesia. Importantly, Pn3a's inhibitory effect over I_{Ca} was additive to that of sub-therapeutic opioid receptor agonists highlighting concerted inhibition of HVA by Pn3a/opioids as a potential component of the antinociceptive effects observed in animal pain models.

METHODS

Dorsal Root Ganglion Isolation and Culture

Rats were purchased from the Animal Resources Center (Perth, Australia; 3–5 weeks old male Sprague Dawley rats) kept in groups of four, on a 12 h–12 h light–dark cycle at 22 ± 2°C with environment enrichment inside individually ventilated cages. Food and water were provided *ad libitum*. In total, DRG neurons from 30 rats were used in this study. To extract neurons, rats were decapitated under anesthesia with 4% isoflurane in the air. Experiments were conducted under the project number 2015/830 approved by the Animals Ethics Committee (AEC) at the University of Sydney, NSW, Australia. AEC guidelines comply with the 'Australian code of practice for the care and use of animals for scientific purposes', the ARRIVE guidelines on reporting experiments involving animals.

Spinal level L3–L5 DRG were removed and placed in ice-cold HEPES-buffered saline (HBS) composed of (in mM): 154 NaCl, 2.5 KCl, 1.8 $CaCl_2$, 1.5 $MgCl_2$, 10 HEPES, and 10 glucose (pH 7.4, 330 ± 5 mOsm). Iridectomy scissors were utilized to cut up ganglia before incubation at 37°C for 15 min in oxygenated HBS containing 5 mg ml^{-1} collagenase type 2 (Worthington Biochemical Corp, Lakewood, NJ, United States) followed by 25 min in oxygenated HBS containing 1 mg ml^{-1} papain (Worthington Biochemical Corp). The enzyme activity was terminated with the addition of HBS containing a combination of 1 mg ml^{-1} bovine serum albumin (BSA) and 1 mg ml^{-1} trypsin inhibitor (Sigma). After enzyme treatment, ganglia were placed in 3 ml of HBS following two room temperature HBS washes. Ganglia were then triturated through fire-polished Pasteur pipettes with decreasing bores to extract cells. Finally, the cells mixed in HBS were plated onto surface modified culture dishes (Corning Primaria™ easy grip). Cells were viable at room temperature for approximately 8 h. DRG cells were pre-treated with 1 μg ml^{-1} Alexa Fluor 488-conjugated *Bandeiraea simplicifolia* IB_4 (Invitrogen) for 5 min at room temperature and washed with HBS for 5 min before fluorescence was examined on the inverted microscope (Olympus, IX50) used for patch clamp recordings.

Cell Culture and Transfection

Human embryonic kidney (HEK293T) cells containing the SV40 Large T-antigen were cultured at 37°C, 5% CO2 in Dulbecco's Modified Eagle's Medium (DMEM, Invitrogen Life Technologies, Australia), supplemented with 10% fetal bovine serum (FBS, Bovigen, Australia), 1% GlutaMAX and penicillin-streptomycin (Invitrogen, Australia). HEK293 cells were then transiently co-transfected with the different voltage-gated calcium channel isoforms and green fluorescent protein (GFP) for visualization, using the calcium phosphate method. cDNAs encoding $mCa_v1.2$ (a gift from Dr. D. Lipscombe; Addgene plasmid #26572) (Helton et al., 2005), $rCa_v1.3$ (a gift from Dr. D. Lipscombe; Addgene plasmid # 49,333) (Xu and Lipscombe, 2001), $hCa_v2.1$ (a gift from Dr. J. Striessnig), $rCa_v2.2$ (a gift from Dr. D. Lipscombe), $hCa_v2.2$ (a gift from Dr. D. Yue), $hCa_v2.3$ (purchased from GenScript United States Inc.) were co-transfected with β_3, $\alpha_2\delta_1$ and GFP. After transfection, cells were plated on 12 mm cover glass and transferred to a 30°C incubator for 1–3 days.

Electrophysiology of Native High Voltage-Activated (HVA) Calcium Currents

Cell size was determined from an eyepiece graticule. Whole-cell electrophysiology was conducted at room temperature (22–24°C) in culture dishes perfused with room temperature HBS. The intracellular pipette solution contained (mM): 120 CsCl, 10 HEPES, 10 EGTA, 2 $CaCl_2$, 5 MgATP, 5 Na_2GTP, 5 NaCl; pH 7.3 (CsOH); 285 ± 5 mos mol l^{-1}. To isolate I_{Ca}, the extracellular solution contained (mM): 140 tetraethylammonium chloride (TEA-Cl), 2.5 KCl, 1.8 $CaCl_2$, 1.2 $MgCl_2$, 10 HEPES, 10 glucose; pH 7.4 (CsOH); 330 ± 5 mosmol. l^{-1}. The liquid junction potential was 9 mV. The extracellular solution to isolate I_{Na} contained (mM): 110 TEA-Cl, 30 NaCl, 2.5 KCl, 1.8 $CaCl_2$, 1.2 $MgCl_2$, 10 HEPES, 10 D-glucose, 0.1 $CdCl_2$, 0.1 mg ml^{-1} BSA; pH 7.2 (CsOH); 330 ± 5 mosmol. l^{-1}.

An EPC-9 patch-clamp amplifier and corresponding PULSE software from HEKA Electronik (Lambrecht/Pfalz, Germany) were used to make recordings. Currents were sampled at 50 kHz and recorded on a hard disk. Borosilicate glass from AM Systems, Everett, WA, United States were used for patch pipettes. The input resistance of the pipettes ranged from 2 to 4 MΩ. The cell capacitance was between 7 and 20 pF (15–25 μm), while series resistance under 9 MΩ was deemed acceptable. All experiments had a series resistance compensation of at least 80%. A built-in procedure of the HEKA amplifier compensated for the capacitive transient currents. A −**P**/6 protocol was utilized to subtract leak current online. I_{Ca} was generated with the recording protocol which included a depolarization from a holding potential of −80 mV to 0 mV for 10 ms every 30 s. I_{Na} was generated through a recording protocol which included a step depolarization from a holding potential of −80 mV to 0 mV for 10 ms at a frequency of 0.1 Hz. Cells were perfused with the test compound via a pressure driven perfusion system (AutoMate Scientific, United States). Pn3a mediated inhibition was determined by measuring the decrease in peak I_{Na} or $\mathbf{I}_{Ca}$ amplitude from baseline upon perfusion of the compound.

Electrophysiology of Transiently Transfected Ca_vs

Depolarization-activated Ca^{2+} currents (I_{Ca}) in transfected HEK293 cells were recorded in the whole-cell patch clamp configuration. Data were recorded using a MultiClamp 700B amplifier, digitized with a DigiData1440 and controlled using Clampex10.7 software (Molecular Devices, United States). Currents were sampled at 100 kHz and filtered to 10 kHz, with leak and capacitive currents subtracted using a −P/4 protocol. Extracellular recording solution contained as follows (mM): 100 NaCl, 10 $CaCl_2$, 1 $MgCl_2$, 5 CsCl, 30 TEA-Cl, 10 D-glucose and 10 HEPES, pH 7.3 with TEA-OH. Fire-polished borosilicate (1B150F-4, World Precision Instruments, Sarasota, FL, United States) patch pipettes were used with resistance of 1-3 MΩ and compensated > 80%. Intracellular recording solution contained as follows (mM): 140 KGluconate, 5 NaCl, 2 $MgCl_2$, 5 EGTA and 10 HEPES, pH 7.2 with KOH. Cells were continuously perfused with extracellular solution at a rate of ~1.2 ml/min. Depolarization-activated currents were elicited from a holding potential of −90 mV to a test potential (20 ms) for different channel isoforms determined by the peak amplitude elicited during an I-V protocol at a rate of 0.2 Hz Pn3a was superfused over the cell using a syringe pump. Activation curves of $hCa_v2.2$ were generated through a series of test pulses (50 ms) ranging from −30 to +50 mV (Δ5 mV) every 5 s with a holding potential of −90 mV. Steady-state inactivation (SSI) curves for $hCa_v2.2$ were generated by a series of pre-pulse potentials ranging from −120 to +30 mV of 1 s prior to a test pulse (50 ms) of +20 mV.

Data and Statistical Analysis

All data analysis and graphs were generated in OriginPro (Origin Lab Corporation, United States). Concentration-response relationships were built by plotting peak current amplitudes in the presence of Pn3a (I_{Pn3a}), over the current prior to Pn3a application ($I_{Control}$). The resulting curve was fit with a sigmoidal curve according to the following expression:

$$I_{Pn3a}/I_{Control} = 1 + [Pn3a]^n / (IC50^n + [Pn3a]^n)$$

Where IC_{50} is the half-maximal inhibitory concentration and n is the Hill coefficient. Activation and SSI curves were fit by the modified Boltzmann equation:

$$I \text{ or } G = 1 \Big/ \left(1 + \exp\left(\frac{Vm - V_{0.5}}{ka}\right)\right)$$

Where I is the current or G is the conductance, Vm is the pre-pulse potential, $V_{0.5}$ is the half-maximal activation potential and ka is the slope factor.

Statistical significance ($p < 0.05$) was determined using unpaired Student's t-test or 1-way ANOVA followed by a Tukey multiple comparison. All data is presented as mean ± SEM (n), where n is individual cells.

Materials

Naloxone hydrochloride and tetrodotoxin (TTX) were from Tocris (Bristol, United Kingdom) and solubilized in H_2O. [D-Ala^2, N-$MePhe^4$, Gly-ol]-Enkephalin (DAMGO) was from Sigma-Aldrich (St. Louis, MO, United States) and solubilized in H_2O.

Synthetic μ-Theraphotoxin-Pn3a (UniProtKB - P0DM12) was kindly provided by Dr. Irina Vetter's laboratory, Institute for Molecular Bioscience, University of Queensland and solubilized in H_2O.

RESULTS

Pn3a Reduces Rodent High Voltage-Activated Ca^{2+} Currents in Small Dorsal Root Ganglion Neurons

Robust depolarization-activated sodium (I_{Na}) and calcium (I_{Ca}) currents can be elicited in rat small-diameter (7–20 pF) DRG neurons that were inhibited by application of Pn3a (**Figure 1**). Representative isolectin-B4 lightly positive ($IB_4^{\pm}$) and negative (IB_4^{-}) DRG neurons mediated I_{Na} and I_{Ca} whole-cell currents in control (black) and in the presence of Pn3a (colored) are shown in **Figures 1A–C**. To compare channel populations mediating TTXs-I_{Na} and HVA-I_{Ca} active during DRG neuron action potential firing, Pn3a exposure experiments were performed using identical pulse protocols (holding potential, −80 mV to a test potential of 0 mV, 10 ms). It can be appreciated that ~50% of I_{Na} remained after application of 300 nM Pn3a in both small-diameter DRG neuron subtypes tested; whereas 10 μM Pn3a spared half of the HVA I_{Ca} observed in IB_4^{-} DRG neurons. Concentration-response curves (CRC) were generated to compare the potency of Pn3a against I_{Na} and I_{Ca} in these neurons under our experimental conditions (**Figure 1D**).

Pn3a inhibition of (TTX-sensitive) TTXs-I_{Na} in IB_4^{-} or $IB_4^{\pm}$ small-diameter DRG neurons had similar IC_{50}s (0.24 ± 0.03 μM vs. 0.29 ± 0.02 μM, respectively), which were comparable to previously reported values (Deuis et al., 2017), and was fully reversible upon washout (**Supplementary Figure S1**). From these two neuronal subtypes, we concentrated on small-diameter IB_4^{-} DRG neurons, as Pn3a displayed more potent block of I_{Ca} in this neuronal population with a calculated IC_{50} of 6.43 ± 0.53 μM. Thus, Pn3a inhibits HVA I_{Ca} known to be critical for neurotransmitter release and pain signal propagation (Bourinet et al., 2014).

Pn3a Inhibits Most Ca_v Channel Isoforms That Mediate Afferent I_{Ca}

Numerous HVA Ca_v channel isoforms are present in rat DRG neurons. In order to ascertain the channel target underlying Pn3a's activity on neuronal HVA I_{Ca}, Pn3a's activity was initially screened on a panel of representative HVA Ca_v channels typically expressed in

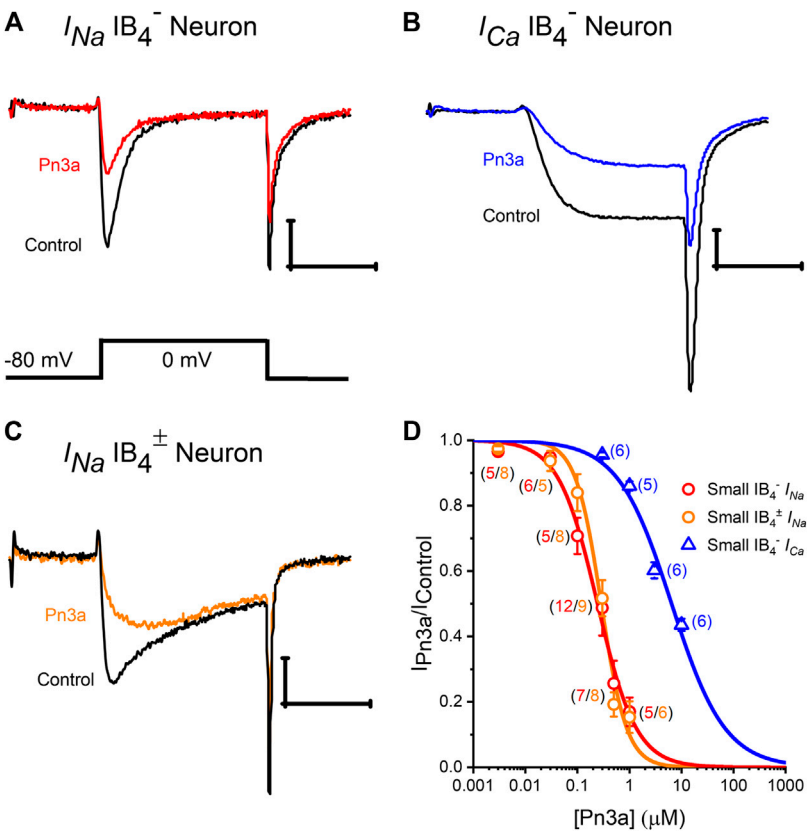

Figure 1 | Pn3a inhibition of TTXs-I_{Na} and high voltage-activated I_{Ca} in rat DRG neurons. **(A–C)** Representative recording of control (black) I_{Na} in IB_4^{-} and $IB_4^{\pm}$ DRG neurons (red and orange, respectively) in the presence of 0.3 μM Pn3a. **(B)** HVA I_{Ca} currents from DRG neurons in control (black) and the presence of 10 μM Pn3a (blue). **(D)** Concentration-response curves obtained for Pn3a inhibition of TTXs-I_{Na} in small-diameter IB_4^{-} (red) and small-diameter (5–60 pF) lightly $IB_4^{\pm}$ (orange) neurons and I_{Ca} in small-diameter IB_4^{-} (blue) neurons (n values shown for each concentration). X scale bar 5 msec; Y scale bar 0.5 nA.

DRG neurons including $Ca_v1.2$, $Ca_v1.3$, $Ca_v2.1$, $Ca_v2.2$, and $Ca_v2.3$. We transiently co-transfected the individual Ca_v channel α-subunits of interest together with β_3 and $\alpha_2\delta_1$ subunits in HEK293 cells and measured whole-cell I_{Ca} currents by patch clamp. I_{Ca} was elicited from a holding potential of −90 mV to a test potential of +20 mV for 20 ms, at a frequency of 0.2 Hz. A large component of I_{Ca} in rat DRG neurons is carried by $Ca_v2.2$ channels therefore we began our screen testing the effects of 10 μM Pn3a on rat and human $Ca_v2.2$ mediated currents (**Figure 2**). Both channel orthologues were similarly suppressed by 69.5 ± 1.0% and 71.8 ± 0.6% (n = 5, *per* orthologue), respectively. Other HVA calcium channels typically expressed in DRG neurons including mouse $Ca_v1.2$, rat $Ca_v1.3$, human Cav2.1, $Ca_v2.2$, and $Ca_v2.3$ were exposed to 10 μM Pn3a and further examined. All but one of the HVA channels studied were sensitive to Pn3a block (**Figure 2**) and fully reversible upon washout (**Supplementary Figure S2**). Specifically, inhibition of $mCa_v1.2$-mediated currents reached 70.3 ± 1.5% (n = 5), $rCa_v1.3$: 65.6 ± 1.8% (n = 5) and $hCa_v2.1$: 58.0 ± 1.8% (n = 5). Interestingly, application of up to 10 μM Pn3a had negligible effects on $hCa_v2.3$ mediated currents (2.2 ± 0.9%, n = 5) (**Figures 2C,F**). The level of Pn3a Ca^{2+} current suppression observed in the recombinant channels was consistent with our observations on HVA I_{Ca} in DRG neurons (56.5 ± 1.9%, n = 6) (**Figure 1D**), suggesting that compounded inhibition of HVA I_{Ca} by Pn3a may be due to its equipotent effects on multiple Ca_v channels rather than a particular isoform.

Pn3a Produces a Hyperpolarizing Shift in $Ca_v2.2$ Steady-State Inactivation

$Ca_v2.2$ is regarded as a major contribution to HVA I_{Ca} in rat DRG neurons and is expressed at a similar level across different DRG neuron sizes/types (Scroggs and Fox, 1992) and, from our screening, a prominent Pn3a target. A concentration-response curve for inhibition of recombinant $hCa_v2.2$ in the presence of Pn3a is shown in **Figure 3A**. The Pn3a CRC was accurately described by a Hill fit with an IC_{50} of 3.7 ± 0.2 μM, and $\mathbf{n}_H$ = 1.16 ± 0.07 (n = 5 *per* concentration). The mechanism of action of Na_v-targeting therapotoxins often involves gating modification (Bosmans and Swartz, 2010), therefore, we investigated in detail the mechanism of inhibition of Pn3a over recombinant $hCa_v2.2$ mediated Ca^{2+} currents. Depolarization-activated $hCa_v2.2$ current kinetics were not altered in the presence of 10 μM Pn3a as observed in **Figures 3B,C** where control and toxin exposed currents have been scaled for ease of comparison. The activation voltage dependence of $hCa_v2.2$ mediated I_{Ca} in the presence of 3 μM Pn3a was slightly shifted from control currents (Control $V_{0.5}$ = 13.4 ± 0.1 mV, ka = 4.4 ± 0.1, and Pn3a $V_{0.5}$ = 11.7 ± 0.1 mV, ka = 3.7 ± 0.1; n = 5; $V_{0.5}$ $p < 0.0001$; **Figures 3D,E**). $Ca_v2.2$ steady-state inactivation was evaluated with a standard protocol (**Figure 3F**) in control and during exposure to 3 μM Pn3a. In the presence of Pn3a, $Ca_v2.2$ mediated currents

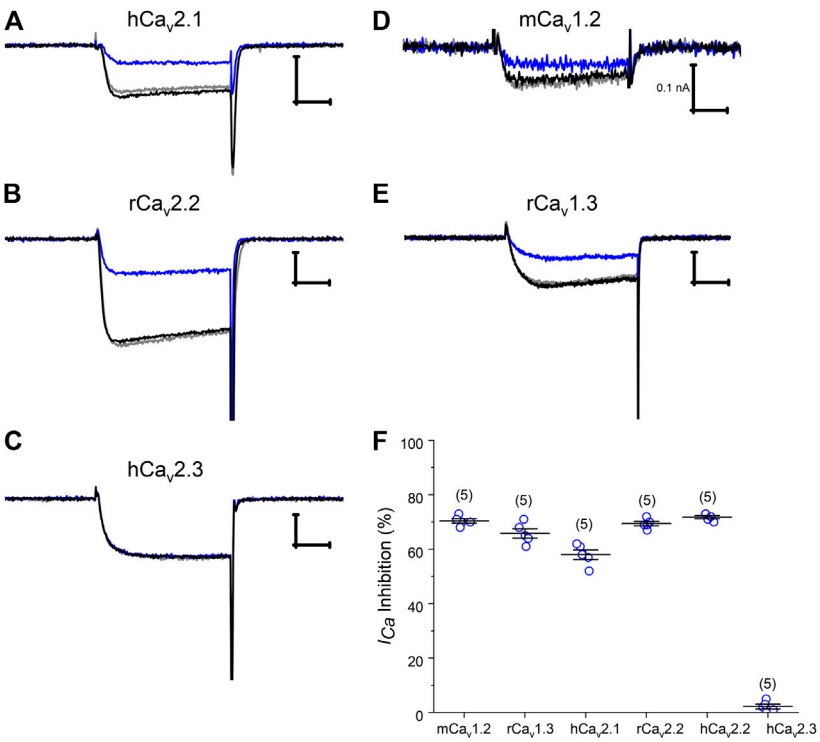

Figure 2 | Pn3a modulation of recombinant HVA Ca_v channels. **(A–E)** Representative current traces of $Ca_v2.1$, $Ca_v2.2$, $Ca_v2.3$, $Ca_v1.2$, and $Ca_v1.3$ mediated Ca^{2+} currents in control (black), in the presence of 10 μM Pn3a (blue), and after washout (gray). **(F)** Summary bar graph comparing 10 μM Pn3a inhibition (%) of heterologously expressed HVA calcium channels predominantly expressed in rodent DRG neurons. Mouse $Ca_v1.2$, rat $Ca_v1.3$, 2.2 and human $Ca_v2.1$, 2.2, 2.3 channels were all co-expressed with human β_3 and $\alpha_2\delta_1$ in HEK293 cells (n = 5 for each channel). X scale bar 5 msec; Y scale bar 0.5 nA, unless noted.

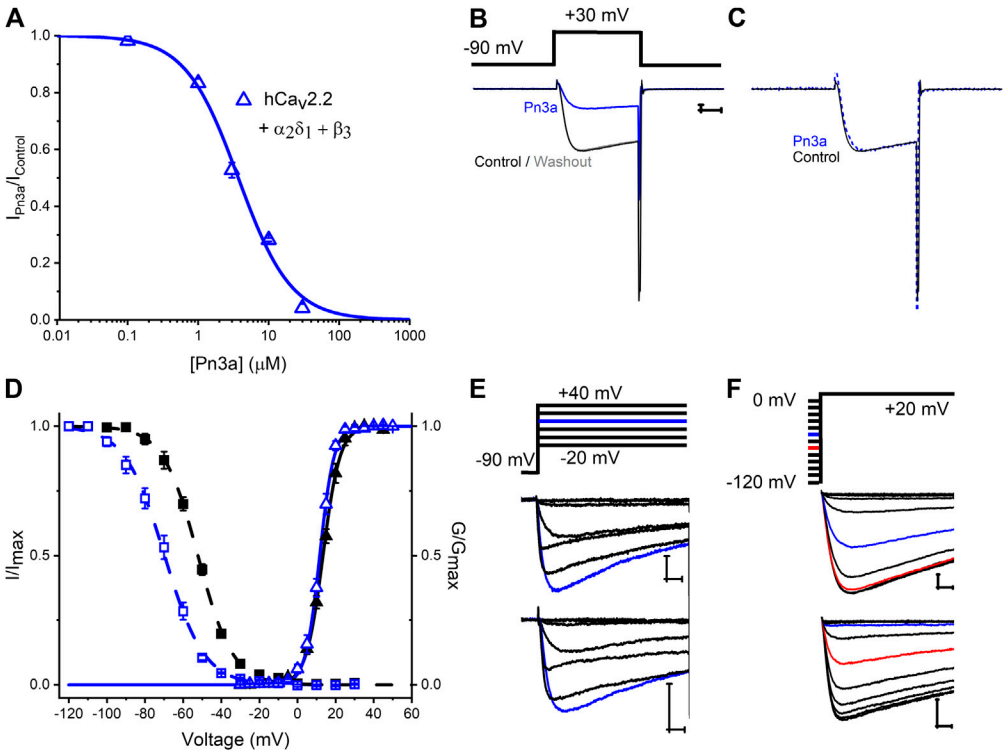

Figure 3 | Characterization of Pn3a effects on Human $Ca_v2.2$ channel-mediated currents. **(A)** Pn3a inhibition of $hCa_v2.2$ currents is described by the concentration-response curve. Hill equation fit gives an IC_{50} = 3.70 ± 0.21 μM, and n_H = 1.16 ± 0.07 (n = 5 for each concentration). **(B)** Representative current traces of $hCa_v2.2$ (β_3/$\alpha_2\delta_1$) recorded in control (black), 10 μM Pn3a (blue), and after peptide washout (gray). **(C)** Normalized peak currents from **(B)** in control (black, solid) and Pn3a (blue, dotted). **(D)** Effect of Pn3a on the voltage dependent kinetics of $Ca_v2.2$. Activation (triangles) and steady-state inactivation (squares) relationships for $hCa_v2.2$ obtained in the absence (▲, ■) and presence of 3 μM Pn3a (△, ⊙). **(E)** Representative currents elicited by the voltage protocol **(top)** in the absence (control, middle) and presence of 3 μM Pn3A **(bottom)** normalized to peak I-V currents (blue trace, +20 mV) used to generate activation curves shown in **(D)**. **(F)** Representative currents from steady-state inactivation (SSI) protocol **(top)** obtained in the absence (control, middle) and presence of 3 μM Pn3a used to generate SSI curves shown in **(D)**. X scale bar 5 msec; Y scale bar 0.5 nA.

displayed enhanced inactivation with a ~18 mV hyperpolarizing shift in SSI (Control $V_{0.5}$ = −52.3 ± 0.2 mV, ka = 9.2 ± 0.2, and Pn3a $V_{0.5}$ = −69.8 ± 0.3 mV, ka = 10.5 ± 0.3; n = 5; $V_{0.5}$ p < 0.0001). Hence, Pn3a appears to inhibit HVA $Ca_v2.2$ by promoting entrance to the inactivated state.

Rat Small IB_4^- DRG Neurons HVA-I_{Ca} is Additively Inhibited by Pn3a and Low Doses of Opioids Agonists but Not Antagonists

To examine a potential contribution of HVA calcium channel inhibition by Pn3a to the reported synergy with opioids observed in animal pain models (Mueller et al., 2019), the effects of co-application of Pn3a and sub-therapeutic doses of opioid modulators DAMGO (OR agonist) and naloxone (OR antagonist) on HVA I_{Ca} from rat DRG neurons were assessed. Co-application of Pn3a (300 nM) and DAMGO (100 nM) resulted in a 14.22 ± 1.72% (n = 8; p < 0.001) (**Figure 4A**) reduction of the total HVA I_{Ca}. This is significantly higher than the inhibition of HVA I_{Ca} achieved with the same concentrations of Pn3a (4.45 ± 0.78%, n = 6; p < 0.001) and DAMGO (6.49 ± 1.07%, n = 6; p > 0.001 applied independently (**Figure 4A**). These results are consistent with the additive inhibition of small-diameter DRG I_{Ca} by activation of ORs using DAMGO and Pn3a. In turn, the suppression of rat neuronal I_{Ca} by individual application of 1 μM Pn3a (13.97 ± 1.39%, n = 5) or co-application with 1 μM naloxone (15.31 ± 0.75%, n = 6) were undistinguishable, whilst on its own 1 μM naloxone minimally affected I_{Ca} (1.68 ± 0.61% inhibition, n = 5; p < 0.001) (**Figure 4B**).

DISCUSSION

This study explored the effects of the analgesic spider venom-derived peptide Pn3a on afferent HVA Ca^{2+} currents revealing that L-, P/Q, and N-type, but not R-type, Ca_v channels are all susceptible to inhibition by this VDP. Pn3a's mechanism of inhibition of $Ca_v2.2$ channels was determined as the major isoform mediating HVA I_{Ca} in nociceptive DRG neurons. Finally, additive suppression of neuronal HVA I_{Ca} by Pn3a and OR agonist, DAMGO was verified.

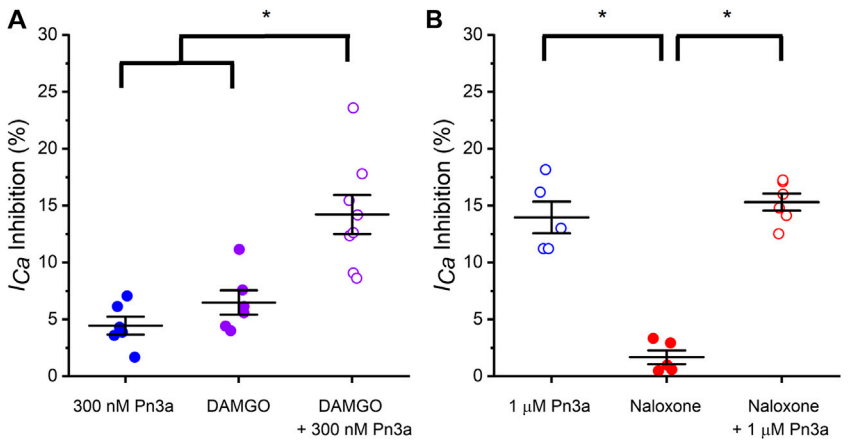

Figure 4 | Pn3a and opioids inhibit rat DRG neurons high voltage-activated I_{Ca}. **(A)** Bar graph summary of I_{Ca} modulation by OR agonist DAMGO and Pn3a in small IB_4^- DRG neurons. 300 nM Pn3a (⊙; $n = 6$), 100 nM DAMGO (⊙; $n = 6$), 100 nM DAMGO +300 nM Pn3a (⊙; $n = 8$) **(B)** Bar graph summary of I_{Ca} modulation by OR antagonist DAMGO and Pn3a in small IB_4^- DRG neurons. 1 μM Pn3a (⊙; $n = 5$), 1 μM naloxone (⊙; $n = 5$) and 1 μM Pn3a +1 μM naloxone (⊙; $n = 6$). One-way Anova results (* = $p < 0.001$).

Pn3a Inhibits High Voltage-Activated Ca_v Channels

Pn3a is a potent ($IC_{50} = 0.9 \pm 0.8$ nM) and selective $Na_v1.7$ gating-modifier spider venom peptides targeting its DII VSD (Deuis et al., 2017). Homology of VGIC voltage sensing domains, and particularly those of Na_v channels, is at the crux of the development of genuinely selective $Na_v1.7$ modulators (Kingwell, 2019). Given the VSD functional importance in neuronal VGICs and their structural homology, it is not surprising that VDPs target related channel families. This, together with Ca_v channels as downstream targets of opioid analgesic drugs (Hescheler et al., 1987), motivated our investigation of Pn3a's modulation of small-diameter DRG neuron HVA calcium channels.

Pn3a was shown to strongly suppress TTXs-I_{Na} in small diameter IB_4^- DRG neurons and reduce c-fibre evoked excitatory post-synaptic currents. These neurons contain large HVA Ca^{2+} currents (**Figure 1B**), which could also contribute to the observed reduction in c-fibre excitatory post-synaptic currents (Deuis et al., 2017). We observed suppression of the HVA Ca^{2+} currents upon application of Pn3a with an IC_{50} value of 6.43 μM, a concentration ~25-fold higher than that required to inhibit I_{Na} in small diameter IB_4^- DRG neurons (**Figure 1D**). HVA I_{Ca} in these neurons is mediated by several Ca_v channel subfamilies, including L-($Ca_v1.2$ and Cav1.3 predominantly), P/Q- ($Ca_v2.1$), N- ($Ca_v2.2$), and R-type ($Ca_v2.3$) (Fuchs et al., 2007). Our experiments with recombinant Ca_v1 and Ca_v2 channels clearly show their sensitivity to Pn3a modulation (**Figure 2**). Earlier work investigating Pn3a (10 μM) activity on endogenous calcium currents in SH-SY5Y cells relied on fluorescence-based (FLIPR) assays of KCl-induced changes in intracellular Ca^{2+} concentration in which the lack of voltage control precludes reliable Ca_v channel activation (Deuis et al., 2017) perhaps missing the Pn3a effects reported here with direct measurement of $Ca_v2.2$-mediated currents.

Pn3a inhibits all the HVA Ca_v isoforms tested here with the notable exception of $Ca_v2.3$, which was minimally affected by up to 10 μM Pn3a (**Figure 2F**). This observation highlights the presence of a conserved Pn3a-binding site in all HVA Ca_v channels but the R-type isoform. Future work is required to attempt to isolate Pn3a's binding site on HVA Ca_v channels, which could provide valuable information for future design of selective $Na_v1.7$, or HVA calcium channel inhibitors, to attempt to dissect out VDP cross talk between these two channel families. A provocative possibility is that analgesic therapeutics may profit from Na_v/Ca_v polypharmacology for which Pn3a may provide a valuable scaffold. This has been shown effective for other potential therapeutic compounds including CNCB-2, a dual $Na_v1.7/Ca_v2.2$ inhibitor that suppresses action potential firing in small diameter DRG neurons, providing long lasting analgesia in postoperative surgical pain and inflammatory pain models (Lee et al., 2019).

Pn3a Inhibition of High Voltage-Activated Ca_vs Differs From That of Na_vs

Pn3a's inhibition of $Na_v1.7$ current is concurrent with a depolarizing shift in the channel's voltage dependence of activation without discernible effects on SSI. Pn3a gating modification of $Na_v1.7$ currents is reported to arise from interactions with one or more $Na_v1.7$ VSDs, as suggested by Pn3a inhibition of $K_v2.1$-$Na_v1.7$ (DII and DIV) VSD chimeras (Bosmans et al., 2008; Deuis et al., 2017). Mammalian Na_v and Ca_v α-subunits are structurally homologous but differ in their gating mechanisms (Kubota et al., 2017). Our analysis of $Ca_v2.2$ inhibition by Pn3a revealed a hyperpolarizing shift in steady-state inactivation without apparent changes in channel activation (**Figure 3D**). Other known gating modifier toxins including Kurtoxin, Hanatoxin, Jingzhaotoxin-I, and Protoxin I/II inhibit both Na_v and Cav channels (Swartz and MacKinnon, 1995;

Chuang et al., 1998; Li-Smerin and Swartz, 1998; Yamamoto and Sakashita, 1998; Middleton et al., 2002; Sidach and Mintz, 2002; Xiao et al., 2005; Bosmans et al., 2008; Bladen et al., 2014). For instance, the scorpion peptide Kurtoxin accelerates deactivation of T-type and L-type Ca_v channels, slows deactivation of P-type calcium channels, with little to no alteration of N-type Ca_v channel kinetics. In contrast, at Na_v channels it slows inactivation of $Na_v1.2$ and $Na_v1.5$ currents thus differentially modifying the gating of individual channel isoforms (Chuang et al., 1998; Olamendi-Portugal et al., 2002; Sidach and Mintz, 2002). Thus peptide interactions with conserved binding pockets on Na_v/Ca_v channel voltage sensor domains can cause distinct changes to various biophysical channel parameters. Examination of other VSD Na_v/Ca_v cross-interacting peptides may help identify the molecular determinants of such polypharmacology.

Pn3a Potency Against Rat DRG Neuron I_{Na} and Recombinant $hNa_v1.7$

The apparent affinity of Pn3a for small-diameter DRG neuronal I_{Na} is ~250 nM (**Figure 1D**), or ~250-fold less potent than reported for recombinant $hNa_v1.7$ channels (Deuis et al., 2017). This is likely due to contribution from Pn3a-insensitive Na_v isoforms that also mediate DRG-I_{Na}, but may also depend on orthologue differences (mouse, rat vs human), and/or dissimilar experimental conditions (recording solutions, pulse protocols, analysis criteria, etc). We evaluated the potency of Pn3a against recombinant $hNa_v1.7$ using the same solutions and pulse protocols applied in our recordings of rat DRG neurons (**Supplementary Figure S3**). Under our experimental condition, Pn3a inhibition of $hNa_v1.7$ channels stably expressed in CHO cells was reliably distinguished from current rundown at concentrations >10 nM (**Supplementary Figure S1A**) and became virtually irreversible at higher concentrations (**Supplementary Figure S1B**). We estimated IC_{50}s of 31.6 ± 1.0 nM (V_h = −80 mV, n = 5) and 15.9 ± 0.4 nM (V_h = −120 mV, n = 5) for Pn3a inhibition of $hNa_v1.7$ mediated currents (**Supplementary Figure S1C**). It has been reported that Pn3a block reaches steady-state after "tens to hundreds of seconds" of exposure (Deuis et al., 2017), thus we surmise that the ~30-fold difference in potency reported by us may arise from differences in experimental approaches.

From our analysis, a ~10-fold higher does Pn3a potency against recombinant $Na_v1.7$ than small-diameter DRG neuron I_{Na} was observed, which is indicative of a large contribution from Pn3a-insensitive Na_v isoforms to the total DRG neuron Na^+ current. This implies that the sole inhibition of $Na_v1.7$ channels would have limited "hyperexcitabilty attenuation" potential in these cells.

Potential Mechanism of Pn3a/Opioid Antinociception

Previous studies showed that Pn3a was antinociceptive when sub-therapeutic concentrations of Pn3a was applied in combination with sub-therapeutic opioid doses. A mechanism for such Pn3a/opioid antinociceptive "synergism" could not be defined as OR modulators had no effects on $Na_v1.7$ nor does Pn3a treatment appear to alter OR signaling (Deuis et al., 2017; Mueller et al., 2020).

Consistently, Pn3a treatment was ineffective in rodent models of acute nociception or inflammatory pain, also in agreement with studies where other $Na_v1.7$ modulators were assayed such as the VSD-peptide ProTx-II (Schmalhofer et al., 2008) and small molecule PF-04856264 (Deuis et al., 2017). The overall contribution of $Na_v1.7$ to pain in some animal behaviour-based models has been questioned (Shields et al., 2018), whereas research and development of multiple potent and selective $Na_v1.7$ inhibitors have failed to recapitulate the pain-free state that characterized CIP in humans (Eagles et al., 2020). Importantly, the genetic ablation of *SCN9A* in mice and in a human CIP patient, the absence of functional $Na_v1.7$ leads to increases in endogenous opioid-dependent analgesia and diminished pain-induced peripheral nociceptive drive (Minett et al., 2015). In the same IB_4^- DRG afferent population, Pn3a suppresses HVA I_{Ca} with an IC_{50} of ~6 μM, which is ~20-fold less potent than toward I_{Na}. Post-surgical additive antinociception was verified by local co-administration of Pn3a with sub-therapeutic oxycodone or baclofen (Mueller et al., 2019). These two compounds are agonists of the opioid and $GABA_B$ receptors (respectively), whose activation leads to G protein signaling cascades that ultimately decrease neuronal HVA Ca_v currents (Hescheler et al., 1987; Page et al., 2006; Sadeghi et al., 2017). The antinociceptive effects of OR agonists such as DAMGO and morphine are enhanced in the presence of Ca_v1 and $Ca_v2.2$ channel inhibitors (Contreras et al., 1988; Barro et al., 1995). We have shown that sub-therapeutic Pn3a when co-applied with the OR activator (DAMGO, **Figure 4A**) additively inhibit HVA I_{Ca}, but not with the OR antagonist (naloxone, **Figure 4B**). With the exception of $Ca_v2.3$, Pn3a equipotently inhibited all HVA-Ca_vs in heterologous expression experiments (**Figure 2**). Altogether, HVA Ca_v's important roles in neuroexcitability, abundant expression, their inhibition by downstream activation of GPCRs and the hereby demonstrated sensitivity to Pn3a are consistent with decreased perception of painful stimuli by sensory neurons at the local and systemic doses reported previously. Hence providing a plausible mechanism for antinociceptive effects observed in various animal pain models as opposed to the exclusive inhibition of $Na_v1.7$ channels.

CONCLUSION

Pn3a inhibits HVA I_{Ca} in small diameter IB_4^- DRG neurons and suppresses recombinant L-, P/Q-, N-, but not R-type Ca_v channels. Pn3a inhibits $Ca_v2.2$ mediated currents by promoting a hyperpolarizing shift in SSI without affecting activation. Finally, Pn3a inhibition of neuronal I_{Ca} is enhanced by opioid receptor activation. Compounded inhibition of afferent HVA Ca^{2+} currents represents a plausible

mechanism behind the antinociceptive effects observed in rodents treated with Pn3a and sub-therapeutic μ-opioid receptor agonists.

DATA AVAILABILITY STATEMENT

The raw data supporting the conclusions of this article will be made available by the authors, without undue reservation.

ETHICS STATEMENT

The animal study was reviewed and approved by University of Sydney.

AUTHOR CONTRIBUTIONS

JM, NM, RF-U, DA, and MC conceived and design the research. JM, NM, and RF-U performed experiments. JM, NM, and RF-U analyzed and interpreted the data. JM, DA, and MC provided reagents. All authors reviewed, revised and approved the final paper.

FUNDING

This work was supported by the National Health and Medical Research Council (NHMRC) Program Grant (APP1072113) to DA and MC, and the Rebecca Cooper Foundation for Medical Research Project Grant (PG2019396) to JM, during the conduct of the study.

ACKNOWLEDGMENTS

Synthetic μ-theraphotoxin-Pn3a was a kind gift from I. Vetter's laboratory, Institute for Molecular Bioscience, University of Queensland. JM and RF-U thank L. Wetto and D. Noonna for insightful discussion and support.

SUPPLEMENTARY MATERIAL

The Supplementary Material for this article can be found online at: https://www.frontiersin.org/articles/10.3389/fphar.2020.633679/full#supplementary-material.

REFERENCES

Barro, M., Ruiz, F., and Hurlé, M. A. (1995). Kappa-opioid receptor mediated antinociception in rats is dependent on the functional state of dihydropyridine-sensitive calcium channels. *Brain Res.* 672 (1-2), 148–152. doi:10.1016/0006-8993(94)01387-w

Bladen, C., Hamid, J., Souza, I. A., and Zamponi, G. W. (2014). Block of T-type calcium channels by protoxins I and II. *Mol. Brain* 7, 36. doi:10.1186/1756-6606-7-36

Bosmans, F., Martin-Eauclaire, M. F., and Swartz, K. J. (2008). Deconstructing voltage sensor function and pharmacology in sodium channels. *Nature* 456 (7219), 202–208. doi:10.1038/nature07473

Bosmans, F., and Swartz, K. J. (2010). Targeting voltage sensors in sodium channels with spider toxins. *Trends Pharmacol. Sci.* 31 (4), 175–182. doi:10.1016/j.tips.2009.12.007

Bourinet, E., Altier, C., Hildebrand, M. E., Trang, T., Salter, M. W., and Zamponi, G. W. (2014). Calcium-permeable ion channels in pain signaling. *Physiol. Rev.* 94 (1), 81–140. doi:10.1152/physrev.00023.2013

Caterina, M. J., Schumacher, M. A., Tominaga, M., Rosen, T. A., Levine, J. D., and Julius, D. (1997). The capsaicin receptor: a heat-activated ion channel in the pain pathway. *Nature* 389 (6653), 816–824. doi:10.1038/39807

Chuang, R. S., Jaffe, H., Cribbs, L., Perez-Reyes, E., and Swartz, K. J. (1998). Inhibition of T-type voltage-gated calcium channels by a new scorpion toxin. *Nat. Neurosci.* 1 (8), 668–674. doi:10.1038/3669

Contreras, E., Tamayo, L., and Amigo, M. (1988). Calcium channel antagonists increase morphine-induced analgesia and antagonize morphine tolerance. *Eur. J. Pharmacol.* 148 (3), 463–466. doi:10.1016/0014-2999(88)90129-x

Cox, J. J., Reimann, F., Nicholas, A. K., Thornton, G., Roberts, E., Springell, K., et al. (2006). An SCN9A channelopathy causes congenital inability to experience pain. *Nature* 444 (7121), 894–898. doi:10.1038/nature05413

Deuis, J. R., Dekan, Z., Wingerd, J. S., Smith, J. J., Munasinghe, N. R., Bhola, R. F., et al. (2017). Pharmacological characterisation of the highly $Na_v1.7$ selective spider venom peptide Pn3a. *Sci. Rep.* 7, 40883. doi:10.1038/srep40883

Dib-Hajj, S. D., Yang, Y., and Waxman, S. G. (2008). Genetics and molecular pathophysiology of Na(v)1.7-related pain syndromes. *Adv. Genet.* 63, 85–110. doi:10.1016/S0065-2660(08)01004-3

Eagles, D. A., YuenChow, C., and King, G. F. (2020). Fifteen years of $Na_v1.7$ as an analgesic target: why has excellent in vitropharmacology not translated into *in vivo* analgesic efficacy? *Br. J. Pharmacol.* [Epub ahead of print]. doi:10.1111/bph.15327

Finol-Urdaneta, R. K., McArthur, J. R., Korkosh, V. S., Huang, S., McMaster, D., Glavica, R., et al. (2019). Extremely potent block of bacterial voltage-gated sodium channels by μ-conotoxin PIIIA. *Mar. Drugs* 17 (9), 510. doi:10.3390/md17090510

Finol-Urdaneta, R. K., Belovanovic, A., Micic-Vicovac, M., Kinsella, G. K., McArthur, J. R., and Al-Sabi, A. (2020). Marine toxins targeting Kv1 channels: pharmacological tools and therapeutic scaffolds. *Mar. Drugs*. 18 (3), 173. doi:10.3390/md18030173

Fuchs, A., Rigaud, M., Sarantopoulos, C. D., Filip, P., and Hogan, Q. H. (2007). Contribution of calcium channel subtypes to the intracellular calcium signal in sensory neurons: the effect of injury. *Anesthesiology* 107 (1), 117–127. doi:10.1097/01.anes.0000267511.21864.93

Gui, J., Liu, B., Cao, G., Lipchik, A. M., Perez, M., Dekan, Z., et al. (2014). A tarantula-venom peptide antagonizes the TRPA1 nociceptor ion channel by binding to the S1-S4 gating domain. *Curr. Biol.* 24 (5), 473–483. doi:10.1016/j.cub.2014.01.013

Helton, T. D., Xu, W., and Lipscombe, D. (2005). Neuronal L-type calcium channels open quickly and are inhibited slowly. *J. Neurosci.* 25 (44), 10247–10251. doi:10.1523/JNEUROSCI.1089-05.2005

Hescheler, J., Rosenthal, W., Trautwein, W., and Schultz, G. (1987). The GTP-binding protein, Go, regulates neuronal calcium channels. *Nature*. 325 (6103), 445–447. doi:10.1038/325445a0

Hui, K., Lipkind, G., Fozzard, H. A., and French, R. J. (2002). Electrostatic and steric contributions to block of the skeletal muscle sodium channel by mu-conotoxin. *J. Gen. Physiol.* 119 (1), 45–54. doi:10.1085/jgp.119.1.45

Kingwell, K. (2019). Nav1.7 withholds its pain potential. *Nat. Rev. Drug Discov.* 18, 321–333. doi:10.1038/d41573-019-00065-0

Kubota, T., Durek, T., Dang, B., Finol-Urdaneta, R. K., Craik, D. J., Kent, S. B., et al. (2017). Mapping of voltage sensor positions in resting and inactivated mammalian sodium channels by LRET. *Proc. Natl. Acad. Sci. U.S.A.* 114 (10), E1857–E1865. doi:10.1073/pnas.1700453114

Kuenzi, F. M., and Dale, N. (1996). Effect of capsaicin and analogues on potassium and calcium currents and vanilloid receptors in Xenopus embryo spinal neurones. *Br. J. Pharmacol.* 119 (1), 81–90. doi:10.1111/j.1476-5381.1996.tb15680.x

Lee, S., Jo, S., Talbot, S., Zhang, H. B., Kotoda, M., Andrews, N. A., et al. (2019). Novel charged sodium and calcium channel inhibitor active against neurogenic inflammation. *Elife*. 8, e48118. doi:10.7554/eLife.48118

Leipold, E., Ullrich, F., Thiele, M., Tietze, A. A., Terlau, H., Imhof, D., et al. (2017). Subtype-specific block of voltage-gated K. *Biochem. Biophys. Res. Commun.* 482 (4), 1135–1140. doi:10.1016/j.bbrc.2016.11.170

Li-Smerin, Y., and Swartz, K. J. (1998). Gating modifier toxins reveal a conserved structural motif in voltage-gated Ca^{2+} and K^+ channels. *Proc. Natl. Acad. Sci. U.S.A.* 95 (15), 8585–8589. doi:10.1073/pnas.95.15.8585

McArthur, J. R., Ostroumov, V., Al-Sabi, A., McMaster, D., and French, R. J. (2011). Multiple, distributed interactions of μ-conotoxin PIIIA associated with broad targeting among voltage-gated sodium channels. *Biochemistry*. 50 (1), 116–124. doi:10.1021/bi101316y

McArthur, J. R., Finol-Urdaneta, R. K., and Adams, D. J. (2019). Analgesic transient receptor potential vanilloid-1-active compounds inhibit native and recombinant T-type calcium channels. *Br. J. Pharmacol.* 176 (13), 2264–2278. doi:10.1111/bph.14676

Middleton, R. E., Warren, V. A., Kraus, R. L., Hwang, J. C., Liu, C. J., Dai, G., et al. (2002). Two tarantula peptides inhibit activation of multiple sodium channels. *Biochemistry*. 41 (50), 14734–14747. doi:10.1021/bi026546a

Minett, M. S., Pereira, V., Sikandar, S., Matsuyama, A., Lolignier, S., Kanellopoulos, A. H., et al. (2015). Endogenous opioids contribute to insensitivity to pain in humans and mice lacking sodium channel Nav1.7. *Nat. Commun.* 6, 8967. doi:10.1038/ncomms9967

Mueller, A., Starobova, H., Morgan, M., Dekan, Z., Cheneval, O., Schroeder, C. I., et al. (2019). Antiallodynic effects of the selective $Na_v1.7$ inhibitor Pn3a in a mouse model of acute postsurgical pain: evidence for analgesic synergy with opioids and baclofen. *Pain* 160 (8), 1766–1780. doi:10.1097/j.pain.0000000000001567

Mueller, A., Dekan, Z., Kass, Q., Agwa, A. J., Starobova, H., Alewood, P. F., et al. (2020). Mapping the molecular surface of the analgesic $Na_v1.7$-selective peptide Pn3a reveals residues essential for membrane and channel interactions. *ACS Pharmacol. Transl. Sci.* 3 (3), 535–546. doi:10.1021/acsptsci.0c00002

Olamendi-Portugal, T., Garcia, B. I., Lopez-Gonzalez, I., Van Der Walt, J., Dyason, K., Ulens, C., et al. (2002). Two new scorpion toxins that target voltage-gated Ca^{2+} and Na^+ channels. *Biochem. Biophys. Res. Commun.* 299 (4), 562–568. doi:10.1016/s0006-291x(02)02706-7

Page, A. J., O'Donnell, T. A., and Blackshaw, L. A. (2006). Inhibition of mechanosensitivity in visceral primary afferents by $GABA_B$ receptors involves calcium and potassium channels. *Neuroscience* 137 (2), 627–636. doi:10.1016/j.neuroscience.2005.09.016

Sadeghi, M., McArthur, J. R., Finol-Urdaneta, R. K., and Adams, D. J. (2017). Analgesic conopeptides targeting G protein-coupled receptors reduce excitability of sensory neurons. *Neuropharmacology* 127, 116–123. doi:10.1016/j.neuropharm.2017.05.020

Schmalhofer, W. A., Calhoun, J., Burrows, R., Bailey, T., Kohler, M. G., Weinglass, A. B., et al. (2008). ProTx-II, a selective inhibitor of Nav1.7 sodium channels, blocks action potential propagation in nociceptors. *Mol. Pharmacol.* 74 (5), 1476–1484. doi:10.1124/mol.108.047670

Scroggs, R. S., and Fox, A. P. (1992). Calcium current variation between acutely isolated adult rat dorsal root ganglion neurons of different size. *J. Physiol.* 445, 639–658. doi:10.1113/jphysiol.1992.sp018944

Shields, S. D., Deng, L., Reese, R. M., Dourado, M., Tao, J., Foreman, O., et al. (2018). Insensitivity to pain upon adult-onset deletion of Nav1.7 or its blockade with selective inhibitor. *J. Neurosci.* 38 (47), 10180–10201. doi:10.1523/JNEUROSCI.1049-18.2018

Sidach, S. S., and Mintz, I. M. (2002). Kurtoxin, a gating modifier of neuronal high- and low-threshold ca channels. *J. Neurosci.* 22 (6), 2023–2034. doi:10.1523/JNEUROSCI.22-06-02023.2002

Swartz, K. J., and MacKinnon, R. (1995). An inhibitor of the Kv2.1 potassium channel isolated from the venom of a Chilean tarantula. *Neuron*. 15 (4), 941–949. doi:10.1016/0896-6273(95)90184-1

Xiao, Y., Tang, J., Hu, W., Xie, J., Maertens, C., Tytgat, J., et al. (2005). Jingzhaotoxin-I, a novel spider neurotoxin preferentially inhibiting cardiac sodium channel inactivation. *J. Biol. Chem.* 280 (13), 12069–12076. doi:10.1074/jbc.M411651200

Xu, W., and Lipscombe, D. (2001). Neuronal Ca(V)1.3alpha(1) L-type channels activate at relatively hyperpolarized membrane potentials and are incompletely inhibited by dihydropyridines. *J. Neurosci.* 21 (16), 5944–5951. doi:10.1523/JNEUROSCI.21-16-05944.2001

Yamamoto, T., and Sakashita, Y. (1998). Differential effects of intrathecally administered N- and P-type voltage-sensitive calcium channel blockers upon two models of experimental mononeuropathy in the rat. *Brain Res.* 794 (2), 329–332. doi:10.1016/s0006-8993(98)00306-0

Yuan, C., Yang, S., Liao, Z., and Liang, S. (2007). Effects and mechanism of Chinese tarantula toxins on the Kv2.1 potassium channels. *Biochem. Biophys. Res. Commun.* 352 (3), 799–804. doi:10.1016/j.bbrc.2006.11.086

Conflict of Interest: The authors declare that the research was conducted in the absence of any commercial or financial relationships that could be construed as a potential conflict of interest.

frontiers in Pharmacology

ORIGINAL RESEARCH
published: 20 April 2021
doi: 10.3389/fphar.2021.611433

Comparison of Pancreatic Damage in Rats for Two Methods of Paraquat Administration

Yanxia Gao[1], Linlin Hou[1], Yibo Wang[1], Yan Zhang[1], Shoutao Zhang[2], Yi Li[3], Yanan Jiang[4], Changju Zhu[1], Tongwen Sun[1], Guoyu Duan[1] and Ding Yuan[1]**

[1]Emergency Department, The First Affiliated Hospital of Zhengzhou University, Zhengzhou, China, [2]Henan Key Laboratory of Bioactive Macromolecules, School of Life Sciences, Zhengzhou, China, [3]Emergency Department, Chinese Academy of Medical Sciences, Peking Union Medical College Hospital, Beijing, China, [4]Department of Pathophysiology, School of Basic Medical Sciences, Zhengzhou University, Zhengzhou, China

It is noted that elevated serum amylase levels suggesting pancreatic damage has an association with prognosis in PQ patients. This study aimed to determine whether PQ can cause pancreatic damage. The two conventional models (intragastric infusion (iG) and intraperitoneal injection (iP)) may exhibit different effects on the pancreas depending on whether or not they pass through the digestive tract. In this study, the rats were divided into four groups: the intragastric infusion group (PQ-iG, $n = 45$), intraperitoneal injection group (PQ-iP, $n = 53$), normal control group 1 (NC-iG, $n = 6$) and normal control group 2 (NC-iP, $n = 6$). Pancreatic damage was compared between groups using serum amylase activity assay, hematoxylin and eosin (H&E) staining, TUNEL assay, and transmission electron microscopy (TEM). Serum amylase levels in group PQ-iG were significantly higher than in group PQ-iP ($p < 0.05$). Examination of the H&E sections showed damage to the pancreas. Both experimental groups were displayed inflammatory infiltration within 9 h of PQ treatment. After 9 h, patchy necrosis was observed in group PQ-iP, when inflammatory infiltration was still the dominant pathology. Necrosis appeared and gradually worsened in group PQ-iG, in which necrosis was the dominant pathology. The TUNEL assay showed significantly higher numbers of apoptotic cells in the pancreas of PQ-groups than in the control NC- groups ($p < 0.05$). TEM showed expansive endoplasmic reticulum lumens and mitochondria swelling in the pancreas of the PQ-groups. It is concluded that both methods of modeling could cause pancreatic damage and the type and degree of damage would change over time. Note that pancreatic damage in group PQ-iG was more severe than that in group PQ-iP. Therefore, clinical practitioners should pay close attention to pancreatic damage caused by PQ, especially when the route of PQ administration was oral.

Keywords: paraquat poisoning, pancreatic damage, multiple organ damage, intragastric infusion, intraperitoneal injection

OPEN ACCESS

Edited by:
Jean-Marc Sabatier, Aix-Marseille Université, France

Reviewed by:
Milladur Rahman, Lund University, Sweden
József Maléth, University of Szeged, Hungary

****Correspondence:***
Yanxia Gao
gaoyanxiazzu@163.com
Ding Yuan
yuanding198879@163.com

Specialty section:
This article was submitted to Translational Pharmacology, a section of the journal Frontiers in Pharmacology

Received: *29 September 2020*
Accepted: *01 February 2021*
Published: *20 April 2021*

Citation:
Gao Y, Hou L, Wang Y, Zhang Y, Zhang S, Li Y, Jiang Y, Zhu C, Sun T, Duan G and Yuan D (2021) Comparison of Pancreatic Damage in Rats for Two Methods of Paraquat Administration. Front. Pharmacol. 12:611433. doi: 10.3389/fphar.2021.611433

INTRODUCTION

Paraquat (PQ) ingestion can lead to multiple organ failure (Melchiorri et al., 1995; Adachi et al., 2000; Zhang X. et al., 2019; Liu et al., 2019; Mirzaee et al., 2019). There is no specific antidote for PQ poisoning, and even small doses of PQ can cause death; the fatality rate of PQ is as high as 50–80% (Zhang L. et al., 2019; Zhang X. et al., 2019; Wu et al., 2019). The cause of PQ poisoning deaths is

usually recorded as acute respiratory failure (Wu et al., 2019; Gao F. et al., 2020). Some clinical studies have shown elevated serum amylase levels in PQ poisoning patients, which suggests that PQ may cause pancreatic damage (Soontornniyomkij and Bunyaratvej, 1992; Wang and Qian, 2005; Gong et al., 2016). It has been shown that patients diagnosed with PQ poisoning who have elevated levels of serum amylase have a worse prognosis than other patients (Gil et al., 2009; Li et al., 2015; Huang et al., 2020).

In clinical patients, PQ is usually taken orally. However, in experimental studies, PQ is often administered by intraperitoneal injection (iP) because it is easy to use and the dose is controllable (Wunnapuk et al., 2013; Chen et al., 2015; Zhang et al., 2018). The biggest difference between iP and iG is in passage through the digestive tract. The pancreas is a digestive organ that is anatomically close to the digestive tract. In our previous animal model study, in which PQ was administered to rats by intragastric infusion (iG), we found that PQ poisoning increased serum amylase levels in the rats; histopathological examination of rat pancreas showed that the pancreas presented inflammatory cell infiltration and cell necrosis (Gao Y. et al., 2020). Regarding pancreatic damage, there is still a controversy in academia. Some researchers believe that PQ poisoning-induced increased amylase may be caused by gastrointestinal damage, which is not strong evidence that pancreatic damage exists (Huang et al., 2020). However, others maintain that PQ in the digestive tract may retrograde into the pancreatic duct due to causes like vomiting and gastric lavage after PQ poisoning, leading to pancreatic damage (Gong et al., 2016). Further investigation of whether PQ poisoning by iP leads to pancreatic damage and differences in the progression of PQ poisoning between administration by iG and iP is merited.

In this study, we observed and compared pancreatic damage caused by PQ when administered by iG and iP, which had not been studied before. The results showed that PQ could cause pancreatic damage when it was either administered by iG or iP; the type and degree of damage would change over time, and there were differences between the two groups. Thus, clinical practitioners are recommended to pay attention to pancreatic damage caused by PQ.

MATERIALS AND METHODS

Animal Protocol

Healthy male Sprague-Dawley (SD) rats, purchased from Beijing Vital River Laboratory Animal Technology Co., Ltd., weighing 180–220 g, were used in this study. The rats were fed under a 12 h light/12 h dark cycle with unlimited food and water for one week prior to the experiment. Ethical approval for this study was obtained from the Animal Ethics Committee of Zhengzhou University in accordance with institutional guidelines for the care and use of animals for scientific purposes (permit number 2019-KY-191).

A total of 110 rats were divided into four groups: normal control group 1 (NC-iG, $n = 6$), normal control group 2 (NC-iP, $n = 6$), intragastric infusion group (PQ-iG, $n = 45$) and intraperitoneal injection group (PQ-iP, $n = 53$). Rats in group NC-iG received 1 ml 0.9% normal saline by iG. Rats in NC-iP group received 1 ml 0.9% normal saline by iP. PQ powder (Sigma-Aldrich, United States) was suspended and dissolved in 0.9% normal saline. The PQ-iG group was administered PQ by iG infusion at a dose of 120 mg/kg in a total volume of 1 ml 0.9% normal saline, and the PQ-iP group was administered PQ by iP injection at a dose of 35 mg/kg in a total volume of 1 ml 0.9% normal saline. The dose was determined with reference to the half lethal dose of PQ poisoning induced by iG and iP in rats (Dinis-Oliveira et al., 2008). The rats were deeply anesthetized by intraperitoneal injection of 50 mg/kg pentobarbital sodium and sacrificed randomly at 3, 6, 9, 12, 24, 48 and 72 h after PQ administration, at least three rats were randomly selected from each group at each time point. The serum was isolated and stored in a −80°C refrigerator for later use; pancreas were harvested and soaked in 4% paraformaldehyde.

Amylase Activity Assay

Levels of rat serum amylase were measured using an amylase activity assay kit (Cat.MAK009, Sigma-Aldrich, United States). The experimental procedure strictly followed the kit manufacturer's instructions.

Hematoxylin and Eosin (H&E) staining

Rat tissues were fixed in 4% paraformaldehyde and embedded in paraffin. The specimens were then sectioned at a thickness of 5 μm, dewaxed using xylene, dehydrated using an alcohol gradient, and stained with H&E. The sections were counterstained with hematoxylin and mounted. The stained sections were examined using an optical microscope (Leica, Germany). The scoring method described by Schmidt et al. was used to evaluate pancreatic histopathology in the rat tissue (Schmidt et al., 1992).

TUNEL Assay

Apoptosis of pancreatic acinar cells was investigated using a TUNEL apoptosis assay (Promega, United States) according to the manufacturer's instructions. The section was dewaxed with xylene and dehydrated with alcohol with a reduced concentration gradient. After dehydration, tissue sections were digested with 2% protease K, incubated at 37°C for 20 min, and then washed 3 times with phosphate buffer saline (PBS). Each section was drizzled with 40 μL TDT (1:10) and incubated for 120 min at 37°C. After washing 3 times with PBS, the section was stained with 50 μL DAPI (1:100), incubated at 37°C for 2 min, and then soaked in PBS 3 times, for 5 min each time. The slices were all sealed with an anti-fluorescence quenching agent, and images were collected under a fluorescence microscope (Leica).

Transmission Electron Microscopy

The rat pancreas were imaged using transmission electron microscopy (TEM) to observe mitochondria and endoplasmic reticulum morphology. Pancreatic tissue from all experimental groups was immediately fixed in 2.5% glutaraldehyde (Solarbio, Beijing, China). The dissected pancreatic tissue was washed with PBS and post-fixed in 2% osmium tetroxide for 2 h at room

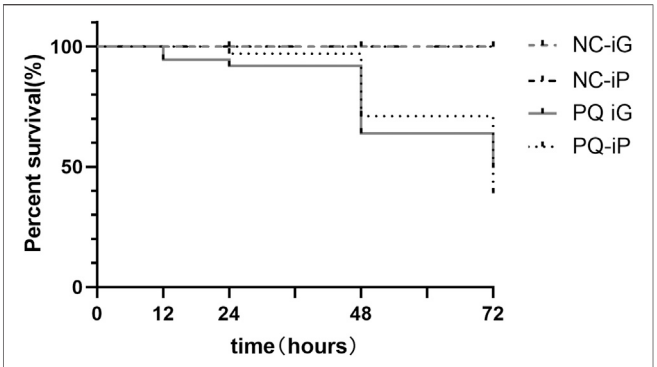

FIGURE 1 | Survival curves of rats in all groups after PQ administration.

temperature. Fixed tissue was dehydrated in a series of graded alcohols and embedded in Epon resin. The resin was polymerized, and blocks were sectioned on a microtome (Leica). The sections were double-stained with uranyl acetate and lead citrate and then examined and imaged with a transmission electron microscope (Leica).

Statistical Analysis

SPSS software version 21.0 (SPSS Inc., United States) was used for statistical analysis. The Kolmogorov–Smirnov test was used to assess the normality of the distribution. The measurement data conforming to the normal distribution were described as mean plus or minus standard deviation (mean ± SD). Samples from two groups were compared using independent sample *t*-tests and correlation analysis, and samples from four groups were compared using one-way analysis of variance (ANOVA), followed by the least significant difference (LSD) test. Measurement data that did not conform to the normal distribution were described by the median and interquartile range [M(p25, p75)]. The Wilcoxon rank-sum test was used for comparison between two groups, and the Kruskal–Wallis rank-sum test was used for comparisons between three or four groups, followed by the Bonferroni test. Differences were considered significant at $p < 0.05$.

RESULTS

Rat Mortality

During the experiment, we recorded the number of animals in the four groups that had died at each time point and drew a cumulative survival curve (**Figure 1**). Rats in the NC- groups survived until they were sacrificed at the end of the experiment. **Figure 1** shows cumulative survival after exposure to PQ. A sharp increase in mortality was observed at 48 h after PQ administration. At 48 h, the cumulative mortality rates were 40% in group PQ-iG and 29% in group PQ-iP. At 72 h, the two groups had similar cumulative mortality rates: the cumulative mortality rates were 56% in group PQ-iG and 61% in group PQ-iP.

Pathological Changes in Pancreas and Serum Amylase Activity

Serum amylase levels were measured (**Figure 2C**). Amylase activity for rats in group PQ-iG was higher than in group NC-iG; the difference was statistically significant ($p < 0.05$) after 24 h. Amylase activity did not significantly increase in group PQ-iP over group NC-iP ($p = 0.12$). There was no statistically significant difference between the two NC- groups ($p = 0.086$). Group PQ-iG showed higher levels than group PQ-iP, and the difference was statistically significant ($p < 0.05$).

The pancreas tissue was stained with H&E at each observation time point to enable us to observe and compare changes in pancreatic damage between the two methods of PQ administration (iG and iP). **Figure 2A** shows that there was no obvious pathological damage in the NC- groups; the pancreatic lobule was intact, the demarcation was clear, and there was almost no inflammatory cell infiltration, necrosis, or hemorrhage. In group PQ-iG, inflammatory cell infiltration had occurred at 3 h, acinar cell fusion and necrosis had occurred at 9 h, and vascular rupture and hemorrhage had occurred at 24 h. In group PQ-iP, inflammatory cell infiltration had occurred at 3 h, and acinar cell fusion and necrosis had occurred at 6 h. Before 9 h, inflammatory infiltration was the predominant presentation in both groups. After 9 h, patchy necrosis was observed in group PQ-iP, in which inflammatory infiltration was still predominant. Necrosis appeared and gradually increased in group PQ-iG to become predominant.

We allocated pathological damage scores according to the scoring method given by Schmidt et al. (Schmidt et al., 1992) to quantify the pancreatic damage (**Figure 2B**). There was no difference in pathological damage scores between the NC- groups ($p = 0.174$). The pathological damage scores of the PQ- groups were higher than those of the corresponding NC- groups. In group PQ-iG, the difference in scores at 24 h, when compared with the group NC-iG, was statistically significant ($p < 0.05$). In group PQ-iP, the difference in scores at 48 h, when compared with the group NC-iP, was statistically significant ($p < 0.05$). At 3 and 6 h, the score of group PQ-iP was higher than that of group PQ-iG; at 9 h and thereafter, the score of group PQ-iG was higher than that of group PQ-iP. The scores for the NC- groups at 0 h were taken as the baselines. These results suggest PQ administration by both iG and iP causes pancreatic damage. The initial pancreatic damage in group PQ-iP was more severe than in group PQ-iG but pancreatic damage at 72 h was less severe than in group PQ-iG.

Effects of PQ Poisoning on Pancreatic Tissue Apoptosis

Apoptosis is a hallmark of pancreatitis (Wang et al., 2019; Zhou et al., 2019). **Figure 2B** showed that the pathological damage scores of PQ-groups stabilized at 48 h. Thus we selected

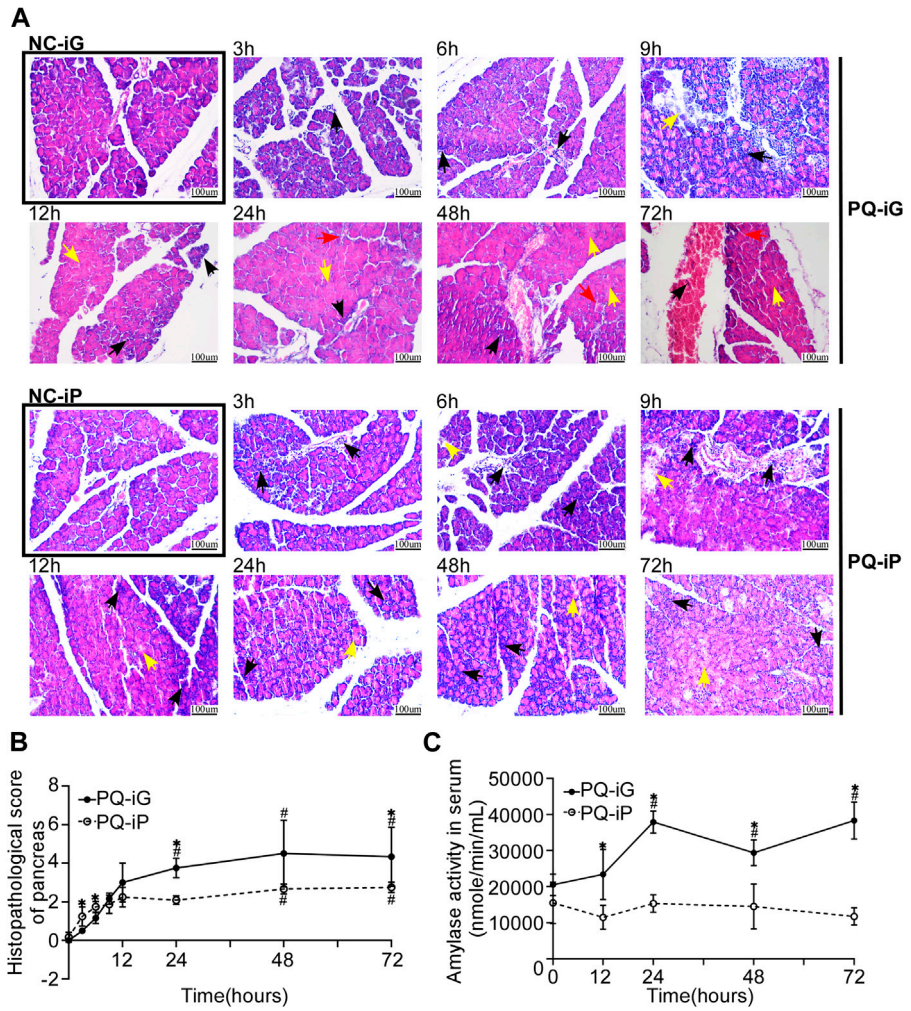

FIGURE 2 | Changes in the pancreas due to iG and iP administration of PQ. **(A)** Typical pathological changes in H&E stained pancreatic tissue sections in groups PQ-iG and PQ-iP at various times of observation (magnification ×200; scale bar: 100 μm; black arrow = inflammatory cell infiltration; yellow arrow = necrotic cell; red arrow = hemorrhage); **(B)** Pathological damage scores of rat pancreas in groups PQ-iG and PQ-iP at each observation time point; **(C)** Serum amylase activity (nmole/ min/ ml) of rats in groups PQ-iG and PQ-iP. The corresponding NC- groups values were taken for 0 h after PQ treatment. $^{*}p < 0.05$: the difference between the PQ-iG and PQ-iP groups was statistically significant at this time point; $^{\#}p < 0.05$: the difference was statistically significant in comparison with the corresponding NC group. PQ paraquat; iG: intragastric infusion; iP: intraperitoneal injection.

pancreatic wax blocks from 48 h after PQ administration for TUNEL assay to quantify the degree of apoptosis. In **Figure 3A**, green indicates the apoptotic cells and increased green fluorescence indicates increased cell apoptosis in tissue. The number of TUNEL-positive cells for each group was calculated by ImageJ (**Figure 3B**); there was no difference between the NC-iG and NC-iP groups. Significantly higher TUNEL-positive cell numbers were found in the PQ-groups than in the corresponding NC- groups ($p < 0.05$). The TUNEL-positive cell count for group PQ-iG was higher than for group PQ-iP; there was no statistically significant difference between the two groups ($p = 0.4589$).

Changes in Pancreatic Organelles

TEM was used to examine changes in the ultrastructure, particularly cellular organelles, of pancreatic tissue 48 h after exposure to PQ. Pancreas sections in the NC- groups had regular structures in the nuclei, with evenly distributed endoplasmic reticulum and normal mitochondria that were intact. In the PQ-groups, endoplasmic reticulum lumen and endoplasmic reticulum disorder were observed, the endoplasmic reticulum showed mild to moderate diffuse endoplasmic reticulum lumen dilation in PQ-iG groups, and mild local endoplasmic reticulum lumen dilation in PQ-iP groups. Mitochondria showed mild local edema in PQ-iG groups and in PQ-iP groups (**Figure 4**).

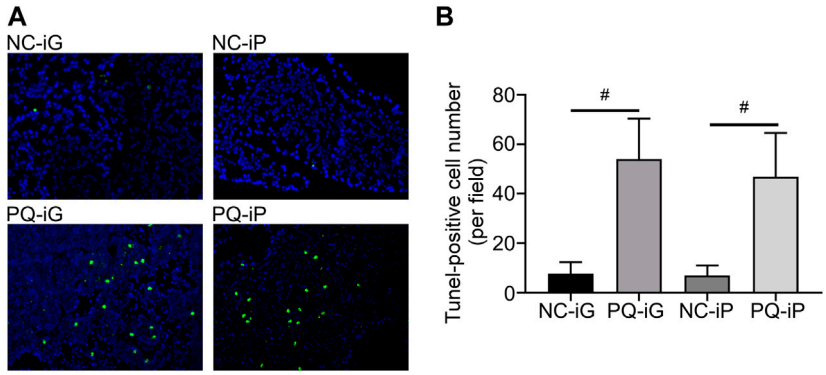

FIGURE 3 | TUNEL staining assay was used to determine apoptosis in pancreatic tissue. **(A)** Typical TUNEL assay results for pancreatic tissue in each group (magnification ×200); **(B)** TUNEL stained apoptotic cell numbers. $^{\#}p < 0.05$: the difference was statistically significant when compared to the corresponding NC- group.

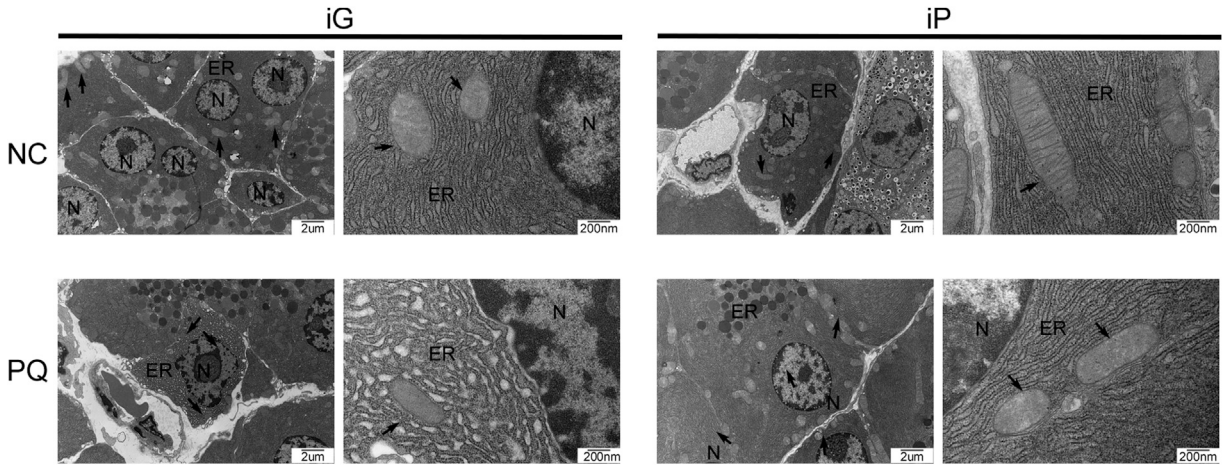

FIGURE 4 | Typical TEM photos of pancreatic tissue sections (bar = 2 μm or 200 nm); N: nucleus, mt: mitochondria, black arrow: mitochondria, ER: endoplasmic reticulum, TEM: transmission electron microscopy, NC: normal control, PQ: paraquat poisoning, iG: intragastric infusion, iP: intraperitoneal injection.

DISCUSSION

In this study, we have focused on pancreatic damage due to PQ poisoning in two conventional rat models. The main findings of our study are: 1. PQ could cause pancreatic damage when it was administered either by iG or iP. Pancreatic damage in group PQ-iG was more severe than that in group PQ-iP; 2. the type and degree of damage would change over time, and there were differences between the two groups.

Some previous studies had reported the abnormal pancreatic enzymes, but few studies have focused on pancreas (Soontornniyomkij and Bunyaratvej, 1992; Wang and Qian, 2005; Li et al., 2015; Gong et al., 2016). There are only two previous basic studies of pancreatic damage due to PQ poisoning. One is our previous study (Gao Y. et al., 2020), a rat model of PQ poisoning by iG administration. The other is the report of an experiment by Silfeler et al. (Silfeler et al., 2015), who induced PQ poisoning in rats by iP administration. In this study, we found that serum amylase levels increased significantly in group PQ-iG but not in group PQ-iP compared with the corresponding NC- groups. PQ poisoning by iG administration led to elevated levels of serum amylase, which is consistent with our previous research (Gao Y. et al., 2020) and clinical reports (Soontornniyomkij and Bunyaratvej, 1992; Wang and Qian, 2005; Gong et al., 2016). Serum amylase levels did not significantly increase in group PQ-iP compared with group NC-iP, a finding that is consistent with that of Silfeler et al. The fact that the increased serum amylase levels in group PQ-iG is more significant than that in group PQ-iP can be explained as follows: 1. pancreatic damage in group PQ-iG was more severe than in group PQ-iP; 2. the increased serum amylase levels in group PQ-iG may have been caused in part by gastrointestinal damage (Liu et al., 2016; Huang et al., 2020).

Silfeler et al. found inflammatory cell infiltration, edema, and congestion in pancreatic tissue. We found in this study that

inflammatory infiltration was predominant in both groups within 9 h of PQ administration. After 9 h, patchy necrosis was observed in group PQ-iP, in which inflammatory infiltration was still predominant; necrosis appeared and gradually increased in group PQ-iG to become predominant. The pathological damage score for group PQ-iP was higher than for group PQ-iG at 9 h after PQ administration; after 9 h, the score for group PQ-iG was higher than for group PQ-iP. The type and degree of damage changed over time, and there were differences between the two groups. The reason the score for group PQ-iP was higher than for group PQ-iG may be that PQ was absorbed directly within the peritoneal cavity in rats in group PQ-iP but absorbed into the blood through the digestive tract in rats in group PQ-iG. The reason pancreatic damage in group PQ-iG was more severe than in group PQ-iP may be that there are two pathways for pancreatic damage to occur in group PQ-iG: through corrosion of gastrointestinal tract and microecology (Cen et al., 2018), and by inflammatory reaction and oxidative stress in response to PQ absorbed in the bloodstream. PQ administered by iP causes pancreatic damage only through inflammatory reaction and oxidative stress due to PQ absorbed into the bloodstream. We thus suggest that the animal model method made by iG is much closer to the pancreatic damage caused by PQ poisoning in the clinical study.

PQ causes cell apoptosis in lungs (Seo et al., 2014; Cui et al., 2019; Zhang et al., 2020), kidneys (Hu et al., 2019), liver (El-Boghdady et al., 2017; Qian et al., 2019) and nerves (Fujimori et al., 2012; Ju et al., 2019). There have been no studies into whether PQ causes apoptosis in pancreatic cells. We observed in this study that PQ causes pancreatic cell apoptosis. The TUNEL assay results show higher apoptotic cell numbers were found in PQ-groups in contrast with the corresponding NC- groups.

The pancreas is a digestive organ that synthesizes many digestive enzymes. Pancreatic acinar cells are rich in endoplasmic reticulum and mitochondria (Habtezion et al., 2019). Dysfunction of the endoplasmic reticulum and mitochondria indicates impaired pancreatic function. We also observed, through TEM, changes in pancreatic organelles caused by PQ. The results of TEM showed that the endoplasmic reticulum showed mild to moderate diffuse endoplasmic reticulum lumen dilation in PQ-iG groups, and mild local endoplasmic reticulum lumen dilation in PQ-iP groups. Mitochondria showed mild local edema in PQ-iG groups and in PQ-iP groups. TEM also confirmed that PQ can cause pancreatic damage.

CONCLUSION

In conclusion, PQ could cause pancreatic damage and its type and degree would change over time. Pancreatic damage in group PQ-iG was more severe than that in group PQ-iP. Clinical practitioners should focus on pancreatic damage caused by PQ, especially when the route of PQ administration was oral.

DATA AVAILABILITY STATEMENT

The raw data supporting the conclusions of this article will be made available by the authors, without undue reservation, to any qualified researcher.

ETHICS STATEMENT

The animal study was reviewed and approved by the Animal Ethics Committee of Zhengzhou University in accordance with the institutional guidelines for the care and use of animals for scientific purposes (permit number 2019-KY-191).

AUTHOR CONTRIBUTIONS

YG, YL, YJ, CZ, SZ and TS conceived and designed the experiments. GD, LH and YW performed the experiments. LH and DY were involved in experimental analysis and data acquisition. YL, DY and YZ assisted in the manuscript preparation. YG and LH wrote the manuscript. All authors contributed to the article and approved the submitted version.

FUNDING

This work was supported by the National Natural Science Foundation of China (grant number: 81701893), the National Science and Technology Major Project (grant number: 2017ZX10103005-009), the Joint Construction Project of Henan Province Medical Science and Technology Research Plan (grant number: SB201901006), the Key Scientific Research Projects of Institutions of Higher Learning in Henan Province (20A320046), and the CAMS Innovation Fund for Medical Sciences(grant number: 2020-I2M-C&T-B-014).

REFERENCES

Adachi, J., Tomita, M., Yamakawa, S., Asano, M., Naito, T., and Ueno, Y. (2000). 7-Hydroperoxycholesterol as a marker of oxidative stress in rat kidney induced by paraquat. *Free Radic. Res.* 33, 321–327. doi:10.1080/10715760000301491

Cen, M.-E., Wang, F., Su, Y., Zhang, W.-J., Sun, B., and Wang, G. (2018). Gastrointestinal microecology: a crucial and potential target in acute pancreatitis. *Apoptosis* 23, 377–387. doi:10.1007/s10495-018-1464-9

Chen, J. L., Dai, L., Zhang, P., Chen, W., Cai, G. S., Qi, X. W., et al. (2015). Methylene blue attenuates acute liver injury induced by paraquat in rats. *Int. Immunopharmacology* 28, 808–812. doi:10.1016/j.intimp.2015.04.044

Cui, S., Nian, Q., Chen, G., Wang, X., Zhang, J., Qiu, J., et al. (2019). Ghrelin ameliorates A549 cell apoptosis caused by paraquat via p38-MAPK regulated mitochondrial apoptotic pathway. *Toxicology* 426, 152267. doi:10.1016/j.tox.2019.152267

Dinis-Oliveira, R. J., Duarte, J. A., Sánchez-Navarro, A., Remião, F., Bastos, M. L., and Carvalho, F. (2008). Paraquat poisonings: mechanisms of lung toxicity, clinical features, and treatment. *Crit. Rev. Toxicol.* 38, 13–71. doi:10.1080/10408440701669959

El-Boghdady, N. A., Abdeltawab, N. F., and Nooh, M. M. (2017). Resveratrol and Montelukast Alleviate Paraquat-Induced Hepatic Injury in Mice: Modulation of Oxidative Stress, Inflammation, and Apoptosis. *Oxid Med Cell Longev* 2017, 9396425. doi:10.1155/2017/93964252017

Fujimori, K., Fukuhara, A., Inui, T., and Allhorn, M. (2012). Prevention of paraquat-induced apoptosis in human neuronal SH-SY5Y cells by lipocalin-type prostaglandin D synthase. *J. Neurochem.* 120, 279–291. doi:10.1111/j.1471-4159.2011.07570.x

Gao, F., Zhang, Y., Yang, Z., Wang, M., Zhou, Z., Zhang, W., et al. (2020). Arctigenin Suppressed Epithelial-Mesenchymal Transition through Wnt3a/beta-Catenin Pathway in PQ-Induced Pulmonary Fibrosis. *Front. Pharmacol.* 11, 584098. doi:10.3389/fphar.2020.584098

Gao, Y., Hou, L., Wang, Y., Guo, S., Yuan, D., Jiang, Y. n., et al. (2020). Octreotide alleviates pancreatic damage caused by paraquat in rats by reducing inflammatory responses and oxidative stress. *Environ. Toxicol. Pharmacol.* 80, 103456. doi:10.1016/j.etap.2020.103456

Gil, H. W., Yang, J. O., Lee, E. Y., and Hong, S. Y. (2009). The level and clinical significance of pancreatic enzymes in survivors of acute paraquat poisoning. *Clin. Toxicol.* 47, 308–311. doi:10.1080/15563650902834497

Gong, Z., Ke, J., Huang, J., et al. (2016). Clinical analysis of 85 cases of acute paraquat poisoning complicated with acute pancreatic injury %. *J. Trauma Emerg.* 4, 43–45. [in Chinese, with English summary].

Habtezion, A., Gukovskaya, A. S., and Pandol, S. J. (2019). Acute pancreatitis: A multifaceted set of organelle and cellular interactions. *Gastroenterology* 156, 1941–1950. doi:10.1053/j.gastro.2018.11.082

Hu, X., Chen, L., Li, T., and Zhao, M. (2019). TLR3 is involved in paraquat-induced acute renal injury. *Life Sci.* 223, 102–109. doi:10.1016/j.lfs.2019.03.029

Huang, C., Bai, L., Xue, X., Peng, L., Jiang, J., and Zhang, X. (2020). Hyperamylasemia as an early predictor of mortality in patients with acute paraquat poisoning. *J. Int. Med. Res.* 48, 300060520910037. doi:10.1177/0300060520910037

Ju, D. T., Sivalingam, K., Kuo, W. W., Ho, T. J., Chang, R. L., Chung, L. C., et al. (2019). Effect of vasicinone against paraquat-induced MAPK/p53-mediated apoptosis via the IGF-1R/PI3K/AKT pathway in a parkinson's disease-associated SH-SY5Y cell model. *Nutrients* 11. doi:10.3390/nu11071655

Li, Y., Wang, M., Gao, Y., Yang, W., Xu, Q., Eddleston, M., et al. (2015). Abnormal pancreatic enzymes and their prognostic role after acute paraquat poisoning. *Sci. Rep.* 5, 17299. doi:10.1038/srep17299

Liu, B., Chen, A., Lan, J., Ren, L., Wei, Y., and Gao, L. (2019). Protective mechanism of 1-methylhydantoin against lung injury induced by paraquat poisoning. *PLoS One* 14, e0222521. doi:10.1371/journal.pone.0222521

Liu, S., Wang, Q., Zhou, R., Li, C., Hu, D., Xue, W., et al. (2016). Hyperamylasemia as an early predictor of mortality in patients with acute paraquat poisoning. *Med. Sci. Monit.* 22, 1342–1348. doi:10.12659/msm.897930

Melchiorri, D., Reiter, R. J., Attia, A. M., Hara, M., Burgos, A., and Nistico, G. (1995). Potent protective effect of melatonin on in vivo paraquat-induced oxidative damage in rats. *Life Sci.* 56, 83–89. doi:10.1016/0024-3205(94)00417-q

Mirzaee, S., Mansouri, E., Shirani, M., Zeinvand-Lorestani, M., and Khodayar, M. J. (2019). Diosmin ameliorative effects on oxidative stress and fibrosis in paraquat-induced lung injury in mice. *Environ. Sci. Pollut. Res.* 26, 36468–36477. doi:10.1007/s11356-019-06572-2

Qian, J. Y., Deng, P., Liang, Y. D., Pang, L., Wu, L. C., Yang, L. L., et al. (2019). 8-Formylophiopogonanone B antagonizes paraquat-induced hepatotoxicity by suppressing oxidative stress. *Front. Pharmacol.* 10, 1283. doi:10.3389/fphar.2019.01283

Schmidt, J., Rattner, D. W., Lewandrowski, K., Compton, C. C., Mandavilli, U., Knoefel, W. T., et al. (1992). A better model of acute pancreatitis for evaluating therapy. *Ann. Surg.* 215, 44–56. doi:10.1097/00000658-199201000-00007

Seo, H. J., Choi, S. J., and Lee, J.-H. (2014). Paraquat induces apoptosis through cytochrome c release and erk activation. *Biomolecules Ther.* 22, 503–509. doi:10.4062/biomolther.2014.115

Silfeler, I., Alp, H., Ozgur, T., Evlioglu, O., Celik, M., Er, M., et al. (2015). Protective effects of caffeic acid phenethyl ester on dose-dependent intoxication of rats with paraquat. *Toxicol. Ind. Health* 31, 1000–1007. doi:10.1177/0748233713484658

Soontornniyomkij, V., and Bunyaratvej, S. (1992). Fatal paraquat poisoning: a light microscopic study in eight autopsy cases. *J. Med. Assoc. Thai* 75 (Suppl. 1), 98–105.

Wang, L., and Qian, Y. Y. (2005). A deceased case report of paraquat ingestion induced severe pancreatic injury %. *J. Zhong Guo Yao Wu Ying Yong He Jian Che.* 1, 37–38.

Wang, N., Ma, J., Ren, Y., Xiang, S., and Jia, R. (2019). Erratum: Secreted klotho from exosomes alleviates inflammation and apoptosis in acute pancreatitis. *Am. J. Transl Res.* 11, 6701.

Wu, L., Cen, Y., Feng, M., Zhou, Y., Tang, H., Liao, X., et al. (2019). Metformin activates the protective effects of the ampk pathway in acute lung injury caused by paraquat poisoning. *Oxid Med. Cel Longev* 2019, 1709718. doi:10.1155/2019/1709718

Wunnapuk, K., Liu, X., Peake, P., Gobe, G., Endre, Z., Grice, J. E., et al. (2013). Renal biomarkers predict nephrotoxicity after paraquat. *Toxicol. Lett.* 222, 280–288. doi:10.1016/j.toxlet.2013.08.003

Zhang, L.Li, Q., Liu, Z., Wang, Y., and Zhao, M. (2019). The protective effects of bone mesenchymal stem cells on paraquat-induced acute lung injury via the muc5b and ERK/MAPK signaling pathways. *Am. J. Transl Res.* 11, 3707–3721.

Zhang, L. C., Wang, Y., Liu, W., Zhang, X. M., Fan, M., and Zhao, M. (2018). Protective effects of SOD2 overexpression in human umbilical cord mesenchymal stem cells on lung injury induced by acute paraquat poisoning in rats. *Life Sci.* 214, 11–21. doi:10.1016/j.lfs.2018.10.020

Zhang, X.Xu, X., Li, S., Li, L., Zhang, J., and Wang, R. (2019). A synthetic receptor as a specific antidote for paraquat poisoning. *Theranostics* 9, 633–645. doi:10.7150/thno.31485

Zhang, Z., Nian, Q., Chen, G., Cui, S., Han, Y., and Zhang, J. (2020). Klotho alleviates lung injury caused by paraquat via suppressing ros/p38 mapk-regulated inflammatory responses and apoptosis. *Oxid Med Cell Longev* 2020, 1854206. doi:10.1155/2020/1854206

Zhou, L., Tan, J. H., Cao, R. C., Xu, J., Chen, X. M., Qi, Z. C., et al. (2019). ATF6 regulates the development of chronic pancreatitis by inducing p53-mediated apoptosis. *Cell Death Dis.* 10, 662. doi:10.1038/s41419-019-1919-0

Conflict of Interest: The authors declare that the research was conducted in the absence of any commercial or financial relationships that could be construed as a potential conflict of interest.

frontiers in Pharmacology

REVIEW
published: 13 May 2021
doi: 10.3389/fphar.2021.655981

Non-Peptidic Small Molecule Components from Cone Snail Venoms

Zhenjian Lin[1], Joshua P. Torres[1], Maren Watkins[1], Noemi Paguigan[1], Changshan Niu[1], Julita S. Imperial[1], Jortan Tun[1], Helena Safavi-Hemami[1,2], Rocio K. Finol-Urdaneta[3], Jorge L. B. Neves[4], Samuel Espino[1], Manju Karthikeyan[1], Baldomero M. Olivera[1] and Eric W. Schmidt[1]**

[1]Departments of Medicinal Chemistry and Biochemistry, School of Biological Sciences, University of Utah, Salt Lake City, UT, United States, [2]Faculty of Health and Medical Sciences, Department of Biomedical Sciences, University of Copenhagen, Copenhagen, Denmark, [3]Illawarra Health and Medical Research Institute, University of Wollongong, Wollongong, NSW, Australia, [4]Interdisciplinary Centre of Marine and Environmental Research, CIIMAR/ CIMAR, Faculty of Sciences, University of Porto, Porto, Portugal

Venomous molluscs (Superfamily Conoidea) comprise a substantial fraction of tropical marine biodiversity (>15,000 species). Prior characterization of cone snail venoms established that bioactive venom components used to capture prey, defend against predators and for competitive interactions were relatively small, structured peptides (10–35 amino acids), most with multiple disulfide crosslinks. These venom components ("conotoxins, conopeptides") have been widely studied in many laboratories, leading to pharmaceutical agents and probes. In this review, we describe how it has recently become clear that to varying degrees, cone snail venoms also contain bioactive non-peptidic small molecule components. Since the initial discovery of genuanine as the first bioactive venom small molecule with an unprecedented structure, a broad set of cone snail venoms have been examined for non-peptidic bioactive components. In particular, a basal clade of cone snails (*Stephanoconus*) that prey on polychaetes produce genuanine and many other small molecules in their venoms, suggesting that this lineage may be a rich source of non-peptidic cone snail venom natural products. In contrast to standing dogma in the field that peptide and proteins are predominantly used for prey capture in cone snails, these small molecules also contribute to prey capture and push the molecular diversity of cone snails beyond peptides. The compounds so far characterized are active on neurons and thus may potentially serve as leads for neuronal diseases. Thus, in analogy to the incredible pharmacopeia resulting from studying venom peptides, these small molecules may provide a new resource of pharmacological agents.

Keywords: secondary metabolites, conus, gastropod, prey capture, conopeptides, natural products, venom, nicotinic acetylcholine receptor

OPEN ACCESS

Edited by:
Patrick Michael McNutt, Wake Forest Institute for Regenerative Medicine, United States

Reviewed by:
Manuel B. Aguilar, Universidad Nacional Autónoma de México, Mexico
Santiago J. Ballaz, Yachay Tech University, Ecuador

****Correspondence:***
Baldomero M. Olivera
olivera@biology.utah.edu
Eric W. Schmidt
ews1@utah.edu

Specialty section:
This article was submitted to Neuropharmacology, a section of the journal Frontiers in Pharmacology

Received: *19 January 2021*
Accepted: *15 March 2021*
Published: *13 May 2021*

Citation:
Lin Z, Torres JP, Watkins M, Paguigan N, Niu C, Imperial JS, Tun J, Safavi-Hemami H, Finol-Urdaneta RK, Neves JLB, Espino S, Karthikeyan M, Olivera BM and Schmidt EW (2021) Non-Peptidic Small Molecule Components from Cone Snail Venoms. Front. Pharmacol. 12:655981. doi: 10.3389/fphar.2021.655981

INTRODUCTION

The venomous cone snails comprise a biodiverse lineage of marine gastropods (~1,000 living species) that specialize on the spectrum of prey (fish, other gastropod molluscs, or polychaete worms) envenomated by each species. The cone snails can be grouped into distinct clades, based on molecular phylogenetic data; these divisions generally correlate with the prey specialization of each

FIGURE 1 | (A) Cone shells of *Stephanoconus* species. Left top, *Conus regius* (Florida); Left bottom, *Conus archon* (West Mexico); Center, *Conus imperialis* (Philippines); Right top, *Conus genuanus* (West Africa); Right bottom, *Conus chiangi* (Philippines, 150–250 m). **(B)** Variation in Indo-Pacific *Stephanoconus*. From left to right: *Conus imperialis fuscatus* (sometimes called *viridulus*; Zanzibar, East Africa); *Conus zonatus* (Laccadive Islands, India); *Conus imperialis* variety (Reunion Island); *Conus imperialis* variety (Balicasag Island, Philippines, gill nets, 70–120 fathoms). All four forms may represent different species from the *Conus imperialis* specimen shown in **A**, but only *Conus zonatus* is generally accepted as being different (Photography by Sam Watson and Sam Espino.)

clade (Nam et al., 2009; Kraus et al., 2011). Despite the enormous range of biology evolved across the entire group, there is a general feature characteristic of the entire family (Conidae): all cone snails have complex venoms each with its own distinctive complement of typically 100–200 bioactive venom components (Olivera et al., 2014). The venoms are produced in a long venom gland, lined with secretory epithelial cells where the biosynthesis of venom components takes place. The venom is injected by extending a proboscis from the anterior gut, through a highly -specialized radular tooth that serves as a hypodermic needle (Kohn et al., 1999).

No matter what the prey type, many venom components are encoded by a few well-characterized gene superfamilies expressed in the venom glands and distributed through all of the diverse lineages of cone snails (Robinson and Norton, 2014). One such example of a well-characterized group of venom peptides are the α-conopeptides that belong to the A-gene superfamily: the bioactive post-translationally processed gene products are typically small (10–25 amino acids) peptides with two disulfide bonds (Puillandre et al., 2010). The mature peptides are encoded at the C-terminal end of a canonical precursor with a conserved signal sequence and an intervening propeptide region. The gene structure that encodes this family of venom components is conserved; a large fraction of the peptides encoded by this gene superfamily share their general targeting specificity—these inhibit nicotinic acetylcholine receptors of various types (McIntosh et al., 1999). Cone snail venom peptides of this type have now been studied for many decades and are increasingly well characterized (Azam and McIntosh, 2009).

The purpose of this article is to balance the perception that the bioactive components of cone snail venoms are all small peptides

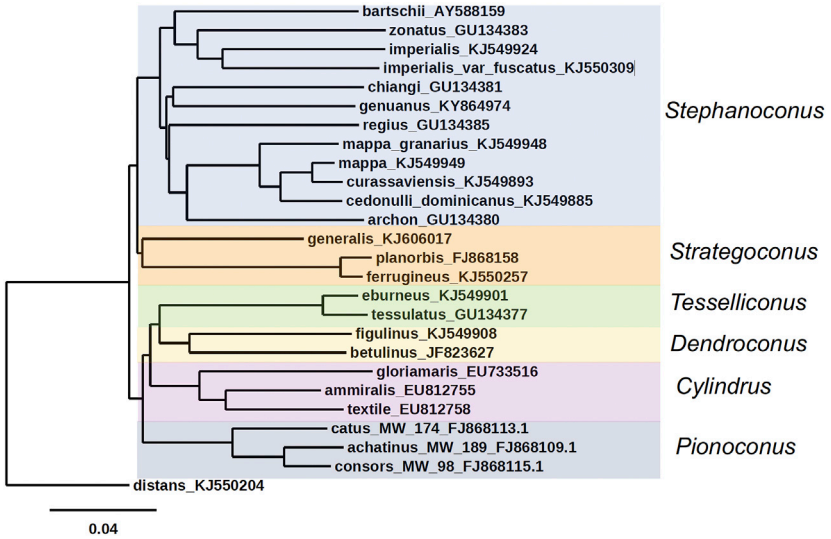

FIGURE 2 | Phylogenetic tree of *Stephanoconus*, *Strategoconus*, *Dendroconus*, *Tesselliconus* (vermivorous), *Cylindrus* (molluscivorous), and *Pionoconus* (piscivorous) clades of *Conus* species, using mitochondrial cytochrome oxidase C (COI) marker. *Conus distans* used as outgroup. Genbank accession numbers KJ549885, KJ549949, KJ549924, KJ549948, KJ549893, KJ549901, KJ5499908, KJ550257, KJ550309, and KJ550204 (Puillandre et al., 2014); GU134380, GU134381, GU134383, and GU134385 (Watkins et al., 2010); AY588159 (Duda and Rolan, 2005); KY864974 (Abalde et al., 2019); FJ868158 (Biggs et al., 2010); KJ606017 (Aman et al., 2015); FJ868109, FJ868113, and FJ868115 (Kantor and Taylor, 2000; Puillandre et al., 2010); EU733516, EU812755, EU812758, and GU134377 (Nam et al., 2009); JF823627 (Cabang et al., 2011; Olivera et al., 2015).

(typified by the α-conopeptides). Much less well-recognized is the emerging evidence that non-peptidic small molecules are used by certain lineages of cone snails as part of their strategy of envenomation. Since the literature is so dominated by studies of conopeptides, we review the expanding literature on small molecule venom components, and present an overview framework for one lineage within the family Conidae, the subgenus *Stephanoconus*, a well-characterized group of vermivorous cone snails. The small molecule strategy of this group is being actively investigated, and we will both review the existing literature and unpublished data, as well as provide a potential framework for future research directions.

THE *STEPHANOCONUS* CLADE: PHYLOGENY AND BIOLOGY

We will describe small molecule natural products broadly across diverse cone snail groups, but the major lineage of cone snails that will be a focus of this article is the *Stephanoconus* clade. Examples of the shells of species in this clade are illustrated in **Figure 1**. These species are not treated in a taxonomically consistent manner in the literature — we regard *Stephanoconus* as a subgenus of *Conus*, within the family Conidae (Puillandre et al., 2014). Other workers (Tucker and Tenorio, 2009; Monnier et al., 2018) have raised *Stephanoconus* to the level of a full genus, and have variously subdivided this group into smaller units (proposing genera such as *Tenorioconus*, *Tarenteconus*, *Rhombiconus*, which we will treat as synonyms of *Stephanoconus*). Some of these proposed genera are recognized as an "alternate representation" by the World Register of Marine Organisms, while others are listed as "unaccepted" (Board, 2020). The molecular data are consistent with including all of the species in **Figure 1** in a single clade, *Stephanoconus*.

An unusual feature of *Stephanoconus* is that the species included have a cosmopolitan distribution, comprising species from the Indo-Pacific, Panamic, Caribbean and Eastern Atlantic marine provinces. There is no other lineage of *Conus* with such a broad geographic distribution (Peters et al., 2013). In most phylogenetic trees, *Stephanoconus* appears as one of the basal lineages within the genus *Conus* (all of the basal lineages are specialists on different types of polychaete worms) (Duda et al., 2001). The phylogenetic tree for the whole genus *Conus* suggests that fish-hunting and mollusc-hunting groups evolved sometime in the Miocene from worm-hunting ancestors (Aman et al., 2015; Olivera et al., 2015). In most of the prior taxonomic literature, the species *Conus genuanus* from the eastern Atlantic has been included in the *Kalloconus* clade (Cunha et al., 2005). However, as noted by Abalde et al. (2019), this was caused by a misidentification, and *C. genuanus* is more closely related to *Conus imperialis*. Despite this, both Abalde et al. (2019) and Tenorio et al. (2020) give *C. genuanus* the genus name *Genuanoconus*. We recently resolved this problem by using many further *Stephanoconus* sequences than are present in those trees, clearly embedding *C. genuanus* within the *Stephanoconus* (**Figure 2**) (Torres et al., 2021), an assignment that will be supported by additional biochemical data presented in this study. Although observations of prey capture are not available for every species within *Stephanoconus*, all of the records in the literature suggest that this group has specialized on amphinomid polychaetes as their major prey (a group widely

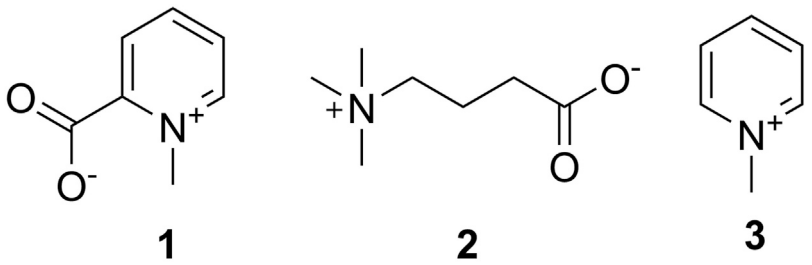

FIGURE 3 | First small molecules identified in cone snails. These compounds were found by Kohn in 1960 in *C. textile*, *C. striatus*; **1** was identified in *C. litteratus*, *C. marmoreus*, and *C. magus*.

known as fireworms, which have painful stinging bristles). This literature has been summarized by Kohn (Kohn, 2014).

The biodiversity of the genus *Conus* is generally richest in the Indo-Pacific marine province, which is not surprising, since this encompasses a vast tract of the tropical marine environment from the Hawaiian Islands to Madagascar. Notably, as Kohn has pointed out, *Stephanoconus* is an apparent exception to this generalization (Kohn, 2014). There were traditionally only two species of *Stephanoconus* recognized from the Indo-Pacific, *C. imperialis* and *Conus zonatus* and three Panamic species: *Conus archon*, *Conus bartschi*, and *Conus brunneus*. In contrast, the speciation in the Western Atlantic and the Caribbean province has been remarkable, and although there are differences of opinion regarding which forms are truly different species (compare the treatment of Kohn (2014) to Monnier et al. (2018), it seems that almost every island group has evolved its own endemic *Stephanoconus* species or subspecies (Kohn, 2014; Monnier et al., 2018). At present, *C. genuanus* is the only member of this clade known from the Eastern Atlantic/Mediterranean province.

All of the non-Indo-Pacific forms of *Stephanoconus* are found in relatively shallow-water marine environments, and have been collected by divers. There is however, one deep-water species group whose biology is poorly known, and these are represented by a set of relatively small Western Pacific species. The best characterized of these is *Conus chiangi* (Watkins et al., 2010). Other small deep-water species such as *Conus polongimarumai* and *Conus suduirauti* likely belong to this group as well. A curious feature of the phylogeny shown in **Figure 2** is that *C. chiangi*, a deep-water Indo-Pacific species, does not appear to branch with the shallow Indo-Pacific species, suggesting that the divergence between deep and shallow-water Indo-Pacific *Stephanoconus* may have occurred before the ancestor of all shallow-water forms radiated out of the Indo-Pacific. Unfortunately, because of their relative rarity, and the difficulty in collecting these deep-water forms, little is known at the present time about their biology or biochemistry.

The division between deep and shallow-water groups can also be observed in the Indo-Pacific *Stephanoconus*. Two different populations comprise *C. imperialis*, which are genetically distinct enough that they may be different species (Torres et al., 2021). One of these occupies shallow, warmer waters, while the other appears to be a deeper-water specialist that may have radiated to cooler Indo-Pacific marine habitats.

NON-PEPTIDIC SMALL MOLECULES REPORTED FROM CONE SNAIL VENOMS

The first identification of non-peptidic venom components in cone snails was the work of Kohn et al. (1960) (**Figure 3**). The presence of homarine (**1**), γ-butyrobetaine (**2**), and *N*-methylpyridinium (**3**) in *Conus textile* and *Conus striatus* venom was established. *Conus marmoreus*, *Conus litteratus*, and *Conus magus* contained **1** as well. In this early work, it was proposed that small molecules might be important for prey capture, a prescient idea that was largely forgotten with the discovery of the conopeptides as the major active components in venom glands.

Following Kohn's pioneering work, a number of small molecule natural products have been observed in diverse cone snail venom glands and other tissues. The identification of serotonin (**4**) in the venom of *C. imperialis* (McIntosh et al., 1993) was the first report where a non-peptide venom component was purified using a bioactivity-based assay (**Figure 4**). However, the first novel non-peptidic compound with a new chemical structure was characterized relatively recently from *C. genuanus* (Neves et al., 2015). Genuanine (**5**), a derivative of guanine with some unique chemical features, had neuroactivity using several different assays.

Neves investigated the small molecules from *Conus genuanus* because he noticed that its venom gland had two different colors, each with different constituents (Neves et al., 2015). The proximal venom gland was the characteristic dull yellow found in most cone snails, and it was dominated by conopeptides. By contrast to most cones, but as is common in *Stephanoconus*, the distal venom gland was deep red in color. Instead of conopeptides, the gland contained mostly small molecules. Neves speculated that these might be important to predation because he observed that when *Conus genuanus* injects its venom into prey polychaetes, the red coloration from the distal venom gland can be readily followed from gland to prey body. The molecule responsible for red coloration has so far eluded structure determination.

Similarly, in a study of *Stephanoconus* feeding behavior, Kohn observed the red coloring from shallow-water *C. imperialis* as it

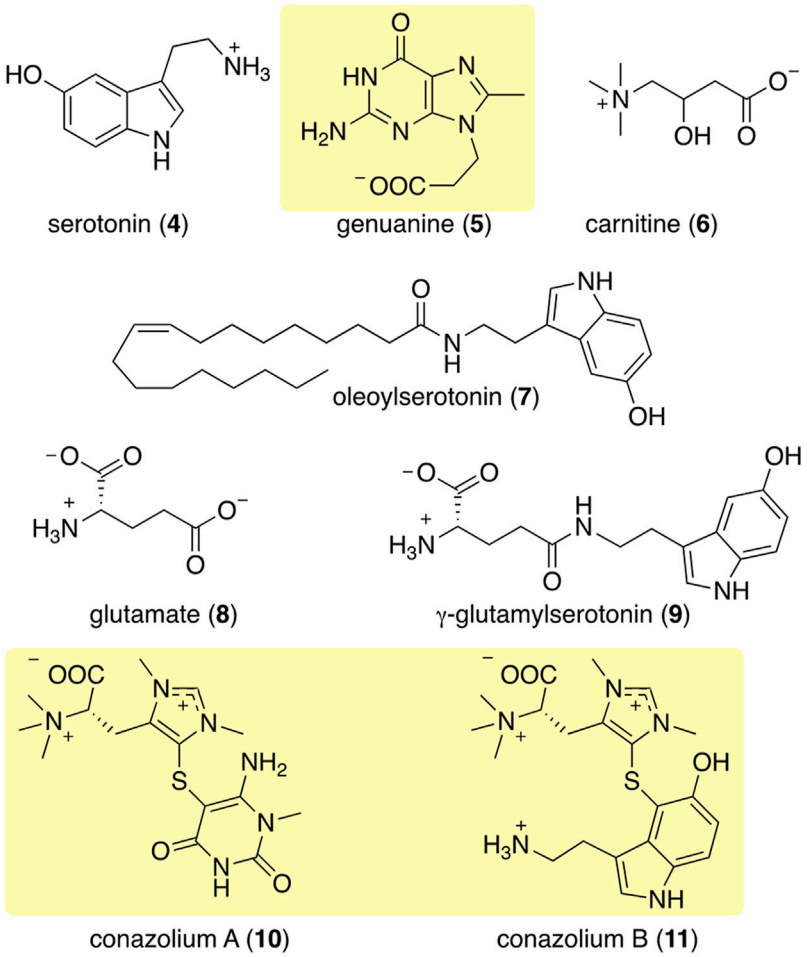

FIGURE 4 | Some of the most abundant compounds discovered in the colored venoms of *Stephanoconus* snails. Those in shaded yellow are compounds so far found only in *Stephanoconus*.

was injected into prey polychaetes (Kohn and Hunter, 2001). Like *C. genuanus*, *C. imperialis* has a bifurcated venom gland, where the proximal end is yellowish while the distal end is deeply pigmented. Because of these similarities, *C. imperialis* chemistry was investigated and compared to that of *C. genuanus* in a metabolomics study (Torres et al., 2021). It should be noted that, at the time we did this study, the close phylogenetic relationship between *C. genuanus* and *C. imperialis* was not known. Like *C. genuanus*, the distal venom gland of *C. imperialis* contains almost solely small molecules, while the proximal venom gland contains mostly conopeptides. Shallow-water *C. imperialis* generally has a dark red distal venom gland, while its deep-water relative has a deep greenish distal gland. In keeping with this color difference, *C. imperialis* had notably different constituents depending upon whether the specimen belonged to the deep- or shallow-water clade, and *C. genuanus* harbored yet another set of compounds.

Using mass spectrometry and nuclear magnetic resonance analyses, the only compounds held in common by all three types of cones were γ-butyrobetaine (**2**), carnitine (**6**), and genuanine (**5**) (**Figures 4**, **5**). The small-molecule constituents of the three types of *Stephanoconus* were quite distinct. As previously shown (McIntosh et al., 1993), shallow-water *C. imperialis* contained the neurotransmitter serotonin (**4**), which was absent from deep-water specimens. The shallow-water specimens also tended to be rich in other neurotransmitters and their derivatives, such as oleoylserotonin (**7**), glutamate (**8**), and γ-glutamylserotonin (**9**) (Torres et al., 2021). These compounds were present in sufficient abundance that they would certainly exhibit activity in prey animals. Essentially, these are cocktails of diverse, neuroactive small molecules, several of which are potently active in annelids.

While they did not contain abundant serotonin or glutamate, the deep-water *C. imperialis* specimens had their own distinctive chemistry. In particular, they were dominated by abundant novel compounds, conazoliums A (**10**) and B (**11**) (Torres et al., 2021). The conazoliums are elaborate derivatives of the antioxidant, ovothiol, which is a common component in marine animals. Indeed, ovothiol and uracil are used by polychaetes as mating pheromones (Zeeck et al., 1996; Zeeck et al., 1998a; Zeeck et al., 1998b; Watson et al., 2000). Based upon that observation, Torres

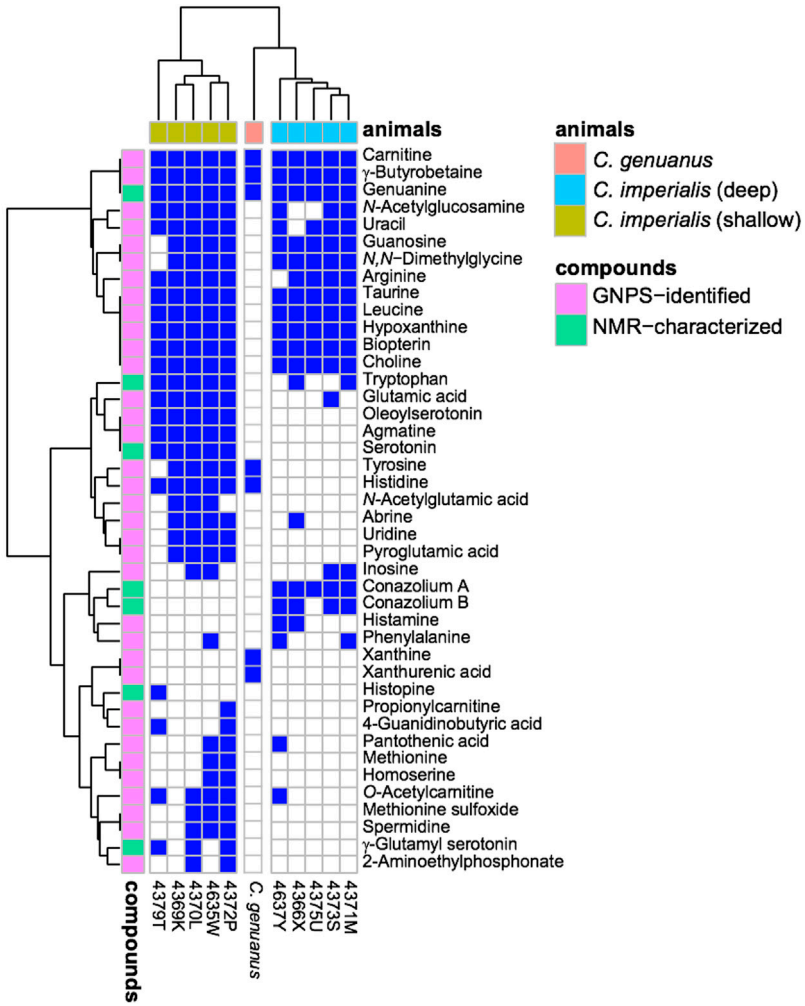

FIGURE 5 | Small molecules in *Stephanoconus* are highly species specific. This chart indicates where each small molecule is found (blue), showing that the deep/shallow *C. imperialis* species and *C. genuanus* contain distinctly different small molecule chemistry in their colored venom glands. GNPS: Global Natural Product Social Molecular Networking.

proposed that conazolium A (**10**) and the uric acid analog genuanine (**5**) might be used in a polychaete prey-capture strategy (Torres et al., 2021). The compounds are highly abundant, with for example **10** comprising ~20% of the dry weight of the venom gland. Addition of conazolium A (**10**) to seawater containing female worms caused the worms to initiate mating behavior. When genuanine (**5**) was added to the seawater near male worms, it led to rapid sperm release. While the normal polychaete hormones are readily degraded both enzymatically and oxidatively, conazolium A (**10**) and genuanine (**5**) are likely stable to common metabolic routes. The resulting worm behaviors suggest a role for these small molecules in attracting prey, in luring them from their burrows, or in interfering with an unknown neuronal target.

In contrast to certain *Stephanoconus* species, other cones generally have venom glands with a single color, which are dominated by conopeptides. While performing bioassay-guided small molecule discovery, we found that in 20 species of cone snails the major compounds present were guanosine (**12**), and the monophosphates of guanosine (**13**) and adenosine (**14**), and often homarine (**1**). These types of compounds are found in *C. imperialis* (Torres et al., 2021) and *C. genuanus* (Neves et al., 2015) as part of a more complex cocktail, but in other species they are the most abundant small molecules (**Table 1**, unpublished data). Since purinosines are signaling molecules involved in pain and other sensory transmission (Burnstock, 2007), it is possible that such components could be involved in predation, although this has yet to be investigated. Purines are involved in spider venoms, for example (Schroeder et al., 2008). An early interpretation of these data, awaiting further work, is that outside of *Stephanoconus*, small molecules may not be important contributors to venoms.

In recent years, the role of the microbiome in shaping animal chemistry has been increasingly appreciated (Morita and Schmidt, 2018). Indeed, marine animals offered some of the first examples where symbiotic bacteria synthesize molecules

TABLE 1 | The most abundant purine derivatives observed in *Conus* venom glands (plus = present; minus = absent)[a].

Subgenus	Species	Compound Number			
		5	12	13	14
Stephanoconus	*C. imperialis* (shallow)	+	+	+	+
	C. imperialis (deep)	+	+	+	+
	C. genuanus	+	+	+	+
Dendroconus	*C. betulinus*	–	+	+	+
Puncticulus	*C. caracteristicus*	–	+	+	+
Gastridium	*C. geographus*	–	+	+	+
Conus	*C. marmoreus*	–	+	+	+
Pionoconus	*C. striatus*	–	+	+	+
Asprella	*C. sulcatus*	–	+	+	+
Virgiconus	*C. virgo*	–	+	+	+

[a]*For* Stephanoconus *species listed here, genuanine (**5**) is the major component. Other, more common purines (**12**–**14**) from primary metabolism are relatively minor in* Stephanoconus*, but represent the major purines in other cone species.*

isolated from the whole animals. In one study of cone snail symbionts, bacteria were cultivated from *Conus rolani* and *Conus tribblei* (Lin et al., 2013). Novel neuroactive pyrones, the nocapyrones, were isolated from the bacteria (**Figure 6**). Subsequently, the same neuroactive compounds were found concentrated in the mucus secretions and in the venom glands of the cones. These were present in sufficient concentrations to modulate neurons in prey animals. The available data suggested that they likely modulate the activity of sodium channels, although the precise targets are not known.

Small molecules have also been identified in other cone snail tissues beyond the venom gland. Several unusual cholesterol derivatives were found in whole body extracts (which included the venom glands) from *Conus pulicarius*, *Conus leopardus*, *Conus ebraeus*, and *Conus tessulatus* (Aknin et al., 1998; Lee et al., 2017).

In summary, although there is still a paucity of literature in the area, current data show that at least some cone snail venom glands are rich in small-molecules, including novel natural products. Many of these are neuroactive in various models, and some directly target the hormonal systems of prey polychaetes. A majority of compounds isolated so far are alkaloids, betaines, neurotransmitters, or purines, with only a small number of non-nitrogenous compounds described. Most of the interesting novel compounds so far found have been concentrated in the single subgenus, *Stephanoconus*, suggesting that members of this group will be a rich source for further discovery.

BIOSYNTHESIS OF CONE SNAIL VENOM SMALL MOLECULES

The conopeptides that are the primary constituents of most cone snail venoms are synthesized in epithelial cells lining the venom gland (Buczek et al., 2005; Safavi-Hemami et al., 2011). Of the biosynthetic mechanisms that are known, they fall squarely into standard eukaryotic metabolic space, and they are encoded in the snail genomes (Arnison et al., 2013). Similarly, of the components so far discovered in cone snail venoms, most are products of common eukaryotic metabolism, and thus are likely made in the venom glands. A few, such as γ-glutamylserotonin (**9**), are relatively restricted in phylogenetic distribution. γ-Glutamylserotonin (**9**) is found in annelids and in the gastropod mollusc *Aplysia californica*, where it was shown to be an enzymatic product of serotonin (**4**) catabolism (McCaman et al., 1985; Sloley, 1994; Stuart et al., 2003). A few of the *Stephanoconus* products are specialized metabolites found so far only in those cones: genuanine (**5**) and the conazolium (**10**–**11**) family of alkaloids. Genuanine (**5**) consists of guanine that has been *C*-methylated, with the addition of *N*-propionate.

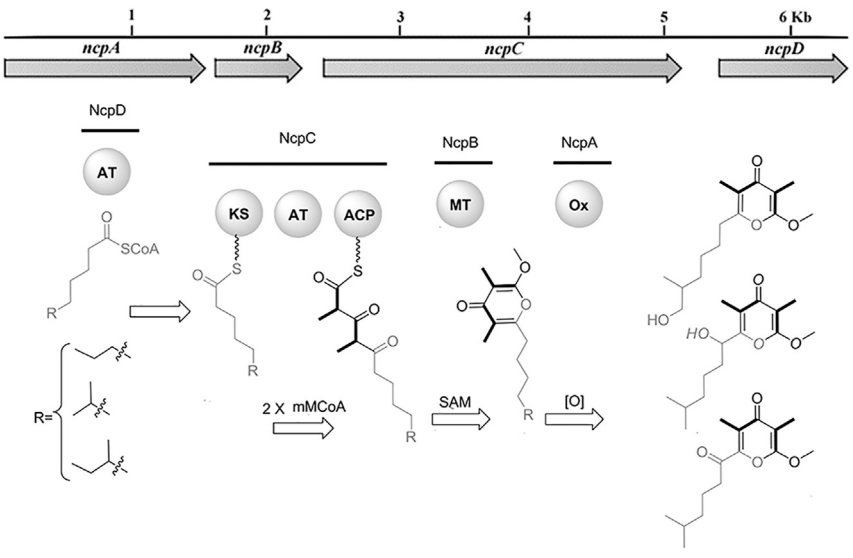

FIGURE 6 | Bacterial biosynthesis of nocapyrones. A genetic locus in *Nocardiopsis* sp. bacteria is responsible for producing ion channel modulators found in the whole snails, *C. rolani* and *C. tribblei*. Bold wedges within chemical structures indicate incorporation of methylmalonate. Figure from Lin et al. (2013).

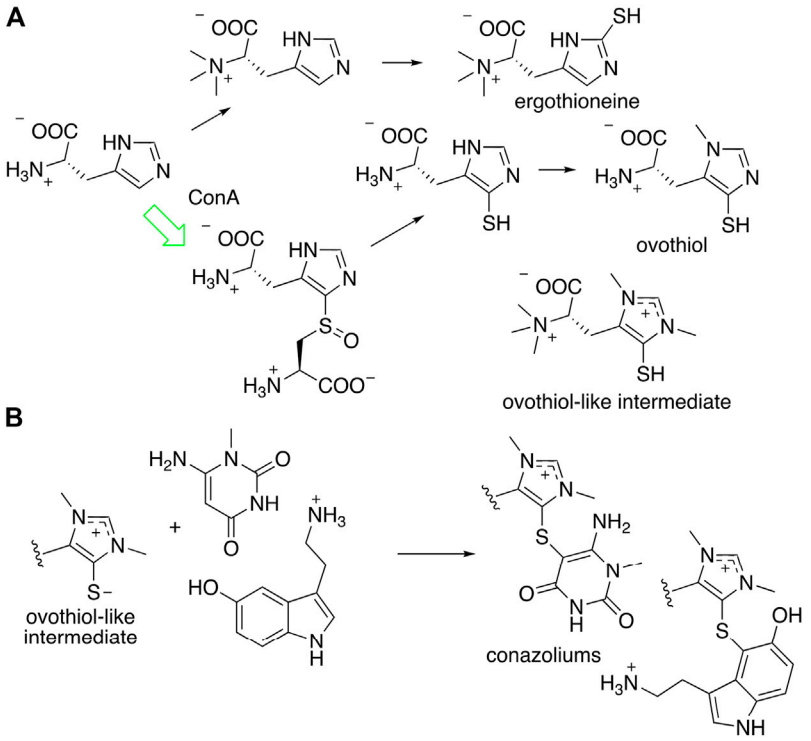

FIGURE 7 | Proposed biosynthesis of conazolium. **(A)** Known routes to antioxidants ergothioneine and ovothiol. The synthesis of an "ovothiol-like intermediate" that is the precursor to conazoliums has features of both pathways, but with an additional methylation on the imidazole ring. The arrow in green indicates a reaction that was characterized using the *C. imperialis* enzyme, ConA. **(B)** The "ovothiol-like intermediate" reacts with electrophilic metabolites to create the conazoliums (**10**–**11**).

The latter is an unprecedented modification in nature, but both the *N*- and *C*-modifications are reminiscent of radical-mediated chemistry (Grove et al., 2011).

Conazoliums (**10**–**11**) are derived from a combination of an ovothiol-like alkaloid and an aromatic residue (**Figure 7**) (Torres et al., 2021). The ovothiol-like side has an unprecedented combination of features. The alpha amine is trimethylated, which is as found in ergothioneine, whereas the imidazole head group is thiolated in the ovothiol position. Both imidazole nitrogens are methylated, forming an imidazolium cation that may have some carbene character. This feature is found in several natural products from marine animals. The biosynthesis of ovothiol has been studied; in animals, the first reactions in the biosynthetic pathway are genetically conserved, but later reactions are not, and for the most part remain unknown. An *ovoA*-like gene, *conA*, is expressed in the colored venom gland of *C. imperialis*. The ConA protein was produced recombinantly in *Escherichia coli* bacteria and purified to homogeneity. When it was treated with the normal substrates of OvoA, ConA produced the expected product, a known intermediate on the ovothiol pathway. Thus, it was shown that the venom glands of *C. imperialis* have the capacity to synthesize the precursor of conazoliums (Torres et al., 2021).

Ovothiol and the related antioxidant ergothioneine have highly nucleophilic sulfur residues that detoxify cells during oxidative stress by removing reactive electrophilic species (Castellano and Seebeck, 2018). In the case of conazoliums (**10**–**11**), the reaction between the ovothiol-like moiety and the aromatic substituents are at the most electrophilic carbon in the molecule. Thus, it is possible that this reaction may even be non-enzymatic. In conazolium A (**10**), an ovothiol-like moiety has reacted with aminomethyluracil, a compound not previously found anywhere in nature, while in conazolium B the uracil moiety has been replaced with serotonin. Natural products featuring ovothiol or its close congeners conjugated with an electrophilic second species have been identified in octopus, sponges, and echinoderms (Castellano and Seebeck, 2018).

Overall, most of the specialized natural products found in cone snail venoms are likely to be made there, using the eukaryotic enzymes in cells lining the venom gland. An exception to this trend may be found in the nocapyrone polyketides, found in both the mucus and the venom glands of *C. rolani* and *C. tribblei*. The biosynthetic locus was identified not in the snails, but in bacteria living within the snails (**Figure 6**; Lin et al., 2013). To provide evidence that the correct locus was identified, the bacterial methyltransferase was expressed in *E. coli*, and the purified enzyme was used in a reaction with the native pyrone substrate, performing the predicted reaction. An unusual polyketide synthase was present in the bacterial locus, but it has not been further investigated.

The specialized metabolites found in cone snail venoms, whether eukaryotic or bacterial in origin, represent a resource for discovering new compounds and biochemical modifications. In the case of conazoliums, for example, although the core

structure is derived from the common metabolite ovothiol, the additional decorations derive from novel biochemical adaptations. It will be of great interest to determine the origin and evolution of these novel compounds and biochemical reactions and the molecular adaptations that take place during their recruitment into the venom gland. In the evolution of venom insulins in cone snails, duplication of an ancestral insulin gene generated two copies, one that retained its endogenous signaling function and another one that experienced neofunctionalization and diversification upon its recruitment into the venom gland (Safavi-Hemami et al., 2016b). Similar mechanisms were shown for enzymes that are important for conopeptide biosynthesis. For example, duplication of an ancestral protein disulfide isomerase (PDI) gene gave rise to a large family of conopeptide-specialized PDIs (csPDIs) that rapidly evolved and diversified to assist in the folding of diverse conopeptide structural disulfide scaffolds (Safavi-Hemami et al., 2016a). It is possible that a similar mechanism comes into play in the origin of venom small molecules (specifically, in the origin of their biosynthetic enzymes), although this has yet to be investigated.

PHARMACOLOGY OF CONE SNAIL VENOM SMALL MOLECULES

The peptide components of cone snail venoms are well known, and their pharmacological properties have been studied for decades (Olivera et al., 2014). By contrast, our understanding of cone snail small molecule pharmacology is in its infancy. Many of the previously described compounds found in cone snail venoms are either neurotransmitters, close relatives of neurotransmitters, or their activities on neurons have been well characterized. Nocapyrones, found in some cone snails in various tissues including venom ducts, are potent modulators of mouse dorsal root ganglion neurons, with IC_{50}s around 2 μM (Lin et al., 2013).

Only two compounds found so far are unique to cone snail venom ducts and are present in sufficient quantities to perform pharmacological studies; these compounds (genuanine (**5**) and conazolium A (**10**)) both have neuromodulatory effects. At a dose of 40 nmol/mouse, genuanine (**5**) paralyzed mice when injected intracranially (Neves et al., 2015). Paralysis was fully reversible after a period of about 2 h. The molecular target leading to paralysis is so far not known. By contrast, conazolium A (**10**) had no obvious effects upon intracranial injection or when loaded onto primary cultures of DRG neurons. Instead, **10** inhibited the human α7 nicotinic acetylcholine receptor with an IC_{50} of 24.4 μM (Torres et al., 2021). This assay was attempted because of the distant resemblance of **10** to urochanycholine (see below), making it likely that this is not the most pharmacologically relevant target. Instead, these findings provide proof-of-concept that, as found with the many well-characterized cone snail venom peptides, the small molecules also exhibit activity on neurons or neuronal targets. These results suggest that cone snail venom small molecules may provide rich sources for further discovery.

CONTEXT AND FUTURE DIRECTIONS

The presence of small molecules in cone snail venoms is far from unique, but is rather a property of diverse venomous animals. Animals such as insects and spiders often contain alkaloids, neurotransmitters, and nucleoside derivatives as major venom components. Although the constituents differ from what we have found in cone snails, the overall pattern is quite similar. What is not always completely clear from the literature is the biological roles that the compounds perform in nature.

Of more interest to drug discovery are the unique, specialized metabolites that are found only in a few species or groups of organisms. These compounds are often highly evolved for specific targets or ecological niches. Thus far, most work has been done in ants and spiders, where unique compounds with human disease-treating potential have been discovered. For example, fire ant-derived solenopsins have been investigated for their potential in treating psoriasis, while spider polyamines have been examined for treating pain and other conditions (Estrada et al., 2007; Arbiser et al., 2017). These and many other alkaloids from spiders and insects are potent, toxic components of offensive/defensive systems (Touchard et al., 2016). Additionally, hydroid and jellyfish venoms are rich in unique small molecules, at least some of which are involved in chemical defense (Stachowicz and Lindquist, 2000; Lindquist, 2002; Reinicke et al., 2020).

Gastropod molluscs have been extensively studied for their bioactive and defensive small molecules, although with little focus on venoms. Much of the work has focused on soft-bodied molluscs. For example, dorid nudibranchs contain diverse small molecules that defend the shell-less molluscs from predation (Faulkner, 1992). Some molluscs, such as *Navanax*, engage in chemical communication and signaling using small molecules (Sleeper and Fenical, 1977). In addition, many molluscs famously bioaccumulate various types of toxins, presumably for defense.

Within the shelled gastropods, data on non-venom compounds have been recently reviewed (Turner et al., 2018). What is evident is that many tissues beyond the venom gland are critical in the chemical ecology of shelled gastropods. For example, a number of choline derivatives, especially urocanycholine (murexine), are secreted from the salivary glands of muricid molluscs (Erspamer and Glasser, 1957; Roseghini et al., 1996). Urocanycholine was briefly under study as a potential therapeutic muscle relaxant because of its nicotinic acetylcholine receptor blocking properties. The hypobranchial gland has also emerged as the locus of defensive compounds. For example, a brominated tryptamine betaine, isolated from the hypobranchial gland defensive secretion of *Calliostoma canaliculatum*, inhibits potassium channels (Kelley et al., 2003). Both murexine and tyrian purple are likely synthesized in the hypobranchial glands of muricids, and subsequently distributed to target tissues where they play different biological roles (Rudd et al., 2015).

However, in contrast to the arthropods where venom small molecules have been intensively studied, relatively little is yet known about the small molecule contribution to gastropod venoms. A few exceptions exist: for example, the blue-ringed octopus envenomates prey with tetrodotoxin (Sheumack et al., 1978). Here, we describe how cone snails, well known for their diverse peptide toxins, also contain small molecules that are used in hunting, and possibly in defense. In particular, the colored venoms of *Stephanoconus* have proved to be a rich source, although even from *Stephanoconus* only a few species have been explored. Most of the >40 cone snail sub-genera comprising the majority of species have not yet been examined. Since there are likely to be hundreds of thousands of venomous animals, the rich known examples of venom small molecules represent just a small part of the chemical potential from venoms. Thus, further examination of these species should yield new bioactive compounds that are used in nature and that might have relevance to human medicine.

One of the major limitations of looking at venom chemistry has been the very small sample sizes available, necessitating cutting-edge instrumentation and a relatively large number of venom glands in order to characterize chemistry. The ability to obtain sufficient biomass has been greatly improved by technological advances in collection such as *lumum-lumun* and tangle nets, methods invented and deployed by Filipino fishermen to collect relatively rare specimens for the collectors trade (Seronay et al., 2010). Another advance is a return to the biology-first approach to drug discovery. In cones, complex hunting strategies are used, where both the behaviors and the chemicals used are highly elaborate and specialized to their habitats (Olivera et al., 2015; Olivera et al., 2017). Conazolium A and genuanine were discovered by chemistry first, but later their role in subduing prey was elucidated. By following the unique behaviors of different cone snail species, we believe that this process could be greatly accelerated.

AUTHOR CONTRIBUTIONS

ZL, NP, and CN performed new chemical analyses described in this study. JPT has worked on all aspects described here. MW performed phylogenetic analysis. JI and JN provided extracts of cone snail venoms. SE took the cone snail photos in **Figure 1**. JT, HS, RF, and MK have participated in our venom small molecules initiative. BO and ES wrote the manuscript.

FUNDING

The ES and BO lab work in this area has been supported by NIH R35GM122521, NIH U19TW008163, NIH P01GM48677, and DOD CDMRP W81XWH-17-1-0413. JN's work is supported by H2020 778069-EMERTOX. RKF-U was supported by grant funding from the National Health & Medical Research Council (NHMRC Program Grant APP1072113) awarded to Prof. D.J. Adams, Illawarra Health and Medical Research Institute (IHMRI), University of Wollongong, Wollongong.

REFERENCES

Abalde, S., Tenorio, M. J., Uribe, J. E., and Zardoya, R. (2019). Conidae phylogenomics and evolution. *Zool Scr* 48, 194–214. doi:10.1111/zsc.12329

Aknin, M., Viracaoundin, I., Faure, R., and Gaydou, E. M. (1998). 5α,8α-Epidioxycholest-6-en-3-β-ol from three cone snails of the Indian ocean. *J. Amer Oil Chem. Soc.* 75, 1679–1681. doi:10.1007/s11746-998-0111-y

Aman, J. W., Imperial, J. S., Ueberheide, B., Zhang, M.-M., Aguilar, M., Taylor, D., et al. (2015). Insights into the origins of fish hunting in venomous cone snails from studies of *Conus tessulatus*. *Proc. Natl. Acad. Sci. USA* 112 (16), 5087–5092. doi:10.1073/pnas.1424435112

Arbiser, J. L., Nowak, R., Michaels, K., Skabytska, Y., Biedermann, T., Lewis, M. J., et al. (2017). Evidence for biochemical barrier restoration: topical solenopsin analogs improve inflammation and acanthosis in the KC-Tie2 mouse model of psoriasis. *Sci. Rep.* 7 (1), 11198. doi:10.1038/s41598-017-10580-y

Arnison, P. G., Bibb, M. J., Bierbaum, G., Bowers, A. A., Bugni, T. S., Bulaj, G., et al. (2013). Ribosomally synthesized and post-translationally modified peptide natural products: overview and recommendations for a universal nomenclature. *Nat. Prod. Rep.* 30 (1), 108–160. doi:10.1039/c2np20085f

Azam, L., and McIntosh, J. M. (2009). Alpha-conotoxins as pharmacological probes of nicotinic acetylcholine receptors. *Acta Pharmacol. Sin.* 30 (6), 771–783. doi:10.1038/aps.2009.47

Biggs, J. S., Watkins, M., Puillandre, N., Ownby, J.-P., Lopez-Vera, E., Christensen, S., et al. (2010). Evolution of *Conus* peptide toxins: analysis of *Conus californicus* Reeve, 1844. *Mol. Phylogenet. Evol.* 56 (1), 1–12. doi:10.1016/j.ympev.2010.03.029

Board, W. E. (2020). World Register of Marine Species. [Online]. Available at: http://www.marinespecies.org (Accessed January 7, 2020)..

Buczek, O., Bulaj, G., and Olivera, B. M. (2005). Conotoxins and the posttranslational modification of secreted gene products. *Cell. Mol. Life Sci.* 62 (24), 3067–3079. doi:10.1007/s00018-005-5283-0

Burnstock, G. (2007). Physiology and pathophysiology of purinergic neurotransmission. *Physiol. Rev.* 87 (2), 659–797. doi:10.1152/physrev.00043.2006

Cabang, A. B., Imperial, J. S., Gajewiak, J., Watkins, M., Corneli, P. S., Olivera, B. M., et al. (2011). Characterization of a venom peptide from a crassispirid gastropod. *Toxicon* 58 (8), 672–680. doi:10.1016/j.toxicon.2011.09.001

Castellano, I., and Seebeck, F. P. (2018). On ovothiol biosynthesis and biological roles: from life in the ocean to therapeutic potential. *Nat. Prod. Rep.* 35 (12), 1241–1250. doi:10.1039/c8np00045j

Cunha, R. L., Castilho, R., Rüber, L., and Zardoya, R. (2005). Patterns of cladogenesis in the venomous marine gastropod genus *Conus* from the Cape Verde islands. *Syst. Biol.* 54 (4), 634–650. doi:10.1080/106351591007471

Duda, T. F., Jr., and Rolán, E. (2005). Explosive radiation of Cape Verde *Conus*, a marine species flock. *Mol. Ecol.* 14 (1), 267–272. doi:10.1111/j.1365-294X.2004.02397.x

Duda, T. F., Jr., Kohn, A. J., and Palumbi, S. R. (2001). Origins of diverse feeding ecologies within *Conus*, a genus of venomous marine gastropods. *Biol. J. Linn. Soc.* 73, 391–409. doi:10.1006/bijl.2001.0544

Erspamer, V., and Glässer, A. (1957). The pharmacological actions of murexine (urocanylcholine). *Br. J. Pharmacol. Chemother.* 12 (2), 176–184. doi:10.1111/j.1476-5381.1957.tb00117.x

Estrada, G., Villegas, E., and Corzo, G. (2007). Spider venoms: a rich source of acylpolyamines and peptides as new leads for CNS drugs. *Nat. Prod. Rep.* 24 (1), 145–161. doi:10.1039/b603083c

Faulkner, D. J. (1992). "Chemical Defenses of Marine Molluscs," in *Ecological Roles of Marine Natural Products*. Editor V. J. Paul (Ithaca: Cornell University Press), 119–163. doi:10.7591/9781501737435-008

Grove, T. L., Benner, J. S., Radle, M. I., Ahlum, J. H., Landgraf, B. J., Krebs, C., et al. (2011). A radically different mechanism for *S*-adenosylmethionine-dependent methyltransferases. *Science* 332 (6029), 604–607. doi:10.1126/science.1200877

Kantor, Y. I., and Taylor, J. D. (2000). Formation of marginal radular teeth in Conoidea (Neogastropoda) and the evolution of the hypodermic envenomation mechanism. *J. Zool.* 252, 251–262. doi:10.1111/j.1469-7998.2000.tb00620.x

Kelley, W. P., Wolters, A. M., Sack, J. T., Jockusch, R. A., Jurchen, J. C., Williams, E. R., et al. (2003). Characterization of a novel gastropod toxin (6-bromo-2-mercaptotryptamine) that inhibits shaker K channel activity. *J. Biol. Chem.* 278 (37), 34934–34942. doi:10.1074/jbc.M301271200

Kohn, A. J. (2014). Conus *of the Southeastern United States and Caribbean*. Princeton: Princeton University Press..

Kohn, A. J., and Hunter, C. (2001). The feeding process in *Conus imperialis*. *Veliger* 44, 232–234.

Kohn, A. J., Nishi, M., and Pernet, B. (1999). Snail spears and scimitars: a character analysis of *Conus* radular teeth. *J. Mollus. Stud.* 65, 461–481. doi:10.1093/mollus/6510.1093/mollus/65.4.461

Kohn, A. J., Saunders, P. R., and Wiener, S. (1960). Preliminary studies on the venom of the marine snail *Conus**. *Ann. N. Y Acad. Sci.* 90, 706–725. doi:10.1111/j.1749-6632.1960.tb26416.x

Kraus, N. J., Corneli, P. S., Watkins, M., Bandyopadhyay, P. K., Seger, J., and Olivera, B. M. (2011). Against expectation: a short sequence with high signal elucidates cone snail phylogeny. *Mol. Phylogenet. Evol.* 58 (2), 383–389. doi:10.1016/j.ympev.2010.11.020

Lee, Y.-J., Han, S., Kim, S., Lee, H.-S., Shin, H., Lee, J., et al. (2017). Three new cytotoxic steroidal glycosides isolated from *Conus pulicarius* collected in Kosrae, Micronesia. *Mar. Drugs* 15 (12), 379. doi:10.3390/md15120379

Lin, Z., Torres, J. P., Ammon, M. A., Marett, L., Teichert, R. W., Reilly, C. A., et al. (2013). A bacterial source for mollusk pyrone polyketides. *Chem. Biol.* 20 (1), 73–81. doi:10.1016/j.chembiol.2012.10.019

Lindquist, N. (2002). Tridentatols D–H, nematocyst metabolites and precursors of the activated chemical defense in the marine HydroidTridentatamarginata (Kirchenpauer 1864). *J. Nat. Prod.* 65 (5), 681–684. doi:10.1021/np010339e

McCaman, M. W., Stetzler, J., and Clark, B. (1985). Synthesis of ?-Glutamyldopamine and other peptidoamines in the nervous system of *Aplysia californica*. *J. Neurochem.* 45 (6), 1828–1835. doi:10.1111/j.1471-4159.1985.tb10540.x

McIntosh, J. M., Foderaro, T. A., Li, W., Ireland, C. M., and Olivera, B. M. (1993). Presence of serotonin in the venom of *Conus imperialis*. *Toxicon* 31 (12), 1561–1566. doi:10.1016/0041-0101(93)90340-o

McIntosh, J. M., Santos, A. D., and Olivera, B. M. (1999). ConusPeptides targeted to specific nicotinic acetylcholine receptor subtypes. *Annu. Rev. Biochem.* 68, 59–88. doi:10.1146/annurev.biochem.68.1.59

Monnier, E., Limpalaër, L., Robin, A., and Roux, C. (2018). *A taxonomic iconography of living Conidae - Volume 1*. Harxheim, Germany: ConchBooks..

Morita, M., and Schmidt, E. W. (2018). Parallel lives of symbionts and hosts: chemical mutualism in marine animals. *Nat. Prod. Rep.* 35 (4), 357–378. doi:10.1039/c7np00053g

Nam, H. H., Corneli, P. S., Watkins, M., Olivera, B., and Bandyopadhyay, P. (2009). Multiple genes elucidate the evolution of venomous snail-hunting *Conus* species. *Mol. Phylogenet. Evol.* 53 (3), 645–652. doi:10.1016/j.ympev.2009.07.013

Neves, J. L. B., Lin, Z., Imperial, J. S., Antunes, A., Vasconcelos, V., Olivera, B. M., et al. (2015). Small molecules in the cone snail arsenal. *Org. Lett.* 17 (20), 4933–4935. doi:10.1021/acs.orglett.5b02389

Olivera, B. M., Raghuraman, S., Schmidt, E. W., and Safavi-Hemami, H. (2017). Linking neuroethology to the chemical biology of natural products: interactions between cone snails and their fish prey, a case study. *J. Comp. Physiol. A.* 203 (9), 717–735. doi:10.1007/s00359-017-1183-7

Olivera, B. M., Seger, J., Horvath, M. P., and Fedosov, A. E. (2015). Prey-capture strategies of fish-hunting cone snails: behavior, neurobiology and evolution. *Brain Behav. Evol.* 86 (1), 58–74. doi:10.1159/000438449

Olivera, B. M., Showers Corneli, P., Watkins, M., and Fedosov, A. (2014). Biodiversity of cone snails and other venomous marine gastropods: evolutionary success through neuropharmacology. *Annu. Rev. Anim. Biosci.* 2, 487–513. doi:10.1146/annurev-animal-022513-114124

Peters, H., O'Leary, B. C., Hawkins, J. P., Carpenter, K. E., and Roberts, C. M. (2013). *Conus*: first comprehensive conservation red list assessment of a marine gastropod mollusc genus. *PLoS One* 8 (12), e83353. doi:10.1371/journal.pone.0083353

Puillandre, N., Bouchet, P., Duda, T. F., Jr., Kauferstein, S., Kohn, A. J., Olivera, B. M., et al. (2014). Molecular phylogeny and evolution of the cone snails (Gastropoda, Conoidea). *Mol. Phylogenet. Evol.* 78, 290–303. doi:10.1016/j.ympev.2014.05.023

Puillandre, N., Watkins, M., and Olivera, B. M. (2010). Evolution of *Conus* peptide genes: duplication and positive selection in the A-superfamily. *J. Mol. Evol.* 70 (2), 190–202. doi:10.1007/s00239-010-9321-7

Reinicke, J., Kitatani, R., Masoud, S. S., Galbraith, K. K., Yoshida, W., Igarashi, A., et al. (2020). Isolation, structure determination, and synthesis of cyclic tetraglutamic acids from box jellyfish species *Alatina alata* and *Chironex yamaguchii*. *Molecules* 25 (4), 883. doi:10.3390/molecules25040883

Robinson, S., and Norton, R. (2014). Conotoxin gene superfamilies. *Mar. Drugs* 12 (12), 6058–6101. doi:10.3390/md12126058

Roseghini, M., Severini, C., Erspamer, G. F., and Vittorio, E. (1996). Choline esters and biogenic amines in the hypobranchial gland of 55 molluscan species of the neogastropod Muricoidea superfamily. *Toxicon* 34 (1), 33–55. doi:10.1016/0041-0101(95)00104-2

Rudd, D., Ronci, M., Johnston, M. R., Guinan, T., Voelcker, N. H., and Benkendorff, K. (2015). Mass spectrometry imaging reveals new biological roles for choline esters and Tyrian purple precursors in muricid molluscs. *Sci. Rep.* 5, 13408. doi:10.1038/srep13408

Safavi-Hemami, H., Li, Q., Jackson, R. L., Song, A. S., Boomsma, W., Bandyopadhyay, P. K., et al. (2016a). Rapid expansion of the protein disulfide isomerase gene family facilitates the folding of venom peptides. *Proc. Natl. Acad. Sci. U S A* 113 (12), 3227–3232. doi:10.1073/pnas.1525790113

Safavi-Hemami, H., Lu, A., Li, Q., Fedosov, A. E., Biggs, J., Showers Corneli, P., et al. (2016b). Venom insulins of cone snails diversify rapidly and track prey taxa. *Mol. Biol. Evol.* 33 (11), 2924–2934. doi:10.1093/molbev/msw174

Safavi-Hemami, H., Siero, W. A., Gorasia, D. G., Young, N. D., Macmillan, D., Williamson, N. A., et al. (2011). Specialisation of the venom gland proteome in predatory cone snails reveals functional diversification of the conotoxin biosynthetic pathway. *J. Proteome Res.* 10 (9), 3904–3919. doi:10.1021/pr1012976

Schroeder, F. C., Taggi, A. E., Gronquist, M., Malik, R. U., Grant, J. B., Eisner, T., et al. (2008). NMR-spectroscopic screening of spider venom reveals sulfated nucleosides as major components for the brown recluse and related species. *Proc. Natl. Acad. Sci. U. S. A.* 105 (38), 14283–14287. doi:10.1073/pnas.0806840105

Seronay, R. A., Fedosov, A. E., Astilla, M. A. Q., Watkins, M., Saguil, N., Heralde, F. M., 3rd, et al. (2010). Accessing novel conoidean venoms: biodiverse lumun-lumun marine communities, an untapped biological and toxinological resource. *Toxicon* 56 (7), 1257–1266. doi:10.1016/j.toxicon.2009.12.002

Sheumack, D., Howden, M., Spence, I., and Quinn, R. (1978). Maculotoxin: a neurotoxin from the venom glands of the octopus *Hapalochlaena maculosa* identified as tetrodotoxin. *Science* 199 (4325), 188–189. doi:10.1126/science.619451

Sleeper, H. L., and Fenical, W. (1977). Navenones A-C: trail-breaking alarm pheromones from the marine opisthobranch Navanax inermis. *J. Am. Chem. Soc.* 99 (7), 2367–2368. doi:10.1021/ja00449a072

Sloley, B. D. (1994). γ-Glutamyl conjugation of 5-hydroxytryptamine (serotonin) in the earthworm (Lumbricus terrestris). *Neurochem. Res.* 19 (2), 217–222. doi:10.1007/BF00966819

Stachowicz, J. J., and Lindquist, N. (2000). Hydroid defenses against predators: the importance of secondary metabolites versus nematocysts. *Oecologia* 124 (2), 280–288. doi:10.1007/s004420000372

Stuart, J. N., Zhang, X., Jakubowski, J. A., Romanova, E. V., and Sweedler, J. V. (2003). Serotonin catabolism depends upon location of release: characterization of sulfated and γ-glutamylated serotonin metabolites in Aplysia californica. *J. Neurochem.* 84 (6), 1358–1366. doi:10.1046/j.1471-4159.2003.01617.x

Tenorio, M. J., Abalde, S., Pardos-Blas, J. R., and Zardoya, R. (2020). Taxonomic revision of West African cone snails (Gastropoda: Conidae) based upon mitogenomic studies: implications for conservation. *Ejt* 663, 1–89. doi:10.5852/ejt.2020.663

Torres, J. P., Lin, Z., Watkins, M., Floréz Salcedo, P., Baskin, R. P., Elhabian, S., et al. (2021). Small molecule mimicry hunting strategy in the imperial cone snail, *Conus imperialis*. *Sci. Adv.* 7 (11), eabf2704. doi:10.1126/sciadv.abf2704

Touchard, A., Aili, S., Fox, E., Escoubas, P., Orivel, J., Nicholson, G., et al. (2016). The biochemical toxin arsenal from ant venoms. *Toxins* 8 (1), 30. doi:10.3390/toxins8010030

Tucker, J. K., and Tenorio, M. J. (2009). *Systemic classification of recent and fossil gastropods*. Hackenheim: Conchbooks..

Turner, A., Craik, D., Kaas, Q., and Schroeder, C. (2018). Bioactive compounds isolated from neglected predatory marine gastropods. *Mar. Drugs* 16 (4), 118. doi:10.3390/md16040118

Watkins, M., Cornell, P. S., Hillyard, D., and Olivera, B. M. (2010). Molecular phylogeny of *Conus chiangi* (Azuma, 1972) (Gastropoda: Conidae). *Nautilus* 124 (3), 129–136.

Watson, G., Langford, F., Gaudron, S., and Bentley, M. (2000). Factors influencing spawning and pairing in the scale worm *Harmothoe imbricata* (Annelida: Polychaeta). *Biol. Bull.* 199 (1), 50–58. doi:10.2307/1542706

Zeeck, E., Harder, T., and Beckmann, M. (1998a). Inosine, L-glutamic acid and L-glutamine as components of a sex pheromone complex of the marine polychaete Nereis succinea (Annelida: Polychaeta). *Chemoecology* 8, 77–84. doi:10.1007/PL00001807/

Zeeck, E., Harder, T., Beckmann, M., and Müller, C. T. (1996). Marine gamete-release pheromones. *Nature* 382, 214. doi:10.1038/382214a0

Zeeck, E., Harder, T., and Beckmann, M. (1998b). Uric acid: the sperm release pheromone of the marine polchaete *Platynereis dumerilii*. *J. Chem. Ecol.* 24, 13–22. doi:10.1023/A:1022328610423

Conflict of Interest: The authors declare that the research was conducted in the absence of any commercial or financial relationships that could be construed as a potential conflict of interest.

Advantages of publishing in Frontiers

OPEN ACCESS
Articles are free to read for greatest visibility and readership

FAST PUBLICATION
Around 90 days from submission to decision

HIGH QUALITY PEER-REVIEW
Rigorous, collaborative, and constructive peer-review

TRANSPARENT PEER-REVIEW
Editors and reviewers acknowledged by name on published articles

Frontiers
Avenue du Tribunal-Fédéral 34
1005 Lausanne | Switzerland

Visit us: www.frontiersin.org
Contact us: frontiersin.org/about/contact

REPRODUCIBILITY OF RESEARCH
Support open data and methods to enhance research reproducibility

DIGITAL PUBLISHING
Articles designed for optimal readership across devices

FOLLOW US
@frontiersin

IMPACT METRICS
Advanced article metrics track visibility across digital media

EXTENSIVE PROMOTION
Marketing and promotion of impactful research

LOOP RESEARCH NETWORK
Our network increases your article's readership